



Universitat
de les Illes Balears

DOCTORAL THESIS

2016

**STUDIES ON MOLECULAR CAVITIES:
SYNTHESIS, CHARACTERIZATION AND
APPLICATIONS**

Elena Sanna Martínez



Universitat
de les Illes Balears

DOCTORAL THESIS

2016

**Doctoral Programme of Chemical Science and
Technology**

**STUDIES ON MOLECULAR CAVITIES:
SYNTHESIS, CHARACTERIZATION AND
APPLICATIONS**

Elena Sanna Martínez

Thesis supervisor: Dr. Antoni Costa Torres

Thesis supervisor: Dra. Carmen Rotger Pons

Doctor by the Universitat de les Illes Balears



Universitat
de les Illes Balears

Dr Antoni Costa Torres and Dr Carmen Rotger Pons, of University of Balearic Islands

WE DECLARE:

That the thesis entitled *Studies on Molecular Cavities: Synthesis, Characterization and Applications*, presented by Elena Sanna Martínez to obtain a doctoral degree, has been completed under our supervision and meets the requirements to opt for a European Doctorate.

For all intents and purposes, we hereby sign this document.

Signature

Dr. Antoni Costa

Dra. M^a Carmen Rotger

Palma de Mallorca, 15/01/2016

The results derived from this thesis have resulted in the publication of the following scientific articles:

1. Soberats, B.; Sanna, E.; Martorell, G.; Rotger, C.; Costa, A. Programmed Enzyme-Mimic Hydrolysis of a Choline Carbonate by a Metal-Free 2-Aminobenzimidazole-Based Cavitand.

Org. Lett. **2014**, *16*, 840-843.

2. Sanna, E.; Escudero, E. C.; Bauza, A.; Ballester, P.; Frontera, A.; Rotger, C.; Costa, A. A crystalline sponge based on dispersive forces suitable for X-ray structure determination of included molecular guests.

Chem. Sci. **2015**, *6*, 5466-5472.

3. Sanna, E.; López, C.; Ballester, P.; Rotger, C.; Costa, A. Unexpected Squaramide-Induced Cleavage of Benzils: Synthesis and Characterization of Mono-Aroyl Squarimides.

Eur. J. Org. Chem. **2015**, *35*, 7656-7660.

Other publications derived from collaborations during this thesis:

1. Sanna, E.; Martínez, L.; Rotger, C.; Blasco, S.; Gonzalez, J.; Garcia-España, E.; Costa, A. Squaramide-Based reagent for selective chromogenic Sensing of Cu(II) through a Zwitterion radical.

Org. Lett. **2010**, *12*, 3840-3843.

2. Martínez, L.; Sampedro, A.; Sanna, E.; Costa, A.; Rotger, C. Synthesis and conformational studies of peptido-squaramide foldable modules: a new class of turn-mimetic compounds.

Org. Biomol. Chem. **2012**, *10*, 1914-1921.

3. Soberats, B.; Martínez, L.; Sanna, E.; Sampedro, A.; Rotger, C.; Costa, A. Janus-Like squaramide-based hosts: dual mode of binding and conformational transitions driven by ion-pair recognition.

Chem. Eur. J. **2012**, *18*, 7533 – 7542.

4. López, C.; Sanna, E.; Carreras, C.; Vega, M.; Rotger, C.; Costa, A. Molecular Recognition of Zwitterions: Enhanced Binding and Selective Recognition of Miltefosine by Squaramide-Based Host.

Chem. Asian J. **2013**, *8*, 84–87.

5. López, C.; Vega, M.; Sanna, E.; Rotger, C.; Costa, A. Efficient microwave-assisted preparation of squaric acid monoamides in water.

RSC Adv. **2013**, *3*, 7249-7253.

Acknowledgements

Esta aventura empezó hace ya unos años. Sinceramente, ni yo tenía confianza en que pudiera hacerlo y, bueno, al final descubrí poco a poco que esto era lo mío. No soy persona de muchas palabras así que, seré breve. En primer lugar me gustaría dar las gracias a mi director de tesis por darme la oportunidad de hacer esta tesis y, sobretodo, por creer en mí. Gracias por las horas discutiendo en tu despacho, por la ayuda que siempre me has dado y, sobre todo, por todo lo que he aprendido. También me gustaría dar las gracias a mi codirectora de tesis por la ayuda que me has dado y las charlas random después de comer.

Igualmente me gustaría dar las gracias a todo el grupo de Química Supramolecular por los buenos ratos, las meriendas, las comidas de grupo y, sobre todo, por hacer más animada la hora de la comida. A mis compis de lab: Manel, Lluís, Ángel, Xisca, Marta, Alberto, Carlos, Ruth. A los “vecinos”: Susana, Paulina, Paulino, Cristina, David, Toni F, Toni B. A los que ya no están: Tomeu, Lucas, Xavi, Carol, Santy. A todos, gracias por hacer que estos años hayan pasado volando y que ahora me cueste decir adiós. Y como no a Kenia, empezamos juntas en esto de la química y ahí seguimos 10 años después.

También me gustaría dar las gracias al Servei Cientifictècnic de la UIB por estar siempre dispuestos a ayudarme. Especialmente a Biel, a Jose, a Juan, a Ferran y a Rosa, gracias por hacerme siempre un hueco.

I want also to thank to Christopher Hunter to let me stay in his lab for a few months and to the entire Hunter group for make me feel like at home.

Quiero también a agradecer a la Conselleria d'Educació, Cultura i Universitats del Govern Balear y al Fondo Social Europeo la beca concedida sin la que esta aventura no hubiera sido posible.

Y, sobre todo, quiero agradecer a mis padres y a mis hermanas todo su apoyo (aunque todavía no entiendan muy bien lo que hago). Pero, en especial, a mis dos princesitas rubias por ayudarme siempre a desconectar y despertarme siempre con una sonrisa.

Gracias a todos.

Pero ante todo: STOP DRAMAS!!!



Universitat
de les Illes Balears



An investigator starts research in a new field with faith, a foggy idea, and a few wild experiments. Eventually the interplay of negative and positive results guides the work. By the time the research is completed, he or she knows how it should have been started and conducted.

DONALD J. CRAM

Chemical abbreviations

DHB	2,5-Dihydroxybenzoic acid
2-ABI	2-aminobenzimidazole
BOC-ON	[2-(<i>tert</i> -butoxycarbonyloxyimino)-2-phenylacetonitrile]
A	Absorbance
MeCN/ACN	Acetonitrile
AcCho	Acetylcholine
AcChE	Acetylcholinesterase
AD	Acidic drugs
AIDS	Acquired immune deficiency syndrome
a.k.a	Also known as
Å	Ångström
BzPh	Benzyl butyl phthalate
OcPh	Bis(2-ethylhexyl) phthalate
BET	Brunauer–Emmett–Teller
CA	Calix[n]arene
CCDC	Cambridge Crystallographic Data Centre
Cbz	Carboxybenzyl
°C	Celsius degree
δ	Chemical shift
CHCl ₃	Chloroform
Cho	Choline
CT	Computed tomography
COSY	Correlation spectroscopy
J	Coupling constant
COF	Covalent Organic Framework
CTF	Covalent Triazine-based Frameworks
CP MAS	Cross Polarization Magic Angle Spinning
CB	Cucurbit[n]uril
CD	Cyclodextrin
DNA	Deoxyribonucleic acid
NaOD	Deuterated sodium hydroxide
BuPh	Dibutyl phthalate
CH ₂ Cl ₂	Dichloromethane
Et ₂ O	Diethyl ether
EtPh	Diethyl phthalate
SQA/SQ	Diethyl squarate
DTPA	Diethylenetriamine pentaacetate
DMSO	Dimethyl sulfoxide
DAD	Diode array detector
DFT	Discrete Fourier transform
K _d	Dissociation constant
Boc ₂ O	Di- <i>tert</i> -butyl dicarbonate
DOX	Doxorubicin
DCC	Dynamic Covalent Chemistry
DSC	Differential Scanning Calorimetry
DLS	Dynamic Light Scattering
EPR	Electron paramagnetic resonance
ESI-MS	Electrospray Ionisation Mass Spectrometry
EtOH	Ethanol
AcOEt	Ethyl acetate
e. g.	For example
GC	Gas chromatography
GPC	Gel permeation chromatography
ΔG	Gibbs free energy

g	Gram
HMBC	Heteronuclear multiple-bond correlation spectroscopy
HSQC	Heteronuclear single quantum coherence spectroscopy
HRMS	High Resolution Mass Spectrometry
HPLC	High-performance liquid chromatography
IR	Infrared Spectroscopy
IUPAC	International Union of Pure and Applied Chemistry
K	Kelvin degree
Kcal	kilocalories
kJ	kiloJoule
Lys	Lysine
MRI	Magnetic resonance imaging
m/z	Mass-to-charge ratio
MALDI-TOF	Matrix-assisted laser desorption/ionization – Time of Flight
MHz	Megahertz
m.p.	Melting point
MOF	Metal Organic Framework
MeOH	Methanol
MW	Microwave
mL	Millilitres
min	Minute
M	Molarity
DIPEA	N,N-Diisopropylethylamine
DMPD	N,N-Dimethylaminophenylenediamine
DMF	N,N-Dimethylformamide
NMP	N-Methylpyrrolidone
NCI	Non-covalent interaction
NMR	Nuclear magnetic resonance
ns	Number of scans
ORTEP	Oak Ridge Thermal Ellipsoid Plot
ppm	Parts-per-million
Phe	Phenylalanine
P	Pillar[n]arenes
PNPCC	p-Nitrophenylcholine Carbonate
PAMAM	Polyamidoamine dendrimer
PEG	Polyethylene glycol
PLL	Poly-L-Lysine dendrimers
PPI	Polypropylenimine dendrimer
PCP	Porous Coordination Polymers
POMC	Porous Organic Molecular Crystals
τ	Relaxation time
RNA	Ribonucleic acid
r.t.	Room temperature
ROESY	Rotating-frame nuclear Overhauser effect correlation spectroscopy
SEM	Scanning electron microscope
siRNA	Small interference RNA
SQI	Squarimide
DOTA	Tetraazacyclododecane tetraacetic acid
TMS	Tetramethylsilane
TGA	Thermogravimetric analysis
NCS	Thiocyanate
EtSH	Thioethanol
DCTB	Trans-2-[3-(4-tert-Butylphenyl)-2-methyl-2-propenyldiene]malononitrile
Tf	Transferrin
TEA	Triethylamine
TFA	Trifluoroacetic
Tris	Tris(hydroxymethyl)aminomethane

Trp	Tryptophan
Tyr	Tyrosine
UV-Vis	Ultraviolet-visible spectroscopy
λ	Wavelength
WGA	Wheat germ agglutinin

Abstract

This PhD thesis involves compounds that present various types of cavities intended for supramolecular studies. Specifically, the work is divided into five chapters.

Chapter 1. The general introduction offers a general description of the supramolecular chemistry. There is a description of the properties of the fundamental non-covalent interactions and their relevance in host-guest chemistry as well as in self-assembly. This chapter also details the features of the squaramides as the squaramide moiety is a motif repeatedly used in this work to obtain new squaramido-based compounds for supramolecular applications.

Chapter 2. The properties of a 2-aminobenzimidazole functionalized deep cavitand previously synthesized in our laboratory have been studied in solution. The cavitand encapsulates trimethylammonium compounds such as choline and acetylcholine with association constants on the order of 10^4 M in MeCN:H₂O mixtures. As a proof of concept, the catalytic properties of the cavitand have been applied to the study of the hydrolysis of *p*-nitrophenyl choline carbamate. In this case, the hydrolysis was achieved in three steps that were monitored by UV-vis and ¹H-NMR spectroscopy. The first step was the recognition of the choline carbamate by the cavity, followed by the carbamoylation of the cavitand compound and the hydrolysis of this intermediate to yield choline. The formation of the carbamoyl derivate was completed after 18 h while the last step was a very slow process that proceeds in around 30 days. These results suggest that the cavitand acts as a mimic of an acetylcholinesterase inhibitor.

Chapter 3. A new family of imine-based macrocyclic compounds has been synthesized by the condensation of two aromatic dialdehydes (isophthalaldehyde and terephthalaldehyde) with 1,3- and 1,4-propargyldiamines in various solvents such as EtOAc or MeOH. The cycloimine that result of the reaction between terephthalaldehyde and 1,3-phenylene-bis-propargylic diamine crystallizes giving a porous structure that is maintained after desolvation. The apohost was filled with guest molecules of different size and featuring a variety of functional groups, such as nitromethane, diethyl squarate, *p*-xylene, ethylene glycol, *p*-anisaldehyde, cis-stilbene, (R)-(+)-limonene, (S)-(-)-nicotine or diethyl phthalate. Overall, this material can be used as a solid support for the structure determination of guest molecules by the crystalline sponge method developed by Fujita et al. Also, preliminary selectivity studies have been conducted using 1:1 v/v mixtures of four phthalates, namely: diethyl phthalate, dibutyl phthalate, benzyl butyl phthalate and di(2-ethylhexyl) phthalate. Under these conditions, the crystal compound has shown selectivity for diethyl phthalate over the other phthalate derivatives.

Chapter 4. Squaramide-based macrocycles analogs to multifarenes have been prepared by reaction of 1,3-dibromobenzil with a bicyclic squaramide derivative in DMF in the presence of Cs₂CO₂. However, the synthetic process yielded an inseparable mixture of oligomeric compounds featuring a variable number of squaramide units. In the course of these reactions, unexpectedly, it was observed the formation of aromatic mono-substituted squarimide compounds. These compounds, rarely described in the literature, were produced in fairly good yields by the reaction between 4,4'-benzils with squaramide or N,N-diethyl squaramide in basic medium. This reaction implied the cleavage of the inter-carbonyl bond of the benzil derivative. The p*H* of the NH group of the resulting squarimides determined in H₂O:MeCN 9:1 v/v mixtures resulted more acidic than the equivalent NH of plain squaramide derivatives.

Chapter 5. A new set of squaramido-amino-based dendrimeric compounds intended for future biological applications has been designed and partially prepared. As part of this work, four polyamines with variable chain lengths and branching units were chosen as core molecules. Moreover, two squaramide-based growing units with different chain length were synthesized. First and second generation

compounds could be successfully isolated and characterized by the reaction of each core molecule with the growing units in an alcoholic medium. The larger and more flexible building blocks have been the most promising candidates because they enable a better accommodation of the more branched third and fourth generations of the dendrimers.

Resumen

Esta tesis describe compuestos que presentan diferentes tipos de cavidades para llevar a cabo estudios supramoleculares. Específicamente, el trabajo aquí descrito se encuentra dividido en cinco capítulos.

Capítulo 1. La introducción general ofrece una descripción general de la química supramolecular. Para ello, se describen las propiedades de las principales interacciones no covalentes y su importancia en la química de huésped:hospedador al igual que en procesos de auto-ensamblaje. Este capítulo también describe las características de las escuaramidas ya que el grupo escuaramida se ha utilizado repetidamente en esta tesis para la obtención de nuevos compuestos con aplicaciones supramoleculares.

Capítulo 2. Se han estudiado las propiedades en disolución de un cavitando profundo funcionalizado con grupos 2-aminobenzimidazol previamente sintetizado en nuestro laboratorio. El cavitando encapsula compuestos trimetilamonio como colina y acetilcolina con constantes de asociación del orden de 10^4 M en mezclas MeCN:H₂O. Como prueba de concepto, las propiedades catalíticas del cavitando se han aplicado en el estudio de la hidrólisis del *p*-nitrofenilcarbonato de colina. En este caso, el proceso de hidrólisis tiene lugar en tres pasos que fueron monitorizados por UV-vis y espectroscopia de RMN. El primer paso de la hidrólisis consiste en el reconocimiento del carbamato de colina por parte de la cavidad, seguido de la carbamoilación del cavitando y la hidrólisis de este intermedio para dar colina. La formación del derivado de carbamoil se completó tras 18 horas de reacción mientras que el último paso resultó ser un proceso muy lento que tenía lugar en unos 30 días. Estos resultados sugieren que el cavitando actúa como mímico de un inhibidor de acetilcolinesterasas.

Capítulo 3. Se ha sintetizado una nueva familia de compuestos macrocíclicos basados en enlaces imina como resultado de la condensación de dos aldehídos aromáticos (isofthalaldehído y tereftalaldehído) con 1,3- y 1,4-propargildiaminas en varios disolventes como AcOEt o MeOH. La cicloimina resultante de la reacción entre tereftalaldehído y 1,3-fenilen-bis-propargildiamina cristaliza generando una estructura porosa que se mantiene tras la desolvatación. Los canales del cristal pueden ser ocupados por moléculas de diferente tamaño y que presentan diferentes grupos funcionales, como nitrometano, escuarato de dietilo, *p*-xileno, etilenglicol, *p*-anisalaldehído, *cis*-estilbeno, (R)-(+)-limoneno, (S)-(-)-nicotina o ftalato de dietilo. En general, este material puede utilizarse como soporte sólido para la determinación estructural de moléculas huésped mediante el método de la esponja cristalina desarrollado por Fujita et al. Además, se han llevado a cabo estudios de selectividad utilizando mezclas 1:1 v/v de diferentes ftalatos: ftalato de dietilo, ftalato de dibutilo, ftalato de butil bencilo y ftalato de di-2-etilhexilo. En estas condiciones, el compuesto cristalino ha mostrado selectividad por ftalato de dietilo frente a los otros derivados de ftalato.

Capítulo 4. Se han preparado compuestos supramoleculares basados en escuaramidas análogos a los multifarenos mediante la reacción de 1,3-dibromobenzilo con una escuaramida bicíclica en DMF en presencia de Cs₂CO₃. Sin embargo, el proceso sintético generó una mezcla de productos inseparables con un número variable de unidades escuaramida. Durante el proceso de síntesis, inesperadamente, se observó la formación de compuestos escuarimida aromáticos monofuncionalizados. Estos productos, raramente descritos en la bibliografía, se produjeron con rendimientos aceptables mediante la reacción de benzilos 4,4'- funcionalizados con escuaramida o N,N-dietilescuaramida en medio básico. Esta reacción implica la rotura del enlace intercarbonílico del derivado de benzilo. El pH del grupo NH de las escuarimidas resultantes determinado en mezclas H₂O:MeCN 9:1 v/v resultó ser más ácido que el NH análogo de los derivados de escuaramida.

Capítulo 5. Se ha diseñado y parcialmente preparado un conjunto de compuestos dendriméricos basados en grupos amina y escuaramida para posteriores aplicaciones biológicas. Para este fin, se eligieron cuatro poliaminas con cadenas de diferente tamaño y con diferente nivel de ramificación como moléculas centrales y dos unidades de crecimiento funcionalizadas con grupos escuaramida con longitud de cadena diferente. Así, se han podido aislar y caracterizar satisfactoriamente varias primera y segunda generaciones a partir de la reacción de una molécula central con una unidad de crecimiento en medio alcohólico. Los mejores resultados se lograron con las unidades más grandes y flexibles dado que permiten acomodar mejor la tercera y cuarta generación de dendrímeros.

Resum

Aquesta tesi descriu composts que presenten diferent tipus de cavitats per a dur a terme estudis supramoleculars. Específicament, el treball aquí descrit es troba dividit en cinc capítols.

Capítol 1. La introducció general ofereix una descripció general de la química supramolecular. Així, es descriuen les propietats de les principals interaccions no covalents i la seva importància en la química hoste:hospedador al igual que en processos d'auto-assemblatge. Aquest capítol també descriu les característiques de les escuaramides ja que el grup escuaramida s'ha emprat repetidament en aquesta tesi per a l'obtenció de nous composts amb aplicacions supramoleculars.

Capítol 2. S'han estudiat les propietats en dissolució d'un cavitand profund funcionalitzat amb grups 2-aminobenzimidazol prèviament sintetitzat al nostre laboratori. El cavitand encapsula composts trimetilamoni com colina i acetilcolina amb constants d'associació de l'ordre de 10^4 M en mescles MeCN:H₂O. Com a prova de concepte, les propietats catalítiques del cavitand s'han aplicat en l'estudi de la hidròlisis del *p*-nitrofenilcarbonat de colina. En aquest cas, el procés de hidròlisis té lloc en tres passes que varen ser monitoritzades per UV-vis i espectroscòpia de RMN. El primer pas de la hidròlisis consisteix en el reconeixement del carbamat de colina per part de la cavitat, tot seguit de la carbamoïlació del cavitand i la hidròlisis d'aquest intermedi per a donar colina. La formació del derivat de carbamoïl es va completar després de 18 hores de reacció mentre que la darrera passa va resultar un procés molt lent que tenia lloc en uns 30 dies. Aquests resultats suggereixen que el cavitand actua com a mímec d'un inhibidor de acetilcolinesterases.

Capítol 3. S'ha sintetitzat una nova família de composts macrocíclics basats en enllaços imina com a resultat de la condensació de dos aldehids aromàtics (isofortaldehid i tereftalaldehid) amb 1,3- y 1,4-propargildiamines en varis dissolvents com AcOEt o MeOH. La cicloimina resultant de la reacció entre tereftalaldehid y 1,3-fenilen-bis-propargil diamina cristal·litza generant una estructura porosa que es mantén després de la desolvatació del producte. Els canals del cristall poden ser ocupats per molècules de diferent mida i que presenten diferents grups funcionals, como nitrometà, escuarat de dietil, *p*-xilè, etilenglicol, *p*-anisaldehid, cis-estilbè, (R)-(+)-limonè, (S)-(-)-nicotina o ftalat de dietil. En general, aquest material pot ser emprat com a suport sòlid per a la determinació estructural de molècules hoste mitjançant el mètode de l'esponja cristal·lina desenvolupat per Fujita et al. A més, s'han duit a terme estudis de selectivitat emprant mescles 1:1 v/v de diferents ftalats: ftalat de dietil, ftalat de dibutil, ftalat de butil bencil y ftalat de di-2-etilhexil. En aquestes condicions, el compost cristal·lí ha mostrat selectivitat per ftalat de dietil en front a la resta de derivats de ftalat.

Capítol 4. S'han preparat composts supramoleculars basats en escuaramides anàlogues als multifarens mitjançant la reacció de 1,3-dibromobenzil amb una escuaramida bicíclica en DMF en presència de Cs₂CO₃. Però, el procés sintètic va generar una mescla de productes inseparables amb un número variable de unitats escuaramida. Durant el procés de síntesis, inesperadament, es va observar la formació de composts escuarimida aromàtics monofuncionalitzats. Aquests productes, rarament descrits a la bibliografia, es varen produir amb rendiments acceptables mitjançant la reacció de benzils 4,4'-funcionalitzats amb escuaramida o N,N-dietilescuaramida en medi bàsic. Aquesta reacció implica la ruptura de l'enllaç intercarbonílic del derivat de benzil. El pH del grup NH de les escuarimides resultants determinat en mescles H₂O:MeCN 9:1 v/v va resultar ser més àcid que el mateix NH dels derivats d'escuaramida.

Capítol 5. S'ha dissenyat i parcialment preparat un conjunt de composts dendrimèrics basats en grups amina i escuaramida per a posteriors aplicacions biològiques. Amb aquest fi, es varen elegir quatre poliamines amb cadenes de diferent mida i amb diferent nivell de ramificació com a molècules centrals i

dues unitats de creixement funcionalitzades amb grups escuaramida amb longitud de cadena diferent. Així, s'han pogut aïllar i caracteritzar satisfactoriament vàries primera i segona generacions a partir de la reacció d'una molècula central amb una unitat de creixement en medi alcohòlic. Els millors resultats es varen aconseguir amb les unitats més grans i flexibles degut a que poden acomodar millor la tercera i quarta generació de dendrímers.

Table of contents

1. General Introduction	27
1.1 Supramolecular Chemistry	29
1.2 Non-covalent interactions	29
1.2.1 Electrostatic interactions	30
1.2.2 Hydrogen bond interactions	30
1.2.3 π Interactions	31
1.2.4 Dispersive van der Waals Interactions	36
1.2.5 Hydrophobic effect	36
1.3 Host-guest chemistry	37
1.4 Self-assembly	38
1.4.1 Self-assembly via coordination compounds	39
1.4.2 Self-assembly via hydrogen bonding	40
1.4.3 Self-assembly via interactions between π -systems	41
1.4.4 Self-assembly via hydrophobic effect	43
1.5 Squaramides in molecular recognition	44
1.5.1 Squaric acid	44
1.5.2 Squaramides	45
1.5.3 Squaramides vs ureas as recognition units	47
1.6 Thesis overview	51
2. Chapter 2: Evaluation of a 2-amino benzimidazole cavitand as container molecule	55
2.1 Resorcin[<i>n</i>]arene-based cavitands	57
2.1.1 Host-guest chemistry of cavitands	59
2.1.2 Self-assembly	60
2.1.3 Deep cavitands in catalysis	63
2.2 Aims	65
2.3 Programmed Enzyme-Mimic Hydrolysis of a Choline Carbonate by a Metal-Free 2-Aminobenzimidazole-Based Cavitand (<i>Organic Letters</i> , 2014 , <i>16</i> , 840-843)	67
2.3.1 Abstract	69
2.3.2 Conclusions	74
2.3.3 Acknowledgments	75
2.3.4 Supporting Information	76
2.3.4.1 Experimental	76
2.3.4.2 Synthesis	76
2.3.4.3 Characterization of caviplexes	83
2.3.4.4 MALDI-TOF	87
2.3.4.5 Kinetic study of the interaction of PNPCC with cavitand 1 and with 2-aminobenzimidazole (2-ABI)	88
3. Chapter 3: Development of new crystalline organic porous materials	93
3.1 Porous materials	95
3.2 Porous organic molecular crystals	98
3.2.1 Zero dimensional porous organic molecular crystals (0D)	99
3.2.2 One-dimensional porous organic molecular crystals (1D)	100
3.2.3 Three-dimensional porous organic molecular crystals (3D)	102
3.3 Dynamic covalent chemistry	103
3.4 Aims	107

3.5 A crystalline sponge based on dispersive forces suitable for X-ray structure determination of included molecular guests (<i>Chem. Sci.</i> 2015 , <i>6</i> , 5466-5472)	109
3.5.1 Abstract	111
3.5.2 Introduction	111
3.5.3 Results and discussion	113
3.5.3.1 Synthesis and structure of the microporous material	113
3.5.3.2 Stability and dynamic behavior of the porous material	114
3.5.3.3 Liquid–solid sorption experiments	116
3.5.3.4 Theoretical calculations	118
3.5.4 Conclusions	120
3.5.5 Acknowledgements	121
3.5.6 Supporting Information	122
3.5.6.1. Experimental Section	122
3.6.6.1a. Instrumental Methods	122
3.6.6.1b. Materials and synthesis	123
3.5.6.2 Procedure for guest inclusion	130
3.5.6.3 Crystal Data of solvates	131
3.5.6.4 Representative geometric parameters of solvates 3 @guest	133
3.6.6.5 Quantitative determination of the molar ratio [3 :sample] by ¹ H NMR spectroscopy	134
3.5.7 Theoretical Methods	137
3.5.7.1 Theoretical methods	137
3.6 Porous Macrocyclic Imines: Synthesis and Application to the Selective Adsorption of Phthalates	141
3.6.1 Abstract	143
3.6.2 Results and discussion	143
3.6.3 Conclusions	154
3.6.4 Supporting Information	155
3.6.4.1 Experimental	155
3.6.4.2 Synthesis	155
3.6.4.3 Crystal Data of Solvates	169
3.6.4.4 Desorption studies of EtOAc by gas chromatography	173
3.6.4.5 Quantitative determination of the molar ratio [EtPh: 3] by ¹ H NMR spectroscopy	174
4. Chapter 4: Studies on squaramide-based macrocycles	179
4.1. Macrocyclic compounds	181
4.1.1 Cyclodextrins	182
4.1.2 Calix[n]arenes	183
4.1.3 Cucurbit[n]urils	184
4.1.4 Pillar[n]arenes	185
4.1.5 Multifarenes[m,n]	186
4.2. Applications of macrocyclic compounds	187
4.2.1 Materials science	187
4.2.2 Catalysis	190
4.2.3 Biomedical applications	191
4.2.4 Supramolecular assemblies	192
4.3. Aims	195
4.4 Studies on squaramide-based macrocycles	197
4.4.1 Abstract	199
4.4.2 Introduction	199

4.4.3 Towards squaramide analogs of multifarenes and cucurbiturils	200
4.4.4 Conclusions	205
4.4.5 Supporting information	206
4.4.5.1. X-ray Crystal Structure Analysis	212
4.5 Unexpected Squaramide-Induced Cleavage of Benzils: Synthesis and Characterization of mono-Aroyl Squarimides (<i>Eur. J. Org. Chem.</i> , 2015 , 35, 7656-7660)	213
4.5.1 Abstract	215
4.5.2 Introduction	215
4.5.3 Results and discussion	216
4.5.4 Conclusions	222
4.5.5 Experimental section	222
4.5.6 Acknowledgements	222
4.5.7 Supporting Information	223
4.5.7.1. General methods	223
4.5.7.2. Synthesis and characterization of products	223
4.5.7.3. HPLC (High performance liquid chromatography) method for the analysis of aroyl squarimides	237
4.5.7.4. X-ray Crystal Structure Analyses	239
4.5.7.5. UV-vis pKa determination	241
5. Chapter 5: Synthesis of squaramide-based dendrimers	245
5.1 The Dendritic Family	247
5.2 Dendrimers	247
5.3 Dendrimeric structure	248
5.4 Synthesis of dendrimers	249
5.5 Applications of dendrimers	251
5.5.1 Dendrimers in drug delivery	251
5.5.2 Dendrimers as vectors for biomedical applications	255
5.6 Aims	259
5.7 Design and synthesis of a new family of squaramido-amino-based dendrimers	261
5.7.1 Abstract	263
5.7.2 Introduction	263
5.7.3 Results and discussion	264
5.7.4 Conclusions	270
5.7.5 Experimental	271
5.7.5.1 General methods	271
5.7.5.2 Synthesis and characterization of products	271
6. Conclusions	299

Chapter 1: General Introduction

1.1 Supramolecular Chemistry

The field of supramolecular chemistry emerged during the late 60s with the discovery of crown-ethers¹ and cryptands² done by Pedersen and Lehn together with the work done by Cram on the host-guest chemistry of spherands³ and cavitands.⁴ For this work, they were awarded with the Nobel Prize in Chemistry in 1987.

Jean-Marie Lehn defined supramolecular chemistry as “the chemistry of molecular assemblies and of the intermolecular bonds” referring to the study of complex molecular systems formed by the union of different components held together by reversible attractive interactions. Often, these assemblies are based on non-covalent interactions but also on dynamic covalent bonds.⁵

The synthesis of supramolecular compounds is based on the thermodynamic control over kinetic control. Hence, in supramolecular chemistry, the different components of the supramolecule are mixed to afford the most stable product. This is possible due to the use of reversible bonds. So, well-defined structures can be obtained in only a few reaction steps.

1.2 Non-covalent interactions

The binding of a guest molecule to another complementary molecule, named host for simplicity, occurs through the structural and energetic recognition of a molecule by the receptor. The binding affinity is determined from the experimentally measured binding constant, K :

$$\Delta G = -RT \ln K = \Delta H - T\Delta S \quad \text{Eq. 1}$$

The binding constant is related to the Gibbs free energy of binding (Eq. 1) and measures the affinity of a host for a particular guest forming a supramolecular complex. Supramolecular complexes can be obtained establishing one or more non-covalent interactions in a cooperative manner between complementary molecules. The synergetic use of a number of different interactions in a collaborative way allows maximizing the selectivity and the stability of the complexes.

In covalent chemistry, the binding energies (200-400 kJ·mol⁻¹) are high because they require the overlap of partially occupied orbitals resulting in bond lengths in the order of 2 Å. Non-covalent interactions are considerably weaker than covalent interactions. Non-covalent interactions range from 2 kJ·mol⁻¹, for dispersive interactions, to 300 kJ·mol⁻¹ for pure electrostatic ion-ion interactions. In non-covalent interactions the attraction forces depend on the electric properties of the molecules involved. As a result, the bond length varies within a few Angstroms range.

In general, besides the structural complementarity, the direct non-covalent host-guest interactions are key for success. The most significant direct interactions are electrostatic interactions, hydrogen bonding, aromatic π - π interactions, cation and anion- π interactions, van Waals forces, and hydrophobic effects.

¹ a) Pedersen, C. J. *J. Am. Chem. Soc.* **1967**, *89*, 7017–7036. b) Pedersen, C. J. *J. Am. Chem. Soc.* **1967**, *89*, 2495–2496.

² Dietrich, B.; Lehn, J. M.; Sauvage, J. P. *Tet. Lett.* **1969**, *10*, 2889-2892.

³ Cram, D. J.; Kaneda, T.; Helgeson, R. C.; Lein, G. M. *J. Am. Chem. Soc.*, **1979**, *101*, 6752–6754.

⁴ a) Cram, D. J. *Science*, **1983**, *219*, 1177-1183. b) Moran, J. R.; Karbach, S.; Cram, D. J. *J. Am. Chem. Soc.*, **1982**, *104*, 5826–5828.

⁵ Cragg, P. J. *Supramolecular Chemistry: From Biological Inspiration to Biomedical Applications*. Springer Science + Business media B. V., **2010**.

1.2.1 Electrostatic Interactions

Electrostatic interactions can be classified as: ion-ion interactions, ion-dipole interactions and dipole-dipole interactions. Ion-ion interactions are non-directional forces based on the Coulombic attraction between charges of opposite sign. It is the strongest non-covalent interaction with strengths in the order of 50-300 kJ·mol⁻¹. In the case of ion-dipole and dipole-dipole interactions, the dipole has to be oriented for an optimal interaction. Ion-dipole interactions are stronger than dipole-dipole interactions (50-200 and 5-50 kJ·mol⁻¹, respectively).

The interaction of Fe(CN)₆³⁻ with the tricationic tripodal receptor shown in Figure 1 is an example of ion-ion interaction.⁶ The complexes of crown ethers with cations are based on ion-dipole interactions in which a lone pair of the oxygen atoms interacts with the alkali metal.⁷ Meanwhile, the attraction between the dipoles of carbonyl groups is an example of dipole-dipole interaction that exhibits energies in the order of 5-50 kJ·mol⁻¹.

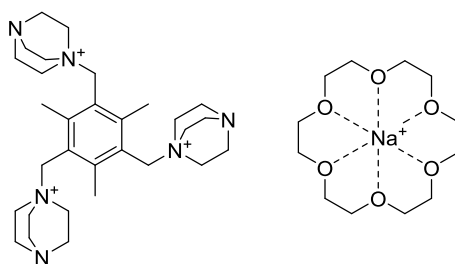


Figure 1. Left: Tripodal receptor able to interact with anions. Right: Na⁺ crown ether complex.

Electrostatic interactions are very important in the understanding of the factors that influence the binding affinities between molecules. They are particularly important in biological systems because they are present in a large number of recognition processes such as the interaction between an enzyme and a substrate.

1.2.2 Hydrogen bond interactions

Hydrogen bonding is a particular strong (4-120 kJ·mol⁻¹) case of dipole-dipole interaction. It is formed when a hydrogen atom is bonded to an electron-rich atom (such as nitrogen or oxygen) leading to the polarization of the bond making that hydrogen electropositive. Then, this hydrogen can be attracted by a neighbour atom with electron-withdrawing atoms (e.g. carbonyl moieties) as is shown in Figure 2. The resulting hydrogen bond is weak, but the sum of multiple interactions results in very stable complexes.

⁶ Garratt, P. J.; Ibbett, A. J.; Ladbury, J. E.; O'Brien, R.; Hursthouse, M. B.; Malik, K. M. A. *Tetrahedron* **1998**, *54*, 949-968.

⁷ Steed, J. W.; Atwood, J. L. *Supramolecular Chemistry* 2nd Edition. John Wiley & Sons Ltd., **2009**.

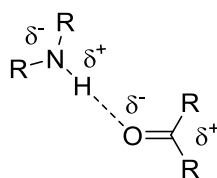


Figure 2. Example of hydrogen bond between a carbonyl group (acceptor) and an amine (donor).

Hydrogen bonds are very important in nature. There are a great number of natural sources of hydrogen bond donor and acceptor molecules such as amino acids, carbohydrates, nucleobases, etc. They are the responsible for: protein folding participating in the formation of α -helix and β -sheet secondary structures, the selective recognition of substrates by enzymes and the formation of the double helix of DNA through the establishment of hydrogen bonds along with π - π interactions between complementary purine and pyrimidine bases (Figure 3), among other important biological processes.

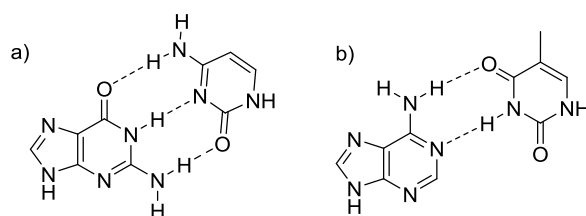


Figure 3. Hydrogen bonding pattern between base-pairs in DNA: a) Guanine-Cytosine, b) Adenine-Thymine.

In the field of supramolecular chemistry hydrogen bonding is the most significant non-covalent interaction used in the synthesis of a wide variety of supramolecular architectures.

1.2.3 π Interactions

There are three main π -interactions: cation- π interactions, anion- π interactions, and π - π interactions.

π - π interactions or π - π stacking forces are established between two aromatic systems ($10 \text{ kJ}\cdot\text{mol}^{-1}$) in which one is a relatively electron-rich π system, and the other is electron-poor. The aromatic rings can be arranged in two different orientations. In these geometries, π - σ attractions overcome π - π repulsions. Although electrostatic forces are very important, there are additional forces such as induced dipoles, polarizability, dispersion or charge transfer that have major energetic contribution.⁸ The edge-to-face or T-shaped geometry implies the interaction between a hydrogen atom of one phenyl ring in a perpendicular orientation with the center of another ring. The other orientation is the displaced face-to-face geometry in which the center of one ring interacts with the corner of another (Figure 4).⁹

⁸ Hunter, C. A.; Lawson, K. R.; Perkins, J.; Urch, C. J. *J. Chem. Soc., Perkin Trans. 2*, **2001**, 651-669.

⁹ a) Hunter, C. A.; Sanders, J. K. M. *J. Am. Chem. Soc.* **1990**, *112*, 5525-5534. b) Meyer, E. A.; Castellano, R. K.; Diederich, F. *Angew. Chem. Int. Ed.* **2003**, *42*, 1210-1250. c) Carver, F. J.; Hunter, C. A.; Jones, P. S.; Livingstone, D. J.; McCabe, J. F.; Seward, E. M.; Tiger, P.; Spey, S. E. *Chem. Eur. J.* **2001**, *7*, 4854-4862.

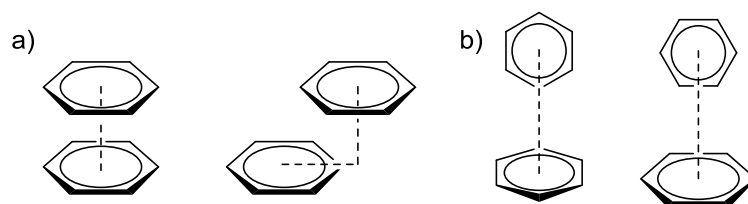


Figure 4. Representations of π - π interactions between arene-arene ring: a) face-to-face and parallel displaced and b) T-shaped and edge-to-face geometry.

These stacking interactions can be affected by modifications in the aromatic system as is illustrated in Figure 5. Thus, the functionalization of the ring with electron donating substituents increases the electron density of the aromatic system, making it suitable for interactions with electron-poor compounds. Conversely, electron-poor aromatic systems are obtained when the ring system is functionalized with electron-withdrawing substituents generating a relative electron deficiency in the core of the ring. In this case, the interaction with electron-rich systems is favoured through face-to-face interactions. The interactions in which electron-rich and electron-poor aromatic rings stack in an alternate fashion are also known as aromatic donor-acceptor interactions.¹⁰ In many cases, this interaction generates charge transfer complexes.¹¹

Several methods have been developed to measure aromatic interactions such as the “molecular torsion balance” reported by Wilcox et al.¹² or the “double mutant cycles” used by Hunter et al.¹³

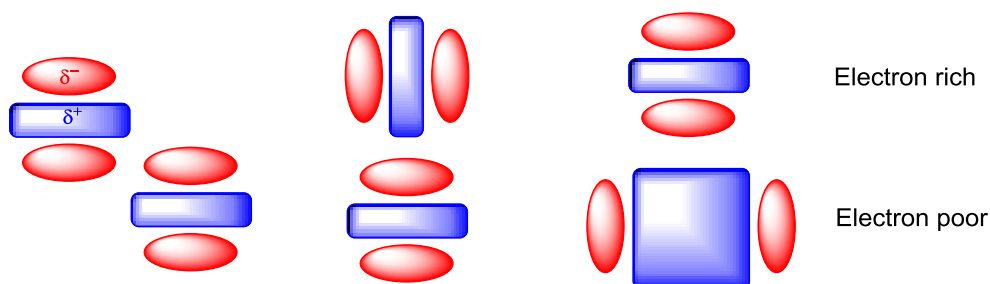


Figure 5. Stacking interactions between aromatic systems.

Systems based on π - π interactions have been widely used in supramolecular chemistry for the preparation of catenanes,¹⁴ rotaxanes¹⁵ or Borromean rings¹⁶ among others. The self-assembly process of these systems is driven by π - π interactions and, to a lesser extent, by weak hydrogen bonds and edge-

¹⁰ Martinez, C. R.; Iverson, B. L. *Chem. Sci.* **2012**, *3*, 2191-2201.

¹¹ a) Talukdar, P.; Bollot, G.; Mareda, J.; Sakai, N.; Matile, S. *J. Am. Chem. Soc.* **2005**, *127*, 6528-6529. b) Yushchenko, O.; Villamaina, D.; Sakai, N.; Matile, S.; Vauthey, E. *J. Phys. Chem. C* **2015**, *119*, 14999-15008. c) Beaumont, T. G.; Davis, K. M. C. *Nature* **1968**, *218*, 865. d) Kodis, G.; Terazono, Y.; Liddell, P. A.; Andréasson, J.; Garg, V.; Hambourger, M.; Moore, T. A.; Moore, A. L.; Gust, D. *J. Am. Chem. Soc.* **2006**, *128*, 1818-1827.

¹² Paliwal, S.; Geib, S.; Wilcox, C. S. *J. Am. Chem. Soc.* **1994**, *116*, 4497-4498.

¹³ Adams, H.; Carver, F. J.; Hunter, C. A.; Morales, J. C.; Seward, E. M. *Angew. Chem. Int. Ed.* **1996**, *35*, 1542-1544.

¹⁴ a) Gil-Ramírez, G.; Leigh, D. A.; Stephens, A. J. *Angew. Chem. Int. Ed.* **2015**, *54*, 6110-6150. b) Claessens, C. G.; Stoddart, J. F. *J. Phys. Org. Chem.* **1997**, *10*, 254-272.

¹⁵ Xue, M.; Yang, Y.; Chi, X.; Yan, X.; Huang, F. *Chem. Rev.* **2015**, *115*, 7398-7501.

¹⁶ a) Pease, A. R.; Jeppesen, J. O.; Stoddart, J. F.; Luo, Y.; Collier, C. P.; Heath, J. R. *Acc. Chem. Res.* **2001**, *34*, 433-444. b) Nepogodiev, S. A.; Stoddart, J. F. *Chem. Rev.* **1998**, *98*, 1959-1976. c) Chichak, K. S.; Cantrill, S. J.; Pease, A. R.; Chiu, S. -H.; Cave, G. W. V.; Atwood, J. L.; Stoddart, J. F. *Science* **2004**, *304*, 1308-1312.

to-face or T-shaped stacking interactions. Typically, the π - π interaction occurs between a π -electron deficient aromatic unit and a π -electron rich aromatic system. For example, Borromean rings were described by Stoddart et al. in 2004. The Borromean system was composed by three interlocked rings generated through dynamic covalent chemistry that lead to the formation of the thermodynamic more stable product. This approach implies the use of molecules with a high number of recognition units and optimized coordination geometries to facilitate the self-assembly process. Specifically, the Borromean rings were constructed by the [2+2] macrocyclization process through acid catalyzed imine bond reaction between a 2,6-diformylpyridine and a 2,2'-bipyridine group using zinc acetate as template. The resulting compound shown in Figure 6 is stabilized by 12 π - π stacking interactions between the aromatic rings and 30 dative bonds between Zn(II) and the nitrogen atoms. When the reaction is carried out without the templating agent, a mixture of macrocyclic and polymeric products was observed.

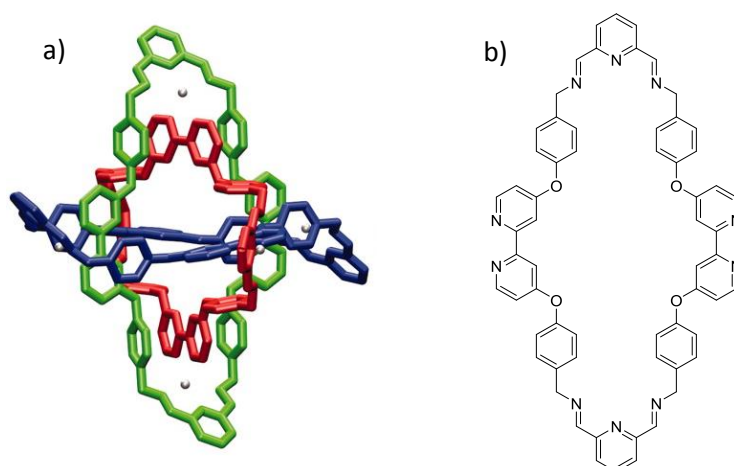


Figure 6. a) Molecular Borromean rings reported by Stoddart et al. b) Chemical structure of the Borromean units.

Stacking interactions can also be used in the construction of folded structures.¹⁷ For example, Huc et al. reported the synthesis of β -sheets foldamers stabilized by π - π interactions that is shown in Figure 7.¹⁸ The structure involved linear aromatic segments and hairpin turns to align the aromatic parts for a correct interaction. Specifically, 2,5-dialkoxy-terephthalic acid units were used as linear segments and 4,6-dinitro-1,3-phenylenediamine derivatives as turn units. The folded structure was confirmed by X-ray analysis being stable in chlorinated solution showing no evidence of aggregation.

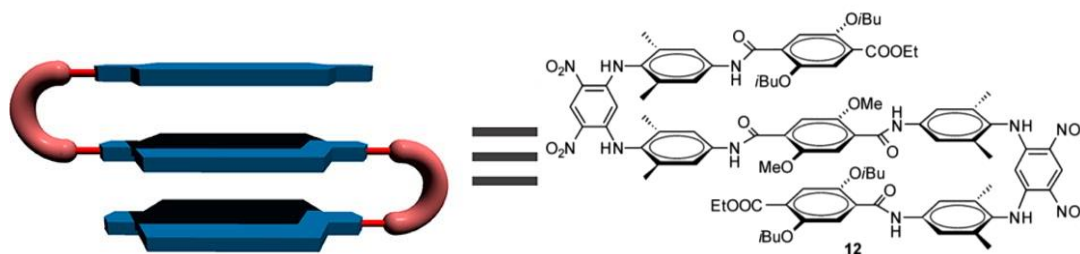


Figure 7. Example of folded structure reported by Huc et al. based on π - π interactions.

¹⁷ Petitjean, A.; Cuccia, L. A.; Schmutz, M.; Lehn, J. M. *J. Org. Chem.* **2008**, *73*, 2481-2495.

¹⁸ Sebaoun, L.; Maurizot, V.; Granier, T.; Kauffmann, B.; Huc, I. *J. Am. Chem. Soc.* **2014**, *136*, 2168-2174.

Cation- π interactions are strong interactions ($5\text{--}80\text{ kJ}\cdot\text{mol}^{-1}$) established between a cation and the face of a π system of an aromatic ring. An example is the interaction between benzene with different anions in gas phase.¹⁹

Table 1. Binding energies for simply cations to benzene in gas phase.²⁰

M^+	$-\Delta G^\circ$ (kJ/mol)
Li^+	165
Na^+	102
K^+	80
Rb^+	66

Cation- π interactions constitute an important force in molecular recognition. They are part of protein structures in which cationic amino acids Lys and Arg interact with the aromatic groups of Phe, Tyr or Trp. They are also used in the binding sites of supramolecular ligands such as cyclophanes or calixarenes.²¹ For example, cation- π interactions are the main force for the development of the supramolecular complex shown in Figure 8. In this case, the structure is stabilized by the interaction of a K^+ situated at the crown ether center and under the influence of the phenolic side chains of two tyrosine molecules.²²

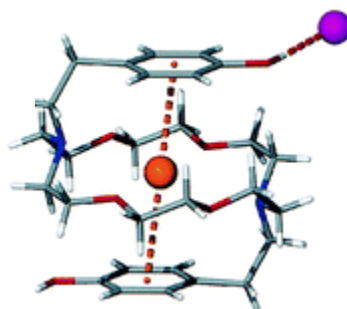


Figure 8. Structure of cation- π supramolecular system presented by Gokel.

A priori, anion- π interactions are expected to be repulsive because they require the interaction between an anion with an electron-rich system. However, during the last years, the attractive interaction of electron deficient (π -acidic) aromatic systems such as triazines, or perfluoroarenes with anions has been reported.²³ In general, this interaction presents electrostatic and anion-induced polarization contributions, but dispersion contributions as well.²⁴ For example, Ballester et al. have reported the quantification of the interaction between the anion chloride with the π -system of different meso-tetraaryl calix[4]pyrrole receptors in acetonitrile (see Table 2).²⁵ It was found that the $\text{Cl}\cdots\pi$ interaction was repulsive in all cases, except for the para-nitro substituted calixpyrrole.

¹⁹ a) Kumpf, R. A.; Dougherty, D. A. *Science* **1993**, *261*, 1708-1710. b) Ma, J. C.; Dougherty, D. A. *Chem. Rev.*, **1997**, *97*, 1303-1324.

²⁰ Kumpf, R. A.; Dougherty, D. A. *Science* **1993**, *261*, 1708-1710.

²¹ Dougherty, D. A. *Acc. Chem. Res.* **2013**, *46*, 885-893.

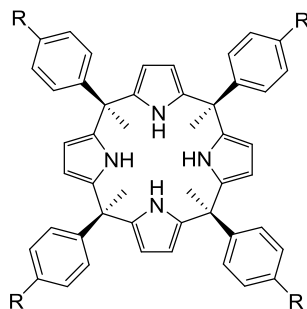
²² DeWall, S. L.; Barbour, L. J.; Gokel, G. W. *J. Am. Chem. Soc.* **1999**, *121*, 8405-8406.

²³ a) Wang, D. -X.; Zheng, Q. -Y.; Wang, Q. -Q.; Wang, M. -X. *Angew. Chem. Int. Ed.* **2008**, *47*, 7485-7488, b) Albrecht, M.; Müller, M.; Mergel, O.; Rissanen, K.; Valkonen, A. *Chem. Eur. J.* **2010**, *16*, 5062-5069.

²⁴ a) Quiñero, D., Garau, C., Rotger, C., Frontera, A., Ballester, P., Costa, A. and Deyà, P. M. *Angew. Chem. Int. Ed.* **2002**, *41*, 3389-3392. b) Schottel, B. L.; Chifotides, H. T.; Dunbar, K. R. *Chem. Soc. Rev.* **2008**, *37*, 68-83.

²⁵ Gil-Ramírez, G.; Escudero-Adán, E. C.; Benet-Buchholz, J.; Ballester, P. *Angew. Chem. Int. Ed.* **2008**, *47*, 4114-4118.

Table 2. Chemical structure of calix[4]pyrroles reported by Ballester et al. and free energy values (ΔG and $\Delta\Delta G$) for the 1:1 chloride: π interactions determined in MeCN at 298K.



R	$\Delta G / \text{kcal mol}^{-1}$	$\Delta\Delta G / \text{kcal mol}^{-1}$
OMe	-2.9	1.0
H	-3.1	0.9
COOMe	-4.1	0.7
Br	-4.8	0.5
CN	-6.2	0.1
NO ₂	-7.2	-0.1

Aromatic interactions are crucial in the biological field. Typical examples are the interaction between base pairs in the coil structure of DNA or between amino acid side chains in the folding of proteins as well as in the molecular recognition processes occurring in enzymes. Additionally, stacking interactions play important roles in material chemistry involved in crystal engineering or in liquid crystals.²⁶ Self-assembled crystalline structures based on π - π interactions can be synthesized increasing the aromatic surface of the building blocks that comprises the structure. An example is the grid network reported by Isaacs et al. in which the building blocks of the lattice are composed of a π surface (pink), H-donors (blue) and H-bond acceptor groups (red) as is shown in Figure 9.²⁷

²⁶ a) Salonen, L. M.; Ellermann, M.; Diederich, F. *Angew. Chem. Int. Ed.* **2011**, *50*, 4808-4842. b) Escudero, D.; Estarellas, C.; Frontera, A.; Quiñonero, D.; Deyà, P. M. *Chem. Phys. Lett.* **2009**, *468*, 280-285.

²⁷ She, N. -F.; Gao, M.; Meng, X. -G.; Yang, G. -F.; Elemans, J. A. A. W.; Wu, A. -X.; Isaacs, L. J. *Am. Chem. Soc.* **2009**, *131*, 11695-11697.

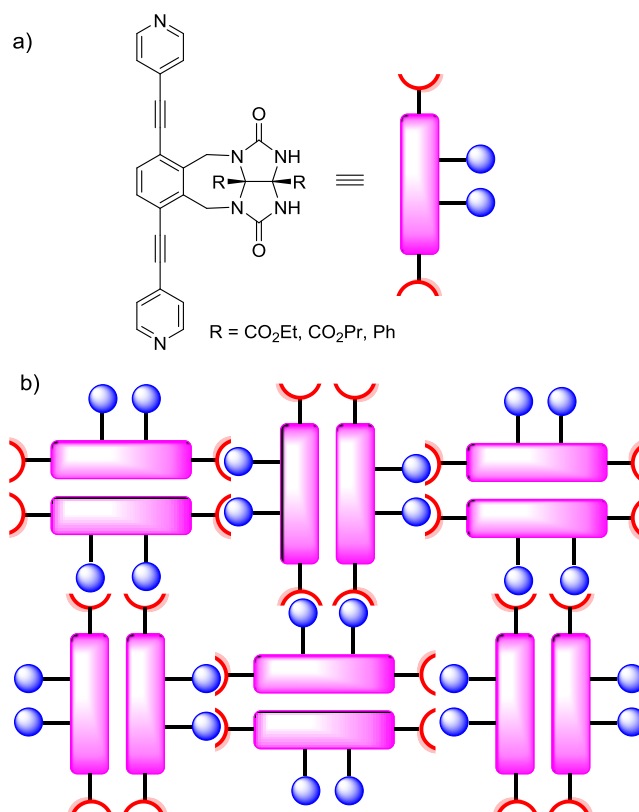


Figure 9. a) Chemical structure of the building blocks used by Isaacs et al. b) Schematic representation of the crystal lattice.

1.2.4 Dispersive van der Waals interactions

Van der Waals forces are non-directional attractive interactions between induced dipoles. They are produced by the polarization of the electron cloud of neighbouring molecules resulting in a weak ($< 2 \text{ kJ}\cdot\text{mol}^{-1}$) interaction.²⁸

These interactions can be divided basically into two contributions. London dispersion forces in which the interaction takes place between two induced dipoles and permanent-induced dipole and Debye forces that consist in the interaction between a permanent dipole and an induced dipole.

The resulting van der Waals forces are subtle but cumulative. For this reason, they have a limited role in the design of supramolecular receptors. However, van der Waals interactions are critical in the formation of inclusion compounds, in which the guest compounds are encapsulated into permanent cavities or included in crystal lattices.

1.2.5 Hydrophobic effect

Hydrophobic effect is responsible of the association of apolar molecules in polar mediums. In nature, for example, the hydrophobic effect is crucial to regulate the folding of globular proteins. Upon folding, the

²⁸ Echeverría, J.; Aullón, G.; Danovich, D.; Shaik, S.; Alvarez, S. *Nat. Chem.* **2011**, *3*, 323-330.

nonpolar amino acids of the protein are located towards the center of the protein avoiding contact with water molecules.

Hydrophobic interactions also play an important role in Supramolecular Chemistry. For example, they are important in the binding of guest molecules by cyclodextrins, cyclophanes, cavitands or cucurbiturils. So, in a highly polar medium, such as water, apolar compounds can displace water molecules from the interior of the apolar cavity to the bulk solvent resulting in an increase of the entropy of the system (Figure 10).

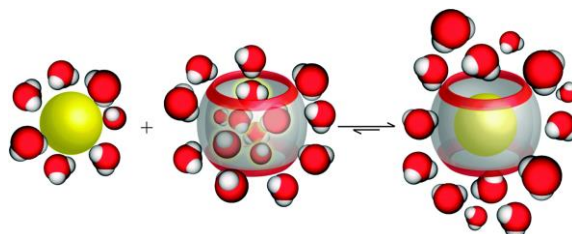


Figure 10. Schematic representation of the displacement of water molecules inside the apolar cavity of a cucurbituril compound by an apolar molecule in polar medium.²⁹

1.3 Host-guest chemistry

Supramolecular chemistry can be split into two broad categories, host-guest chemistry, and self-assembly. If a molecule is significantly larger than another and can wrap around it, then it is termed the "host", and the smaller molecule is named the "guest". According to a definition of Donald Cram, a host component is defined as an organic molecule or ion whose binding sites converge in the complex.³⁰ The guest component is any molecule or ion whose binding sites diverge in the complex. Commonly, the host molecule is a cyclic or concave compound with a cavity able to bind guests or, alternatively, a large molecule with different recognition sites. These systems can be compared with an enzyme that possesses different functionalities able to recognize selectively different substrates.

Weak interactions used for the preparation of supramolecular systems are quite sensitive to the medium. Accordingly, a very strong interaction in chloroform can be inexistent in more polar solvents such as DMSO or water.

For this reason, complementarity and preorganization principles are key issues in the design of new supramolecular systems. The principle of complementarity implies that the host must have different binding sites able to interact with binding sites of the guest without repulsion. In many cases, complementarity is not sufficient for complex formation. Then, some degree of preorganization is necessary. At the same time, the accumulation of a large number of interactions in the formation of these supramolecules yields more stable complexes.

²⁹ Assaf, K.I.; Nau, W.M. *Chem. Soc. Rev.* **2015**, *44*, 394-418.

³⁰ Anslyn, E. V.; Dougherty, D. A. *"Modern Physical Organic Chemistry"*. Edwards Brothers, Inc., **2006**.

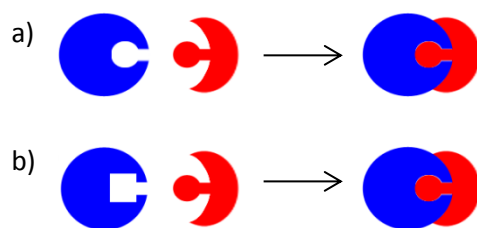


Figure 11. Schematic representation of a) lock-and-key principle and b) Induced fit theory.

In early studies, the recognition process was described as a lock and key image in which receptor and substrate were rigid structures perfectly complementary that interact with a high level of selectivity. However, many systems are not fully preorganized and require conformational changes in the recognition process. For this reason, the initial lock-and-key concept was replaced by the “induced fit” theory in which the host acts as an enzyme changing its conformation slightly to accommodate the guest as is illustrated in Figure 11.

1.4 Self-assembly

Self-assembly is the spontaneous and reversible association of two or more components to form a larger, non-covalently bound aggregate. Self-assembly allows the construction of complex systems held together only by non-covalent interactions. The complexity of the resulting structures implies a high degree of complementarity.

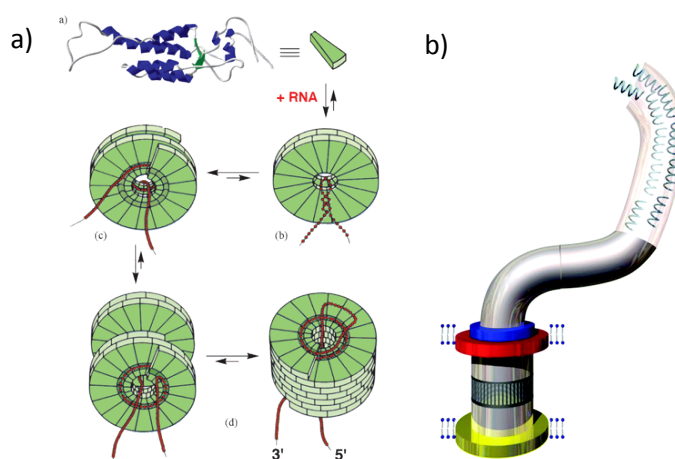


Figure 12. a) Representation of the self-assembly process of tobacco mosaic virus.³¹ b) General structure of the flagellum of a Gram-negative bacterium.

Two important examples of self-assembled molecules are DNA and RNA, but we can find many other examples in biology as the paradigmatic case of tobacco mosaic virus that is represented in Figure 12a. In this case, the virus is formed by 2130 identical subunits forming a helical structure around an RNA single strand that possesses all the genetic information. Another biological example is the self-assembly

³¹ Greig, L. M; Philip, D. *Chem. Soc. Rev.* **2001**, *30*, 287-302.

of the bacterial flagellum that consists of a large number of protein units or flagellins that assembly into a helical structure (Figure 12b).³² This helical structure is the responsible of the movement of the bacteria.

The objective of supramolecular chemistry is the formation of self-assembled structures with analogous precision to that found in biological systems.³³ For this reason, systems are designed to make the self-assembly process reversible. The process begins with the molecular recognition of two assemblies followed by the sequential growth of the supramolecule. In the course of the assembly, the molecules can be assembled and disassembled to correct possible mistakes until reaching the thermodynamic minimum of energy. Self-assembled systems of different shapes and sizes can be obtained varying the reaction and condition parameters. These systems find applications in molecular recognition, transport and catalysis.³⁴

1.4.1 Self-assembly via coordination compounds

Different non-directional hydrogen-bonding, van der Waals, and other weak interactions are responsible for the self-assembly of biological systems. Instead, the use of the stronger and directional metal-ligand bonds let to obtain self-assembled structures that mimic the size, shape and structural properties of many biological entities.³⁵

The use of coordination bonds in self-assembly implies the use of rigid complementary building blocks with defined angles and symmetry and the mix of these precursors in appropriate ratios. The final products are influenced by the choice of the reaction conditions (solvent, temperature, and stoichiometry).

There are two different approaches to the synthesis of supramolecular structures via the use of directional bonds. The edge-directed method implies the use of precursors that define the edges of the resulting compound. The other approach is the face-directed self-assembly in which the linkers used for the formation of the supramolecule form the walls of the cage.

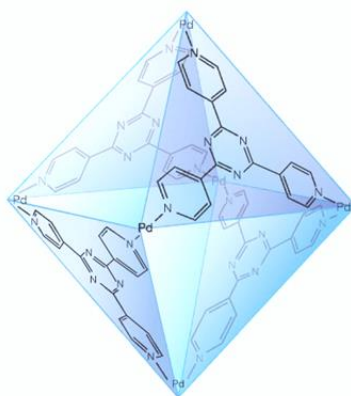


Figure 13. Self-assembled octahedral cage described by Fujita et al.

³² a) Rest, C.; Kandaneli, R.; Fernández, G. *Chem. Soc. Rev.* **2015**, *44*, 2543-2572, b) Yonekura, K.; Maki, S.; Morgan, D. G.; DeRosier, D. J.; Vonderviszt, F.; Imada, K.; Namba, K. *Science* **2000**, *290*, 2148-2152.

³³ Philp, D.; Stoddart, J. F. *Angew. Chem. Int. Ed.* **1996**, *35*, 1154-1196.

³⁴ Whitesides, G. M.; Grzybowski, B. *Science* **2002**, *295*, 2418-2421.

³⁵ Seidel, S. R.; Stang, P. J. *Acc. Chem. Res.* **2002**, *35*, 972-983.

An example of self-assembly via the use of coordination bonds is shown in Figure 13. In this case, an octahedral cage quantitatively self-assembles by mixing end-capped Pd(II) ions with the triangular ligand 1,3,5-tris(4-pyridyl)triazine in a 6:4 ratio.³⁶ The resulting cationic cage encapsulates different organic guests in aqueous media. The substitution of the end-capping groups of the metal ligand forms cages with different properties.

1.4.2 Self-assembly via hydrogen bonding

Very complex 3D structures can be obtained from simple building blocks using hydrogen bond interactions due to their cooperative strength, orientation, and specificity. The combination of multiple hydrogen bonds in a cooperative fashion in the same structure reinforces the stability of the product.

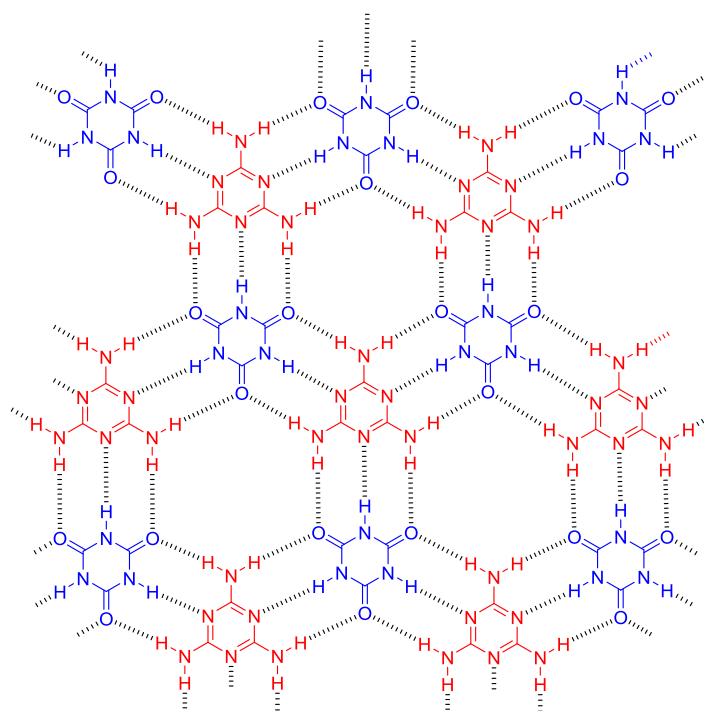


Figure 14. Lattice structure obtained from the self-assembly of cyanuric acid (blue) and melamine (red).

One of the best known and more studied systems is the three-dimensional structure obtained from the direct assembly of melamine and cyanuric acid that generates the “rosette” structure represented in Figure 14.³⁷ The direct reaction of cyanuric acid and melamine forms an insoluble 1:1 complex stabilized by several complementary hydrogen bonds between both compounds. There is a high level of positive cooperativity in the formation process. Larger and more complex supramolecular systems can be obtained from slight variations of the two building blocks mentioned above.³⁸ For example, a 3:3 “bisrosette” complex stabilized by 36 hydrogen bonds was obtained when a bismelamine unit and a bulkier isocyanurate were used as building units.

³⁶ Fujita, M.; Oguro, D.; Miyazawa, M.; Oka, H.; Yamaguchi, K.; Ogura, K. *Nature* **1995**, *378*, 469-471.

³⁷ Seto, C. T.; Whitesides, G. M. *J. Am. Chem. Soc.* **1990**, *112*, 6409-6411.

³⁸ Mathias, J. P.; Simanek, E. E.; Whitesides, G. M. *J. Am. Chem. Soc.* **1994**, *116*, 4326-4340.

The benzene-1,3,5-tricarboxamide (BTA) family constitutes another example that self-assembles through intermolecular hydrogen bonds established between the C=O groups of one unit with the NH groups of another BTA unit. Depending on the functionalization of the BTA, different assemblies can be obtained. So, long and columnar chiral aggregates stabilized through three hydrogen bonds between two adjacent units were obtained in apolar solvents when N,N',N''-tris(2-methoxyethyl)-1,3,5-benzene-tricarboxamide was used under diluted conditions. Conversely, the pyridine BTA derivative shown in Figure 15 crystallizes forming a two-dimensional honeycomb grid of bilayer sheets. In this case, the structure is composed by intermolecular hydrogen bonds between the pyridyl moieties of one molecule with the NH groups of the adjacent molecules. The bilayer sheets form a 3D porous structure with pore diameter of one nanometer.³⁹ These compounds present applications in biomedicine and in materials science.⁴⁰

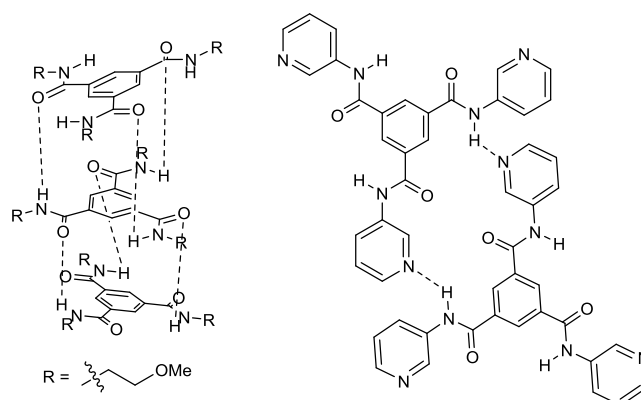


Figure 15. Hydrogen bond interaction patterns that give rise to columnar assemblies (left) and bilayers (right).

1.4.3 Self-assembly via interactions between π -systems

Several examples of self-assembled structures mainly based on stacking interactions can be found in the literature. Recently, Würthner et al. have reported the self-assembly of perylene bisimide (PBI) dyads.⁴¹ Here, the dyad is composed by two PBI chromophores functionalized with alkyl chains and connected by acetylene units. Depending on the number of acetylene units present in the backbone, dimers or elongated π -stacked structures can be obtained as shown in Figure 16.

³⁹ Palmans, A. R. A.; Vekemans, J. A. J. M.; Kooijman, H.; Spek, A. L.; Meijer, E. W. *Chem. Commun.* **1997**, 2247-2248.

⁴⁰ Cantekin, S.; Greef, T. F. A.; Palmans, A. R. A. *Chem. Soc. Rev.* **2012**, 41, 6125-6137.

⁴¹ Shao, C.; Stolte, M.; Würthner, F. *Angew. Chem. Int. Ed.* **2013**, 52, 7482-7486, b) Shao, C.; Stolte, M.; Würthner, F. *Angew. Chem. Int. Ed.* **2013**, 52, 10463-10467.

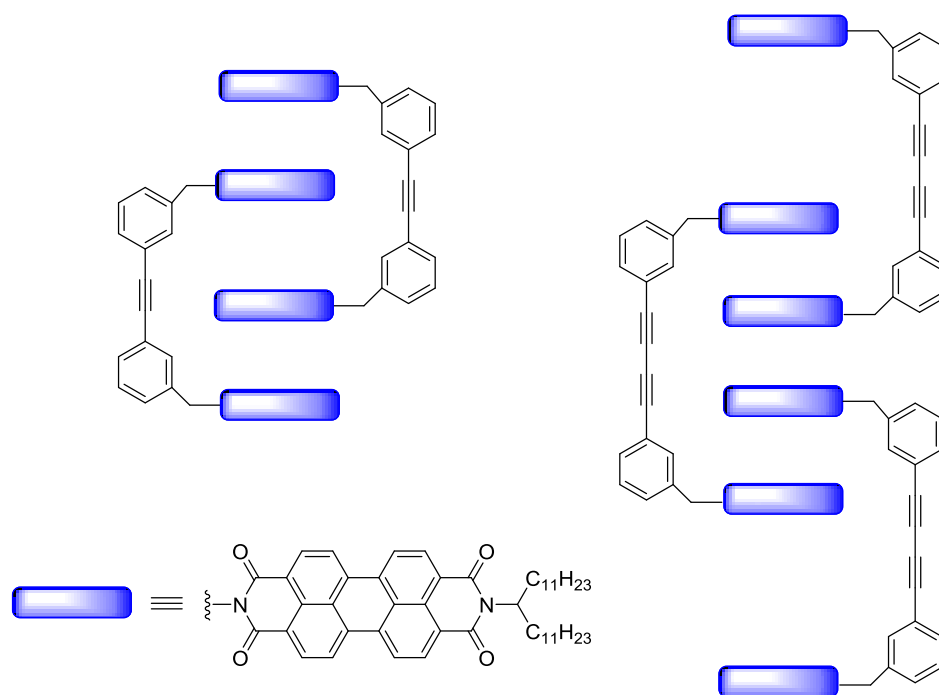


Figure 16. Schematic representation of the dimeric and oligomeric structures described by Würthner et al.

The preparation of complex ring systems as catenanes, rotaxanes or molecular knots is another goal of supramolecular chemistry. The concepts of supramolecular chemistry and molecular recognition have been used to rationalize the preparation of these compounds. In some cases, these systems are based on π donor-acceptor effects in which the preorganization is an important factor.⁴² In others, the aromatic building blocks are held together using metal coordination. In these cases, the ion is removed from the solution after the assembly.⁴³ In Figure 17, it is shown an example of catenane reported by Sanders et al.⁴⁴ Here, the first step for the formation of the self-assembled compound through the interaction between the π -electron-deficient aromatic ring of the diimide derivative and the π -electron-rich aromatic ether compound followed by an intermolecular oxidative coupling between the terminal alkyne units of the two self-assembled compounds in DMF that yields the final catenane structure.

⁴² Spruell, J. M.; Coskun, A.; Friedman, D. C.; Forgan, R. S.; Sarjeant, A. A.; Trabolsi, A.; Fahrenbach, A. C.; Barlin, G.; Paxton, W. F.; Dey, S. K.; Olson, M. A.; Benítez, D.; Tkatchouk, E.; Colvin, M. T.; Carmielli, R.; Caldwell, S. T.; Rosair, G. M.; Hewage, S. G.; Duclairoir, F.; Seymour, J. L.; Slawin, A. M.; Goddard III, W. A.; Wasielewski, M. R.; Cooke, G.; Stoddart, J. F. *Nat. Chem.* **2010**, *2*, 870-879.

⁴³ Forgan, R. S.; Sauvage, J. -P.; Stoddart, J. F. *Chem. Rev.* **2011**, *111*, 5434-5464.

⁴⁴ a) Hamilton, D. G.; Sanders, J. K. M.; Davis, J. E.; Clegg, W.; Teat, S. J. *Chem. Commun.* **1997**, 897-898. b) Gil-Ramírez, G.; Leigh, D. A.; Stephens, A. J. *Angew. Chem. Int. Ed.* **2015**, *54*, 6110-6150.

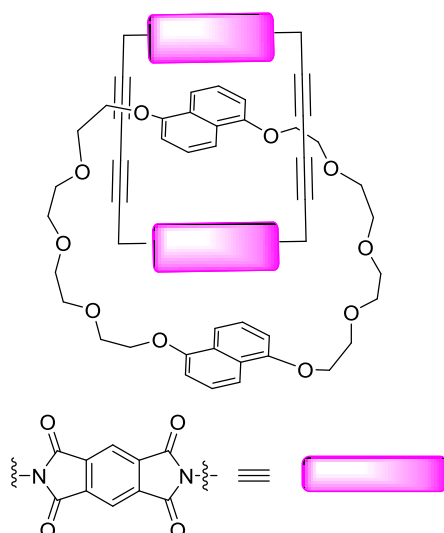


Figure 17. Example of a catenane reported by Sanders.

1.4.4 Self-assembly via hydrophobic effect

Due to the polar nature of the water molecule, self-assembly processes of compounds with non-polar groups in this medium are highly influenced by the hydrophobic effect. Hence, non-polar compounds tend to aggregate to minimize the interaction with the solvent. Several supramolecular systems based on the aggregation of amphiphilic compounds in water have been synthesized following this approach. Recently, the self-assembly of the highly hydrophobic compound shown in Figure 18 has been reported.⁴⁵ In this case, the aggregate precipitated when a 30% of water was added to a solution of the compound in THF. Microscopic and SLD studies showed that the precipitate was composed of spherical assemblies of the monomeric unit.

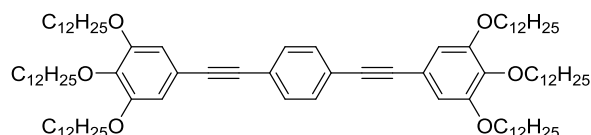


Figure 18. Chemical structure of the hydrophobic compounds reported by Fernández et al.

Additionally, container compounds with closed structures able to encapsulate a wide variety of guest molecules in their inner cavity by non-covalent interactions are important in molecular recognition. There are two types of container compounds. In the first type, the inner cavity is formed through the covalent union of the components such is the case of calixarenes, cavitands, cryptophans or cucurbituril compounds. However, the cavity can also be formed by a spontaneous self-assembly process. An example of a self-assembled system is the symmetrical capsular complex obtained after the addition of guest molecules such as steroids or hydrocarbons into solutions of the water soluble deep-cavity shown

⁴⁵ Mayoral, M. J.; Rest, C.; Schellheimer, J.; Stepanenko, V.; Fernández, G. *Chem. Eur. J.* **2012**, *18*, 15607-15611.

in Figure 19.⁴⁶ The cavity has also been used as a nanoscale reaction vessel for the study of photochemical processes.⁴⁷

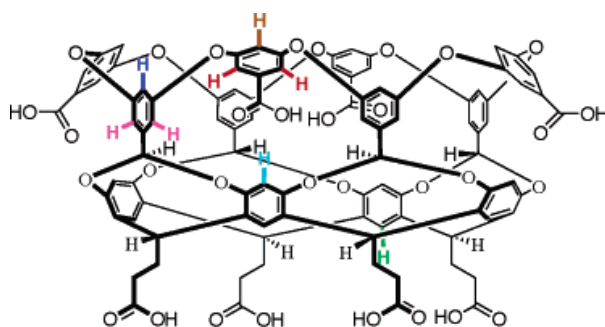


Figure 19. Structure of the deep cavitaand able to self-assemble in the presence of steroids or hydrocarbons.

1.5 Squaramides in molecular recognition

1.5.1 Squaric acid

The 3,4-dihydroxycyclobut-3-ene-1,2-dione also known as squaric acid is a member of the oxocarbon family.⁴⁸ It is currently synthesized by acid hydrolysis of hexachlorocyclobutene. Squaric acid is a very strong acid with pK_a values of 0.5 and 3.5, respectively (Figure 20).⁴⁹ The formation of the conjugate base causes the increase of the aromaticity of the squaric ring.

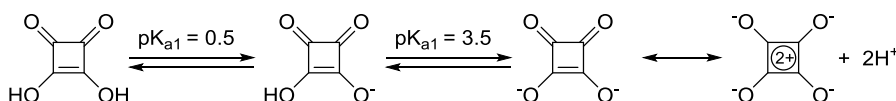


Figure 20. Ionization equilibrium of squaric acid.

The squaric di-anion can act as mono- or bidentate ligand as shown in Figure 21, but so far only monodentate complexes have been reported.

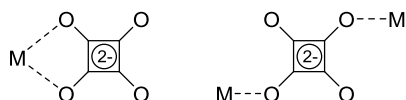


Figure 21. Possible metal coordination geometries for the squaric di-anion.

⁴⁶ Gibb, C. L.; Gibb, B. C. *J. Am. Chem. Soc.* **2004**, *126*, 11408-11409.

⁴⁷ Liu, S.; Gibb, B. C. *Chem. Commun.* **2008**, 3709-3716.

⁴⁸ Seitz, G.; Imming, P. *Chem. Rev.* **1992**, *92*, 1227-1260.

⁴⁹ Storer, R. I.; Aciro, C.; Jones, L. H. *Chem. Soc. Rev.* **2011**, *40*, 2330-2346.

Squaric acid derivatives such as alkyl squarates or squaramides can be considered as isosters of different functional groups, such as carboxylic acids,⁵⁰ amino acids,⁵¹ phosphates⁵² and ureas (Figure 22).⁵³ Due to these properties, squaric acid derivatives have found application in the fields of medicinal and material chemistry, as bioactive compounds, advanced materials, and catalysts in asymmetric synthesis.

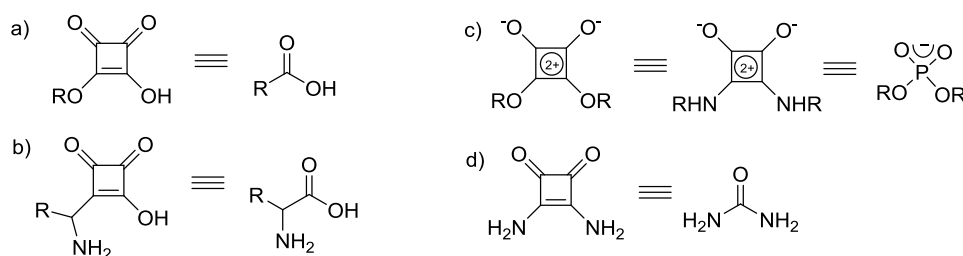


Figure 22. Schematic representation of the isosterism of squaric derivatives and: a) carboxylic acid, b) amino acids, c) phosphates, and d) ureas.

1.5.2 Squaramides

Squaramides are the 3,4 diamino derivatives of squaric acid. In a certain way, they can be seen as vinyl analogous of amides. The squaramides have a high ability to form hydrogen bonds due to the delocalization of the electron pair of the nitrogen atoms through the cyclobutene-1,2-dione ring as represented in the resonant structures shown in Figure 23. For this reason, the C-N bonds of squaramides show restricted rotation. The squaramide ring is a planar, rigid, and polarizable structure.

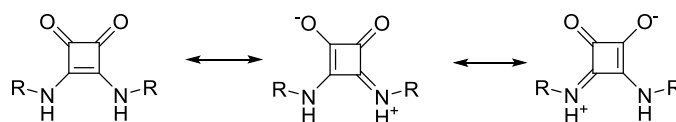


Figure 23. Resonant forms of squaramides.

These compounds have the ability to act as hydrogen bond donors through the NH groups, and also, as hydrogen bond acceptors through the two adjacent carbonyl groups. Hence, squaramide motifs have been used in the design of supramolecular receptors for the recognition of cations,⁵⁴ anions⁵⁵ or ion pairs.⁵⁶

⁵⁰ Ballatore, C.; Huryn, D. M.; Smith, A. B. *ChemMedChem* **2013**, *8*, 385-395.

⁵¹ Campbell, E.; Park, A.; Kinney, W.; Fengl, R.; Liebeskind, L. J. *Org. Chem.* **1995**, *60*, 1470-1472.

⁵² a) Niewiadomski, S.; Beebejaun, Z.; Denton, H.; Smith, T. K.; Morris, R. J.; Wagner, G. K. *Org. Biomol. Chem.* **2010**, *8*, 3488-3499. b) Seio, K.; Miyashita, T.; Sato, K.; Sekine, M. *Eur. J. Org. Chem.* **2005**, 5163-5170.

⁵³ Amendola, V.; Bergamaschi, G.; Boiocchi, M.; Fabbrizzi, L.; Milani, M. *Chem. Eur. J.* **2010**, *16*, 4368-4380.

⁵⁴ Tomàs, S.; Prohens, R.; Vega, M.; Rotger, M. C.; Deyà, P. M.; Ballester, P.; Costa, A. *J. Org. Chem.* **1996**, *61*, 9394-9401.

⁵⁵ a) Prohens, R.; Tomàs, S.; Morey, J.; Deyà, P. M.; Ballester, P.; Costa, A. *Tet. Lett.* **1998**, *39*, 1063-1066. b) Jin, C.; Zhang, M.; Wu, L.; Guan, Y.; Pan, Y.; Jiang, J.; Lin, C.; Wang, L. *Chem. Commun.* **2013**, *49*, 2025-2027.

⁵⁶ Soberats, B.; Martínez, L.; Sanna, E.; Sampedro, A.; Rotger, C.; Costa, A. *Chem. Eur. J.* **2012**, *18*, 7533-7542.

Because of the restricted rotation of the C-N bond ($63 \text{ kJ}\cdot\text{mol}^{-1}$), squaramides can exist in the different conformations showed in Figure 24. The E,E rotamer is the less favourable configuration due to the steric hindrance of the NH substituents. From the point of view of molecular recognition, the Z,Z conformer is preferred. This conformer allows the formation of supramolecular complexes by establishing cooperative hydrogen bond interactions with a variety of guest molecules.

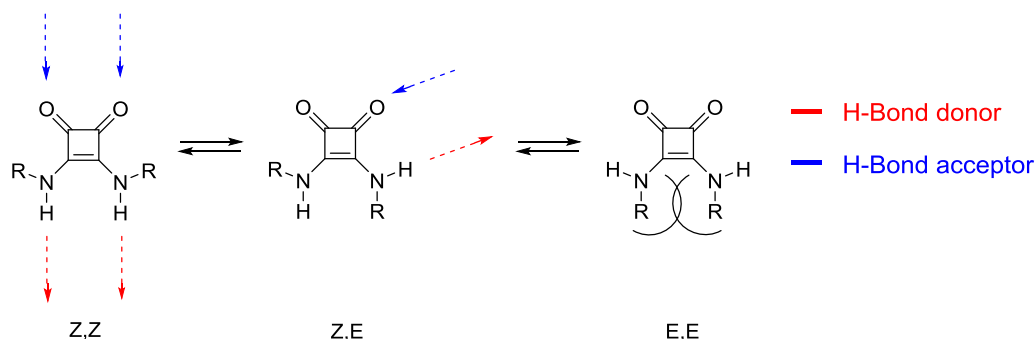


Figure 24. Schematic representation of the different conformations for a disquaramide in solution.

Meanwhile, the Z,E conformation can be stabilized by the formation of intramolecular hydrogen bonds, making these compounds good candidates for the design of folded structures. Recently, our group has reported the use of a squaramide-based module able to induce the formation of hairpin structures that mimics the action of the proline amino acid in the β -turn of proteins, thus rendering peptidomimetic structures.⁵⁷ In this case, the turning module is formed by the direct condensation of diethyl squarate and (2-aminoethyl)methylamine (Figure 25).

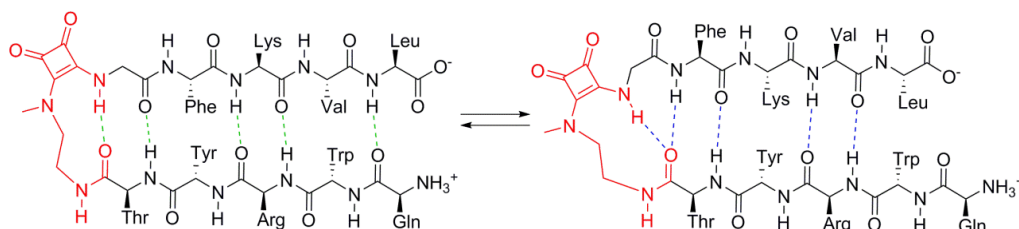


Figure 25. Representation of the conformational equilibrium of the squaramide based decapeptidomimetic presented by Rotger et al.

Our group had already used these characteristics to study macrocyclization processes on squaramide compounds.⁵⁸ Specifically, we have described the condensation of oligosquaramides with diethyl squarate in a polar solvent (EtOH or MeOH) without the need of high-dilution conditions (Figure 26). In this work, we described several oligosquaramides of different lengths with a donor atom (N, O) in the δ position of the alkyl chain directly linked to the squarate ring. The donor atom stabilizes the folded conformation (Z/E) as in the previous case. The stability of the oligomers increases with the chain length, therefore favoring the macrocyclization of oligosquaramides containing 2 to 7 squaramide units.

⁵⁷ a) Martínez, L.; Martorell, G.; Sampedro, A.; Ballester, P.; Costa, A.; Rotger, C. *Org. Lett.* **2015**, *17*, 2980-2983. b) Martínez, L.; Sampedro, A.; Sanna, E.; Costa, A.; Rotger, C. *Org. Biomol. Chem.* **2012**, *10*, 1914-1921.

⁵⁸ Rotger, C.; Piña, M. N.; Vega, M.; Ballester, P.; Deyà, P. M.; Costa, A. *Angew. Chem. Int. Ed.* **2006**, *45*, 6844-6848.

The resulting macrocycles have shown interesting activities as antitumor agents on several cancer lines.⁵⁹ Remarkably, one cyclic oligosquaramide conjugates showed very effective cell internalization.⁶⁰

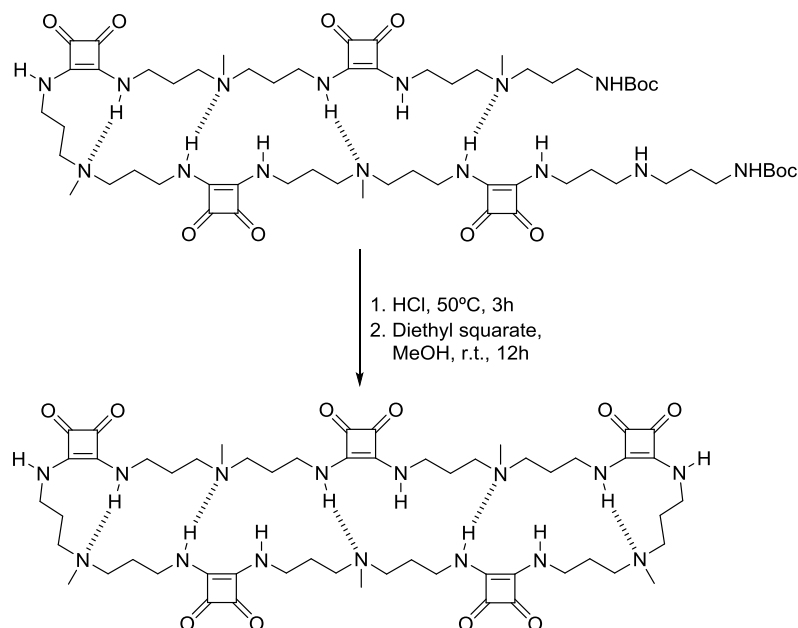


Figure 26. Macrocyclization reaction for the preparation of a macrocycle with 5 squaramide units.

1.5.3 Squaramides vs ureas as recognition units

The ability of squaramide to form hydrogen bonds has been compared to that of urea. Both have demonstrated to be good H-bonding donors. The association constants (K_{as}) for urea complexes with tetraalkylammonium carboxylates in DMSO are in the range 50-150 M^{-1} . In comparison, the K_{as} of several squaramides with tetramethyl ammonium acetate in DMSO is 217-1980 M^{-1} .⁶¹ These data highlights the superior H-bond donor ability of the squaramide moiety compared to urea. This is likely due to the increased aromaticity of the squaramide ring after complexation. Besides, the squaramides possess two adjacent carbonyl groups that allow stronger hydrogen bond acceptor interactions than ureas (Figure 27).⁶²



Figure 27. Comparison of the size and internitrogen distances for urea and squaramide moieties.

⁵⁹ Villalonga, P.; Fernández de Mattos, S.; Ramis, G.; Obrador-Hevia, A.; Sampedro, A.; Rotger, C.; Costa, A. *ChemMedChem* **2012**, *7*, 1472-1480.

⁶⁰ Sampedro, A.; Villalonga-Planells, R.; Vega, M.; Ramis, G.; Fernández de Mattos, S.; Villalonga, P.; Costa, A.; Rotger, C. *Bioconjugate Chem.* **2014**, *25*, 1537-1546.

⁶¹ Amendola, V.; Bergamaschi, G.; Boiocchi, M.; Fabbri, L.; Milani, M. *Chem. Eur. J.* **2010**, *16*, 4368-4380.

⁶² Alemán, J.; Parra, A.; Jiang, H.; Jørgensen, K. A. *Chem. Eur. J.* **2011**, *17*, 6890-6899.

The dipolar character of squaramide and urea allow the formation of 3D structures hold in place by hydrogen bonding interactions between the N-H and the C=O groups of adjacent molecules in a head-to-tail packing as is shown in Figure 28.

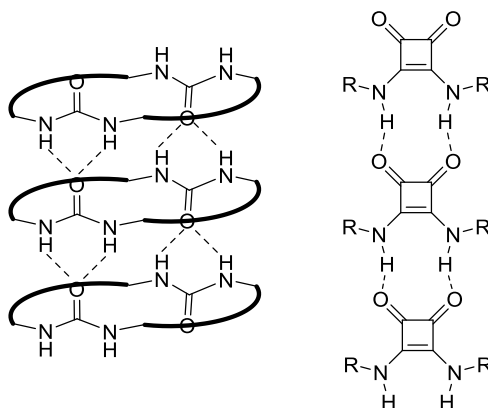


Figure 28. Head-to-tail complexes of ureas⁶³ (left) and squaramides⁶⁴ (right).

The hydrogen bonding ability of squaramides has been used in the design and synthesis of mixed structures containing both, urea and squaramide. The resulting compound dimerizes giving a structure that resembles guanine derivatives (Figure 29).⁶⁵

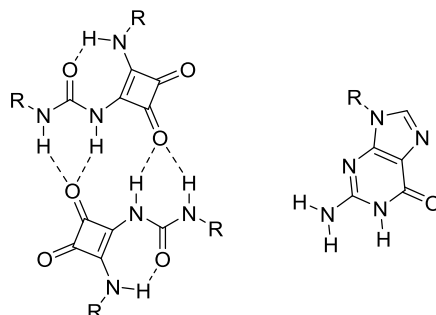


Figure 29. Structure comparison between squaramido-urea compounds and guanidine.

Particularly attractive in supramolecular chemistry are anion receptors. Urea and squaramide are used in the design of synthetic anion receptors due to the two NH groups of their structure. These two NH groups can bind anions via formation of six and seven-membered chelate rings^{62,66} and oxoanions through the formation of eight and nine-membered rings (Figure 30).

⁶³ a) Bowers, C. R.; Dvoyashkin, M.; Salpage, S. R.; Akel, C.; Bhase, H.; Geer, M. F.; Shimizu, L. S. *ACS Nano* **2015**, *9*, 6343-6353. b) Shimizu, L. S.; Smith, M. D.; Hughes, A. D.; Shimizu, K. D. *Chem. Commun.* **2001**, 1592-1593.

⁶⁴ Rotger, C.; Soberats, B.; Quiñero, D.; Frontera, A.; Ballester, P.; Benet-Buchholz, J.; Deyà, P. M.; Costa, A. *Eur. J. Org. Chem.* **2008**, 1864-1868.

⁶⁵ Davis, A. P.; Draper, S. M.; Dunne, G.; Ashton, P. *Chem. Commun.* **1999**, 2265-2266.

⁶⁶ Quiñero, D.; Prohens, R.; Garau, C.; Frontera, A.; Ballester, P.; Costa, A.; Deyà, P. M. *Chem. Phys. Lett.* **2002**, *351*, 115-120.

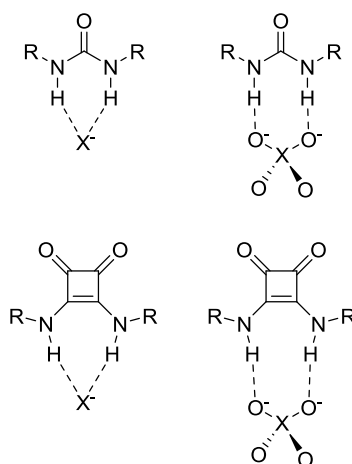


Figure 30. Schematic structures of complexes between ureas or squaramides and anions.

The design of synthetic receptors for carboxylate recognition is critical due to their biological importance. Typical receptors for anions relies on polyamine,⁶⁷ guanidinium,⁶⁸ amides, urea/thiourea,⁶⁹ pyrrol⁷⁰ and natural amino acid groups.⁷¹ The design and evaluation of squaramide, bis-squaramides and tris-squaramides able to bind mono-, di- and tricarboxylates have been reported.⁷²

Molecular systems for the simultaneous recognition of anions and cations have also been reported. One example is the macrocyclic unit described by Micheloni et al. (Figure 31).⁷³ In this case, one binding unit is a tetra-aza macrocycle base having four nitrogen atoms to coordinate different metals as a function of the pH. The other is formed by two squaramide units capable of simultaneously binding the guest anions.

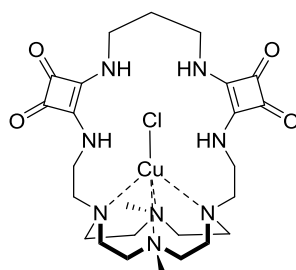


Figure 31. Schematic representation of the complex between CuCl and the macrocyclic cryptand described by Micheloni.

⁶⁷ Choj, K.; Hamilton, A. D. *J. Am. Chem. Soc.* **2003**, *125*, 10241-10249.

⁶⁸ Busschaert, N.; Caltagirone, C.; Van Rossom, W.; Gale, P. A. *Chem. Rev.* **2015**, *115*, 8038-8155.

⁶⁹ Andrews, N. J.; Haynes, C. J. E.; Light, M. E.; Moore, S. J.; Tong, C. C.; Davis, J. T.; Harrell Jr., W. A.; Gale, P. A. *Chem. Sci.* **2011**, *2*, 256-260.

⁷⁰ Sessler, J. L.; Katayev, E.; Pantos, G. D.; Scherbakov, P.; Reshetova, M. D.; Khurstalev, V. N.; Lynch, V. M.; Ustynyuk, Y. A. *J. Am. Chem. Soc.* **2005**, *127*, 11442-11446.

⁷¹ Niu, L.-Y.; Guan, Y.-S.; Chen, Y.-Z.; Wu, L.-Z.; Tung, C.-H.; Yang, Q.-Z. *Chem. Commun.* **2013**, *49*, 1294-1296.

⁷² a) See reference 55a. b) Frontera, A.; Morey, J.; Oliver, A.; Piña, M. N.; Quiñonero, D.; Costa, A.; Ballester, P.; Deyà, P. M.; Anslyn, E. V. *J. Org. Chem.* **2006**, *71*, 7185-7195.

⁷³ Ambrosi, G.; Formica, M.; Fusi, V.; Giorgi, L.; Guerri, A.; Micheloni, M.; Paoli, P.; Pontellini, R.; Rossi, P. *Chem. Eur. J.* **2007**, *13*, 702-712.

Acyclic squaramide receptors for the recognition of ion pairs have also been studied. One example is the Janus-like compound reported by our investigation group that is shown in Figure 32.⁷⁴ The semi-rigid tripod-like receptor consisted of a tris-aminopropargylbenzene unit functionalized with bis-dissecondary squaramide moieties. This compound acts as tris-heteroditopic ligand forming 1:3 host-guest complexes based on the establishment of hydrogen bonds with NR₄I ion pairs.

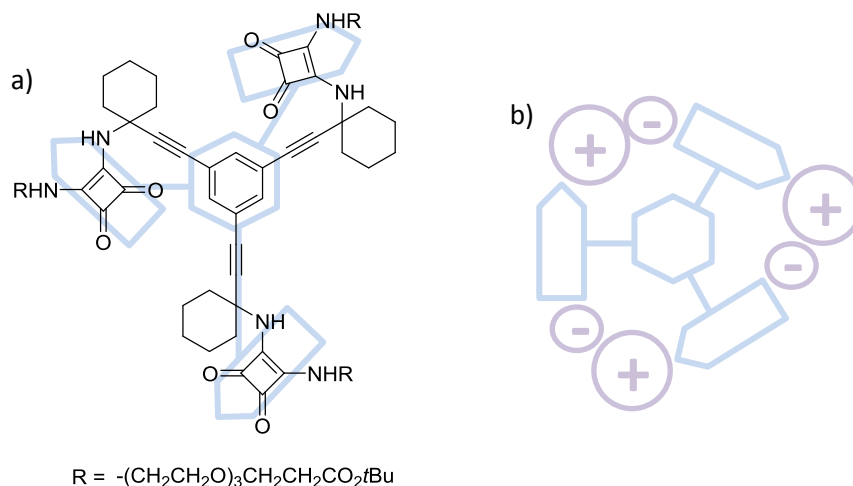


Figure 32. a) Tripodal receptor for ion pair binding. b) Schematic representation of the complexes.

The functionalization of the amine residues of squaramides allows the modulation of the binding properties of the anionic receptors. Thus, the addition of functional groups such as carbonyl groups has reported to act as a molecular switch (Figure 33).⁷⁵ In this case, the two carbonyl groups of the benzophenone unit act as molecular valves. In polar solvents, the intramolecular H-bonds are disfavoured allowing the binding to chloride anions but in apolar solvents, the cavity is closed causing the release of the anion.

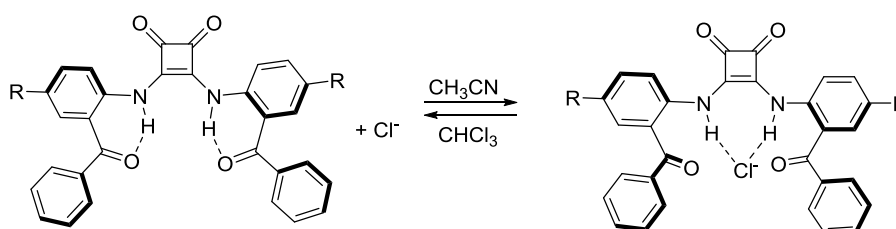


Figure 33. An example of a molecular valve based on a squaramide unit.

Squaramides have also shown the ability to transport anions⁷⁶ and natural amino acids⁷⁷ through lipid bilayers via mobile carrier and anion exchange mechanisms with better results than urea and thiourea. The higher transport activity of squaramides is probably due to their lower lipophilicity that results in a higher binding affinity.

⁷⁴ See reference 56.

⁷⁵ Ramalingam, V.; Domaradzki, M. E.; Jang, S.; Muthyala, R. S. *Org. Lett.* **2008**, *10*, 3315-3318.

⁷⁶ Busschaert, N.; Kirby, I. L.; Young, S.; Coles, S. J.; Horton, P. N.; Light, M. E.; Gale, P. A. *Angew. Chem. Int. Ed.* **2012**, *51*, 4426-4430.

⁷⁷ Wu, X.; Busschaert, N.; Wells, N. J.; Jiang, Y.-B.; Gale, P. A. *J. Am. Chem. Soc.* **2015**, *137*, 1476-1484.

1.6 Thesis overview

In a general context of supramolecular chemistry, the work reported in this thesis is focused on the exploration of new molecules featuring intrinsic cavities, voids or holes that could be applied as artificial receptors or porous materials. Our motivation is to provide new molecular tools for researchers who want to develop practical and/or technological applications. For this reason in selected favorable cases, we will show their potential by developing demonstrative applications in molecular recognition as well as in catalysis and molecular transport.

Chapter 2: Evaluation of a 2-amino benzimidazole cavitand as container molecule.

Chapter 2 continues a synthetic effort initiated by Dr. B. Soberats, a former member of the research group. In this case, we study the ability of a deep-wall cavitand as catalyst. To this end, first we determined the solubility and the conformation, kite or vase, of the functionalized cavitand as a function of the solvent and the pH of the medium. Then, we measured the host-guest affinities of these compounds with trimethyl ammonium derivatives by ITC and $^1\text{H-NMR}$. Finally, the cavitand will be used as a catalyst for enzyme-like acetylation and hydrolysis reactions.

Chapter 3: Development of new crystalline organic porous materials.

Recently, the preparation of porous organic materials through the use of reversible bonds has become a field of interest. In chapter 3, we describe the synthesis of crystalline cycloimine compounds through the condensation of propargyldiamines with dialdehydes or trialdehydes. We evaluated the porosity of the resulting molecular structures by X-ray, SEM, OM and gas sorption analysis. This chapter analyzes the influence of changing the reaction conditions, such as the solvents and the temperature, on the outcome of the resulting material. Also, and more interesting, we describe the application of a new porous material based on dispersive interactions, as the solid support to obtain X-ray data of non crystallizable liquid molecules.

Chapter 4: Studies on squaramide-based macrocycles.

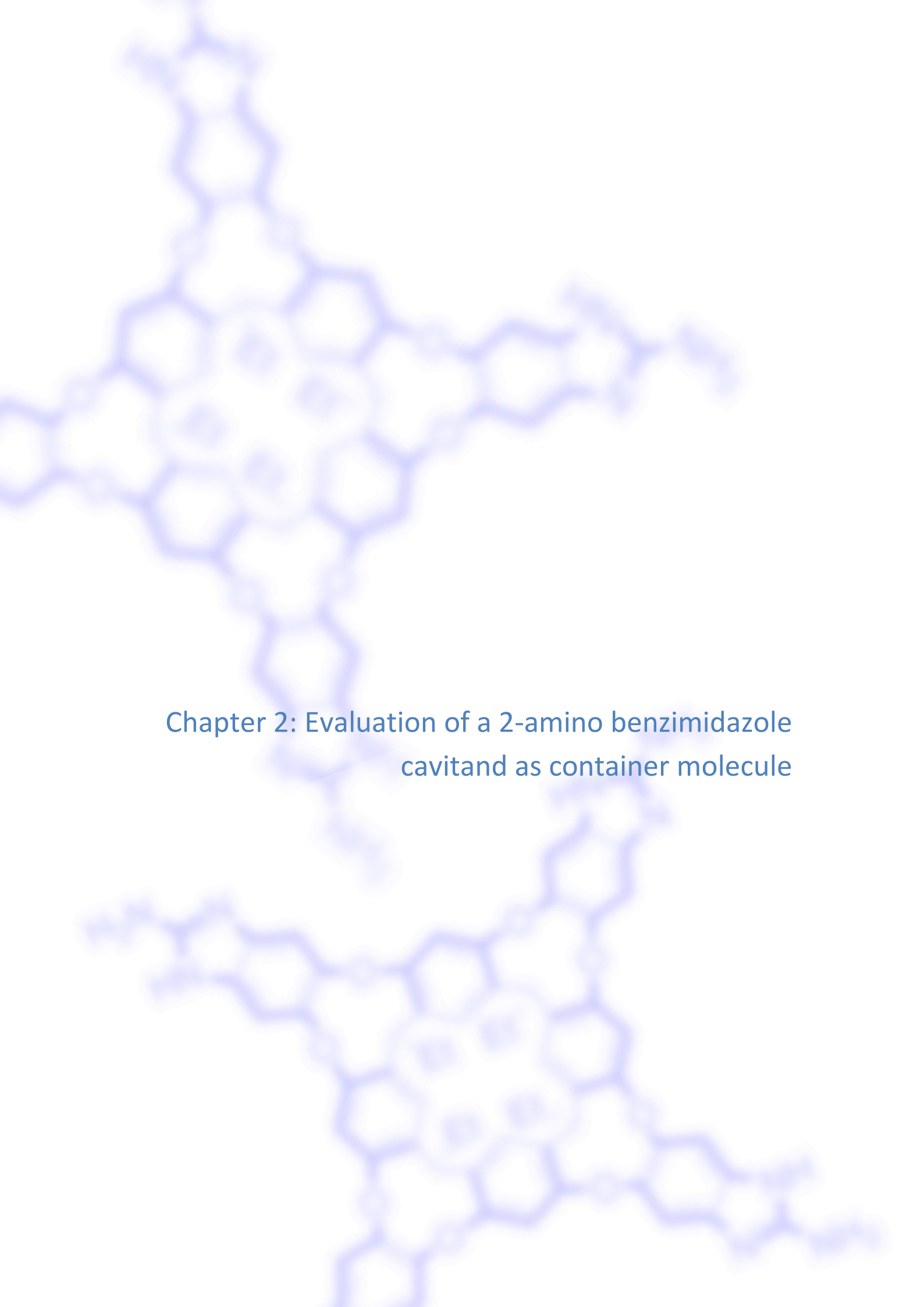
Cucurbiturils are glycoluril-based macrocycles widely used in supramolecular chemistry with applications in molecular recognition and catalysis. On the other hand, squaramides have shown to be isosters of different functionalities such as carboxylic acids, amino acids or ureas, among others. Specifically, squaramides are more effective than ureas in related host-guest complexes. Given the similarities between squaramides and ureas, the aim of this work is the synthesis of squaramide-based glycoluril analogues. The idea behind is to use these building blocks for the construction of unprecedented squaramide-based macrocycles. This chapter describes the incomplete characterization of several macrocycles as well as the difficulties to reach all the objectives initially planned.

Chapter 5: Synthesis of squaramide-based dendrimers.

Polyamino-based dendrimers are water soluble compounds that encapsulate different guests as a function of the pH due to the proton sponge effect. These compounds are useful for molecular transport in drug delivery and gene therapy. In this chapter, we want to explore a new set of polyamino-

squaramide-based dendrimers that combines the properties of a classic polyamino dendrimer with the host-guest properties of the squaramide units. The synthesis of these molecules will be carried out following both, convergent and divergent approaches. The resulting materials will be characterized by mass spectrometry, 2D-NMR spectroscopy, AFM, DLS and zeta potential measurements. The DLS, AFM and DOSY experiments carried out in H₂O at different pH will inform us about the size and shape of the new dendrimeric materials.

PART I

A large, faint, blue molecular structure is visible in the background, consisting of interconnected hexagonal and pentagonal rings, resembling a complex organic or inorganic framework.

Chapter 2: Evaluation of a 2-amino benzimidazole cavitand as container molecule

2.1. Resorcin[*n*]arene-based cavitands

Calix[*n*]arenes are a family of macrocyclic compounds that result from the condensation reaction between phenol, resorcinol or pyrogallol with aldehydes. In particular, resorcin[*n*]arenes are macrocyclic compounds derived from the direct condensation of resorcinol and benzaldehyde with the consequent loss of water molecules without any extra template or high dilution. The *n* indicates the number of resorcinol units present in the macrocycle. Cyclic compounds with even number of resorcinol units (*n* = 4, 6 and 8) are easily obtained, being resorcin[4]arene the most common. These compounds are highly soluble in basic aqueous solutions due to the deprotonation of one hydroxyl group of each aromatic ring giving a cone-shaped structure stabilized by intramolecular hydrogen bonds as shown in Figure 34.

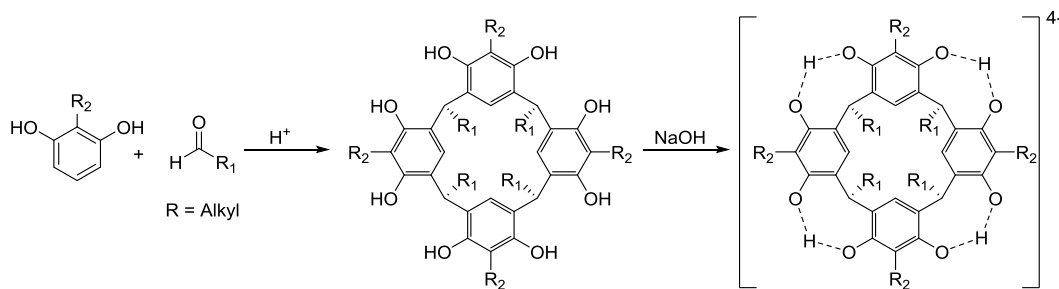


Figure 34. General synthesis of tetraanionic resorcin[*n*]arenes functionalized with alkyl groups in the bottom rim suitable for cationic guest inclusion.

The presence of eight hydroxyl groups on the surface of the upper rim makes these compounds suitable to interact with a wide variety of guests. It has been reported that they can bind cationic guests with high association constants (10^4 - 10^5 M⁻¹).⁷⁸ The host-guest interaction is affected by changes in the electrical charge of guests and the ionic strength or the polarity of the medium. For example, the association constant of the complex of methyl trialkylammonium cation and the resorcin[4]arene with R₁ = Me, R₂ = H is 3×10^4 M⁻¹ in 0.5N NaOD.⁷⁹ Conversely, the interaction of the same resorcin[4]arene with *tert*-butylphenol under the same conditions is only $K = 7$ M⁻¹ showing that the interaction with electroneutral guests is very weak.

Resorcin[4]arene molecules self-assemble giving large hexameric crystalline capsules.⁸⁰ In these cases, the structures are stabilized by sixty hydrogen bonds: forty-eight intra- and intermolecular hydrogen bonds between resorcinarene units, and twelve additional intermolecular hydrogen bonds with eight water molecules. The cavity has an interior volume of 1375 Å³. Moreover, there are four **free** hydrogen atoms as shown in Figure 35, able to interact with potential guest molecules of different sizes.

⁷⁸ Biros, S. M.; Rebek, J. Jr. *Chem. Soc. Rev.* **2007**, *36*, 93-104.

⁷⁹ Timmerman, P.; Verboom, W.; Reinhoudt, D. N. *Tetrahedron*, **1996**, *52*, 2663-2704.

⁸⁰ a) MacGillivray, L. R.; Atwood, J. L. *Nature*, **1997**, *389*, 469-472. b) Adriaenssens, L.; Ballester, P. *Chem. Soc. Rev.* **2013**, *42*, 3261-3277.

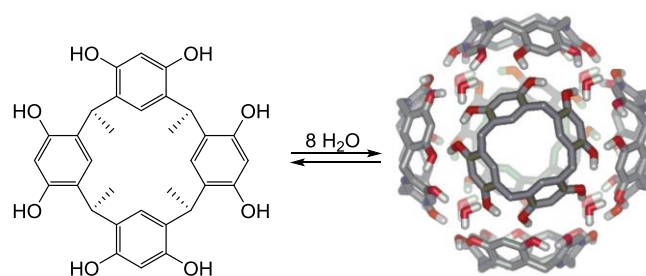


Figure 35. Self-assembled structure observed for resorcin[4]enes in the presence of traces of water.

Resorcin[4]arene-based calix[4]arenes can be used as starting material for the synthesis of deep cavitands through the modification of the hydroxyl groups of the upper rim of the resorcinarene with aromatic groups.⁸¹ The first example of deep cavitand was reported by Cram et al. using quinoxaline spacers to obtain the bowl-shaped compound shown in Figure 36.⁸² These compounds possess larger cavities and less flexibility than the respective starting materials. Further modifications of the upper and bottom rims allow the modulation of their solubility, and their binding and catalytic properties.

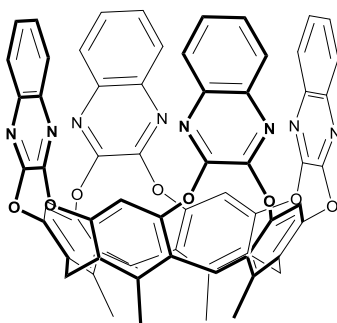


Figure 36. Chemical structure of calixarene reported by Cram et al.

Calixarenes or cavitand compounds display rigid structures wherein the aromatic groups can occupy axial or equatorial positions resulting in two different conformations, named vase and kite (Figure 37). The vase form, with C_{4v} symmetry, implies the formation of a hydrophobic cavity closed at the bottom rim, but with open portals at the upper rim that allow the binding of different guests. On the contrary, the kite conformation has C_{2v} symmetry. Here, the spacers are located in the same plane, resulting in a more extended surface. Both conformations are in equilibria in solution and can be differentiated by NMR techniques.⁸³ Switching between conformations can be done with variations of pH, temperature, concentration of metal ions or redox processes. The equilibrium between the vase and the kite form is a function of the temperature, and it can be displaced by addition of acid or metal ions to the solution enabling the capture and release of guest molecules.

⁸¹ Cram, D. J. *Science* **1983**, *219*, 1177–1183.

⁸² Moran, J. R.; Karch, S.; Cram, D. J. *J. Am. Chem. Soc.* **1982**, *104*, 5826–5828.

⁸³ Moran, J. R.; Ericson, J. L.; Dalcanale, E.; Bryant, J. A.; Knobler, C. B.; Cram, D. J. *J. Am. Chem. Soc.* **1991**, *113*, 5707–5714.

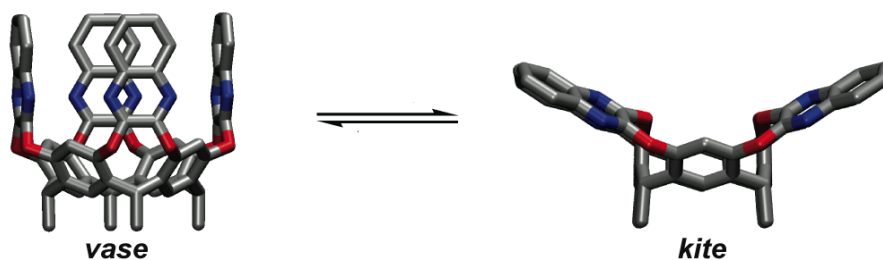


Figure 37. Representation of the two possible conformations of cavitan compounds. This example corresponds to a quinoxaline-bridged resorcin[4]arene cavitan reported by Cram et al.⁸⁴

2.1.1 Host-guest chemistry of cavitands

Resorcinarene cavitands are dynamic cavities assembled using a combination of covalent bonds and non-covalent interactions capable of reversibly bind molecules with an appropriate size, shape and chemical properties. The optimal binding is achieved when the guest molecule occupies the 55% of the cavity volume.⁸⁵

The inner cavity of these compounds is formed by the π -system of the aromatic rings that provide an electron-rich surface. For this reason, cavitan compounds present affinity for cationic and neutral molecules as a function of the dimensions and the functionalization of the cavity.

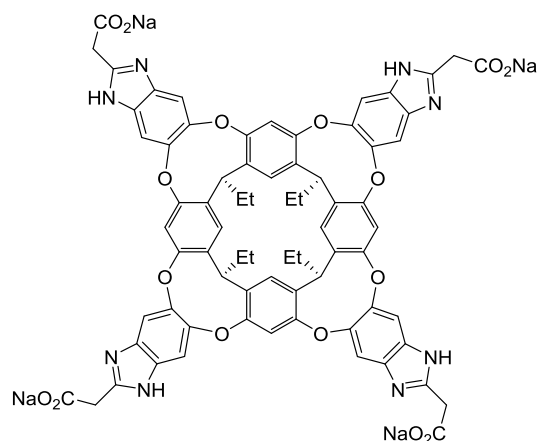


Figure 38. Structure of water-soluble deep cavitan synthesized by Rebek et al.

There are many different examples of cavitands able to encapsulate and transport biologically relevant molecules. For example, Rebek et al. have synthesized the water-soluble cavitan shown in Figure 38. This cavitan shows high affinities in front of different quaternary ammonium salts in aqueous media.⁸⁶

⁸⁴ a) See reference 82. b) Azov, V. A.; Beeby, A.; Cacciarini, M.; Cheetham, A. G.; Diederich, F.; Frei, M.; Gimzewski, J. K.; Gramlich, V.; Hecht, B.; Jaun, B.; Lатыchevskaia, T.; Lieb, A.; Lill, Y.; Marotti, F.; Schlegel, A.; Schlittler, R. R.; Skinner, P. J.; Seiler, P.; Yamakoshi, Y. *Adv. Funct. Mater.* **2006**, *16*, 147-156.

⁸⁵ Mecozzi, S.; Rebek, J. Jr. *Chem. Eur. J.* **1998**, *4*, 1016-1022.

⁸⁶ a) Purse, B. W.; Rebek, J. Jr. *Proc. Natl. Acad. Sci. U.S.A.* **2005**, *102*, 10777-10782. b) Hof, F.; Trembleau, L.; Ullrich, E. C.; Rebek, J. Jr. *Angew. Chem. Int. Ed.* **2003**, *42*, 3150-3153, c) Biros, S. M.; Ulrich, E. C.; Hof, F.; Trembleau, L.; Rebek Jr., J. *J. Am. Chem. Soc.* **2004**, *126*, 2870-2876.

The association constants of the various complexes are shown in Table 3. Remarkably, the higher values correspond to those obtained with choline derivatives. This effect can be explained due to the competitive effect of the solvent on the guests. In the case of the choline derivatives, the hydrophobic effect of the cavity stabilizes more efficiently the guest molecules than the solvent.

Table 3. Association constants for some ammonium salts in water.

Guest	K, M ⁻¹
Me ₄ NBr	3800±600
Et ₄ NBr	12000±900
EtMe ₃ NBr	>10000
Choline chloride	26000±700
Acetylcholine chloride	15000±1200
L-carnitine	150±10

2.1.2 Self-assembly

The presence of donor and acceptor hydrogen bond functional groups at the upper rim of the cavity, together with the partial rigidity of the compounds promotes the formation of cylindrical capsules between two more cavitands. These capsules can be generated by non-covalent interactions leading to the reversible formation of the capsule favouring the encapsulation and release of guest molecules under mild conditions.

Capsules formed by non-covalent interactions are quite common. For example, in 1998, Rebek et al. described the self-assembly of a deep cavitand stabilized by eight bifurcated hydrogen bonds between the imide protons of one cavitand molecule and the carbonyl moieties of another.⁸⁷ Additionally, this compound has shown the ability to extend the cylinder by the addition of four glycoluril molecules between the ends of the two cavitand molecules as is illustrated in Figure 39.⁸⁸ The new capsule is large enough to accommodate long alkane chains (C₁₄-C₁₆) in their extended conformations. Smaller guests as cyclopropane can also be encapsulated showing mobility on the NMR time scale.

⁸⁷ Heinz, T.; Rudkevich, D. M.; Rebek, J. Jr. *Nature* **1998**, *394*, 764-766.

⁸⁸ Ajami, D.; Rebek, J. Jr. *Nat. Chem.* **2009**, *1*, 87-90.

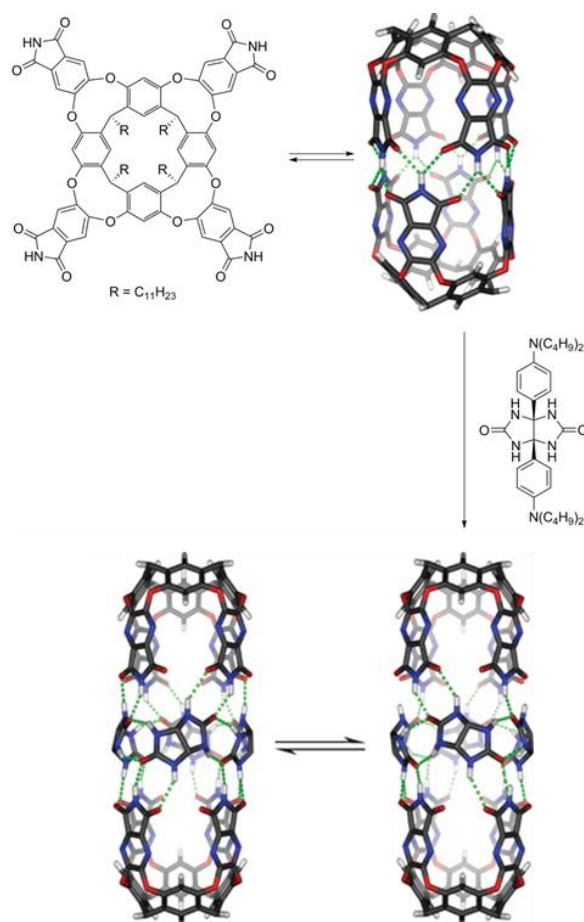


Figure 39. Self-assembled capsule reported by Rebek et al. The addition of glycoluril causes the intercalation thereof between the calixarene molecules with the consequent enlargement of the assembly.

Complementary heterodimeric capsules can also be formed. For example, in the presence of larger guests such as azobenzene, the previous cavitan dimerize with the azo compound as templating agent. If the complex is heated for 5 minutes at 150 °C in the presence of a resorcinarene compound and 1,1' - dimethylferrocene, the azo compound isomerizes causing the breakage of the capsule. Under these conditions the formation of a heterocapsule between the resorcinarene and the calixarene with ferrocene in the inner cavity is favoured. The irradiation of the solution for 150 minutes at 360 nm causes the recovering of the homocapsule, thus proving the reversibility of the process (Figure 40).⁸⁹

⁸⁹ Lux, J.; Rebek, J. Jr. *Chem. Commun.* **2013**, 49, 2127-2129.

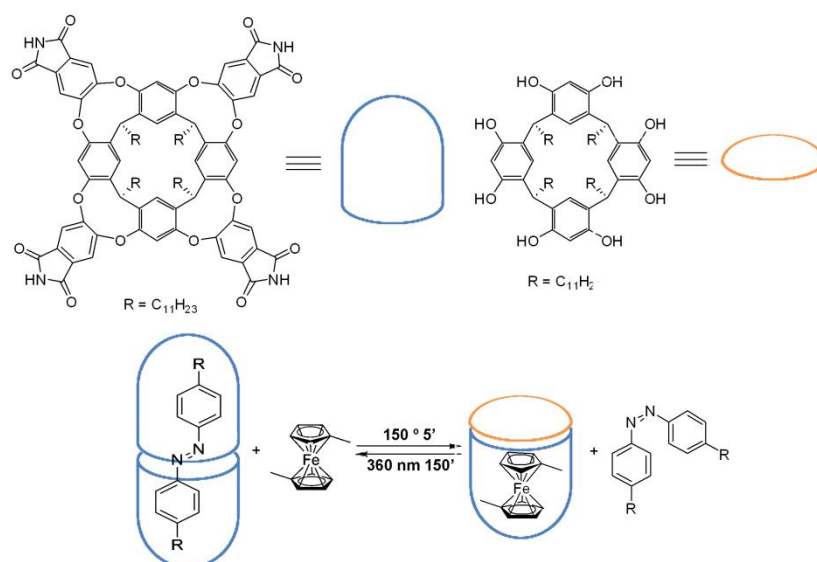


Figure 40. Schematic representation of the switching process in the formation of the homo and heterodimeric capsules.

Cavitand-based capsular assemblies can also be formed using dynamic covalent chemistry (DCC). This approach has some advantages in supramolecular chemistry because it combines the strength of covalent bonds with the reversibility of non-covalent interactions. The acid catalysed condensation of a resorcinarene cavitand functionalized with aldehyde groups in the upper rim with 1,2-ethylenediamine has been reported.⁹⁰ When the reaction is performed in chloroform, an octahedral cage composed of six resorcinarenes and twelve diamines with a cavity volume of 1700 Å³ is isolated (Figure 40). On the contrary, if the reaction is carried out in THF a tetrahedral cage composed of four resorcinarenes and eight diamine molecules is obtained.

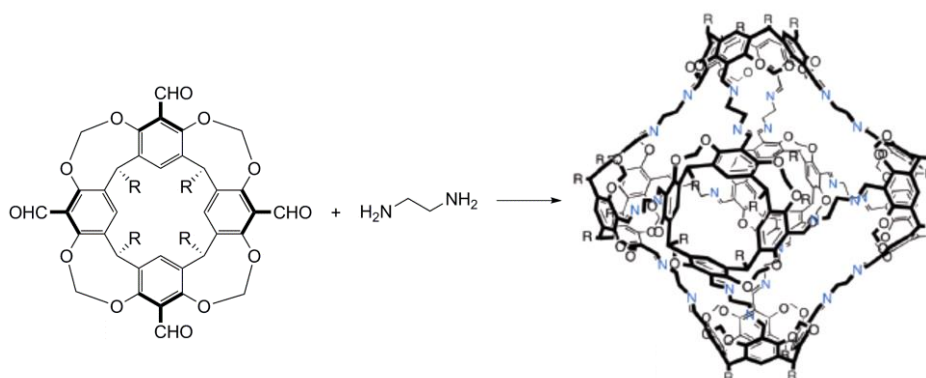


Figure 41. Octahedral cage formed by dynamic covalent bonds described by Warmuth.

Three-dimensional supramolecular structures can be also obtained from the self-assembly of calixarene compounds. For example, supramolecular polymeric chains can be synthesised in apolar solvents by the direct assembly of tetraurea calixarene molecules functionalized with di-L-lysine chains showing a

⁹⁰ a) Liu, X.; Liu, Y.; Li, G.; Warmuth, R. *Angew. Chem. Int. Ed.* **2006**, *45*, 901-904. b) Kobayashi, K.; Yamanaka, M. *Chem. Soc. Rev.* **2015**, *44*, 449-466.

dimerization constant of $K_d > 10^6 \text{ M}^{-1}$. The functionalization of the carboxylic residue of the amino acid with hexamethylenamine generates a compound with two free amino groups, the amino of the hexamethylenamine and the α -amino of the amino acid. When CO_2 is bubbled into the solution, the gas reacts with both amines causing a reversible cross-linking process that generates the 3D structure shown in Figure 42.⁹¹

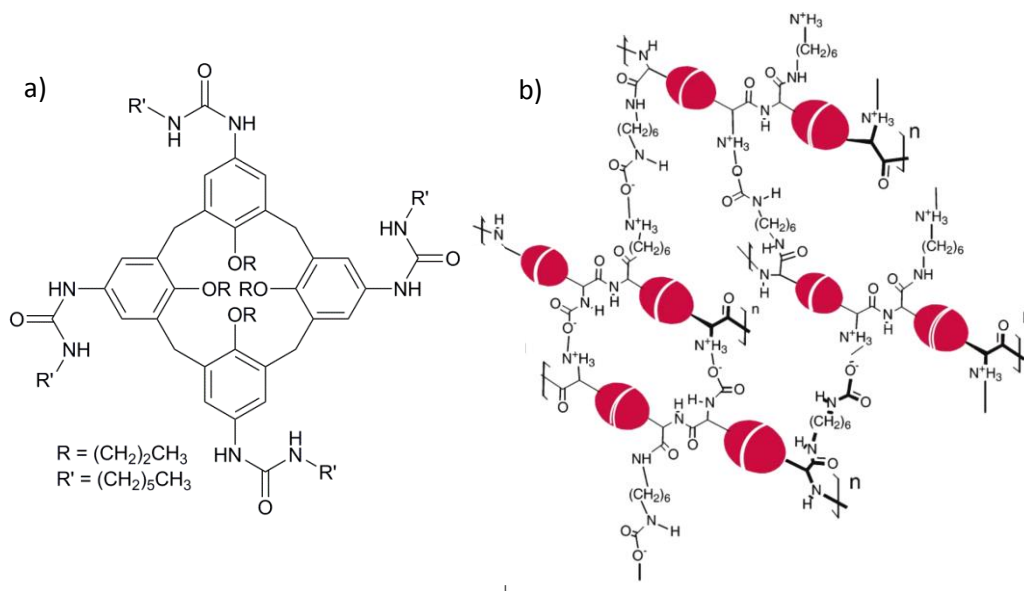


Figure 42. a) Tetraurea calixarene structure. b) Cross-linked structure described by Rudkevich et al.

2.1.3 Deep cavitands in catalysis

Enzymes stabilise transition states enabling the rapid formation of reaction intermediates, and very high rate reactions. The interior of cavitand compounds shows a limited space with tunable walls that can mimic the action of catalytic sites by placing reactants in an appropriate spatial configuration to carry out reactions with very high regio- and stereoselectivity.

In the example shown in Figure 43, an imide-pyrazine-bridged cavitand has been proposed as catalyst for the 1,3-dipolar cycloaddition reaction of phenylacetylene and phenylazide showing a factor of 30000 in rate enhancement.⁹² In this case, only the formation of the 1,4 regioisomer was observed.

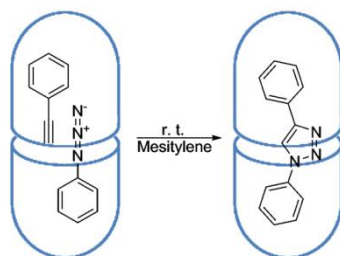


Figure 43. [2+3] cycloaddition of phenylacetylene and phenylazide.

⁹¹ Rudkevich, D. M.; Xu, H. *Chem. Commun.* **2005**, 2651-2659.

⁹² Yoshizawa, M.; Klosterman, J. K.; Fujita, M. *Angew. Chem. Int. Ed.* **2009**, *48*, 3418-3438.

Usually, reaction intermediates are very unstable species that hinder the study of certain reaction steps. Cavitands have been used to encapsulate these compounds and extend their lifetimes allowing their characterization. For example, a deep cavitand compound has been used as mimic of a DRP aldose enzyme able to entrap the reaction intermediate. Here, the cavity binds the target amine isolating it from the bulk solution. Then, an aldehyde functionality situated at the upper rim of the cavity is positioned over the amine favouring the formation of the hemiaminal with a half-life from several minutes to hours that can be followed by NMR spectroscopy under mild conditions (Figure 44).⁹³

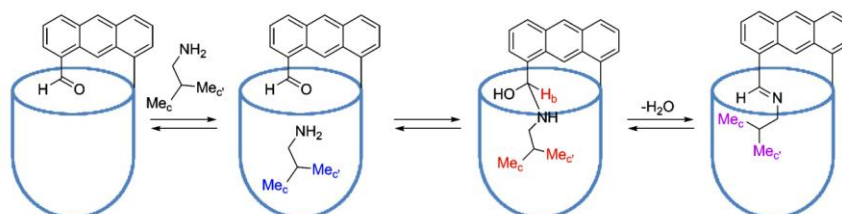


Figure 44. Representation of hemiaminal and imine formation into a cavitand compound.

⁹³ a) Iwasawa, T.; Hooley, R. J.; Rebek, J. Jr. *Science* **2007**, *317*, 493-496. b) Hooley, R. J.; Rebek, J. Jr. *Chem. Biol.* **2009**, *16*, 255-264.

2.2 Aims

The main goal of this chapter is to explore the properties of a resorcinarene cavitand previously synthesized in our group. The specific aims of this work are:

- The NMR study of the conformation equilibria of the cavitand compound in different solvents, mixture of solvents and pH conditions by NMR.
- The determination of the affinities of this cavitand toward cationic compounds. In particular, the determination of the binding constants of complexes formed by the cavitand with various choline derivatives by NMR spectroscopy.
- The evaluation of the inner cavitand cavity as a catalytic site. Specifically, the study of the hydrolysis of choline carbonate derivatives by NMR and UV-vis spectroscopy.

Programmed Enzyme-Mimic Hydrolysis of a Choline Carbonate by a Metal-Free 2-Aminobenzimidazole-Based Cavitand

Bartolomé Sobrats,[†] Elena Sanna,[†] Gabriel Martorell,[‡] Carmen Rotger[†] and Antoni Costa^{*,†}

[†] *Departament de Química, Universitat de les Illes Balears, Ctra. Valldemossa, km 7.5, 07122 Palma de Mallorca, Spain.*

[‡] *Serveis Científicotècnics, Universitat de les Illes Balears, Ctra. Valldemossa, km 7.5, 07122 Palma de Mallorca, Spain.*

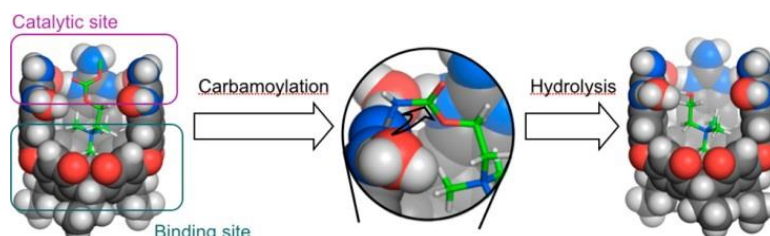
***Organic Letters*, 2014, 16, 840-843**

Received: December 13, 2013

Published: January 13, 2014

2.3.1 Abstract

The hydrolysis of a choline carbonate through a metal-free, enzyme-like mechanism has been achieved using a 2-aminobenzimidazole-based deep cavitand as catalyst. The supramolecular catalysis involves three steps: host-guest binding, carbamoylation and enzyme-like hydrolysis. Interestingly the rate-determining step proceeds through a programmed hydrolysis of carbamoylcholine-cavitand intermediate that may be driven by water molecules surrounding the benzimidazole walls of the cavity.



The development of artificial enzymes has recently attracted a lot of attention due to their applications in chemistry, biology, and medicine.⁹⁴ It is well-known that natural enzymes bind their substrates through weak interactions and selectively place the appropriate functional groups to achieve the catalysis. This approach helps chemists to design supramolecular systems that are able to simulate specific enzymatic roles. A number of supramolecular catalysts based on polymers,⁹⁵ cages,⁹⁶ cavities,⁹⁷ and macrocycles,⁹⁸ among others, have demonstrated enzyme like activity in a wide variety of reactions. However, only a few examples of supramolecular catalysis that mimic the enzymatic mechanisms and kinetics have been reported.⁹⁹ Herein, we report the metal-free, enzyme-like hydrolysis of p-nitrophenylcholine carbonate (PNPCC) catalyzed by the supramolecular cavitand **1** (Figure 45). This reaction involves three steps, i.e. host-guest binding, covalent bonding, and a rate-determining hydrolysis that proceeds in days. It is remarkable that the final hydrolysis may proceed by the nucleophilic attack of the hydrogen bonded water molecules located between the 2-aminobenzimidazole (2-ABI) walls of the cavity.

⁹⁴ (a) Dong, Z.; Luo, Q.; Liu, J. *Chem. Soc. Rev.* **2012**, *41*, 7890-7908. (b) Wei, H.; Wang, E. *Chem. Soc. Rev.* **2013**, *42*, 6060-6093. (c) Hupp, J. T. *Nat. Chem.* **2010**, *2*, 432-433. (d) Nanda, V.; Koder, R. L. *Nat. Chem.* **2009**, *2*, 15-24. (e) Zhao, H.; Foss, F. W., Jr; Breslow, R. *J. Am. Chem. Soc.* **2008**, *130*, 12590-12591. (f) Breslow, R. *J. Biol. Chem.* **2009**, *284*, 1337-1342. (g) D'Souza, V. T.; Bender, M. L. *Acc. Chem. Res.* **1987**, *20*, 146-152.

⁹⁵ (a) Darbre, T.; Reymond, J. -L. *Acc. Chem. Res.* **2006**, *39*, 925-934. (b) Klotz, I. M., Suh, J. *In Evolution of Synthetic Polymers with Enzymelike Catalytic Activities*; Breslow, R. Ed.; Wiley-VCH, Verlag GmbH & Co. KGaA, Weinheim, FRG, **2005**; pp 63-88. (c) Chi, Y.; Scroggins, S. T.; Fréchet, J. M. J. *J. Am. Chem. Soc.* **2008**, *130*, 6322-6323.

⁹⁶ (a) Murase, T.; Nishijima, Y.; Fujita, M. *J. Am. Chem. Soc.* **2012**, *134*, 162-164. (b) Wiester, M. J.; Ulmann, P. A.; Mirkin, C. A. *Angew. Chem., Int. Ed.* **2011**, *50*, 114-137. (c) Ajami, D.; Rebek, J. *Top. Curr. Chem.* **2012**, *319*, 57-78.

⁹⁷ (a) Ballester, P.; Vidal-Ferran, A.; van Leeuwen, P. W. N. M. *Modern Strategies in Supramolecular Catalysis. In Advances in Catalysis*; Gates, C., Knözinger, H., Eds.; Elsevier: **2011**; Vol. 54; pp 63-126. (b) Hooley, R. J.; Rebek, J., Jr. *Chem. Biol.* **2009**, *16*, 255-264.

⁹⁸ (a) Thordarson, P.; Bijsterveld, E. J.; Rowan, A. E.; Nolte, R. J. *Nature* **2003**, *424*, 915-918. (b) D'Souza, V. T. *Supramol. Chem.* **2003**, *15*, 221-229. (c) Mertes, M. P.; Mertes, K. B. *Acc. Chem. Res.* **1990**, *23*, 413-418. (d) Breslow, R.; Dong, S. D. *Chem. Rev.* **1998**, *98*, 1997-2012.

⁹⁹ (a) Klöck, C.; Dsouza, R. N.; Nau, W. M. *Org. Lett.* **2009**, *11*, 2595-2598. (b) Pluth, M. D.; Bergman, R. G.; Raymond, K. N. *J. Am. Chem. Soc.* **2008**, *130*, 1142-1143. (c) Richeter, S.; Rebek, J., Jr. *J. Am. Chem. Soc.* **2004**, *126*, 16280-16281.

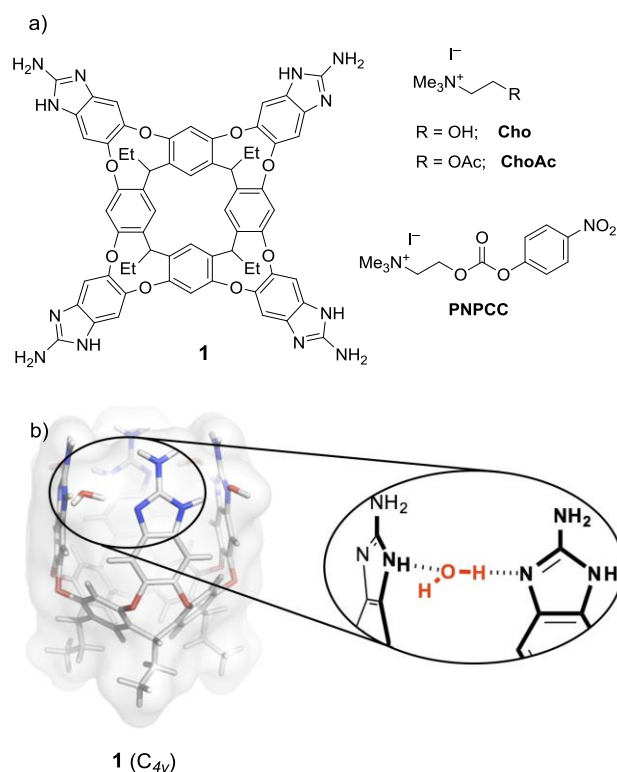


Figure 45. (a) Chemical structures of 2-aminobenzimidazole-based cavitaand **1**, Choline (Cho), Acetylcholine (ChoAc), and *p*-nitrophenylcholine carbonate (PNPCC) iodide salts. (b) Energy-minimized (PM3) perspective side view of cavitaand **1** (C_{4v}) including four hydrogen bonded water molecules on the upper rim.

Resorcin[4]arene cavitaands having extended aromatic walls have been shown to be effective receptors for improved binding to charged and neutral small guests.¹⁰⁰ Work done mainly by Rebek et al. have demonstrated that deep cavitaands decorated with a variety of functional groups at the upper rim fulfill specialized functions, such as encapsulation,¹⁰¹ catalysis,¹⁰² or as nanocontainers designed to stabilize unstable intermediates.¹⁰³ In particular, benzimidazole-based cavitaands are very effective as hosts for alkylammonium compounds¹⁰⁴ and hydrocarbons¹⁰⁵ of suitable size and shape. The reason for the notable binding capabilities of benzimidazole cavities lies in their stable vase conformations under humid conditions due to the presence of hydrogen bonded water molecules bridging two consecutive benzimidazole walls that fix the vase conformation (Figure 45b).

¹⁰⁰ (a) Amrhein, P.; Shivanyuk, A.; Johnson, D. W.; Rebek, J. J. *Am. Chem. Soc.* **2002**, *124*, 10349-10358. (b) Purse, B. W.; Rebek, J. *Proc. Natl. Acad. Sci. U.S.A.* **2005**, *102*, 10777-10782. (c) Xiao, S.; Ajami, D.; Rebek, J., Jr. *Org. Lett.* **2009**, *11*, 3163-3165.

¹⁰¹ (a) Haino, T.; Rudkevich, D. M.; Shivanyuk, A.; Rissanen, K.; Rebek, J., Jr. *Chem.-Eur. J.* **2000**, *6*, 3797-3805. (b) Purse, B. W.; Rebek, J., Jr. *Proc. Natl. Acad. Sci. U.S.A.* **2006**, *103*, 253-257.

¹⁰² (a) Byron, W.; Gissot, A.; Rebek, J., Jr. *J. Am. Chem. Soc.* **2005**, *127*, 11222-11223. (b) Byron, W.; Ballester, P.; Rebek, J., Jr. *J. Am. Chem. Soc.* **2003**, *125*, 1468-1469. (c) Sarmentero, M. A.; Fernández-Pérez, H.; Zuidema, E.; Bo, C.; Vidal-Ferran, A.; Ballester, P. *Angew. Chem. Int. Ed.* **2010**, *49*, 7489-7492.

¹⁰³ (a) Shenoy, S. R.; Pinacho Crisóstomo, F. R.; Iwasawa, T.; Rebek, J., Jr. *J. Am. Chem. Soc.* **2008**, *130*, 5658-5659. (b) Hooley, R. J.; Van Anda, H. J.; Rebek, J. J. *Am. Chem. Soc.* **2007**, *129*, 13464-13473.

¹⁰⁴ (a) Biro, S. M.; Ullrich, E. C.; Hof, F.; Trembleau, L.; Rebek, J. J. *Am. Chem. Soc.* **2004**, *126*, 2870-2876. (b) Lledo, A.; Hooley, R. J.; Rebek, J. Jr. *Org. Lett.* **2008**, *10*, 3669-3671.

¹⁰⁵ (a) Hooley, R. J.; Van Anda, H. J.; Rebek, J. J. *Am. Chem. Soc.* **2007**, *129*, 13464-13473.

Our intention here is to use a benzimidazole-based cavitand as the catalyst for a stepwise hydrolysis of choline carbonates. The new extended resorcinarene **1**, bearing (2-ABI) groups, was designed to offer an appropriate environment to accommodate the ammonium group of the choline derivative inside the cavity owing to the stable vase conformation of the cavitand. Concomitantly, the 2-ABI moieties and their hydrogen bonded structural water molecules may promote the hydrolysis of choline carbonates in the upper rim of the supramolecular pocket (see abstract image).

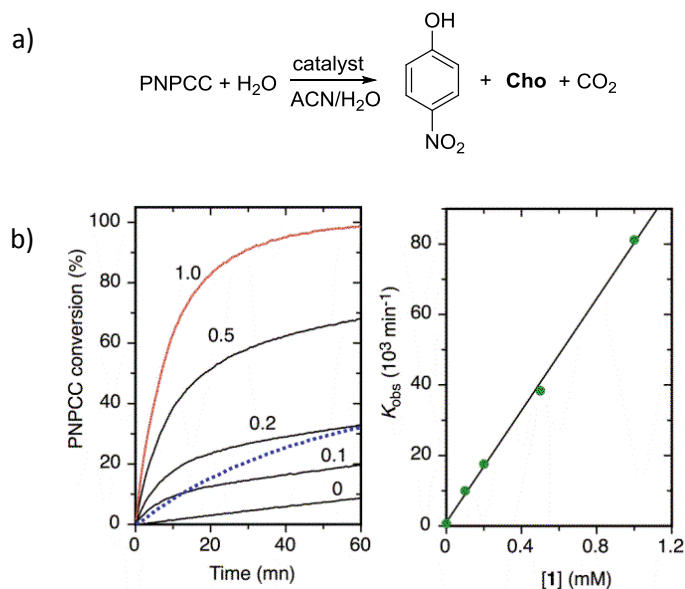


Figure 46. (a) Ideal catalyzed hydrolysis of PNPCC. (b) Real-time UV-vis kinetic conversion curves at 298 K of a solution of PNPCC (0.1 mM) in MeCN/H₂O (99:1 v/v) buffered with 10 mM EtN(*i*-Pr)₂ and 5 mM CF₃CO₂H containing cavitand **1** at different molar ratios: 0, 0.1, 0.2, 0.5, and 1.0 with respect to PNPCC. Blue dashed line: time course for 2-aminobenzimidazole (2-ABI) (0.1 mM). (b) Dependence of the apparent first-order rate constant on cavitand concentration (0.01–0.1 mM). The data were fitted to a straight line ($R^2 = 0.998$), with the second-order rate constant of hydrolysis defined by the slope of the line.

Previously, the hydrolysis of PNPCC was achieved through supramolecular catalysts based on cavitands or cyclodextrin bearing Zn(II) as an active Lewis acid. In these complexes, the metal center was key to modulating both the binding event and the hydrolysis.^{99c;106} However, natural cholinesterases do not include any metal ion in the active center.

In this work, we prepared a metal-free cavitand **1**, which was obtained in moderate yields by a stepwise synthetic procedure (see the Supporting Information). The ¹H NMR of **1** showed the diagnostic methine proton as a sharp triplet at 5.52 ppm in D₂O/MeCN-*d*₃, indicating the existence of **1** in the vase (C_{4v}) form (Figure 47a). The addition of choline (Cho) or acetylcholine (ChoAc) to **1** induces their complexation. The large upfield shifts observed for the N(CH₃)₃ and NCH₂ protons and ¹H–¹⁴N HSQC experiments prove that the trimethylammonium groups of choline derivatives were located deep inside the cavity.^{104a} The affinity of **1** for choline derivatives was assessed by integration of the resonances of free and bound guests. Both complexes, namely **1**·Cho⁺ and **1**·ChoAc⁺, afforded values well above 10⁴ M⁻¹ that preclude their exact determination by ¹H NMR titrations. These complexes were also observed by MALDI-TOF mass spectrometry at *m/z* 1220.56 and 1262.56 assigned to caviplexes **1**·Cho⁺ and **1**·ChoAc⁺,

¹⁰⁶ Zhou, Y.-H.; Zhao, M.; Mao, Z.-W.; Ji, L.-N. *Chem.-Eur. J.* **2008**, *14*, 7193-7201.

respectively, thus confirming that cavitand **1** forms tight complexes with choline derivatives (see the Supporting Information).

Table 4. Kinetic parameters for the reaction of PNPCC (0.1 mM) in the presence of variable amounts of cavitand **1** or 2-ABI

Entry	Catalyst	[PNPCC]/[1]	$k_{\text{obs}} \times 10^{-3} \text{ min}^{-1}$	$k_{\text{obs}}/k_{\text{uncat}}$
1	none	-	0.7 ± 0.2	-
2	1	0.1	10.0 ± 2.1	14
3	1	0.2	17.6 ± 5.4	25
4	1	0.5	38.4 ± 13.5	55
5	1	1	81.2 ± 24.3	116
6	2-ABI	-	21.5 ± 6.4	30

Kinetic studies of PNPCC hydrolysis with **1** were performed in acetonitrile–water mixtures by adaptation of reported procedures.^{99c,107} Hydrolysis of PNPCC under basic conditions generally affords choline, CO₂, and *p*-nitrophenol (Figure 46a) which can be easily monitored by UV spectroscopy. Reactions of cavitand **1** with PNPCC were carried out in MeCN/H₂O (99:1 v/v) buffered with EtN(*i*-Pr)₂/CF₃CO₂H at different concentrations of **1**, and the formation of the *p*-nitrophenolate anion was followed at 405 nm by UV measurements. The experimental kinetic curves obtained for different concentrations of cavitand are shown in Figure 46b. Pseudo-first-order rate constants (k_{obs}) evaluated from the initial slopes were in line with previous reports.¹⁰⁸ Table 4 shows that the amount of cavitand has a marked effect on the initial rates of the reaction (entries 1–5). The linear dependence of the pseudo-first-order rate constants with the concentration of cavitand indicates its participation in the reaction. The apparent second-order rate constant was $79.3 \pm 0.2 \text{ M}^{-1} \text{ min}^{-1}$. It is noteworthy that the effectiveness of cavitand **1** is higher than that of 2-ABI alone (entry 6). 2-ABI also catalyzes the reaction of PNPCC, though less effectively, thus confirming the active role of the 2-aminobenzimidazole units of **1** in the event.

It was expected that the catalytic hydrolysis of PNPCC afforded Cho, CO₂, and *p*-nitrophenol (Figure 46a). However, ¹H NMR experiments ran on mixtures of **1** and PNPCC reveals that the reaction presented here does not proceed through a single reaction step. Instead, a stepwise mechanism involving the formation and subsequent hydrolysis of a 1-cholinecarbamate intermediate takes place under these conditions. The time course of a solution of **1** (0.5 mM) and PNPCC (0.5 mM) in unbuffered MeCN–D₂O (95:5 v/v) was followed by ¹H NMR spectroscopy, and the representative results are shown in Figure 47. To slow down the reaction between **1** and PNPCC and to detect the formation of **1**·PNPCC⁺, the spectrum at *t* = 10 min was registered at 278 K. Figure 47b shows the characteristic upfield signal at –1.28 ppm corresponding to the (⁺NMe₃) of bound PNPCC deep inside of **1**. The coexisting methine protons of **1**·PNPCC⁺ and unbound **1** were also observed at 5.63 and 5.53 ppm, respectively. Formation of the **1**·PNPCC⁺ complex was confirmed by MALDI-TOF mass spectrometry, with *m/z* 1385.423 assigned to [**1**·PNPCC]⁺. Thereafter, the extensive carbamoylation of **1** to give the N-benzimidazolylcarbamate **2** was evident, and it was complete after 18 h (Figure 47c). ¹H NMR spectra taken during this period shows the progressive loss of the C_{4v} symmetry characteristic of **1** and **1**·PNPCC. MALDI-TOF mass spectrometry also revealed the majority presence of a peak at *m/z* 1246.502 corresponding to **2**. The broadened ¹H NMR spectra and the absence of any significant signal at negative shifts indicate that the trimethylammonium “knob” is outside the aromatic pocket. Interestingly, the cavitand portion remains always unchanged in vase form as indicated by a permanent diagnostic signal at around 5.6 ppm. This intermediate slowly hydrolyzes affording the final complex **1**·Cho⁺ which recovers the symmetric

¹⁰⁷ Cuevas, F.; Di Stefano, S.; Magrans, J. O.; Prados, P.; Mandolini, L.; de Mendoza, J. *Chem.-Eur. J.* **2000**, *6*, 3228-3234.

¹⁰⁸ Zelder, F. H.; Rebek, J., Jr. *Chem. Commun.* **2006**, 753-754.

appearance expected for a cavitand–choline complex (Figure 47d,e). It is relevant that the complete decarbamylation of **2** proceeds in a period of around 30 days at 298 K.

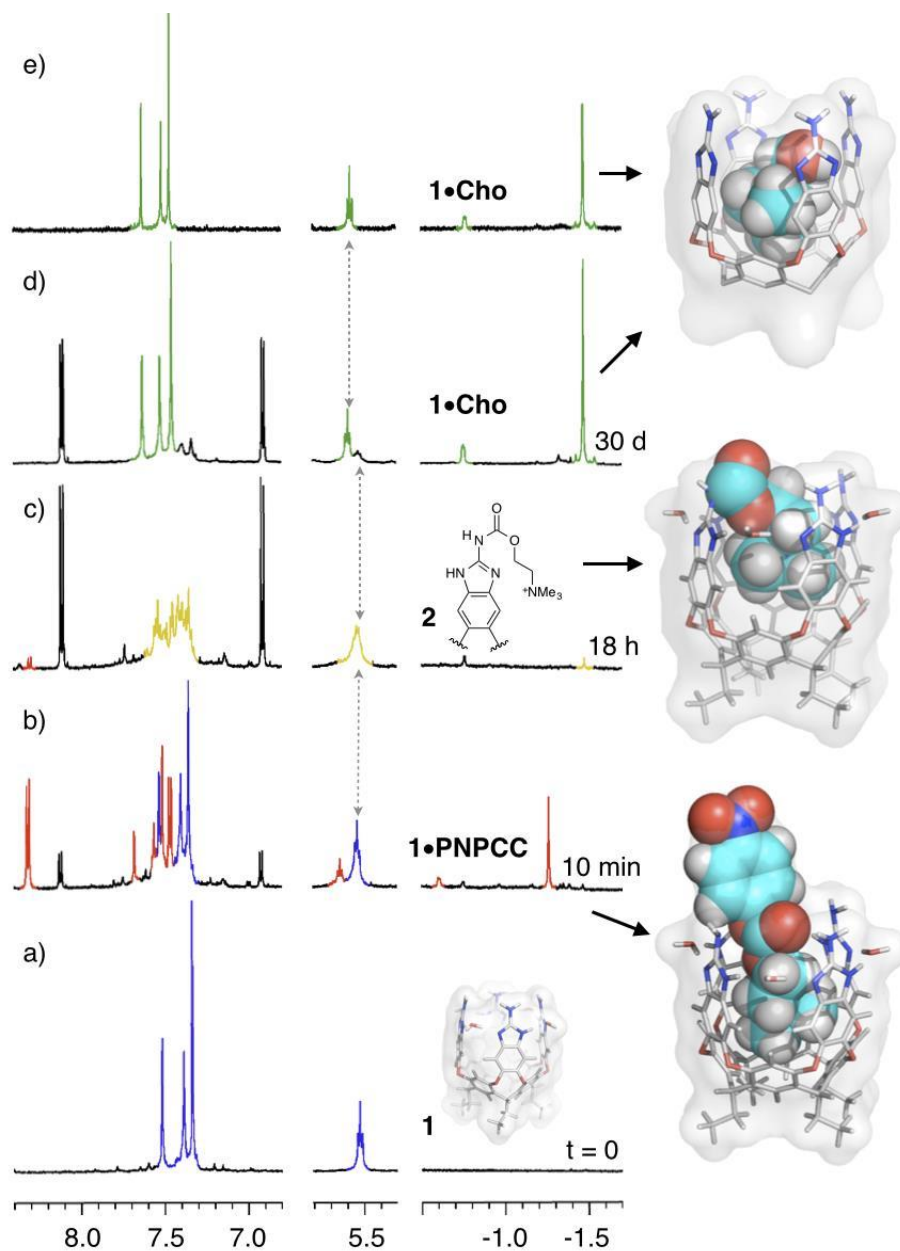


Figure 47. Representative ¹H NMR spectra (600 MHz) of selected regions of a stoichiometric solution containing **1** (0.5 mM) and PNPCC in MeCN-*d*₃/D₂O (95:5 v/v) recorded at different time intervals. Colored resonances are diagnostic signals for free **1** (a, blue), **1**•PNPCC⁺ caviplex (b, red), carbamoylated cavitand (c, khaki), and bound choline **1**•Cho⁺ (d, green). The spectrum of **1**•Cho⁺, prepared independently, is included for comparison (e, green).

Remarkably, carbamylation followed by slow decarbamylation is the mechanism of inhibition operating in certain cholinergic drugs used for treatment of dementia, Parkinson's, and Alzheimer's diseases.¹⁰⁹ Rivastigmine is a paradigmatic example of this behavior. Inhibition of acetylcholinesterases (AcChE) with rivastigmine occurs by a mechanism that includes (i) initial formation of a complex with

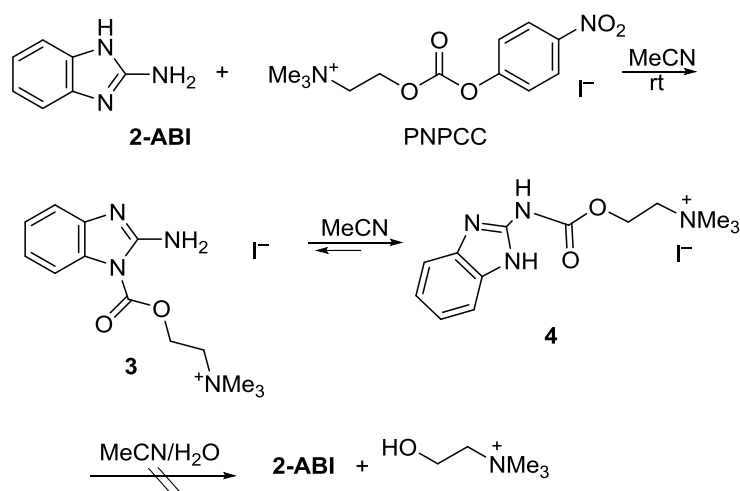
¹⁰⁹ Bar-On, P.; Millard, C. B.; Harel, M.; Dvir, H.; Enz, A.; Sussman, J. L.; Silman, I. *Biochemistry* **2002**, *41*, 3555-3564.

AChE prior to carbamylation, (ii) stoichiometric carbamylation of a histidine residue in the catalytic triad of AChE, and (iii) very slow (hours to days) decarbamylation of the enzyme.¹⁰⁹ Due to the slow decarbamylation process, rivastigmine is classified as a “pseudoirreversible” inhibitor of AChE. These results closely parallel those of PNPCC with cavitand **1**.

The reaction of PNPCC with 2-aminobenzimidazole (2-ABI) and the subsequent hydrolysis were also investigated for comparison (Scheme 1). Depending on the experimental conditions, the addition of PNPCC to a solution of 2-ABI in MeCN–D₂O (95:5 v/v) gave the benzimidazole carbamates **3** and **4** (see the Supporting Information).¹¹⁰ However, in striking contrast with the carbamoyl-cavitand intermediate **2** these carbamates, obtained by direct condensation of 2-ABI and PNPCC, do not hydrolyze even after extended periods at room temperature.

These results suggest that hydrolysis of carbamate intermediate **2** does not proceed by simple nucleophilic attack of the water molecules in the solvent matrix. Hence, decarbamylation of **2** to afford **1·Cho⁺** may be enabled by water molecules located near the upper rim of the cavitand. Molecular modeling of **2** reveals that the trimethylammonium group is outside the cavity and that the carbamoyl group adopts a planar conformation. In this conformation, the carbonyl group of the carbamate is susceptible to hydrolysis by pseudo-intramolecular nucleophilic attack of water molecules lying in the interstice between benzimidazole walls.

Scheme 1. Reaction of PNPCC with 2-ABI



2.3.2 Conclusions

In conclusion, this new metal-free cavitand provides the appropriate environment to promote the stepwise PNPCC hydrolysis in an enzyme-like process. It is of special interest that the hydrolysis of PNPCC takes place slowly due to the combined effect of the supramolecular recognition event and nucleophilic attack of water molecules confined at the outer rim of the carbamoylated cavitand **2**. This is a unique example of quasi-irreversible catalyst inhibition found in cavitands.

¹¹⁰ (a) Fife, T. H. *Acc. Chem. Res.* **1993**, *26*, 325-331. (b) Norberto, F. P.; Santos, S. P.; Iley, J.; Silva, D. B.; Real, M. C. J. *Braz. Chem. Soc.* **2007**, *18*, 171-178.

2.3.3 Acknowledgments

Financial support from the Spanish Ministry of Economy and Competitiveness (CTQ2011-27512/BQU and CONSOLIDER-INGENIO 2010 CSD2010-00065, FEDER funds) and the “Direcció General de Recerca, Desenvolupament Tecnològic i Innovació del Govern Balear” (CAIB, Project 23/2011, FEDER funds) are gratefully acknowledged. E.S. and B.S. thank CAIB and FSE for a predoctoral fellowship.

2.3.4 Supporting Information

2.3.4.1 Experimental

All reagents were purchased commercially and used without further purification. Mass spectra were registered on a MICROMASS Autospec3000 spectrometer equipped with an electrospray module or with a Bruker Autoflex (MALDI-TOF) using trans-2-[3(4-*t*-butylphenyl)-2-methyl 2-propenylidene]malononitrile (DCTB) as matrix. ^1H and ^{13}C spectra were recorded on Bruker AVANCE 300 (^1H at 300 MHz and ^{13}C at 75 MHz) and on Bruker AVANCE III 600 equipped with a cryoprobe, in DMSO-*d*6 or MeCN-*d*3 solvents and using the residual proton signal as reference. Chemical shifts (δ) are in ppm and coupling constants (J) in Hz.

2.3.4.2 Synthesis

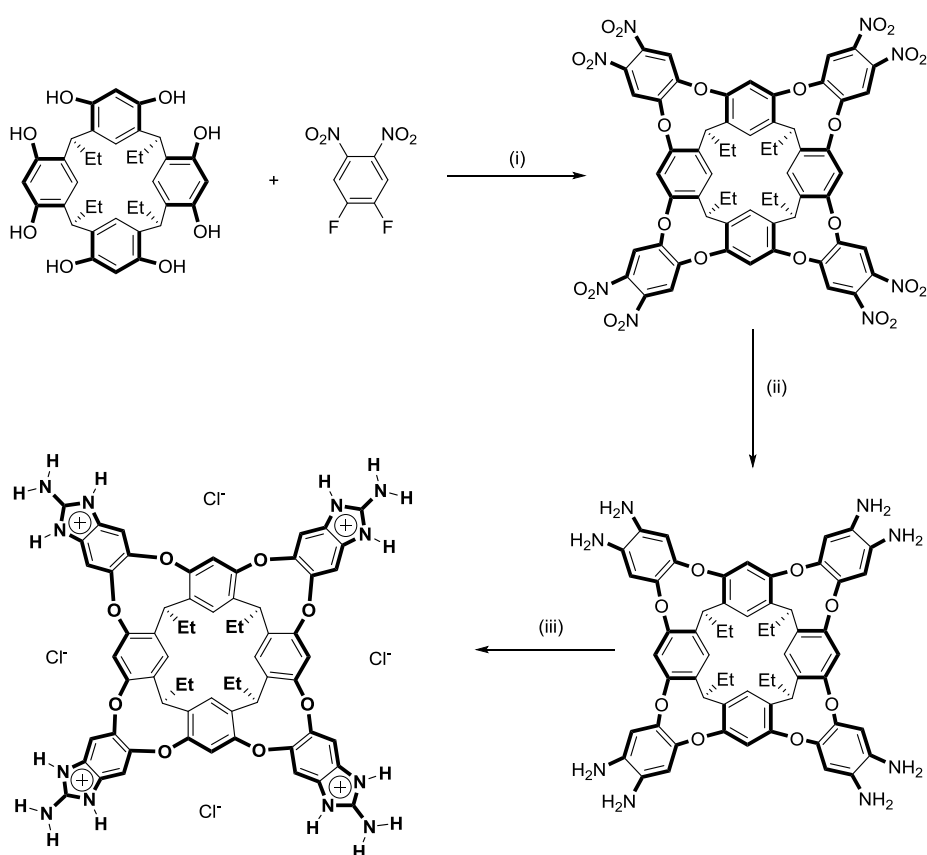


Figure S1. Synthesis of cavitand 1 (hydrochloride salt). (i) Et_3N , DMF, 16h, 70 °C; (ii) $\text{SnCl}_2 \cdot 2\text{H}_2\text{O}$, HCl, EtOH, 16 h, 70 °C; (iii) a) BrCN, EtOH, 20h; b) HCl-diethyl ether, MeOH.

Preparation of the octanitro cavitand

This compound was prepared by an adaptation of a reported procedure.¹¹¹ Tetraethyl calix[4]resorcinarene¹¹² (5g, 8.3 mmol) and 1,2-difluoro-3,4-dinitrobenzene (6.8 g, 33.3 mmol) were suspended in 300 mL of anhydrous DMF and 11 mL of triethylamine were added dropwise. The mixture was heated to 70 °C for 16 h. The solution was cooled and poured into ice (500 g) inducing precipitation of a yellow solid. The solid was collected by filtration, suspended in methanol and sonicated for 5 min. After filtration, the precipitate was washed with methanol (10 mL) and digested with dichloromethane (20 mL) for 1h. The insoluble portion was collected by filtration to afford octanitrocavitand as a yellow solid (9 g, 7.1 mmol) in 86 % yield.

¹H NMR (300 MHz, (CD₃)₂CO): δ 8.14 (s, 16H, Ar-H), 7.36 (s, 4 H, ArH), 4.24 (broad s, 4H, CH), 2.29 (m, 8H, CH₂), 0.92 (t, J=6.8 Hz, 12H, CH₃).

Preparation of the octaamino cavitand

50 mL of concentrated HCl and SnCl₂·2H₂O (6.7 g, 29.8 mmol) were added to a suspension of octanitro cavitand (0.5 g, 0.4 mmol) in 40 mL of ethanol. The mixture was stirred for 16 h at 70 °C. After cooling the resulting precipitate was collected by centrifugation and washed with a 1:1 mixture of water:ethanol to give a solid. The white solid was suspended in 200 mL of ethyl acetate and 150 mL of NH₃ (28 % in H₂O) and the mixture was stirred for 30 min. at room temperature The organic layer was separated, dried over Na₂SO₄ and concentrated to afford the octaamino cavitand (395 mg, 0.4 mmol) in 98 % yield. This compound showed gradual decomposition in contact to air and therefore was rapidly used in the next step.

¹H NMR (300 MHz, DMSO-*d*₆), δ = 7.59 (s, 4 H, ArH), 7.05 (4 H, s, Ar-H), 6.63 (s, 4H, ArH) 5.33 (s broad, 4H, CH), 4.16 (s broad, 8H, NH₂) 2.26 (m, 8H, CH₂), 0.81 (m, 12H, CH₃).

Preparation of tetra(2-aminobenzimidazole) cavitand (1)

A) tetra(2-aminobenzimidazolium chloride salt

Octaamino cavitand (454 mg, 0.44 mmol) was suspended in 80 mL of ethanol and stirred for 15 min. A solution of cyanogen bromide¹¹³ (300 mg, 2.83 mmol) in EtOH (5 mL) was added dropwise within a period of 30 min and the mixture was stirred for 20 h at r.t. After this period, the mixture was cooled at 0 °C and NaOH (1 M) was added until pH > 7. The solvent was removed by rotatory evaporation and the solid was washed with cold water (3×10 mL) and dried under vacuum. The crude was dissolved in methanol (10 mL) and hydrogen chloride in ether (1M) was added to dropwise, a white precipitate was formed. The solid was collected by filtration and washed with EtOH (3 × 20 mL) and MeOH (2×10 mL) to obtain tetra(2-aminobenzimidazolium chloride) cavitand as a white powder (113 mg, 0.09 mmol) in 20 % yield.

¹H NMR (300 MHz, DMSO-*d*₆), δ: 12.1 (s, 8H; NH), 8.7 (s, 8H; NH), 7.79 (s, 4H, ArH), 7.73 (s, 8H, Ar-H), 7.65 (s, 4H, Ar-H), 5.33(t, J = 7.8 Hz, 4H; CH), 2.24 (m, 8 H; CH₂), 0.85 (t, J = 7.2 Hz, 12H; CH₃); ¹³C NMR

¹¹¹ T. Haino, D. M. Rudkevich, A. Shivanyuk, K. Rissanen, J. Rebek, Jr. *Chem. Eur. J.* **2000**, *6*, 3797-3805.

¹¹² L. M. Tunstad, J. A. Tucker, E. Dalcanale, J. Weiser, J. A. Bryant, J. C. Sherman, R. C. Helgeson, C. B. Knobler and D. J. Cram, *J. Org. Chem.* **1989**, *54*, 1305-1312.

¹¹³ Cyanogen bromide is a very toxic reagent and must be handled with care within a fume hood.

(75 MHz, DMSO- d_6) δ : 155.9, 152.0, 148.7, 135.6, 130.3, 127.1, 125.3, 117.1, 107.4, 35.7, 30.2, 25.2; ESI-HMRS: calc. $C_{64}H_{53}C_{14}N_{12}O_8$: 1117.41; exp. 1117.47 $[M+H]^+$.

B) Tetra(2-aminobenzimidazole) cavitand as free base (1), was obtained by precipitation of the benzimidazolium salt from an aqueous solution of the tetrachlorhydrate upon addition of NaOH 1M (10 mL). The mixture was stirred for 30 min at r.t. and the resulting solid was collected by filtration, washed with cold water (3×10 mL) and dried under vacuum.

1H NMR (300 MHz, MeCN- d_3 :D $_2$ O), δ : 7.56 (s, 8H; NH), 7.42 (s, 4H, Ar-H), 7.38 (s, 8H, Ar-H), 7.65 (s, 4H, Ar-H), 5.56 (t, $J = 4.5$ Hz, 4H; CH), 2.36 (m, $J = 3.9$ Hz; 8 H; CH $_2$), 0.97 (t, $J = 3.6$ Hz, 12H; CH $_3$). HRMS (MALDI-TOF): calc. $C_{64}H_{53}N_{12}O_8$: 1117.41038; exp. 1117.40603 $[M-H]^+$.

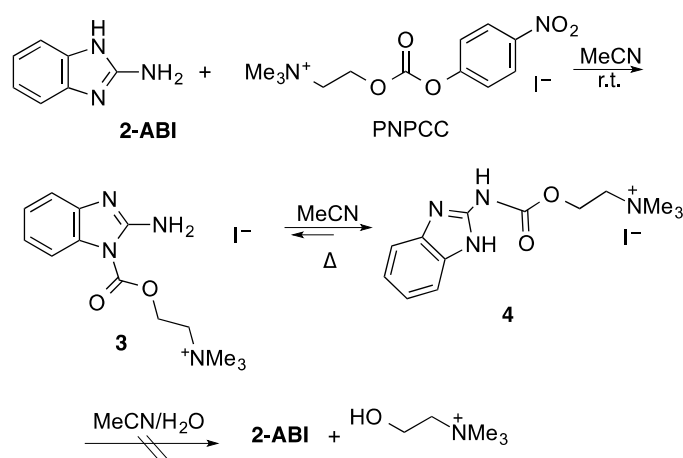


Figure S2. Synthesis of carbamate derivatives from 2-ABI and PNPCC **3** and **4**.

Preparation of 2-((2-amino-1H-benzo[d]imidazole-1-carbonyloxy)-N,N,N-trimethylethanaminium iodide (**3**)

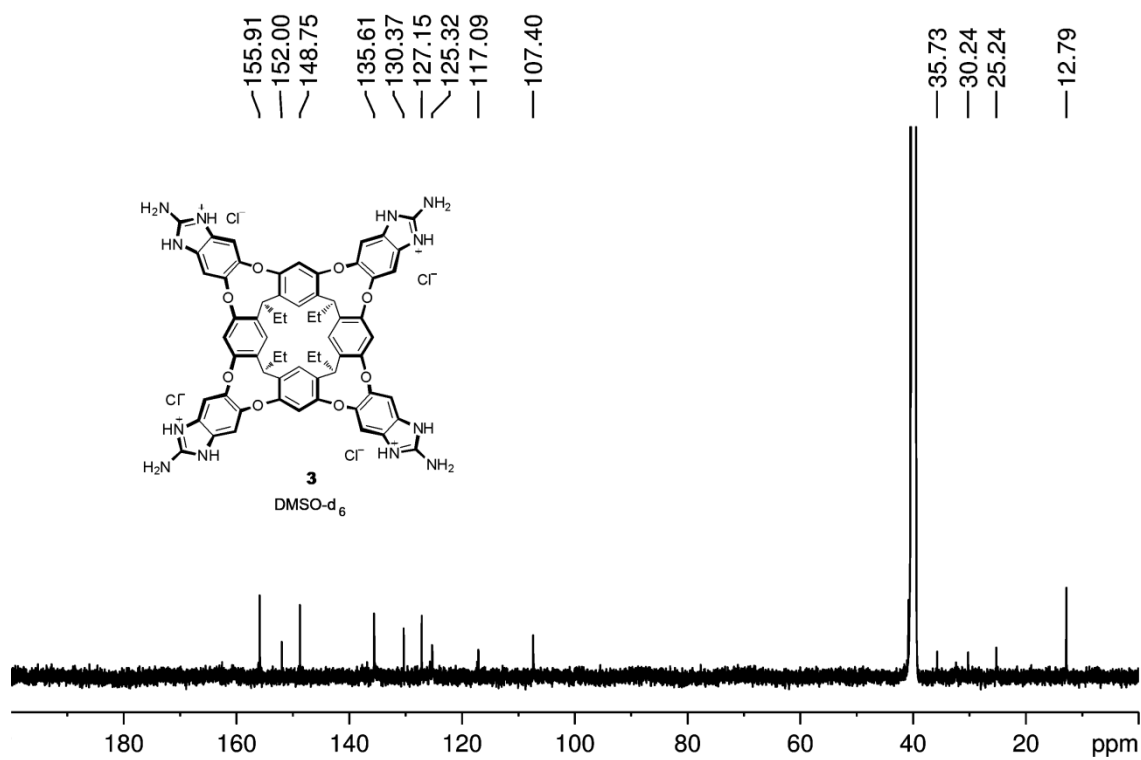
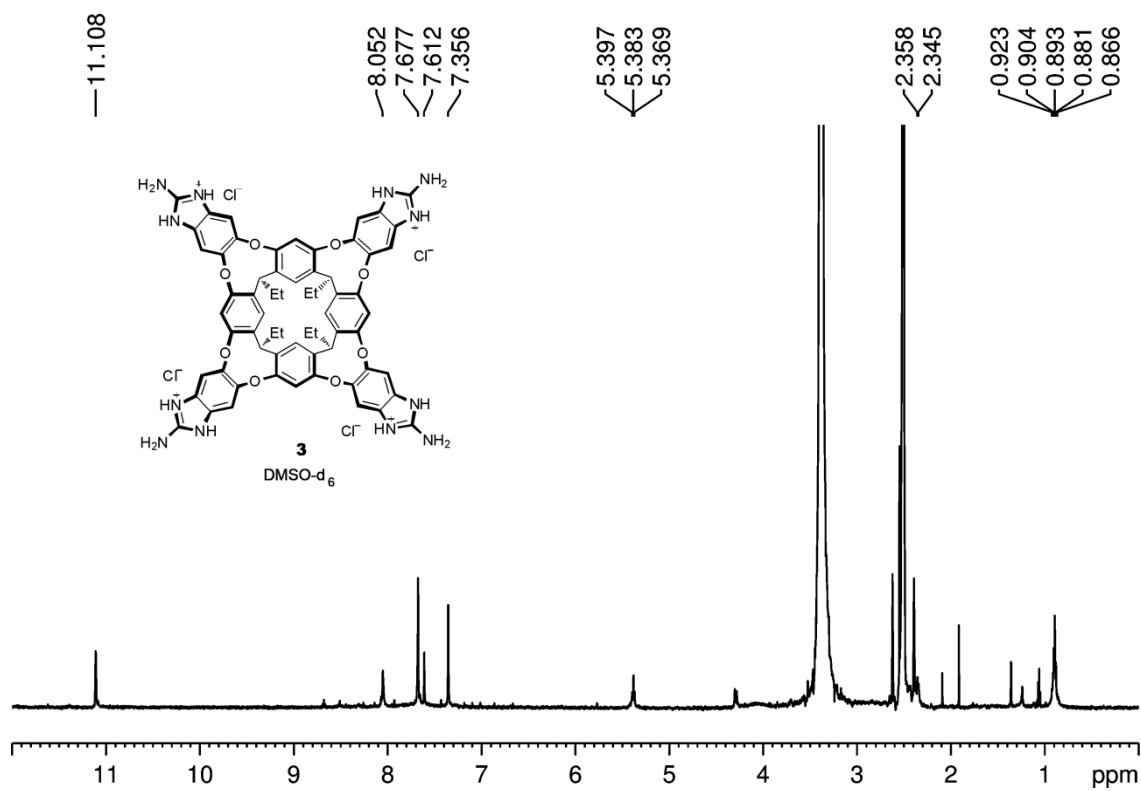
PNPCC (100 mg, 0.248 mmol) in MeCN (25 mL) was added dropwise at 0°C to a stirred solution of 2-aminobenzimidazole (51 mg, 0.372 mmol) in 25 mL of MeCN. The solution was stirred three hours at this temperature. Then, 25 mL of toluene and 8.3 mL of cyclohexane were added at room temperature (resulting mixture MeCN:toluene:cyclohexane 6:3:1). After five days yellow crystals of **3** (83 mg, 83 %) were collected by filtration.

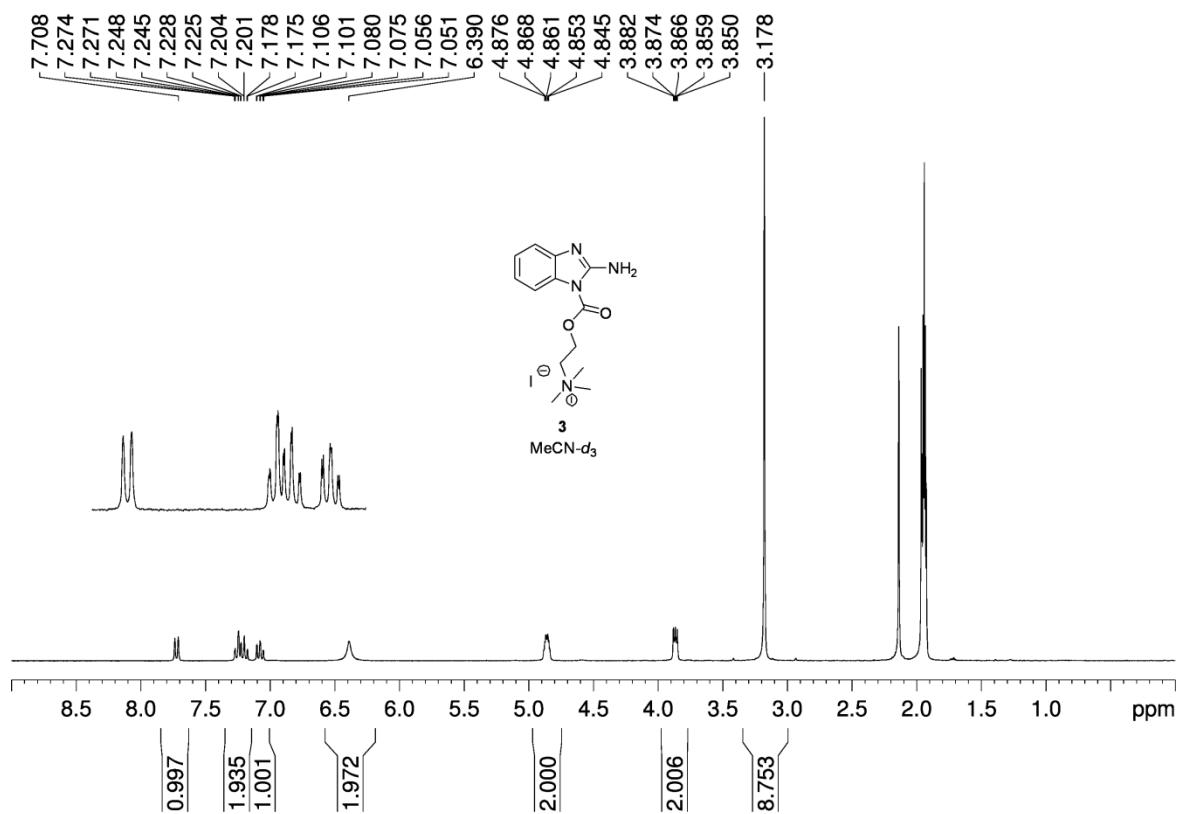
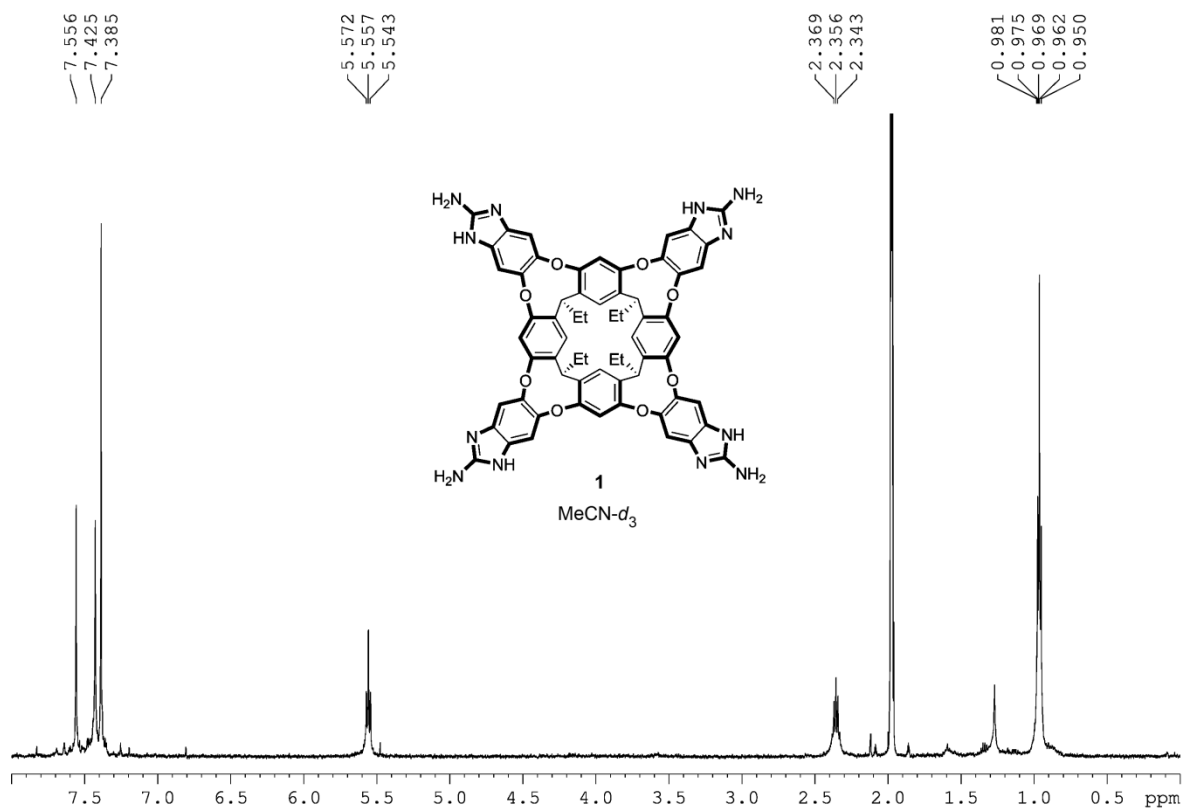
1H -NMR (300 MHz, MeCN- d_3), δ : 3.178 (s, 9H), 3.87 (m, $J = 4.8$ Hz, 2H), 4.86 (m, $J = 4.8$ Hz, 2H), 6.39 (s, 2H), 7.08 (m, $J = 7.2$ Hz, 1H), 7.20 (m, $J = 7.8$ Hz, 1H), 7.24 (m, $J = 7.8$ Hz, 1H), 7.72 (d, $J = 7.2$ Hz, 1H); ^{13}C NMR (75 MHz, MeCN- d_3), δ : 154.5, 152.1, 144.0, 131.2, 125.6, 121.7, 117.1, 115.0, 65.2, 61.9, 54.8. ESI-HMRS: calc. $C_{13}H_{19}N_4O_2$: 263.1508; exp. 263.1510 $[M]^+$.

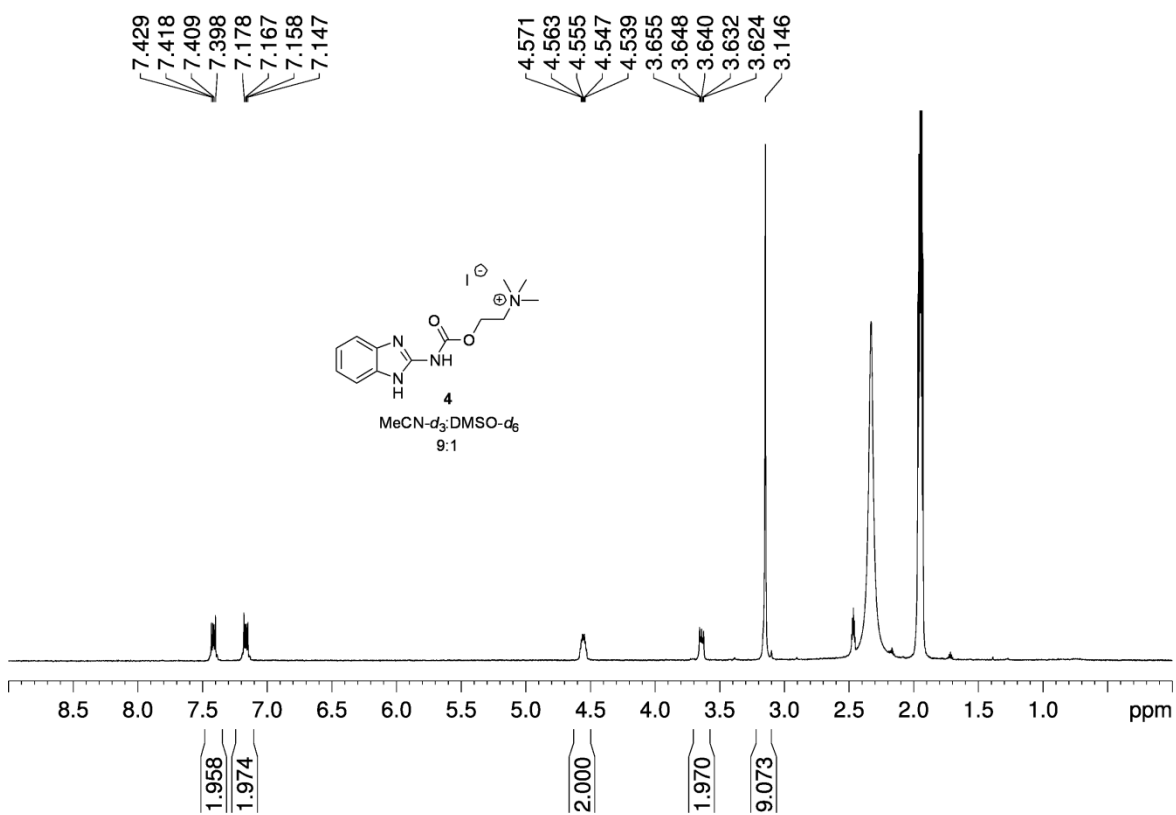
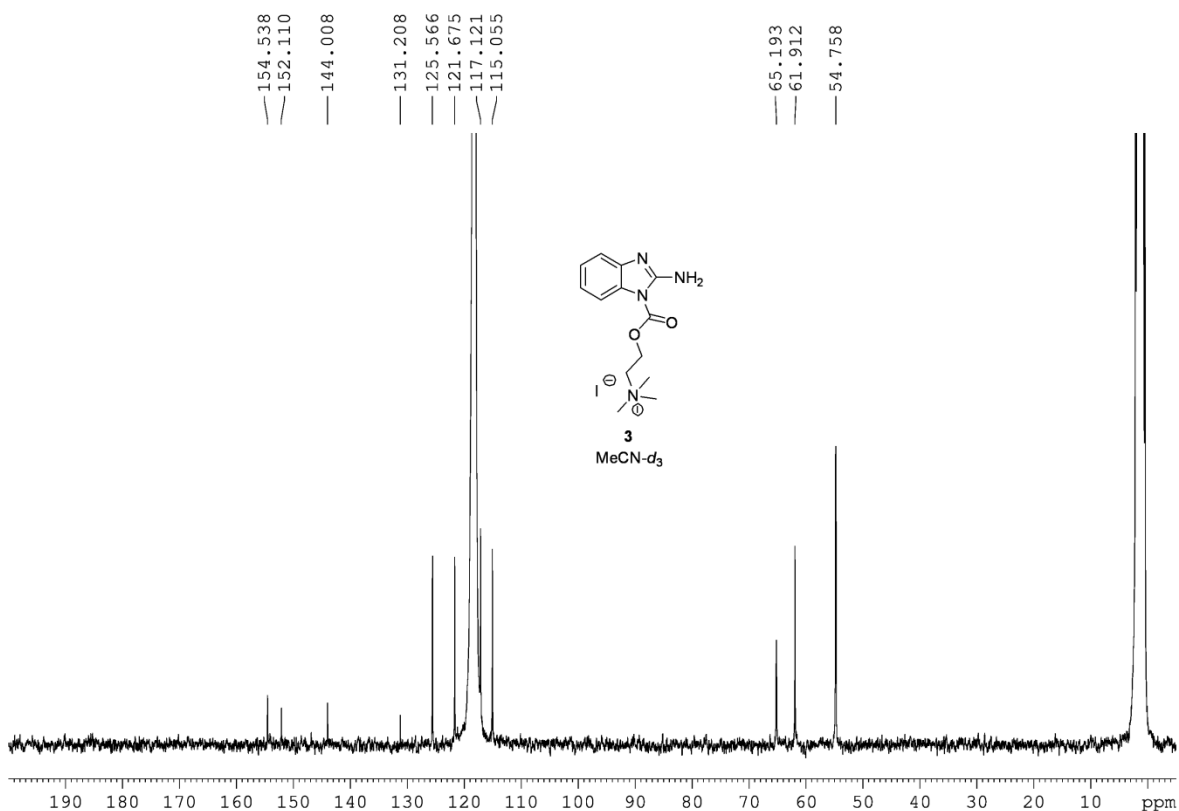
Preparation of 2-(((1H-benzo[d]imidazol-2-yl)carbamoyl)oxy)-N,N,N-trimethylethanaminium iodide (4)

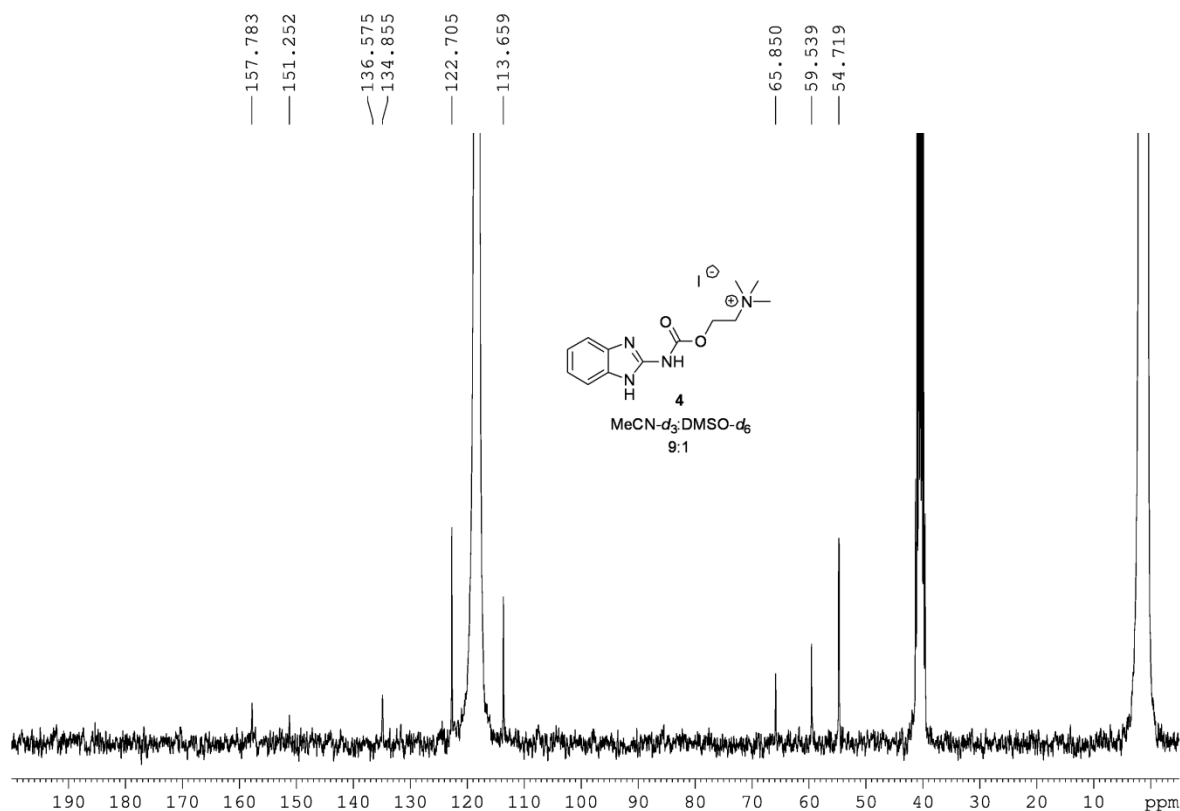
PNPCC (400 mg, 1.01 mmol) in anhydrous MeCN (10 mL) was added to a solution of 2-aminobenzimidazole (200 mg, 1.46 mmol) and potassium carbonate (200 mg, 1.46 mmol) in 10 mL of anhydrous MeCN at room temperature. The mixture was stirred for 2.5 hours. After this period, the solution was evaporated on a rotary evaporator and the resulting solid recrystallized from MeCN:toluene:cyclohexane 6:3:1 at -4 °C, affording **4** (79 mg, 80 %) as yellow solid.

¹H-NMR (300 MHz, MeCN-*d*₃:DMSO-*d*₆), δ : 3.146 (s, 9H), 3.64 (m, *J* = 4.8 Hz, 2H), 4.55 (m, *J* = 4.8 Hz, 2H), 7.16 (m, *J* = 3.3 Hz, 2H), 7.41 (m, *J* = 3.3 Hz, 2H); ¹³C NMR (75 MHz, MeCN-*d*₃:DMSO-*d*₆), δ : 157.8, 151.2, 136.6, 134.8, 122.7, 113.7, 65.8, 59.5, 54.7. ESI-HMRS: calc. C₁₃H₁₉N₄O₂: 263.1508; exp. 263.1509 [M⁺].









2.3.4.3 Characterization of caviplexes

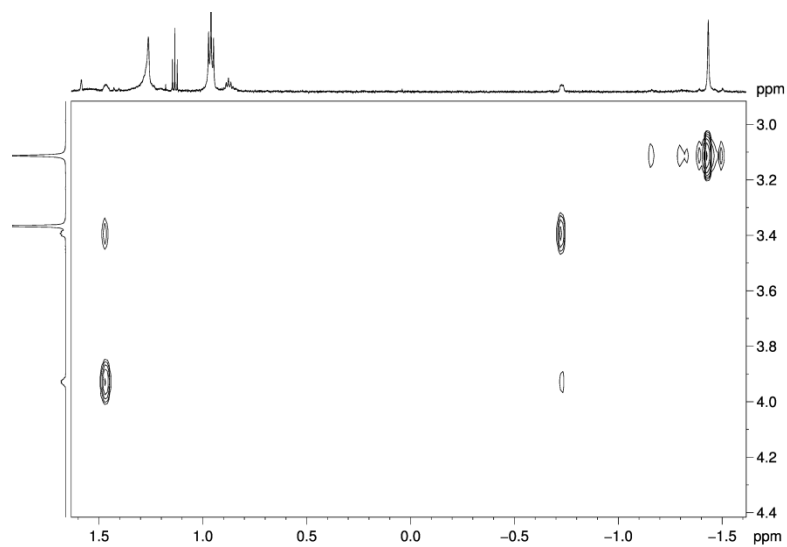


Figure S3. Partial 2D ROESY spectrum of a mixture containing **1** (0.5 mM) and choline (Cho) (5 mM) in MeCN-*d*₃:D₂O at 278 K. The spectrum shows the exchange between bound and free choline.

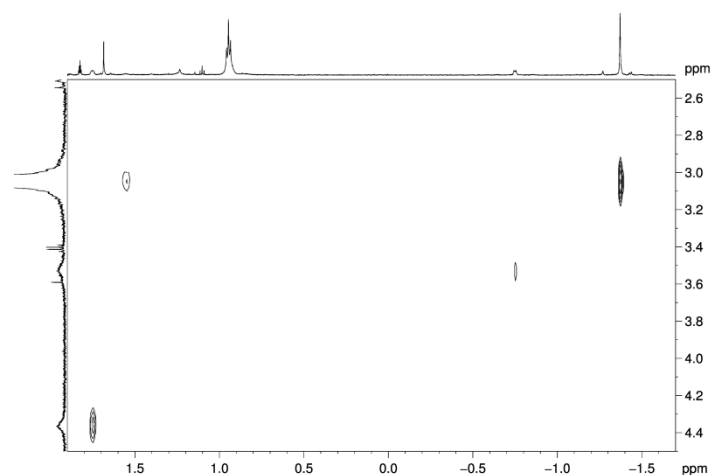


Figure S4. Partial 2D ROESY spectrum of a mixture containing **1** (0.5 mM) and acetylcholine (**AcCho**) (1 mM) in MeCN- d_3 :D $_2$ O at 278 K. The spectrum shows the exchange between bound and free acetylcholine.

^1H - ^{14}N HSQC experiments use the long-range coupling (2J and 3J) networks between ^1H and ^{14}N in choline. The sensitivities in these experiments are comparable to those of standard ^1H - ^{13}C HMBC experiments. The signal intensities varied with the values of INEPT evolution time (τ).¹¹⁴ Referencing indirect dimension (^{14}N) was made following IUPAC recommendations¹¹⁵, δ value for ^{14}N was calculated using 380.23 ppm¹¹⁶ as the position of the resonance of CH $_3$ NO $_2$, as a secondary reference, relative to the primary reference ^{14}N of liquid NH $_3$ and 0 ppm for TMS in 1H dimension.

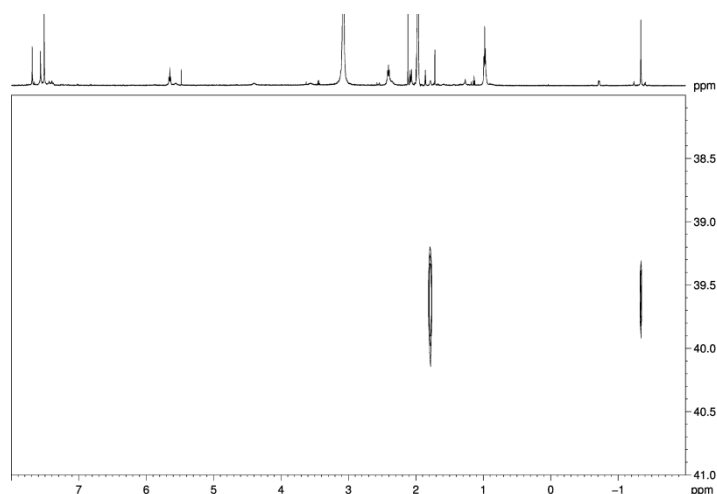


Figure S5. ^1H - ^{14}N HSQC experiment (CD $_3$ CN:D $_2$ O 95:5, 278 K) of a mixture of **1** (0.7 mM) and acetylcholine (**AcCho**) (0.2 mM, τ = 15.6 ms). Bound AcCho: δ = 39.6 ppm.

¹¹⁴ (a) Mao, J.; Jiang, L.; Jiang, B.; Liu, M.; Mao, X. A. *J. Am. Chem. Soc.* **2010**, *132*, 17349-17351. (b) Mao, J.; Jiang, L.; Jiang, B.; Liu, M.; Mao, X. A. *J. Magn. Reson.* **2010**, *206*, 157-160.

¹¹⁵ Harris, R.K.; Becker, E.D.; Cabral de Menezes, S.M.; Goodfellow, R.; Granger, P. *Pure Appl. Chem.* **2001**, *73*, 1795-1818.

¹¹⁶ Live, D.H.; Davis, D.G.; Agosta, W.C.; Cowburn, D. *J. Am. Chem. Soc.* **1984**, *106*, 1939-1941.

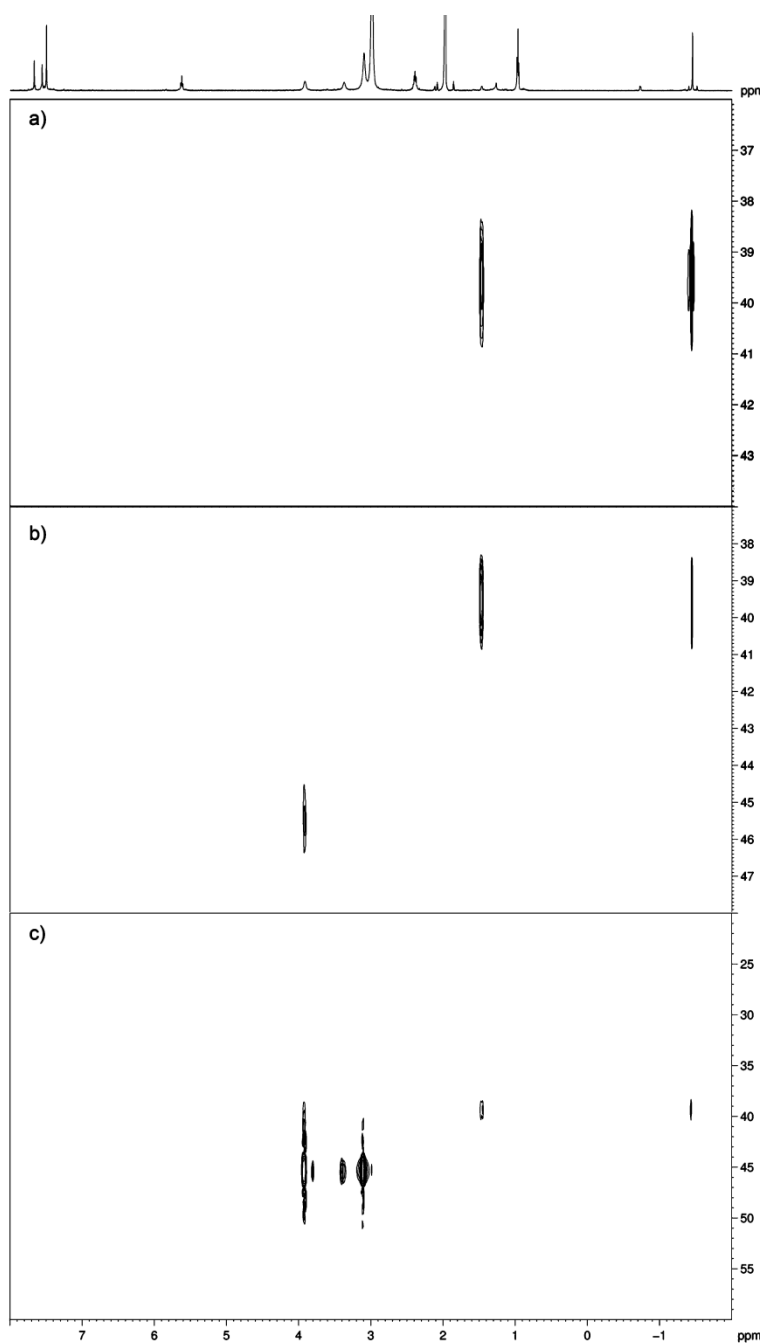


Figure S6. Representative ^1H - ^{14}N HSQC experiments ($\text{CD}_3\text{CN}:\text{D}_2\text{O}$ 95:5, 278 K) of a mixture of **1** (0.5 mM) and increasing amounts of choline (**Cho**); a) **Cho** (0.5mM, $\tau = 41.7$ ms, $ns=64$); b) **Cho** (2mM, $\tau = 15.6$ ms, $ns=64$); c) **Cho** (3mM, $\tau = 15.6$ ms, $ns=64$). The spectra show that the intensity of cross peaks heavily depends on the evolution time. Free choline: $\delta = 45.4$ ppm and bound choline: $\delta = 39.5$ ppm.

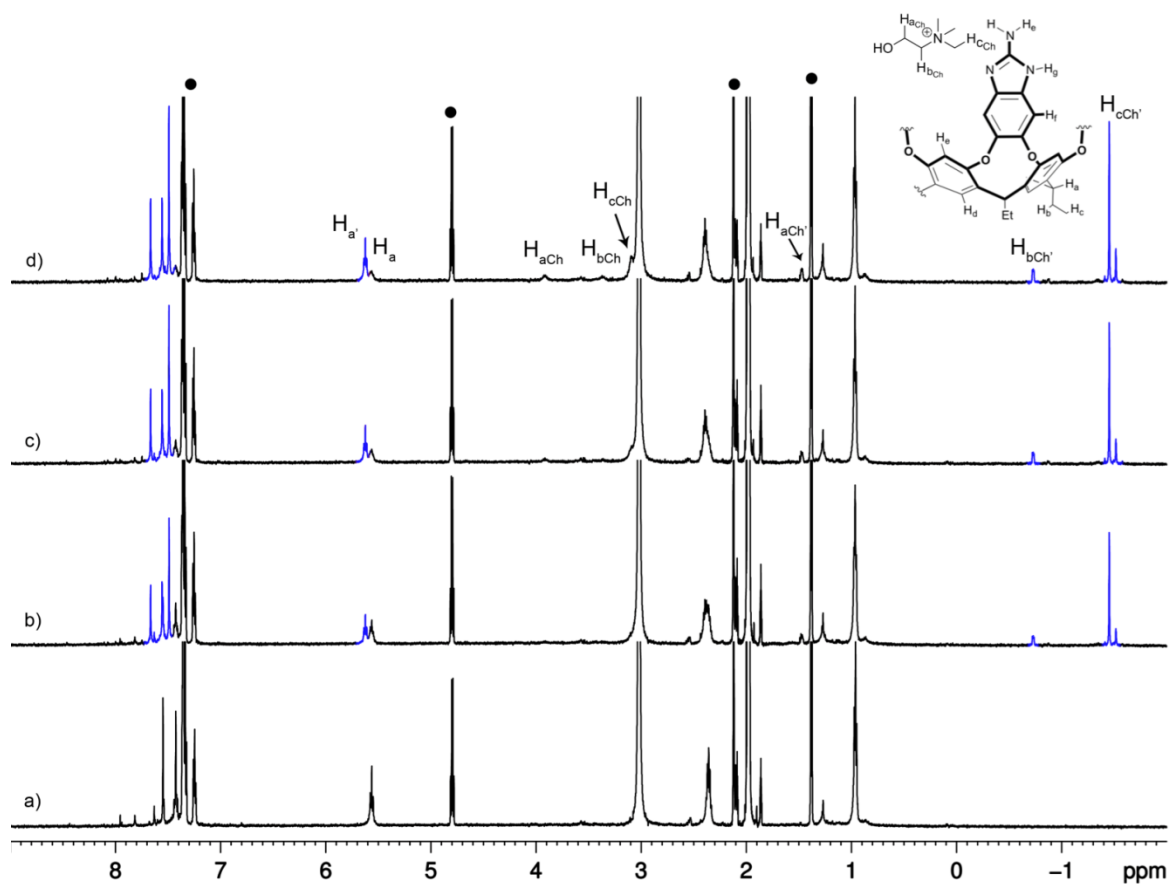
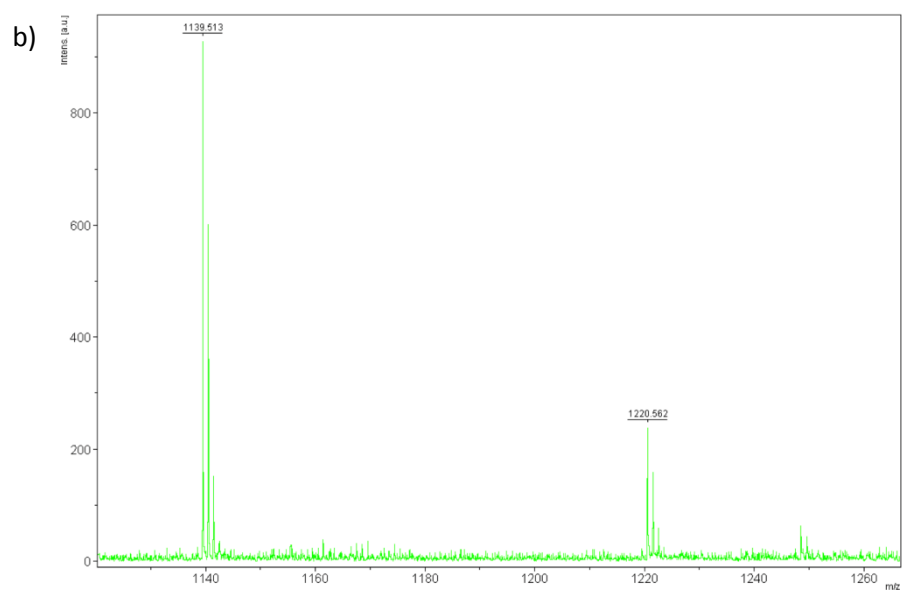
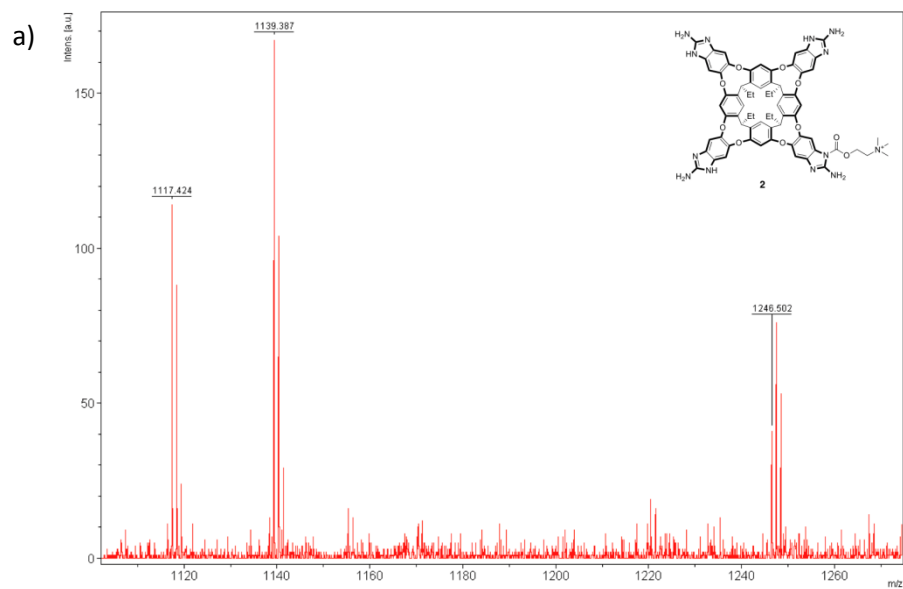


Figure S7. Representative ^1H NMR spectra ($\text{CD}_3\text{CN}:\text{D}_2\text{O}$ 95:5, 278 K) acquired during titration of **1** (0.5 mM) with incremental amounts of Choline (iodide salt): a) 0; b) 0.18; c) 0.24; d) 0.3 equiv. in the presence of 1-phenylethanol (0.7 mM ●) as internal calibration. Colored (blue) resonances correspond to the $\mathbf{1}\cdot\text{Cho}^+$ caviplex.

2.3.4.4 MALDI-TOF (DCTB matrix)



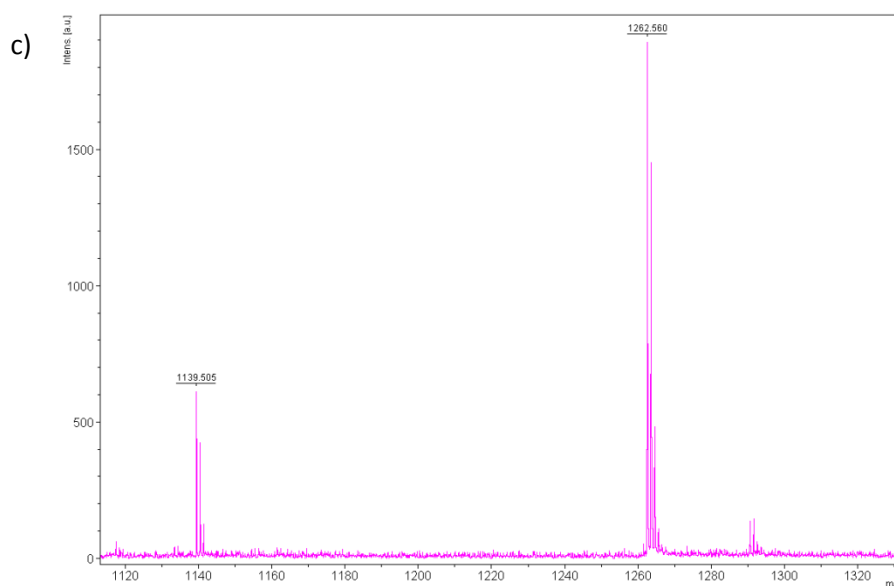


Figure S8. MALDI-TOF mass spectra of a) Carbamoylcavitand **2**: $[1+H]^+$ 1117.42, $[1+Na]^+$ 1139.39, $[2]^+$ 1246.50; b) **1•Cho**: $[1+Na]^+$ 1139.51, $[1•Cho]^+$ 1220.56 and c) **1•AcCho**: $[1+Na]^+$ 1139.50, $[1•AcCho]^+$ 1262.56, in DCTB with NaTFA in a MeCN:H₂O 95:5 mixture.

2.3.4.5 Kinetic study of the interaction of PNPCC with cavitand **1** and with 2-aminobenzimidazole (2-ABI)

All reagents were purchased commercially and used without further purification. The PNPCC was synthesized as previously described.¹¹⁷ Kinetic experiments were performed in 3 mL quartz cells (10 mm) in a UV-visible Varian Cary 300Bio spectrophotometer using the Varian Cary Win-UV Kinetic Application.

Typical conditions used for the experiments were 0.1 mM of PNPCC in a MeCN:H₂O 99:1 mixture buffered with an organic buffer (10 mM DIPEA and 5 mM of TEA) at 298 K. A stock solution of **1** (0.2 mM) was also prepared in the same mixture. For each experiment, a new solution of PNPCC was prepared.

In a representative experiment, the different components are: 0.4 mL of PNPCC solution, V mL of **4** solution and 2-V mL of buffer solution. The volume of **1** depends of the desired percentage of **1** (for example 0.1 mL of catalyst solution used of 10% of catalyst/PNPCC). For the blank experiments no catalyst solutions was added.

The PNPCC was added at the last moment and immediately upon mixing, the sample was placed in the UV-vis spectrometer at 405 nm and the reaction monitored by periodic absorbance acquisition (every 30 seconds during 60 minutes). Each experiment was repeated at least two times.

¹¹⁷ S. Richeter, J. Rebeck Jr. *J. Am. Chem. Soc.* **2004**, *126*, 16280-16281.

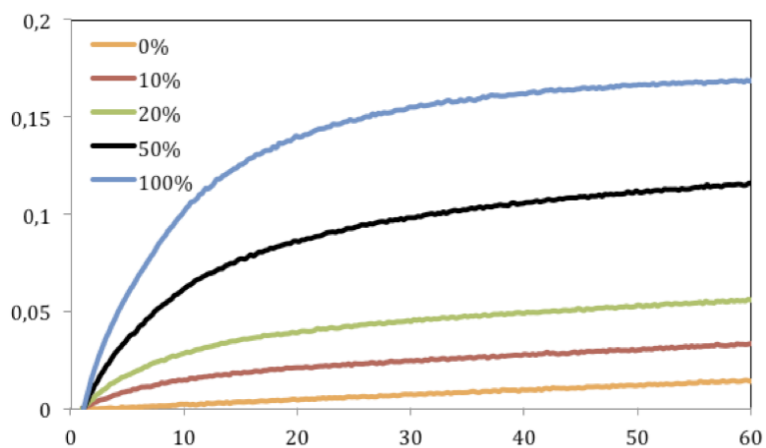


Figure S9. Experimental kinetics curves obtained for PNPCC 0.1 mM. The percentage of cavitaand **1** respect to **1** is indicated in the graphic.

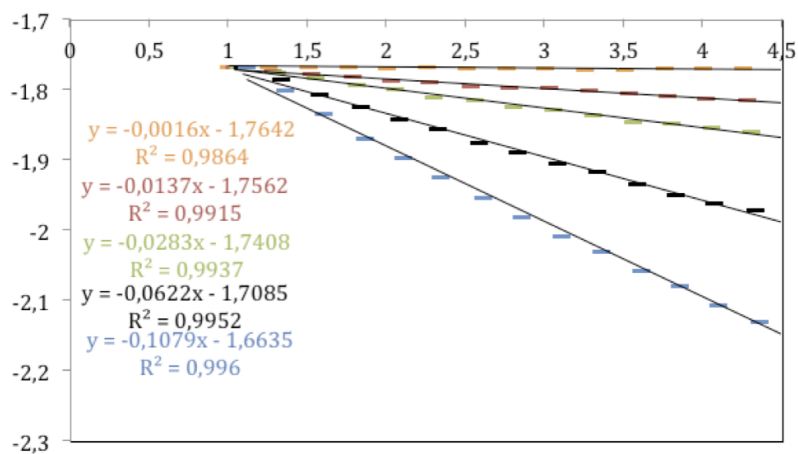


Figure S10. First order rate in PNPCC was determined by plotting $\ln(A_{\max} - A)$ vs. time. A_{\max} corresponds to the maximum absorbance of PNPCC in the buffer mixture. The rates were evaluated from the slopes of the lines obtained by linear correlation on a common time window (orange, blank reaction; red, 10% of **1**; green, 20% of **1**; black 50% of **1**; blue 100 % of **1**).

PART II



Chapter 3: Development of new crystalline
organic porous materials

3.1 Porous materials

Over the last years, the preparation of new porous materials has become of increasing interest among the scientific community owing to their technological applications in molecular separation, gas storage, and catalysis. Traditionally, porous materials used for these applications have been crystalline inorganic frameworks such as zeolites or, alternatively, amorphous structures, such as silica gel or activated carbon.

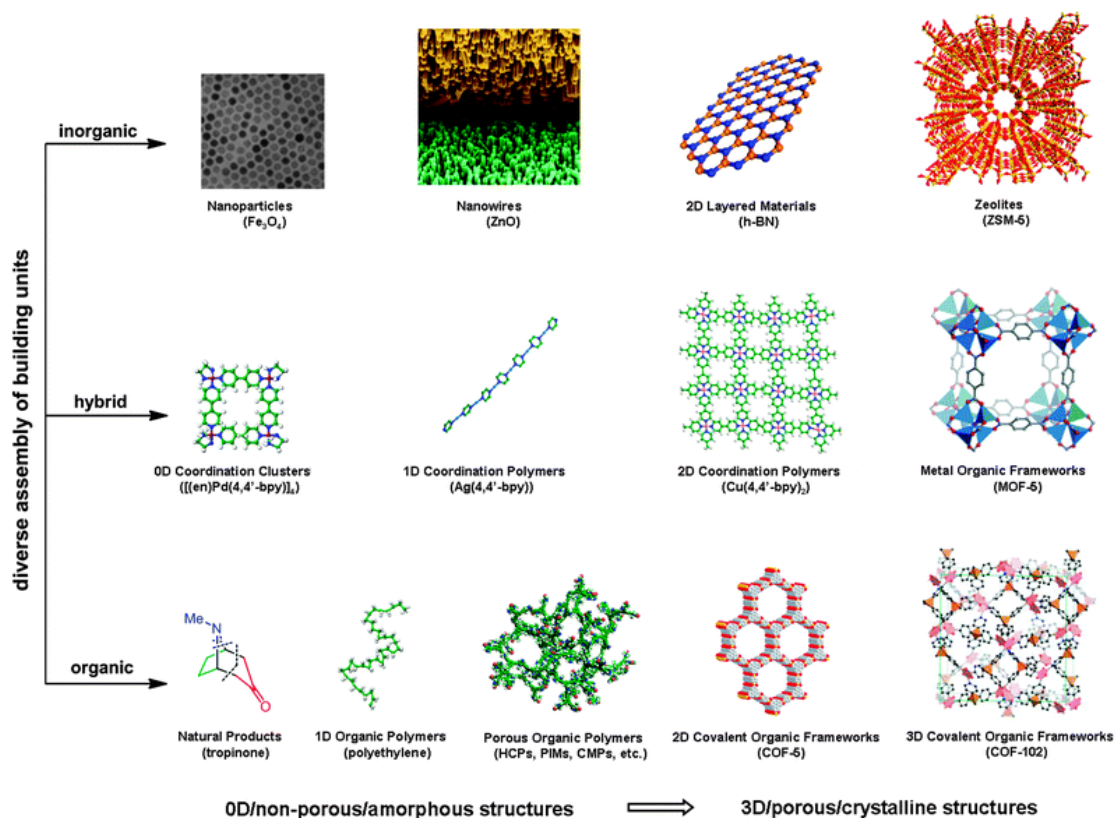


Figure 48. Examples of diverse assembly of building blocks to the preparation of porous materials.¹¹⁸

The main types of nanoporous materials include metal-organic frameworks (MOFs)¹¹⁹, covalent organic frameworks (COFs)¹²⁰ and organic nanoporous polymers.¹²¹

These compounds possess extended 3D frameworks with nanopores normally occupied by solvent molecules arising from the reaction media. In the case of inorganic materials, such as zeolites and MOFs, the removal of solvent molecules yields structures with interconnected channels and cavities.¹²²

¹¹⁸ Ding, S.-Y.; Wang, W. *Chem. Soc. Rev.* **2013**, *42*, 548–568.

¹¹⁹ Eddaoudi, M.; Kim, J.; Rosi, N.; Vodak, D.; Wachter, J.; O'Keefe, M.; Yaghi, O. M. *Science* **2002**, *295*, 469–472.

¹²⁰ Côté, A. P.; Benin, A. I.; Ockwig, N. W.; O'Keefe, M.; Matzger, A. J.; Yaghi, O. M. *Science* **2005**, *310*, 1166–1170.

¹²¹ Dawson, R.; Cooper, A. I.; Adams, D.J. *Prog. Polym. Sci.* **2012**, *37*, 530–563.

¹²² Wales, D. J.; Grand, J.; Ting, V. P.; Burke, R. D.; Edler, K. J.; Bowen, C. R.; Mintova, S.; Burrows, A. D. *Chem. Soc. Rev.* **2015**, *44*, 4290–4321.

Conversely, the desolvation of organic COF materials, in some cases, causes the collapse of the structure with the consequent loss of porosity.¹²³

Porous organic materials, exclusively constructed from organic molecules, are particularly interesting over the rest in that their properties can be tuned by functionalization to interact with different guest molecules. The functionalization can be done following two distinct approaches.

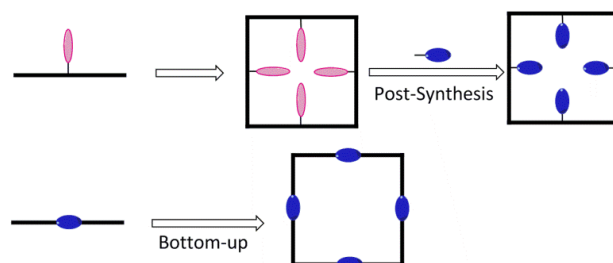


Figure 49. Schematic representation of the two possible routes for the functionalization of porous materials.

The first approach, also known as post-synthetic route, implies the functionalization of the material after the crystallization process. The integration of functional groups easily modifiable in the structure of the porous solid is the most used methodology. For example, recently a crystalline porous COF stable in water and strong acid and base solutions has been reported (see Figure 50).¹²⁴ The inclusion of methoxy groups on the walls of the COF material reinforces the interaction between layers stabilizing the entire structure. Post-synthetic modification of this material through copper(I) catalysed click reactions generate a new crystalline porous compound with a very high BET (Brunauer-Emmett-Teller) surface area of 2105 m²·g⁻¹. This COF has been tested as the heterogeneous catalyst for asymmetric transformations. Specifically, it has been reported the Michael reaction between β -nitrostyrene derivatives and cyclohexanone using this new catalyst in water at 25°C and 1 bar showing excellent enantioselectivity and diastereoselectivity.

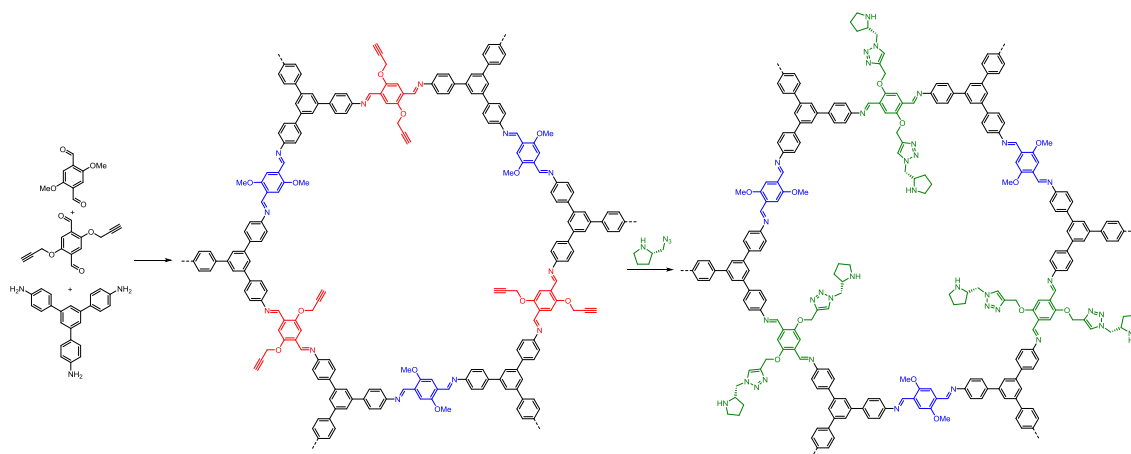


Figure 50. Example of the post-functionalization process is a COF compound.

¹²³ Mastalerz, M.; *Chem. Eur. J.* **2012**, *18*, 10082-10091.

¹²⁴ Xu, H.; Gao, J.; Jiang, D. *Nat. Chem.* **2015**, *7*, 905-912.

The second methodology is a bottom-up process. Here, the functionalization of the different building blocks is a step previous to the formation of the porous material. An advantage of this approach is the homogeneous distribution of the functional groups of the porous structure. This process can change the properties of the resulting compounds conducting to non-crystalline products or different polymorphic crystalline structures. To avoid these drawbacks, a throughout control over the rigidity and shape of the building units is critical.

Using this route, various libraries of COF compounds can be synthesized. Recently, a new family of covalent triazine-based frameworks (CTFs) has been reported. In this case, polymeric structures constructed from the most branched monomers shown in Figure 51 have higher surface areas.¹²⁵

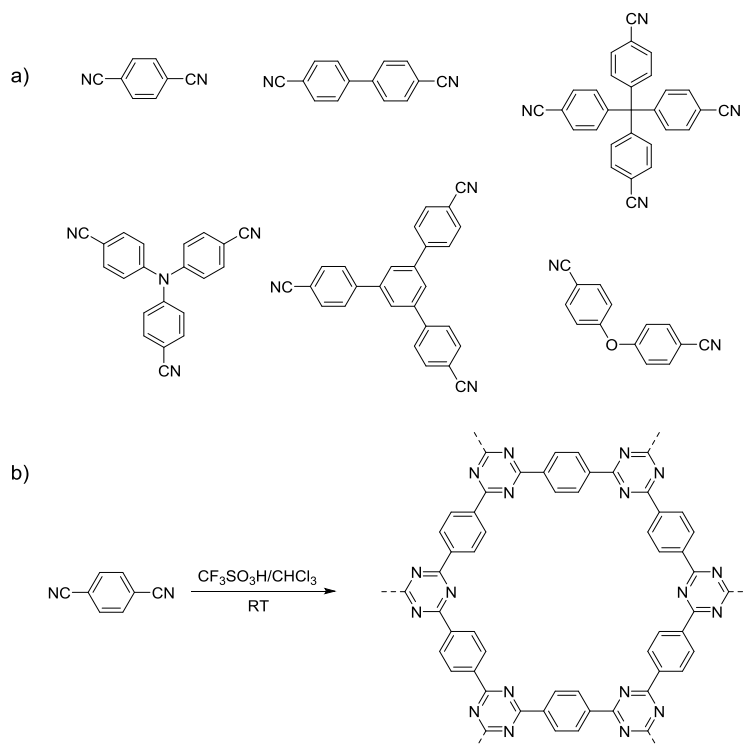


Figure 51. a) Monomeric units used for the synthesis of CTFs by Cooper et al. b) Synthetic route.

Gas sorting, storage¹²⁶ and catalysis¹²⁷ are typical applications of porous materials, but new developments are coming in this field. For instance, recently Fujita et al. have developed two MOFs with chemical formulas $\{[(\text{Co}(\text{NCS})_2)_3(\mathbf{1})_4] \cdot x(\text{solvent})\}_n$ and $\{[(\text{Zn})_3(\mathbf{1})_2] \cdot x(\text{solvent})\}_n$, respectively. Remarkably, these materials can adsorb molecules from a solution into their pores in an ordered fashion. Once included in the solid support, the molecular structures of the included guests can be analyzed by X-ray diffractometry. Hence, these materials are named as "crystalline sponges".¹²⁸ Obviously, the sorption process implies a complete displacement of the molecules present in the pores by the new guests when the crystals are soaked in the guest solution. The procedure is effective even working at very low concentrations.

¹²⁵ Ren, S.; Bojdys, M. J.; Dawson, R.; Laybourn, A.; Khimyak, Y. Z.; Adams, D. J.; Cooper, A. I. *Adv. Mater.* **2012**, *24*, 2357-2361.

¹²⁶ Doonan, C. J.; Tranchemontagne, D. J.; Glover, G. T.; Hunt, J. R.; Yaghi, O. M. *Nat. Chem.* **2010**, *2*, 235-238.

¹²⁷ Kaur, P.; Hupp, J. T.; Nguyen, S. *ACS Catal.* **2011**, *1*, 819-835.

¹²⁸ Inokuma, Y.; Yoshioka, S.; Ariyoshi, J.; Arai, T.; Hitora, Y.; Takada, K.; Matsunaga, S.; Rissanen, K.; Fujita, M. *Nature* **2013**, *495*, 461-466.

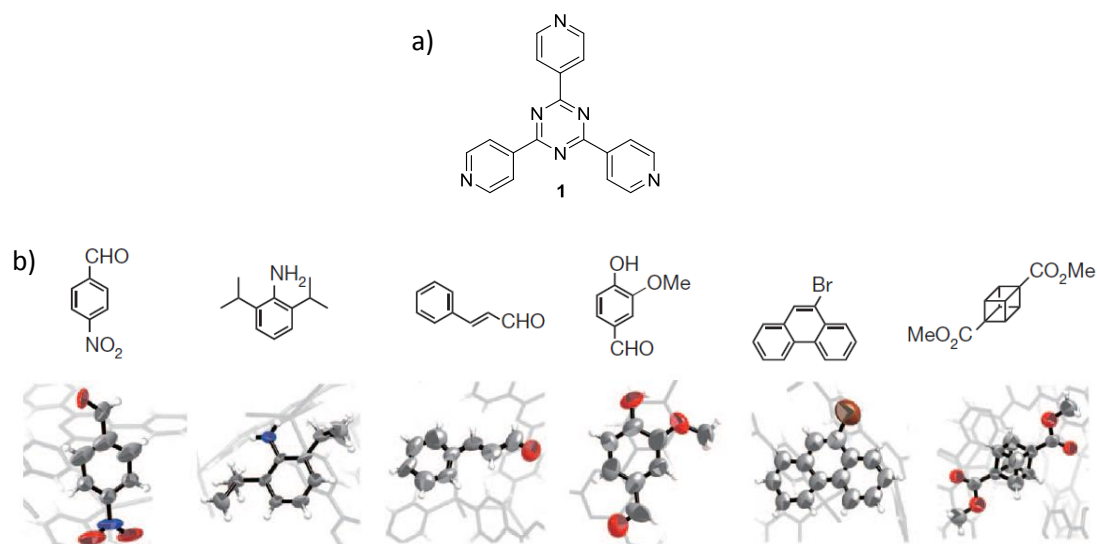


Figure 52. a) Chemical structure of tris(4-pyridyl)-1,3,5-triazine (1). b) X-ray structures of different guest molecules determined after their inclusion in MOF $\{[(Zn)_3(1)_2] \cdot x(\text{solvent})\}_n$.

The "crystalline sponge" method of Fujita relies on the use of MOFs for determination of the X-ray structures of molecules without the requirement of obtaining a crystal of the target molecule. In this protocol, the crystallization step is rendered unnecessary. Inspired by this work, in this thesis we describe for the first time a porous organic material (POM) as solid support for the "crystalline sponge method".

3.2 Porous organic molecular crystals

A minor group of porous materials are porous organic materials (POMs). POMs are based on discrete molecules that crystallize through weak non-covalent interactions forming defined pore channels. In optimal conditions, the organic molecules can construct crystals with zero-dimension (0D),¹²⁹ one-dimensional (1D)¹³⁰ or three-dimensional (3D) structures.¹³¹ An example of 0D structure is shown in Figure 53. In this case, the porous crystals result from the inefficient packing of a calix[4]arene derivative. The resulting microcavities in the range of 27-115 Å³ can trap freons, methane or dichloromethane among other guests.

¹²⁹ Kane, C. M.; Ugono, O.; Barbour, L. J.; Holman, K. T. *Chem. Mater.* **2015**, *27*, 7337-7354.

¹³⁰ a) Mastalerz, M.; Oppel, I. M. *Angew. Chem. Int. Ed.* **2012**, *51*, 5252-5255. b) Natarajan, R.; Bridgland, L.; Sirikulajorn, A.; Lee, J. -H.; Haddow, M. F.; Magro, G.; Ali, B.; Narayanan, S.; Strickland, P.; Charmant, J. P. H.; Orpen, A. G.; McKeown, N. B.; Bezzu, C. G.; Davis, A. P. *J. Am. Chem. Soc.* **2013**, *135*, 16912-16925.

¹³¹ a) Slater, A. G.; Cooper, A. I. *Science* **2015**, *348*. DOI: 10.1126/science.aaa8075, b) Moorthy, J. N.; Natarajan, R.; Venugopalan, P. *J. Org. Chem.* **2005**, *70*, 8568-8571.

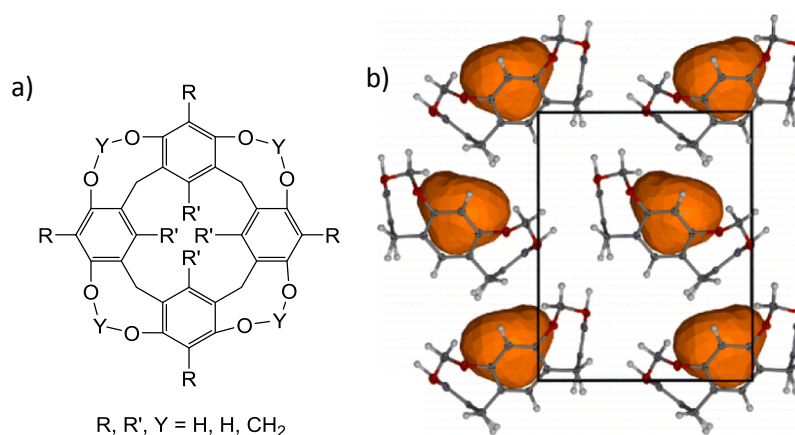


Figure 53. a) Chemical structure of calix[4]arene reported by Holman et al. b) 0-D crystalline structure. The unoccupied intrinsic microcavities are indicated in orange.

The synthesis of porous organic materials is more complicated than that from inorganic counterparts. The materials based on inorganic crystals are formed by extended coordination complexes or by covalent frameworks. However, for POMs, it is necessary to start from already rigid structures provided with functionalities able to preserve the pores only by the tiny forces arising from the weak intermolecular interactions between the single molecules of the crystal lattice. In general, the desolvation of the porous organic material can cause the collapse of the structure to give non-porous and denser polymorphic structures or amorphous materials.¹³²

In porous organic molecular solids, permanent porosity is rare because molecules tend to pack forming minimal voids. There are two types of POMs.¹³³ In one type, the porosity is related to discrete molecules such as macrocycles, cages, and related structures featuring intrinsic pre-defined cavities and pore windows that form the crystal. In a second type, the extrinsic porosity is constructed from voids accessible to solvent or guest molecules. These voids are generated as a result of the inefficient packing of the organic molecules during the crystallization process. In the extrinsic porous materials, the porosity is maintained even after solvent removal. In some cases, there are materials featuring both types of porosity as a function of the crystallization procedure used.¹³⁴

3.2.1 Zero dimensional porous organic molecular crystals (0D)

Zero dimensional POMs are nonporous crystals with isolated voids. In the case of inorganic compounds, these voids are usually inaccessible because the structures are too narrow and too rigid to allow the guest exchange at room temperature. Some zeolites able to entrap gases in their microcavities are examples of inorganic 0D materials.¹³⁵

¹³² Giri, N.; Davidson, C. E.; Melaugh, G.; Del Pópolo, M. G.; Jones, J. T. A.; Hasell, T.; Cooper, A. I.; Horton, P. N.; Hursthouse, M. B.; James, S. L. *Chem. Sci.* **2012**, *3*, 2153-2157.

¹³³ Barbour, L. J. *Chem. Commun.* **2006**, *11*, 1163-1168.

¹³⁴ a) Bojdys, M. J.; Briggs, M. E.; Jones, J. T. A.; Adams, D. J.; Chong, S. Y.; Schmidtman, M.; Cooper, A. I. *J. Am. Chem. Soc.* **2001**, *123*, 16566-16571. b) Holst, J. R.; Trewin, A.; Cooper, A. I. *Nat. Chem.* **2010**, *2*, 915-920.

¹³⁵ Corbin, D. R.; Abrams, L.; Jones, G. A.; Smith, M. L.; Dybowski, C. R.; Hriljacc, J. A.; Parise, J. *Chem. Commun.* **1993**, 1027-1029.

As noted above, organic structures such as calixarenes and cavitands have shown the ability to form OD POMs as the result of the inefficient crystal packing of the rigid bowl-shaped compounds.¹³⁶ Calixarene-based nanocrystals reported by Ripmeester are an example.¹³⁷ Here, two molecules of *p*-hexanoylcalix[4]-arene and *p*-octanoylcalix[4]-arene form a crystalline nanocapsule stabilized through Van der Waals interactions between acyl moieties. The resulting capsule allows gas diffusion processes. Posterior studies demonstrated that the compound has affinity for hydrocarbons, Xenon and CO₂ over N₂ or O₂. Recently, different cavitand compounds with microcavity volumes in the range of 27–115 Å³ able to store different guest molecules as fluoromethane gas have also been described.¹²

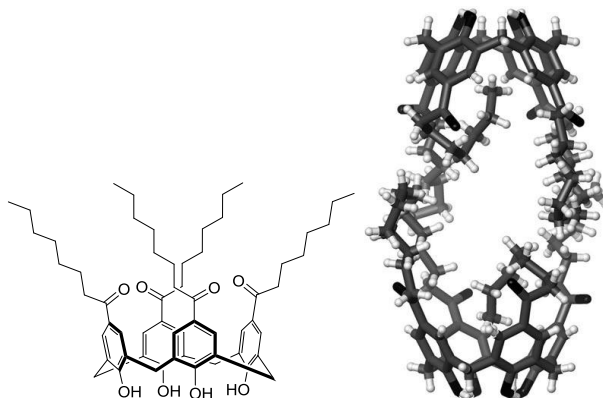


Figure 54. Structure of the capsule of para-octanoylcalix[4]arene and its crystalline lattice.¹³⁸

3.2.2 One-dimensional porous organic molecular crystals (1D)

Many crystalline nanoporous molecular materials show a network of infinite linear channels in which the sorption of gases tends to be a fast equilibration process. For example, bis-urea macrocycles crystallize into a columnar structure stabilized by hydrogen bonds through the urea molecules. The macrocyclic structure is constructed with different aromatic building blocks that provide rigidity to the structure favouring the columnar packing by additional π - π interactions.¹³⁹ The compound, shown in Figure 55, can reversibly transport ¹²⁹Xe through the channels by a single-file transport mechanism.

¹³⁶ a) Kane, M. C.; Ugono, O.; Barbour, L. J.; Holman, T. *Chem. Mater.* **2015**, *27*, 7337–7354.

¹³⁷ Ananchenko, G. S.; Udachin, K. A.; Dubes, A.; Ripmeester, J. A.; Perrier, T.; Coleman, A. W. *Angew. Chem. Int. Ed.* **2006**, *45*, 1585–1588.

¹³⁸ Ananchenko, G. S.; Moudrakovski, I. L.; Coleman, A. W.; Ripmeester, J. A. *Angew. Chem. Int. Ed.* **2008**, *47*, 5616–5618.

¹³⁹ Bowers, C. R.; Dvoyashkin, M.; Salpage, S. R.; Akel, C.; Bhase, H.; Geer, M. F.; Shimizu, L. S. *ACS Nano* **2015**, *9*, 6343–6353.

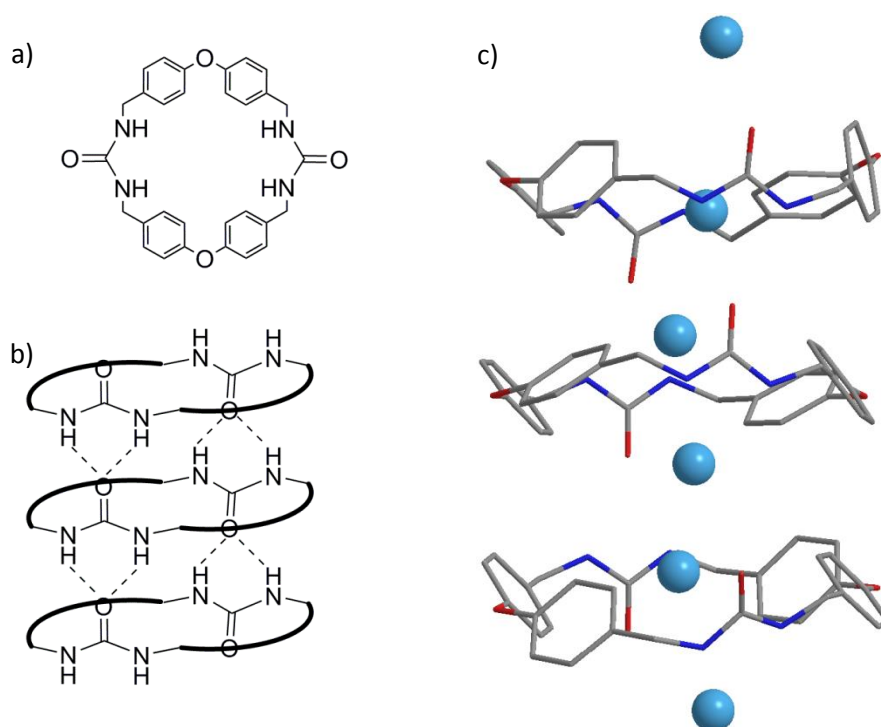


Figure 55. a) Chemical structure of bis-urea macrocycle. b) Schematic representation of the 1D channels formed through the interaction between bis-urea macrocycles. c) Representation of the Xe atom (blue balls) diffusion through the channels.

Other organic macrocyclic compounds as cucurbiturils or pillaranes, generally used in supramolecular chemistry to encapsulate guests, can also crystallize forming 1D nanochannels. These porous structures entrap and release different guests as a function of the functionalization of the cycle.

For example, cucurbit[6]uril (CB[6]) and cucurbit[8]uril (CB[8]) crystallize from acid-water solutions generating 1D water-filled channels.¹⁴⁰ The resulting X-ray analysis shows that cucurbiturils crystallize forming columnar arrangements perfectly aligned. In the case of CB[8], the composition of the crystals consists of 60 molecules of water per macrocycle and eight additional HNO₃ molecules that are situated between the 1D channels. This structure is relatively fragile and tends to crack after exposure to air. Recently, it has been measured the proton conductivities of the water-acid filled channels of CB[6] and CB[8] crystals showing to be comparable or superior to most MOFs or organic proton conductors.¹⁴¹

For its part, pillar[*n*]arenes have also shown to crystallize forming channels. As an example, a *per*-hydroxylated pillar[6]arene crystallize from acetone in an up-to-down manner forming infinite 1D channels along the *b* axis as is shown in Figure 56.¹⁴² In this case, the macrocyclic structure is stabilized by hydrogen bonds between de hydroxyl groups of the aryl units. This compound forms 1:1 host-guest complexes with bispyridinium salts in acetone to form [2] pseudorotaxanes. Specifically, the 1:1 complex with paraquat was isolated in a crystalline manner by slow diffusion of *n*-pentane into the acetone

¹⁴⁰ a) Bardelang, D.; Udachin, K. A.; Leek, D. M.; Ripmeester, J. A. *CrystEngComm* **2007**, *9*, 973-975. b) Bardelang, D.; Udachin, K. A.; Leek, D. M.; Margeson, J. C.; Chan, G.; Ratcliffe, C. I.; Ripmeester, J. A. *Cryst. Growth Des.* **2011**, *11*, 5598-5614.

¹⁴¹ Yoon, M.; Suh, K.; Kim, H.; Kim, Y.; Selvapalam, N.; Kim, K. *Angew. Chem. Int. Ed.* **2011**, *50*, 7870-7873.

¹⁴² Ma, Y.; Chi, X.; Yan, X.; Liu, J.; Yao, Y.; Chan, W.; Huang, F.; Hou, J. -L. *Org. Lett.* **2012**, *14*, 1532-1535.

solution showing the disruption of the pillar structure. Other pillar[5]arene derivatives have also been crystallized forming 1D channels filled with water molecules.¹⁴³

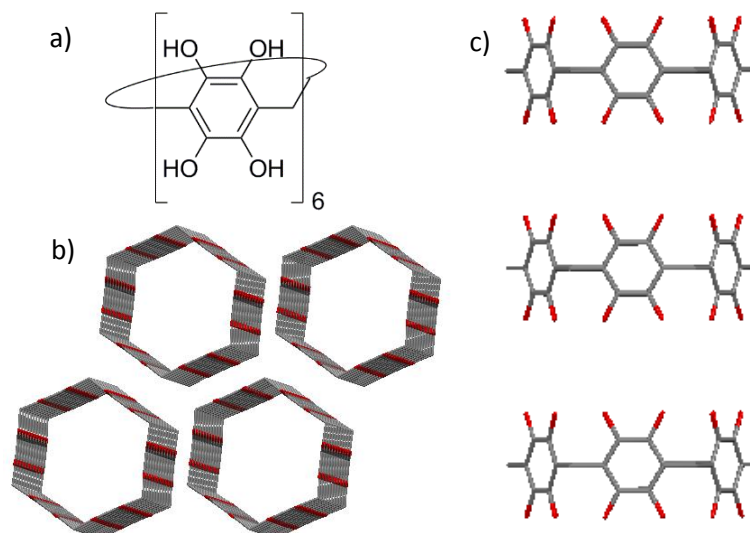


Figure 56. a) Chemical structure of *per*-hydroxylated pillar[6]arene. b) Partial structure of the 1D crystalline channels and c) packing mode.

3.2.3 Three-dimensional porous organic molecular crystals (3D)

Usually, three-dimensional POMs are formed by interconnected channels that allow the guest exchange. In 2005 Tedesco et al. reported the first example of 3D channel structure in porous molecular crystals; wherein the crystals were formed by the direct assembly of 1,2-dimethoxy-*p*-*tert*-butylcalix[4]dihydroquinone through a combination of H-bonding and van der Waals interactions.¹⁴⁴ As a result of the crystal packing, it was obtained a structure having hydrophobic cavities and channels filled with water. After water removal by thermal treatment, the porous structure was maintained. This material showed selective uptake of CO₂ and CH₄ over H₂.

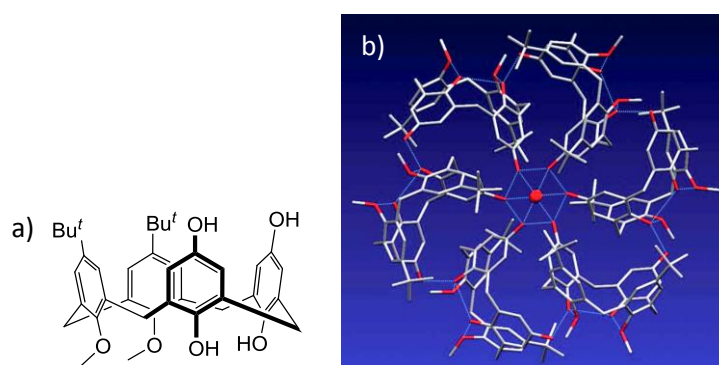


Figure 57. a) Chemical structure of 1,2-dimethoxy-*p*-*tert*-butylcalix[4]dihydroquinone, b) 3D x-ray structure.

¹⁴³ Si, W.; Hu, X. -B.; Liu, X. -H.; Fan, R.; Chen, Z.; Weng, L.; Hou, J. -L. *Tet. Lett.* **2011**, *52*, 2484-2487.

¹⁴⁴ Tedesco, C.; Immediata, I.; Gregoli, L.; Vitagliano, L.; Immirzi, A.; Neri, P. *CrystEngComm* **2005**, *7*, 449.

Recently, rigid organic cage compounds have also shown the ability to form porous molecular crystals. For example, Mastalerz et al. have reported a new set of imine-based 3D cage compounds. These compounds were obtained by the reaction of a triamine with each of the different dialdehydes (compounds **a-e**) in THF at room temperature as shown in Figure 58.¹⁴⁵ The imine arising from the dialdehyde **c** was isolated directly from the solution as a crystalline material. However, the dialdehydes **b**, **d**, and **e** yielded the corresponding imines as amorphous materials and required a subsequent crystallization step in THF. Gas-sorption studies revealed that the BET (Brunauer-Emmett-Teller) surface area was lower when the peripheral groups of the dialdehydes were bulkier.

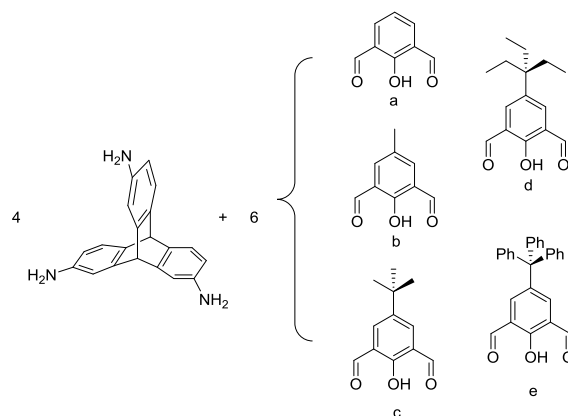


Figure 58. Schematic pathway followed by Mastalerz et al. to the synthesis of 3D cages compounds with different functionalization.

3.3 Dynamic covalent chemistry

Dynamic covalent chemistry (DCC), introduced by Jean-Marie Lehn,¹⁴⁶ implies the use of reversible covalent bond-forming reactions, such as imine metathesis, olefin metathesis, or boronic acid condensation, among others, to arrive at the thermodynamically most favoured species.¹⁴⁷ This approach offers the possibility to generate porous materials by the use of reversible covalent bonds such as imine, hydrazine, boronate or borosilicates in one-step reactions as shown in Figure 59. Numerous authors, as Cooper,¹⁴⁸ Mastalerz,¹⁴⁹ Warmuth,¹⁵⁰ Gawronski,¹⁵¹ Severin¹⁵² or Zhang¹⁵³ have described porous materials based on DCC intended for gas sorption.¹⁵⁴

¹⁴⁵ Schneider, M. W.; Oppel, I. M.; Ott, H.; Lechner, L. G.; Hauswald, H. –J. S.; Stoll, R.; Mastalerz, M. *Chem. Eur. J.* **2012**, *18*, 836-847.

¹⁴⁶ a) Corbett, P. T.; Leclaire, J.; Vial, L.; West, K. R.; Wietor, J. –L.; Sanders, J. K. M.; Otto, S. *Chem. Rev.* **2006**, *106*, 3652-3711.

¹⁴⁷ Belowich, M. E.; Stoddart, J. F. *Chem. Soc. Rev.* **2012**, *41*, 2003-2024.

¹⁴⁸ Tozawa, T.; Jones, J. T. A.; Swamy, S. I.; Jiang, S.; Adams, D. J.; Shakespeare, S.; Clowes, R.; Bradshaw, D.; Hasell, T.; Chong, S. Y.; Tang, C.; Thompson, S.; Parker, J.; Trewin, A.; Bacsá, J.; Slawin, A. M. Z.; Steiner, A.; Cooper, A. I. *Nat. Mater.* **2009**, *8*, 973-978.

¹⁴⁹ Zhang, G.; Mastalerz, M., *Chem. Soc. Rev.* **2014**, *43*, 1934-1947.

¹⁵⁰ Liu, X.; Liu, Y.; Li, G.; Warmuth, R. *Angew. Chem. Int. Ed.* **2006**, *45*, 901-904.

¹⁵¹ Skowronek, P.; Warzajtis, B.; Rychlewska, U.; Gawronski, J. *Chem. Commun.* **2013**, *49*, 2524-2526.

¹⁵² Granzhan, A.; Riis-Johannessen, T.; Scopelliti, R.; Severin, K. *Angew. Chem. Int. Ed.* **2010**, *49*, 5515-5518.

¹⁵³ Jin, Y.; Voss, B. A.; Noble, R. D.; Zhang, W., A. *Angew. Chem. Int. Ed.* **2010**, *49*, 6348-6351.

¹⁵⁴ Buyukcakir, O.; Seo, Y.; Coskun, A. *Chem. Mater.* **2015**, *27*, 4149-4155.

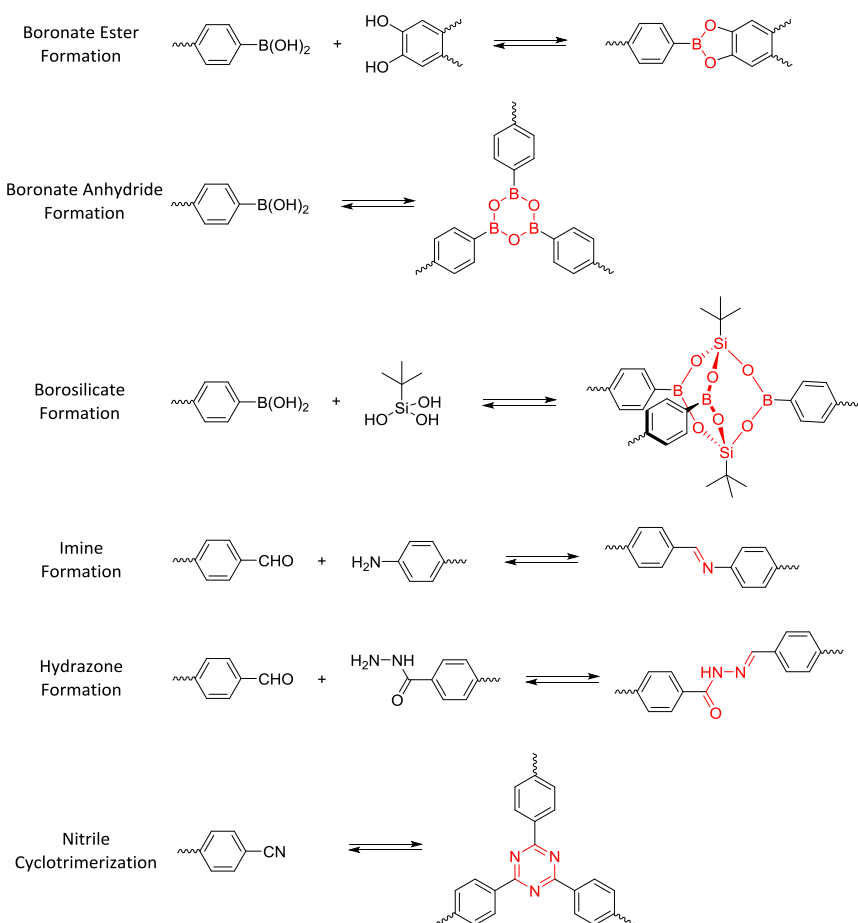


Figure 59. Examples of reversible reactions used in DCC.

The imine bond is one of the most used reversible bonds in dynamic covalent chemistry. This approach does not require the use of catalysts and usually give high reaction yields. The first example of a cage compound based on imine bonds was a shape-persistent hemicarcerand formed by the [2+4] condensation of a tetraformilcavitand with 1,3-diaminobenzene presented by Cram in 1991.¹⁴⁹ Since then, many imine cage compounds have appeared in the literature.

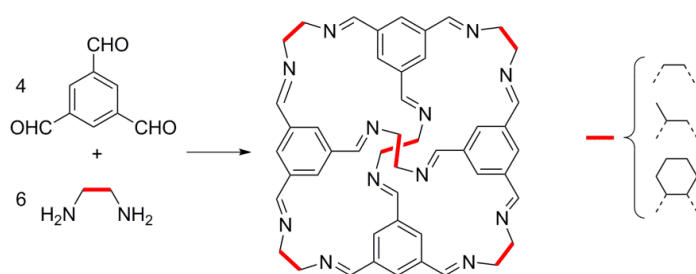


Figure 60. Synthesis of cycloimine cage compounds described by Cooper et al.

In 2009, Atwood and Cooper reported, a purely organic porous compound synthesized through DCC. These authors described an amorphous porous material based on a noria cyclic oligomer derivative that

shows affinity for CO₂ over N₂ or H₂.¹⁵⁵ Meanwhile, Cooper reported three different [4+6] imine-linked tetrahedral cages formed from 1,3,5-triformylbenzene and three different diamines (1,2-ethylenediamine, 1,2-propylenediamine and (R,R)-1,2-diaminocyclohexane) in ethyl acetate at room temperature. In this case, the crystals were obtained from the reaction media directly without any further purification step. The desolvated cage compounds showed the ability to adsorb different gases.¹⁴⁸

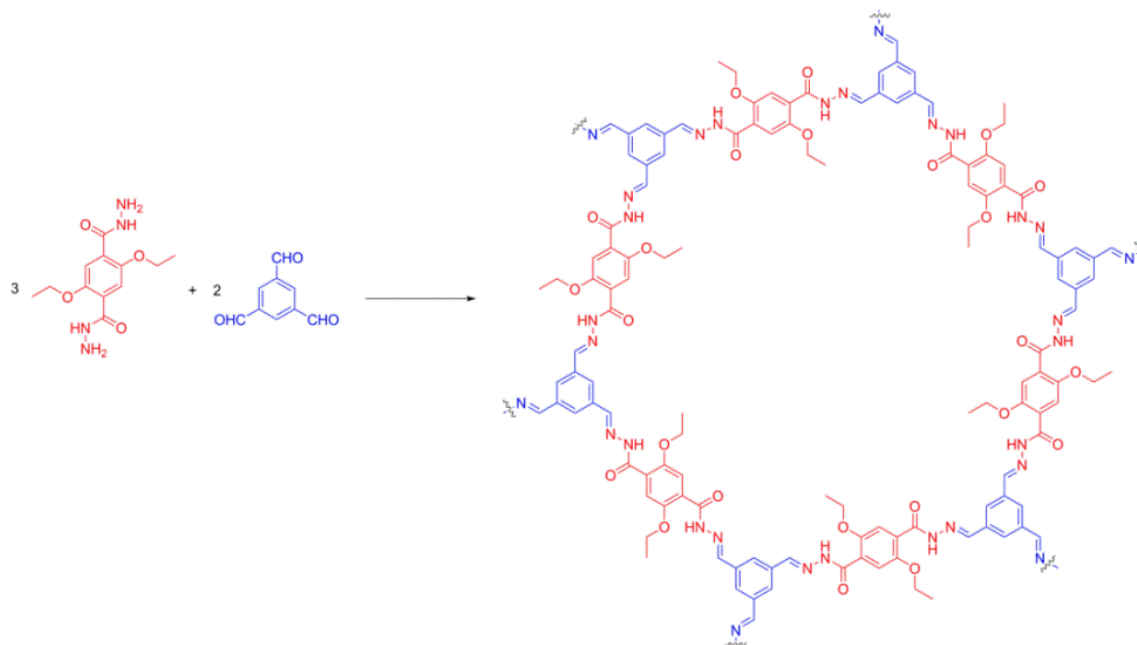


Figure 61. Structure of COF-42 based on hydrazone bonds presented by Yaghi.¹⁵⁶

Hydrazone-linked bonds are another type of imine-based materials. Yaghi et al. used a DCC strategy based on hydrazones for the formation of COF molecules by the condensation of aldehydes with hydrazides (Figure 61).

Mastalerz¹⁵⁷ and Cooper¹⁵⁸ reported several purely organic interlocked crystalline cages obtained through DCC based on boronic acid and imine bonds, respectively. For example, Cooper describes an interlocked system obtained by the direct condensation of 1,3,5-triformylbenzene and several diamines in acetonitrile in the presence of trifluoroacetic acid (See Figure 62). In this case, the catenane compound was stabilized by π - π interactions between aromatic groups of two different cages.

¹⁵⁵ Tian, J.; Thallapally, P. K.; Dalgarno, S. J.; McGrail, P. B.; Atwood, J. L. *Angew. Chem. Int. Ed.* **2009**, *48*, 5492–5495.

¹⁵⁶ Uribe-Romo, F. J.; Doonan, C. J.; Furukawa, H.; Oisaki, K.; Yaghi, O. M. *J. Am. Chem. Soc.* **2011**, *133*, 11478–11481.

¹⁵⁷ Zhang, G.; Presly, O.; White, F.; Oppel, I. M.; Mastalerz, M. *Angew. Chem. Int. Ed.* **2014**, *53*, 1516–1520.

¹⁵⁸ Hasell, T.; Wu, X.; Jones, J. T. A.; Bacsá, J.; Steiner, A.; Mitra, T.; Trewin, A.; Adams, D. J.; Cooper, A. I. *Nat. Chem.* **2010**, *2*, 750–755.

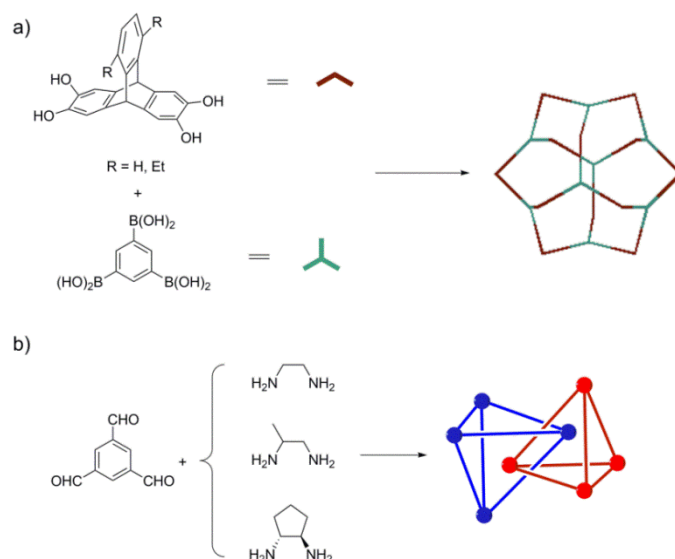


Figure 62. a) [12+8] boronic acid-based cage of Mastalerz. b) Interlocked [12+8] imine based cage of Cooper.

Self-sorting processes can be used in dynamic covalent chemistry to obtain very stable cage compounds from mixtures of components avoiding multistep reactions. Recently, Mukherjee et al. have reported the first example of self-sorting imines by mixing two similar dialdehydes and two triamines. These starting products yield four different cages (**1-4**) when they were mixed by pairs in CHCl_3 -EtOH (1:10 v/v) mixtures. However, the direct mixture of all the above components yielded only two cages (**2** and **3**). Remarkably, cage-to-cage transformations to the most stable product were also observed when the cage compounds were mixed in solution.¹⁵⁹

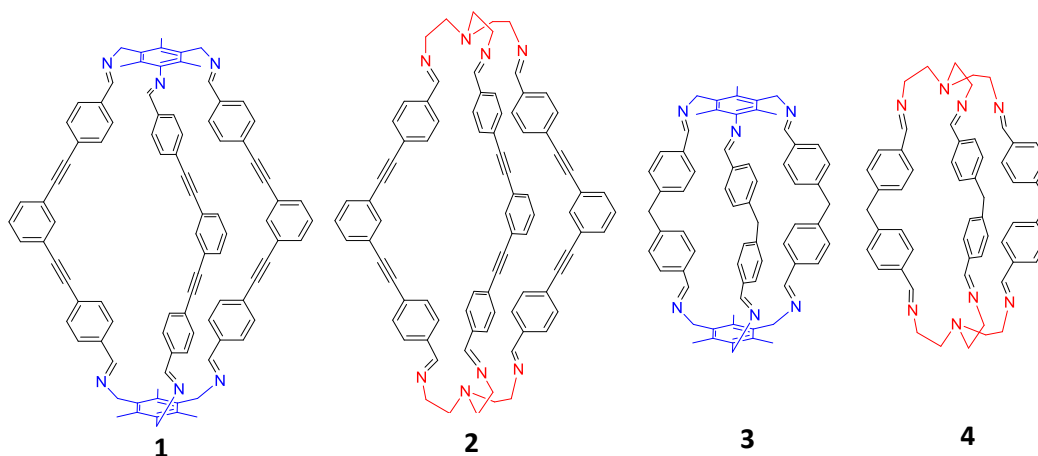


Figure 63. Structure of the four imine-based compounds reported by Mukherjee.⁴¹

¹⁵⁹ a) Acharyya, K.; Mukherjee, P. S. *Chem. Eur. J.* **2014**, *20*, 1646–1657. b) Acharyya, K.; Mukherjee, S.; Mukherjee, P. S. *J. Am. Chem. Soc.* **2013**, *135*, 554–557.

3.4 Aims

Continuing with our efforts toward the development of new molecular containers, in this chapter, we focus our attention on the design, synthesis, and evaluation of a new family of imine-based porous materials. Specifically, the goals are:

- To design and synthesise a new set of crystalline imine-based compounds constructed by the condensation of propargyl diamines with dialdehydes or trialdehydes. The proposed research encompasses the optimization of the reaction conditions including the influence of the solvent, the use or not of catalysts, and the time of reaction.
- To characterise the new compounds by NMR spectroscopy, mass spectrometry, and X-ray diffraction analysis.
- To study the adsorption and desorption of different selected guests by NMR, gas chromatography and or UV-vis techniques.

A crystalline sponge based on dispersive forces suitable for X-ray structure determination of included molecular guests

Elena Sanna,^a Eduardo C. Escudero-Adán,^b Antonio Bauzá,^a Pablo Ballester,^b Antonio Frontera,^a Carmen Rotger^a and Antonio Costa^{*a}

^a *Departament de Química. Universitat de les Illes Balears, Palma, 07122, Spain. Email: antoni.costa@uib.es; Fax: +34 971 172436; Tel: +34 971 173266.*

^b *Institut of Chemical Research of Catalonia (ICIQ). Avda. Països Catalans 16, 43007 Tarragona (Spain).*

^c *Catalan Institution for Research and Advanced Studies (ICREA). Passeig Lluís Companys 23, 08010, Barcelona (Spain).*

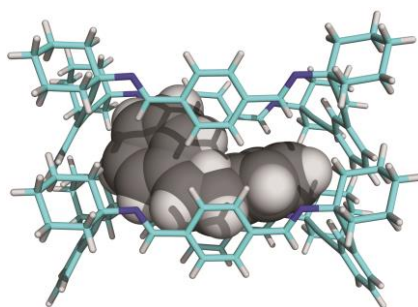
Chemical Science, 2015, 6, 5466-5472

Received: May 21, 2015

Accepted: July 13, 2015

3.5.1 Abstract

A crystalline porous material showing one-dimensional (1-D) rectangular micropores ($12 \times 9 \text{ \AA}^2$) has been assembled from a semirigid macrocyclic tetraimine and EtOAc as the templating agent. The 1-D nature of the material is intrinsic to the conformationally rigid structure of a macrocyclic sub-unit bearing four cyclohexylidene residues. The multiple dispersive forces established among the aliphatic residues glutted the 1-D channels and provided thermal stability to the material at temperatures below $160 \text{ }^\circ\text{C}$. Upon removal of the template, the structure of the empty solid exhibited permanent microporosity ($S_{\text{BET}} = 342 \text{ m}^2 \text{ g}^{-1}$). Being a true molecular sponge, the channel framework of this material allowed the inclusion of a variety of molecular sample guests without compromising its crystalline nature. Remarkably, this crystalline material enabled the structure determination by X-ray diffraction of the included molecules. Theoretical studies demonstrated the vital role played by the dispersive forces in the overall stabilization of the crystal packing.



3.5.2 Introduction

Porous organic materials¹⁶⁰ are currently of growing interest owing to their potential applications in diverse fields such as storage and separation of gases,¹⁶¹ molecular sorting¹⁶² and catalysis.¹⁶³ In this context, the synthesis of porous materials constructed from discrete molecules¹⁶⁴ is particularly attractive. This approach takes advantage of the structural versatility provided by organic synthesis and the possibility to obtain porous solid materials simply by crystallization.¹⁶⁵ The molecular components of porous organic molecular crystals (POMC) lacking an extended directional covalent or coordination bonding are held together only by weak intermolecular forces. Hence, molecular materials based on non-directional intermolecular forces are metastable and tend to collapse upon removal of the template

¹⁶⁰ (a) McKeown, N. B. *J. Mater. Chem.* **2010**, *20*, 10588–10597; (b) Jones, J. T.; Hasell, T.; Wu, X.; Bacsá, J.; Jelfs, K. E.; Schmidtman, M.; Chong, S. Y.; Adams, D. J.; Trewin, A.; Schiffman, F.; Cora, F.; Slater, B.; Steiner, A.; Day, G. M.; Cooper, A. I. *Nature*, **2011**, *474*, 367–371; (c) Pantos, G. D.; Pengo, P.; Sanders, J. K. *Angew. Chem. Int. Ed.*, **2007**, *46*, 194–197.

¹⁶¹ (a) Kim, H.; Kim, Y.; Yoon, M.; Lim, S.; Park, S. M.; Seo, G.; Kim, K. *J. Am. Chem. Soc.*, **2010**, *132*, 12200–12202; (b) Jin, Y.; Voss, B. A.; Noble, R. D.; Zhang, W. *Angew. Chem. Int. Ed.* **2010**, *49*, 6348–6351; *Angew. Chem.* **2010**, *122*, 6492–6495; (c) Farha, O. K.; Bae, Y. -S.; Hauser, B. G.; Spokoynny, A. M.; Snurr, R. Q.; Mirkin, C. A.; Hupp, J. T. *Chem. Commun.* **2010**, *46*, 1056–1058; (d) He, Y.; Xiang, S.; Chen, B. *J. Am. Chem. Soc.* **2011**, *133*, 14570–14573; (e) Yang, W.; Greenaway, A.; Lin, X.; Matsuda, R.; Blake, A. J.; Wilson, C.; Lewis, W.; Hubberstey, P.; Kitagawa, S.; Champness, N. R. *J. Am. Chem. Soc.* **2010**, *132*, 14457–14469; (f) Li, P.; He, Y.; Guang, J.; Weng, L.; Zhao, J. C.; Xiang, S.; Chen, B. *J. Am. Chem. Soc.* **2014**, *136*, 547–549.

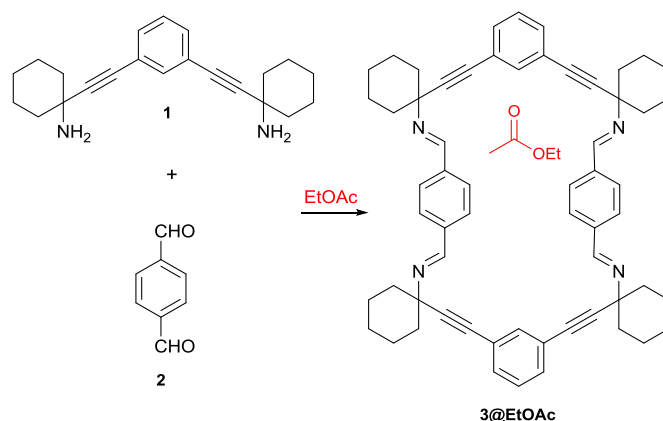
¹⁶² Mitra, T.; Jelfs, K. E.; Schmidtman, M.; Ahmed, A.; Chong, S. Y.; Adams, D. J.; Cooper, A. I. *Nat. Chem.* **2013**, *5*, 276–281.

¹⁶³ (a) Zhang, Y.; Riduan, S. N. *Chem. Soc. Rev.* **2012**, *41*, 2083–2094; (b) Kaur, P.; Hupp, J. T.; Nguyen, S. T. *ACS Catal.* **2011**, *1*, 819–835.

¹⁶⁴ Mastarlerz, M. *Chem.–Eur. J.* **2012**, *18*, 10082.

¹⁶⁵ Holst, J. R.; Trewin, A.; Cooper, A. I. *Nat. Chem.* **2010**, *2*, 915–920.

agents used to stabilize the voids of their porous crystalline structures.¹⁶⁶ Related materials exclusively stabilized by weak dispersive interactions are scarce. In this regard, Atwood and Barbour's contributions are particularly significant. These authors showed that interstitial van der Waals interactions could be employed as the main component for the design of porous host-guest assemblies.¹⁶⁷ A logical development of this approach that produced more stable porous molecular materials relied on the use of molecules interacting through hydrogen bonding and aromatic interactions, either separately or in combination.^{160d-f,165} Using this strategy, Shimizu and colleagues reported a microporous crystalline bis-urea macrocyclic host that self-assembled by hydrogen bonding and aromatic stacking interactions. In this example, the macrocyclic ureas aligned into columnar 1-D assemblies and maintained its porous structure even upon guest removal.¹⁶⁸



Scheme 2. Synthesis of macrocyclic tetraimine **3**.

In this work, we present a new organic material featuring permanent porosity based on the macrocyclic tetraimine **3** (Scheme 2). A key aspect of our design is the use of multiple weak dispersive interactions as the glue element to organize and maintain together the components of the stable porous molecular material. Our report constitutes a paradigmatic example of the so-called Gulliver's principle¹⁶⁹ applied to the design of porous organic materials.

Previously, we have described the synthesis of the 1,3-phenylene-bis-propargylic diamine **1** used in this work as rigid spacer to avoid the collapse of the macrocycle **3**.¹⁷⁰ The hierarchical self-assembly of the macrocycle **3** into a porous material arises from the combination of multiple van der Waals and aromatic interactions.¹⁷¹ These interactions are established between the phenyl and cyclohexylidene residues, the “sticky groups” of **3**. The resulting porous material displays 1-D channels that are large enough for liquid–solid sorption applications.¹⁷²

¹⁶⁶ (a) Raatikainen, K.; Rissanen, K. *Chem. Sci.* **2012**, *3*, 1235–1239; (b) Barbour, L. J. *Chem. Commun.*, **2006**, 1163–1168; (c) Brunet, P.; Simard, M.; Wuest, J. D. *J. Am. Chem. Soc.*, **1997**, *119*, 2737–2738; (d) Mastalerz, M.; Opperl, I. M. *Angew. Chem. Int. Ed.*, **2012**, *51*, 5252–5255.

¹⁶⁷ (a) Dalgarno, S. J.; Thallapally, P. K.; Barbour, L. J.; Atwood, J. L. *Chem. Soc. Rev.* **2007**, *36*, 236–245; (b) Atwood, J. L.; Barbour, L. J.; Jerga, A. *Science*, **2002**, *296*, 2367–2369.

¹⁶⁸ Dewal, M. B.; Lufaso, M. W.; Hughes, A. D.; Samuel, S. A.; Pellechia, P.; Shimizu, L. S. *Chem. Mater.* **2006**, *18*, 4855–4864.

¹⁶⁹ Prins, L.; Reinhoudt, D. N.; Timmerman, P. *Angew. Chem. Int. Ed.*, **2001**, *40*, 2382–2426.

¹⁷⁰ Soberats, B.; Martínez, L.; Vega, M.; Rotger, C.; Costa, A. *Adv. Synth. Catal.* **2009**, *351*, 1727–1731.

¹⁷¹ Martinez, C. R.; Iverson, B. L. *Chem. Sci.* **2012**, *3*, 2191–2201.

¹⁷² (a) Natarajan, R.; Bridgland, L.; Sirikulajorn, A.; Lee, J. -H.; Haddow, M. F.; Magro, G.; Ali, B.; Narayanan, S.; Strickland, P.; Charmant, J. P. H.; Orpen, A. G.; McKeown, N. B.; Bezzu, C. G.; Davis, A. P. *J. Am. Chem. Soc.* **2013**, *135*, 16912–16925; (b) Jacobs, T.; Barbour, L. J. *CrystEngComm*, **2013**, *15*, 1512–1514.

More specifically, we were interested in knowing if a crystalline porous material based only on dispersive forces, could be used as the crystalline solid support in X-ray diffraction studies by applying the “crystalline sponge method” developed by Fujita.¹⁷³ In this method, accurate molecular structures of samples can be obtained by analyzing the diffraction patterns of single crystals without requiring the crystallization of the samples. However, the crystalline sponges reported so far are based on metal-organic frameworks (MOFs) that include electron-rich atoms, such as iodine, bromine, chlorine as well as transition metals in their structures.¹⁷⁴ These atoms contribute heavily to the overall diffraction pattern masking the information available for the guest. From this point of view, our system based only in light-atoms, could offer an alternative to MOF-based crystalline sponges.

3.5.3 Results and discussion

3.5.3.1 Synthesis and structure of the microporous material

The macrocyclic tetraimine **3** was prepared by Schiff base condensation of the diamine **1** with terephthalaldehyde **2** in EtOAc solution. On standing at room temperature, single crystals of **EtOAc@3** slowly grew from the solution (yield 50%).¹⁷⁵ The solid material was characterized by single crystal X-ray diffraction,¹⁷⁶ ¹³C CP MAS NMR and thermogravimetric analysis (TGA).

The single crystal X-ray structure showed the macrocycle **3** molecules stacked one on top of another forming a columnar assembly. The solid material displayed one-dimensional channels with distorted rectangular morphology along the b axis (Fig. 64). The total solvent accessible void volume within the channels calculated from PLATON/Squeeze, was 1096 Å³ (274 Å³ per each macrocyclic imine) representing 19.4% of the unit cell volume.¹⁷⁷ We observed that the channels were filled with partially disordered EtOAc molecules (Fig. 64a). In the crystal packing, the four aromatic rings of **3** were tilted ca. 60° with regard to the plane of the macrocycle. Furthermore, the two phenyl rings located at the wider sides of **3** oscillated between two positions (75:25 occupancy) and acted as revolving doors (Fig. 64b).

¹⁷³ (a) Inokuma, Y.; Yoshioka, S.; Ariyoshi, J.; Arai, T.; Hitora, Y.; Takada, K.; Matsunaga, S.; Rissanen, K.; Fujita, M. *Nature*, **2013**, *495*, 461–466; (b) Inokuma, Y.; Arai, T.; Fujita, M. *Nat. Chem.* **2010**, *2*, 780–783.

¹⁷⁴ (a) Yoshioka, S.; Inokuma, Y.; Hoshino, M.; Sato, T.; Fujita, M. *Chem. Sci.* **2015**, *6*, 3765; (b) Inokuma, Y.; Yoshioka, S.; Ariyoshi, J.; Arai, T.; Fujita, M. *Nat. Protoc.* **2014**, *9*, 246; (c) Kubota, R.; Tashiro, S.; Shiro, M.; Shionoya, M. *Nat. Chem.* **2014**, *6*, 913; (d) Ramadhar, T. R.; Zheng, S. –L.; Chen, Y. –S.; Clardy, J. *Chem. Commun.* **2015**, *51*, 11252–11255; (e) Zigon, N.; Hoshino, M.; Yoshioka, S.; Inokuma, Y.; Fujita, M. *Angew. Chem. Int. Ed.*, **2015**, *54*, 9033–9037.

¹⁷⁵ Crystal data for **EtOAc@3** (CCDC no. 1012389): C_{65.36}H_{70.72}N₄O_{2.68}, *M* = 955.18, monoclinic, *a* = 34.794(16) Å, *b* = 5.836(3) Å, *c* = 28.131(14) Å, α = 90.00°, β = 97.862(11)°, γ = 90.00°, *V* = 5659(5) Å³, *T* = 100(2) K, space group *C2/c*, *Z* = 4, 35400 reflections measured, 10696 independent reflections (*R*_{int} = 0.0434). The final *R*₁ values were 0.0597 (*I* > 2σ(*I*)). The final *wR*(*F*²) values were 0.1624 (*I* > 2σ(*I*)). The final *R*₁ values were 0.0931 (all data). The final *wR*(*F*²) values were 0.1931 (all data). Crystal data for **3(I)**, (CCDC no. 1012398): C₆₀H₆₀N₄, *M* = 837.12, monoclinic, *a* = 34.8696(19) Å, *b* = 5.8099(3) Å, *c* = 28.1212(16) Å, α = 90°, β = 98.143(2)°, γ = 90°, *V* = 5639.6(5) Å³, *T* = 100(2) K, space group *C2/c*, *Z* = 4, 26236 reflections measured, 8377 independent reflections (*R*_{int} = 0.0577). The final *R*₁ values were 0.0602 (*I* > 2σ(*I*)). The final *wR*(*F*²) values were 0.1686 (*I* > 2σ(*I*)). The final *R*₁ values were 0.0825 (all data). The final *wR*(*F*²) values were 0.1883 (all data). Crystal data for **3(II)**, (CCDC no. 1012399): C₃₀H₃₀N₂, *M* = 418.56, triclinic, *a* = 6.5695(4) Å, *b* = 13.4759(8) Å, *c* = 14.1239(9) Å, α = 91.0310(10)°, β = 99.2650(10)°, γ = 91.6850(10)°, *V* = 1233.21(13) Å³, *T* = 100(2) K, space group *P*₁, *Z* = 2, 13275 reflections measured, 13275 independent reflections (*R*_{int} = 0.0000). The final *R*₁ values were 0.0529 (*I* > 2σ(*I*)). The final *wR*(*F*²) values were 0.1334 (*I* > 2σ(*I*)). The final *R*₁ values were 0.0860 (all data). The final *wR*(*F*²) values were 0.1550 (all data).

¹⁷⁶ CCDC codes 1012389, 1012398 and 1012399, contain the crystal data for **EtOAc@3**, **3(I)** and **3(II)**, respectively.

¹⁷⁷ van der Sluis, P.; Spek, A. L. *Acta Crystallogr., Sect. C: Cryst. Struct. Commun.* **1990**, *A46*, 194–201.

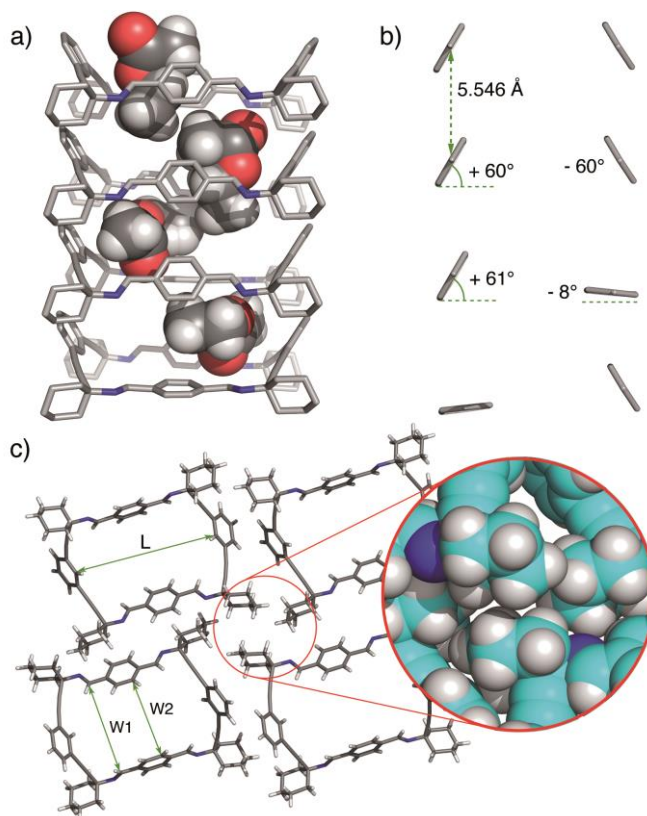


Figure 64. (a) Representative X-ray perspective side-view in *b* direction of **3@EtOAc** crystals displaying disordered EtOAc molecules inside the channel. (b) Partial view showing the relative orientation of the 1,4-phenylene rings (see text). (c) Top view of a molecular cell unit of the monoclinic crystals ($V_c \frac{1}{4} 5642 \text{ \AA}^3$, $Z = 4$) of **AcOEt@3** ($D_c = 1.121 \text{ g cm}^{-3}$; $L \sim 11.98 \text{ \AA}$, $W1 \sim 9.13 \text{ \AA}$; $W2 \sim 6.11\text{--}6.90 \text{ \AA}$) (CCDC no. 1012389). Disorder and EtOAc solvent molecules are removed for clarity. The inset shows multiple van der Waals contacts between cyclohexylidene residues.

From this structure, it became clear that the combined action of intermolecular displaced π - π aromatic stacking, as well as multiple CH (sp^3)-CH (sp^3) van der Waals interactions extending throughout the channel, provided the necessary stabilization of the assembly.

The results obtained in ^{13}C CP-MAS NMR experiments confirmed the role of EtOAc as guest template. The carbon signals of the relatively mobile molecules of EtOAc included in the solid, but not those of the host tetraimine **3** that formed the porous framework were observed in the standard mode ^{13}C MAS spectra (Fig. S17 in ESI†).

3.5.3.2 Stability and dynamic behavior of the porous material

Guest solvent molecules were completely removed by treating the solvate **EtOAc@3** under vacuum for several hours at room temperature (12 h, 2×10^{-2} mm Hg). This treatment afforded a new crystalline material, the apohost **3(I)**. The X-ray structure of **3(I)** (Fig. 65) revealed the absence of electron density in the channels previously filled with EtOAc. The lack of EtOAc in the crystalline structure was also confirmed by registering the ^1H NMR spectra of single crystals of **3(I)** dissolved in CDCl_3 .

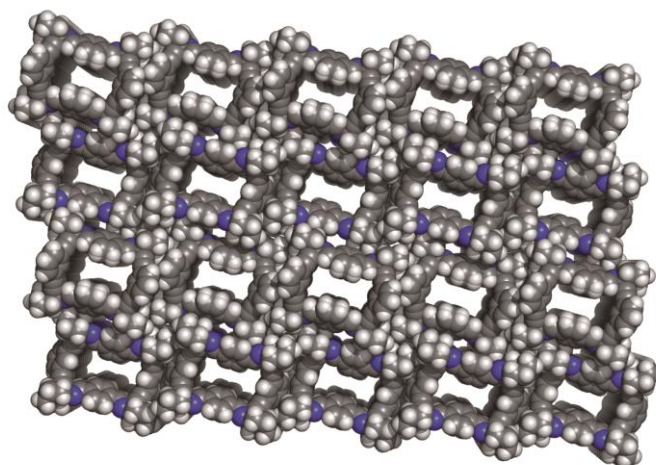


Figure 65. X-ray perspective top-view of the apohost **3(I)** ($V_c = 5639 \text{ \AA}^3$, $Z = 4$) ($D_c = 0.9859 \text{ g cm}^{-3}$; $L \sim 11.98 \text{ \AA}$, $W1 \sim 9.20 \text{ \AA}$; $W2 \sim 6.90 \text{ \AA}$) (CCDC no. 1012398).

More important, the crystal packing of **3(I)** was almost identical to that of the **EtOAc@3** solvate (see Table S1 in ESI[†]), indicating that the porous structure remained intact after vacuum treatment.

The relatively easy removal of the included EtOAc molecules at room temperature implied that they were weakly retained in the channels.

Remarkably, the **EtOAc@3** solvate could be regenerated by simply soaking crystals of the empty material **3(I)** in EtOAc. These findings were consistent with the absence of strong dipole–dipole or hydrogen bonding interactions between the cycloimine **3** and the included EtOAc molecules.

The dynamic nature of the guest exchange constituted an essential feature of this material. The kinetics of the guest exchange process was monitored by using ^{13}C NMR. Crystals of ^{13}C -[1.2]-EtOAc@**3** obtained by treating **3(I)** with ^{13}C labelled EtOAc were suspended in unlabelled EtOAc.

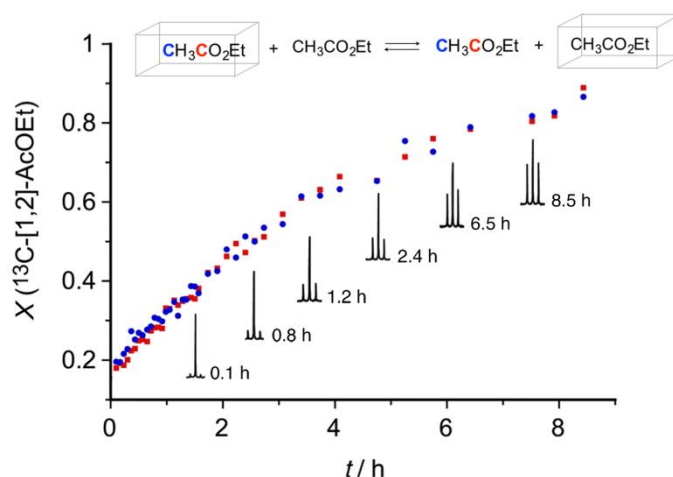


Figure 66. Plot representing the fraction of ^{13}C -[1.2]-EtOAc in a solution of EtOAc. This plot was obtained from 50 mg of labelled ^{13}C -[1.2]-EtOAc@**3** suspended in 0.5 mL of EtOAc at 298 K, by integration of the ^{13}C satellites with respect to the ^{12}C signal and assuming the complete replacement of ^{13}C -[1.2]-EtOAc. The inset shows representative increasing carbonyl doublet resonances (169.7 ppm, $J_{\text{C-C}} = 59.5 \text{ Hz}$) used to extract the integral data.

We observed that the combined integral values of the isotopic ^{13}C doublet grew steadily with time and reached a plateau after 8–10 h (Fig. 66). This experiment demonstrated that the almost complete exchange of the included ^{13}C labeled EtOAc was slow in the human time-scale. Desolvation of EtOAc was also monitored using thermogravimetry. The TGA trace of **EtOAc@3** revealed an 11.8% weight loss in a temperature range from room temperature to 175 °C. This weight loss corresponded to the vaporization of 1.3 molecules of EtOAc per macrocycle, therefore indicating the 3:4 stoichiometry found for this complex (see Fig. S19 in ESI[†]). In complete agreement, the differential scanning calorimetry (DSC) thermogram of **EtOAc@3** exhibited an endothermic peak at around 160 °C due to vaporization of the entrapped guest solvent (Fig. 67b).

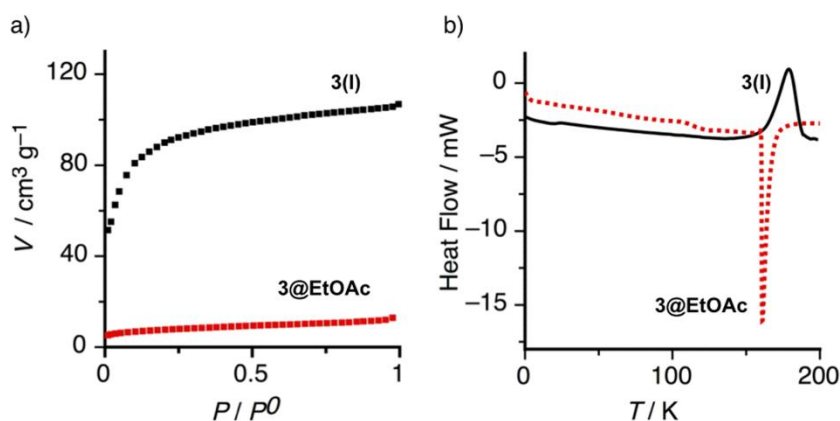


Figure 67. (a) Adsorption isotherm of N₂ for the solvate **3@EtOAc** compared to the empty solid **3(I)** ($T = 77\text{ K}$, $P^0 = 1\text{ atm}$). (b) DSC traces of **3@EtOAc** displaying an endothermic peak at 160 °C due to solvent vaporization (red dotted line) and of **3(I)** showing an exothermic peak at 177 °C assigned to irreversible phase transition to **3(II)**.

On the other hand, the porosity of **3(I)** was also confirmed by gas absorption of nitrogen at 77 K (Fig. 67a). The empty solid **3(I)** exhibited a typical type I adsorption isotherm indicative of a microporous (<2 nm) structure with significant specific surface area ($S_{\text{BET}} = 342\text{ m}^2\text{ g}^{-1}$).¹⁷⁸ In addition, the DSC trace of the apohost **3(I)** displayed an exothermic and irreversible process at around 175 °C (Fig. 67b and S20[†]), which we assigned to a monotropic solid-phase transition of **3(I)**. In both cases, the X-ray structure analysis of the material obtained after thermal treatment above 160 °C, revealed the formation of a new nonporous polymorphic form **3(II)**.

The X-ray structure of **3(II)** (see Fig. S21 in ESI[†]) showed densely packed layers of displaced macrocyclic imine units **3** ($D_{\text{C}} = 1.127\text{ g cm}^{-3}$) and the concomitant loss of the columnar assembly characteristic of the **3(I)** polymorphic form.

3.5.3.3 Liquid–solid sorption experiments

The void volumes of the porous frameworks exhibited by the crystalline materials **EtOAc@3** and **3(I)** are sufficiently large to include a variety of molecular guests. This characteristic, together with the absence of polar groups that can be displayed to the included guests and the high thermal stability of the

¹⁷⁸ Sing, K. S. V.; Everett, D. H.; Haul, R. A. W.; Moscou, L.; Pierotti, R. A.; Rouquerol, J.; Siemieniowska, J. *Pure Appl. Chem.* **1985**, *57*, 603–619.

crystalline materials, suggested us the potential use of **EtOAc@3** and **3(I)** as suitable supports for X-ray diffraction studies by the crystalline sponge method.^{179, 180}

To test this functionality, we soaked single crystals of **EtOAc@3** and **3(I)** in different neat liquid samples with molecular volumes ranging from 55–60 Å³ i.e. nitromethane and ethylene glycol, to >200 Å³ of Z-stilbene (see, Table S2 in ESI†). In favourable cases, i.e. less than 5 min for nitromethane, the initially floating crystals of **EtOAc@3** gradually sank to the bottom of the vial providing a visual indication of the exchange status. During the process, we did not observe any apparent degradation of the crystal integrity. The exchange of the guest samples was confirmed by ¹H NMR of CDCl₃ solutions of the solvates. Also, ¹³C CP-MAS NMR experiments confirmed the inclusion of the liquid guests within the porous framework. The carbon signals of non-volatile guests (i.e. diethyl squarate) appeared slightly upfield shifted (0.5–2 ppm) with respect to those of diethyl squarate in the bulk (Fig. S18 in ESI†).

Owing to the poor solubility of the solvates in CDCl₃, the molar ratios were better evaluated by digesting the solvates with DCl/D₂O (50 mL) before registering the ¹H NMR spectra in a mixture of DMSO-*d*₆:CDCl₃ (2.5:1 v/v, 600 mL) (see, ESI†).^{173c} In general, the molar ratios of **3**:sample evaluated by ¹H NMR after a common period of 72 h, agree well with the crystallographic stoichiometries (Table S2 in ESI†). In one case, the average experimental molar ratio calculated for Z-stilbene of 0.8 was consistently inferior to that expected for a 1:1 **Z-stilbene@3** solvate. This result is likely due to the incomplete inclusion of Z-stilbene within the channels of the **3(I)**. Therefore, the molecular volume of Z-stilbene of 216 Å³, approaching the maximum available void volume of 274 Å³ per macrocycle calculated using PLATON/Squeeze,¹⁷⁶ suggested us a practical upper limit for the effective inclusion of samples in **3(I)**.

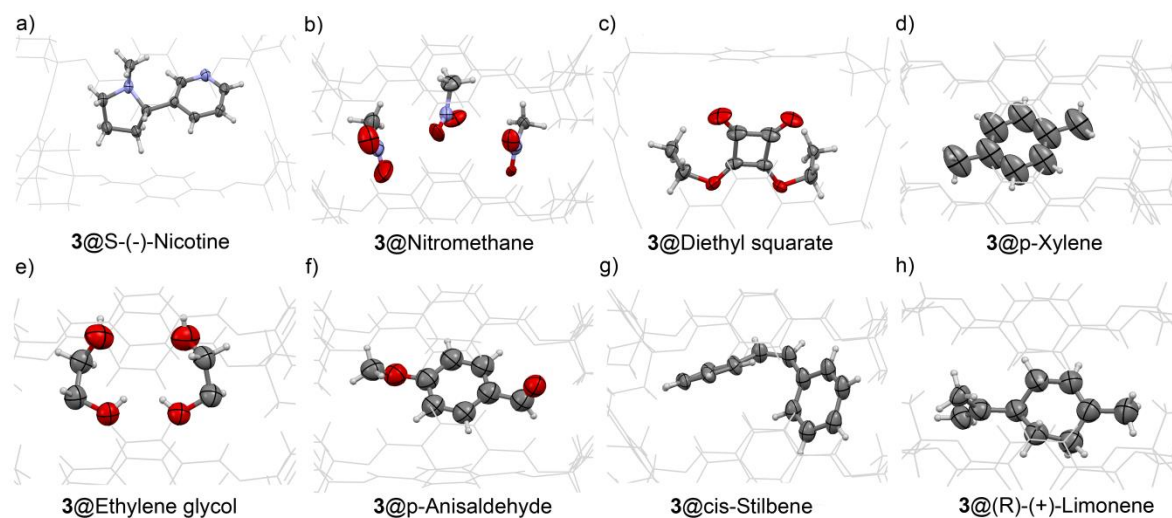


Figure 68. (a to h) ORTEP views of different liquid molecules diffused into the channel structure of **3(I)** with thermal ellipsoids set at 50% probability. Disorder is removed for clarity. CCDC codes 1012389 to 1012397 and 1063714 contain the structural X-ray data (see ESI for RX structural details†).

¹⁷⁹ a) Inokuma, Y.; Yoshioka, S.; Ariyoshi, J.; Arai, T.; Hitora, Y.; Takada, K.; Matsunaga, S.; Rissanen, K.; Fujita, M. *Nature*, **2013**, *495*, 461–466. b) Inokuma, Y.; Arai, T.; Fujita, M.; *Nat. Chem.* **2010**, *2*, 780–783.

¹⁸⁰ a) Yoshioka, S.; Inokuma, Y.; Hoshino, M.; Sato, T.; Fujita, M. *Chem. Sci.* **2015**, *6*, 3765–3768. b) Inokuma, Y.; Yoshioka, S.; Ariyoshi, J.; Arai, T.; Fujita, M. *Nat. Protoc.* **2014**, *9*, 246–252. c) Kubota, R.; Tashiro, S.; Shiro, M.; Shionoya, M.; *Nat. Chem.* **2014**, *6*, 913–918. d) Ramadhar, T. R.; Zheng, s. –L.; Chen, Y. –S.; Clardy, J. *Chem. Commun.* **2015**, *51*, 11252–11255. e) Zigon, N.; Hoshino, M.; Yoshioka, S.; Inokuma, Y.; Fujita, M. *Angew. Chem. Int. Ed.* **2015**, *54*, 9033–9037.

Fig. 68a–h, depict ORTEP views of representative X-ray structures obtained by guest exchange from single crystals of **EtOAc@3** or alternatively, by soaking a single crystal of the empty apohost **3(I)** with ca. 1 mL of the liquid sample. Both methods produced identical results in all tested cases (see ESI for X-ray structural data†). Both, the empty material **3(I)** and the solvate **EtOAc@3** allowed the formation of inclusion solid complexes (solvates) with aromatic, unsaturated and aliphatic neutral substrates bearing a variety of functional groups such as hydroxy, aldehyde, ester and nitro groups, among others.

Since the included guests could, eventually, establish hydrogen bonds or dipole–dipole interactions with **3** that would lead to degradation of the porous structure of the solids, the obtained results in the guest exchange/inclusion experiments confirmed that the interactions established between **3** and the incoming sample guests must be feeble.

Remarkably, the inclusion of the different guests into the crystal lattice did not disrupt the pore size significantly ($\Delta L < 2\%$; $\Delta W1 < 2.6\%$). However, to obtain a better fit between the size and shape of the pore and those of the included molecules (induce fit), the two opposite phenyl rings located on the wider sides of the macrocycle **3** oscillated with a mechanism that resembles the functioning of the revolving doors. The adaptation process experienced by the pore was revealed by careful analysis of the X-ray structures of **EtOAc@3**, **p-anisaldehyde@3**, and **S(-)-nicotine@3(I)** ($\Delta W2 \sim 20\%$).

The induced fit process, in which the width of the channels responded to the size and shape of the included sample guests took place without any loss of crystal integrity (Table S1 in ESI†). In contrast, the X-ray structure of the non-porous polymorphic form **3(II)** displayed a narrowed entrance of the pore that can be referred as “closed” doors. Most likely, this structural change was responsible for inhibiting the guest sorption of liquid guests ($W1 \sim 9.91 \text{ \AA}$; $W2 \sim 5.54 \text{ \AA}$).

3.5.3.4 Theoretical calculations

(a) Host–host interactions. In order to rationalize the sorption properties of **EtOAc@3** and **3(I)**, we first studied the non-covalent interactions responsible for the formation of the one-dimensional channels and the columnar assembly in the crystal packing. We fully optimized a dimer of the macrocycle **3** starting from the crystallographic coordinates of **3(I)** and evaluated its interaction energy. The dimerization energy was large and negative ($-34.3 \text{ kcal mol}^{-1}$), indicating a strong binding (Fig. 69). The geometry of the energy-optimized dimer **3₂** was very similar to the one found in the solid state.

In addition, the interaction energy computed for the dimer using the crystallographic coordinates (without optimization) gave a very similar value ($-32.9 \text{ kcal mol}^{-1}$). Removal of the cyclohexylidene residues led to a significant reduction of the interaction energy ($-14.5 \text{ kcal mol}^{-1}$). This finding supported the strong influence exerted by the C–H/H–C interactions to the stability of the porous material.¹⁸¹

The energy difference calculated for the two energy-minimized dimers ($18.4 \text{ kcal mol}^{-1}$) represented an estimation of the contribution of these interactions to the overall dimerization process. Since four cyclohexylidene residues are present in the macrocycle **3**, each intermolecular cyclohexylidene/cyclohexylidene interaction contributes in $4.6 \text{ kcal mol}^{-1}$. This value was in good agreement with previously reported high level ab initio results for dodecahedrane.¹⁷⁸

¹⁸¹ J. Echeverría, G. Aullón, D. Danovich, S. Shaik and S. Alvarez, *Nat. Chem.* **2011**, *3*, 323–330.

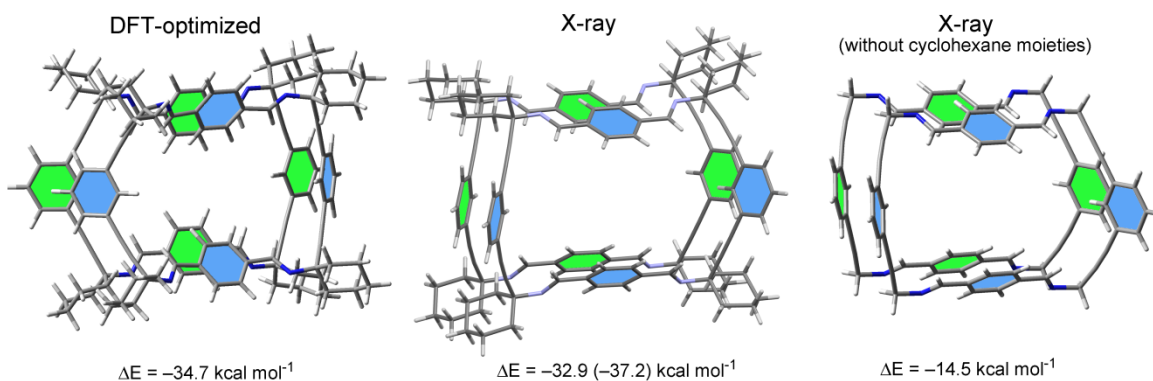


Figure 69. Comparison of the X-ray and DFT-D3 optimized structures of **3(I)** and interaction energies at the BP86-D3/def2-TZVP level of theory (value in parenthesis corresponds to the BP86-D3/def2-SVP level).

To further analyze the non-covalent interactions in the dimer **3**₂ we used the NCI (Non Covalent Interaction) index.¹⁸² This visualization index enables the identification and visualization of weak non-covalent interactions efficiently.

The isosurfaces corresponded to both favorable and unfavorable interactions, as differentiated by the sign of the second density Hessian eigenvalue and defined by the isosurface color. NCI analysis allowed an assessment of host-guest complementarity and the extent to which weak interactions stabilize a complex. Fig. 70, shows the representation of the NCI plot computed for the dimer **3**₂. In addition to a panoply of C-H/H-C interactions, two weak equivalent and oppositely located parallel-displaced π - π interactions and four C H/ π interactions involving the p-system of the triple bond were also observed. The largest isosurface was located around the cyclohexylidene rings that established a multitude of C-H/H-C interactions with another cyclohexylidene and the aromatic ring.

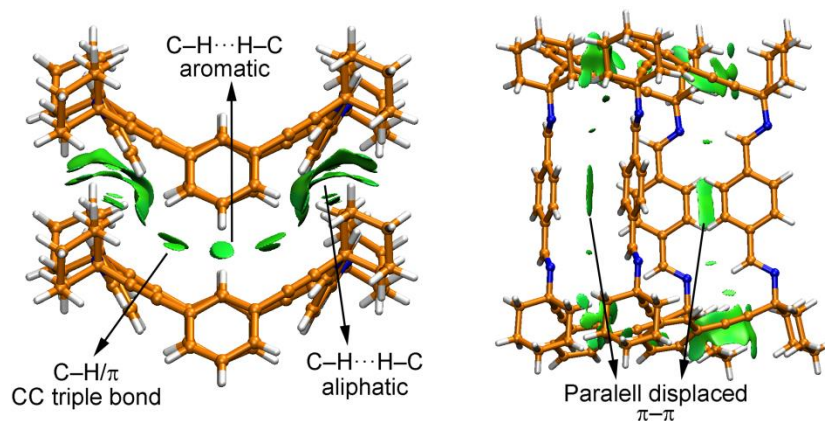


Figure 70. NCI surfaces of a dimer of **3** used as a minimalist model of the 1-D channel. The isosurfaces (pale and dark green) correspond to favourable.

(b) Substitution analysis. We theoretically analyzed the progressive substitution of EtOAc by diethyl squarate (SQA) inside the channel using a minimalist model of **EtOAc@3**. This exchange process was experimentally favorable. In our model system, we started from a minimal representative channel

¹⁸² E. Johnson, S. Keinan, P. Mori-Sánchez, J. Contreras-García, A. Cohen and W. Yang, *J. Am. Chem. Soc.* **2010**, *132*, 6498–6506.

composed of only three macrocyclic imines complexed to three EtOAc molecules and locating one diethyl squarate (SQA) molecule at one end of the channel. We energetically evaluated the process of inserting the SQA molecule through this end and, simultaneously, removing one included EtOAc molecule out.

The process was favorable by $4.1 \text{ kcal mol}^{-1}$ (Fig. 71). Subsequently, we assessed the energy required to exchange the expelled EtOAc by a new SQA molecule. This second process was also favorable by 3 kcal mol^{-1} . This sequence was repeated to evaluate the energy of the exchange processes of the second and third molecules of EtOAc by SQA molecules (see Fig. S25–S27 in ES†).

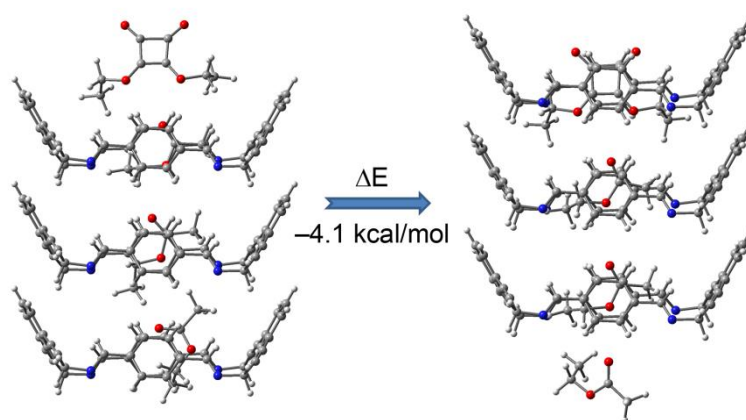


Figure 71. Favourable energy change due to the substitution of one EtOAc molecule by one diethyl squarate molecule in a minimalist representative channel of **3@EtOAc**.

These processes were also energetically favorable and showed similar magnitudes for the exchange energies. Hence, the results of this theoretical study agreed well with the aforementioned experimental results and supported the viability of the liquid–solid guest exchange process.

3.5.4 Conclusions

In summary, we have synthesized an unprecedented conformationally semirigid macrocyclic tetraimine **3** that is decorated with four peripheral cyclohexylidene substituents. The tetraimine **3** crystallized from EtOAc solutions affording a porous crystalline material **EtOAc@3** composed of one-dimensional channels filled with solvent molecules. The crystal packing of **EtOAc@3** was stabilized mainly by dispersive interactions. We have demonstrated that the templating EtOAc solvent molecules can be removed in vacuo to yield an empty but crystalline and porous solid **3(I)**, which can be considered as a polymorphic form of **EtOAc@3**. Both solid materials **EtOAc@3** and **3(I)**, are rare examples of porous crystalline structures stabilized exclusively by dispersive forces. We confirmed the use of these solid crystalline materials for X-ray structure determination of molecular guests included in their pores by the crystalline sponge method. Finally, using high-level theoretical calculations we evaluated the strength of the cohesive interactions responsible for the porous structure, as well as the favorable energy change produced by guest exchange of molecules in the pores. Because porous materials based on dispersive forces have energetic advantages for the reversible storage of polar molecules in comparison to porous materials containing polar groups that can be presented to the included guests, we anticipate an emergence of materials of the former type in the near future.

3.6.5 Acknowledgements

This work was supported by Ministry of Economy and Competitiveness grants (CTQ2014-57393-C2-1-P, Severo Ochoa Excellence Accreditation 2014–2018 SEV-2013-0319 and Consolider-Ingenio CSD2010-00065, FEDER funds). E. S. thanks CAIB and FSE for a predoctoral fellowship.

3.5.6 Supporting Information

3.5.6.1. Experimental Section

3.5.6.1a. Instrumental Methods

NMR. Solution ^1H and ^{13}C spectra were recorded on Bruker AVANCE 300 (^1H at 300 MHz and ^{13}C at 75 MHz) and on Bruker AVANCE III 600 (^1H at 600 MHz and ^{13}C at 150.9 MHz) equipped with a cryoprobe, in CDCl_3 using the residual proton signal as reference. Chemical shifts (δ) are in ppm and coupling constants (J) in Hz.

Thermogravimetric Analysis. TG analyses were carried out using a SDT2960 TGA analyzer (TA instruments) with an automated vertical overhead thermobalance. The experiments were performed on 10 - 20 mg samples, over a temperature range of 25-600 °C at a constant heating rate of 10 °C min^{-1} , with a purge of dry nitrogen flowing at 30 mL min^{-1} . The samples were crushed, blotted dry and placed in open Pt pans for TG experiments.

Differential Scanning Calorimetry. DSC were carried out using a DSC2920 modulated DSC (TA instruments). The experiments were performed on 10 -15 mg samples over a temperature range of 0 – 175 °C at a constant heating rate of 10 °C min^{-1} , with a purge of dry nitrogen flowing at 30 mL min^{-1} . The samples were crushed, blotted dry and placed in crimped but vented aluminium pans for DSC experiments.

Nitrogen Adsorption Isotherms. Surface areas were measured by nitrogen adsorption and desorption at 77.3 K using a Autosorb IQ volumetric adsorption analyzer. Solid **3(I)** were degassed offline at room temperature °C for 24 h under high vacuum 10^{-6} mmHg, before analysis, followed by degassing on the analysis port under vacuum, for 30 °C. The isotherm of compound **EtOAc@3** was registered without previous treatment at vacuo.

Single Crystal X-ray Diffraction. Data were collected at 100K on a Bruker-Nonius FR591 Mo $K\alpha$ rotating anode single crystal diffractometer equipped with an Apex II CCD area detector and Montel mirrors and an Oxford Cryostream Plus 700 Series. For the data collection the software *Apex2 V2010.7-0* (Bruker AXS 2010) was used. The data reduction was performed using Saint + Version 7.60A (Bruker AXS 2008) and the absorption correction using *SADABS V. 2008/1*¹⁸³ (CCDC 1012391, 101392, 101393, 101396, 101398 and 101399) and *TWINABS V. 2008/4*¹⁸⁴ (CCDC 1012389, 1063714, 101394, 101395 and 101397). The structures were solved using the program *SIR2011*¹⁸⁵ and refined by full matrix least squares using *SHELXL-97*¹⁸⁶ (CCDC 101389-101394 and 101399) and *SHELXL2013*¹⁸³ (CCDC 101395-101398).

¹⁸³ G. M. Sheldrick, **2008**.

¹⁸⁴ M. C. Burla, R. Caliendo, M. Camalli, B. Carrozzini, G. L. Cascarano, C. Giacovazzo, M. Mallamo, A. Mazzone, G. Polidori, R. Spagna, *J. Appl. Cryst.* **2012**, *45*, 357-361.

¹⁸⁵ G. M. Sheldrick, *Acta Cryst. A* **2008**, *64*, 112-122.

¹⁸⁶ G. M. Sheldrick, SHELXL2013. University of Göttingen, Germany. **2013**.

In order to gain greater insight into the disordered structure of the starting solvate, the X-ray structure of **EtOAc@3** was acquired at higher resolution (CCDC no. 1012389). Data collection: full sphere single crystal X-ray diffraction data were collected at 90 K on a Rigaku XtaLab P200 Mo $K\alpha$ rotating anode equipped with a Pilatus 200K detector and an Oxford Cryostream 700 low temperature device. For data collection, data reduction and absorption correction the software CrystalClear 2.1 B29 (Rigaku, 2013)¹⁸⁷ was used. The structure was solved using the program SIR2014¹⁸⁸ and refined using SHELXTL Version 2014/3.¹⁸⁹

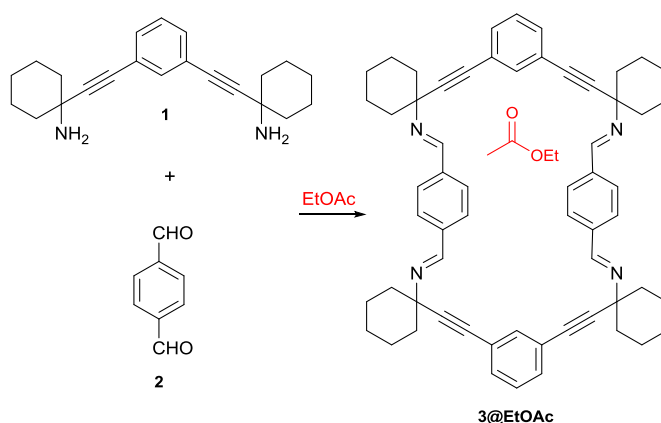
3.6.6.1b. Materials and synthesis

Materials

Ethyl acetate (EtOAc) HPLC quality purchased from Scharlau or Aldrich was used as received. 1,3-bispropargylic diamine **1** was prepared as described previously.¹⁹⁰ Terephthalaldehyde **2** and all other chemicals were purchased from Sigma-Aldrich and used as received.

Synthesis of the macrocyclic tetraimine **3@EtOAc** solvated and the apohost **3(I)**

The macrocyclic tetraimine **3** was prepared by slow Schiff condensation of the diamine **1**¹⁸⁷ with terephthalaldehyde **2**. A typical procedure was as follows: a solution of the diamine **1** (400 mg, 1.248 mmol) and the dialdehyde **2** (169 mg, 1.248 mmol) in 120 mL of AcOEt was placed in a 250 mL erlenmeyer flask. The flask was covered with parafilm and let aside at room temperature for evolution. After four to ten weeks, prismatic crystals of **EtOAc@3** separated slowly from the solution. The crystals were harvested carefully from the bottom of the flask using a spatula, washed with fresh EtOAc and dried in the air to give an initial crop of **EtOAc@3** (135 mg, 15 % yield). Further quantities were obtained in successive crops from the mother solution to reach *c.a.* (410 mg, 50% yield).



Crystals of **EtOAc@3** (CCDC no. 1012389) are soluble in mesitylene and slightly soluble in chloroform but insoluble in a variety of common organic solvents such as: methanol, ethanol, dimethylsulfoxide, ethyl

¹⁸⁷ J. W. Pflugrath, *Acta Crystallographica Section D-Biological Crystallography* **1999**, *55*, 1718-1725.

¹⁸⁸ M. C. Burla, R. Caliendo, B. Carrozzini, G. L. Casciarano, C. Cuocci, C. Giacovazzo, M. Mallamo, A. Mazzone, G. Polidori, *J. Appl. Cryst.* **2015**, *48*, 306-309.

¹⁸⁹ G. M. Sheldrick, *Acta Crystallographica Section C-Structural Chemistry* **2015**, *71*, 3-8.

¹⁹⁰ B. Soberats, L. Martínez, M. Vega, C. Rotger, A. Costa, *Adv. Syn. Catal.* **2009**, *351*, 1727-1731.

acetate, diethyl ether, tetrahydrofuran, toluene and hexane. Other solvents already tested such as cyclohexane and dichloromethane cause degradation of the crystal integrity.

To prepare the unsolvated material **3(I)** (CCDC no. 1012398) crystals of **EtOAc@3** were evacuated at 5×10^{-2} mmHg at room temperature for 12 h.

3(I): m.p. > 250 °C (dec.). ^1H NMR (CDCl_3), δ (ppm from TMS): 8.82 (s, 4H), 7.88 (s, 8H), 7.68 (s, 2H), 7.47 (d, $J = 7.5$ Hz, 4H), 7.32 (t, $J = 7.8$ Hz, 2H), 1.82 (m, 20H). ^{13}C NMR in CDCl_3 (δ , ppm): 157.7, 138.5, 134.6, 131.5, 128.7, 128.6, 123.7, 91.7, 88.8, 63.9, 39.8, 25.6, 23.2. ESI-HRMS (+) m/z (%): calc. $\text{C}_{60}\text{H}_{61}\text{N}_4$ 837.4896; exp. 837.4902 $[\text{M}+\text{H}]^+$. Anal. Calcd. for $\text{C}_{60}\text{H}_{60}\text{N}_4$: C, 86.08; H, 7.22; N, 6.69. Found: C, 85.48; H, 7.17; N, 6.65.

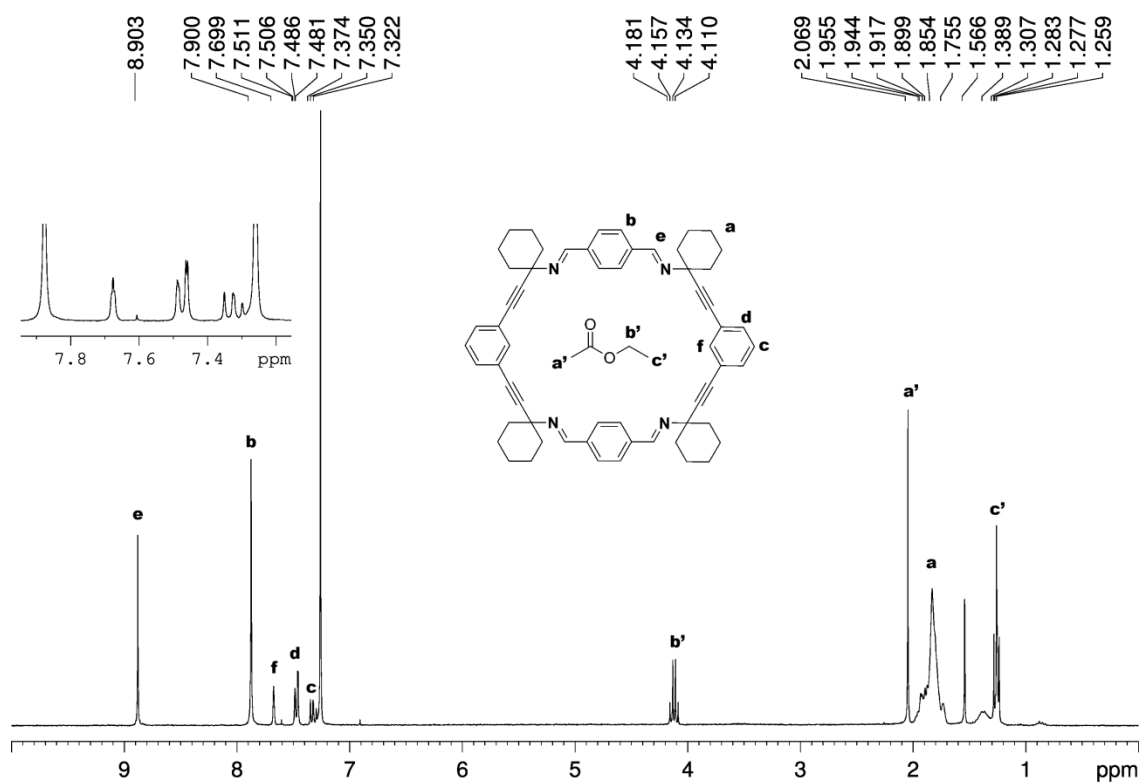


Figure S11. ^1H NMR spectrum of EtOAc@3 dissolved in CDCl_3

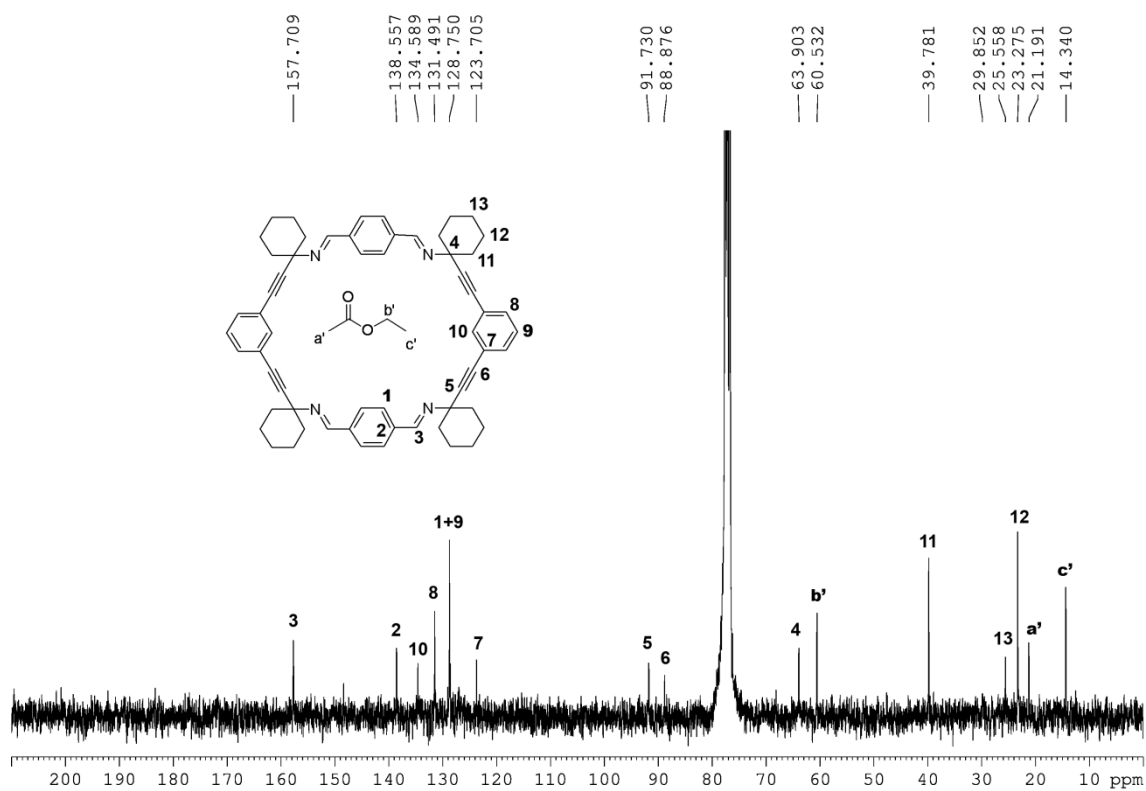


Figure S12. ^{13}C NMR spectrum of EtOAc@3 dissolved in CDCl_3

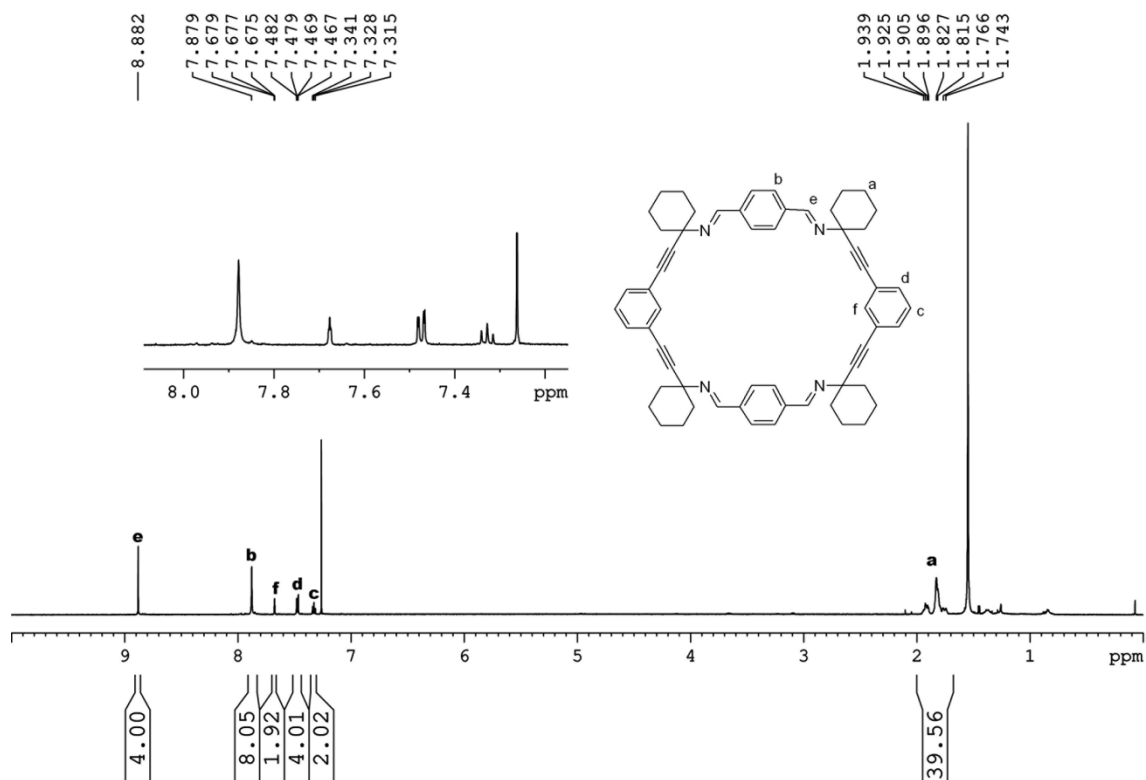


Figure S13. ^1H NMR spectrum of **3(I)** dissolved in CDCl_3

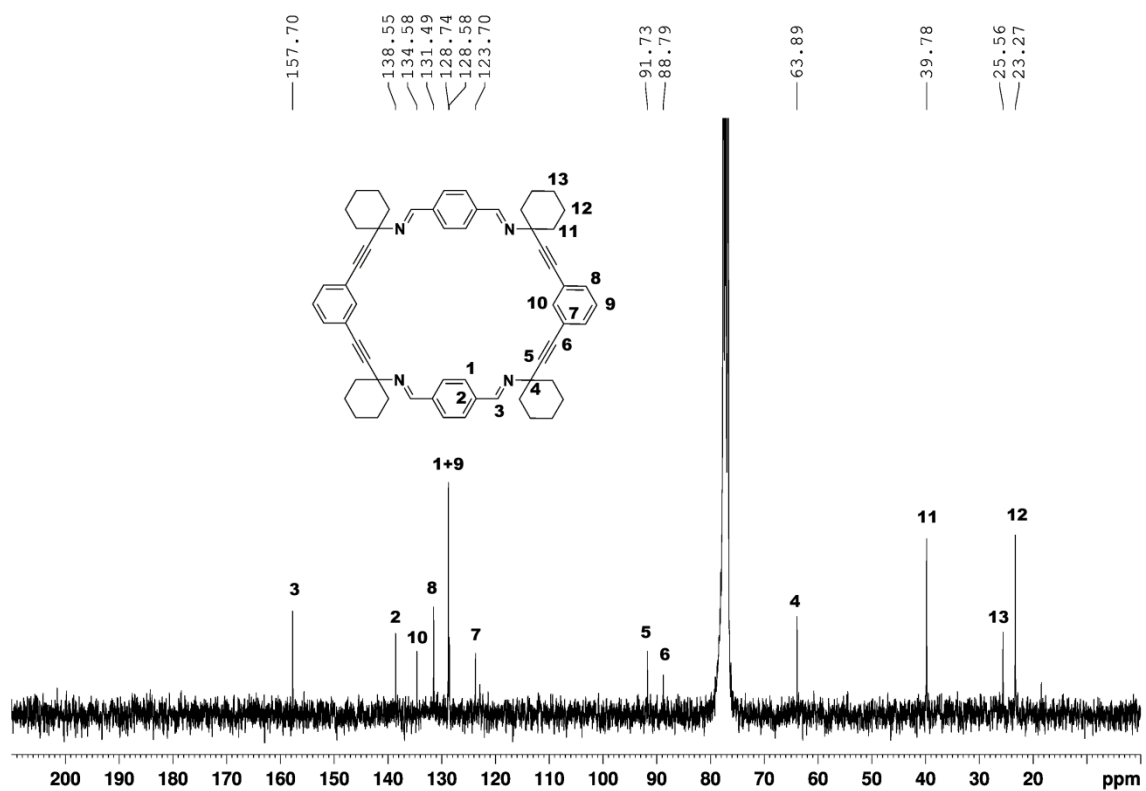


Figure S14. ^{13}C NMR spectrum of **3(I)** dissolved in CDCl_3

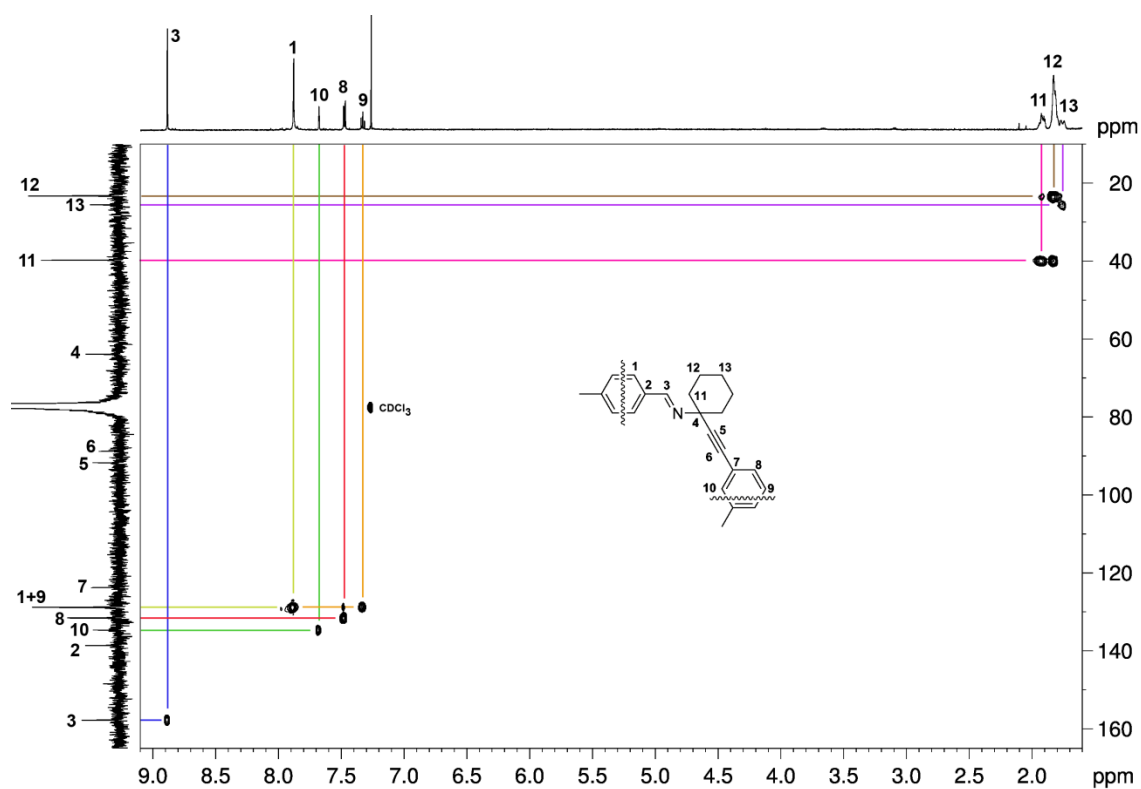


Figure S15. Heteronuclear single quantum correlation (HSQC) spectrum of tetraimine **3(I)** in CDCl_3 at 298 K

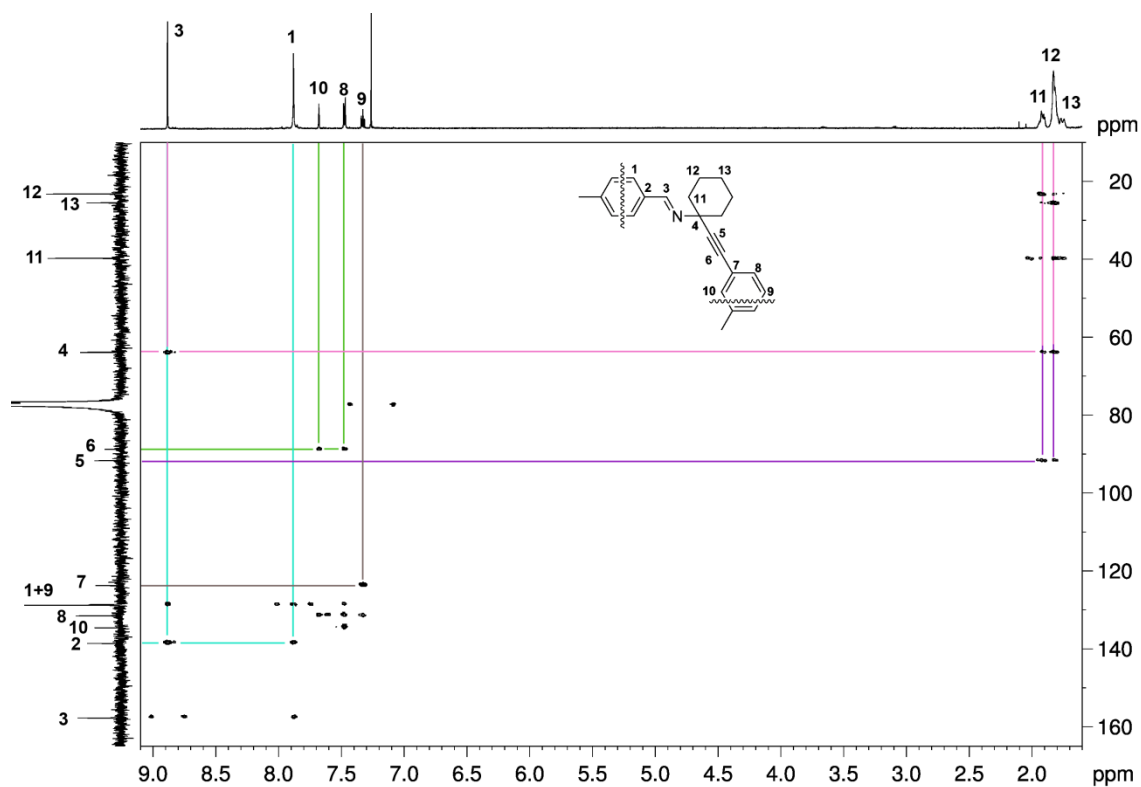


Figure S16. Heteronuclear multiple bond correlation (HMBC) spectrum of the tetraimine **3(I)** in CDCl_3 at 298 K

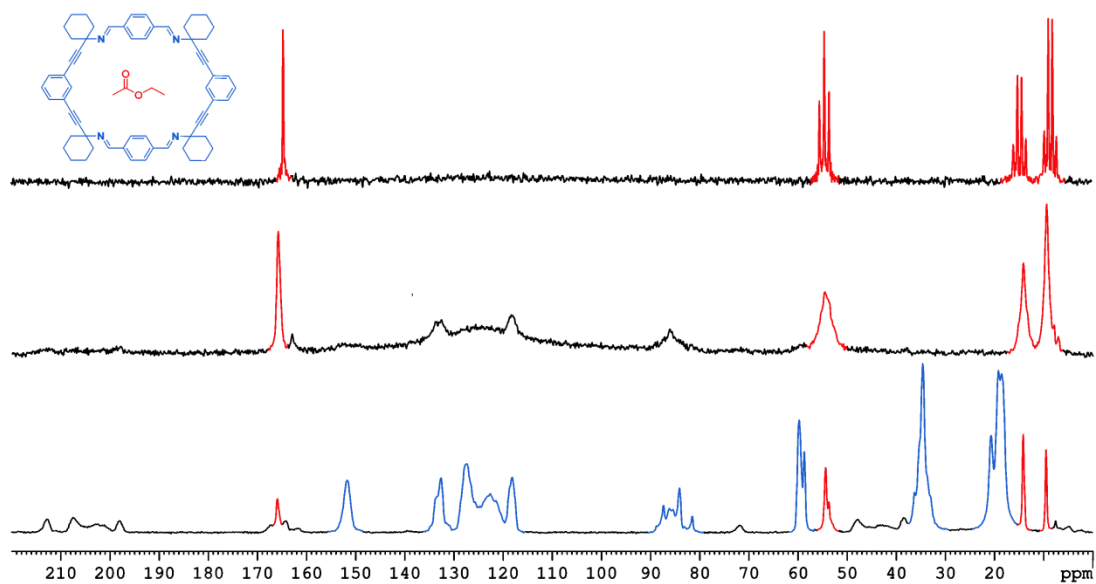


Figure S17. (a) ^{13}C CP-MAS spectra of **EtOAc@3**, EtOAc peaks in red. (b) ^1H undecoupled normal mode (without cross polarization) ^{13}C MAS spectra **EtOAc@3**. In this mode, only the mobile EtOAc peaks appear (in red) (c) ^1H undecoupled normal mode ^{13}C MAS spectra of liquid AcOEt.

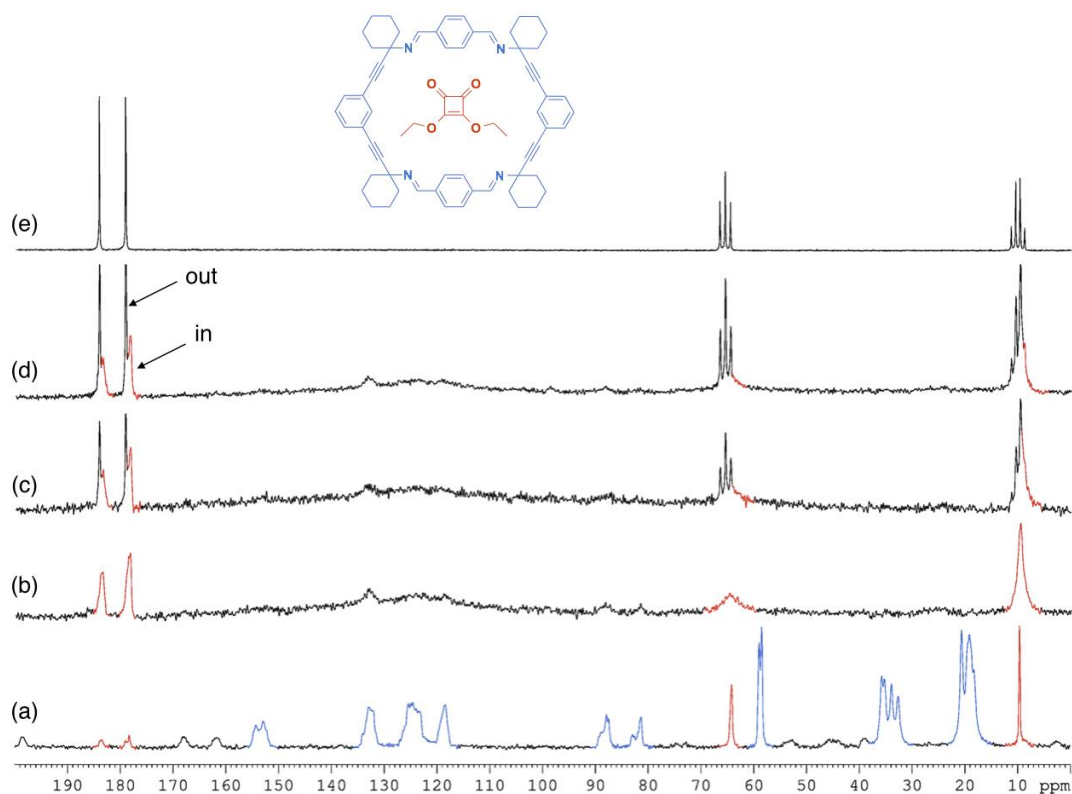


Figure S18. (a) ^{13}C CP-MAS (^{13}C - ^1H , decoupled) spectrum of **Diethyl squarate@3** (50 mg), diethyl squarate peaks in red. (b) ^1H undecoupled normal mode (without cross polarization) ^{13}C MAS spectrum of **Diethyl squarate@3**. In this mode, only the included diethyl squarate resonances appeared as broad peaks (in red) (c) *Idem*, after addition of 2 μL of liquid diethyl squarate; (d) *Idem*, after addition of 4 μL of liquid diethyl squarate; (e) ^1H undecoupled normal mode ^{13}C MAS spectra of liquid diethyl squarate.

TGA and DSC

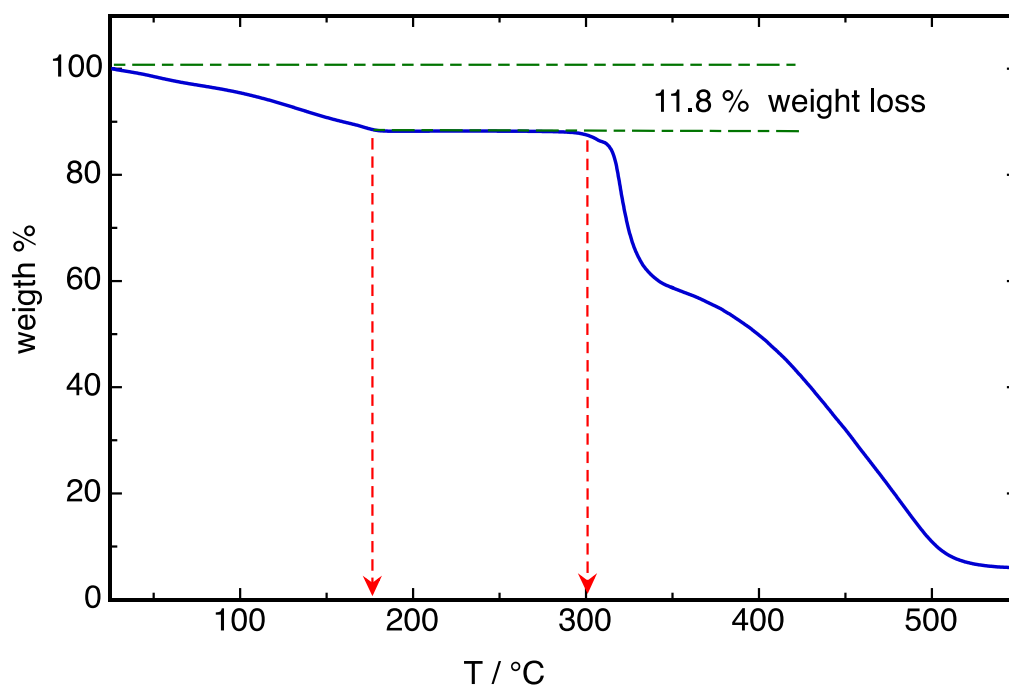


Figure S19. Thermogravimetric analysis of EtOAc@3. A $10\text{ }^{\circ}\text{C}\cdot\text{min}^{-1}$ ramp was used.

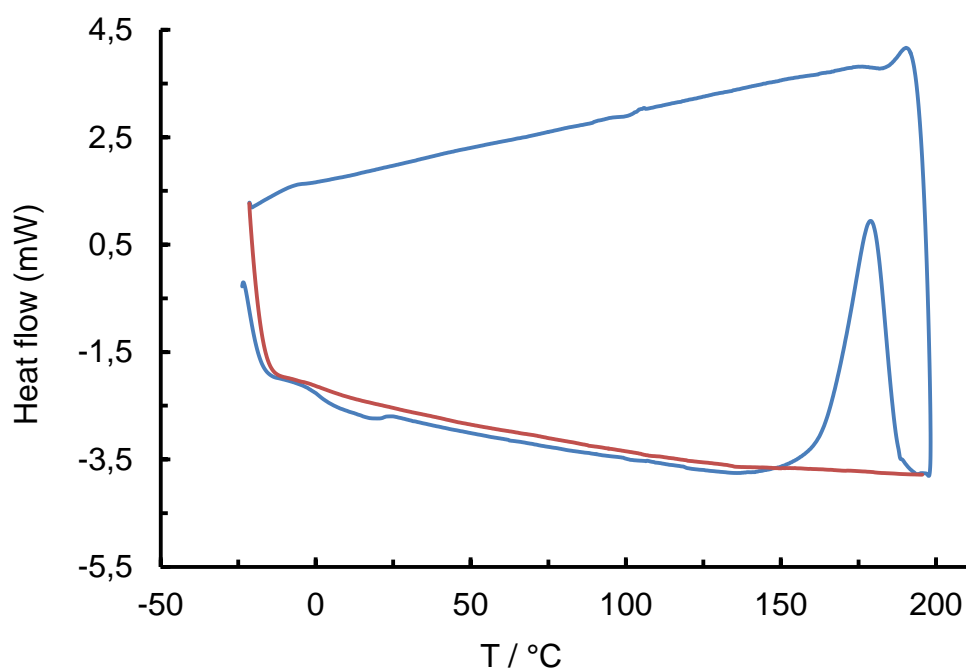


Figure S20. DSC trace of the empty crystal **3(I)** showing the irreversible transition occurring at 177°C (blue line). Second cycle (red). The analysis was run with a $10\text{ }^{\circ}\text{C}\cdot\text{min}^{-1}$ ramp.

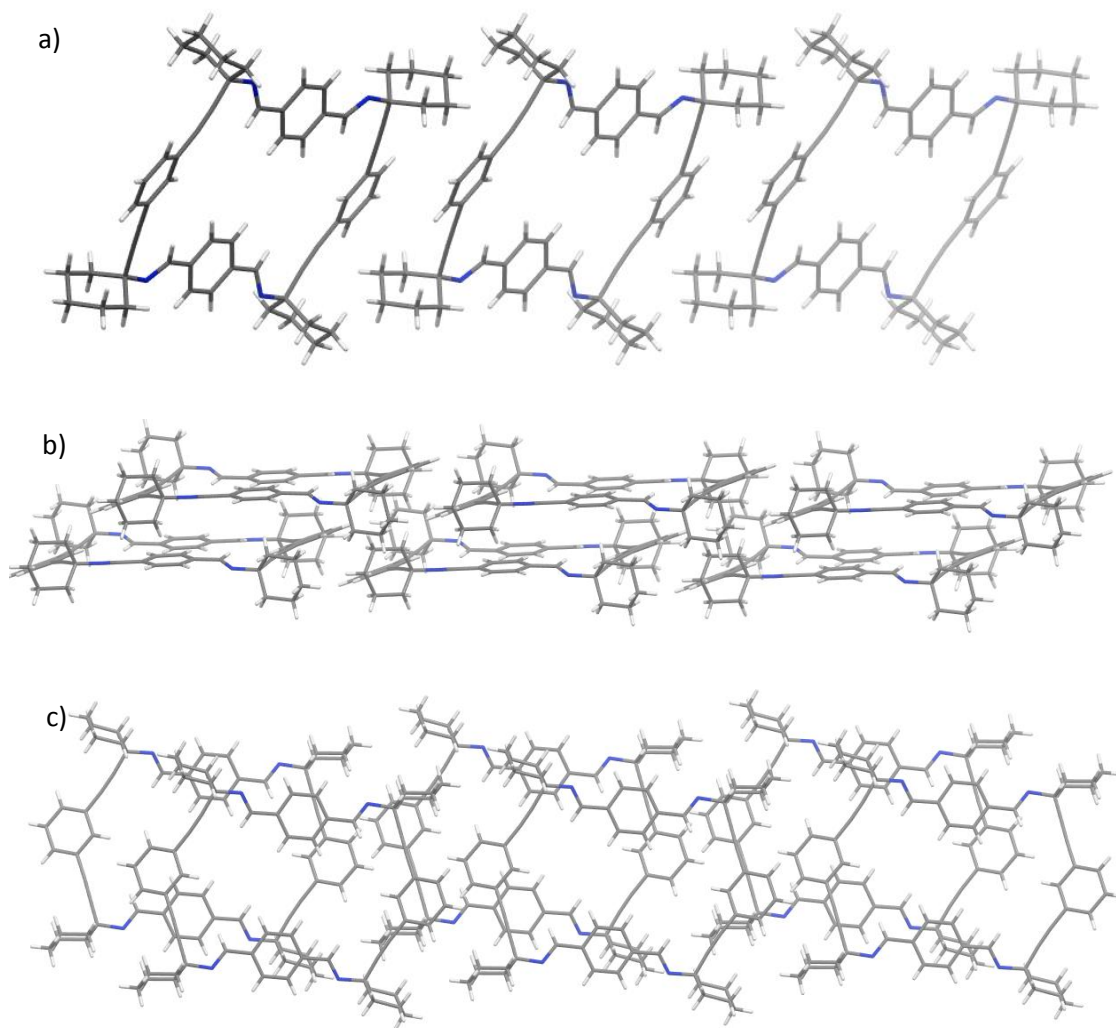


Figure S21. X-ray structure, (a) along the a-axis, (b) side view, (c) top view of the more dense, thermally stable, polymorph **3(II)** (triclinic, P-1, $D_c = 1.127 \text{ g cm}^{-3}$; CCDC no. 1012399).

3.5.6.2 Procedure for guest inclusion

One single crystal of the vacuum treated crystallization harvest of the cycloimine was dipped in approx. 1mL of the neat solvent to be included in the channels of the solid. The period required for the diffusion of the guest into the solid is highly dependent on the guest sample. The exact range varies from less than five minutes for nitromethane to 48-72 h for nicotine and stilbene. After this period, the crystal was removed and rapidly cooled to -100 K before the X-ray diffraction analysis.

3.5.6.3 Crystal Data of solvates

Crystal data for **S(-)-Nicotine@3** (CCDC no.1063714): $C_{70}H_{74}N_6$, $M = 999.34$, monoclinic, $a = 35.689(4)$ Å, $b = 5.9481(6)$ Å, $c = 28.840(3)$ Å, $\alpha = 90^\circ$, $\beta = 97.562(6)^\circ$, $\gamma = 90^\circ$, $V = 6069.0(11)$ Å³, $T = 100(2)$ K, space group $C2$, $Z = 4$, 90524 reflections measured, 17187 independent reflections ($R_{int} = 0.1126$). The final R_1 values were 0.0768 ($I > 2\sigma(I)$). The final $wR(F^2)$ values were 0.2101 ($I > 2\sigma(I)$). The final R_1 values were 0.0931 (all data). The final $wR(F^2)$ values were 0.2312 (all data).

Crystal data for **Nitromethane @3** (CCDC no.1012393): $C_6H_6N_7O_6$, $M = 1020.25$, monoclinic, $a = 34.875(4)$ Å, $b = 5.7940(6)$ Å, $c = 28.028(3)$ Å, $\alpha = 90.00^\circ$, $\beta = 98.453(2)^\circ$, $\gamma = 90.00^\circ$, $V = 5602.0(10)$ Å³, $T = 100(2)$ K, space group $C2/c$, $Z = 4$, 39875 reflections measured, 11756 independent reflections ($R_{int} = 0.0370$). The final R_1 values were 0.0610 ($I > 2\sigma(I)$). The final $wR(F^2)$ values were 0.1765 ($I > 2\sigma(I)$). The final R_1 values were 0.0742 (all data). The final $wR(F^2)$ values were 0.1876 (all data).

Crystal data for **Diethyl squarate@3** (CCDC no.1012391): $C_{68}H_{71}N_4O_{4.50}$, $M = 1016.29$, monoclinic, $a = 34.814(2)$ Å, $b = 5.8498(4)$ Å, $c = 27.956(2)$ Å, $\alpha = 90.00^\circ$, $\beta = 98.517(2)^\circ$, $\gamma = 90.00^\circ$, $V = 5630.7(7)$ Å³, $T = 100(2)$ K, space group $C2/c$, $Z = 4$, 68338 reflections measured, 16500 independent reflections ($R_{int} = 0.0255$). The final R_1 values were 0.0579 ($I > 2\sigma(I)$). The final $wR(F^2)$ values were 0.1626 ($I > 2\sigma(I)$). The final R_1 values were 0.0733 (all data). The final $wR(F^2)$ values were 0.1751 (all data).

Crystal data for **p-Xylene@3** (CCDC no.1012395): $C_{68}H_{70}N_4$, $M = 943.28$, triclinic, $a = 5.8032(7)$ Å, $b = 17.6171(18)$ Å, $c = 28.095(3)$ Å, $\alpha = 82.852(4)^\circ$, $\beta = 89.950(4)^\circ$, $\gamma = 81.848(4)^\circ$, $V = 2820.8(5)$ Å³, $T = 100(2)$ K, space group $P1$, $Z = 2$, 10911 reflections measured, 10911 independent reflections ($R_{int} = 0.0751$). The final R_1 values were 0.0788 ($I > 2\sigma(I)$). The final $wR(F^2)$ values were 0.1961 ($I > 2\sigma(I)$). The final R_1 values were 0.1480 (all data). The final $wR(F^2)$ values were 0.2277 (all data).

Crystal data for **Ethylene glycol@3** (CCDC no.1012392): $C_{63}H_{69}N_4O_3$, $M = 930.22$, monoclinic, $a = 34.994(5)$ Å, $b = 5.7712(9)$ Å, $c = 28.005(5)$ Å, $\alpha = 90.00^\circ$, $\beta = 97.696(5)^\circ$, $\gamma = 90.00^\circ$, $V = 5604.9(15)$ Å³, $T = 100(2)$ K, space group $C2/c$, $Z = 4$, 20328 reflections measured, 9168 independent reflections ($R_{int} = 0.0449$). The final R_1 values were 0.0681 ($I > 2\sigma(I)$). The final $wR(F^2)$ values were 0.1908 ($I > 2\sigma(I)$). The final R_1 values were 0.0978 (all data). The final $wR(F^2)$ values were 0.2163 (all data).

Crystal data for **p-Anisaldehyde@3** (CCDC no.1012394): $C_{68}H_{68}N_4O_2$, $M = 973.26$, monoclinic, $a = 35.119(8)$ Å, $b = 5.8515(13)$ Å, $c = 28.129(6)$ Å, $\alpha = 90.00^\circ$, $\beta = 96.944(5)^\circ$, $\gamma = 90.00^\circ$, $V = 5738(2)$ Å³, $T = 100(2)$ K, space group $C2/c$, $Z = 4$, 9090 reflections measured, 9090 independent reflections ($R_{int} = 0.0999$). The final R_1 values were 0.1199 ($I > 2\sigma(I)$). The final $wR(F^2)$ values were 0.3229 ($I > 2\sigma(I)$). The final R_1 values were 0.1489 (all data). The final $wR(F^2)$ values were 0.3400 (all data).

Crystal data for **cis-Stilbene@3** (CCDC no.1012397): $C_{74}H_{72}N_4$, $M = 1017.35$, triclinic, $a = 5.8111(13) \text{ \AA}$, $b = 17.553(4) \text{ \AA}$, $c = 28.328(5) \text{ \AA}$, $\alpha = 82.080(6)^\circ$, $\beta = 89.417(6)^\circ$, $\gamma = 83.086(6)^\circ$, $V = 2841.2(10) \text{ \AA}^3$, $T = 100(2) \text{ K}$, space group $P1, \bar{1}$, $Z = 2$, 21469 reflections measured, 21469 independent reflections ($R_{int} = 0.0621$). The final R_1 values were 0.0949 ($I > 2\sigma(I)$). The final $wR(F^2)$ values were 0.2375 ($I > 2\sigma(I)$). The final R_1 values were 0.1388 (all data). The final $wR(F^2)$ values were 0.2665 (all data).

Crystal data for **R-(+)-Limonene@3** (CCDC no.1012396): $C_{70}H_{76}N_4$, $M = 973.34$, monoclinic, $a = 34.833(4) \text{ \AA}$, $b = 5.8219(7) \text{ \AA}$, $c = 28.205(3) \text{ \AA}$, $\alpha = 90^\circ$, $\beta = 98.490(5)^\circ$, $\gamma = 90^\circ$, $V = 5657.1(12) \text{ \AA}^3$, $T = 100(2) \text{ K}$, space group $C2$, $Z = 4$, 25503 reflections measured, 11682 independent reflections ($R_{int} = 0.0803$). The final R_1 values were 0.0699 ($I > 2\sigma(I)$). The final $wR(F^2)$ values were 0.1761 ($I > 2\sigma(I)$). The final R_1 values were 0.1361 (all data). The final $wR(F^2)$ values were 0.2142 (all data).

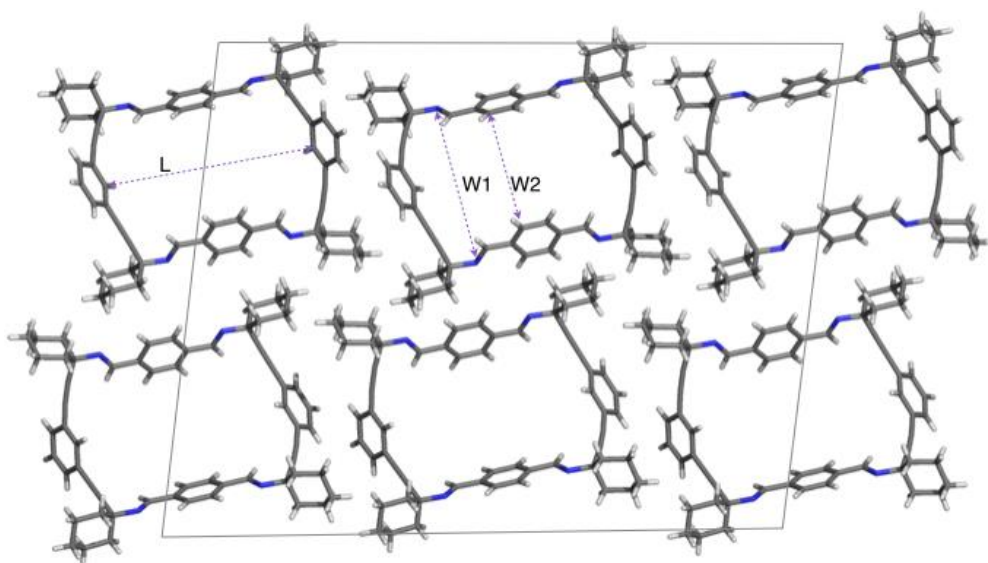
3.5.6.4 Representative geometric parameters of solvates **3**@guest (L; W1; W2)

Table S1. Comparison of stoichiometry (*S*), calculated density (D_c) and pore dimensions: length (*L*) and width (*W1* and *W2*) of different inclusion complexes.

	Structure	CCDC	S^a	D_c^b	<i>L</i>	<i>W1</i>	<i>W2</i>
		No		g cm^{-3}	Å	Å	Å
1	3(I) ^c	1012398	–	0.99	11.98	9.20	6.90
2	3(II) ^d	1012399	–	1.13	12.14	9.91	5.54
3	EtOAc@3	1012389	3:4	1.12	11.97	9.23	6.11 - 6.91 ^g
4	S(-)-Nicotine@3(I) ^f	1063714	1:1	1.09	12.22	9.52	7.35
5	Diethyl Squarate@3	1012391	1:1	1.20	11.97	9.11	6.66
6	Ethylene Glycol@3	1012392	2:3	1.11	12.06	9.09	6.12 - 6.71 ^g
7	Nitromethane@3	1012393	1:3	1.21	12.10	9.09	6.67
8	p-Anisaldehyde@3	1012394	1:1	1.20	12.00	9.34	6.35 - 7.34 ^g
9	p-Xylene@3	1012395	2:3	1.11	12.00	9.18	6.72
10	Z-Stilbene@3(I) ^e	1012397	1:1	1.01	12.02	9.34	7.57
11	(R)-(+)-Limonene@3(I) ^f	1012396	1:1	1.14	12.01	9.21	6.92

^a *S* = Crystallographic stoichiometry (**3**:guest). ^b Crystallographic densities. ^c **3(I)**: Porous empty crystal. ^d **3(II)**: Non porous empty crystal, triclinic space group *P*-1, obtained by heating **3(I)** below to 160°C. ^e Obtained from **3(I)**, triclinic space group *P*-1. ^f Obtained from **3(I)**, space group *C*2 due to the asymmetry of the guest. ^g Indicate disorder of phenyl rings between two limiting positions.

3.6.6.5 Quantitative determination of the molar ratio [3:sample] by ^1H NMR spectroscopy

A single monocrystal of **EtOAc@3** was soaked in 100 μL of guest (neat) for 72 h at room temperature. After this period, the solution was removed and the crystal was washed with EtOAc ($2 \times 0.5 \text{ mL}$) and MeOH ($3 \times 0.5 \text{ mL}$), respectively, and dried under vacuum for 10 minutes.

If the crystal was small (length $< 0.5 \text{ mm}$) it was dissolved in 0.6 mL of CDCl_3 followed by ^1H NMR measurement. The stoichiometry of the crystal was determined based on the integral ratios of the signal of the imine protons and the corresponding protons of the guest molecule (see Figure S22). This procedure is slow ($>24 \text{ h}$) and due to the poor solubility of cycloimine **3** it is only suitable for relatively small crystals (length $< 0.2\text{-}0.3 \text{ mm}$).

For bigger crystals (length $> 0.4 \text{ mm}$) the complete dissolution of the crystal in CDCl_3 was unsuitable due to the low solubility of **3** in CDCl_3 . In these cases, it was necessary the destruction of the imine macrocycle **3** by adding 50 μL of $\text{DCI}/\text{D}_2\text{O}$ (37%) to the sample and, then diluting with a mixture of $\text{DMSO-}d_6:\text{CDCl}_3$ (2.5:1 v/v, 600 μL). The stoichiometries of the inclusion complexes were determined based on the integral ratios of well-separated proton signals of the macrocyclic tetraimine and the guest (i.e. protons of the resulting dialdehyde from **3**) (see Figure S23).

Table S2. Comparison of molar ratios [guest:3] obtained by X-ray diffraction and ¹H NMR of the different inclusion complexes.

Sample	Sample Volume ^a Å ³	Solvate	Crystallographic molar ratio ^b	¹ H-NMR molar ratio ^c
EtOAc	100,7	EtOAc@3	1:1.34	1:1.36
S-(-)-Nicotine	187,0	S-(-)-Nicotine@3(I)^f	1:1	1:0.90
Diethyl Squarate	173,5	Diethyl Squarate@3	1:1	1:1.04
Ethylene glycol	66,7	Ethylene Glycol@3	1:1.5	1:1.54
Nitromethane	55,6	Nitromethane@3	1:3	1:3.4
<i>p</i> -Anisaldehyde	147,8	<i>p</i>-Anisaldehyde@3	1:1	1:0.93
<i>p</i> -Xylene	136,2	<i>p</i>-Xylene@3	1:1.5	1:1.24
Z-Stilbene	216,0	Z-Stilbene@3(I)^e	1:1	1:0.8
R-(+)-Limonene	177,3	(R)-(+)-Limonene@3(I)^f	1:1	1:0.96

^a CPK molecular volumes were calculated from DFT (EDF1) energy-minimized structures using MacSpartan'14 (v. 1.1.4). ^b Calculated from the crystallographic formula. ^c Calculated by integration of the corresponding proton signals.

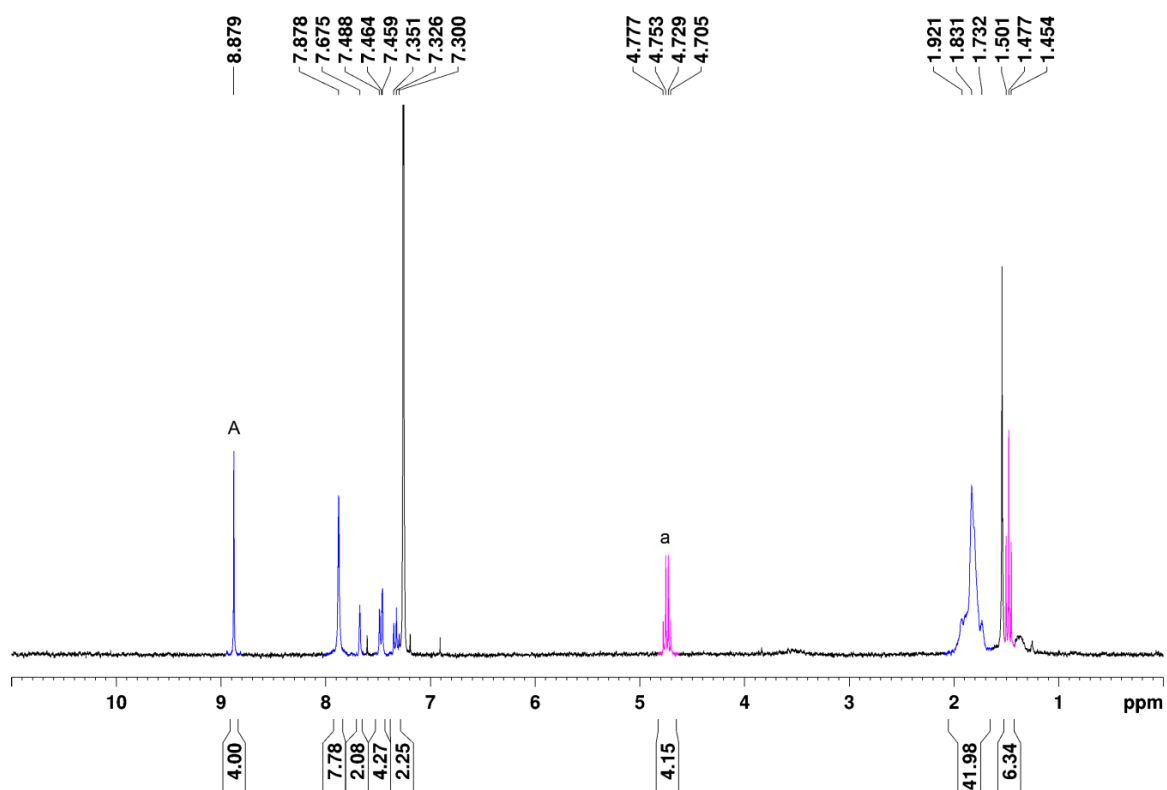


Figure S22. Molar ratio of **guest:3** determined by direct dissolution of the inclusion complex in CDCl_3 .

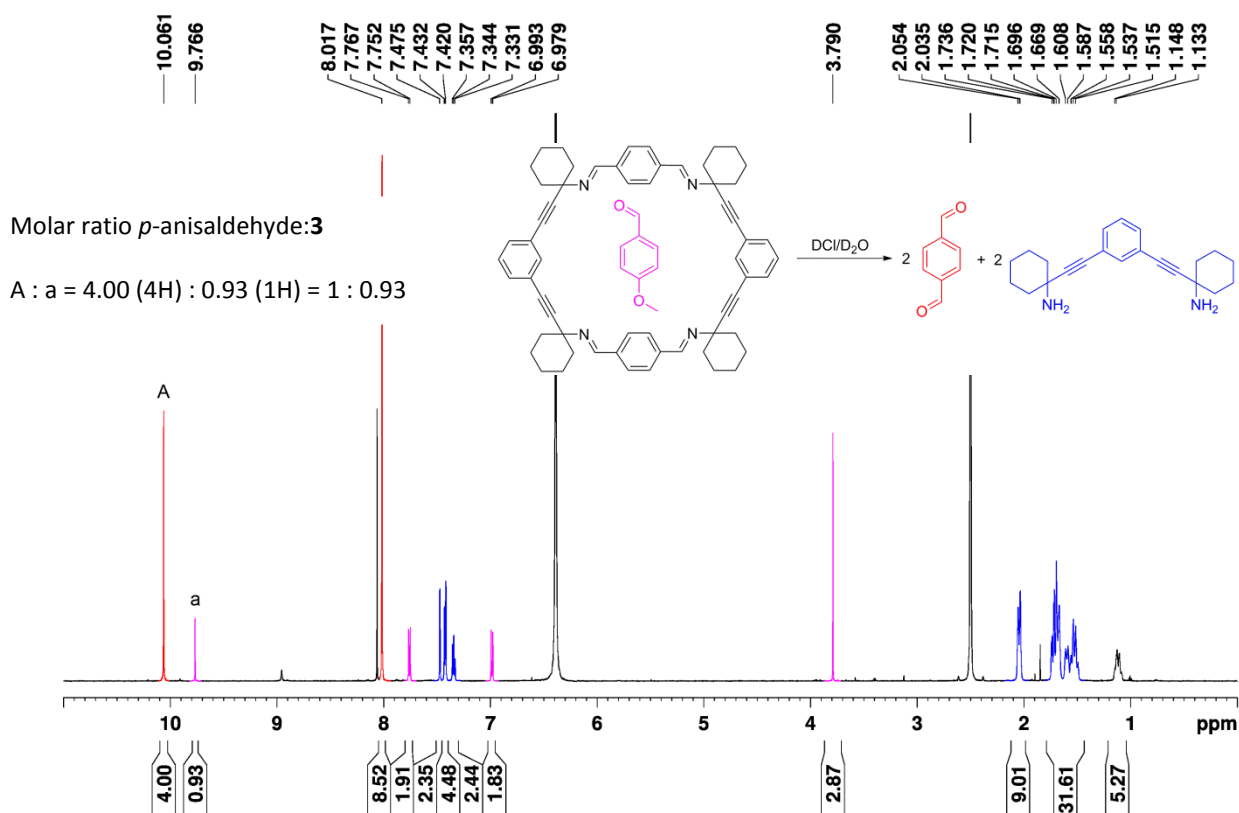


Figure S23. Molar ratio of **guest:3** determined by previous hydrolysis of the cycloimine **3** in $\text{DCl/D}_2\text{O}$.

3.5.7 Theoretical Methods

3.5.7.1 Theoretical methods.

The 1:1 complexes were completely optimized at the BP86-D3/def2-SVP and BP86-D3/def2-TZVP levels of theory using Turbomole 6.4 program.⁹ The substitution, diffusion and cooperativity studies were performed only at the BP86-D3/def2-SVP level of theory due to the large number of atoms. In these studies, a model of the channel (formed by three host units) is used, which has been constructed from the crystallographic coordinates and kept frozen during the optimizations.

We have used the NCI method¹⁹¹ to study the noncovalent interactions observed in the host-guest complexes. This method relies on two scalar fields to map local bonding properties: the electron density (ρ) and the reduced-density gradient (RDG, σ). It is able of mapping real-space regions where non-covalent interactions are important and is based exclusively on the electron density and its gradient. The information provided by NCI plots is essentially qualitative, i.e. which molecular regions interact. The color scheme is a red-green-blue scale with red for ρ^+ cut (repulsive) and blue for ρ^- cut (attractive).

Channel-Guest interactions. The interaction energies of the channel and three different guests were computed from a macrocycle trimer (denoted as **3CM**) that has been kept frozen during the optimizations at the BP86-D3/def2-SVP level of theory.

Table S3. Interaction energies (E , kcal mol⁻¹) for complexes between the channel model **3CM** and three different guests at different stoichiometric ratios.

	n = 1	n = 2	n = 3
3CM ⋯(EtOAc) _n	-17.1	-37.8	-60.5
3CM ⋯(SQA) _n	-30.8	-65.1	-96.7

¹⁹¹ Johnson, E.; Keinan, S.; Mori-Sánchez, P.; Contreras-García, J.; Cohen, A.; Yang, W. *J. Am. Chem. Soc.* **2010**, *132*, 6498–6506 (NCI).

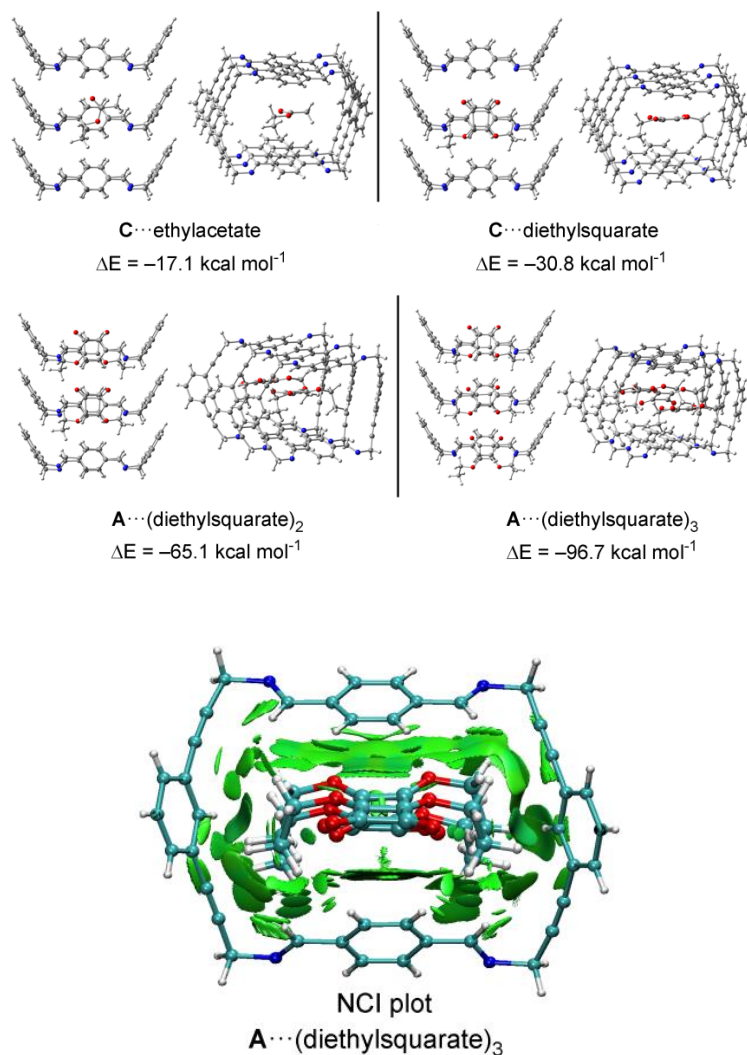


Figure S24. Optimized geometries of the complexes between the channel (**3CM**) and different guests. The NCI surfaces for the **3CM**...(SQA)_n complex is also represented.

Diffusion analysis. To measure the facility of the guest to move inside the channel we have performed a DFT theoretical study (BP86-D3/def2-SVP) where we move the guest inside the channel as a reaction coordinate using steps separated by 1 Å and computing the interaction energy every step. In each point the energy of the system is relaxed (apart from the reaction coordinate) keeping the channel frozen. The diffusion energy estimated using this theoretical model is probably overestimated because the channel is not allowed to relax. However, our purpose is not to compute the exact diffusion barrier, instead we use the estimated energies for comparison purposes and provide qualitative results.

Figures S25-S26 show the reaction coordinates for EtOAc and diethyl squarate moving inside the channel. The first point of the coordinate corresponds to the energy of the system locating the guest at more than 5 angstroms from the entrance of the channel. In the second point of the coordinate the guest is located at 2 Å away from the entrance and the reaction coordinate follows with steps of 1 Å and finishes when the guest is out of the channel at 4 Å from the exit.

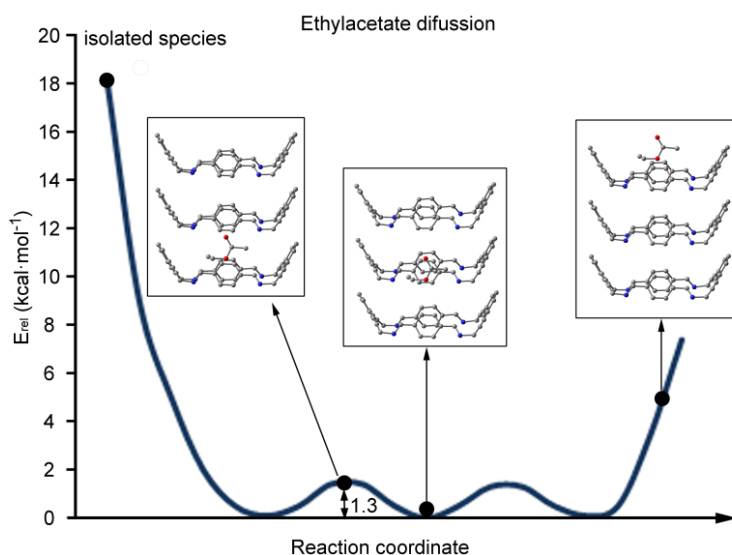


Figure S25. Reaction coordinate for EtOAc moving inside the channel. Hydrogen atoms have been omitted in the representation of several points of the coordinate. The diffusion barrier of ethylacetate is very small ($1.3 \text{ kcal mol}^{-1}$). Therefore it can freely move inside the channel with a high diffusion rate and is expected to be replaced by any of the other two guests easily and rapidly.

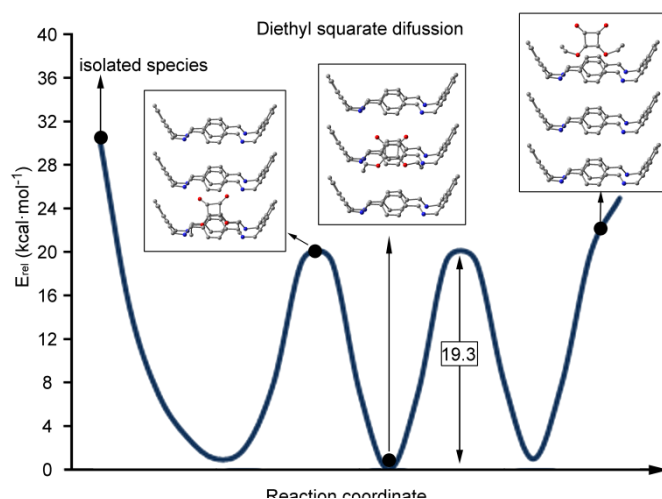


Figure S26. Reaction coordinate for diethylsquarate moving inside the channel. Hydrogen atoms have been omitted in the representation of several points of the coordinate. Diethylsquarate presents the highest diffusion barrier and the interaction energy is smaller than that of diethylphtalate.

Substitution analysis.

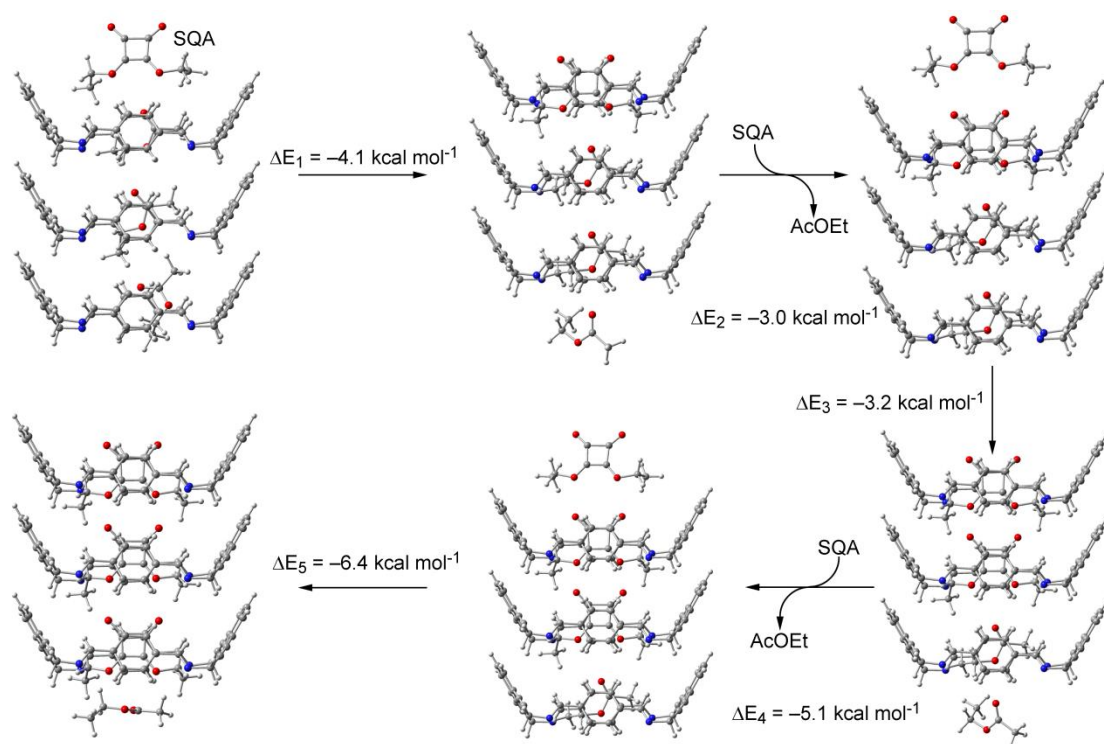


Figure S27. Proposed pathway for the progressive substitution of EtOAc by SQA and the energies associated to each step.

Porous Macrocyclic Imines: Synthesis and Application to the Selective Adsorption of Phthalates

Elena Sanna,^a Eduardo C. Escudero-Adán,^{b,c} Pablo Ballester,^{b,c} Carmen Rotger^a and Antonio Costa^{*a}

^a *Departament de Química. Universitat de les Illes Balears, Palma, 07122, Spain. Email: antoni.costa@uib.es; Fax: +34 971 172436; Tel: +34 971 173266.*

^b *Institut of Chemical Research of Catalonia (ICIQ). Avda. Països Catalans 16, 43007 Tarragona (Spain).*

^c *Catalan Institution for Research and Advanced Studies (ICREA). Passeig Lluís Companys 23, 08010, Barcelona (Spain).*

Manuscript in preparation

3.5.1 Introduction

During the last decades, the interest in obtaining organic porous materials has been increased. The synthesis of molecules that pack in a crystalline form or in an amorphous state to generate permanent microporosity have shown multiple potential applications.¹⁹² Zeolites, mesoporous silicates, MOFs (Metal Organic Frameworks) and PCPs (Porous Coordination Polymers) can be included in this group.¹⁹³

There are innumerable crystal structures based on porous inclusion compounds, but only a few have demonstrated to have permanent porosity implying that the structure is maintained after solvent removal.¹⁹⁴ These compounds crystallize forming zero-dimension, one-dimension or three-dimensional pore structures. Usually, the loss of the solvent causes the collapse of the structure, rendering amorphous materials or more densely packed materials. Indeed, the rigidity seems to be necessary to obtain porous materials with high specific surface areas.¹⁹⁵

The development of dynamic covalent chemistry has let to obtain thermodynamically stable porous compounds.¹⁹⁶ Specifically, imines have shown to be promising candidates for this purpose. Recently, Cooper and Mastalerz have reported some examples of three-dimensional cycloimine cages with high capability for the adsorption of different substrates.^{192a, 197} In this instance, the pore size and the surface area are closely related to the reaction conditions (temperature, solvent, concentration) and the structural units that form the material.

3.5.2 Results and discussion

The aim of this work was the synthesis and evaluation of a new set of cycloimine compounds. With this objective in mind, we studied the condensation reaction of two dialdehydes (**2** and **4**) with four different diamines (**1**, **5**, **6** and **7**) at room temperature using the solvent as unique template.

¹⁹² a) Culshaw, J. L.; Cheng, G.; Schmidtmann, M.; Hasell, T.; Liu, M.; Adams, D. J.; Cooper, A. I.; *J. Am. Chem. Soc.* **2013**, *135*, 10007-10010. b) Holst, J. R.; Trewin, A.; Cooper, A. I. *Nat. Chem.* **2010**, *2*, 915-920. c) Bradshaw, D.; Prior, T. J.; Cussen, E. J.; Claridge, J. B.; Rosseinsky, M. J. *J. Am. Chem. Soc.* **2004**, *126*, 6106-6114. d) Eddaoudi, M.; Li, H.; Reineke, T.; Fehr, M.; Kelley, D.; Groy, T. L.; Yaghi, O. M. *Topics in Catalysis*, **1999**, *9*, 105-111.

¹⁹³ a) Bellussi, G.; Carati, A.; Rizzo, C.; Millini, R. *Catal. Sci. Technol.* **2013**, *3*, 833-857. b) Chun, J.; Kang, S.; Park, N.; Park, E. J.; Jin, X.; Kim, K. -D.; Seo, H. O.; Lee, S. M.; Kim, H. J.; Kwon, W. H.; Park, Y. -K.; Kim, J. M.; Kim, Y. D.; Son, S. U. *J. Am. Chem. Soc.* **2014**, *136*, 6786-6789, c) Navarro, J. A. R.; Barea, E.; Salas, J. M.; Masciocchi, N.; Galli, S.; Sironi, A.; Ania, C. O.; Parra, J. B. *J. Mat. Chem.* **2007**, *17*, 1939-1946.

¹⁹⁴ Mastalerz, M.; *Chem. Eur. J.* **2012**, *18*, 10082-10091

¹⁹⁵ Schneider, M. W.; Oppel, I. M.; Mastalerz, M. *Chem, Eur. J.* **2012**, *18*, 4156-4160.

¹⁹⁶ Acharyya, K.; Mukherjee, P. S. *Chem. Eur. J.* **2013**, *19*, 1-13

¹⁹⁷ a) Chen, L.; Reiss, P. S.; Chong, S. Y.; Holden, D.; Jelfs, K. E.; Hasell, T.; Little, M. A.; Kewley, A.; Briggs, M. E.; Stephenson, A.; Thomas, K. M.; Armstrong, J. A.; Bell, J.; Busto, J.; Noel, R.; Liu, J.; Strachan, D. M.; Thallapally, P. K.; Copper, A. I. *Nat. Chem.* **2014**, *13*, 954-960, b) Mastalerz, M.; Schneider, M. W.; Oppel, I. M.; Presly, O. *Angew. Chem, Int. Ed.* **2011**, *50*, 1046-1051.

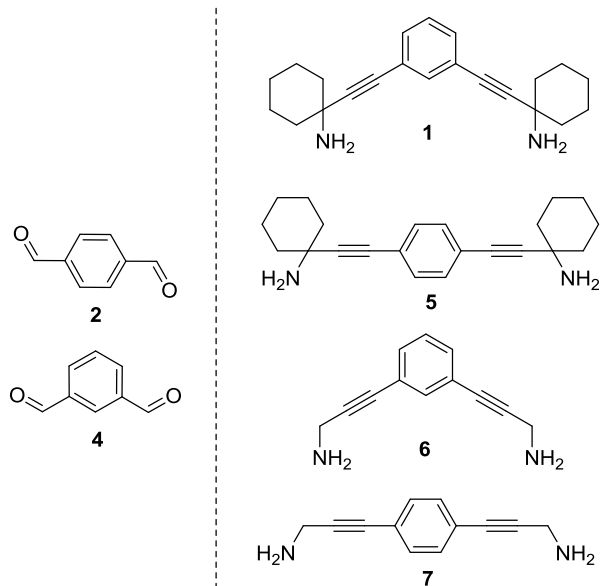


Figure 72. Chemical structure of the diamines and aldehydes used for this study.

The slow condensation reaction of a dialdehyde and a diamine derivative in EtOAc at room temperature for 7-60 days gives semi-rigid compounds that, once crystallized, could establish stacking interactions between the adjacent superposed macrocycles. All the imine macrocycles derived from the combination of the dialdehydes **2** and **4** with the cyclohexylidene propargylamines **1** and **5** were obtained in moderate to good yields ranging from 16 to 50% isolated yields. Compounds **3** and **8** were soluble in chloroform and mesitylene. Macrocycles **9** and **10** were also soluble in chloroform, but they could not be isolated in pure form.

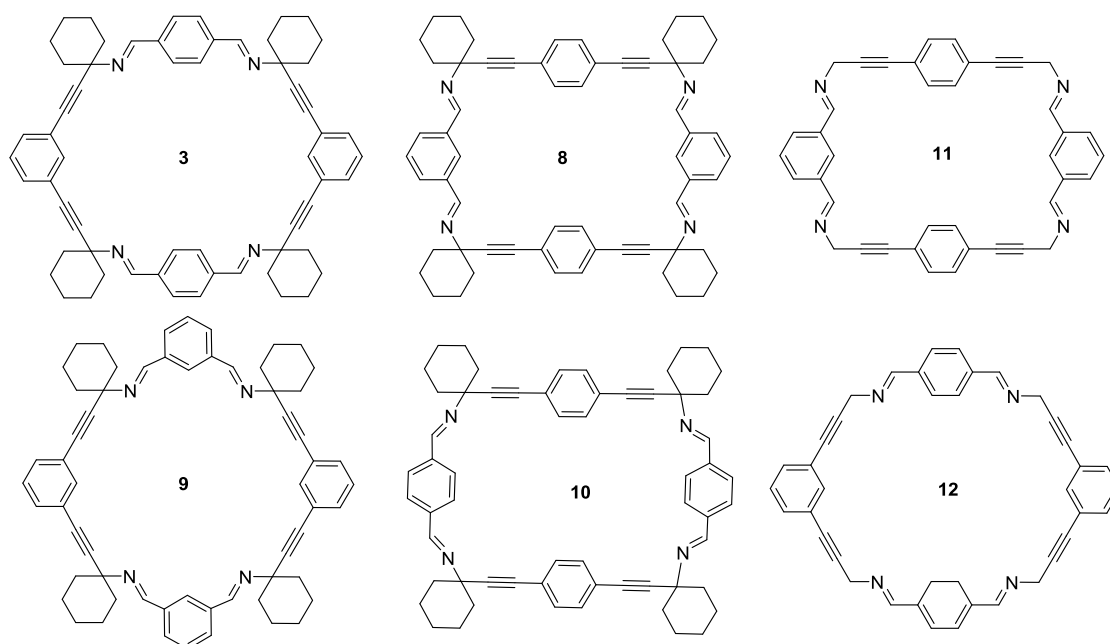


Figure 73. Chemical structure of the different cycloimines synthesized.

On the other hand, the unsubstituted propargylamines **6** and **7** yielded the cycloimine compounds **11** and **12**. These macrocycles are almost insoluble in chloroform. Hence, we decided to continue our studies using only the macrocycles **3** and **8**.

To optimize the yields of cycloimine, the condensation reaction of the dialdehydes with the diamines was performed in solvents of different polarity such as EtOAc, MeOH, acetonitrile, or dichloromethane (Table 5). In general, the cycloimines were obtained with moderate yields. However, when the reaction was performed in CH₂Cl₂ the yields of the cycloimine were clearly lower. Crystals suitable for X-ray analysis were obtained from the reaction performed in EtOAc without the need of a further crystallization step.

Table 5. Synthesis conditions proved. *Yield obtained after several crystallizations.

Solvent	3	8
EtOAc	50% ^{198,*}	25%
MeOH (reflux)	10%	23%
MeCN	16%	25%
MeCN/TFA	35%	25%
CH ₂ Cl ₂	No reaction	8%

The X-ray analysis revealed that compound **3** crystallizes in the C2/c space group forming one-dimensional pores filled with disordered molecules of EtOAc. This macrocycle has effective dimensions of 6.901 Å, measured between the aromatic CH of the 1,4-diethynylbenzene moiety, and of 11.979 Å between the aromatic CH of the benzaldimine rings. The triple bonds deviate slightly from linearity with C≡C-C angles of 173.65-177.17°. The cycloimines pack by cooperative stacking and dispersive interactions arising from the cyclohexylidene residues, thus stabilizing the pore structure. Remarkably, the pore structure of **3** is maintained even after the desolvation of the crystals under vacuum to afford the apohost **3(I)**.

The crystallographic structures of **3** show local crystallographic disorder affecting the para-substituted aromatic rings due to the “revolving doors” movement of the aromatic rings along the bisethynyl axis, to accommodate the guests.¹⁹⁹

¹⁹⁸ Sanna, E.; Escudero-Adán, E. C.; Bauzá, A.; Ballester, P.; Frontera, A.; Rotger, C.; Costa, A. *Chem. Sci.* **2015**, *6*, 5466-5472.

¹⁹⁹ Martí-Gastaldo, C.; Antypov, D.; Warren, J. E.; Briggs, M. E.; Chater, P. A.; Wiper, P. V.; Miller, G. J.; Khimyak, Y. Z.; Darling, G. R.; Berry, N. G.; Rosseinsky, M. J.; *Nat Chem.* **2014**, *6*, 343-351.

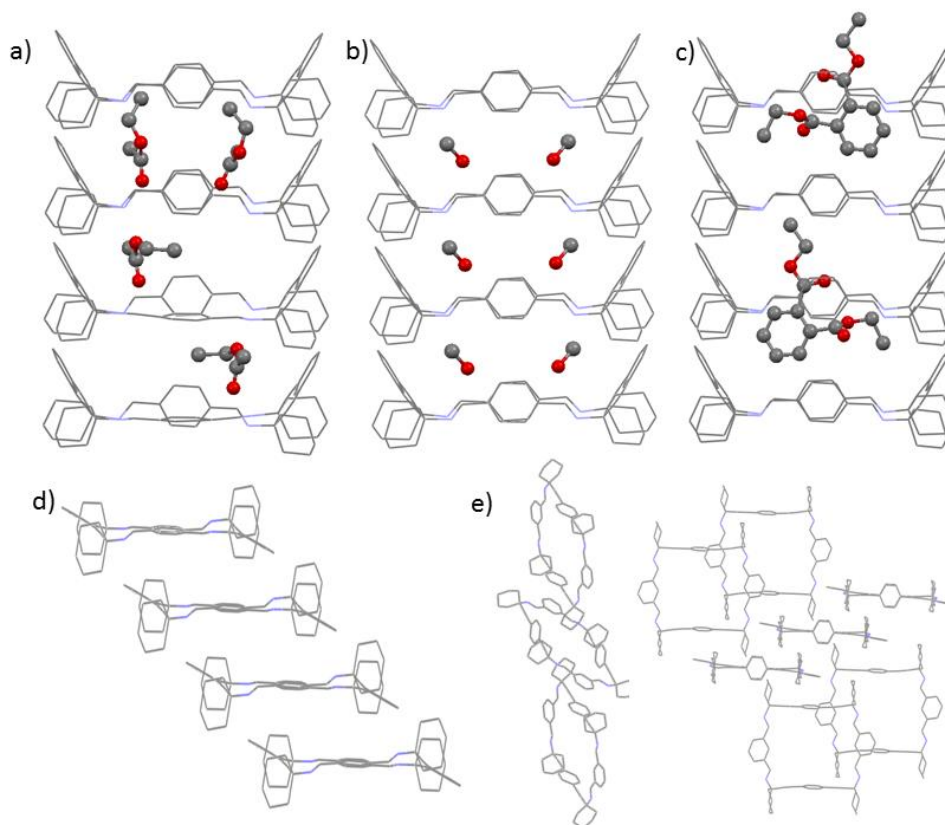


Figure 74. X-ray structure of: a) **EtOAc@3**, b) **MeOH@3**, c) **EtPh@3**, d) **3(II)** and e) **8**. Hydrogen atoms have been omitted for clarity.

The porosity shown by the apohost **3(I)** was lost by soaking the crystals in MeOH for 12 hours. X-ray analysis of the resulting non-porous but still crystalline material **3(II)**, shows that the crystal changed from monoclinic (C2/c) to triclinic (P1) space groups. At the same time, the crystal density of **3(II)** 1.127 mg/m³ is higher than that of the porous **3(I)** 0.986 mg/m³ due to a more compact structure of **3(II)** compared to **3(I)**. As for **3(I)**, the crystalline structure of **3(I)** was held together by CH- π interactions between the cyclohexylydene substituents and the aromatic group of the macrocycle. Due to the slow rate of decomposition of **3(I)** in MeOH, it was possible to solve the crystal of **3** with MeOH inside the pores (**MeOH@3**). The stoichiometry of the resulting complex was 3:1 MeOH:**3** still maintaining the C2/c space group.

Compound **8** was also crystallized from EtOAc. The crystal structure was solved by single-crystal X-ray diffraction. Cycloimine **8** crystallizes in the monoclinic space group P21/c. It consists of distorted cycloimine layers forming a 2D network with perpendicular cycloimine units. However, the structure **8** is non-porous. Attempted crystallization of cycloimines **9**, **10**, **12** in EtOAc, CHCl₃ and mesitylene produced amorphous materials. Macrocyclic imine **11**, crystallized in EtOAc as fibrous "cotton-like" crystals unsuitable for X-ray analysis.

Table 6. Summary of crystallographic data and parameters for isolated crystals.

	AcOEt@3	3(I)	3(II)
Empirical formula	C ₃₂ H ₃₄ N ₂ O	C ₆₀ H ₆₀ N ₄	C ₃₀ H ₃₀ N ₂
Formula weight	462.61	837.12	418.56
Temperature (K)	100(2)	100(2)	100(2)
Wavelength (Å)	0.71073 Å	0.71073	0.71073
Crystal system, space group	Monoclinic, C2/c	Monoclinic, C2/c	Triclinic, P-1
Unit cell dimensions	a = 34.850(6) b = 5.8331(10) c = 28.030(6) α = 90.00 β = 97.906(8) γ = 90.00	a = 34.8696(19) b = 5.8099(3) c = 28.1212(16) α = 90.00 β = 98.143(2) γ = 90.00	a = 6.5695(4) b = 13.4759(8) c = 14.1239(9) α = 91.0310(10) β = 99.2650(10) γ = 91.6850(10)
Volume (Å ³)	5643.9(18)	5639.6(5)	1233.21(13)
Z	8	4	2
Calculated density (mg/m ³)	1.089	0.986	1.127
Absorption coefficient	0.065	0.057	0.065
F(000)	1984	1792	448
Crystal size (mm)	0.25 x 0.10 x 0.03	0.25 x 0.10 x 0.03	0.20 x 0.20 x 0.15
θ range for data collection	1.47 -27.61°	1.180-30.547°	2.92-38.71 °
Reflections collected (unique)	23533/6479 [R(int) = 0.0795]	23533/8377 [R(int) = 0.0577]	13275/13275 [R(int) = 0.00]
Completeness to theta	98.6%	96.9%	94.3%
Max. and min. transmission	0.9980 and 0.9839	0.994 and 0.884	0.9903 and 0.9870
Data / restraints / parameters	6479 / 190 / 454	8377/ 91/ 325	13275 / 0 / 290
Goodness-of-fit on F ²	1.054	1.071	1.014
Final R indices [I>2σ(I)]	R ₁ = 0.0879 , wR ₂ = 0.2484	R ₁ = 0.0602 , wR ₂ = 0.1686	R ₁ = 0.0529 , wR ₂ = 0.1334
R indices (all data)	R ₁ = 0.1341 , wR ₂ = 0.2846	R ₁ = 0.0825 , wR ₂ = 0.1883	R ₁ = 0.0860 , wR ₂ = 0.1550

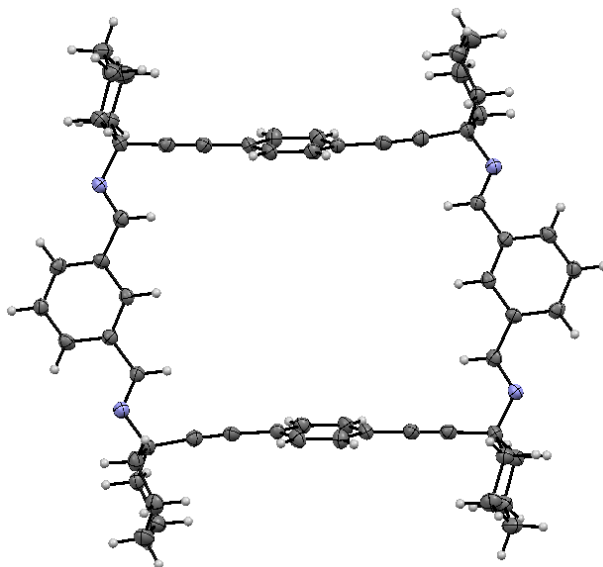


Figure 75. ORTEP representation of **8**. Displacement ellipsoids are drawn at the 50% probability level.

In refluxing MeOH besides the two target cycloimines **3** and **8**, we observed the formation of two isomeric products **3'** and **8'**. These additional, and somehow unexpected, products were stereoisomers of **3** and **8**, respectively, as evidenced by $^1\text{H-NMR}$, ESI-MS, and TGA. The $^1\text{H-NMR}$ spectra of **3+3'** and **8+8'** mixtures showed unique resonances (e and e') for the imine and also for other diagnostic signals of the macrocycles. Assuming a rapid interconversion of protons on the NMR time scale, the simplicity of the spectra evidenced that the two pairs of products were essentially symmetrical.

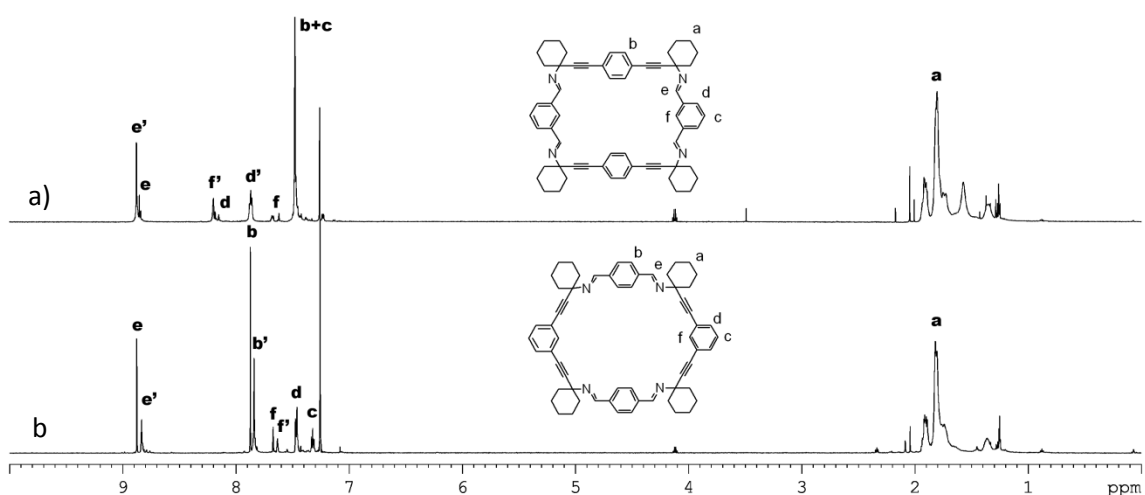


Figure 76. $^1\text{H-NMR}$ spectra of the mixture of stereoisomers: a) **8+8'** and b) **3+3'**.

The analysis of the 2D-NMR spectra (ROESY, COSY) allowed in each case the assignation of two independent sets of cycloimine signals. In addition, the mass spectra of **3+3'** and of **8+8'** showed, in each case, the same molecular ions at m/z 837.5201 for **3+3'** and 837.4905 for **8+8'**, respectively. Remarkably,

upon gentle heating at 50 °C for 24 hours in CDCl₃, both products **3'** and **8'** were smoothly converted into **3** and **8**, respectively (Figure 77). The thermal conversion of the above mixtures into pure products, proved the dynamic nature of the macrocyclization to afford the thermodynamically most stable macrocyclic imine. Unfortunately, all the attempts to isolate the kinetic stereoisomers **3'** and **8'** in pure forms, by preferential crystallization or HPLC, were unsuccessful due to partial conversion to the stable stereoisomers during the separation and/or the purification steps.

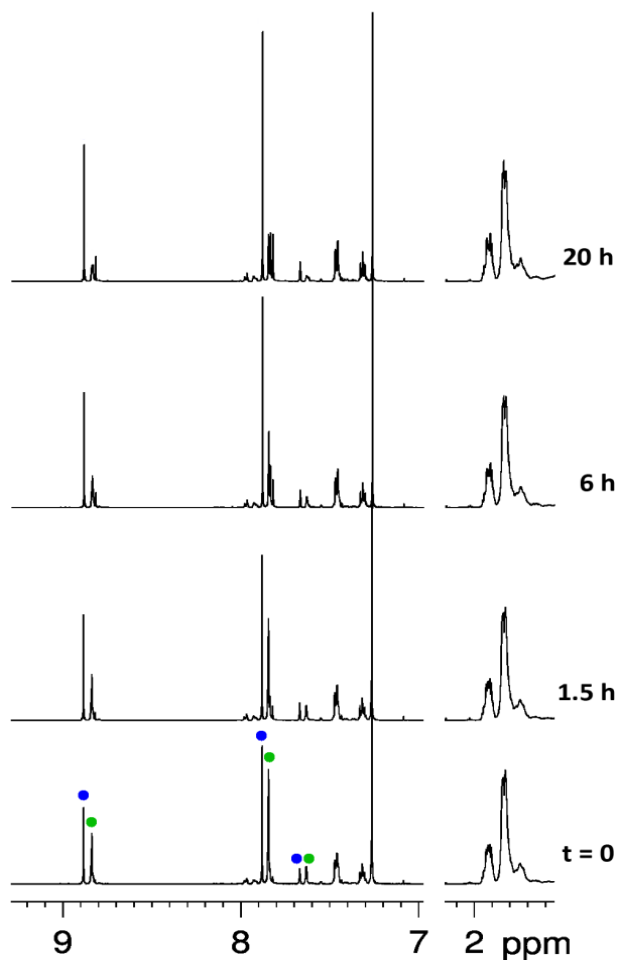


Figure 77. ¹H-NMR spectra showing the evolution with time of the mixture of isomers of **3** (blue) and **3'** (green) in CDCl₃ at 50 °C.

At this point, we hypothesized that the formation of two stereomeric mixtures of cycloimines could be due to the formation of cycloimines as mixtures of Z and E imine bonds or, alternatively, to the formation of two diastereomeric boat-like and chair-like cycloimines, both having similar energies (Figure 78). In both cases, given the thermal equilibrium favouring the lowest energy stereoisomer, these results could be accounted for by assuming the interconversion of the two stereoisomeric cycloimines through an open intermediate. This mechanism would be a direct consequence of the dynamic character of the imine bonds. Noticeably, the formation of stereoisomeric cycloimines has recently been described.²⁰⁰

²⁰⁰ Acharyya, K.; Mukherjee, P. S. *Chem. Commun.* **2015**, *51*, 4241-4244.

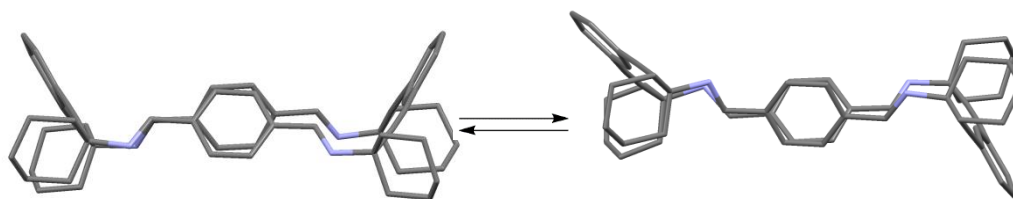


Figure 78. Proposed structural equilibrium between "boat-like" **3** (left) and "chair-like" **3'** (right) diastereoisomers.

In order to shed some light on the mechanism of interconversion between the two diastereomers, first we investigated the possible formation of mixtures of imines containing both, Z and E imine bonds. To this end, we synthesized the open bis imine compounds **13** and **14** by a condensation reaction in refluxing MeOH between benzaldehyde with the diamines **1** and **5**, respectively (Figure 79a). We found that, in both cases, only one imine product was isolated. This result supports the idea that the stereoisomeric mixtures observed namely **3+3'** and **8+8'**, resulted from the macrocyclization step. The bis imine **14** could be crystallized in chloroform.

The X-ray analysis of diimine **14** shows that the two imine bonds of **14** have the E configuration. As is illustrated in Figure 79, the molecules of the diimine are packed together by means of C-H \cdots π interactions between the aromatic rings of two neighbouring molecules and by C-H \cdots C=N interactions between an aromatic ring of one molecule and the π system of C=N groups of another.

To demonstrate the dynamic nature that governs the observed isomerization processes, we investigated the uncatalyzed transimination (imine metathesis) between the macrocyclic imine **3** and n-butylamine. It has recently reported the catalytic effect of the presence of primary amines on the imine metathesis.²⁰¹

A mixture containing the cycloimine **3** and a fivefold molar excess of n-butylamine in CDCl₃ was prepared and the reaction was monitored by ¹H-NMR at 50°C. After 15 hours, only the product of transimination **15** and the diamine **1** were observed (See Figure 80). A similar result was obtained when the experiment was carried out in a mixture of the two isomers **3 + 3'** (See Supporting Information). Both results support the idea that the macrocyclization implies that the thermal equilibrium between macrocycles occurs through an open intermediate and that the posterior reclosing afford the thermodynamic product.

The one-dimensional porous structure of the macrocycle **3** allows us to evaluate **3** for liquid-solid sorption applications. To demonstrate this functionality, we planned to study the selective diffusion of a particular guest compound inside the pores. In general, the adsorption depends on (i) the size of the guest in relation to the size of the pores and (ii) the interaction of the guest with the walls of the pore.²⁰²

The sorption experiments were carried out by soaking crystals of pure **3**, either solvated with EtOAc or desolvated, into a liquid guest. We found that the rate of the exchange heavily varied as a function of the guest. In control experiments, the exchange rates were in the range of minutes (i.e. for nitromethane) to hours (i.e. for diethyl squarate).

²⁰¹ (a) Ciaccia, M.; Pilati, S.; Cacciapaglia, R.; Mandolini, L.; Di Stefano, S. *Org. Biomol. Chem.* **2014**, *12*, 3282-3287.
(b) Ciaccia, M.; Cacciapaglia, R.; Mencarelli, P.; Mandolini, L.; Di Stefano, S. *Chem. Sci.* **2013**, *4*, 2253-2261.

²⁰² Kubota, R.; Tashiro, S.; Shiro, M.; Shionoya, M. *Nat. Chem.* **2014**, *6*, 913-918.

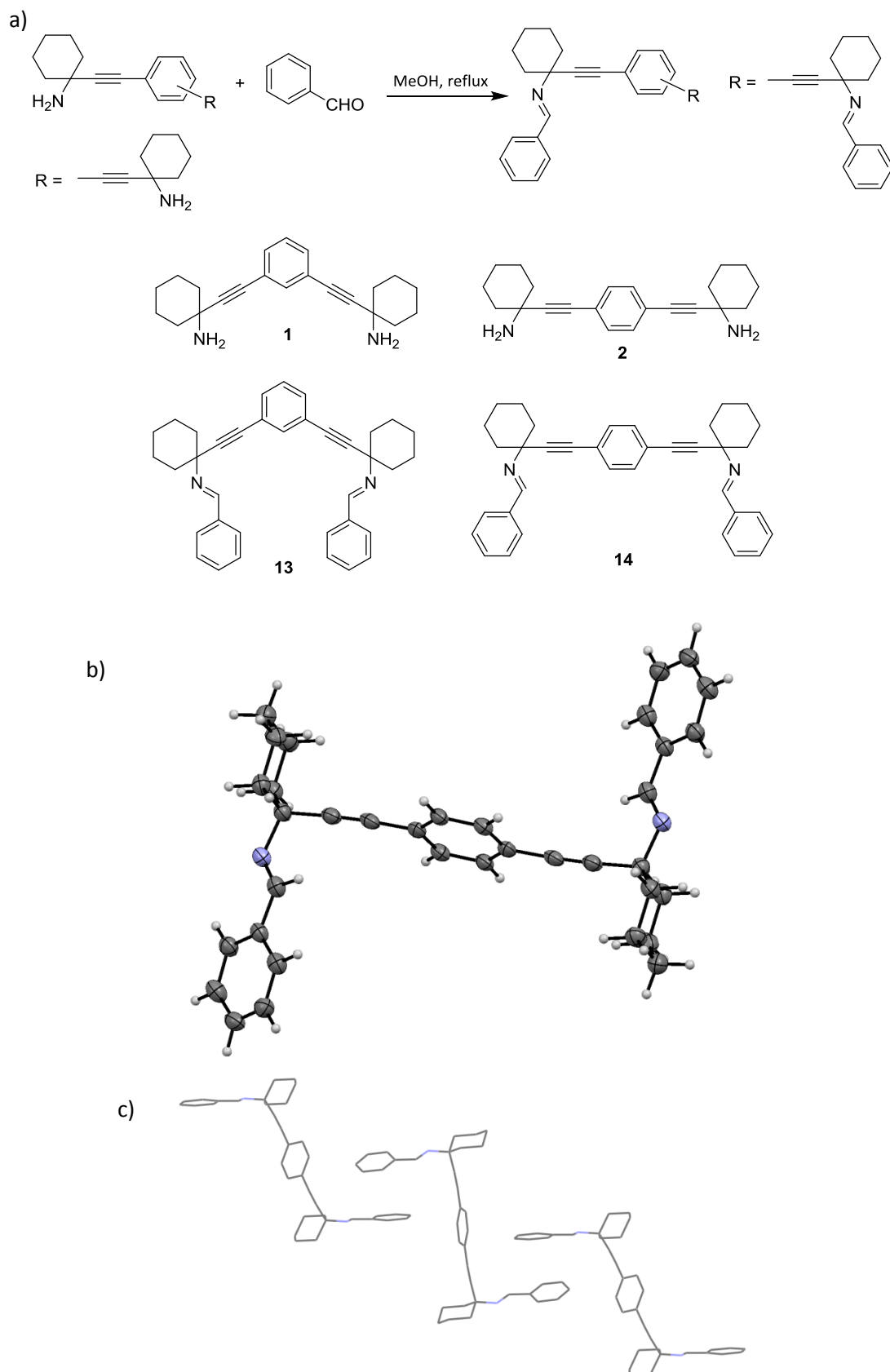


Figure 79. a) General procedure for the synthesis of diimine compounds **13** and **14**. b) ORTEP representation of **14**. Displacement ellipsoids are drawn at the 50% probability level. c) Crystal packing of **14** in which hydrogens have been omitted for clarity.

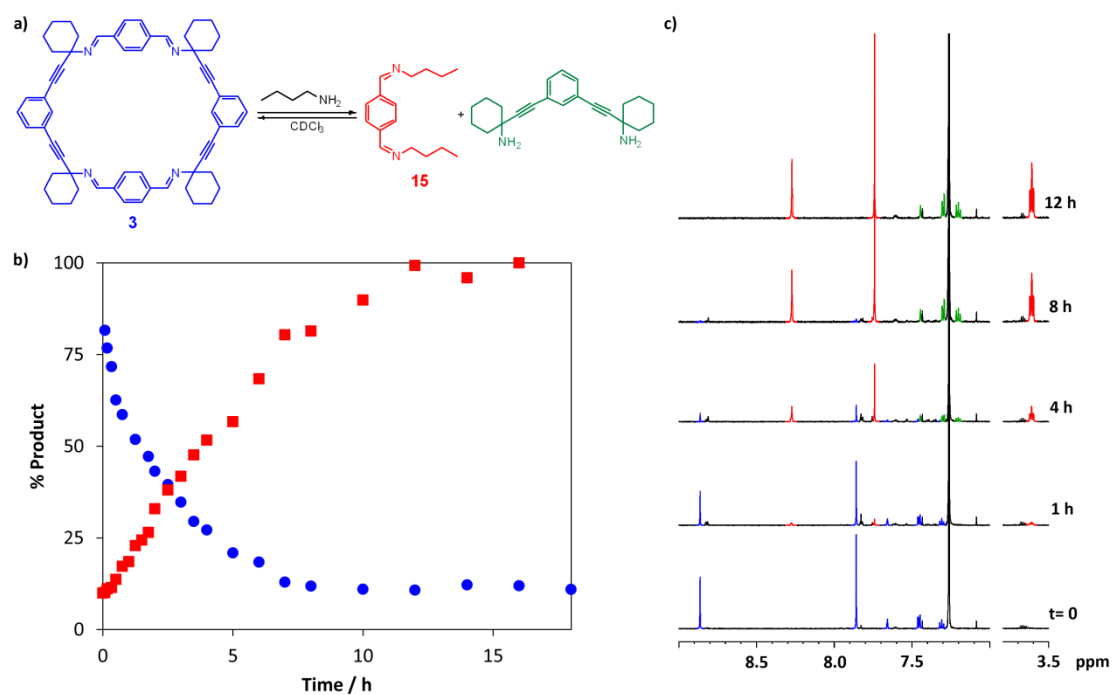


Figure 80. a) Transimination reaction between **3** (blue) and butylamine to give 2 mols of the transimination product represented in red and 2 mols of the propargyldiamine represented in green. b) Percentage of **3** (blue) and **15** at different reaction times. c) Some ¹H-NMR spectra for comparison. The time of reaction is indicated in each case.

Among the different potential guests, phthalates are interesting due to environmental and health issues. The experiments were carried out by soaking several crystals of EtPh@**3** in 1 mL of the phthalate under test. Among the phthalates tested, namely diethyl phthalate (EtPh, 232 Å³), dibutyl phthalate (BuPh, 305 Å³), dibenzyl phthalate (BnPh, 363 Å³), and 2-diethylhexylphthalate (OcPh, 451 Å³), we only observed the incorporation of EtPh into the pores of the cycloimine compound **3**. The crystalline structure of the solvate was solved by single-crystal X-ray diffraction showing a 1:2 **EtPh@3** crystallographic stoichiometry. This stoichiometry was confirmed by a weight loss of 10.86 % in the thermogravimetric analysis (TGA, See Supporting Information). In this case, the sorption of EtPh could be visually monitored (Figure 81). On the other hand, the diffusion process was followed by gas chromatography (GC) by monitoring the peak corresponding to the desorbed EtOAc (See Figure 81c, Supporting Information). An adsorption time course experiment showed that the process was completed after five hours. The NMR registered in CDCl₃ on dissolved samples of **EtPh@3** also demonstrated the 1:2 stoichiometry and the full exchange of EtOAc by EtPh.

Once exchanged with EtPh for the first time, the former crystals filled with EtOAc were recovered again if the above crystals were immersed in EtOAc for three additional days (See Supporting Information). Remarkably, we did not observe any morphological alteration of the crystal structure of **3** after several EtOAc-EtPh exchanging cycles. However, when crystals of **EtPh@3** were soaked in MeOH instead of EtOAc, the process turned irreversible. Here, the EtPh release was monitored by ¹H-NMR spectroscopy showing that the desorption process was complete after 12 hours, as shown in Figure 81b. The X-ray analysis of the remaining crystals showed that **3** evolved to the non-porous and denser polymorphic form **3(II)**.

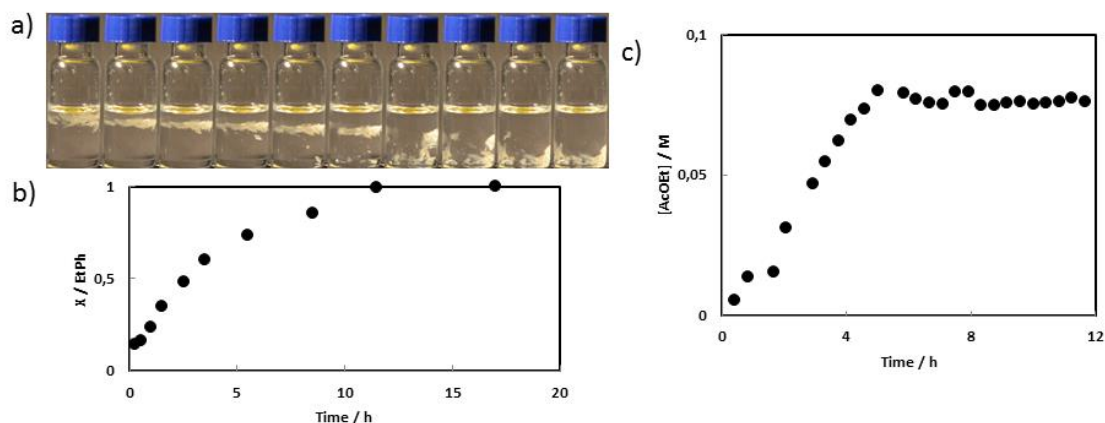


Figure 81. a) Sequential images showing **AcOEt@3** crystals that gradually sank as a function of the diethyl phthalate uptake. The images were taken every 5 min ($t_{\text{tot}} = 50$ min). b) Molar fraction of EtPh during time displaced from **EtPh@3** channels by MeOH followed by NMR. c) GC evaluation of the displacement of EtOAc molecules from **EtOAc@3** due to the exchange by EtPh.

The thermal stability, fluidity and low volatility of the higher molecular weight phthalate esters make them highly widely used as plasticizers. Phthalates are everywhere, and the health risks cause increasing concern. For these reasons, we decided to realize a preliminary test to evaluate the ability of the cycloimine **3** to absorb four of the most used phthalates in the industry, namely: diethyl phthalate (EtPh), dibutyl phthalate (BuPh), benzyl butyl phthalate (BBPh) and bis(2-ethylhexyl) phthalate (OcPh). With this objective in mind, we assayed the selective adsorption between pairs of phthalates. Sorption studies performed with compound **3** and 1:1 v/v mixtures of phthalates revealed that only EtPh was capable of displacing the EtOAc from the pores (See Figure 82). Hence, the macrocycle **3** selectively adsorb EtPh over other phthalates.

Early work on **3**, suggested the relation between the maximum available void volume per macrocycle of **3** (274 \AA^3) and the guest volume. Given the 2:1 stoichiometry for **EtPh@3** and the volume of EtPh (232 \AA^3), the packing coefficient is 0.40. This value is within the 0.55 packing limit established by Rebek for the encapsulation of guests in solution.²⁰³

²⁰³ Mecozzi, S.; Rebek Jr, J. *Chem. Eur. J.* **1998**, *4*, 1016-1022.

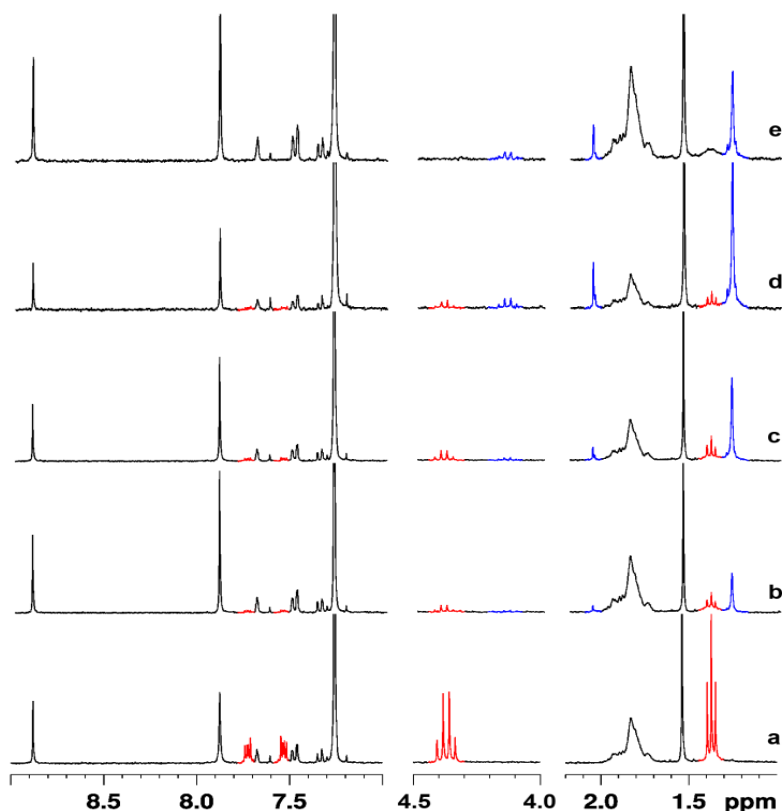


Figure 82. ¹H-NMR spectra of **EtOAc@3** after immersion during 1 day in neat EtPh (a) and in 1:1 v/v mixtures of: EtPh/BuPh (b) EtPh/BBPh (c); EtPh/OcPh (d) and BuPh/BBPh (e). In each case, the resulting crystals were washed with MeOH and dried under vacuum to remove the excess of phthalate before registering the spectra.

3.6.3 Conclusions

In conclusion, we have synthesized a set of cycloimine compounds from the condensation of aromatic propargyldiamines with aromatic dialdehydes. Most part of the obtained macrocycles was insoluble or slightly soluble in common solvents, but some of them were obtained as crystals suitable for their analysis by X-ray diffraction. Specifically, compound **3** crystallizes from the bulk EtOAc solution to form a porous structure composed of channels filled with EtOAc. It has also been demonstrated that the macrocyclic cycloimine **3** absorbs preferentially diethyl phthalate over other phthalates with bigger volume than EtPh. The phthalate sorption and desorption is a reversible process that retains the nanoporous structure of the crystals. Due to the fact that only one structure has been obtained as a crystalline porous material, we hope that modifications in the aromatic structure of the cycloimines in future work will provide crystalline materials with different porosity as well as interlocked systems for applications in catalysis, sensing or separations.

3.6.4 Supporting Information

3.6.4.1 Experimental

All reagents were purchased commercially and used without further purification. Mass spectra were registered on a MICROMASS Autospec3000 spectrometer equipped with an electrospray module or with a Bruker Autoflex (MALDI-Tof). ^1H and ^{13}C spectra were recorded on Bruker AVANCE 300 (^1H at 300 MHz and ^{13}C at 75 MHz) and on Bruker AVANCE III 600 equipped with a cryoprobe, in CDCl_3 and using the residual proton signal as reference. Chemical shifts (δ) are in ppm and coupling constants (J) in Hz. Elemental analyses (C, H, N) were conducted by the "Centro de Microanálisis Elemental" of the "Universidad Complutense de Madrid" (Spain). TG analyses were carried out using a SDT2960 TGA analyzer (TA instruments) with an automated vertical overhead thermobalance. The experiments were performed on 10 - 20 mg samples, over a temperature range of 25-600 °C at a constant heating rate of 10 °C min^{-1} , with a purge of dry nitrogen flowing at 30 mL min^{-1} . The samples were crushed, blotted dry and placed in open Pt pans for TG experiments. Single Crystal X-ray Diffraction data were collected at 100K on a Bruker-Nonius FR591 Mo $K\alpha$ rotating anode single crystal diffractometer equipped with an Apex II CCD area detector and Montel mirrors and an Oxford Cryostream Plus 700 Series. For the data collection the software *Apex2 V2010.7-0* (Bruker AXS 2010) was used.

3.6.4.2 Synthesis

General procedure for the preparation of the cycloimines

The cycloimines were prepared by slow Schiff condensation of the appropriate diamine²⁰⁴ with the corresponding dialdehyde. A typical procedure was as follows: a solution of the diamine (400 mg, 1.248 mmol) and the dialdehyde (169 mg, 1.248 mmol) in 120 mL of EtOAc was placed in a 250 mL Erlenmeyer flask. The flask was covered with parafilm and let aside at room temperature for evolution. After few days to ten weeks, the precipitated products were isolated by simple decantation of the solution. The solid amorphous or crystalline was washed with fresh EtOAc and dried.

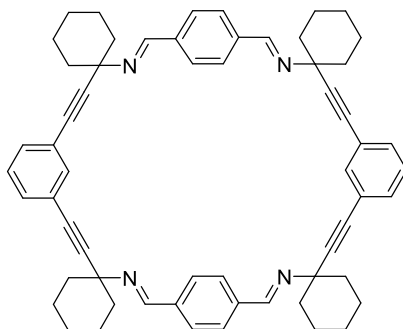
General procedure for the preparation of 3' and 8': A mixture of 1,1'-(1,3-phenylenebis(ethyne-2,1-diyl))bis(cyclohexan-1-amine) (0.468 mmol) and terephthalaldehyde (0.468 mmol) in MeOH (55 mL) was refluxed for 5 hours. After being cooled to room temperature, the precipitate formed was isolated by filtration.

The obtained solid was suspended in EtOAc (25 mL) and centrifuged. The supernatant was placed in an Erlenmeyer flask and reserved. After 2-3 days crystals of **7** were obtained from the solution (38 mg, 10% yield).

General procedure for the preparation of the diimine compounds

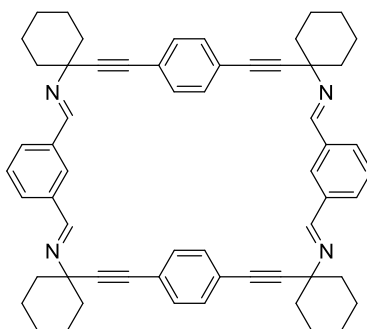
0.21 g (0.655 mmol) of diamine were dissolved in 20 mL of MeOH with 0.139 μL of benzaldehyde. The resulting solution was refluxed for 8 hours. After being cooled to room temperature the precipitation of a solid was observed. The product was filtered, washed with MeOH and dried under vacuum.

²⁰⁴ Soberats, B.; Martínez, L.; Vega, M.; Rotger, C.; Costa, A. *Adv. Synth. Catal.* **2009**, *351*, 1727-1731.



Macrocyclic tetraimine compound 3. It has been synthesized following a previous reported procedure.²⁰⁵

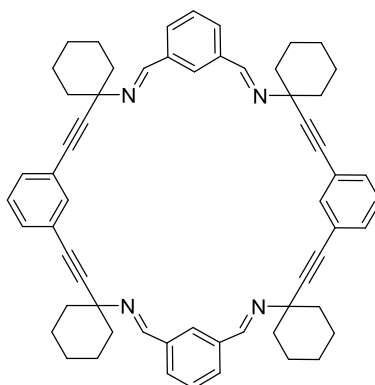
Macrocyclic tetraimine compound 3+3'. 10% yield (from EtOAc). m.p. > 250 °C (dec.). ¹H NMR (600 MHz, CDCl₃), δ (ppm): 8.87 (s, 4H), 8.83 (s, 4H), 7.87 (s, 8H), 7.84 (s, 8H), 7.67 (s, 2H), 7.63 (s, 2H), 7.47 (d, *J* = 6 Hz, 8H), 7.32 (t, *J* = 7.6 Hz, 2H), 1.82 (m, 20H). ESI-MS (+) *m/z* (%): calc. C₆₀H₆₁N₄ 837.4896; exp. 837.5201 [M+H]⁺. Anal. Calcd. for C₆₀H₆₀N₄: C, 86.08; H, 7.22; N, 6.69. Found: C, 84.32; H, 7.09; N, 6.51.



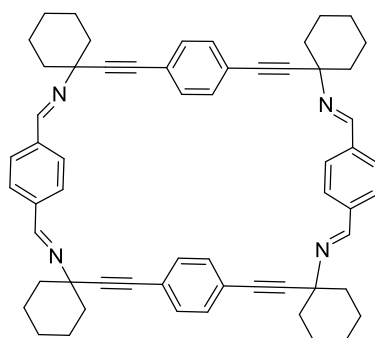
Macrocyclic tetraimine compound 8. 25% yield (from EtOAc). m.p. > 250 °C (dec.). ¹H NMR (600 MHz, CDCl₃), δ (ppm): 8.85 (s, 4H), 8.19 (d, *J* = 7.2 Hz, 4H), 7.62 (s, 2H), 7.48 (s, 10H), 1.81 (m, 40H); ¹³C NMR (75 MHz, CDCl₃) δ 157.3, 136.9, 133.1, 131.8, 129.3, 128.2, 123.1, 92.53, 89.5, 63.9, 39.9, 29.8, 25.5, 23.2; ESI-HRMS(+) *m/z* (%): calc. C₆₀H₆₀N₄ 837.4896; exp. 837.4905 [M+H]⁺; IR(KBr) $\tilde{\nu}$ = 3416.6, 3045.6, 2928.5, 2852.9, 1907.9, 1737.5, 1704.2, 1638.0, 1505.5, 1444.8, 1403.1, 1354.7, 1337.1, 1260.1, 1162.6, 1099.9, 1059.0, 972.1, 948.4, 923.0, 902.4, 854.0, 835.1, 803.9, 690.9, 649.5 cm⁻¹. Anal. Calcd. for C₆₀H₆₀N₄: C, 86.08; H, 7.22; N, 6.69. Found: C, 84.08; H, 7.14; N, 6.53.

Macrocyclic tetraimine compound 8+8'. 23% yield (from EtOAc). m.p. > 250 °C (dec.). ¹H NMR (600 MHz, CDCl₃), δ (ppm): 8.87 (s, 4H), 8.85 (s, 4H), 8.19 (d, *J* = 6 Hz, 4H), 7.86 (d, *J* = 7.2 Hz, 6H), 7.61 (d, *J* = 7.4 Hz, 2H), 7.47 (s, 10H), 1.81 (m, 40H); ESI-HRMS(+) *m/z* (%): calc. C₆₀H₆₀N₄ 837.4896; exp. 837.4905 [M+H]⁺; IR(KBr) $\tilde{\nu}$ = 3421.7, 3061.8, 3036.7, 2929.8, 2853.3, 1702.9, 1639.8, 1505.3, 1444.6, 1337.2, 1298.4, 1262.3, 1161.4, 1149.5, 1054.8, 971.2, 946.3, 903.1, 835.0, 793.8, 721.7, 689.9, 648.5 cm⁻¹. Anal. Calcd. for C₆₀H₆₀N₄: C, 86.08; H, 7.22; N, 6.69. Found: C, 84.32; H, 7.11; N, 6.56.

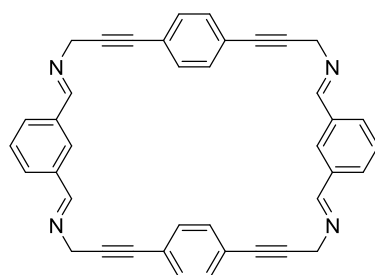
²⁰⁵ Sanna, E.; Escudero-Adán, E. C.; Bauzá, A.; Ballester, P.; Frontera, A.; Rotger, C.; Costa, A. *Chem. Sci.* **2015**, *6*, 5466-5472.



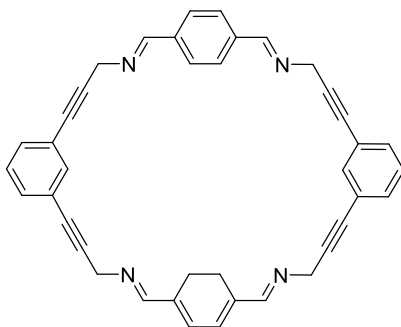
Macrocyclic tetraimine compound 9. 16% yield (from EtOAc). m.p. > 250 °C (dec.). ^1H NMR (600 MHz, CDCl_3), δ (ppm): 8.87 (s, 4H), 8.19 (s, 2H), 7.86 (s, $J = 7.8$ Hz, 4H), 7.63 (s, 2H), 7.45 (d, $J = 7.5$ Hz, 4H), 7.32 (t, $J = 4.8$ Hz, 4H), 1.80 (m, 40H); ESI-HRMS(+) m/z (%): calc. $\text{C}_{60}\text{H}_{61}\text{N}_4$ 837.4890; exp. 837.4891 $[\text{M}+\text{H}]^+$.



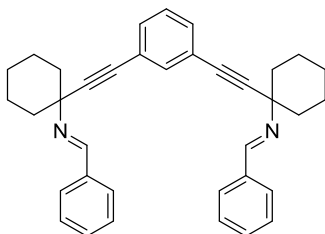
Macrocyclic tetraimine compound 10. 21% yield (from EtOAc). m.p. > 250 °C (dec.). ^1H NMR (600 MHz, CDCl_3), δ (ppm): 8.84 (s, 4H), 7.85 (s, 8H), 7.47 (s, 8H), 1.83 (m, 40H); ESI-HRMS(+) m/z (%): calc. $\text{C}_{60}\text{H}_{61}\text{N}_4$ 837.4896; exp. 837.4885 $[\text{M}+\text{H}]^+$.



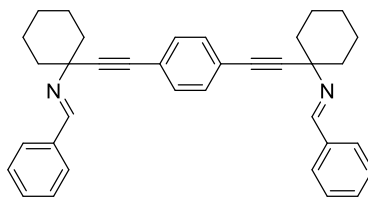
Macrocyclic tetraimine compound 11. 22% yield (from EtOAc). m.p. > 250 °C (dec.). ^1H NMR (600 MHz, CDCl_3), δ (ppm): 8.75 (s, 4H), 8.01 (d, $J = 7.8$ Hz, 4H), 7.97 (s, 2H), 7.51 (t, $J = 7.2$ Hz, 2H), 7.47 (s, 8H), 4.81 (s, 8H); ESI-HRMS(+) m/z (%): calc. $\text{C}_{40}\text{H}_{29}\text{N}_4$ 565.2392; exp. 565.2373 $[\text{M}+\text{H}]^+$; Anal. Calcd. for $\text{C}_{40}\text{H}_{28}\text{N}_4$: C, 85.08; H, 5.00; N, 9.92. Found: C, 83.15; H, 4.99; N, 10.11.



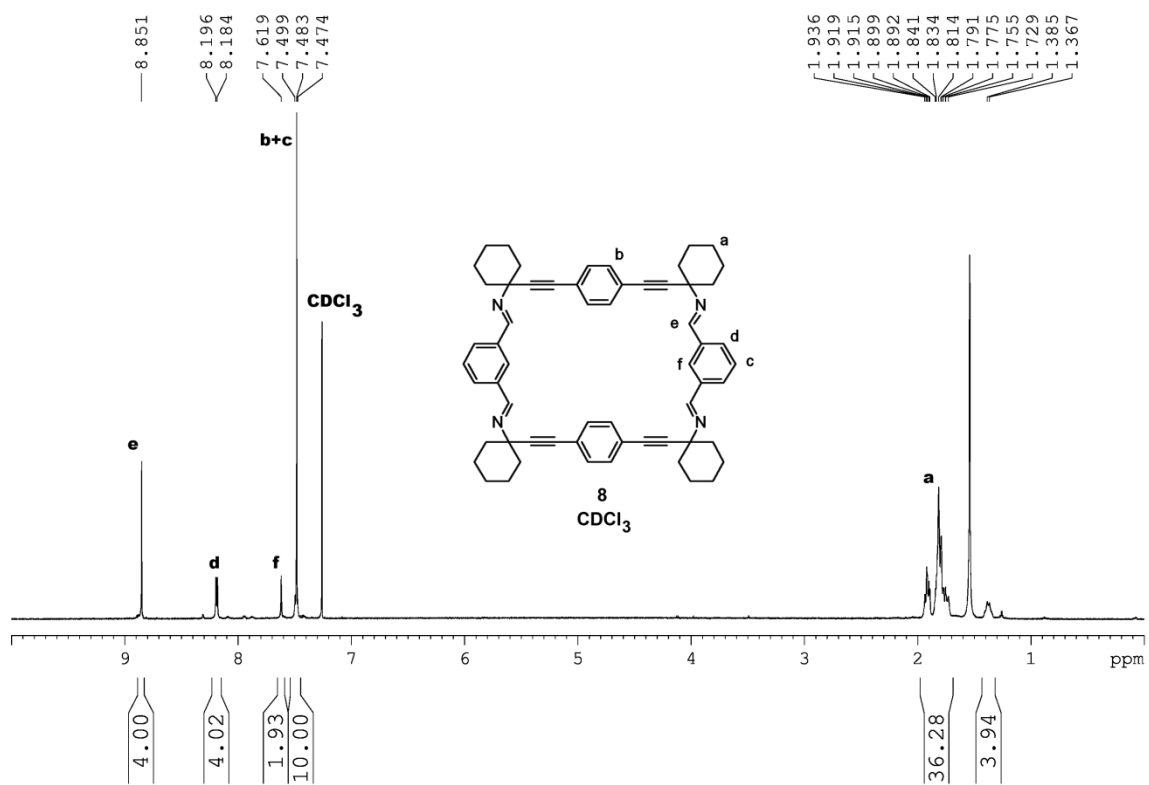
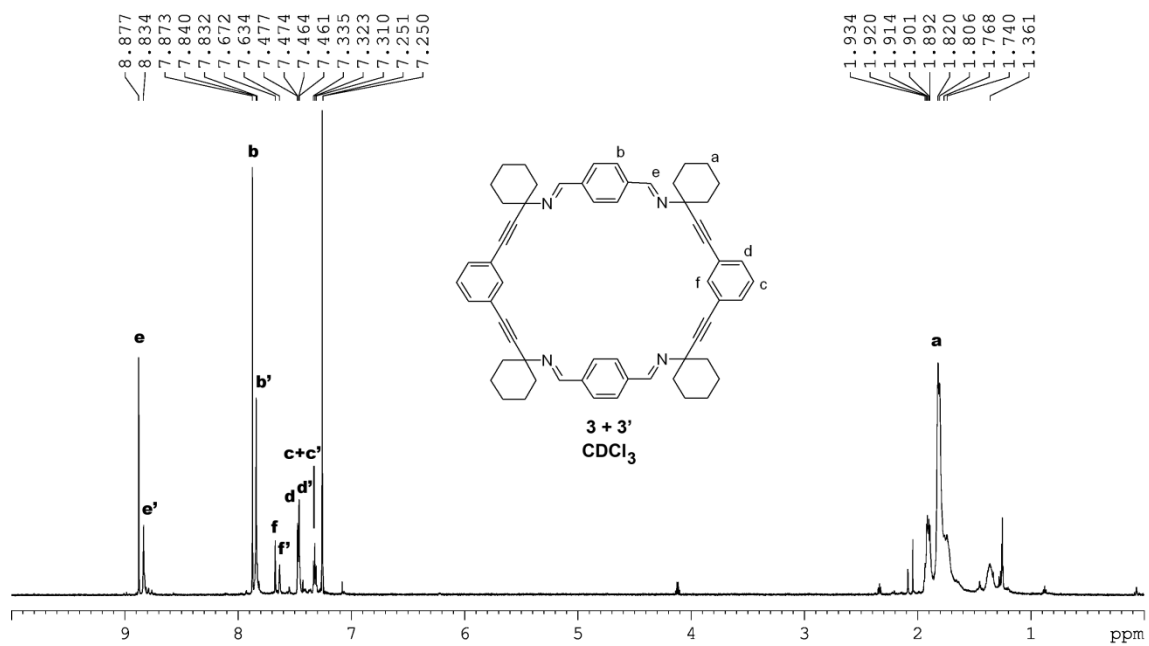
Macrocyclic tetraimine compound 12. 15% yield (from EtOAc). m.p. > 250 °C (dec.). ^1H NMR (600 MHz, CDCl_3), δ (ppm): 8.69 (s, 4H), 7.88 (s, 8H), 7.71 (s, 2H), 7.40 (t, $J = 6.9$ Hz, 6H), 4.77 (s, 8H); ESI-HRMS(+) m/z (%): calc. $\text{C}_{40}\text{H}_{29}\text{N}_4$ 565.2392; exp. 565.2379 $[\text{M}+\text{H}]^+$.

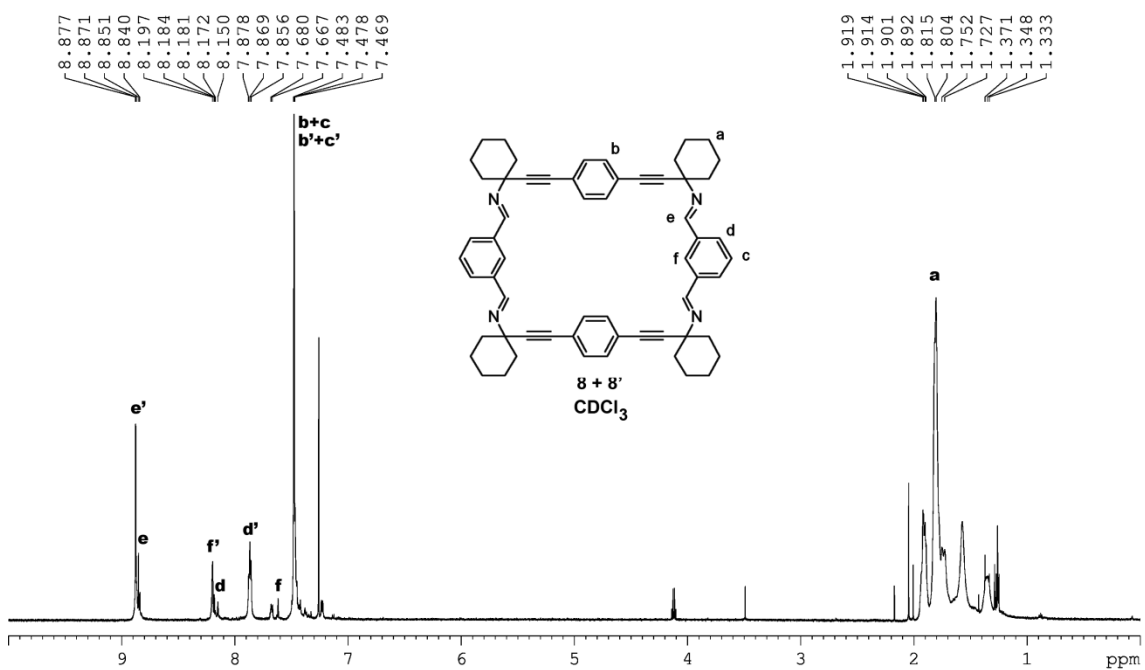
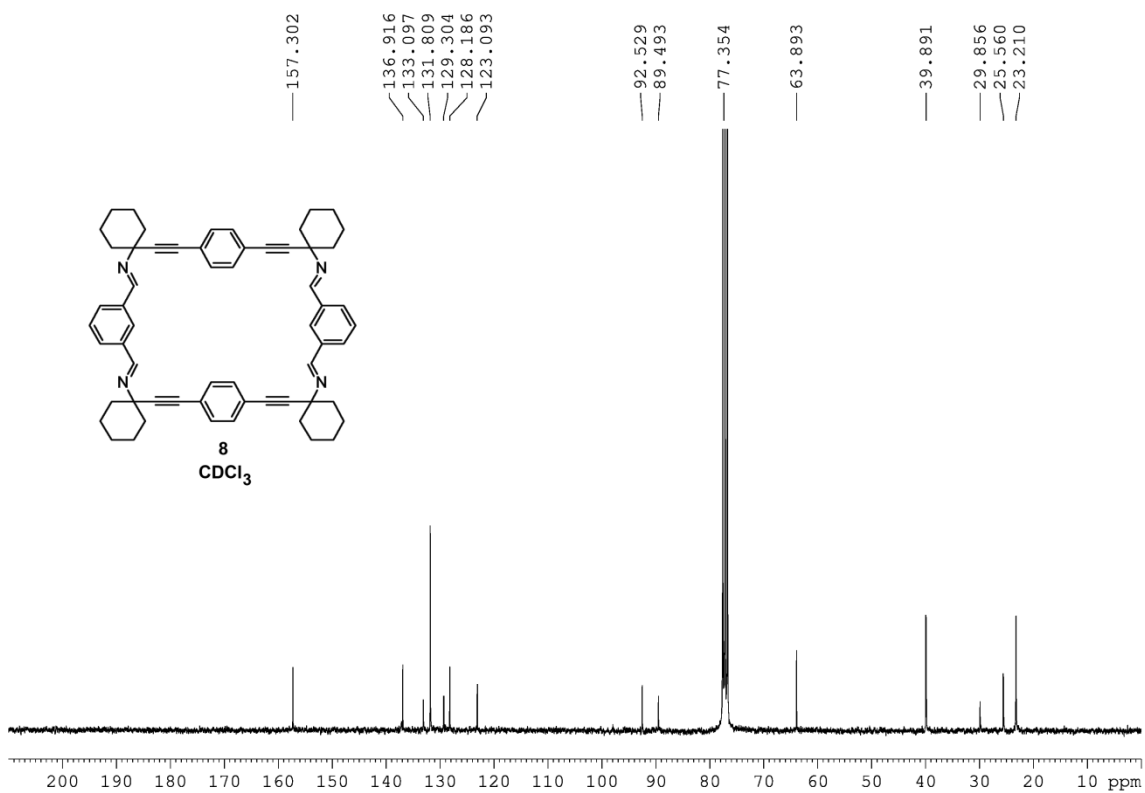


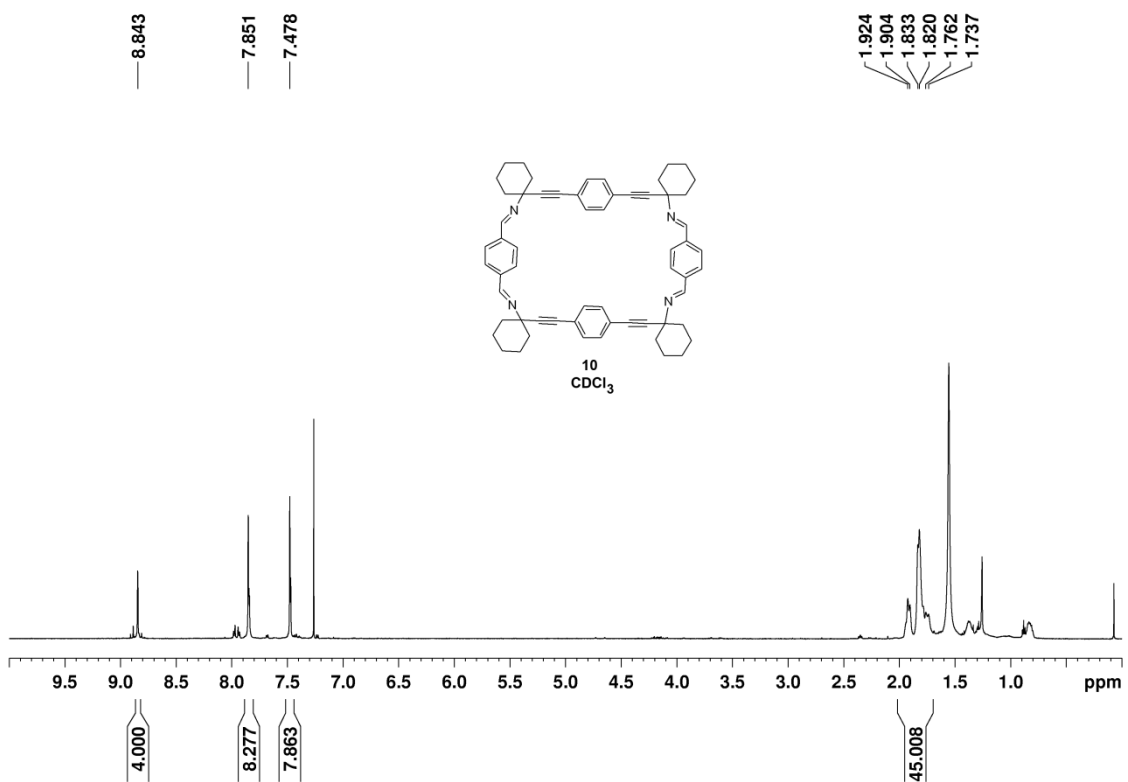
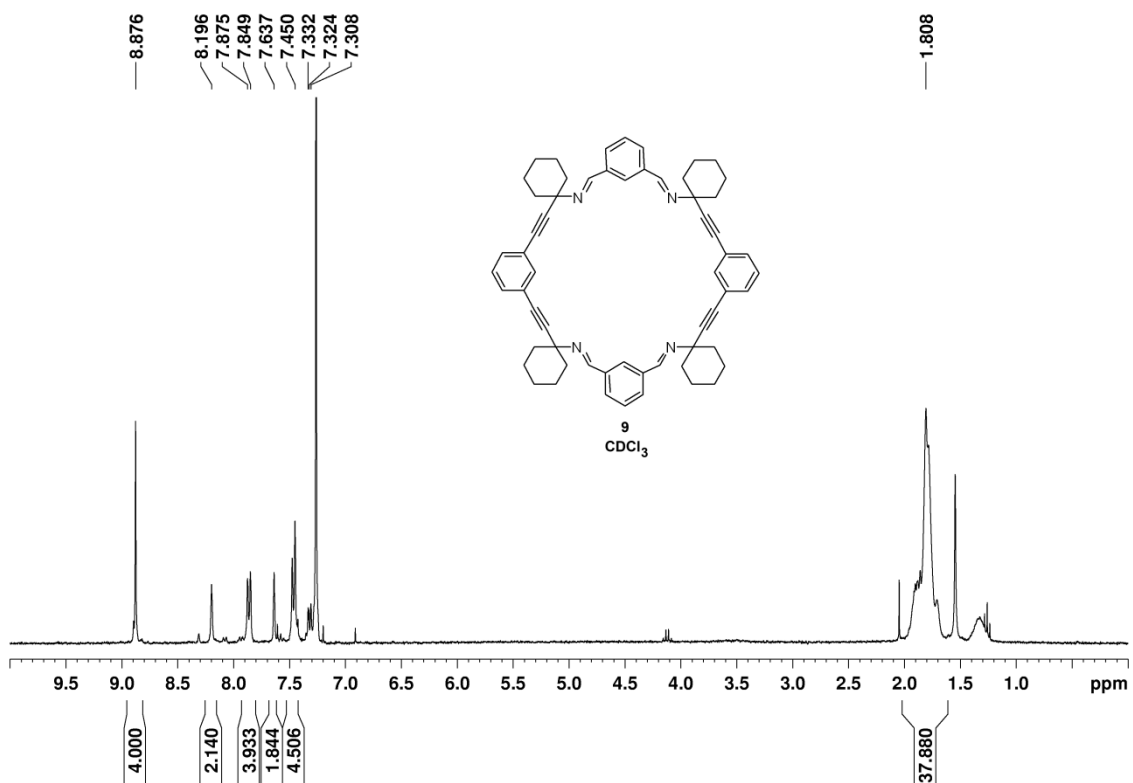
(1E,1'E)-N,N'-((1,3-phenylenebis(ethyne-2,1-diyl))bis(cyclohexane-1,1-diyl))bis(1-phenylmethanimine) (13). 61% yield. m.p. = 121-124 °C. ^1H NMR (300 MHz, CDCl_3) δ 8.84 (s, 2H), 7.82 (m, 4H), 7.64 (s, 1H), 7.47 (d, $J = 7.2$ Hz, 2H), 7.42 (m, 6H), 7.33 (t, $J = 7.95$ Hz, 1H), 1.87 (m, 20H); ^{13}C NMR (75 MHz, CDCl_3) δ 158.2, 136.7, 134.9, 131.5, 130.6, 128.7, 128.5, 123.7, 92.01, 88.7, 63.7, 39.9, 25.6, 23.3; ESI-HRMS(+) m/z (%): calc. $\text{C}_{36}\text{H}_{37}\text{N}_2$ 497.2957; exp. 497.2949 $[\text{M}+\text{H}]^+$. Anal. Calcd. for $\text{C}_{36}\text{H}_{36}\text{N}_2$: C, 87.05; H, 7.31; N, 5.64. Found: C, 86.44; H, 7.21; N, 5.71.

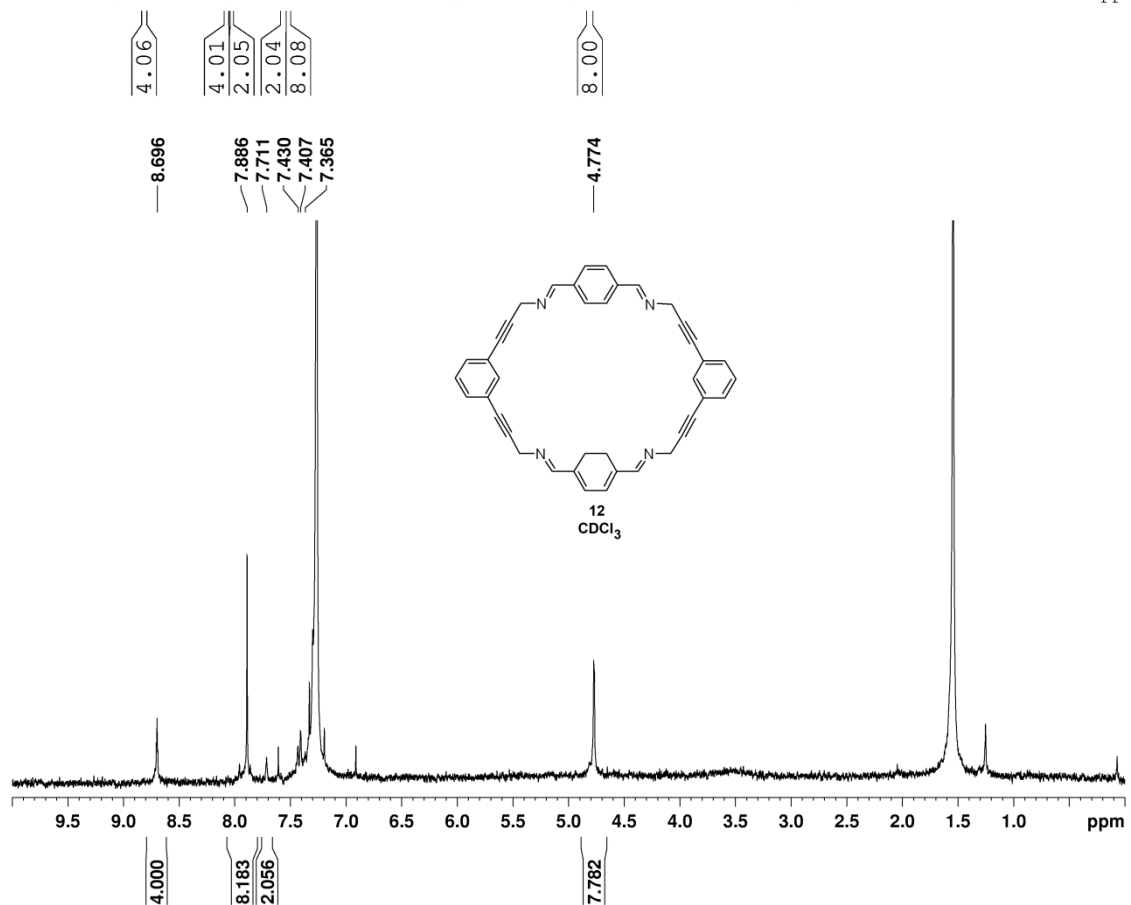
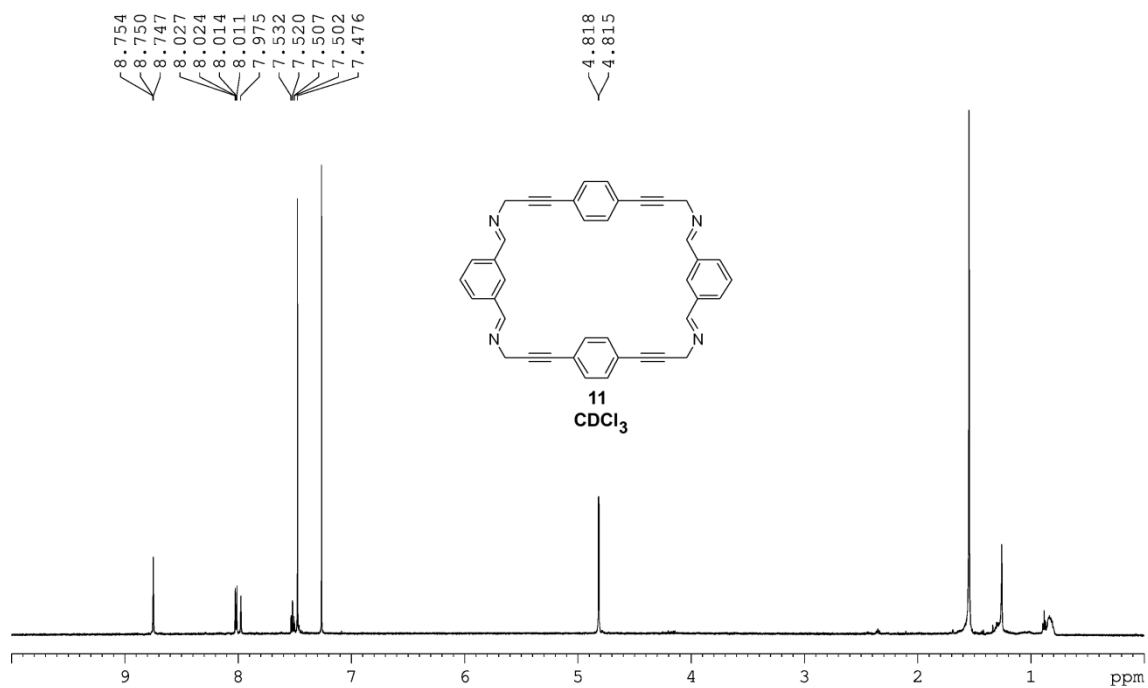


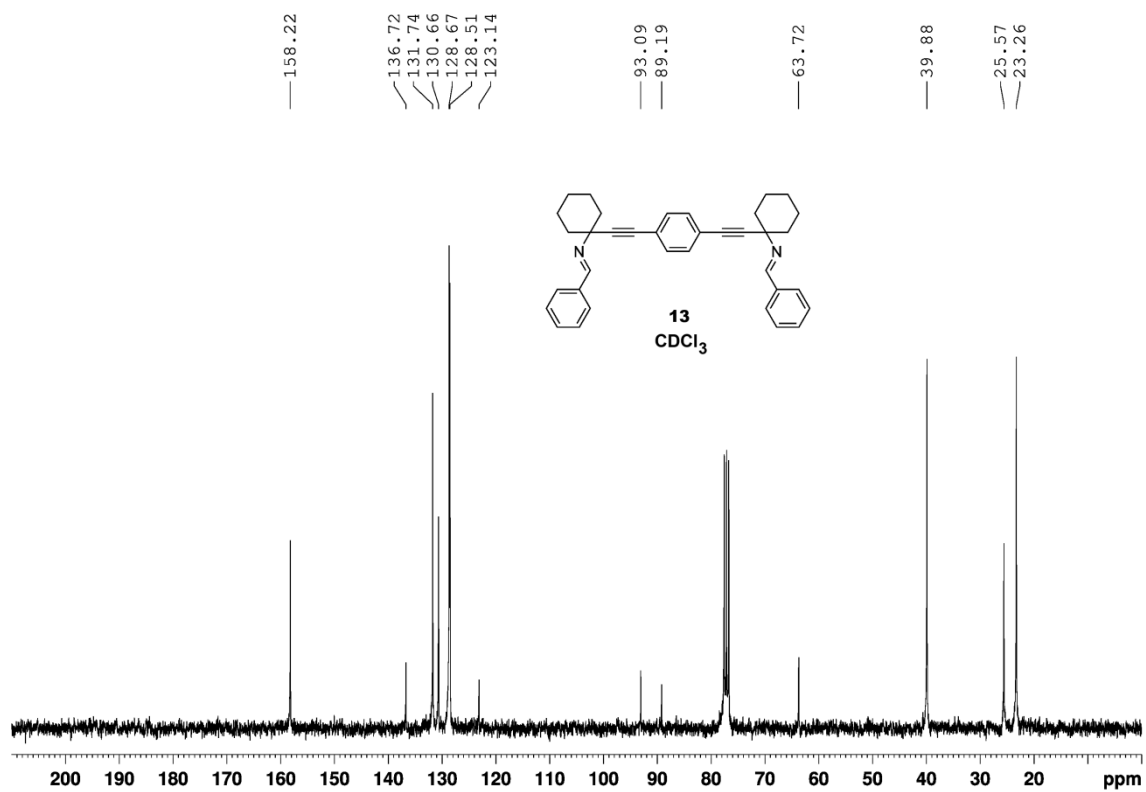
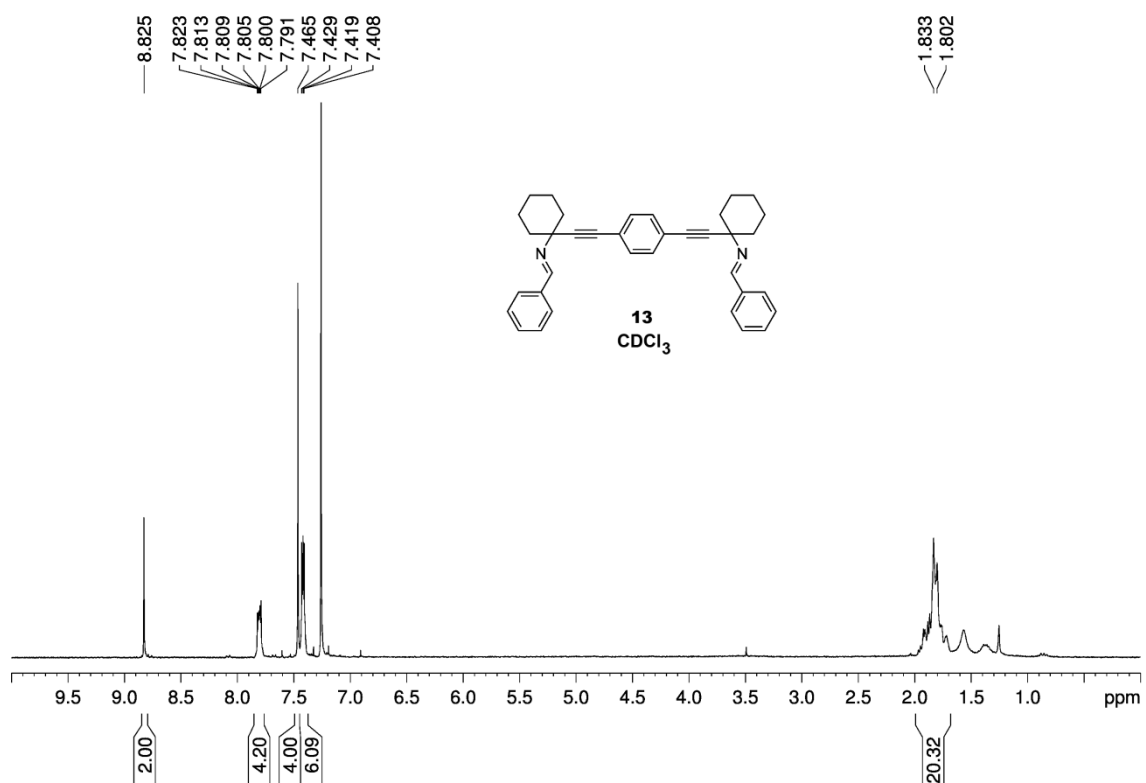
(1E,1'E)-N,N'-((1,4-phenylenebis(ethyne-2,1-diyl))bis(cyclohexane-1,1-diyl))bis(1-phenylmethanimine) (14). 72% yield. mp = 110-112 °C; ^1H NMR (300 MHz, CDCl_3) δ 8.86 (s, 2H), 7.84 (m, 4H), 7.50 (s, 4H), 7.45 (t, $J = 3$ Hz, 6H), 1.87 (m, 20H); ^{13}C NMR (75 MHz, CDCl_3) δ 158.2, 136.7, 131.7, 130.7, 128.7, 128.5, 123.1, 93.1, 89.2, 63.7, 39.9, 25.6, 23.3; ESI-HRMS(+) m/z (%): calc. $\text{C}_{36}\text{H}_{36}\text{NaN}_2$ 519.2776; exp. 519.2770 $[\text{M}+\text{Na}]^+$. Anal. Calcd. for $\text{C}_{36}\text{H}_{36}\text{N}_2$: C, 87.05; H, 7.31; N, 5.64. Found: C, 85.16; H, 7.22; N, 5.55.

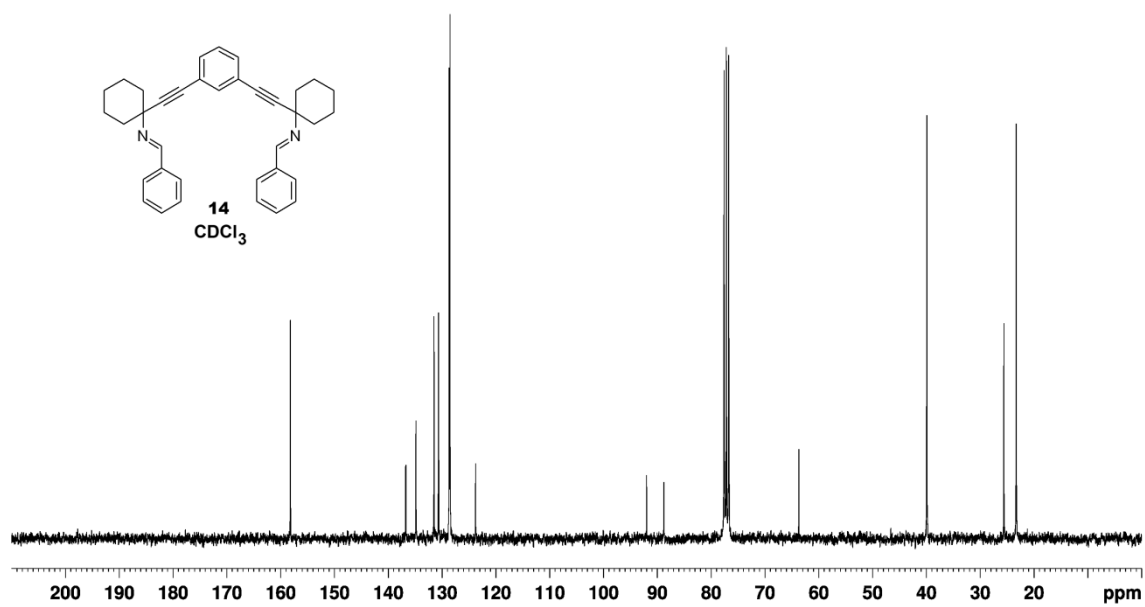
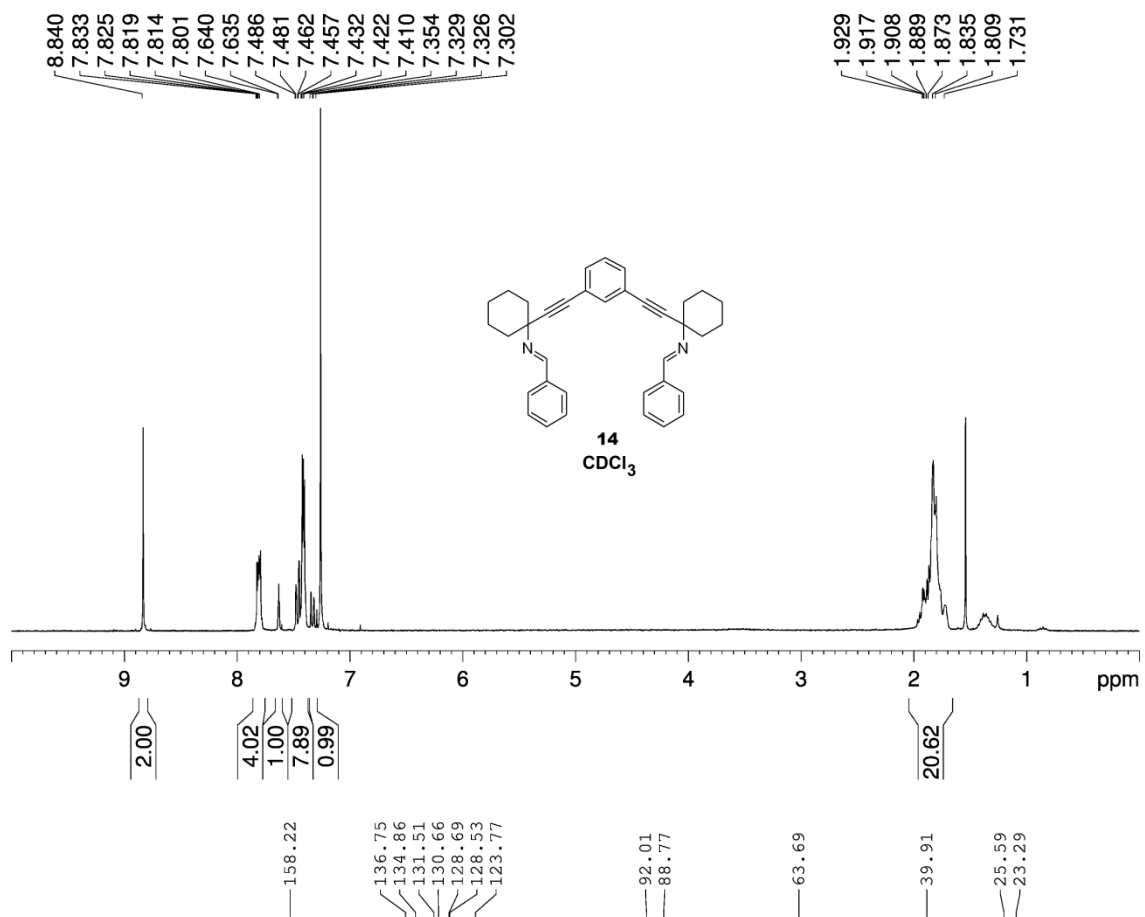












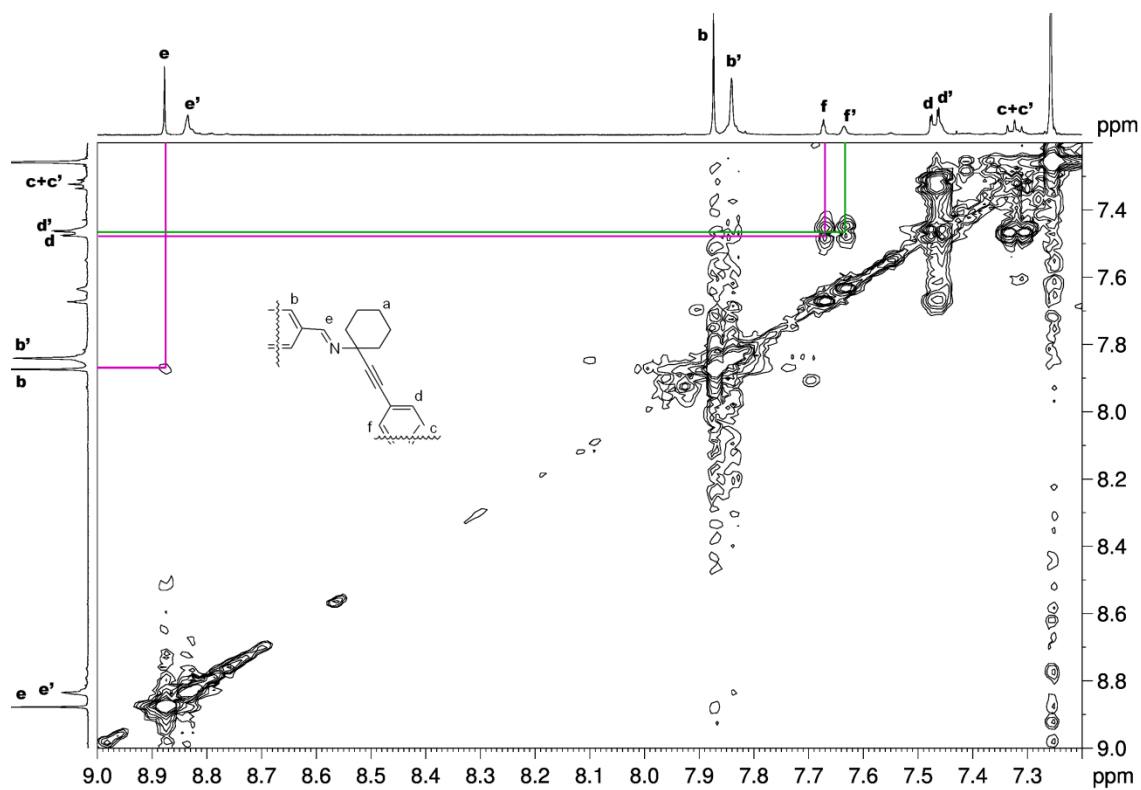


Figure S28. Partial 2D COSY spectrum of **3** (pink) + **3'** (green) in CDCl₃ at 298 K.

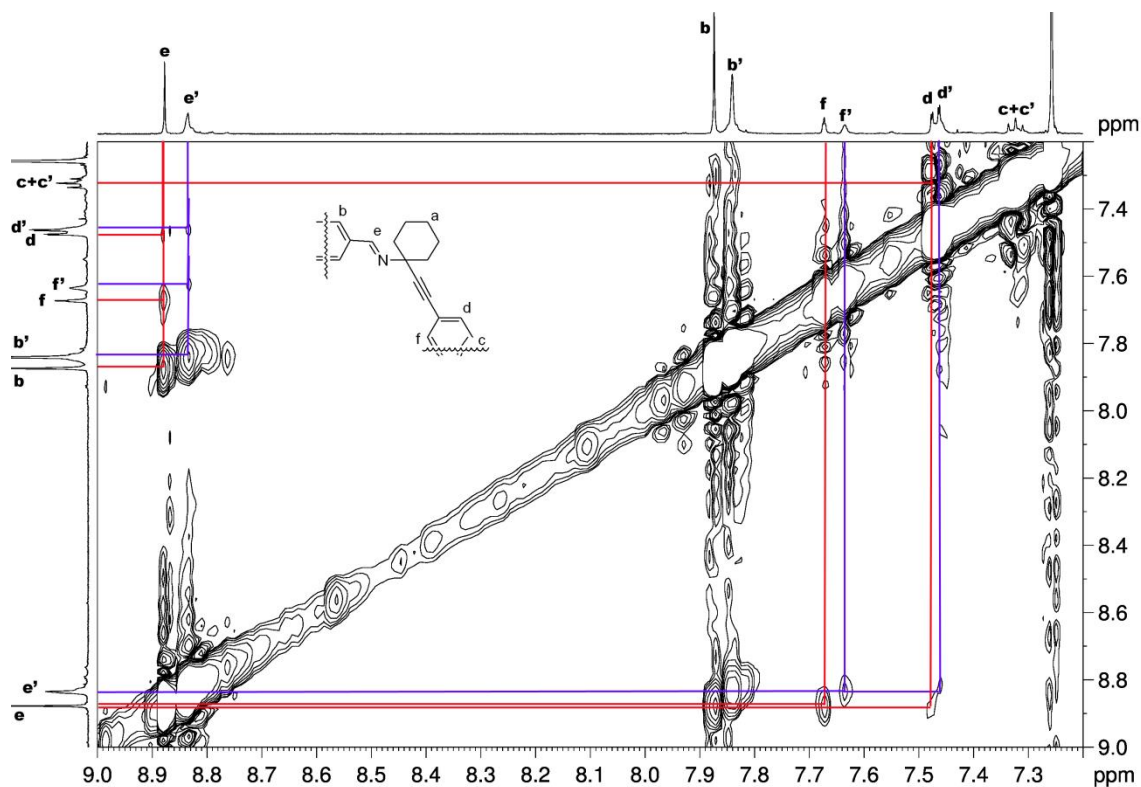


Figure S29. Partial 2D ROESY spectrum of **3** (red) + **3'** (blue) in CDCl₃ at 298 K.

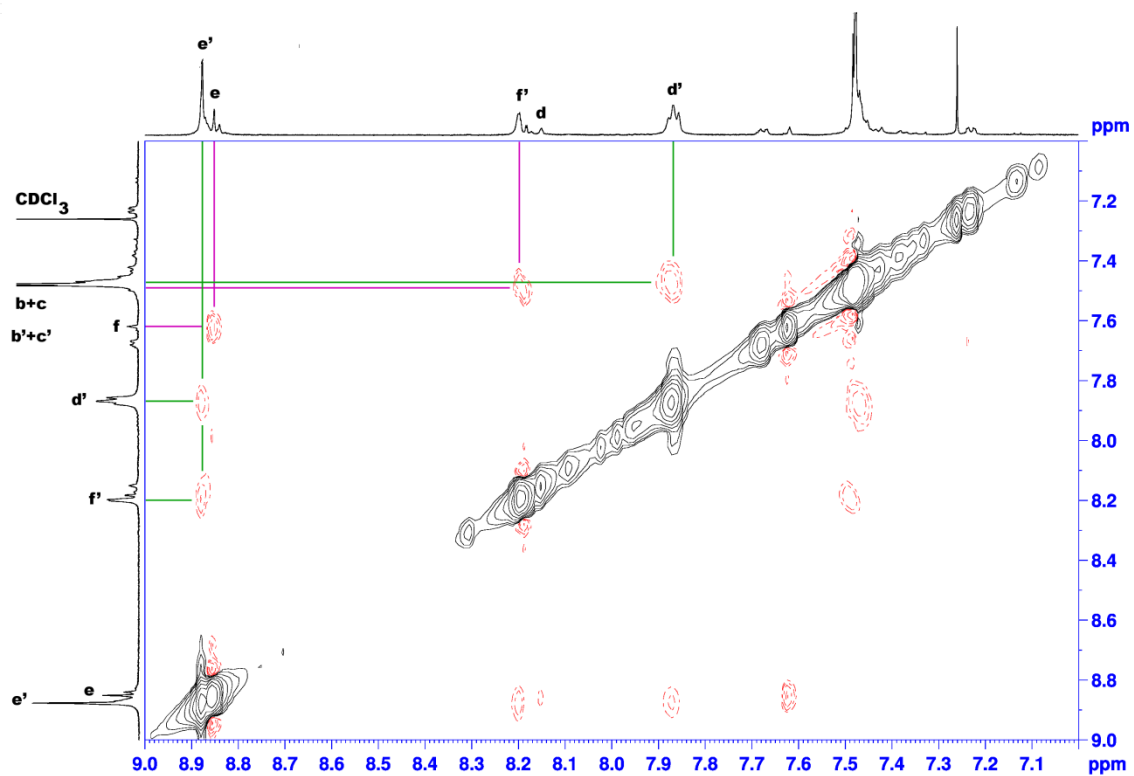


Figure S30. Partial 2D ROESY NMR spectra of compounds: **8** (purple) and **8'** (green).

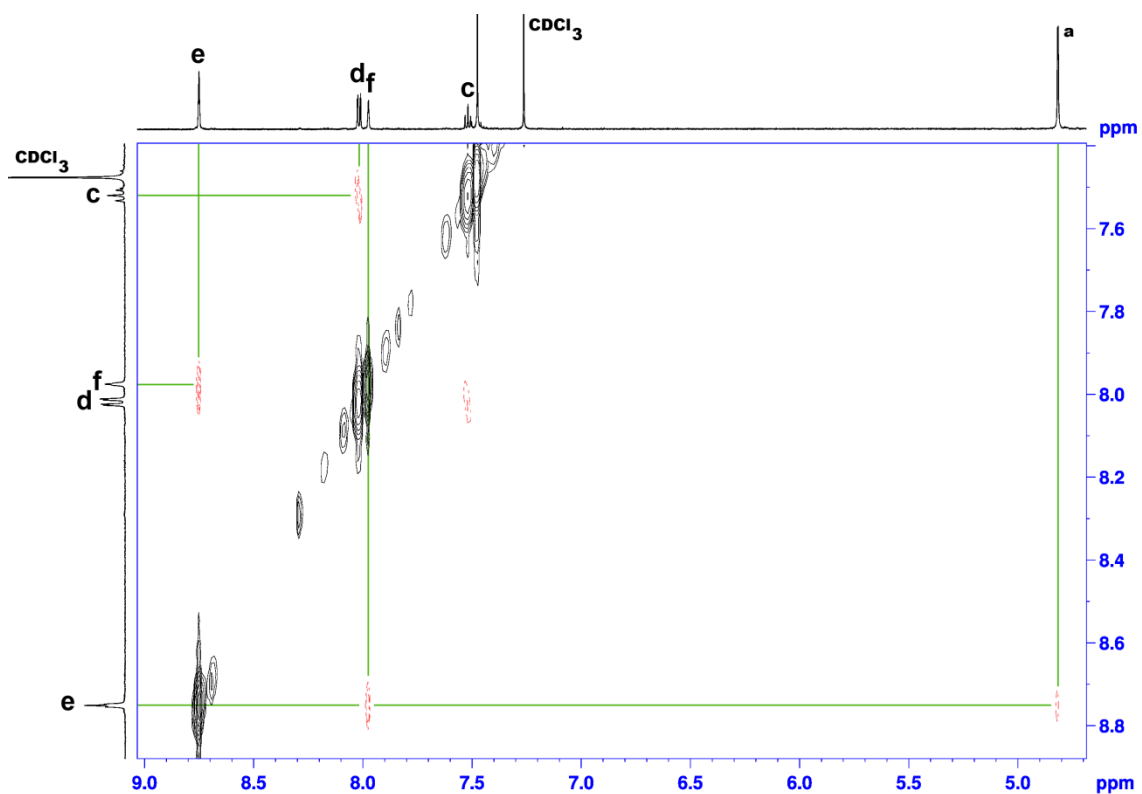


Figure S31. Partial 2D ROESY NMR spectra of compound **11**.

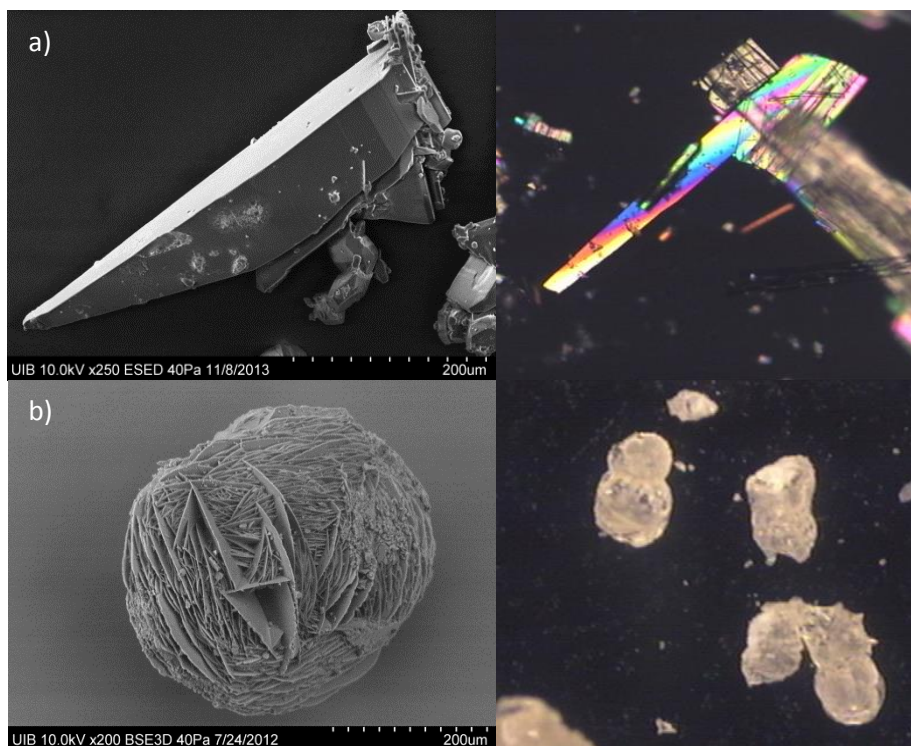


Figure S32. Scanning electron microscope images (left) and optic microscope images (right) of: a) **AcOEt@3** and b) **8**.

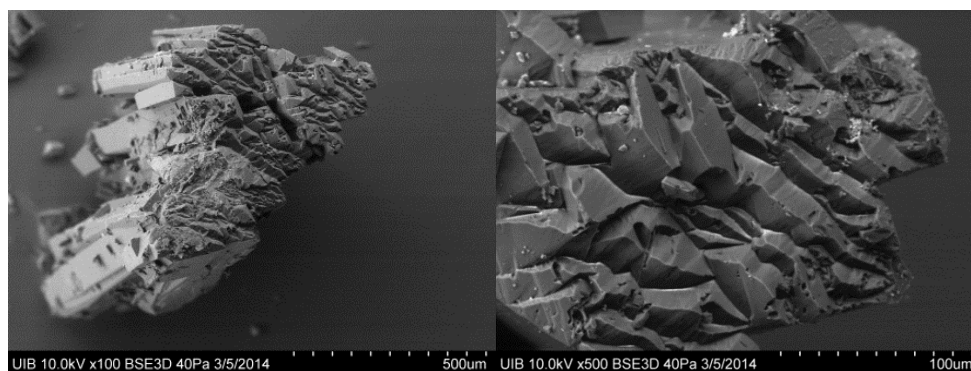
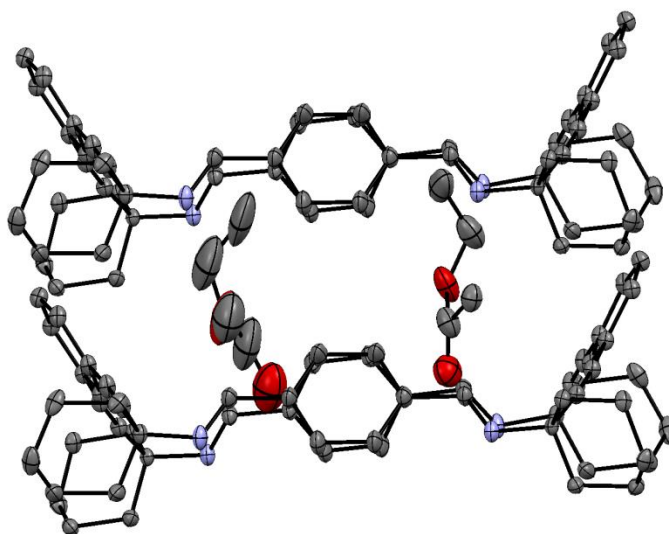
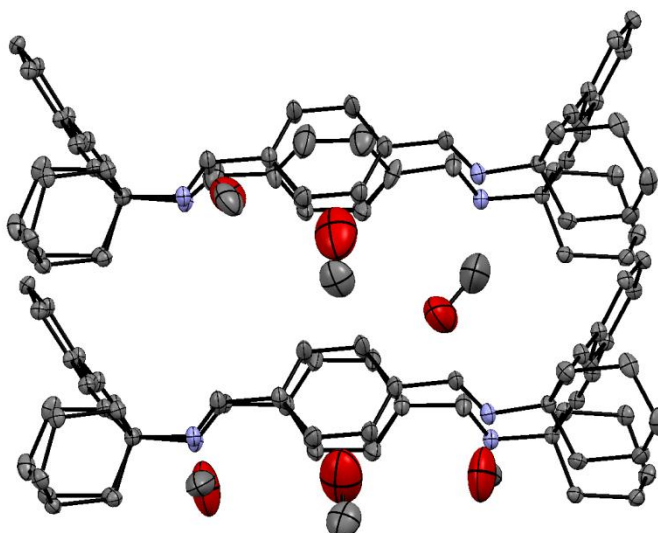


Figure S33. SEM images of a desolvated crystal of **3(II)**.

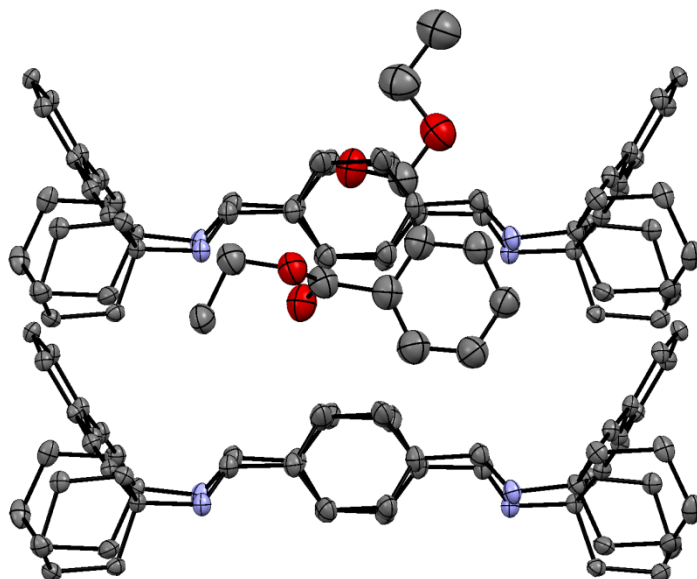
3.6.4.3 Crystal Data of Solvates



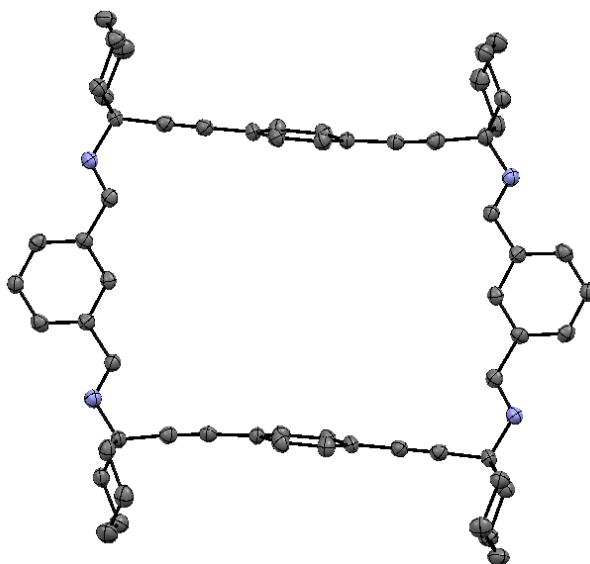
Crystal data for EtOAc@3: $C_{64}H_{68}N_4O_2$, $M = 925.22$, monoclinic, $a = 34.828(3) \text{ \AA}$, $b = 5.8364(5) \text{ \AA}$, $c = 28.023(2) \text{ \AA}$, $\alpha = 90.00^\circ$, $\beta = 97.911(2)^\circ$, $\gamma = 90.00^\circ$, $V = 5642.0(8) \text{ \AA}^3$, $T = 100(2) \text{ K}$, space group $C2/c$, $Z = 4$, 18372 reflections measured, 18372 independent reflections ($R_{int} = 0.0000$). The final R_1 values were 0.0710 ($I > 2\sigma(I)$). The final $wR(F^2)$ values were 0.2048 ($I > 2\sigma(I)$). The final R_1 values were 0.0922 (all data). The final $wR(F^2)$ values were 0.2274 (all data).



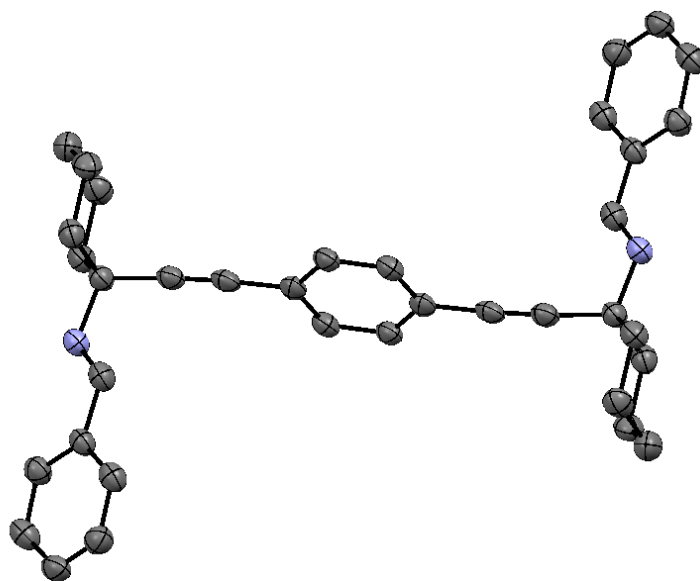
Crystal data for MeOH@3: $C_{63}H_{72}N_4O_3$, $M = 933.25$, monoclinic, $a = 34.830(2) \text{ \AA}$, $b = 5.7840(4) \text{ \AA}$, $c = 28.0834(19) \text{ \AA}$, $\alpha = 90.00^\circ$, $\beta = 98.727(2)^\circ$, $\gamma = 90.00^\circ$, $V = 5592.0(7) \text{ \AA}^3$, $T = 100(2) \text{ K}$, space group $C2/c$, $Z = 4$, 12600 reflections measured, 12600 independent reflections ($R_{int} = 0.0000$). The final R_1 values were 0.0779 ($I > 2\sigma(I)$). The final $wR(F^2)$ values were 0.2029 ($I > 2\sigma(I)$). The final R_1 values were 0.1065 (all data). The final $wR(F^2)$ values were 0.2193 (all data).



Crystal data for EtPh@3: $C_{66}H_{67}N_4O_2$, $M = 948.24$, monoclinic, $a = 34.890(3) \text{ \AA}$, $b = 5.8074(4) \text{ \AA}$, $c = 28.103(2) \text{ \AA}$, $\alpha = 90.00^\circ$, $\beta = 98.310(2)^\circ$, $\gamma = 90.00^\circ$, $V = 5634.4(7) \text{ \AA}^3$, $T = 100(2) \text{ K}$, space group $C2/c$, $Z = 4$, 24070 reflections measured, 24070 independent reflections ($R_{int} = 0.0000$). The final R_1 values were 0.0717 ($I > 2\sigma(I)$). The final $wR(F^2)$ values were 0.2167 ($I > 2\sigma(I)$). The final R_1 values were 0.0841 (all data). The final $wR(F^2)$ values were 0.2318 (all data).



Crystal data for 8: $C_{60}H_{60}N_4$, $M = 837.12$, monoclinic, $a = 10.9226(8) \text{ \AA}$, $b = 10.4233(9) \text{ \AA}$, $c = 20.7193(17) \text{ \AA}$, $\alpha = 90.00^\circ$, $\beta = 97.876(3)^\circ$, $\gamma = 90.00^\circ$, $V = 2336.6(3) \text{ \AA}^3$, $T = 100(2) \text{ K}$, space group $P2(1)/c$, $Z = 2$, 3982 reflections measured, 3982 independent reflections ($R_{int} = 0.0000$). The final R_1 values were 0.0674 ($I > 2\sigma(I)$). The final $wR(F^2)$ values were 0.1751 ($I > 2\sigma(I)$). The final R_1 values were 0.1278 (all data). The final $wR(F^2)$ values were 0.2043 (all data).



Crystal data for 14: $C_{36}H_{36}N_2$, $M = 496.67$, monoclinic, $a = 9.710(10) \text{ \AA}$, $b = 5.980(4) \text{ \AA}$, $c = 24.309(15) \text{ \AA}$, $\alpha = 90^\circ$, $\beta = 92.459(16)^\circ$, $\gamma = 90^\circ$, $V = 1410.3(19) \text{ \AA}^3$, $T = 100(2) \text{ K}$, space group $P2(1)/c$, $Z = 2$, 7581 reflections measured, 2792 independent reflections ($R_{int} = 0.1508$). The final R_1 values were 0.0840 ($I > 2\sigma(I)$). The final $wR(F^2)$ values were 0.1940 ($I > 2\sigma(I)$). The final R_1 values were 0.1611 (all data). The final $wR(F^2)$ values were 0.2341 (all data).

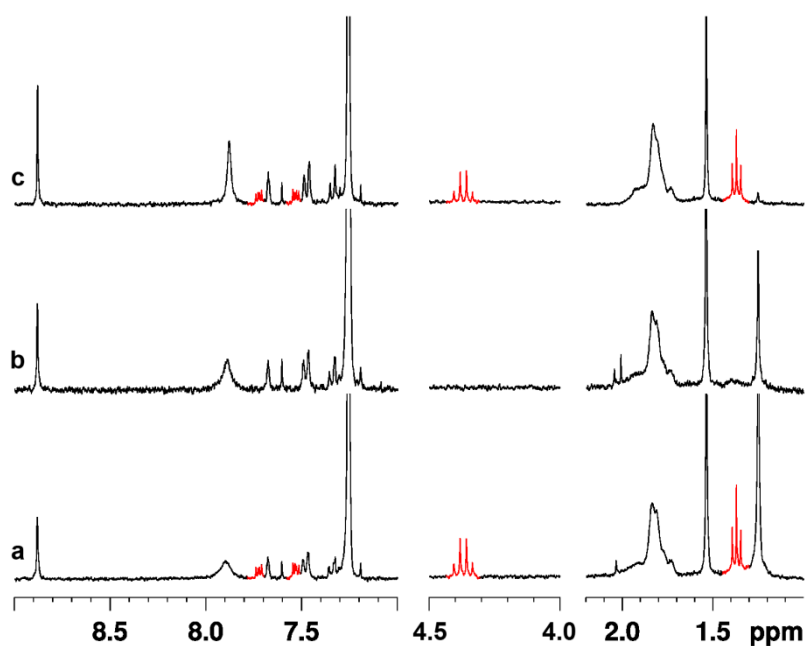


Figure S34. $^1\text{H-NMR}$ spectra of the same crystals of **EtOAc@3** after treatment with: EtPh 3 days (a), EtOAc 4 days (b) and EtPh 3 days (c) showing the reversibility of the process.

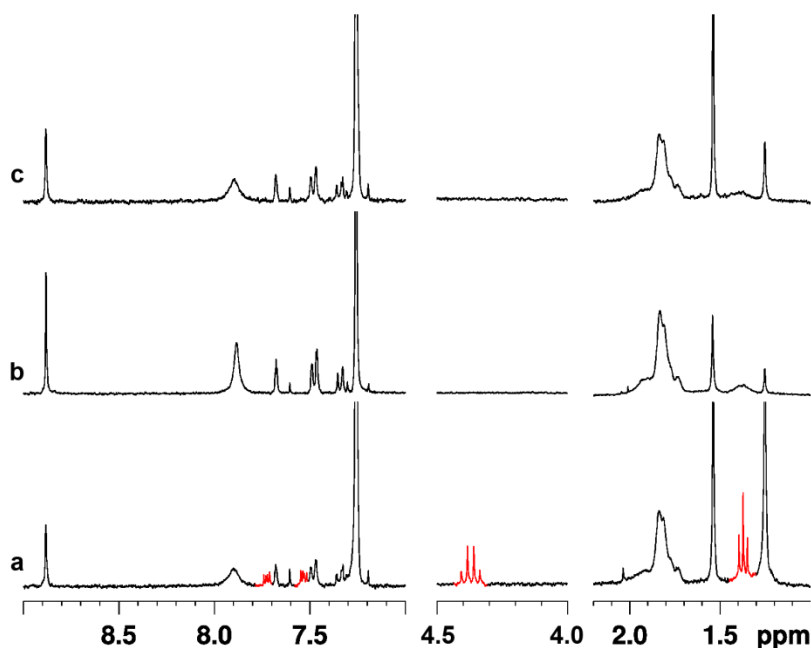


Figure S35. $^1\text{H-NMR}$ spectra of the same crystals of **EtOAc@3** after treatment with: EtPh 3 days (a), MeOH 4 days (b) and EtPh 3 days (c) showing the irreversibility of the process.

3.6.4.4 Desorption studies of EtOAc by gas chromatography

For this study, 50.9 mg of crystals of **3** filled with EtOAc previously washed with *n*-pentane (3×1.5 mL) and dried under vacuum, were soaked in 1.5 mL of EtPh. The gas chromatograms of the sample were recorded every 25 minutes and the area of the peak corresponding to the EtOAc was measured. The total concentration of EtOAc was calculated theoretically from the stoichiometry calculated in the previous work from the X-ray analysis and the $^1\text{H-NMR}$ spectra that corresponds to a 4:3 EtOAc:**3** complex. The concentration of free EtOAc was calculated from extrapolation into the calibration curve previously calculated that is shown in Figure S36.

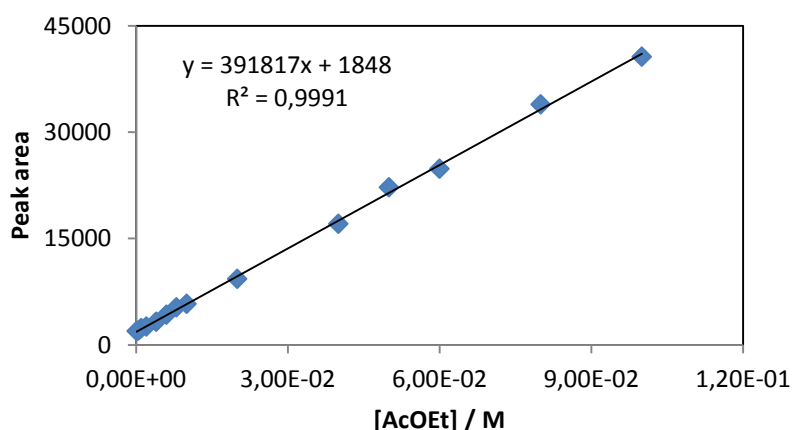


Figure S36. Calibration curve for EtOAc in EtPh calculated by gas chromatography.

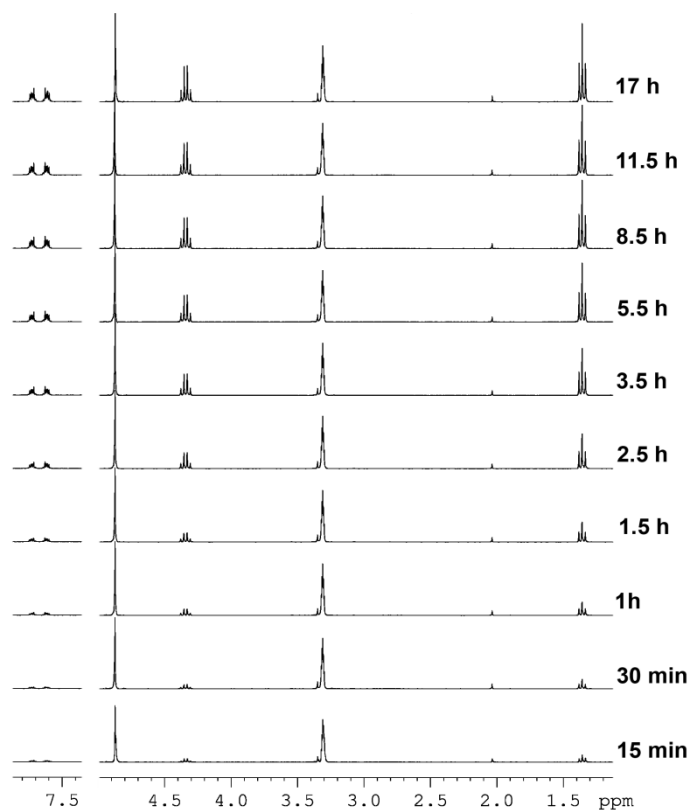


Figure S37. ¹H-NMR spectra of the displacement of EtPh by MeOH.

3.6.4.5 Quantitative determination of the molar ratio [EtPh:3] by ¹H NMR spectroscopy

A single crystal of **EtOAc@3** was soaked in 100 μ L EtPh for 72 h at room temperature. After this period, the solution was removed and the crystal was washed with EtOAc (2×0.5 mL) and MeOH (3×0.5 mL), respectively, and dried under vacuum for 10 minutes.

The crystal was then dissolved in 0.6 mL of CDCl₃ followed by ¹H NMR measurement. The stoichiometry of the crystal was determined based on the integral ratios of the signal of the imine protons and the corresponding protons of the ethyl groups of the EtPh molecule (see Figure S38). The calculated stoichiometries were 1:1.99 from the CH₂ and 1:2.00 from the CH₃ group that corresponds with the measured crystallographic stoichiometry of the complex **EtPh@3**.

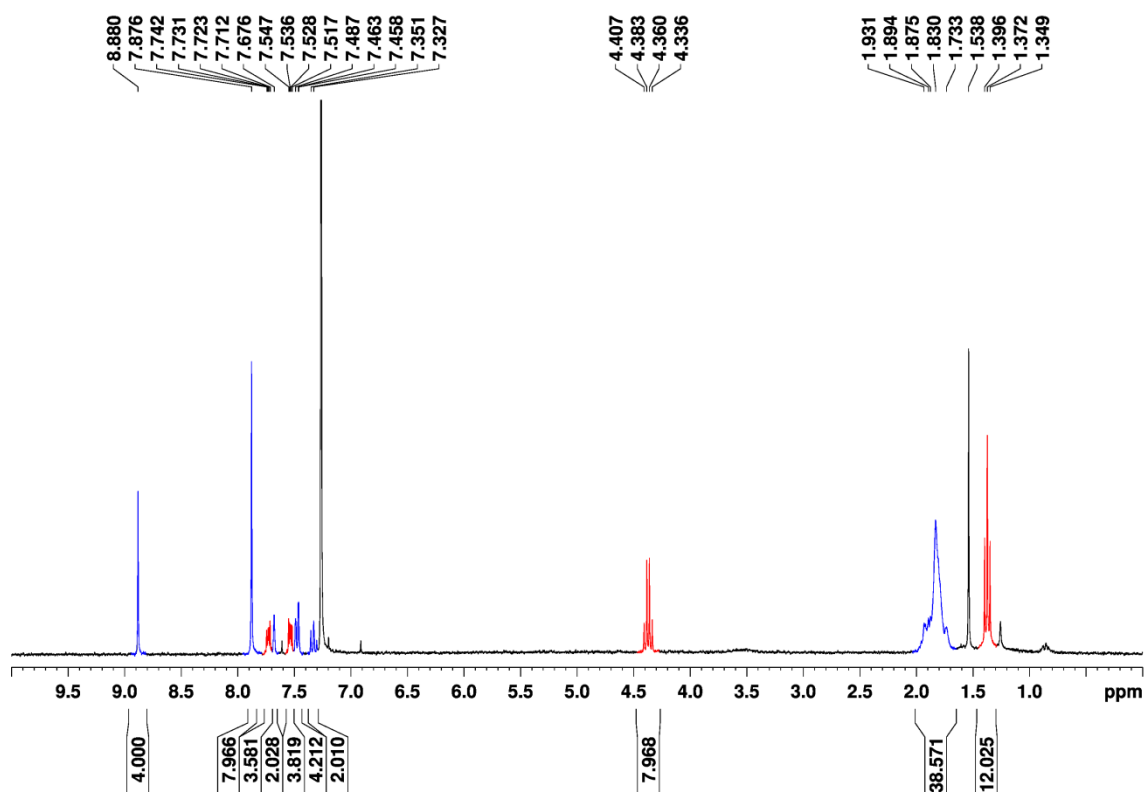


Figure S38. Molar ratio of EtPh:3 determined by direct dissolution of the inclusion complex in CDCl_3 .

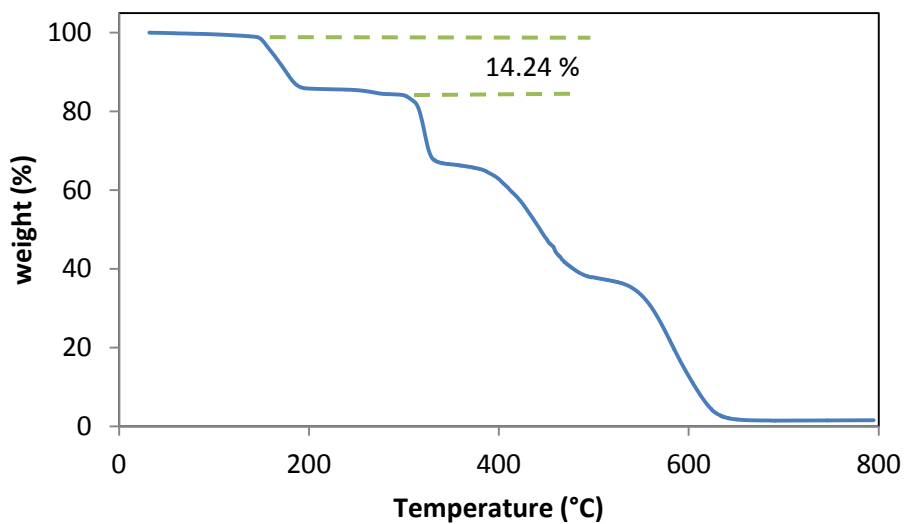


Figure S39. Thermogravimetric analysis of 13.967 mg of EtPh@3. A $10\text{ }^\circ\text{C}\cdot\text{min}^{-1}$ ramp was used. The theoretical loose of mass for a 1:2 EtPh:3 is 11.7%.

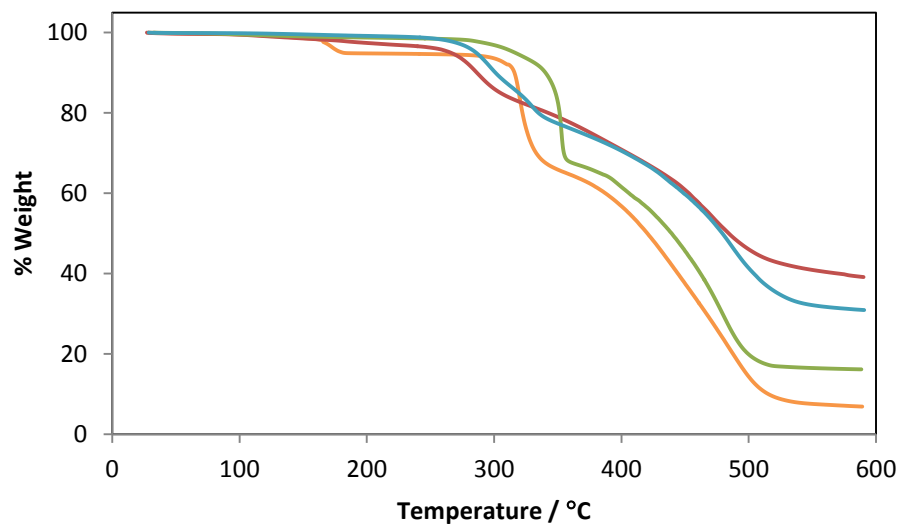


Figure S40. Thermogravimetric analysis of **EtOAc@3** (orange), **3+3'** (red), **8** (green) and **8+8'** (blue).

PART III



Chapter 4: Design and attempted synthesis of squaramide-based cucurbit[*n*]uril analogs

4.1. Macrocyclic compounds

A macrocyclic compound, as defined by IUPAC, is a cyclic macromolecule or a macromolecular cyclic portion of a molecule. Classic examples of macrocyclic compounds are crown ethers, cryptands, spherands or cyclodextrins. More recent examples are calixarenes, resorcinarenes, calixpyrroles, cucurbiturils or pillarenes, among others (See Figure 83).²⁰⁶

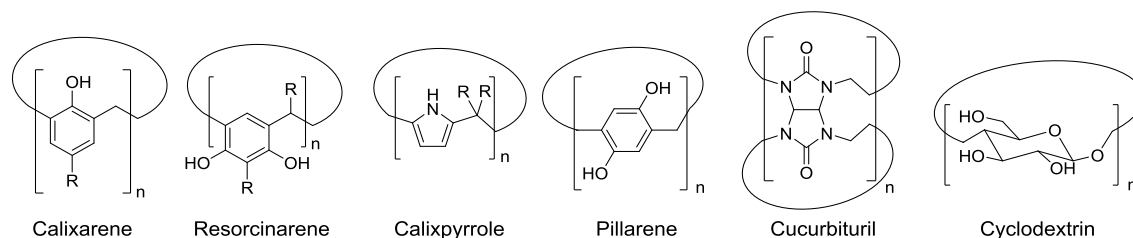


Figure 83. Chemical representations of the main macrocyclic compounds used in supramolecular chemistry.

Usually, these macrocyclic compounds are obtained by oligomerization reactions of a monomeric building block that provides particular properties, substitution patterns, functionalization and solubility to the forming cycles. Particularly, most of the previous macromolecules are obtained from condensation reactions of an aldehyde with a repetitive unit.²⁰⁷

The design and synthesis of new functional macrocyclic compounds is an important goal of organic and, particularly, in supramolecular chemistry for applications in many areas such as the development of new supramolecular architectures, catalysis, environmental sciences, medicinal chemistry or materials chemistry.²⁰⁸

Macrocycles such as crown ethers, cyclodextrins, calixarenes, cucurbiturils or, more recently, pillarenes are increasingly interesting as hosts in the study of molecular recognition processes. For example, the binding constants of host-guest complexes of cyclodextrins are in the range of 10^4 M^{-1} while for cucurbiturils the binding can be as high as 10^{15} M^{-1} in aqueous solution as is illustrated in Table 7.²⁰⁹ Macrocyclic structures are also important in self-assembly processes, in the formation of sophisticated supramolecular structures, and in the preparation of advanced materials.²¹⁰

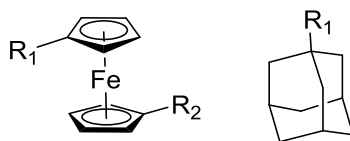
²⁰⁶ Wang, M. –X. *Chem. Commun.* **2008**, 4541-4551.

²⁰⁷ Lisbjerg, M.; Nielsen, B. E.; Milhøj, B. O.; Sauer, S. P. A.; Pittelkow, M. *Org. Biomol. Chem.* **2015**, *13*, 369-373.

²⁰⁸ Parvari, G.; Annamalai, S.; Borovoi, I.; Chechik, H.; Botoshanski, M.; Pappo, D.; Keinan, E. *Chem. Commun.* **2014**, *50*, 2494-2497.

²⁰⁹ Loh, X. J. *Mater. Horiz.*, **2014**, *1*, 185-195.

²¹⁰ Guo, Q. –H.; Zhao, L.; Wang, M. –X. *Angew. Chem. Int. Ed.* **2015**, *54*, 8386-8389.

Table 7. Association constant values of different complexes between CB[7], α -CD and β -CD with different ferrocene and adamantane derivatives in H₂O at 298 K.²¹¹

Host	R1	R2	K (M ⁻¹)
Ferrocene guests			
CB[7]	-CH ₂ OH	-H	3.2 × 10 ⁹
	-CH ₂ N(CH ₃) ₃ ⁺	-CH ₂ N(CH ₃) ₃ ⁺	3.0 × 10 ¹⁵
α -CD	-CH ₃	-H	2.0 × 10 ²
	-(CH ₂) ₇ CO ₂ H	-H	1.2 × 10 ³
Adamantane guests			
CB[7]	-OH	-H	2.3 × 10 ¹⁰
	-NH ₃ ⁺	-H	1.7 × 10 ¹⁴
β -CD	-NH ₃ ⁺	-H	8.3 × 10 ³
	-COO ⁻	-H	3.2 × 10 ⁴

4.1.1 Cyclodextrins

Cyclodextrins (CDs) are cyclic oligosaccharides generated as a result of an intramolecular transglycosylation reaction from the degradation of starch by cyclodextrin glucan transferase (CGTase) enzyme.

Cyclodextrins were discovered by Villiers in 1891²¹² and later studied by Schardinger. These compounds have extensive uses in analytical and enzymatic chemistry, in catalysis and in pharmaceutical applications.²¹³ There are three main cyclodextrins known as α -CD, β -CD and γ -CD with 6, 7 or 8 glucopyranose units, respectively, linked by α -(1,4) bonds. The different cyclodextrins differ in their solubility as well as in the size of the cavity, depending on the number of sugar units, while the depth is always the same as Table 8 shows. The hydroxyl groups of the sugar rings are located on the edges of the macrocycle while the methylene protons are oriented to the inner cavity.²¹⁴ Consequently, cyclodextrins are soluble in water due to their hydrophilic surface, but have a hydrophobic cavity, making them suitable for the formation of complexes with apolar compounds. Specifically, the most used cyclodextrin is β -CD because the cavity of α -CD is too small to encapsulate most of the common drug molecules and γ -CD is too expensive.²¹⁵

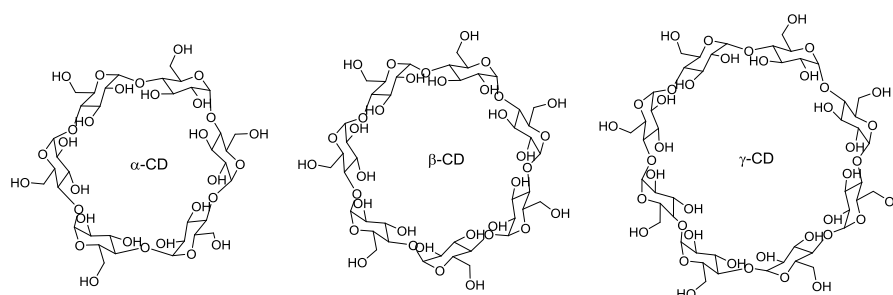
²¹¹ a) Moghaddam, S.; Yang, C.; Rekharsky, M.; Ko, Y. H.; Kim, K.; Inoue, Y.; Gilson, M. K. *J. Am. Chem. Soc.* **2011**, *133*, 3570-3581. b) Rekharsky, M. V.; Inoue, Y. *Chem. Rev.* **1998**, *98*, 1875-1917.

²¹² Villiers, A. *Compt. Rend. Fr. Acad. Sci.* **1891**, 435-438.

²¹³ Tashiro, S.; Shionoya, M. *Bull. Chem. Soc. Jpn.* **2014**, *87*, 643-654.

²¹⁴ Martin del Valle, E. M. *Process Biochem.* **2004**, *39*, 1033-1046.

²¹⁵ Challa, R.; Ahuja, A.; Ali, J.; Khar, R. K. *AAPS PharmSciThec.* **2005**, *6*, E329-E357.

Table 8. Chemical structures and cavity sizes of the most common cyclodextrins.²¹⁶

Macrocycle	Internal diameter (Å)	External diameter (Å)	Height (Å)
CD- α	5.7	13.7	7.8
CD- β	7.8	15.3	7.8
CD- γ	9.5	16.9	7.8

In general, cyclodextrins can bind small neutral molecules but also both cationic and anionic substrates, proteins and polymer chains. Additionally, cationic CDs can be obtained by the functionalization of the rings with amino groups. Consequently, anionic CDs can also be prepared by the modification of the macrocyclic structure with carboxyl methyl or sulfonic groups.²¹⁷

Over the last years, these macrocyclic compounds have been extensively used to increase the solubility in water of a broad range of hydrophobic drugs enhancing their bioavailability in biological media.²¹⁸ As an example, Table 9 summarizes the solubility enhancement of different acidic drugs (AD) and the corresponding binary complexes with cyclodextrins (AD:CD) in water at pH 5.0-6.5.²¹⁹

Table 9. Aqueous solubility of some drugs and their 1:1 complexes with cyclodextrins.

Drug	AD (mg/mL)	AD:CD (mg/mL)
Indomethacin (anti-inflammatory)	0.01	0.1
Piroxicam (anti-inflammatory)	0.3	0.5
Nimesulide (anti-inflammatory)	0.005	0.47
Glicazide (anti-diabetic)	0.01	0.4
Chlorothiazide (diuretic)	0.5	1.0

4.1.2 Calix[n]arenes

Calix[n]arenes or calixarenes (CA) are composed of phenolic units linked by methylene bridges on the ortho positions as previously described in the chapter 2 (Table 10). CAs with even numbers ($n = 4, 6, 8$) are more frequent than their odd counterparts. The lower rim of the macrocycle presents a hydrophilic

²¹⁶ Ma, X.; Zhao, Y. *Chem. Rev.*, **2015**, *115*, 7794-7839

²¹⁷ a) Zhou, J.; Tang, J.; Tang, W. *TrAC Trends Anal. Chem.*, **2015**, *65*, 22-29, b) Zhao, Y. –L.; Li, Z.; Kabehie, S.; Botros, Y. Y.; Stoddart, F. S.; Zink, J. I. *J. Am. Chem. Soc.* **2010**, *132*, 13016-13025, c) Mavridis, I. M.; Yannakopoulou, K. *Int. J. Pharm.* **2015**, *492*, 275-290, d) Sukegawa, T.; Furuike, T.; Niikura, K.; Yamagishi, A.; Monde, K.; Nishimura, S. *Chem. Commun.* **2002**, *7*, 430-431.

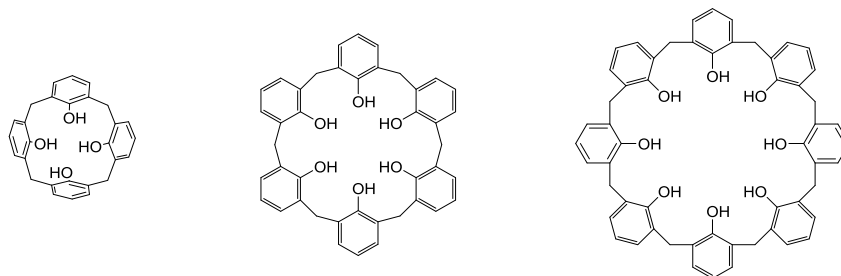
²¹⁸ Brewster, M. E.; Loftsson, T. *Adv. Drug Deliv. Rev.* **2007**, *59*, 645-666.

²¹⁹ Redenti, E.; Szente, L.; Szejtli, J. *J. Pharm. Sci.* **2001**, *90*, 979-986.

character due to their functionalization with phenolic oxygens while the upper rim remains hydrophobic due to the aromatic moiety.

Calix[*n*]arenes can act as a host for a wide variety of guests including organic molecules, ions, sugars or proteins.

Table 10. Chemical structures and cavity sizes of the most common calixarenes.¹¹



Macrocycle	Internal diameter (Å)	External diameter (Å)	Height (Å)
CA[4]	3.0	5.9	11.75
CA[6]	7.6	4.96	16.24
CA[8]	11.7	9.23	22.4

4.1.3 Cucurbit[*n*]urils

Cucurbit[*n*]urils or cucurbiturils (CB) are macrocyclic structures composed of a variable number of glycoluril units doubly linked by methylene bridges. The first report on a cucurbituril was published by Behrend et al. in 1905 with the description of the Behrend's polymer²²⁰ obtained from the acid catalysed condensation of glycoluril and formaldehyde. Upon recrystallization with H₂SO₄, this compound yields cocrystals with different products. However, it was not until 1981 when Mock and coworkers reported its chemical nature and structure.²²¹ Later, Buschmann described the isolation of CB[6] in a one-step reaction in H₂SO₄.²²² Twenty years later, cucurbit[*n*]uril homologues CB[5], CB[7], CB[8] were isolated under milder reaction conditions (80-100 °C in concentrated HCl or 75°C, 10-100h in 9M H₂SO₄) by Kim and Day.²²³ Recently, the structure of the so far biggest CB analogue CB[14] with a twisted configuration has also been reported.²²⁴

Cucurbituril structures provide a hydrophobic interior cavity that is accessible through both sides of the macrocyclic structure. All the macrocycles of the family have the same cavity depth (9.1 Å) but different cavity widths (see Table 11). For this reason, their inner volumes are a function of the number of glycoluril units of the macrocycle. Frequently, cucurbiturils are compared with cyclodextrins due to their similar cavity sizes (CB[6], CB[7] and CB[8] are analogous to α, β and γ-Cyclodextrins).

²²⁰ Behrend, R.; Meyer, E.; Rusche, F. *Justus Liebig's Annalen der Chemie* **1905**, 339, 1–37.

²²¹ Freeman, W. A.; Mock, W. L.; Shih, N. -Y. *J. Am. Chem. Soc.* **1981**, 103, 7367-7368.

²²² Lagona, J.; Mukhopadhyay, P.; Chakrabarti, S.; Isaacs, L. *Angew. Chem. Int. Ed. Engl.* **2005**, 44 (31), 4844.

²²³ Diederich, F.; Stang, P. J.; Tykwinski, R. R. *Modern Supramolecular Chemistry: Strategies for Macrocycle Synthesis*. Wiley-VCH Verlag GmbH & Co. KGaA, **2008**.

²²⁴ Cheng, X.J.; Liang, L.L.; Chen, K.; Ji, N.N.; Xiao, X.; Zhang, J.-X.; Zhang, Y.-Q.; Xue, S.-F.; Zhu, Q.-J.; Ni, X.-L.; Tao, Z. *Angew. Chem. Int. Ed.* **2013**, 125, 7393-7396.

Table 11. Chemical structures and cavity sizes of the most common cucurbiturils.

Macrocycle	Internal diameter (Å)	External diameter (Å)	Height (Å)
CB[5]	4.4	2.4	9.1
CA[6]	5.8	3.9	9.1
CA[7]	7.3	5.4	9.1
CA[8]	8.8	6.9	9.1

The major disadvantage of cucurbiturils is their poor solubility in water and organic media. Typically, CB[6] and CB[8] are insoluble in water while CB[5] and CB[7] are slightly soluble. Water solubility greatly increases in acidic media. For example, CB[6] displays a maximum solubility of 61 mM in a mixture HCOOH/H₂O 1:1 v/v).

The highly symmetric structure, with a hydrophobic cavity and the negatively charged portals make cucurbiturils perfect candidates for molecular recognition processes especially with positively charged guests.²²⁵

4.1.4 Pillar[n]arenes

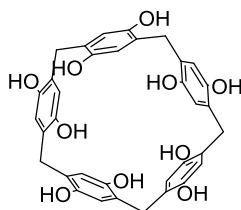
Pillar[n]arenes or pillarenes (P[n]) are 1,4- substituted [1n]-paracyclophanes derived from hydroquinones linked by methylene bridges in the 2,5-positions. They were first described by Tomoki Ogoshi in 2008.²²⁶ The most common technique used for their preparation is by the condensation reaction of 1,4-dimethoxybenzene and formaldehyde in the presence of a Lewis acid such as BF₃·OEt₂.

Pillar[n]arenes are highly symmetric and rigid structures compared with crown ethers and calix[n]arenes. Unlike cucurbit[n]urils and cyclodextrins, pillarenes are soluble in common organic solvents, but they can be easily solubilized in water by functionalization of the benzene rings.

²²⁵ Barrow, S. J.; Kasera, S.; Rowland, M. J.; del Barrio, J.; Scherman, O. A. *Chem. Rev.* **2015**, *115*, 12320-12406.

²²⁶ Ogoshi, T.; Kanai, S.; Fujinami, S.; Yamagishi, T. -A.; Nakamoto, Y. *J. Am. Chem. Soc.* **2008**, *130*, 5022-2023.

Table 12. Representative structure of pillar[5]arene and cavity sizes of the most common pillarenes.²²⁷



Macrocycle	Internal diameter (Å)	External diameter (Å)	Height (Å)
CB[5]	4.7	13.5	7.8
CA[6]	6.7	15.2	7.8
CA[8]	8.7	16.9	7.8

The most common pillar[*n*]arene is P[5] whose size is comparable to CB[6] (Table 12). P[6] and P[7] have also been described with cavity sizes analogous to CB[7] and CB[8], respectively.

Pillar[*n*]arenes act as hosts for positively charged or neutral molecules such as viologen derivatives, (bis)-imidazolium cations, *n*-hexane, alkenediamines and *n*-octyltrimethyl ammonium compounds, among others.²²⁸ They can also form self-assembled structures, rotaxanes, supramolecular polymers or supramolecular dimers, artificial transmembrane proton channels, fluorescent sensors or functional materials.²²⁹

4.1.4 Multifarenes[*m,n*]

Multifarenes[*m,n*] are a new family of macrocyclic compounds recently reported by Keinan et al. in which *m* and *n* are the numbers of the different building blocks used for their preparation (Figure 86).²³⁰ These new compounds are constructed by the condensation reaction of alternated units of 4-*t*-butylphenol and 2-imidazolidinthione with *p*-formaldehyde (see Figure 84). The resulting macrocycles present several thiourea moieties that offer the possibility to bind different types of organic molecules as well as metal ions.

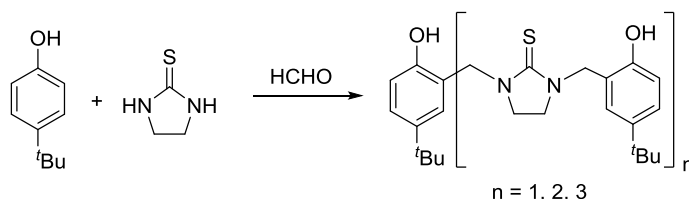


Figure 84. Formation of oligomeric structures.

²²⁷ Xue, M.; Yang, Y.; Chi, X.; Zhang, Z.; Huang, F. *Acc. Chem. Res.* **2012**, *45*, 1294-1308.

²²⁸ a) Tan, L. -L.; Yang, Y. -W. *J. Incl. Phenom. Macrocycl. Chem.* **2015**, *81*, 13-33. b) Strutt, N. L.; Forgan, R. S.; Spruell, J. M.; Botros, Y. Y.; Stoddart, J. F. *J. Am. Chem. Soc.* **2011**, *133*, 5668-5671.

²²⁹ Zhang, H.; Zhao, Y. *Chem. Eur. J.* **2013**, *19*, 16862-16879.

²³⁰ Parvari, G.; Annamalai, S.; Borovoi, I.; Chechik, H.; Botoshansky, M.; Pappo, D.; Keinan, E. *Chem. Commun.* **2014**, *50*, 2494-2497.

Different reaction conditions have been tested. When the reaction is carried out under basic conditions, only oligomeric compounds are obtained. The same result is obtained when the reaction is performed in toluene under acidic conditions (*p*-toluenesulfonic acid) even using different molar ratios of the building blocks. Surprisingly, when a 1:1 molar ratio is used, the multifarene[4,4] is formed with a high yield (67%). Additionally, multifarene[4,4] and multifarene[3,3] can be obtained by the reaction of the previously obtained oligomeric chains with 2-imidazolidiethione.²³¹

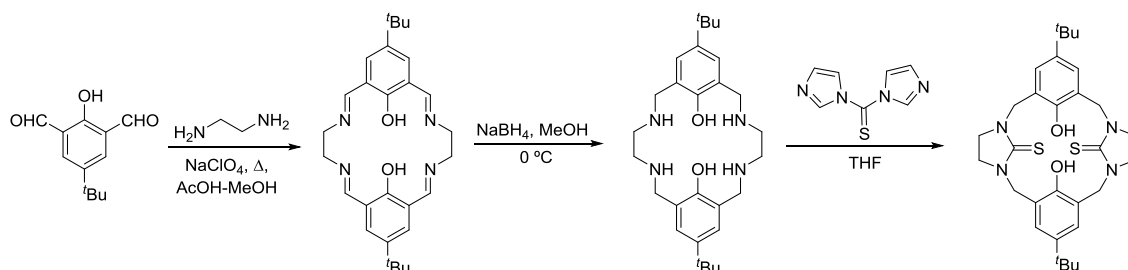


Figure 85. Template synthesis of multifarenes.

The templated synthesis of 4-*t*-butyl-2,6-diformylphenol, 5-(*tert*-butyl)-2-hydroxyisophthalaldehyde and 1,2-diaminoethane in a mixture of methanol and acetic acid in the presence of NaClO_4 afford the tetraimine macrocycle shown in Figure 85. The reduction of the imine groups followed by the functionalization with 1,1'-thiocarbonyldiimidazole in THF yields the three multifarenes.

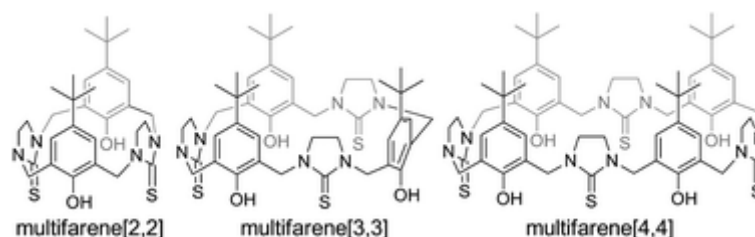


Figure 86. Chemical structure of the different members of the multifarene family.

The X-ray structure of multifarene[2,2] shows the formation of a small hydrophobic cavity similar to calixarenes. Multifarene[3,3] binds diethyl ether into the cavity and multifarene[4,4] ethyl acetate.²³¹

4.2. Applications of macrocyclic compounds

4.2.1 Materials science

Over the last decades, macrocyclic compounds have found increasing uses as hosts for molecular recognition applications in solution. Also, these compounds have been used as building blocks for the formation of porous materials designed for applications such as molecular storage, catalysis or sensing.⁷

Thus, cyclodextrins form channel-type packing structures in crystalline state with head-to-head or head-to-tail columnar stacking stabilized by hydrogen bond interactions between the hydroxyl groups of the

ring units (Figure 87).²³¹ Several types of molecules can be included inside the channels. For example, Stoddart et al. reported a Cyclodextrin-MOF porous crystal based on γ -cyclodextrin and alkaline or alkaline earth metal ions. The resulting porous structures possess nanochannels with the dimensions of the CD cavity. These MOFs were used for adsorption of gases, and they show selectivity for CO₂ over CH₄.²³²

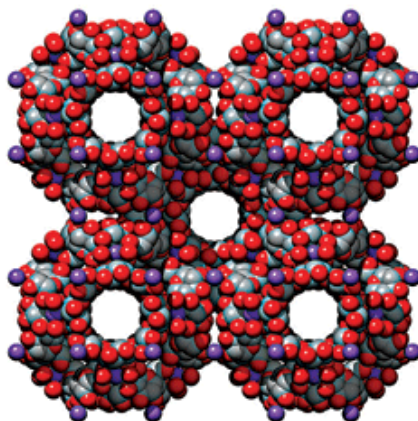


Figure 87. Space-filling representation of a cyclodextrin-based (γ -CD-MOF) structure used for adsorption of gases. The atoms are represented as: carbon gray, oxygen red and potassium purple.

Cucurbit[*n*]urils and their derivatives crystallize forming narrow to wide channels filled with water molecules.²³³ Usually, these structures collapse after solvent removal, but some examples of permanent porous cucurbit[*n*]urils have been reported. For example, a CB[6] derivative maintain its crystallinity after solvent removal and shows high stability to air exposure. This compound crystallizes forming a one-dimensional honeycomb-like structure. The desolvated product can adsorb gases such as N₂O, NO or CO₂,²³⁴ but also a large amount of acetylene gas (4.2 mol of acetylene per mole of CB[6] at 196 K and 1 atm).²³⁵ Another example is the CB[5] structure described by Ratcliffe et al. In this instance, it takes place a single-crystal to single-crystal transformation at room temperature in which the one-dimensional structure is converted in a porous layer structure. The new compound is not very stable at air but can adsorb Xe gas.²⁵

Calix[*n*]arenes can also promote the formation of porous structures. For example, the pentasodium salt of *p*-sulphonatocalix[4]arene crystallizes forming bilayered structures of alternating organic and aqueous layers.²³⁶ Conversely, the use of the three-component system consisting of the pentasodium salt of the *p*-sulphonatocalix[4]arene, pyridine *N*-oxide and a lanthanide metal nitrate (Ln³⁺) in water medium in a 2:2:1 molar ratio yields the dimeric assembly shown in Figure 88.²³⁷ Additionally, a crystalline tubular assembly is obtained when the same molecules are combined in a 2:8:1 molar ratio.

²³¹ Harata, K. *Chem. Rev.* **1998**, *98*, 1803-1828.

²³² Smaldone, R. A.; Forgan, R. S.; Furukawa, H.; Gassensmith, J. J.; Slawin, A. M. Z.; Yaghi, O. M.; Stoddart, J. F. *Angew. Chem. Int. Ed.* **2010**, *49*, 8630-8634.

²³³ Bardelang, D.; Udachin, K. A.; Anedda, R.; Moudrakovski, I.; Leek, D. M.; Ripmeester, J. A.; Ratcliffe, C. I. *Chem. Commun.* **2008**, 4927-4929.

²³⁴ Miyahara, Y.; Abe, K.; Inazu, T. *Angew. Chem. Int. Ed.* **2002**, *41*, 3020-3023.

²³⁵ Lim, S.; Kim, H.; Selvapalam, N.; Kim, K. -J.; Cho, S. J.; Seo, G.; Kim, K. *Angew. Chem. Int. Ed.* **2008**, *47*, 3352-3355.

²³⁶ Atwood, J. L.; Coleman, A. W.; Zhang, H.; Bott, S. G. *J. Inclusion. Phenom.* **1989**, *5*, 203-211.

²³⁷ Orr, G. W.; Barbour, L. J.; Atwood, J. L. *Science* **1999**, *285*, 1049-1052.

In this case, the structure is formed by the arrangement of the calix[4]arene molecules along the cylinder.

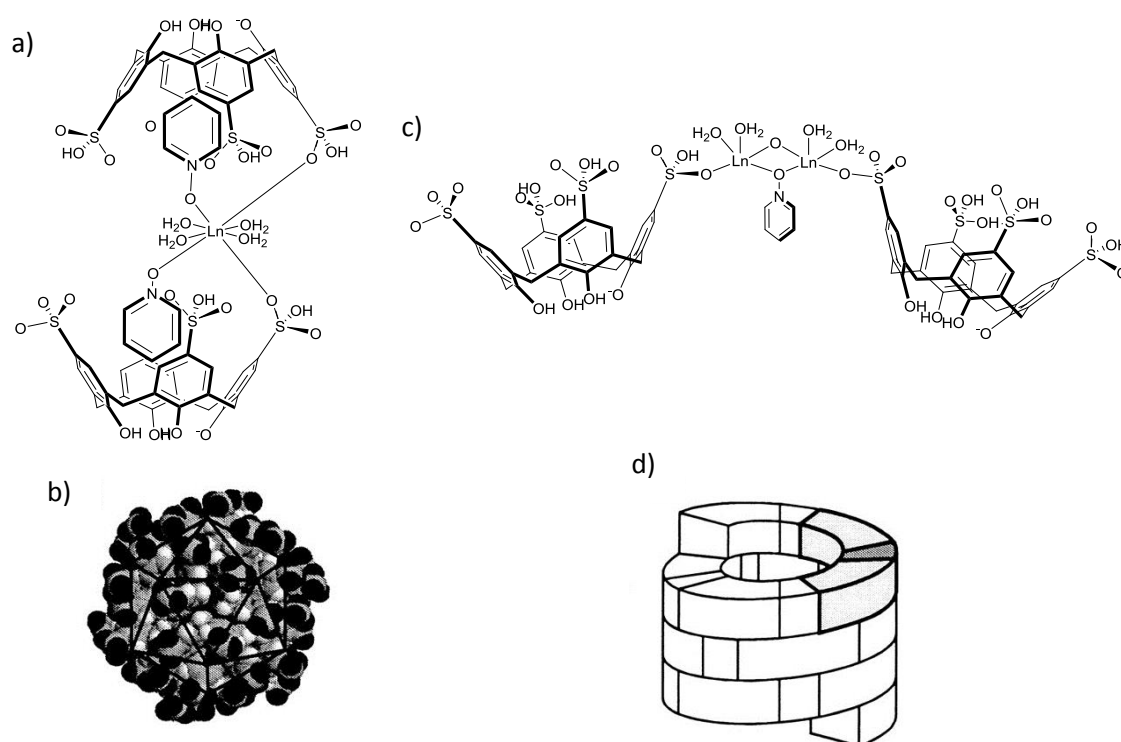


Figure 88. Schematic representation of the self-organization of *p*-sulfonatocalix[4]arene anions, pyridine N-oxide and Ln^{3+} ions: in a 2:2:1 molar ratio (a) that yields the globular structure (b) and in a 2:8:1 molar ratio (c) that yields the tubular assembly (d).

Recently, a novel supramolecular organic framework based on perhydroxyl-pillar[5]arenes that crystallize in an open 3D network has been reported. In this case, the structure is stabilized by hydrogen bonds between the macrocyclic units showing permanent porosity (Figure 89). The resulting porous structure has permanent porosity and shows good selectivity towards CO_2 .²³⁸

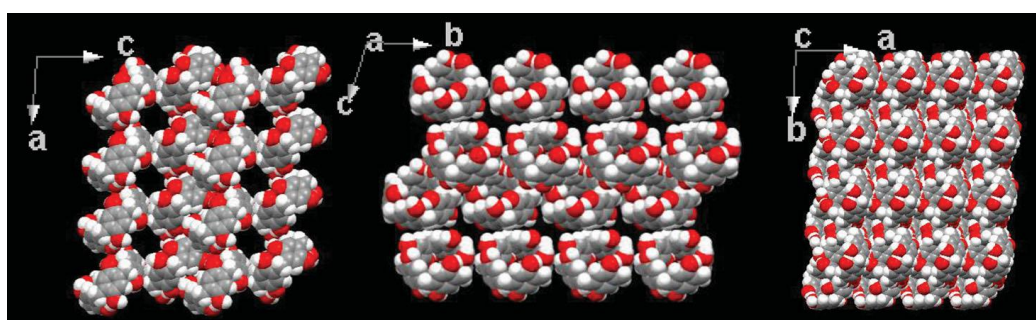


Figure 89. 3-D network of a pillar[5]arene derivative.

4.2.2 Catalysis

²³⁸ Tan, L. -L.; Li, H.; Tao, Y.; Zhang, S. X. -A.; Wang, B.; Yang, Y. -W. *Adv. Mater.* **2014**, *26*, 7027-7031.

The design of catalytic supramolecular systems able to locate reagents together and in the correct conformation has been studied during years. Macrocycles are promising candidates in this field because the reagents can be appropriately oriented into the cavity as in the catalytic site of an enzyme.

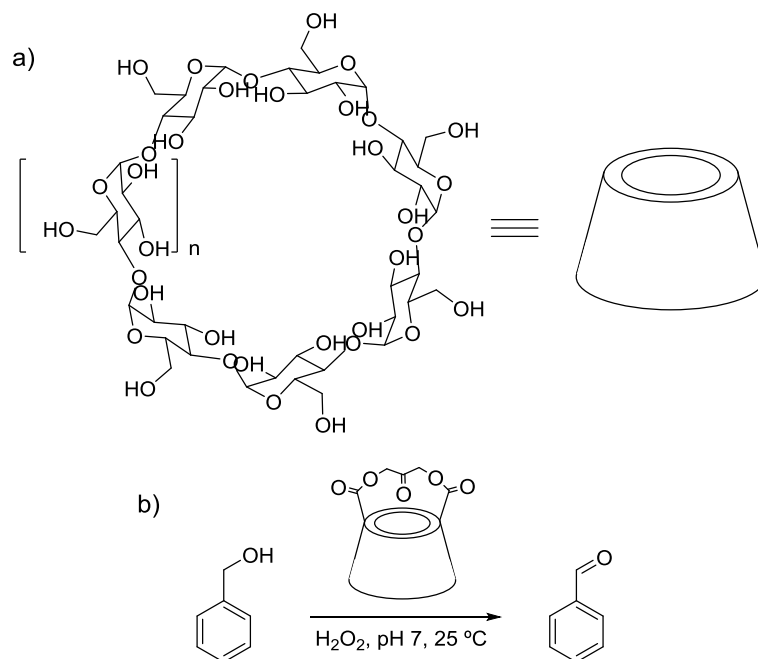


Figure 90. a) Structure of α - and β -CD ($n = 6, 7$), b) Schematic representation of the catalytic oxidation of benzyl alcohols by CD.

Cyclodextrins have been evaluated as catalysts for reactions such as acylation, alkylation or chlorination, cleavage of esters or intramolecular Diels-Alder reactions, among others.²³⁹ Additionally, cyclodextrins have been used as artificial enzymes.²⁴⁰ This is illustrated by functionalized α - or β -cyclodextrins with dihydroxyacetone through ester bonds (Figure 90). This CD catalyzes the transformation of benzyl alcohols into aldehydes in the presence of H_2O_2 under mild aqueous conditions with very high rate enhancements.²⁴¹

The ability of cucurbiturils to form ternary complexes makes them suitable candidates for catalytic purposes. The first example of catalysis inside a cucurbituril cavity was reported by Mock et al.²⁴² They described the [3+2] cycloaddition of various azides and acetylenes (Figure 91).

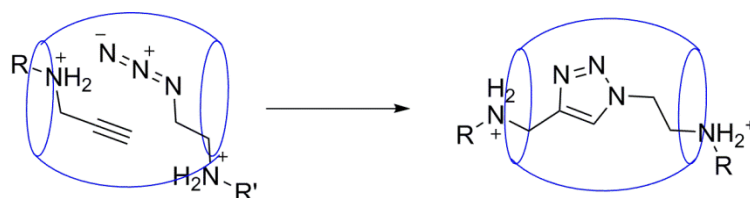


Figure 91. Click reaction catalyzed by CB[6] reported by Mock.

4.2.3 Biomedical applications

²³⁹ Breslow, R.; Dong, S. D. *Chem. Rev.* **1998**, *98*, 1997-2011.

²⁴⁰ Breslow, R. *Acc. Chem. Res.* **1995**, *28*, 146-153.

²⁴¹ Marinescu, L. G.; Bols, M. *Angew. Chem. Int. Ed.* **2006**, *45*, 4590-4593.

²⁴² Mock, W. L.; Shih, N. -Y. *J. Org. Chem.* **1983**, *48*, 3619-3620.

The development of compounds able to enhance the solubility of drug molecules in aqueous media and transport them to target organs is an important goal of supramolecular chemistry. Several macrocyclic compounds have been studied for these purposes.

Owing to their good biocompatibility, cyclodextrins have been used to increase the solubility of hydrophobic drugs in aqueous media. For example, 1:1 complexes between the anticancer drug paclitaxel and β -CD have been used for the treatment of breast cancer cells.²⁴³

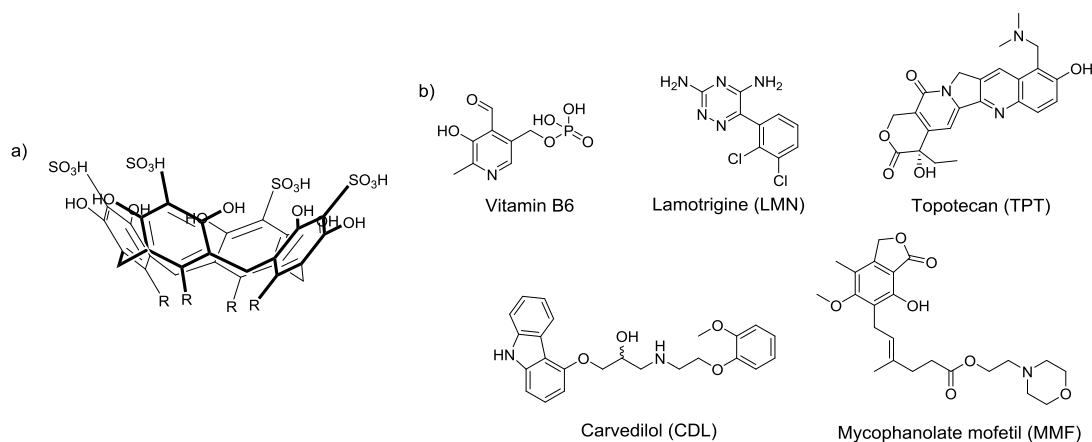


Figure 92. Examples of drug molecules (a) encapsulated by sulphonate functionalized CA (a).

In general, the binding constants of drug-calixarene (CA) complexes are higher than those with CDs. Sulfonation of the upper rim of calixarenes is a common approach to solubilize these compounds in water. The resulting macrocycles can encapsulate drug molecules for drug delivery and other biomedical applications. Figure 92 shows several drug molecules that have been successfully encapsulated into *p*-sulphonatocalix[4]arene.²⁴⁴

An important goal of supramolecular chemistry is the design of systems for gene delivery into target organs for the treatment of various diseases. As an example, a self-assembled tertiary complex between G3, G4 or G5 poly(propyleneimine) dendrimers (PPI-DAB), DNA and a cucurbituril CB[6] has been reported as is shown in Figure 93.²⁴⁵ These complexes can transfect viral genome (DNA) into various types of cell lines with low toxicities.

²⁴³ Jing, J.; Szarpak-Jankowska, A.; Guillot, R.; Pignot-Paintrand, I.; Picart, C.; Auzély-Velty, R. *Chem. Mater.* **2013**, *25*, 3867-3873.

²⁴⁴ a) Song, J.; Li, H.; Chao, J.; Dong, C.; Shuang, S. *J. Incl. Phenom. Macrocycl. Chem.* **2012**, *72*, 389-395, b) Patel, M. B.; Valand, N. N.; Modi, N. R.; Joshi, K. V.; Harikrishnan, U.; Kumar, S. P.; Jasrai, Y. T.; Menon, S. K. *RSC Adv.* **2013**, *3*, 15971-15981, c) Wang, G. -S.; Zhang, H. -Y.; Ding, F.; Liu, Y. *J. Incl. Phenom. Macrocycl. Chem.* **2011**, *69*, 85-89, d) Menon, S. B.; Mistry, B. R.; Joshi, K. V.; Modi, N. R.; Shashtry, D. *J. Incl. Phenom. Macrocycl. Chem.* **2012**, *73*, 295-303, e) Menon, S. K.; Modi, N. R.; Mistry, B.; Joshi, K. *J. Incl. Phenom. Macrocycl. Chem.* **2011**, *70*, 121-128.

²⁴⁵ Lim, J. -B.; Kim, T.; Lee, J. W.; Kim, S. -M.; Kim, H. -J.; Kim, K.; Park, J. -S. *Bioconjug. Chem.* **2002**, *13*, 1181-1185.

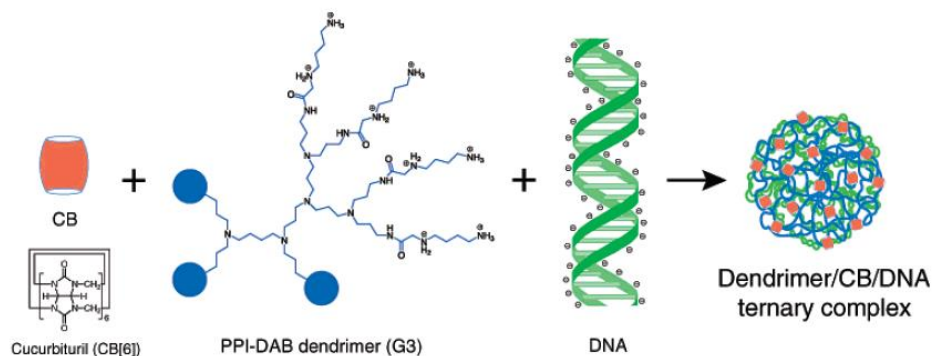


Figure 93. Schematic representation of the formation of the tertiary complex CB:PPI-DAB:DNA.

Another bioapplication of supramolecular systems is the formation of hydrogels (three dimensional cross-linked structures able to entrap large amounts of guest molecules). Cyclodextrins have been extensively applied in this field. They act by the formation of supramolecular polymers,²⁴⁶ or as macrocyclic host molecules conjugated with the side chains of the polymeric structure. In both cases, they have been applied as drug delivery systems for sustained and controlled drug release.²⁴⁷

4.2.3 Supramolecular assemblies

Interlocked molecules featuring several recognition sites attached through non-covalent interactions have a great potential for the construction of molecular switches and motors.

Cucurbiturils are good candidates for these purposes. One example is the molecular switch reported by Salih et al.²⁴⁸ In this case, a [3]rotaxane is formed by a 1,3-cycloaddition reaction inside the CB[6] cavity (Figure 94). The slow addition of NaOH causes the movement of cucurbituril units through the aliphatic region. The addition of HCl to the solution causes the protonation of the amines directly linked to the aliphatic region fixing the cucurbituril positions. The initial state is recovered when the solution is heated.

²⁴⁶ Li, J. J.; Zhao, F.; Li, J. *Adv. Biochem. Eng. Biotechnol.* **2011**, *125*, 207-249.

²⁴⁷ Park, K. M.; Yang, J. -A.; Jung, H.; Yeom, J.; Park, J. S.; Park, K. -H.; Hoffman, A. S.; Hahn, S. K.; Kim, K. *ACS Nano* **2012**, *6*, 2960-2968.

²⁴⁸ Tuncel, D.; Özsar, Ö.; Tiftik, H. B.; Salih, B. *Chem. Commun.* **2007**, 1369-1371.

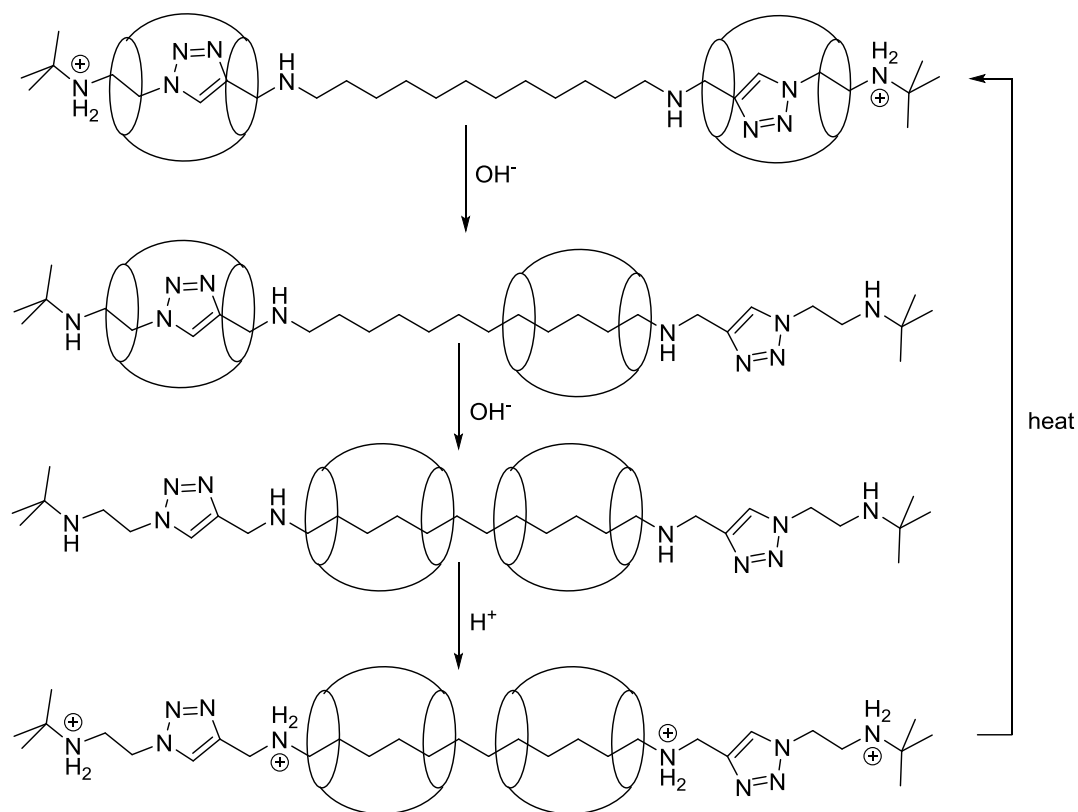


Figure 94. Chemical switch process for the [2]rotaxane shown.

The development of synthetic supramolecular systems for transmembrane transport is also important, but at the same time, a difficult goal to achieve. Pillar[n]arenes have been applied as artificial transmembrane channels for the transport of protons, water, amino acids or ions such as K^+ .²⁴⁹ For instance, hydrazide pillar[5]arenes form pentameric cylinders through intramolecular hydrogen bonds yielding tubular structures that act as single-molecule transmembrane water channels showing transport activity at very low concentrations, as shown in Figure 95.

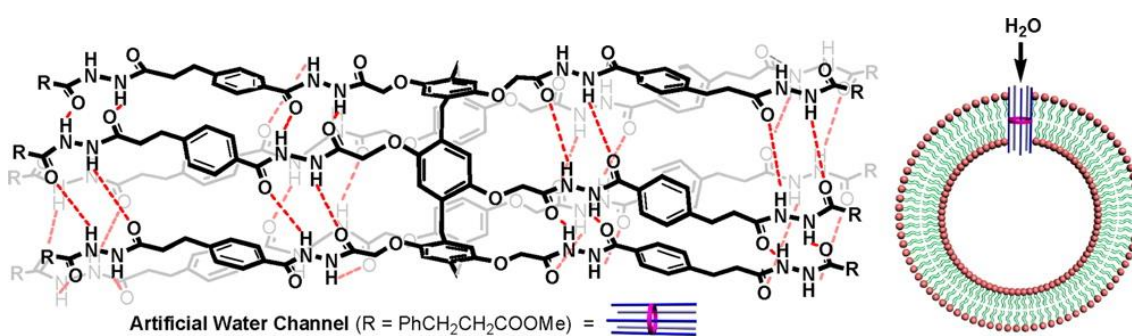


Figure 95. Hydrazide pillar[5]arene derivative used as artificial transmembrane water channels.

²⁴⁹ a) Song, N.; Yang, Y. –W. *Sci. China Chem.* **2014**, *57*, 1185-1198, b) Chen, L.; Si, W.; Zhang, L.; Tang, G.; Li, Z. –T.; Hou, J. –L. *J. Am. Chem. Soc.* **2013**, *135*, 2152-2155, c) Hu, X. –B.; Chen, Z.; Tang, G.; Hou, J. –L.; Li, Z. –T. *J. Am. Chem. Soc.* **2012**, *134*, 8384-8387.

4.3. Aims of this chapter

Owing to the multiple applications and the technological potential of macrocyclic structures, the main goal of this chapter is the design, synthesis, characterization, and evaluation of a new family of squaramide-based macrocycles. Given the analogies existing between ureas and squaramides, in this chapter we will focus our attention on squaramide analogs to multifarenes and cucurbituril compounds.

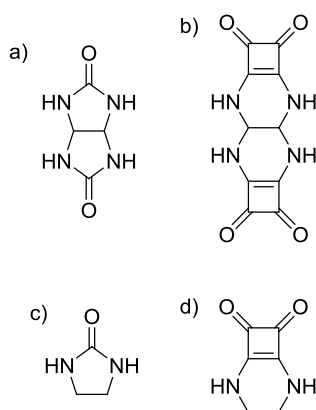


Figure 96. Chemical structures of: a) Glycoluril, b) Squaramide-glycoluril analog, c) imidazolidin-2-one, d) squaramide imidazolidin-2-one analog.

Specifically, the objectives of this chapter are:

- The synthesis and characterization of a bicyclic squaramide, analog to a cyclic urea, as building block to construct squaramide analogs of multifarenes.
- The synthesis and characterization of squaramide multifarene analogs
- The synthesis and characterization of the squaramide-based analog of glycoluril.
- The synthesis and characterization of squaramide-based macrocycles through the condensation of the squaramide analogs of glycoluril with glyoxal.
- The identification of the molecular recognition properties of these new compounds by NMR and mass spectroscopy.
- The initial exploration of the catalytic properties, if any, of the new macrocyclic compounds.

Design and synthesis of a new family of squaramide-based macrocycles

Preliminary unpublished results

4.4.1 Abstract

The development of new macrocyclic systems for applications in molecular recognition and catalysis has attracted great attention. In this regard, squaramides are promising candidates due to their host-guest properties. Here, we present the synthesis of a new set of squaramide-based oligomers and macrocycles analogous to multifarenes. These compounds have been obtained as mixtures of products.

4.4.2 Introduction

There is great interest in the development of building blocks that contain specific information for applications in molecular recognition and catalysis. Specifically, macrocyclic compounds present some advantages due to their highly preorganized structures with oriented functional groups that increase the binding affinity and selectivity over potential guests in comparison with linear analogues.

In this regard, ureas and their N,N'-substituted derivatives have been widely exploited in the design of supramolecular receptors.²⁵⁰ Urea compounds present two parallel NH groups that act as hydrogen bond donors and a carbonyl group with hydrogen bond acceptor character. This hydrogen bonding-interaction pattern has been used for applications in the design of self-assembled molecules,²⁵¹ macrocycles,²⁵² and organic gelators.²⁵³

One of the most important urea derivatives is glycoluril. Glycoluril and its derivatives are prepared by the cyclocondensation reaction of urea with glyoxal or diketones in acidic solution. The resulting compounds present rigid skeletons, high melting points and multiple hydrogen bond donor (NH) and acceptor (C=O) groups making them suitable building blocks for supramolecular applications. For this reason, glycolurils have been used in the formation of rotaxane compounds,²⁵⁴ self-assembled capsules²⁵⁵ and molecular tweezers or clips.²⁵⁶ But the most important application of these compounds has been the synthesis of the cucurbit[n]uril family by condensation reaction with formaldehyde in acidic solution.²⁵⁷

Squaramides are isosters of urea but present some advantages in host-guest chemistry.²⁵⁸ Firstly, squaramides can interact both with cations and anions through the CO or NH groups, respectively, while ureas show preference for anionic guests (Figure 97). The rigidity of the cyclobutene ring is also important to fix the carbon framework of the product. Additionally, the distance between the two NH groups is larger than in ureas in the case of the squaramide moiety allowing a better orientation of the

²⁵⁰ a) Dey, S. K.; Chutia, R.; Das, G. *Inorg. Chem.* **2012**, *51*, 1727-1738. b) Bondy, C. R.; Gale, P. A.; Loeb, S. J. *J. Am. Chem. Soc.* **2004**, *126*, 5030-5031. c) Li, A. -F.; Wang, J. -H.; Wang, F.; Jiang, Y. -B. *Chem. Soc. Rev.* **2010**, *39*, 3729-3745.

²⁵¹ a) Fischer, L.; Guichard, G. *Org. Biomol. Chem.* **2010**, *8*, 3101-3117. b) Schauer, C. L.; Matwey, E.; Fowler, F. W.; Lauher, J. W. *J. Am. Chem. Soc.* **1997**, *119*, 10245-10246.

²⁵² Dawn, S.; Dewal, M. B.; Sobransingh, D.; Paredes, M. C.; Wibowo, A. C.; Smith, M. D.; Krause, J. A.; Pellechia, P. J.; Shimizu, L. S. *J. Am. Chem. Soc.* **2011**, *133*, 7025-7032.

²⁵³ a) Lai, T. -L.; Canevet, D.; Almohamed, Y.; Mévellec, J. -Y.; Barillé, R.; Avarvari, N.; Sallé, M. *New. J. Chem.* **2014**, *38*, 4448-4457. b) van Esch, J.; Schoonbeek, F.; de Loos, M.; Kooijman, H.; Spek, A. L.; Kellogg, R. M.; Feringa, B. L. *Chem. Eur. J.* **1999**, *5*, 937-950.

²⁵⁴ a) Ho, T. -H.; Lai, C. -C.; Liu, Y. -H.; Peng, S. -M.; Chiu, S. -H. *Chem. Eur. J.* **2014**, *20*, 4563-4567. b) Duan, Q.; Xia, W.; Hu, X.; Ni, M.; Jiang, J.; Lin, C.; Pan, Y.; Wang, L. *Chem. Commun.* **2012**, *48*, 8532-8534.

²⁵⁵ a) Rebek, J. Jr. *Acc. Chem. Rev.* **1999**, *32*, 278-286, b) Conn, M. M.; rebek, J. Jr. *Chem. Rev.* **1997**, *97*, 1647-1668.

²⁵⁶ Elemans, J. A. A. W.; Rowan, A. E.; Nolte, R. J. M. *Ind. Eng. Chem. Res.* **2000**, *39*, 3419-3428.

²⁵⁷ a) Jansen, K.; Wego, A.; Buschmann, H. -J.; Schollmeyer, E.; Döpp, D. *Des. Monomers Polym.* **2003**, *6*, 46-55. b) Freeman, W. A.; Mock, W. L.; Shih, N. -Y. *J. Am. Chem. Soc.* **1981**, *103*, 7367-7368.

²⁵⁸ Amendola, V.; Fabbri, L.; Mosca, L. *Chem. Soc. Rev.* **2010**, *39*, 3889-3915.

hydrogen bonds. For all these reasons, squaramides form more stable host-guest complexes with neutral, cationic or anionic guest molecules.

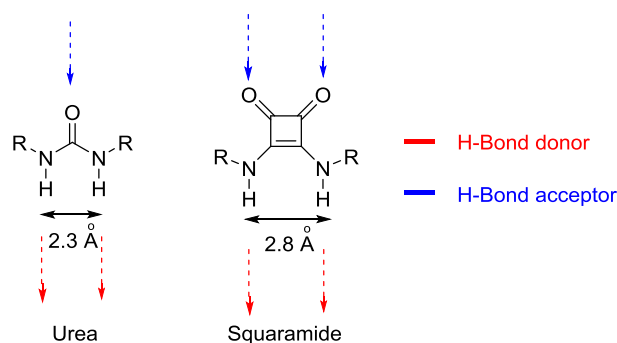


Figure 97. Schematic comparison between hydrogen bonding pattern and NH distances between urea and squaramide units.

The aim of this work is the preparation, characterization and evaluation of new squaramide-based macrocycles analogous to cucurbiturils and multifarenes to test their host-guest properties.

4.4.3 Towards squaramide analogs of multifarenes and cucurbiturils

The preparation of squaramide multifarenes or squaramide-based cucurbituril analogs requires previously the synthesis and characterization of the squaramides **2-4** that we plan to use as building blocks. These compounds are the squaramide analogs of the corresponding cyclic ureas or bicyclic ureas.

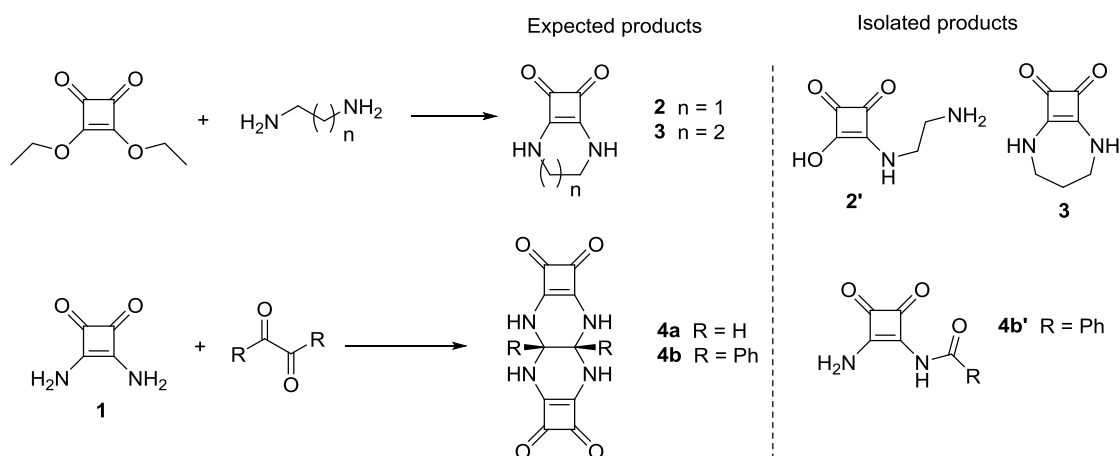


Figure 98. Reactions planned with expected and isolated products.

The reactions conducting to the squaramides **2** and **3** were performed by condensation of diethyl squarate and the corresponding diamine in alcoholic media. Under these experimental conditions, only the monosubstitution product **2'** was detected in the reaction mixture of diethyl squarate with ethylenediamine ($n=1$). This result was confirmed by elemental analysis due to the insolubility of the product in common solvents. This result is likely due to the considerable ring strain anticipated for the

bicyclic squaramide **2**. In accordance, the reaction performed on the homologous 1,3-propanediamine, in the same experimental conditions, yielded nicely the bicyclic squaramide **3** in fairly good yield (75%).

The squaramide **3** is a di-secondary bis-squaramide. The cyclic nature of the squaramide substitution forced the E,E configuration of the two NH squaramido bonds. This is a distinctive structural feature when compared with open squaramides. In particular, all the di-secondary bis squaramides substituted with alkyl or aryl chains are soluble in DMSO and related highly polar solvents, but totally insoluble in water and other usual solvents. This is due to the strong aggregation of the squaramide moiety in a head-to-tail fashion leading to extended ladder structures.²⁵⁹ In stark contrast, the bicyclic squaramide **3** is soluble in water. In fact, the recrystallization of **3** in water afforded crystalline prisms suitable for X-ray structure determination.

The X-ray analysis revealed that cyclic squaramide **3** crystallized together with two water molecules. The structure of [**3**·(H₂O)₂], is almost planar with the exception of the methylene bridge that is out of the molecular plane. The fixed E,E squaramide motif, imposed by the cyclic structure, is capable of creating a one-dimensional architecture held together by NH···O hydrogen bonds. Specifically, the crystal structure of [**3**·(H₂O)₂] contains infinite squaramide ribbons held together by NH···O (NO distance 2.815 Å) hydrogen bonds. These ribbons (Figure 99) are oriented in a zig-zag fashion displaying an invariable, close to ideal, N-H···O angle of 164.8°. There are not hydrogen bonds between neighboring squaramide ribbons located in the same layer. Instead the ribbons are hydrogen bonded to water molecules bridging two adjacent squaramide ribbons (Figure 102). The ribbons of **3** pack in a stacked layer assembly along "b" direction with the squaramide units in an alternate and displaced disposition (Figure 101). In accordance with the dipolar and partial aromatic character of squaramides (Figure 100), the measured intermolecular layer-to-layer distance is 3.25 Å. This value is lower than the sum of the van der Waals radii of carbon atoms (3.40 Å). Therefore, the face-to-face displaced stacking observed is induced by the strong dipolar intermolecular interactions between the squaramide rings.

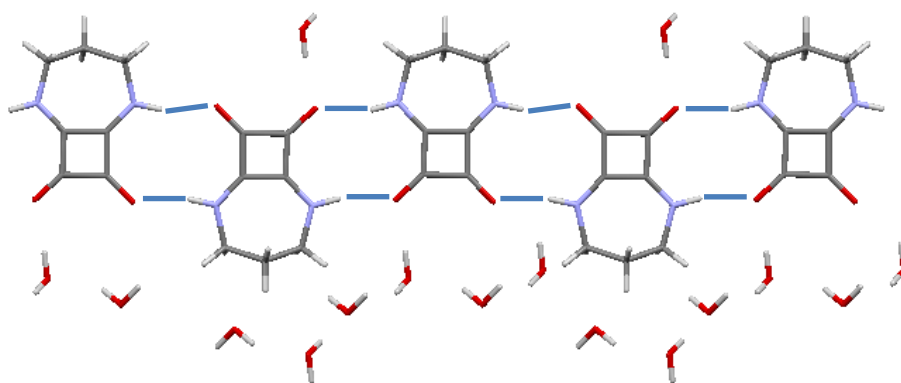


Figure 99. Ribbon of cyclic squaramide **3** generated by NH···O hydrogen bonds (indicated by dashed lines).

²⁵⁹ (a) Rotger, C.; Soberats, B.; Quiñonero, D.; Frontera, A.; Ballester, P.; Benet-Buchholz, J.; Deyà, P. M.; Costa, A. *Eur. J. Org. Chem.* **2008**, 2008, 1864-1868. (b) Prohens, R.; Puigjaner, C.; Barbas, R.; Portell, A.; Font-Bardia, M.; Alcobe, X.; Tomas, S. *CrystEngComm.* **2012**, 14, 5745-5748.

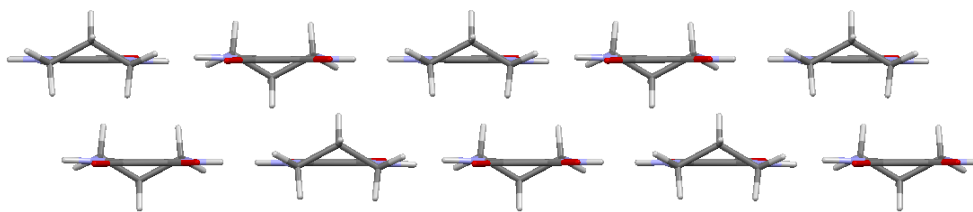


Figure 100. Layer-to-layer arrangement of two superposed squaramide ribbons showing a displaced dipolar interaction between squaramides. The layer-to-layer distance is 3.25 Å.

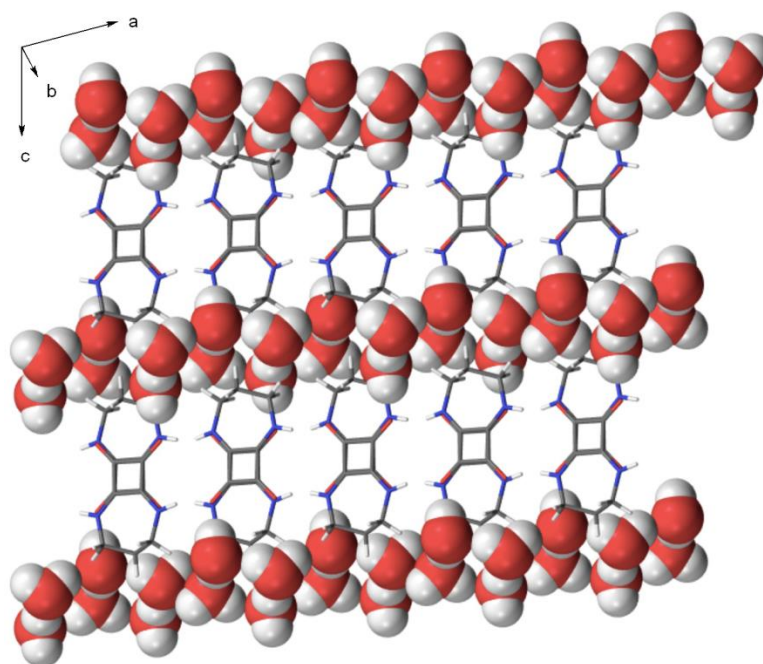


Figure 101. Structure view of $[3 \cdot (\text{H}_2\text{O})_2]$, along the *b* direction showing the arrangement of the squaramide ribbons and water molecules.

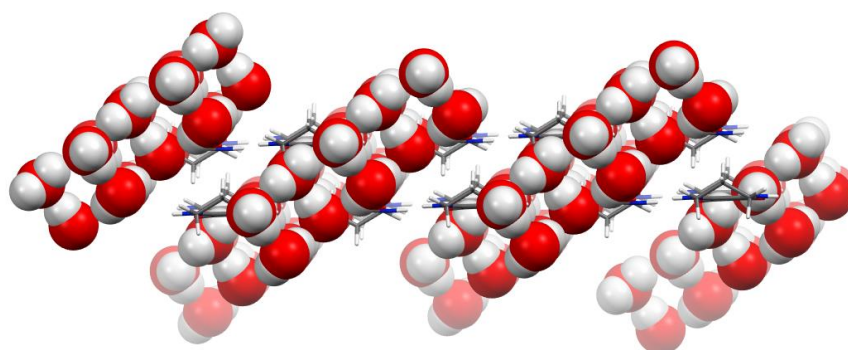


Figure 102. Perspective side view of $[3 \cdot (\text{H}_2\text{O})_2]$, showing the arrangement of the water molecules as ordered chains. These chains are tilted 38° regarding the squaramide layers.

Overall the structure of $[3 \cdot (H_2O)_2]$ is exceptional as it is composed of layers of stacked ribbons and each ribbon is surrounded by water molecules. Although irrelevant to the present work, addressed to the synthesis of multifarenes and cucurbituril analogs of squaramides, the solubility of **3** in water with the concomitant formation of a solid hydrate is certainly interesting and deserves separate future investigations for the design of squaramide-based materials.

The squaramide **3** possesses the structural features required for the oligomerization. Thus, the squaramide **3** was reacted with either formaldehyde or *p*-formaldehyde using typical conditions for cyclization processes (HCl 37%, 100°C, 18h) affording a yellow precipitate. The mass spectrum analysis showed that the solid was an inseparable mixture of oligomers (**5**) with the predominant presence of oligomers having four and five squaramide units (Figure 103). Further treatment with sulphuric acid or with concentrated HCl, to force the cyclization, resulted unsuccessful. The separation of the oligomeric mixtures using chromatographic techniques was not possible.

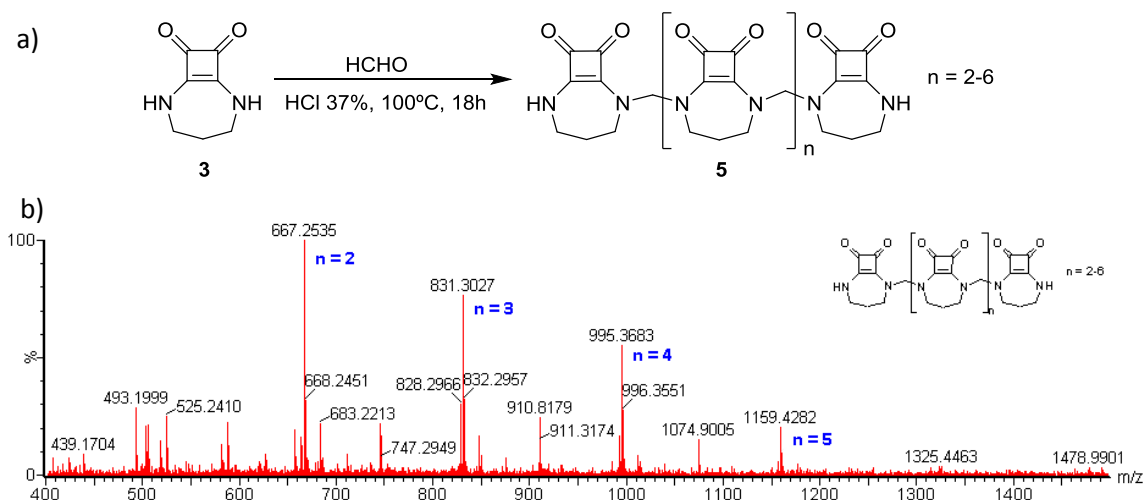


Figure 103. a) Synthesis of oligomeric squaramides **5**. b) ESI-MS mass spectra of **5** recorded in MeOH:DMSO:HCOOH (8:1:1).

Trying to avoid the uncontrolled oligomerization of **3**, we checked an alternative approach by using bromomethylbenzene as a linker between the squaramide units. The alkylation reaction was carried out using conditions previously reported for the synthesis of the product **6** (see Figure 104).

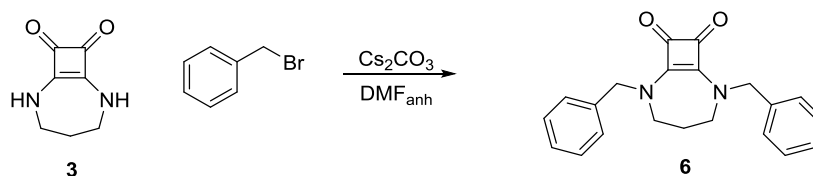


Figure 104. Synthesis of dibenzyl squaramide **6**.

Following the same procedure with 1,3-bis(bromomethyl)benzene, the corresponding macrocyclic compounds (**7a-d**) were identified by mass spectrometry, being the macrocycle **7b** the major product in the crude reaction mixture (Figure 105). When the reaction was carried out under more diluted conditions (see Supporting Information), **7a** was obtained as the major compound in the mixture. However, it was not possible to isolate each macrocycle by either partial precipitation or

chromatography. The resulting macrocycles are squaramide analogues of multifarenes.²⁶⁰ Therefore, this approach afforded the target squaramide macrocycles, unfortunately as inseparable mixtures. Knowing that the synthesis of this type of squaramide macrocycles results feasible, further work addressed to improve the ring size will be necessary before developing any application for them.

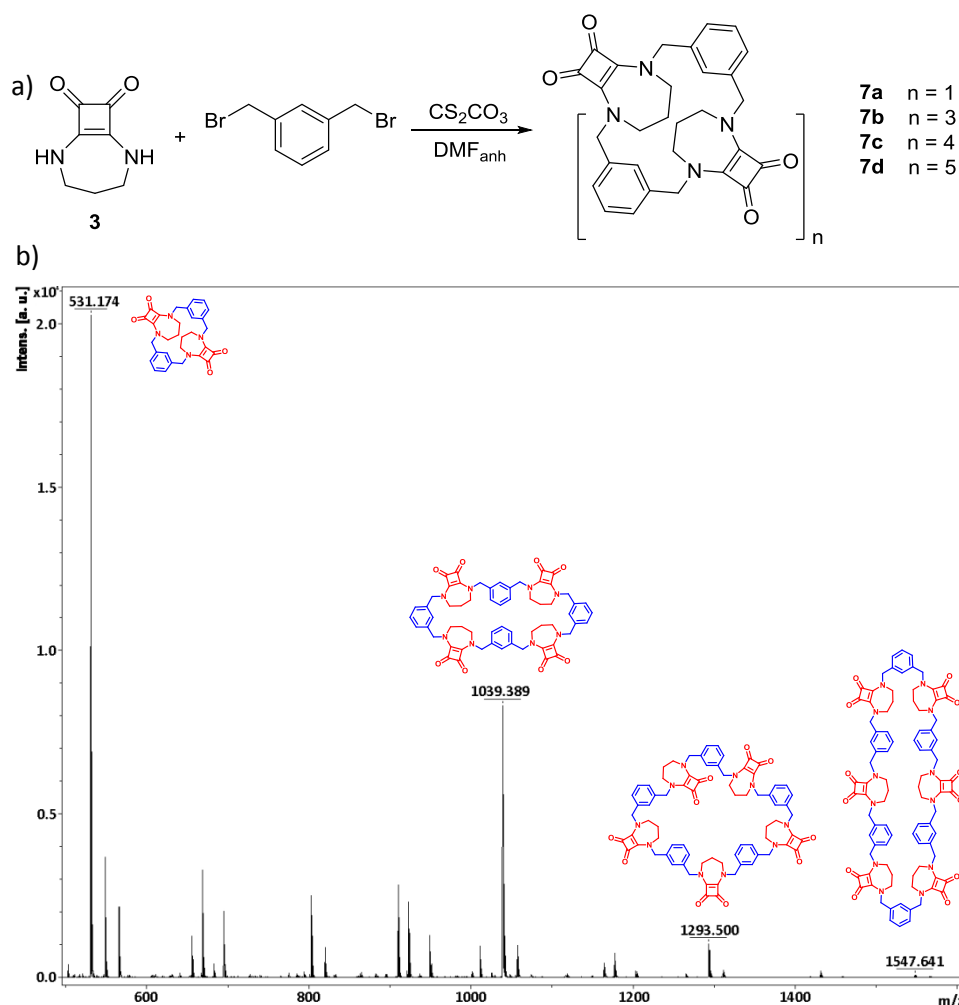


Figure 105. a) Reaction conditions for the synthesis of **7**, b) Maldi-TOF mass spectra of **7** prepared under diluted conditions.

Regarding the synthesis of squaramide analogs of glycolurils, we tried the condensation of 1,3-diaminocyclobut-1-en-1,2-dione (plain squaramide) **1** with several diketone compounds such as oxalaldehyde, 2-oxopropanal, ethyl oxalaldehyde, benzil glyoxal, benzil and 4,4'-dimethylbenzil using neutral (DMSO, r.t., 18h), acidic (benzene, TFA, reflux Dean-Stark, 24 h) or basic media (DMF, Cs₂CO₃, 100 °C, 5h). The structure of some of the expected products (**4a** and **4b**) is shown in Figure 98.

All these attempts resulted unsuccessful, and the squaramide analog of glycoluril has never been detected. Instead, the condensation of squaramide **1** with aromatic benzils leads to an unexpected fragmentation of the intercarbonyl C-C bond of benzils (**4b'**). These reactions are described in the paper next to this section.

²⁶⁰ Parvari, G.; Annamalai, S.; Borovoi, I.; Chechik, H.; Botoshansky, M.; Pappo, D.; Keinan, E. *Chem. Commun.* **2014**, 50, 2494-2497.

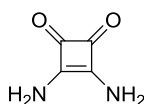
Noticeably, a cucurbituril type macrocycle based on propane diurea instead of glycoluril has recently been reported.²⁶¹

4.4.4 Conclusions

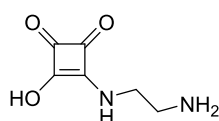
In conclusion, two new series of squaramide-based oligomers and macrocyclic compounds have been synthesised and characterized as a mixture of products. However, the isolation as pure compounds of the different members of both families of compounds has not been possible until now.

²⁶¹ Ustrnul, L.; Kulhanek, P.; Lizal, T.; Sindelar, V. *Org. Lett.* **2015**, *17*, 1022-1025.

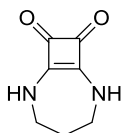
4.4.5 Supporting information



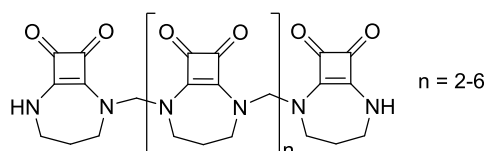
3,4-diaminocyclobut-3-ene-1,2-dione (1). 15 mL (108 mmol) of 7M ammonia solution in methanol were added dropwise to 1.84 g (10.81 mmol) of diethyl squarate in 20 mL of EtOH and the resulting solution was stirred overnight. After the addition of the ammonia, a yellow precipitate was observed. The product was isolated by filtration and washed with EtOH (1.1 g, 91%). m.p. > 210 °C (dec.). ¹³C NMR (75 MHz, DMSO-*d*₆) δ 184.4, 170.9; IR (Film, cm⁻¹): 3298, 3128, 1814, 1661, 1621, 1565, 1502, 1384, 680, 629, 595.



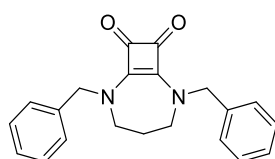
3-((2-aminoethyl)amino)-4-hydroxycyclobut-3-ene-1,2-dione (2'). 0.2 mL (2.94 mmol) of ethylenediamine dissolved in 500 mL of EtOH are slowly added to 0.5 g (2.94 mmol) of diethyl squarate in 10 mL of EtOH during 5 hours with a Harvard pump. The resulting solution is stirred for 24 hours. After this period, the product that has precipitated as white solid, is isolated by filtration and washed with EtOH (0.2 g, 49%). The resulting product is insoluble in common solvents. m.p. > 240 °C (dec.). Anal. Calcd. for C₆H₈N₂O₃: C, 46.15; H, 5.16; N, 17.94. Found: C, 46.24; H, 5.04; N, 18.99.



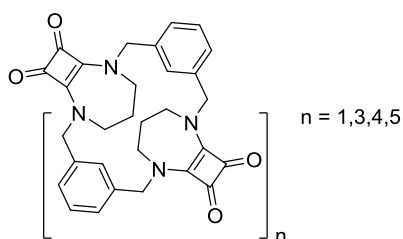
2,6-diazabicyclo[5.2.0]non-1(7)-ene-8,9-dione (3). 2.5 g (14.69 mmol) of diethyl squarate in 100 mL of MeOH and 1.487 mL (17.63 mmol) of propane-1,3-diamine in 100 mL of MeOH were added dropwise simultaneously to 100 mL of MeOH in a 500 mL round-bottom-flask. Immediately, a white precipitate is observed. The solution was stirred at room temperature overnight. The precipitate was then isolated by filtration and washed with MeOH (1.7 g, 75%). m.p. > 250 °C (dec.). ¹H NMR (300 MHz, DMSO-*d*₆) δ 8.44 (s, 2H), 3.34 (t, *J* = 2.7 Hz, 2H), 3.32 (t, *J* = 3 Hz, 2H), 1.90 (m, *J* = 4.8 Hz, 2H); ¹³C NMR (75 MHz, DMSO-*d*₆) δ 182.3, 169.8, 47.2, 31.8; IR (Film, cm⁻¹): 3196, 3052, 2967, 2914, 1807, 1621, 1557, 1364, 1325, 1273, 1207, 1118, 1004, 840, 728, 626; ESI-HRMS(+) *m/z* (%): calc. C₁₄H₁₆N₄O₄Na 327.1069; exp. 327.1064 [2M+Na]⁺. Anal. Calcd. for C₇H₈N₂O₂: C, 55.26; H, 5.30; N, 18.41. Found: C, 54.66; H, 5.31; N, 18.41.



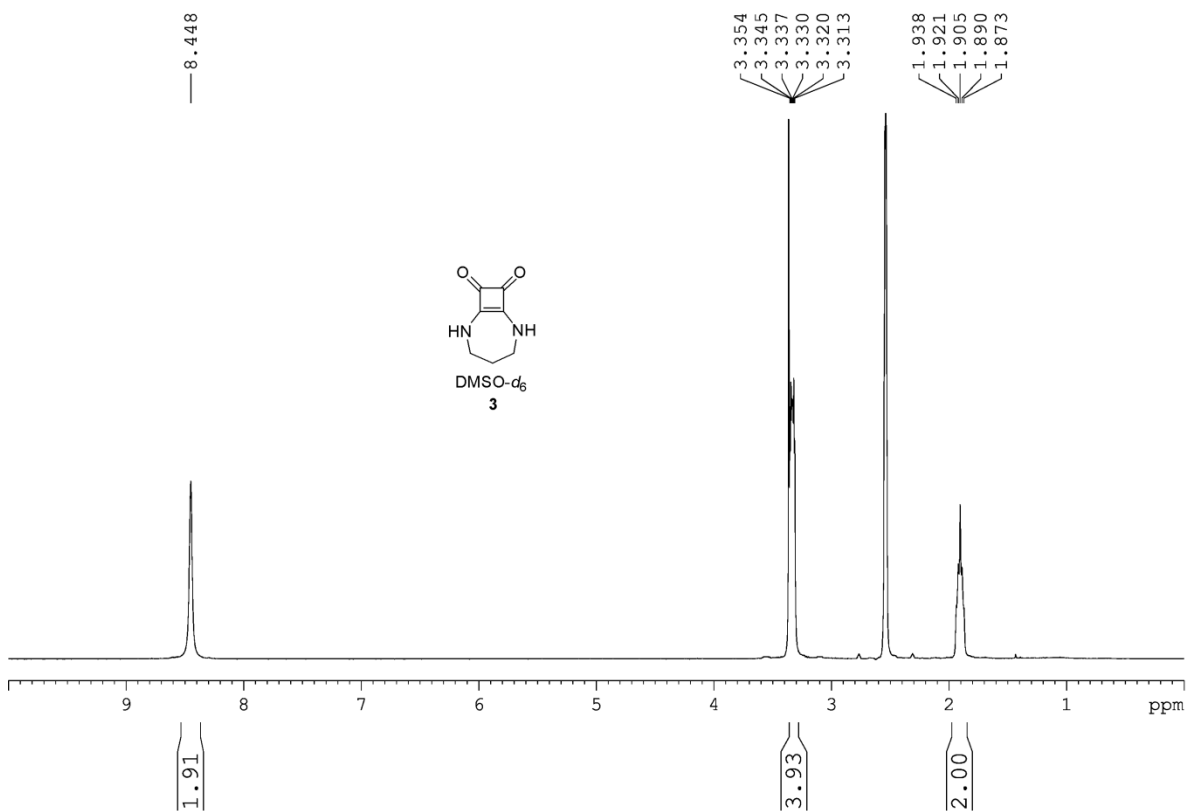
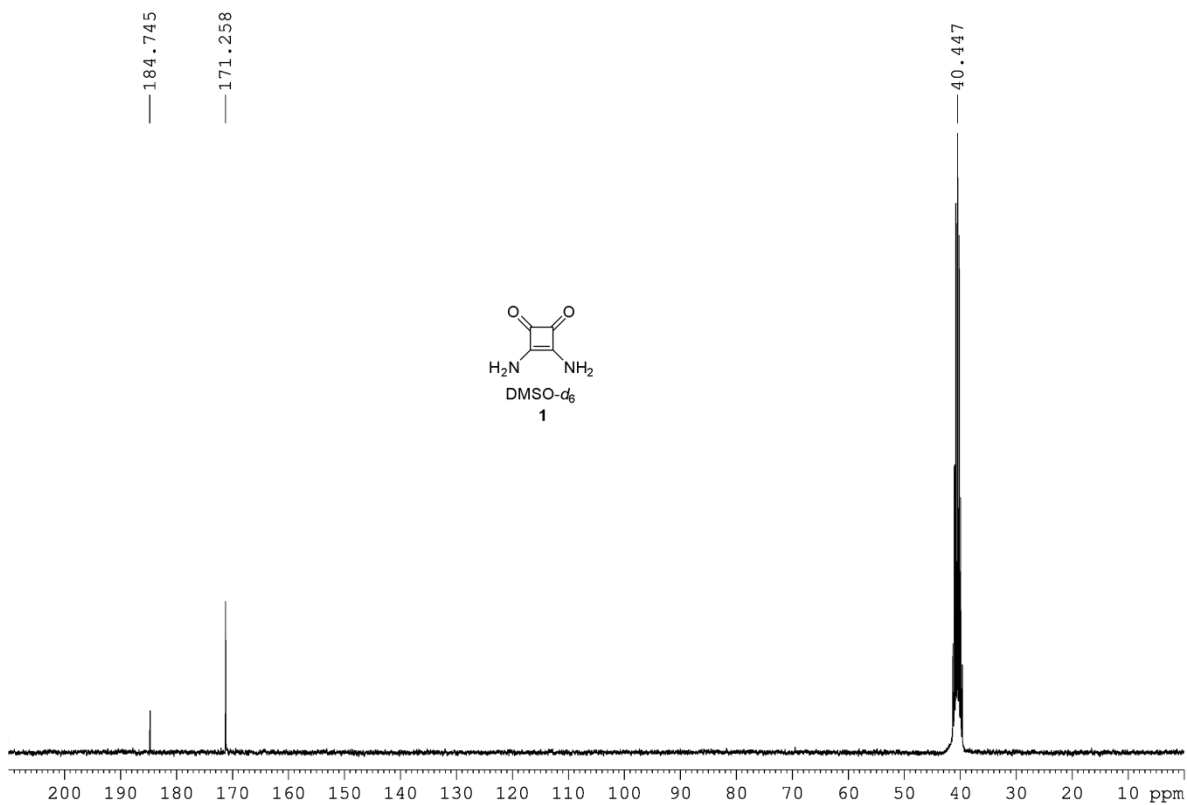
5. 1 g (6.57 mmol) of 2,6-diazabicyclo[5.2.0]non-1(7)-ene-8,9-dione and 0.2 g (6.66 mmol) of paraformaldehyde were dissolved in 0.6 mL of concentrated HCl and stirred at 100°C for 5 hours. After this period, the solution was cooled to room temperature observing the apparition of a grey precipitate. The solid was then isolated by centrifugation and washed with H₂O milliQ (0.89 g, 70%). The product is partially soluble in DMSO and MeCN/H₂O mixtures. m.p. > 210 °C (dec.). ¹H NMR (300 MHz, MeCN-*d*₃:D₂O 8:2 v/v) δ 5.59 (d, *J* = 2.7, 2H), 3.42 (s, 4H), 2.03 (m, 2H); ¹³C NMR (75 MHz, DMSO-*d*₆) δ 181.7, 181.2, 180.2, 167.1, 166.9, 166.6, 62.0, 54.5, 50.0, 37.4, 28.2, 28.0.

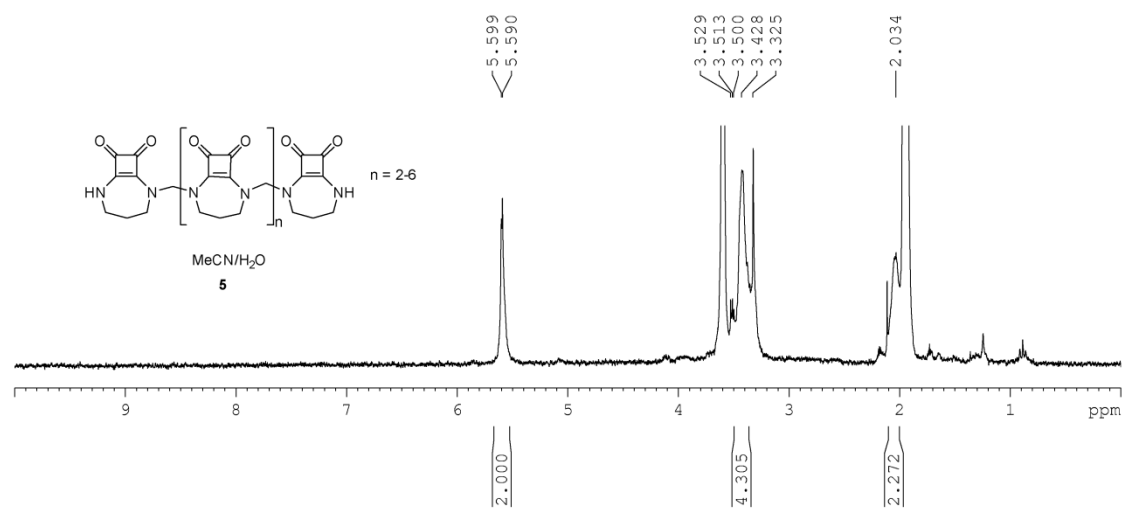
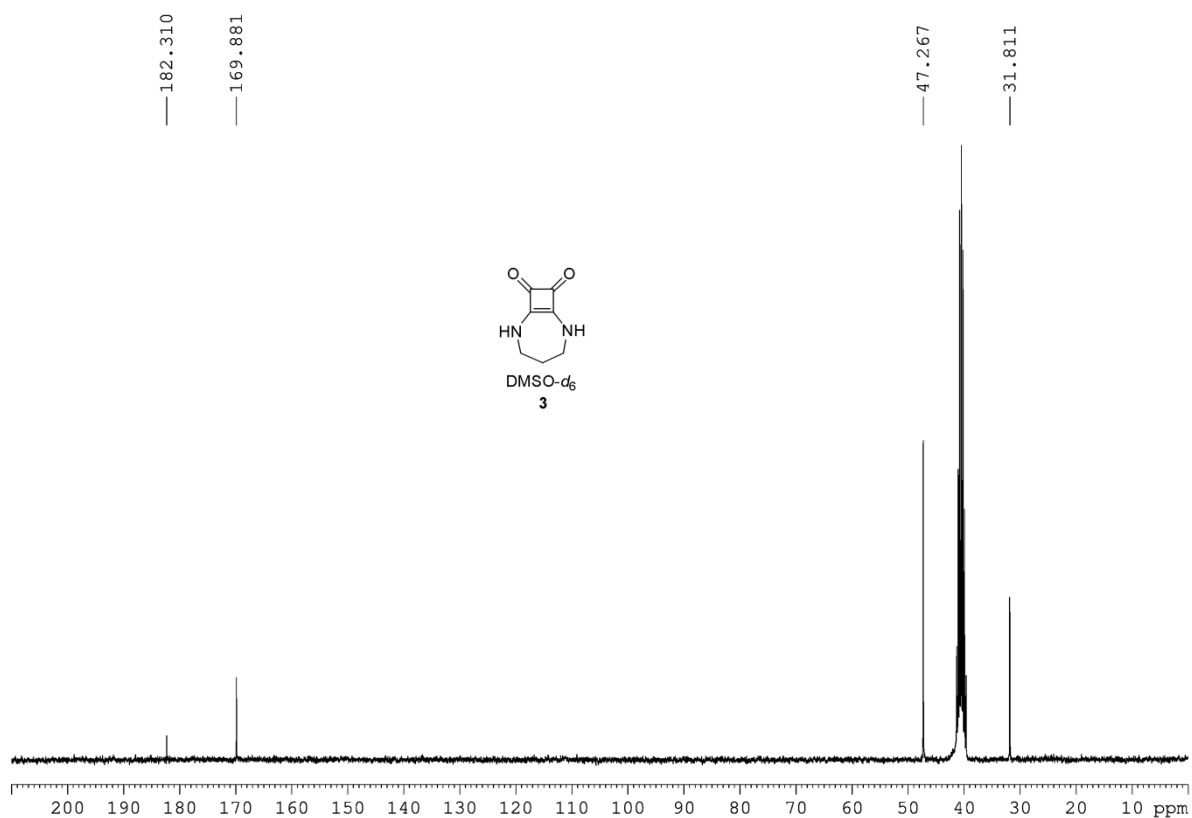


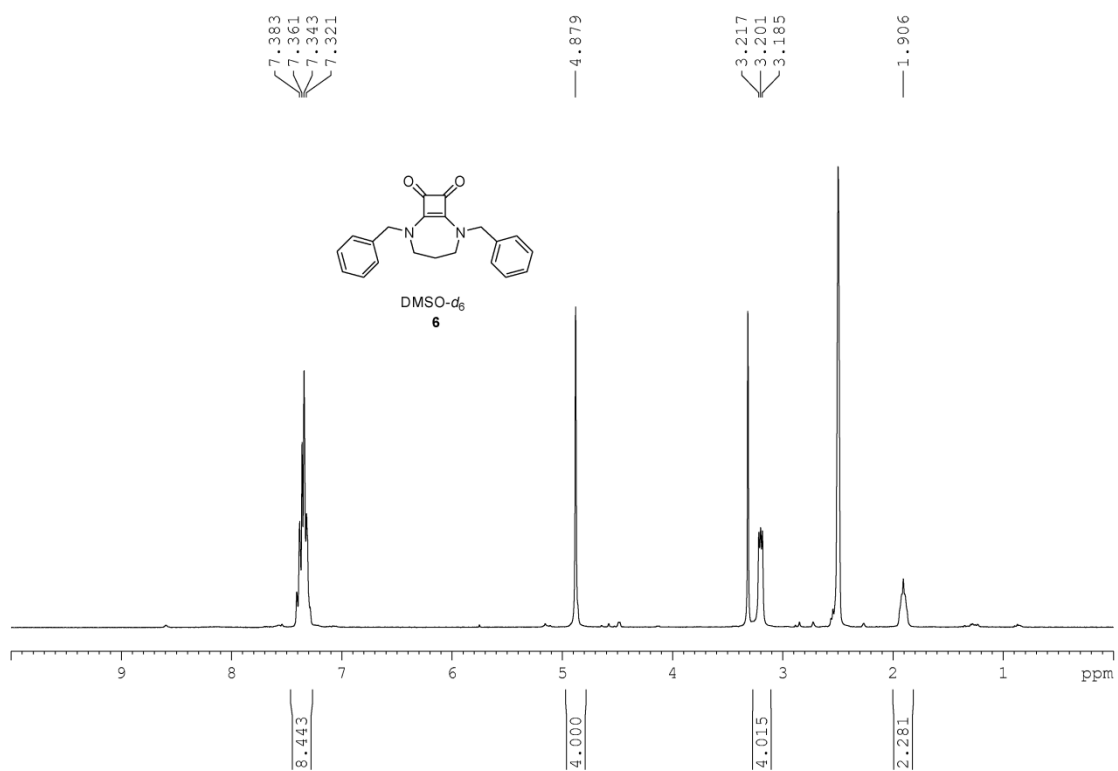
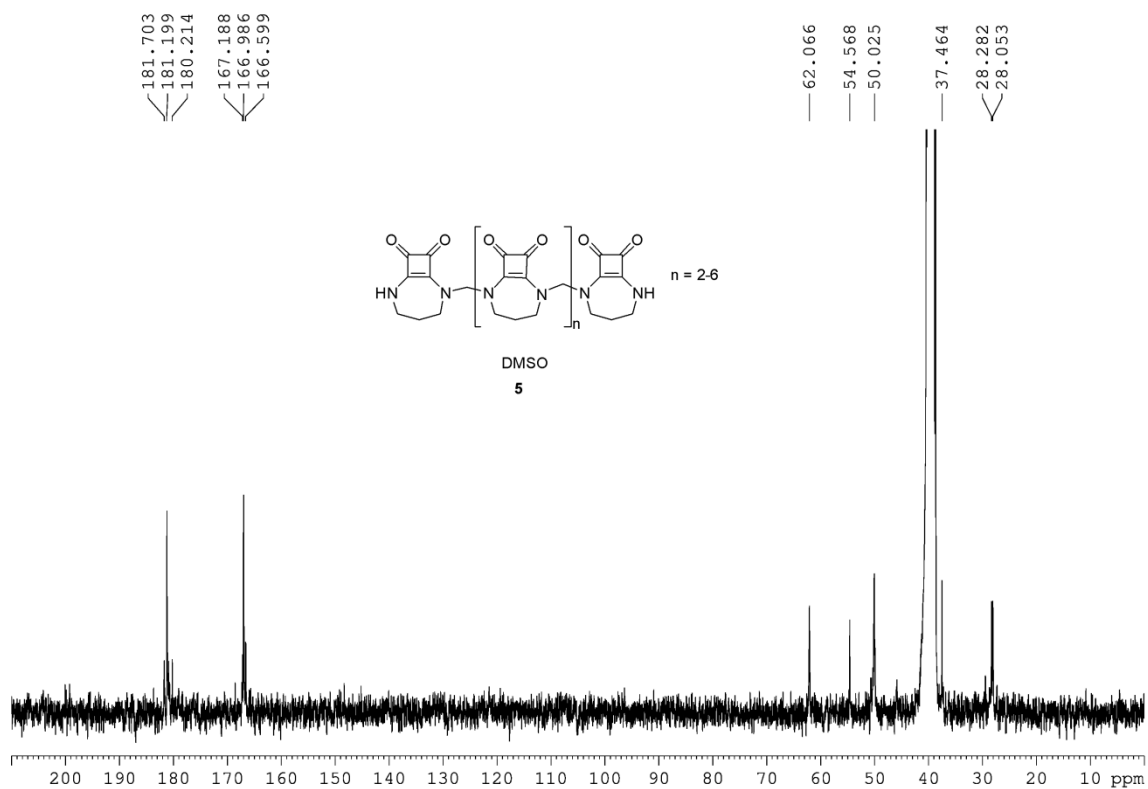
2,6-dibenzyl-2,6-diazabicyclo[5.2.0]non-1(7)-ene-8,9-dione (6). 0.319 mL (2.63 mmol) of (bromomethyl)benzene in 10 mL of anhydrous DMF were added to 0.2 g (1.314 mmol) of 2,6-diazabicyclo[5.2.0]non-1(7)-ene-8,9-dione and 0.857 g (2.63 mmol) of cesium carbonate in 40 mL of anhydrous DMF. The solution was stirred 1 day at room temperature. After this period, the solution was filtered through celite and concentrated. The resultant solid was dissolved in 20 mL of CH₂Cl₂ and washed with brine (2 × 10 mL). The organic phase was dried with Na₂SO₄, filtered and concentrated (0.25 g, 57%). mp 127-130°C. ¹H NMR (300 MHz, DMSO-*d*₆) δ 7.35 (m, 10H), 4.87 (s, 4H), 3.20 (t, *J* = 4.8 Hz, 4H), 1.90 (t, 2H); ¹³C NMR (75 MHz, DMSO-*d*₆) δ 180.9, 166.7, 136.4, 128.7, 128.0, 127.8, 53.1, 51.93, 28.5; ESI-HRMS(+) *m/z* (%): calc. C₂₁H₂₁N₂O₂ 333.1603; exp. 333.1601 [M+H]⁺.

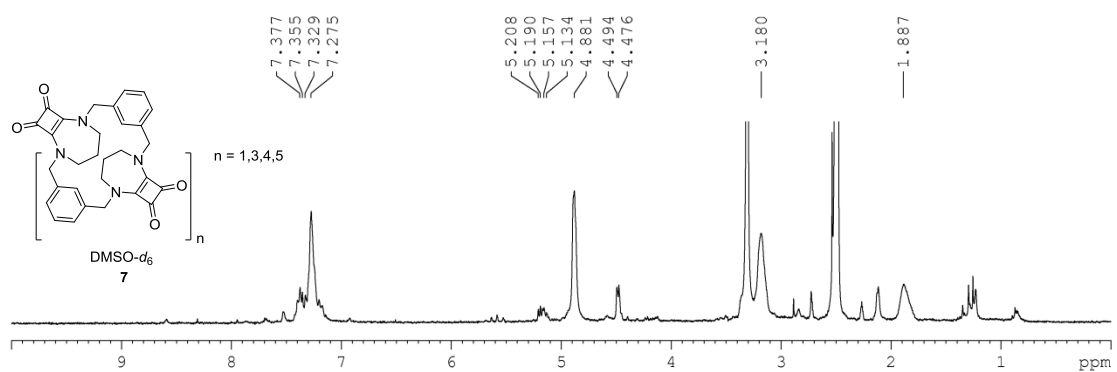
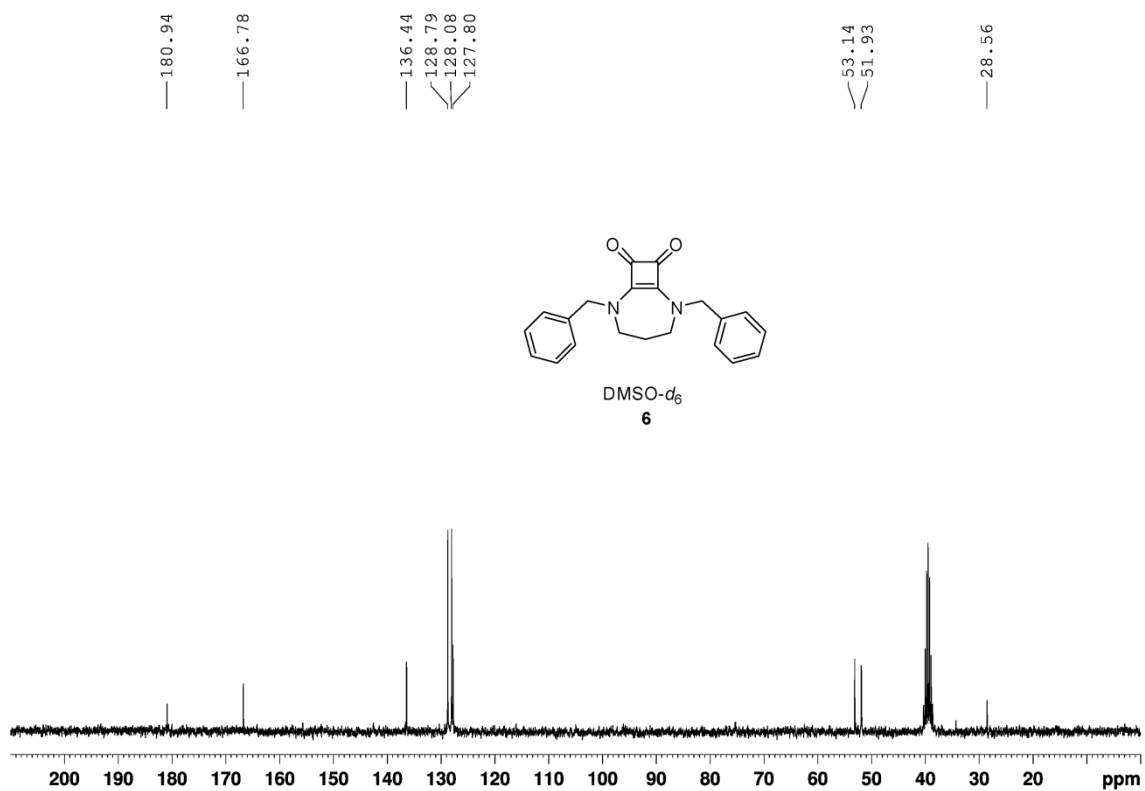


7. 0.179 g (0.657 mmol) of 1,3-bis(bromomethyl)benzene in 10 mL of anhydrous DMF were added to 0.1 g (0.657 mmol) of 2,6-diazabicyclo[5.2.0]non-1(7)-ene-8,9-dione and 0.5 g (1.544 mmol) of cesium carbonate in 15 mL of anhydrous DMF. The solution was stirred at room temperature 6 days. After this period, the solution was filtered through celite, concentrated and washed with diethyl ether. The isolated solid was then dissolved in 20 mL of CH₂Cl₂ and washed with an saturated aqueous solution of LiCl (5 × 10 mL) (15-30%). m.p. > 260 °C (dec.). ¹H NMR (300 MHz, DMSO-*d*₆) δ 7.28 (m, 4 H), (5.20 (m = 0.75 H)), 4.88 (s, 4H), 4.48 (d, *J* = 4.8 Hz, 0.75H), 3.18 (s, 4H), 1.87 (s, 2H); ¹³C NMR (75 MHz, DMSO-*d*₆) δ 181.7, 181.2, 180.2, 167.1, 166.9, 166.6, 62.0, 54.5, 50.0, 37.4, 28.2, 28.0.









4.4.5.1. X-ray Crystal Structure Analysis

Table S4. Crystallographic data of **3**.

Empirical formula	C ₇ H ₁₂ N ₂ O ₄	
Formula weight	188.19	
Temperature (K)	100(2)	
Wavelength (Å)	0.71073	
Crystal system, space group	Triclinic, <i>P</i> -1	
Unit cell dimensions	a = 5.3851(6)	α = 77.366(3)
	b = 7.5472(8)	β = 83.202(3)
	c = 10.9853(11)	γ = 80.882(3)
Volume (Å ³)	428.53(8)	
Z, calculated density (Mg/m ³)	2, 1.458	
Absorption coefficient	0.120	
<i>F</i> (000)	200	
Crystal size (mm)	0.20 x 0.10 x 0.03	
θ range for data collection	1.91-30.06	
Index ranges	-7 ≤ <i>h</i> ≤ 7, -10 ≤ <i>k</i> ≤ 10, -14 ≤ <i>l</i> ≤ 15	
Reflections collected (unique)	2284/2147 [<i>R</i> (int) = 0.0337]	
Completeness to theta = 30.06 °	0.907%	
Max. and min. transmission	0.9964 and 0.9764	
Goodness-of-fit on <i>F</i> ²	1.079	
Final <i>R</i> indices [<i>I</i> > 2σ(<i>I</i>)]	<i>R</i> ₁ = 0.0367, <i>wR</i> ₂ = 0.0993	
<i>R</i> indices (all data)	<i>R</i> ₁ = 0.0385, <i>wR</i> ₂ = 0.1020	

Unexpected Squaramide-Induced Cleavage of Benzils: Synthesis and Characterization of mono-Aroyl Squarimides

Elena Sanna^a, Carlos López^a, Pablo Ballester^{b,c}, Carmen Rotger^a, Antoni Costa^{*a}

^a Department of Chemistry, Universitat de les Illes Balears, Ctra. Valldemossa, km 7.5, 07122 Palma de Mallorca, Spain.

^b Institute of Chemical Research of Catalonia (ICIQ), Avda. Països Catalans 16, 43007 Tarragona (Spain).

^c Catalan Institution of Research and Advanced Studies (ICREA), Passeig Lluís Companys 23, 08010-Barcelona (Spain).

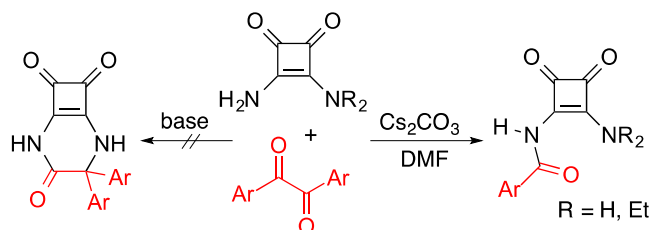
***Eur. J. Org. Chem.*, 2015, 35, 7656-7660**

Received: September 25, 2015

Published: November 10, 2015

4.5.1 Abstract

We report the reaction of 4,4'-substituted benzils with squaramides (SQ) affording mono-squarimides (SQIs). The ^1H NMR and X-ray structures of the SQIs (R=H) revealed the existence of a strong $\text{C}=\text{O}\cdots\text{HN}$ intramolecular hydrogen-bond motif. The unprecedented reaction between SQs and benzils highlights the difference in reactivity between urea and squaramide units.



4.5.2 Introduction

Squaric acid bisamides (a.k.a. squaramides, SQ) are excellent double hydrogen bond donors²⁶² and acceptors²⁶³ displaying excellent chemical stability. The hydrogen bond properties of SQs are critical for the successful application of squaramide units in important areas such as molecular recognition,²⁶⁴ organocatalysis,²⁶⁵ biomimetic transport,²⁶⁶ ion sensing²⁶⁷ and cell labelling.²⁶⁸ The synthesis of SQs is

²⁶² For pioneering works, see: (a) Rotger, C.; Soberats, B.; Quiñonero, D.; Frontera, A.; Ballester, P.; Benet-Buchholz, J.; Deyà, P. M.; Costa, A. *Eur. J. Org. Chem.* **2008**, 2008, 1864-1868. (b) Storer, R. I.; Aciro, C.; Jones, L. H. *Chem. Soc. Rev.* **2011**, 40, 2330-2346. (c) Quiñonero, D.; Frontera, A.; Suñer, G. A.; Morey, J.; Costa, C.; Ballester, P.; Deyà, P. M. *Chem. Phys. Lett.* **2000**, 326, 247-254. (d) Prohens, R.; Rotger, M. C.; Piña, M. N.; Deyà, P. M.; Morey, J.; Ballester, P.; Costa, A. *Tetrahedron Lett.* **2001**, 42, 4933-4936. (e) Prohens, R.; Tomas, S.; Morey, J.; Deyà, P. M.; Ballester, P.; Costa, A. *Tetrahedron Lett.* **1998**, 39, 1063-1066.

²⁶³ For pioneering works, see: (a) Tomás, S.; Prohens, R.; Vega, M.; Rotger, M. C.; Deyà, P. M.; Ballester, P.; Costa, A. *J. Org. Chem.* **1996**, 61, 9394-9401. (b) Quiñonero, D.; Prohens, R.; Frontera, A.; Ballester, P.; Garau, C.; Costa, A.; Deyà, P. M. *Chem. Phys. Lett.* **2002**, 351, 115-120. (c) Tomás, S.; Prohens, R.; Deslongchamps, G.; Ballester, P.; Costa, A. *Angew. Chem. Int. Ed.* **1999**, 38, 2208-2211. (e) Tomás, S.; Rotger, M. C.; González, J.; Deyà, P. M.; Ballester, P.; Costa, A. *Tetrahedron Lett.* **1995**, 36, 2523-2526.

²⁶⁴ For selected examples, see: (a) Alemán, J.; Parra, A.; Jiang, H.; Jørgensen, K. A. *Chem. –Eur. J.* **2011**, 17, 6890-6899. (b) Soberats, B.; Martínez, L.; Sanna, E.; Sampedro, A.; Rotger, C.; Costa, A. *Chem.–Eur. J.* **2012**, 18, 7533-7542. (e) López, C.; Sanna, E.; Carreras, L.; Vega, M.; Rotger, C.; Costa, A. *Chem. –Asian J.* **2013**, 8, 84-87. (g) Jin, C.; Zhang, M.; Wu, L.; Guan, Y.; Pan, Y.; Jiang, J.; Lin, C.; Wang, L. *Chem. Commun.* **2013**, 49, 2025-2027. (h) Carmine Gaeta, C.; Talotta, C.; Della Sala, P.; Margarucci, L.; Casapullo, A.; Neri, P.; *J. Org. Chem.* **2014**, 79, 3704-3708.

²⁶⁵ For selected examples, see: (a) Malerich, J. P.; Hagihara, K.; Rawal, V. H. *J. Am. Chem. Soc.* **2008**, 130, 14416-14417. (b) Tungen, J. E.; Nolsøe, J. M.; Hansen, T. V. *Org. Lett.* **2012**, 14, 5884-5887. (c) Jarava-Barrera, C.; Esteban, F.; Navarro-Ranninger, C.; Parra, A.; Alemán, J. *Chem. Commun.* **2013**, 49, 2001-2003. (d) Wang, X.; Yao, W.; Yao, Z.; Ma, C. *J. Org. Chem.* **2012**, 77, 2959-2965. (e) Min, C.; Han, X.; Liao, Z.; Wu, X.; Zhou, H. -B.; Dong, C. *Adv. Syn. Catal.* **2011**, 353, 2715-2720. (f) Zhu, Y.; Malerich, J. P.; Rawal, V. H. *Angew. Chem. Int. Ed.* **2010**, 49, 153-156. (g) A. G.; Xia, A. B.; Xu, Z. Y. *Chem.–Eur. J.* **2010**, 16, 4177-4180. (h) Zhu, Y.; Malerich, J. P.; Rawal, V. H. *Angew. Chem. Int. Ed. Engl.* **2010**, 49, 153-156. (i) Jiang, H.; Rodríguez-Escrich, C.; Johansen, T. K.; Davis, R. L.; Jørgensen, K. A. *Angew. Chem. Int. Ed. Engl.* **2012**, 51, 10271-10274.

²⁶⁶ (a) Wu, X.; Busschaert, N.; Wells, N. J.; Jiang, Y. B.; Gale, P. A. *J. Am. Chem. Soc.* **2015**, 137, 1476-1484. (b) Busschaert, N.; Kirby, I. L.; Young, S.; Coles, S. J.; Horton, P. N.; Light, M. E.; Gale, P. A. *Angew. Chem. Int. Edit.* **2012**, 51, 4426-4430.

²⁶⁷ (a) Ambrosi, G.; Formica, M.; Fusi, V.; Giorgi, L.; Guerri, A.; Micheloni, M.; Paoli, P.; Pontellini, R.; Rossi, P. *Chem. –Eur. J.* **2007**, 13, 702-712. (b) Prohens, R.; Martorell, G.; Ballester, P.; Costa, A. *Chem. Commun.* **2001**, 1456-1457. (c) Piña, M. N.; Soberats, B.; Rotger, C.; Ballester, P.; Deyà, P. M.; Costa, A. *New J. Chem.* **2008**, 32, 1919-1923. (d) Rostami, A.; Wei, C. J.; Guérin, G.; Taylor, M. S. *Angew. Chem. Int. Ed. Engl.* **2011**, 50, 2059-2062. (e) Song, H. L.; Yuan, K.; Wu, X. Y. *Chem. Commun.* **2011**, 47, 1012-1014. (f) Elmes, R. B.; Turner, P.; Jolliffe, K. A. *Org. Lett.* **2013**, 15, 5638-5641. (g) Piña, M. N.; Rotger, M. C.; Costa, A.; Ballester, P.; Deyà, P. M. *Tetrahedron Lett.* **2004**, 45, 3749-3752.

straightforward, the vast majority of SQs described so far are obtained by condensation of amines with commercially available dialkyl esters of squaric acid.²⁶⁹ This methodology, universally embraced to synthesize SQs, allows the preparation of alkyl and aryl substituted squaramides. The hydrogen bond patterns and properties of these SQ units are modulated by proper selection of the amino substituents attached to the cyclobuten-1,2-dione ring.²⁷⁰ However, synthetic methods leading to other squaric acid derivatives that could potentially broaden the applicability of SQs, are very scarce. In this work, we report the synthesis of mono-squaramide-imide hybrids (SQIs) obtained by reacting simple SQs with benzils.²⁷¹ In a context of hydrogen bonding interactions, the imide functionality is particularly attractive owing to the expected enhanced acidity of the imide NH proton. A previous method for the synthesis of SQIs lead to mixtures of mono- and disubstitution products.²⁷²

4.5.3 Results and discussion

Preliminary experiments were performed with 4,4-dimethylbenzyl **1a** (R = Me) and 3,4-diamino cyclobut-3-en-1,2-dione (squaramide, SQ **2a**, R' = H) in neutral (i.e. DMSO, r.t. 18h) or acid media (EtOH, HCl, reflux, 4h), affording unreacted starting materials or intractable reaction mixtures. However, in the presence of a base, the reaction of **1a** and **2a** evolved through a completely unexpected new route. In principle, the benzil molecule could react in three different ways in the presence of a base:²⁷³ (i) by benzil-benzilic acid rearrangement, (ii) by cleavage of the carbon-carbonyl bond, and (iii) by cleavage of the intercarbonyl single bond of benzil. In addition, given the structural similarities between urea and the simple squaramide **2a**, the condensation of SQ **2a** with benzils to afford products such as (I) and (II), that is the squaramide analogues of glycouryls and hydantoins, could also be envisaged.

To avoid the formation of products originating from the benzilic acid rearrangement and/or the basic hydrolysis of SQ **2a**, we choose to use Cs₂CO₃ in anhydrous DMF as reaction medium.²⁷⁴ Cesium carbonate in DMF solution is basic enough to cause a partial deprotonation of SQ and promote the nucleophilic attack of the SQ **2a** anion on one of the carbonyl groups of the benzils. To our surprise, the reaction of 4,4-dimethylbenzil **1a** and SQ **2a** under the selected initial conditions (rt, 96h, anhydrous DMF, Ar balloon) afforded the mono-aroyl squarimide **3a** that was isolated as a solid in 37% yield simply by filtration (Table 13, entry 1). A careful analysis of the mother liquors revealed the presence in

(h) Sanna, E.; Martínez, L.; Rotger, C.; Blasco, S.; González, J.; García-España, E.; Costa, A. *Org. Lett.* **2010**, *12*, 3840-3843.

²⁶⁸ Rotger, C.; Sampedro, A.; Villalonga, R.; Vega, M.; Ramis, G.; Fernández de Mattos, S.; Villalonga, P.; Costa, A. *Bioconjug. Chem.* **2014**, *25*, 1537-1546.

²⁶⁹ For selected examples, see: (a) Rotger, C.; Piña, M. N.; Vega, M.; Ballester, P.; Deyà, P. M.; Costa, A. *Angew. Chem. Int. Edit.* **2006**, *45*, 6844-6849. (b) Rostami, A.; Colin, A.; Li, X. Y.; Chudzinski, M. G.; Lough, A. J.; Taylor, M. S. *J. Org. Chem.* **2010**, *75*, 3983-3992. (c) Storer, R. I.; Aciro, C.; Jones, L. H. *Chem. Soc. Rev.* **2011**, *40*, 2330-2346. (d) Sato, K.; Seio, K.; Sekine, M. *J. Am. Chem. Soc.* **2002**, *124*, 12715-12724. (e) López, C.; Vega, M.; Sanna, E.; Rotger, C.; Costa, A. *RSC. Adv.* **2013**, *3*, 7249-7253. (f) Sejwal, P.; Han, Y.; Shah, A.; Luk, Y. Y. *Org. Lett.* **2007**, *9*, 4897-4900. (g) Wurm, F.; Steinbach, T.; Klok, H. A. *Chem. Commun.* **2013**, *49*, 7815-7817. (j) Wurm, F. R.; Klok, H. -A. *Chem. Soc. Rev.* **2013**, *42*, 8220-8236.

²⁷⁰ (a) Ramalingam, V.; Domaradzki, M. E.; Jang, S.; Muthyala, R. S. *Org. Lett.* **2008**, *10*, 3315-3318. (b) Porel, M.; Ramalingam, V.; Domaradzki, M. E.; Young, V. G.; Ramamurthy, V.; Muthyala, R. S. *Chem. Commun.* **2013**, *49*, 1633-1635. (c) Rotger, M. C.; Piña, M. N.; Frontera, A.; Martorell, G.; Ballester, P.; Deyà, P. M.; Costa, A. *J. Org. Chem.* **2004**, *69*, 2302-2308. (d) Lim, N. C.; Morton, M. D.; Jenkins, H. A.; Brückner, C. *J. Org. Chem.* **2003**, *68*, 9233-9241. (e) Martínez, L.; Sampedro, A.; Sanna, E.; Costa, A.; Rotger, C. *Org. Biomol. Chem.* **2012**, *10*, 1914-1921. (f) Piña, M. N.; Rotger, C.; Soberats, B.; Ballester, P.; Deyà, P. M.; Costa, A. *Chem. Commun.* **2007**, 963-965.

²⁷¹ For earlier synthesis of SQIs, see: (a) Davis, A. P.; Draper, S. M.; Dunne, G.; Ashton, P.; *Chem. Commun.* **1999**, 2265-2266, (b) Chen, Y.; Li, L.; Li, W.; Yu, L.; Pan, H. *J. Sichuan Univ. Nat. Sci. Ed.* **1996**, *33*, 90.

²⁷² Chen, Y.; Li, J.; Li, W.; Yu, L.; Pan, H. *Sichuan Daxue Xuebao, Ziran Kexueban* **1996**, *33*, 87-90.

²⁷³ Bowden, K.; Fabian, W. M. *J. Phys. Org. Chem.* **2001**, *14*, 794-796.

²⁷⁴ Cella, J. A.; Bacon, S. W. *J. Org. Chem.* **1984**, *49*, 1122.

solution of minor amounts of 4-methylbenzaldehyde and 4-methylbenzoic acid. Inspired by this result, we screened other reaction conditions. The reaction carried out with NMP as solvent afforded **3a** in 45% yield (entry 2). Bases such as Na_2CO_3 or Et_3N in DMF solution were completely ineffective in mediating the reaction, and the starting benzil **1a** was recovered almost unaltered. The addition of 1% water or additives such as EtSH to the DMF solution inhibited the reaction completely.

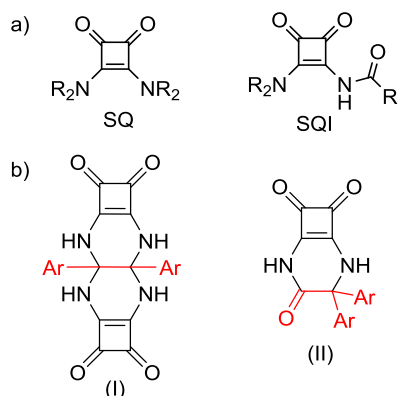
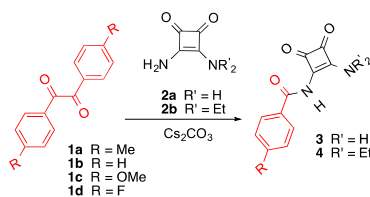


Figure 106. a) General structures of squaramide (SQ) and squarimide (SQI) compounds. b) Expected products from the condensation of squaramides with benzil compounds.

Next, we speculated whether the presence of the two primary amino groups of SQ **2a** were necessary to promote the reaction. To evaluate this possibility we performed the reaction with the N,N-diethylsquaramide **2b** featuring the two NH hydrogens of one amino group replaced by ethyl groups. Noticeably, SQ **2b** also reacted with **1a** but in a moderate yield to give SQI **4a** ($\text{R} = \text{Me}$; $\text{R}' = \text{Et}$) (entry 3). This finding demonstrated that only one primary amine group of the squaramide unit was involved in the reaction. The increased solubility of SQ **2b** allowed the use of less polar solvents. The reaction of **1a** with SQ **2b** in anhydrous MeCN at room temperature and for an extended period (4-5 days) yielded **4a** in 41% (entry 4). The same reaction at reflux for 5 hours results in a marked decrease in yield (entry 5). It is worth noting that the reactions carried out with SQs and other 1,2-dicarbonyl compounds different from benzils, namely: 2,3-butanedione, phenylglyoxal and methylglyoxal mainly resulted in the recovery of the starting materials. On the other hand, the reaction of phenantrene-9,10-quinone with SQ **2a** and of acenaphthenequinone with SQ **2b** afforded complex mixtures containing minor amounts (< 8%) of the double SQIs at m/z 562.9964 and 539.1907 assigned to $[\text{M}(\text{C}_{22}\text{H}_{14}\text{N}_4\text{O}_6)+\text{Cs}]^+$ and $[\text{M}(\text{C}_{28}\text{H}_{28}\text{N}_4\text{O}_6)+\text{Na}]^+$, respectively. Although far from ideal, these results provide an indication that SQ anions added to both carbonyl carbons of the 1,2-diketones. Conversely, the separated reaction of benzils **1a** ($\text{R} = \text{Me}$), **1b** ($\text{R} = \text{H}$), **1c** ($\text{R} = \text{OMe}$) and **1d** ($\text{R} = \text{F}$) with SQs **2a** and **2b** using optimized experimental conditions (DMF, 100°C , 5h) allowed the isolation of the corresponding SQIs **3** and **4** in moderate to good yields (Table 13, entries 6 to 13).

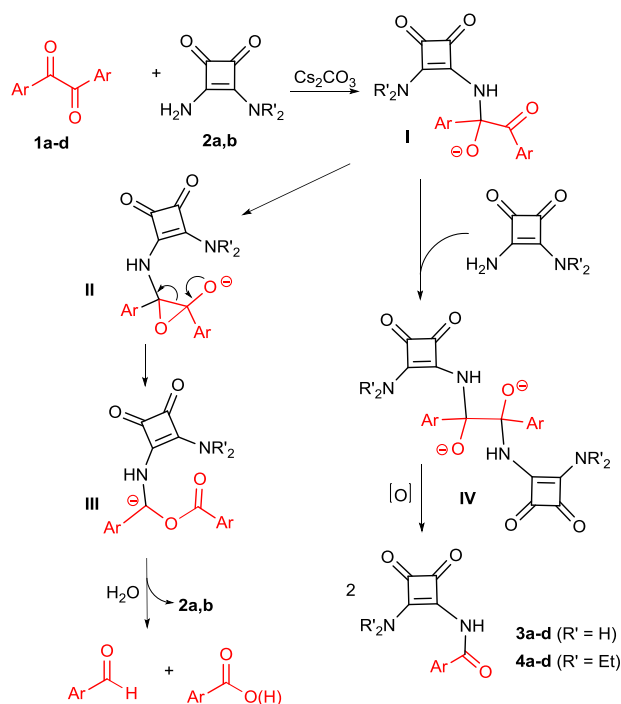
Table 13. Different reaction conditions assayed for the preparation of SQIs.

entry	benzil ^a	SQ	T(°C)/t(h)/solvent	SQI	Yield ^{b,c} (%)
1	1a	2a	rt/96/DMF	3a	37
2	1a	2a	rt/96/NMP	3a	45
3	1a	2b	rt/96/DMF	4a	17
4	1a	2b	rt/96/MeCN	4a	41 ^d
5	1a	2b	Δ /5/MeCN	4a	6 ^d
6	1a	2a	100/5/DMF	3a	65
7	1a	2b	100/5/DMF	4a	61
8	1b	2a	100/5/DMF	3b	54
9	1b	2b	100/5/DMF	4b	67
10	1c	2a	100/5/DMF	3c	32
11	1c	2b	100/5/DMF	4c	31 ^d
12	1d	2a	100/5/DMF	3d	54
13	1d	2b	100/5/DMF	4d	75

^a Reactions performed at 0.22 mmol scale with molar ratios 1:2:6 benzil:SQ:Cs₂CO₃ in DMF (4 mL). ^b Isolated yields of SQIs **3** and **4** were calculated considering the benzil as the limiting reagent able of converting two moles of SQ into product (see supporting information). ^c The purity of SQIs was checked by NMR and HPLC. ^d Determined by HPLC

The formation of SQIs **3** and **4** is surprising since it implies the cleavage of the single bond between the carbonyl groups of the benzils. Intercarbonyl C–C bond cleavage is an unlikely reaction pathway that is observed in benzil-benzilic acid rearrangements of benzils having strong electron-withdrawing substituents in their aryl groups.²⁷⁵ However, in the reaction described here the SQ acted as a strong nucleophile and promoted the intercarbonyl single bond breaking of benzils having electron-donating substituents in their phenyl groups. On the basis of our results and from the inspection of the structures of the resulting SQIs, we propose a plausible mechanistic pathway for the reaction in Scheme 3.

²⁷⁵ Bowden, K.; Williams, K. D. *J. Chem. Soc. Perkin Trans 2* **1994**, 77-81.



Scheme 3. Proposed anionic mechanistic pathway for the formation of SQIs.

Similarly to what is reported for cyanide,²⁷⁶ dimsyl²⁷⁷ and thiazolium carbene²⁷⁸ nucleophiles, the highly nucleophilic squaramide anions generated from SQ **1a** or **1b** and Cs_2CO_3 , attack the carbonyl of a benzil molecule to form the alkoxide anion **I**, which, in turn, evolves to the carbanions **II** and **III** via [1,2]-C to O aroyl shift. Finally, the alkoxide anion **III** affords benzaldehyde and benzoic acid after protonation and retro-nucleophilic addition of the SQ catalyst. This "normal" pathway, present in all experimental conditions already tested, competes with the addition of a second SQ unit to the remaining carbon carbonyl of the benzil to afford the intermediate **IV**. Then, the dianion intermediate **IV** could evolve to SQIs **3** and **4** through C-C oxidative bond cleavage. Although we have no experimental evidence to support the proposed mechanism i.e. isolation of any of the intermediates, it is worth mentioning that O-centered dianions derived from α -dicarbonyl compounds undergo base-induced ionic and radical C-C bond cleavage depending on the reaction conditions.²⁷⁹

The proposed mechanism explain the formation of benzaldehyde and benzoic acid byproducts as well as the detection of the products of double SQ addition to carbonyl with phenantrene-9,10-quinone and acenaphthenequinone. In addition, this mechanistic proposal agrees with the observed 1:2 benzil to SQ stoichiometry of the reaction.

²⁷⁶ (a) Cho, D. G.; Kim, J. H.; Sessler, J. L. *J. Am. Chem. Soc.* **2008**, *130*, 12163-12167, (b) Reardon, W. C.; Wilson, J. E.; Trisler, J. C. *J. Org. Chem.* **1974**, *39*, 1596-1596, (c) Demir, A. S. Reis, O. *Tetrahedron* **2004**, *60*, 3803-3811, (d) Kwart, H.; Baevsky, M. M. *J. Am. Chem. Soc.* **1958**, *80*, 580-588.

²⁷⁷ (a) Ragno, D.; Bortolini, O.; Fantin, G.; Fogagnolo, M.; Giovannini, P. P.; Massi, A. *J. Org. Chem.* **2015**, *80*, 1937-1945, (b) Bortolini, O.; Fantin, G.; Ferretti, V.; Fogagnolo, M.; Giovannini, P. P.; Massi, A.; Pacifico, S.; Ragno, D. *Adv. Syn. Catal.* **2013**, *355*, 3244-3252.

²⁷⁸ Bertolasi, V.; Bortolini, O.; Donvito, A.; Fantin, G.; Fogagnolo, M.; Giovannini, P. P.; Massi, A.; Pacifico, S. *Org. Biomol. Chem.* **2012**, *10*, 6579-6586.

²⁷⁹ Varea, T.; Medio, M.; Ballesteros, R.; Oniga, O.; Asensio, G. *Tetrahedron* **1995**, *51*, 10093-10100.

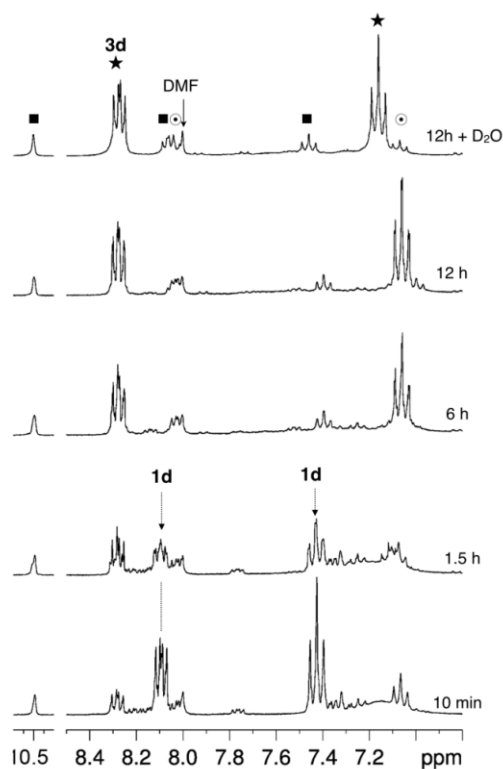


Figure 107. (A) Representative partial spectra showing the progress of the reaction of 4,4-difluorobenzil **1d** (0.05 M) with SQ **2a** (0.1 M) in 0.5 mL of d_7 -DMF at 100 °C. (**1d**) **1d**; (★) **3d**; (n) 4-fluorobenzaldehyde; (x) 4-fluorobenzoic acid (salt).

To make sure that the isolation step does not influence the results we decided to monitor the reaction at regular intervals of time using NMR spectroscopy. An NMR tube containing a solution benzil **1d**, SQ **2a** and Cs_2CO_3 in d_7 -DMF (500 μL) was heated at 100 °C in the NMR probe. After the first 10 min of reaction in which the sample was temperature stabilized and shimmed, we acquired a ^1H NMR spectrum of the solution at regular intervals during the following 12 h. The progress of the reaction was monitored by integrating the separated proton signals of benzil **1d** ($R = \text{F}$) and SQI **3d** ($R = \text{F}$; $R' = \text{H}$) in the series of acquired ^1H NMR spectra. A significant conversion of **1d** had occurred only ten minutes after the initial time count. In addition, the proton signals diagnostic of the presence of the SQI **3d** and 4-fluorobenzaldehyde in the solution were easily detected. We also observed other proton signals probably due to evolving intermediates and/or to the formation of secondary products to a lesser extent. After 6 h, the starting benzil **1d** was entirely consumed but the reaction mixture was still evolving. At the end of the reaction (12 h), the observed proton signals corresponded to a mixture of **3d**, 4-fluorobenzaldehyde, and 4-fluorobenzoic acid (salt) (Figure 107). The formation of **3d** assessed by ^1H NMR results in a 65 % yield, considering a 1:2 benzil to SQ stoichiometry. This value follows the trend of the 54 % calculated as isolated yield in the batch reaction.

The X-ray structures and the NMR data revealed marked conformational differences between type **3** and type **4** SQIs.²⁸⁰ In the following discussion, we selected compounds **3c** ($R = \text{OMe}$; $R' = \text{H}$) and **4c** ($R = \text{OMe}$; $R' = \text{Et}$) as representative examples (Figure 108). In the solid-state, the structure of **3c** is practically planar, and the amino group is coplanar with the C_4 -cycle. This observation indicated the strong conjugation of the lone pair of electrons of the N2 nitrogen atom with the squaramide ring. This

²⁸⁰ **3c** (CCDC ref. 1406379); **4c** (CCDC ref. 1406380).

observation was also substantiated by the observed short distance for the C4–N2 bond (1.308(2) Å). This value is shorter than in the analogous urea bond (NH₂–C=O, 1.334 Å) and close to that found for a C=N covalent double bond (C_{ar}–C=N–C_#, 1.279–1.314 Å).²⁸¹ In the X-ray structure of **3c**, the imide carbonyl is tilted inward forming a strong intramolecular hydrogen bond (N···O length 2.679 Å) with one of the protons of the free amino group of the primary squaramide.

Conversely, the X-ray structure of **4c** showed a non-hydrogen bonded imide proton. The imide group adopted an inverted conformation compared to that in **3c**. The plane formed by the benzoyl imide with respect to the C₄-cycle of the squaramide moiety was *ca* 41°. The NEt₂ group of **4c** is coplanar with the C₄-cycle due to the partial double bond character of the C4–N2 bond although the bond distance was slightly longer in this case (1.3155(8) Å). The planar disposition of the NEt₂ group observed in the solid state was also assisted by the formation of a CH···O intramolecular hydrogen bond.²⁸²

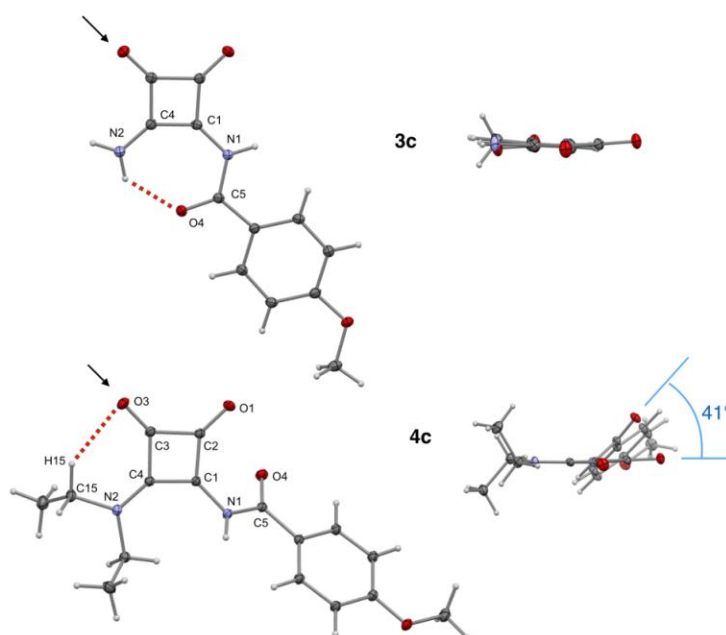


Figure 108. ORTEP front views and side views of SQIs **3c** and **4c**. Selected distances (Å) and angles (°): **3c**: NH(2)···O(4) 2.023, C(4)C(1)N(1)NH(1) torsion angle 179.21. **4c**: H(15)···O(3) 2.406, C(4)C(1)N(1)H(1) torsion angle –41.88. Displacement ellipsoids are drawn at the 50% probability level. The broken red lines indicated the intramolecular hydrogen bonding. The black arrows indicated the direction of the side views.

Finally, the acidic strength of two representative SQIs was determined by spectrophotometric acid-base titration. The pK_a's measurements were made in water containing 10% by volume MeCN. The determined values of the pK_a's for **3c** and **4c** were 9.009 ± 0.005 and 8.195 ± 0.001, respectively. The magnitudes of the pK_a values confirmed the relatively high acidity of the NH protons in SQIs compared to SQs²⁸³ (see supporting information).

²⁸¹ Allen, F. H.; Kennard, O.; Watson, D. G.; Brammer, L.; Orpen, G.; Taylor, R. *J. Chem. Soc. Perkin Trans II* **1987**, S1–S19.

²⁸² (a) Hosein, H. A.; Hall, L. A.; Lough, A. J.; Desmarais, W.; Vela, M. J.; Foxman, B. M. *Inorg. Chem.* **1998**, *37*, 4184–4189. (b) May, E.; Destro, R.; Gatti, C. *J. Am. Chem. Soc.* **2001**, *123*, 12248–12254.

²⁸³ a) López, C.; Vega, M.; Sanna, E.; Rotger, C.; Costa, A. *RSC Adv.* **2013**, *3*, 7249–7253. b) Ni, X.; Li, X.; Wang, Z.; Cheng, J. –P. *Org. Lett.* **2014**, *16*, 1786–1789.

4.5.4 Conclusions

In conclusion, we report the unprecedented cleavage of the intercarbonyl single bond of benzils promoted by squaramide anions. Unlike the formation of hydantoin or glycouryl-type products usually obtained in the reaction of benzils with urea, the described reaction afforded hybrid squarimides in good yields. The prepared SQIs feature characteristic hydrogen bond patterns offering new opportunities for the use of squaric acid derivatives as molecular components of processes governed by hydrogen bonding interactions.

4.5.5 Experimental section

General procedure for the synthesis of aroyl squarimides from 3: In a typical experiment: Squaramide **2a** (0.45 mmol) was dissolved in 3 mL of anhydrous DMF containing Cs₂CO₃ (1.34 mmol). The suspension was stirred for 15 min. A solution of benzil (0.22 mmol) in anhydrous DMF (1 mL) was then added and the mixture was stirred at 100°C 5 hours. The mixture was filtered through celite. Diethyl ether (5 mL) was added to the solution to precipitate the product. The solid isolated by filtration was dissolved in H₂O (pH = 3) and extracted with AcOEt (3×10mL). The combined organic phases were dried over Na₂SO₄, filtered and concentrated under reduced pressure.

General procedure for the synthesis of aroyl squarimides from 4: In a typical experiment: Squaramide compound **2b** (0.45 mmol) was dissolved in 3 mL of anhydrous DMF with Cs₂CO₃ (1.34 mmol). The suspension was stirred for 15 min. A solution of benzil (0.22 mmol) in anhydrous DMF (1 mL) was then added and the mixture was stirred at 100°C 5 hours. The mixture was filtered through celite and the solution concentrated. The crude product was dissolved in H₂O (pH = 3) and extracted with AcOEt (5×10mL). The combined organic phases were dried over Na₂SO₄, filtered and concentrated under reduced pressure. Finally, the product was purified by preparative HPLC when it was necessary.

4.5.6 Acknowledgements

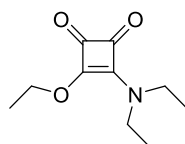
Financial support from the Spanish Ministry of Economy and Competitiveness (CTQ2014-57393-C2-1-P and CONSOLIDER-INGENIO 2010 CSD2010-00065, FEDER funds) are gratefully acknowledged. E. S. and C. L. thank CAIB and FSE for a predoctoral fellowship.

4.4.7 Supporting Information

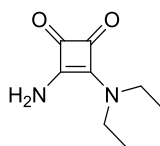
4.4.7.1. General methods

All reagents were purchased commercially and used without further purification. Mass spectra were registered on a MICROMASS Autospec3000 spectrometer equipped with an electrospray module or with a Bruker Autoflex (MALDI-ToF) using 2,5-Dihydroxybenzoic acid (DHB) as matrix. ^1H and ^{13}C spectra were recorded on Bruker AVANCE 300 (^1H at 300 MHz and ^{13}C at 75 MHz) and on Bruker AVANCE III 600 equipped with a cryoprobe, in $\text{DMSO-}d_6$ or $\text{MeCN-}d_3$ solvents and using the residual proton signal as reference. Chemical shifts (δ) are in ppm and coupling constants (J) in Hz. UV-Vis absorption spectra were recorded with a UV-2401PC Shimadzu UV-Vis recording spectrophotometer. pH measurements were carried out on a Crison micropH 2000 pH meter. Elemental analyses (C, H, N) were conducted by the "Centro de Microanálisis Elemental" of the "Universidad Complutense de Madrid" (Spain). Infrared (IR) were obtained on a Bruker Tensor 27 instrument in the solid state. HPLC spectra were registered with a GILSON system equipped with 321 pump and UV-vis-152 detector modules.

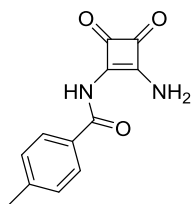
4.4.7.2. Synthesis and characterization of products



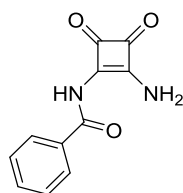
3-(diethylamino)-4-ethoxycyclobut-3-ene-1,2-dione. 1.11 mL (10.68 mmol) of diethylamine in 20 mL of MeCN were added dropwise to a solution of 2g (11.75 mmol) of diethyl squarate in 50 mL of MeCN and the resulting solution was stirred overnight. After this period, the solvent was removed by rotary evaporation and the crude product purified by column chromatography (silica, CH_2Cl_2 :MeOH) to afford the product as white solid (1.8 g, 86%). mp 37°C. ^1H NMR (300 MHz, $\text{DMSO-}d_6$) δ 4.66 (q, J = 7.2 Hz, 2H), 3.63 (q, J = 7.2 Hz, 2H), 3.41 (q, J = 7.2 Hz, 2H), 1.36 (t, J = 7.2 Hz, 3H), 1.16 (t, J = 7.2 Hz, 2H); ^{13}C NMR (75 MHz, $\text{DMSO-}d_6$) δ 189.5, 181.7, 176.7, 171.4, 69.5, 44.4, 43.8, 16.2, 15.0, 14.6; IR (Film, cm^{-1}): 3417, 3298, 3124, 2971, 1816, 1801, 1596, 1438, 1384, 1287, 1078, 1036, 983, 870, 784, 673, 574; MALDI-TOF(+) m/z (%): calc. $\text{C}_{10}\text{H}_{16}\text{NO}_3$ 330.0106; exp. 330.0118 $[\text{M}+\text{H}]^+$. Anal. Calcd. for $\text{C}_{10}\text{H}_{16}\text{NO}_3$: C, 60.90; H, 7.67; N, 7.10. Found: C, 60.84; H, 7.47; N, 7.12.



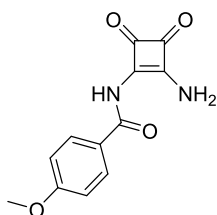
3-amino-4-(diethylamino)cyclobut-3-ene-1,2-dione (2b). 5.6 mL (39.7 mmol) of 7M ammonia solution in methanol were added dropwise to 0.964 g (4.89 mmol) of **3a** in 50 mL of MeOH and the resulting solution was stirred overnight. After this period, the solvent was removed by rotary evaporation affording **3** as yellow solid (0.8 g, 98%). mp 228°C. ^1H NMR (300 MHz, $\text{DMSO-}d_6$) δ 7.56 (s, 2H), 3.50 (s, 4H), 1.10 (t, J = 7.2 Hz, 6H); ^{13}C NMR (75 MHz, $\text{DMSO-}d_6$) δ 183.0, 182.4, 168.6, 167.3, 43.3, 15.0; IR (Film, cm^{-1}): 3340, 3186, 2978, 1791, 1662, 1566, 1511, 1469, 1324, 1171, 1079; MALDI-TOF(+) m/z (%): calc. $\text{C}_8\text{H}_{12}\text{N}_2\text{O}_2$ 301.1015; exp. 300.9948 $[\text{M}+\text{Cs}]^+$. Anal. Calcd. for $\text{C}_8\text{H}_{12}\text{N}_2\text{O}_2$: C, 57.13; H, 7.19; N, 16.66. Found: C, 57.10; H, 7.07; N, 16.55.



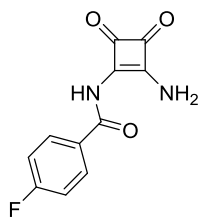
N-(2-amino-3,4-dioxocyclobut-1-en-1-yl)-4-methylbenzamide (3a). 65% yield. ^1H NMR (300 MHz, $\text{DMSO-}d_6$) δ 11.75 (s, 1H), 8.74 (s, 1H), 7.96 (d, $J=7.8$ Hz, 2H), 7.56 (s, 1H), 7.34 (d, $J=7.8$ Hz, 2H), 2.39 (s, 3H); ^{13}C NMR (75 MHz, $\text{DMSO-}d_6$) δ 195.1, 187.2, 178.9, 169.6, 166.1, 148.2, 133.8, 133.6, 25.9; IR (Film, cm^{-1}): 3391, 3248, 1810, 1703, 1679, 1618, 1558, 1524, 1497, 1385, 1322, 1085, 744, 685, 650, 609, 597; MALDI-TOF(+) m/z (%): calc. $\text{C}_{12}\text{H}_{10}\text{N}_2\text{O}_3$ 362.9740; exp. 362.9747 $[\text{M}+\text{Cs}]^+$. Anal. Calcd. for $\text{C}_{12}\text{H}_{10}\text{N}_2\text{O}_3$: C, 62.61; H, 4.38; N, 12.17. Found: C, 62.45; H, 4.45; N, 11.99.



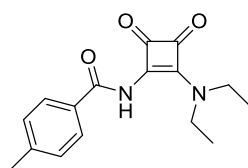
N-(2-amino-3,4-dioxocyclobut-1-en-1-yl)benzamide (3b). 54% yield. ^1H NMR (300 MHz, $\text{DMSO-}d_6$) δ 11.82 (s, 1H), 8.75 (s, 1H), 8.05 (d, $J=7.5$ Hz, 2H), 7.65 (t, $J=7.2$ Hz, 1H), 7.54 (d, $J=7.5$ Hz, 3H); ^{13}C NMR (75 MHz, $\text{DMSO-}d_6$) δ 190.5, 182.4, 174.2, 165.0, 161.3, 133.0, 131.7, 128.7, 128.5; IR (Film, cm^{-1}): 3393, 3261, 1814, 1717, 1688, 1602, 1561, 1518, 1489, 1385, 695, 636; MALDI-TOF(+) m/z (%): calc. $\text{C}_{11}\text{H}_8\text{N}_2\text{O}_3$ 348.9584; exp. 348.9587 $[\text{M}+\text{Cs}]^+$. Anal. Calcd. for $\text{C}_{11}\text{H}_8\text{N}_2\text{O}_3$: C, 61.11; H, 3.73; N, 12.96. Found: C, 60.78; H, 3.73; N, 12.91.



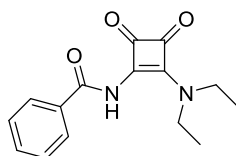
N-(2-amino-3,4-dioxocyclobut-1-en-1-yl)-4-methoxybenzamide (3c). 32% yield. ^1H NMR (300 MHz, $\text{DMSO-}d_6$) δ 11.68 (s, 1H), 8.72 (s, 1H), 8.07 (d, $J=9$ Hz, 2H), 7.55 (s, 1H), 7.07 (d, $J=9$ Hz, 2H), 3.85 (s, 3H); ^{13}C NMR (75 MHz, $\text{DMSO-}d_6$) δ 190.3, 182.2, 173.9, 164.1, 163.0, 161.7, 131.0, 123.7, 113.8, 55.5; IR (Film, cm^{-1}): 3380, 3246, 1807, 1706, 1675, 1614, 1547, 1495, 1413, 1313, 1256, 1176, 1087, 1022, 848, 688, 597; MALDI-TOF(+) m/z (%): calc. $\text{C}_{12}\text{H}_{10}\text{N}_2\text{O}_4$ 378.9689; exp. 378.9680 $[\text{M}+\text{Cs}]^+$. Anal. Calcd. for $\text{C}_{12}\text{H}_{10}\text{N}_2\text{O}_4$: C, 58.54; H, 4.09; N, 11.38. Found: C, 58.36; H, 4.16; N, 11.21.



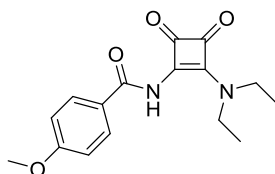
N-(2-amino-3,4-dioxocyclobut-1-en-1-yl)-4-fluorobenzamide (3d). 54% yield. ^1H NMR (300 MHz, $\text{DMSO-}d_6$) δ 11.87 (s, 1H), 8.76 (s, 1H), 8.13 (d, $J=6$ Hz, 2H), 7.55 (s, 1H), 7.38 (d, $J=8.7$ Hz, 2H); ^{13}C NMR (75 MHz, $\text{DMSO-}d_6$) δ 190.4, 182.5, 174.2, 166.5, 163.9, 163.1, 161.3, 131.7 (d, $J=9$ Hz), 128.4 (d, $J=3$ Hz), 115.7, 115.4; IR (Film, cm^{-1}): 3397, 3240, 1821, 1714, 1694, 1655, 1580, 1504, 1402, 1275, 1239, 1162, 1092, 842, 596; MALDI-TOF(+) m/z (%): calc. $\text{C}_{11}\text{H}_7\text{CsN}_2\text{O}_3$ 366.9495; exp. 366.949 $[\text{M}+\text{Cs}]^+$.



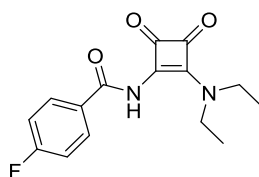
N-(2-(diethylamino)-3,4-dioxocyclobut-1-en-1-yl)-4-methylbenzamide (4a). 61% yield. mp 197 °C. ^1H NMR (300 MHz, $\text{DMSO-}d_6$) δ 11.86 (s, 1H), 7.88 (d, $J=8.4$ Hz, 2H), 7.35 (d, $J=8.1$ Hz, 2H), 3.75 (q, $J=6.9$ Hz, 2H), 3.42 (q, $J=7.2$ Hz, 2H), 1.20 (t, $J=7.2$ Hz, 3H), 1.12 (t, $J=6.9$ Hz, 3H); ^{13}C NMR (75 MHz, $\text{DMSO-}d_6$) δ 192.3, 184.2, 175.7, 173.7, 164.5, 160.3, 142.8, 129.6, 129.1, 128.3, 44.2, 43.7, 21.0, 14.5, 13.9; IR (Film, cm^{-1}): 3416, 3240, 2981, 2936, 1794, 1720, 1671, 1590, 1485, 1301, 1268, 1049, 831, 745, 625; ESI-HRMS(+) m/z (%): calc. $\text{C}_{16}\text{H}_{18}\text{CsN}_2\text{O}_3$ 419.0372; exp. 419.0366 $[\text{M}+\text{Cs}]^+$. Anal. Calcd. for $\text{C}_{16}\text{H}_{18}\text{N}_2\text{O}_3$: C, 67.12; H, 6.34; N, 9.78. Found: C, 66.39; H, 6.32; N, 9.77.



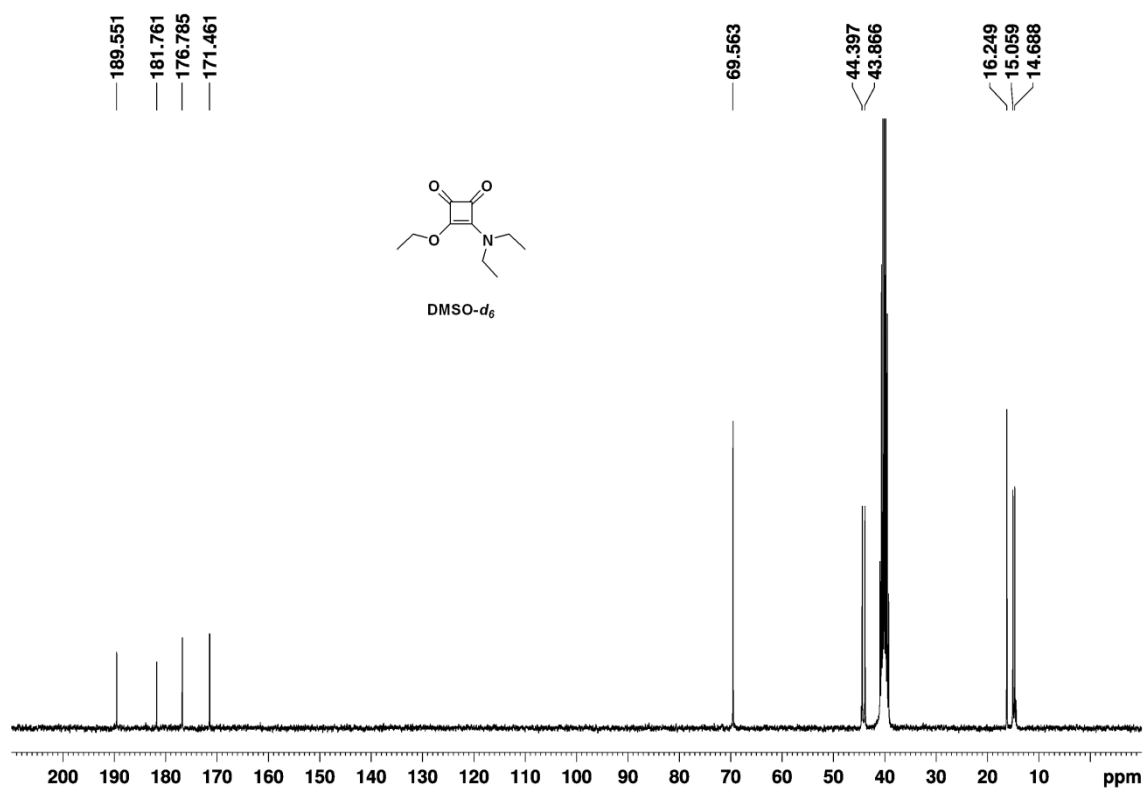
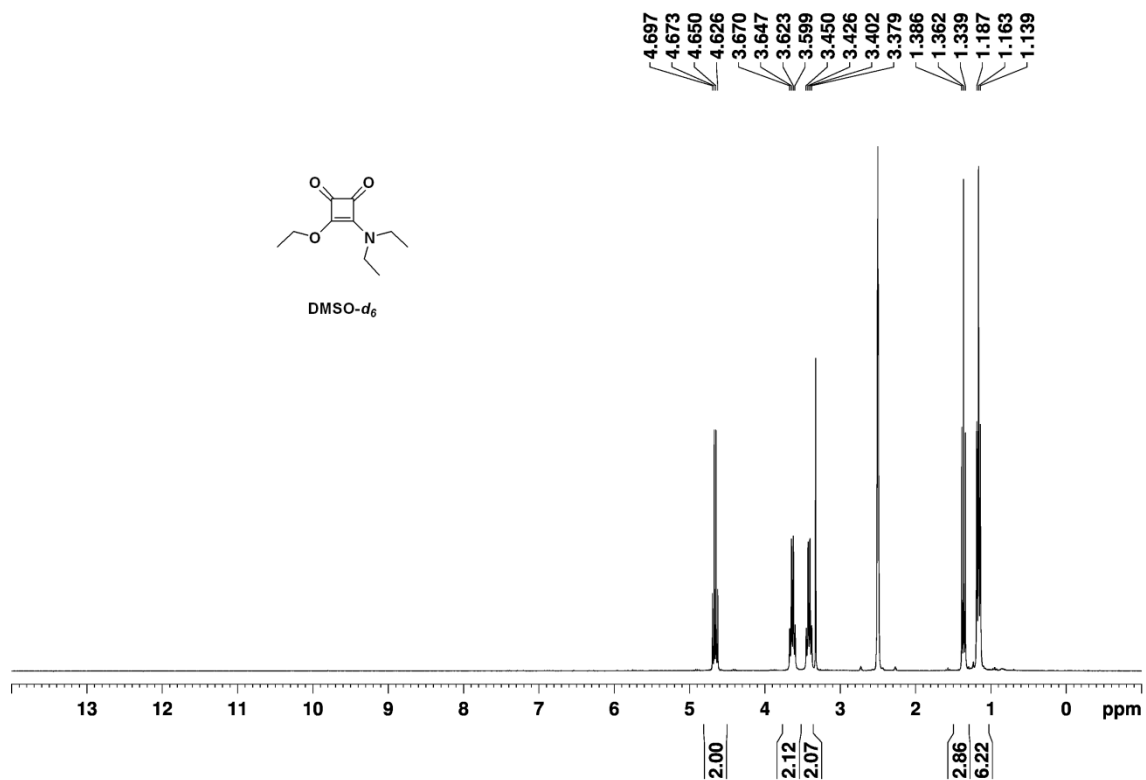
N-(2-(diethylamino)-3,4-dioxocyclobut-1-en-1-yl)benzamide (4b). 67% yield. mp 149 °C. ^1H NMR (300 MHz, $\text{DMSO-}d_6$) δ 10.94 (s, 1H), 7.97 (d, $J=7$ Hz, 2H), 7.65 (t, $J=7.1$ Hz, 1H), 7.54 (t, $J=7.5$ Hz, 2H), 3.73 (q, $J=6.9$ Hz, 2H), 3.45 (q, $J=7.2$ Hz, 2H), 1.21 (t, $J=7.2$ Hz, 3H), 1.13 (t, $J=6.9$ Hz, 3H); ^{13}C NMR (75 MHz, $\text{DMSO-}d_6$) δ 192.0, 184.6, 175.6, 165.0, 161.8, 133.0, 132.0, 128.5, 128.2, 44.0, 43.6, 14.5, 13.9; IR (Film, cm^{-1}): 3416, 3277, 2978, 1801, 1724, 1677, 1610, 1509, 1485, 1384, 1348, 1294, 1269, 1079, 1051, 798, 710, 590, 551; MALDI-TOF(+) m/z (%): calc. $\text{C}_{15}\text{H}_{16}\text{N}_2\text{NaO}_3$ 295.1059; exp. 295.1053 $[\text{M}+\text{Na}]^+$. Anal. Calcd. for $\text{C}_{15}\text{H}_{16}\text{N}_2\text{O}_3$: C, 66.16; H, 5.92; N, 10.29. Found: C, 63.68; H, 5.80; N, 10.01.

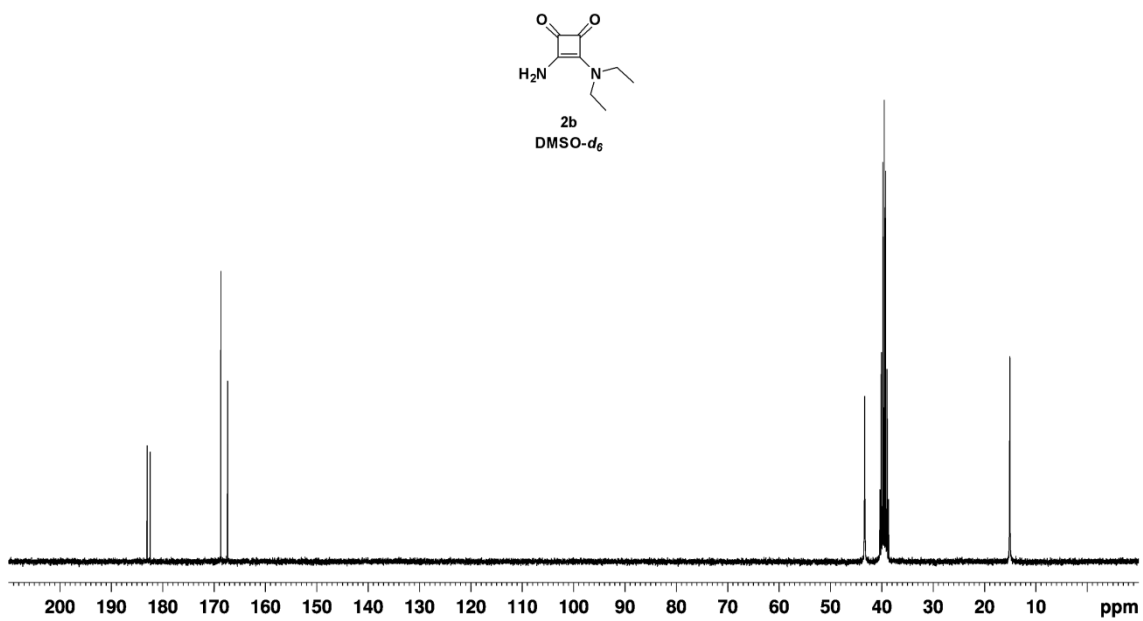
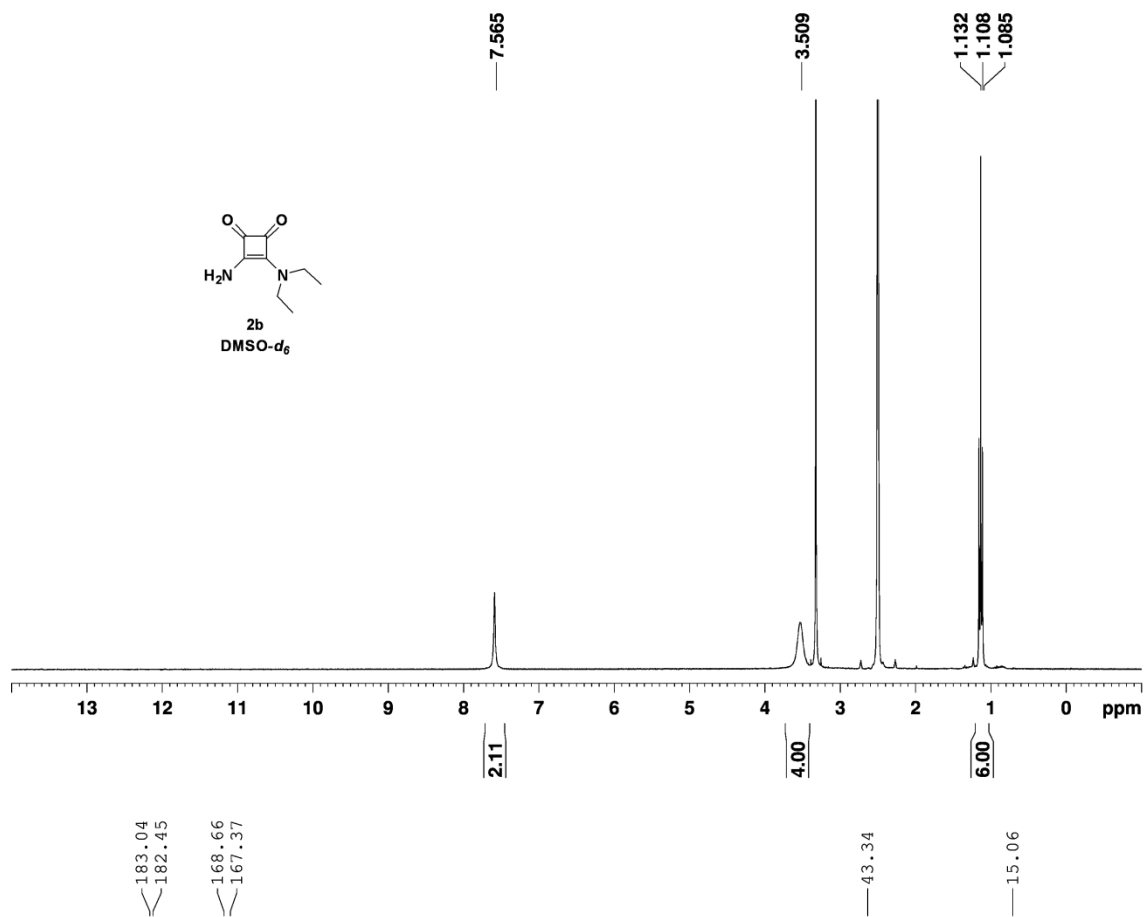


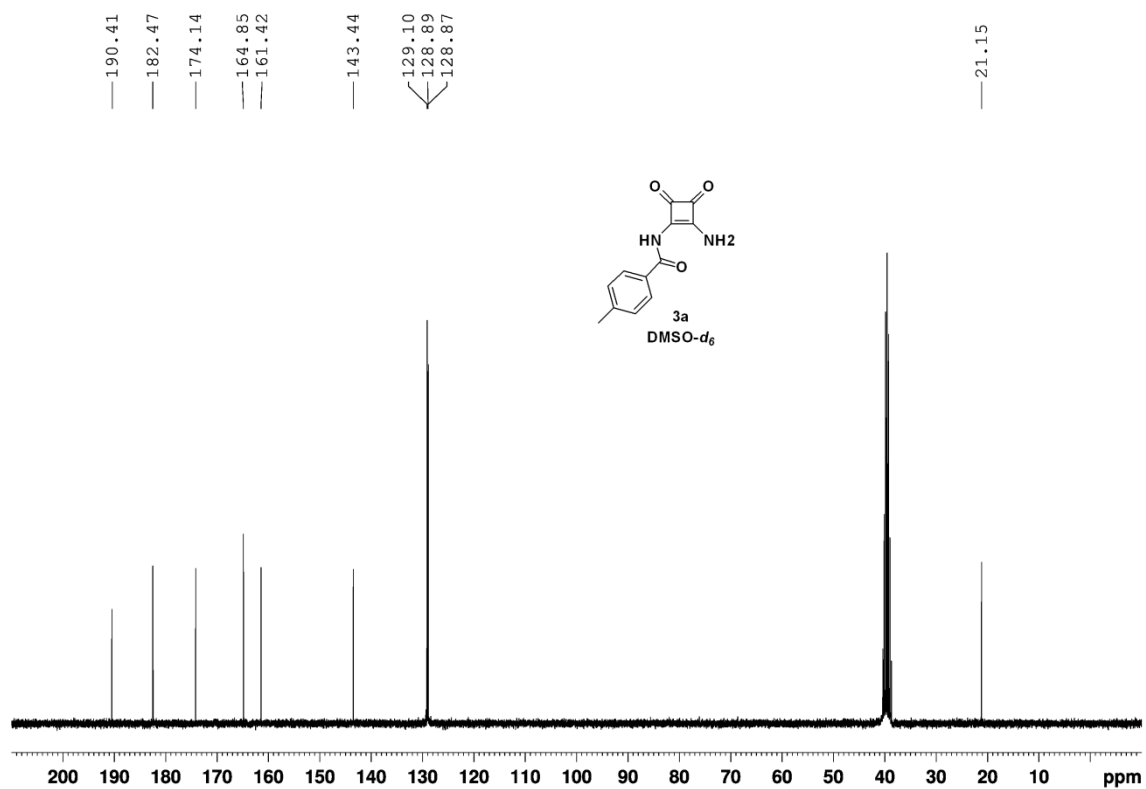
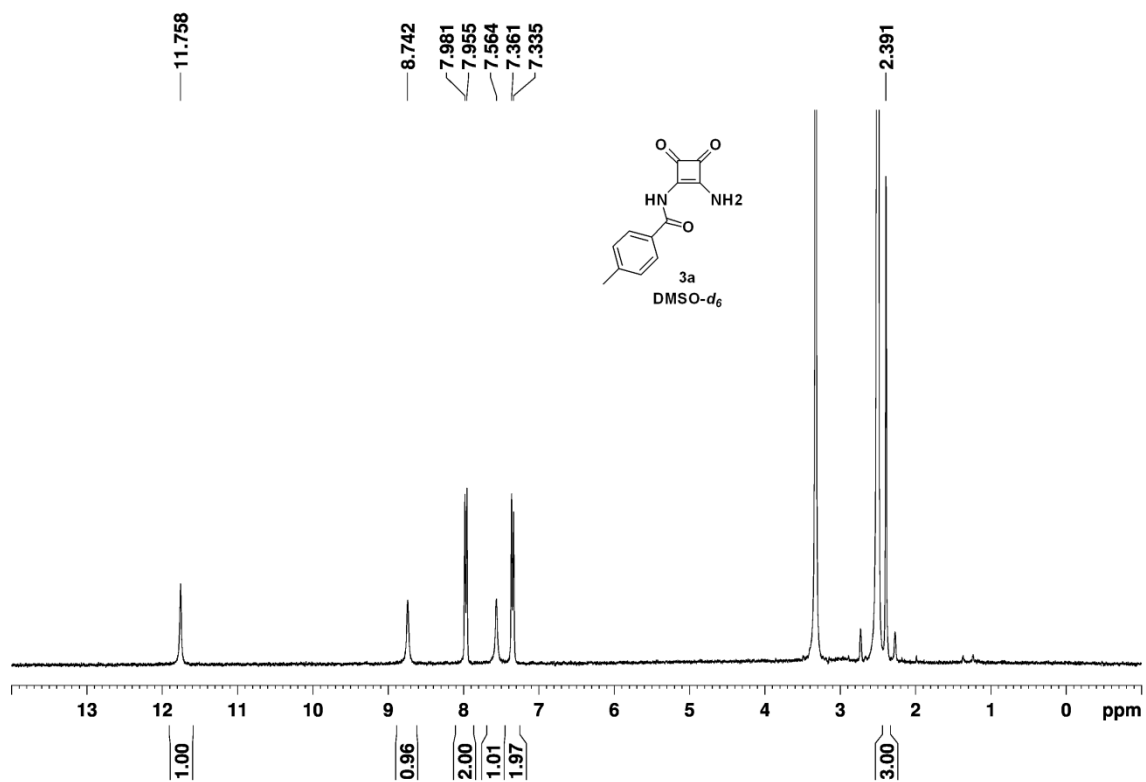
N-(2-(diethylamino)-3,4-dioxocyclobut-1-en-1-yl)-4-methoxybenzamide (4c). 31% yield. mp 130°C. ^1H NMR (300 MHz, $\text{DMSO-}d_6$) δ 10.80 (s, 1H), 7.96 (d, $J=8.7$ Hz, 2H), 7.06 (d, $J=8.7$ Hz, 2H), 3.84 (s, 3H), 3.75 (q, $J=6.6$ Hz, 2H), 3.43 (q, $J=6.9$ Hz, 2H), 1.20 (t, $J=6.6$ Hz, 3H), 1.12 (t, $J=6.6$ Hz, 3H); ^{13}C NMR (75 MHz, $\text{DMSO-}d_6$) δ 192.1, 184.4, 175.7, 164.2, 162.6, 161.1, 130.3, 124.7, 113.8, 55.5, 44.1, 43.6, 14.5, 13.9; IR (Film, cm^{-1}): 3416, 2977, 1789, 1712, 1667, 1604, 1487, 1383, 1296, 1257, 1175, 1054, 1033, 837, 588; ESI-HRMS(+) m/z (%): calc. $\text{C}_{16}\text{H}_{18}\text{N}_2\text{NaO}_4$ 325.1164; exp. 325.1159 $[\text{M}+\text{Na}]^+$.

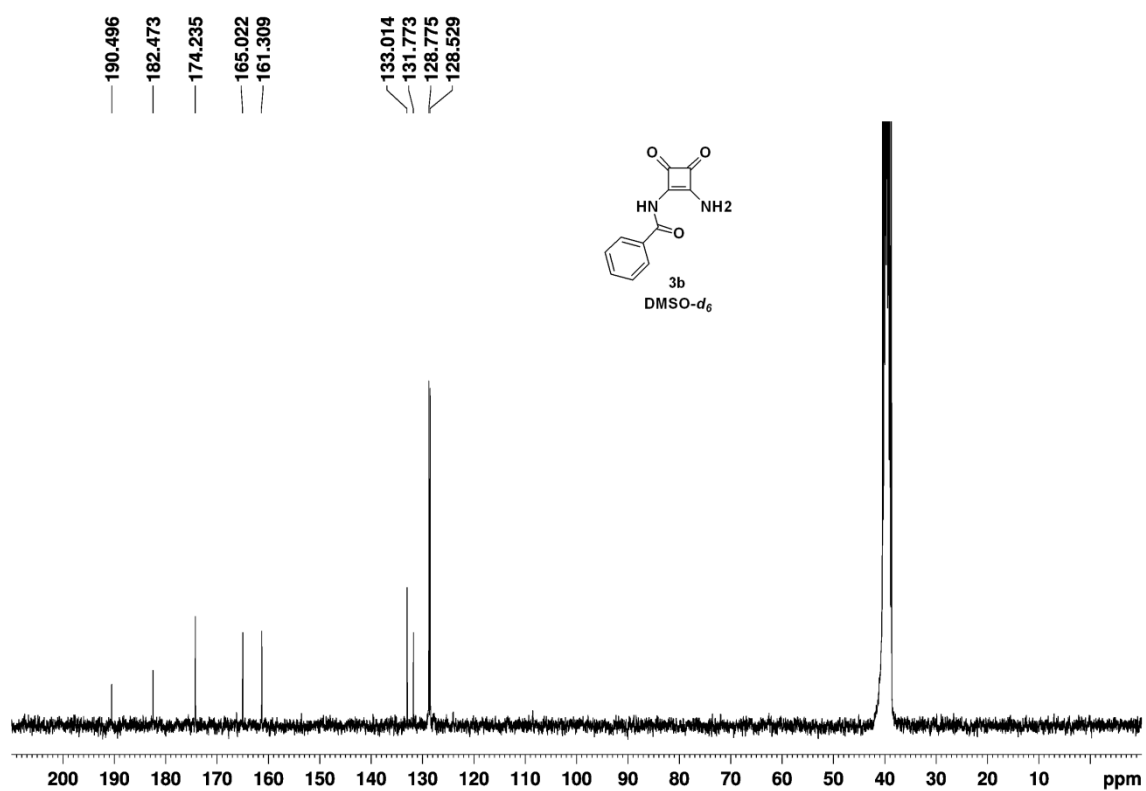
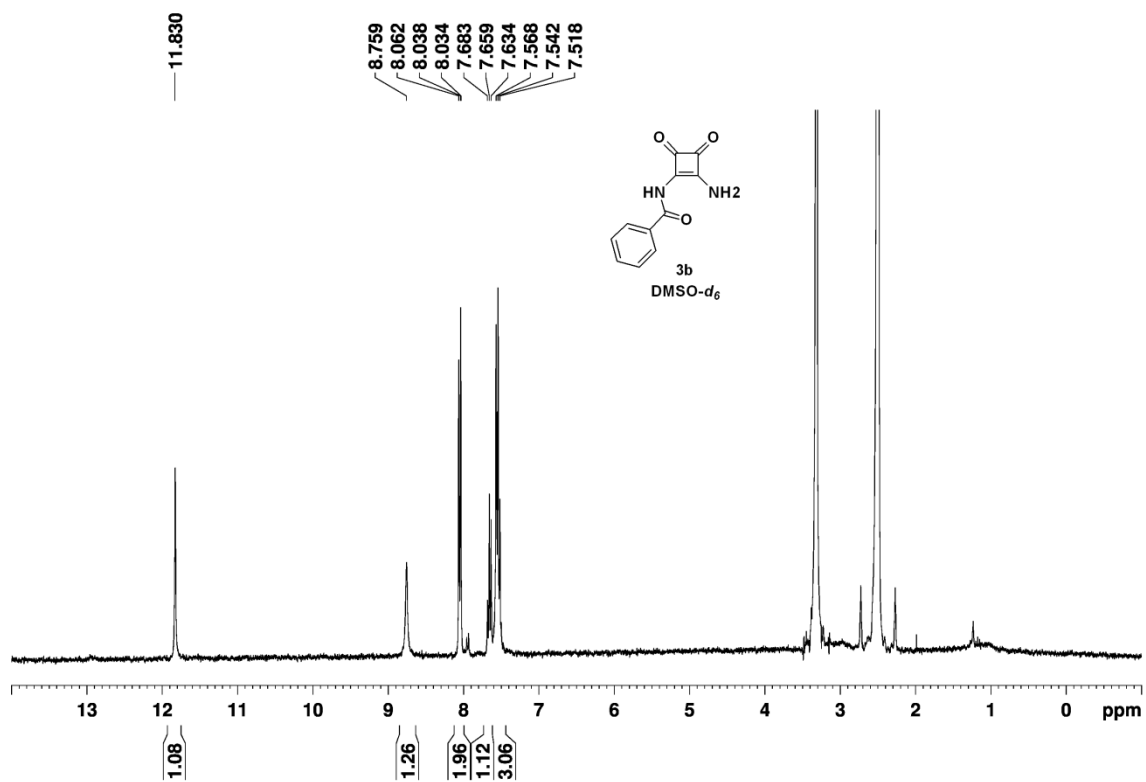


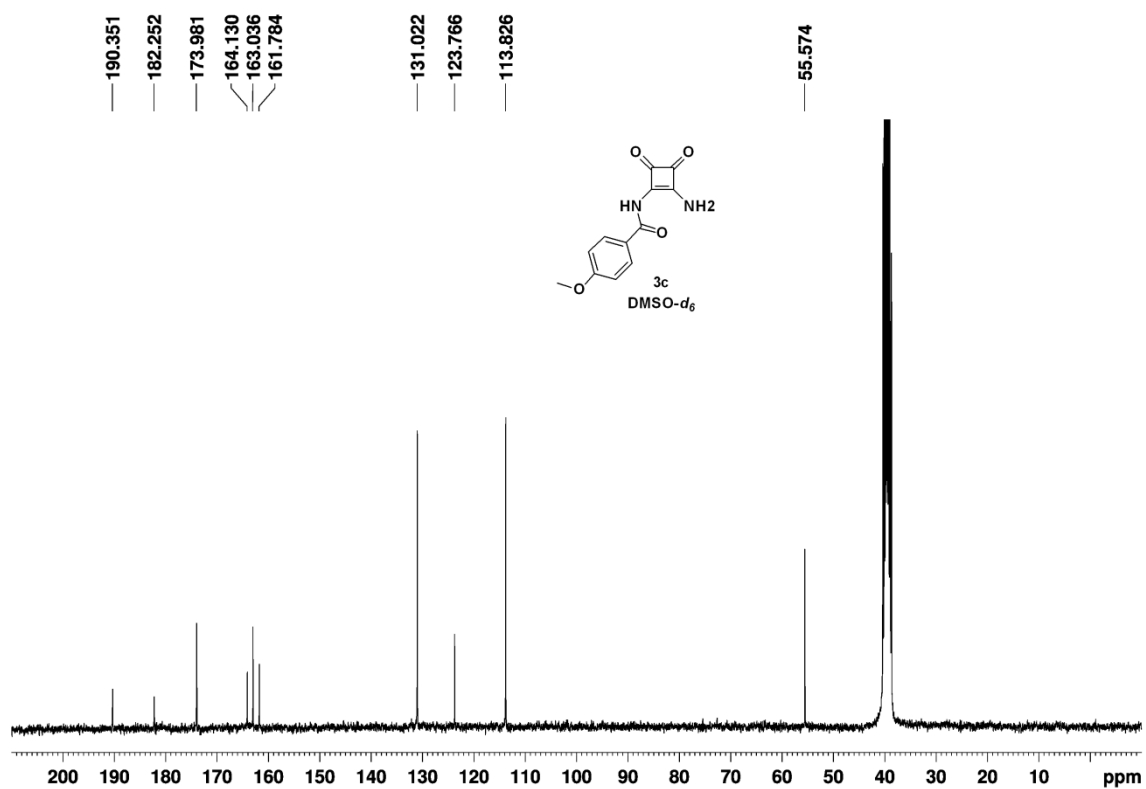
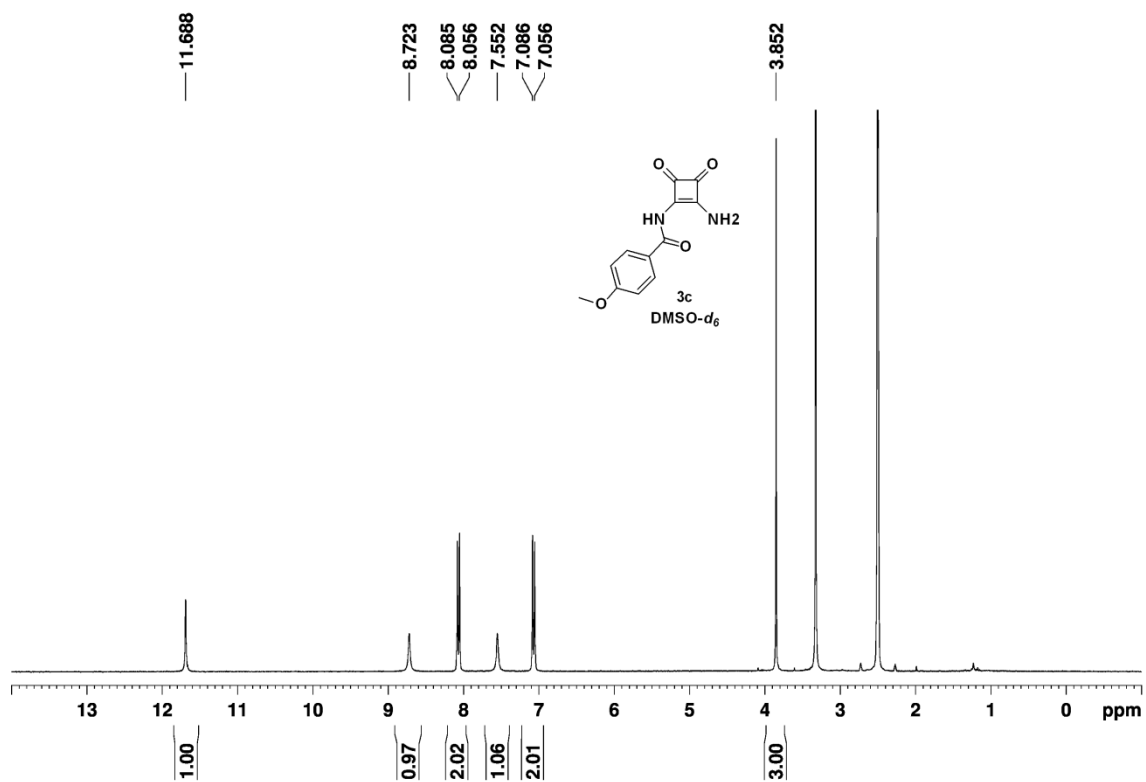
N-(2-(diethylamino)-3,4-dioxocyclobut-1-en-1-yl)-4-fluorobenzamide (4d). 75% yield. mp 224°C. ^1H NMR (300 MHz, $\text{DMSO-}d_6$) δ 10.97 (s, 1H), 8.04 (t, $J=7.2$ Hz, 2H), 7.38 (t, $J=9$ Hz, 2H), 3.75 (q, $J=6.9$ Hz, 2H), 3.44 (q, $J=7.8$ Hz, 2H), 1.20 (t, $J=7.2$ Hz, 3H), 1.13 (t, $J=6.6$ Hz, 3H); ^{13}C NMR (75 MHz, $\text{DMSO-}d_6$) δ 191.9, 184.6, 175.5, 166.1, 164.0, 162.8, 131.1 (d, $J=9$ Hz), 129.7, 115.5, 115.3, 44.0, 43.5, 14.5, 13.9; IR (Film, cm^{-1}): 3213, 2972, 1795, 1717, 1673, 1601, 1491, 1302, 1264, 1230, 1156, 1089, 1055, 850, 759, 688, 599; ESI-HRMS(+) m/z (%): calc. $\text{C}_{15}\text{H}_{16}\text{N}_2\text{O}_3$ 291.1145; exp. 291.1162 $[\text{M}+\text{H}]^+$.

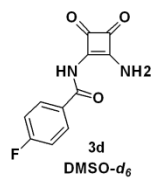
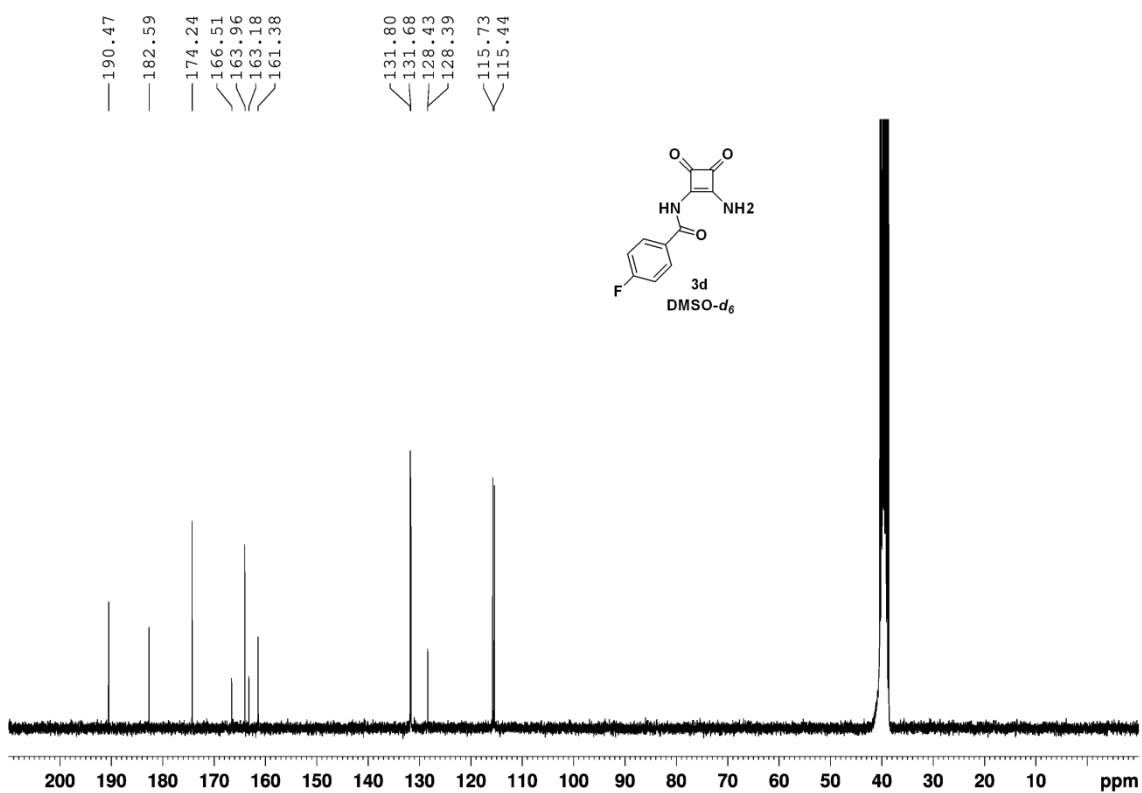
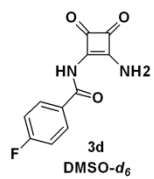
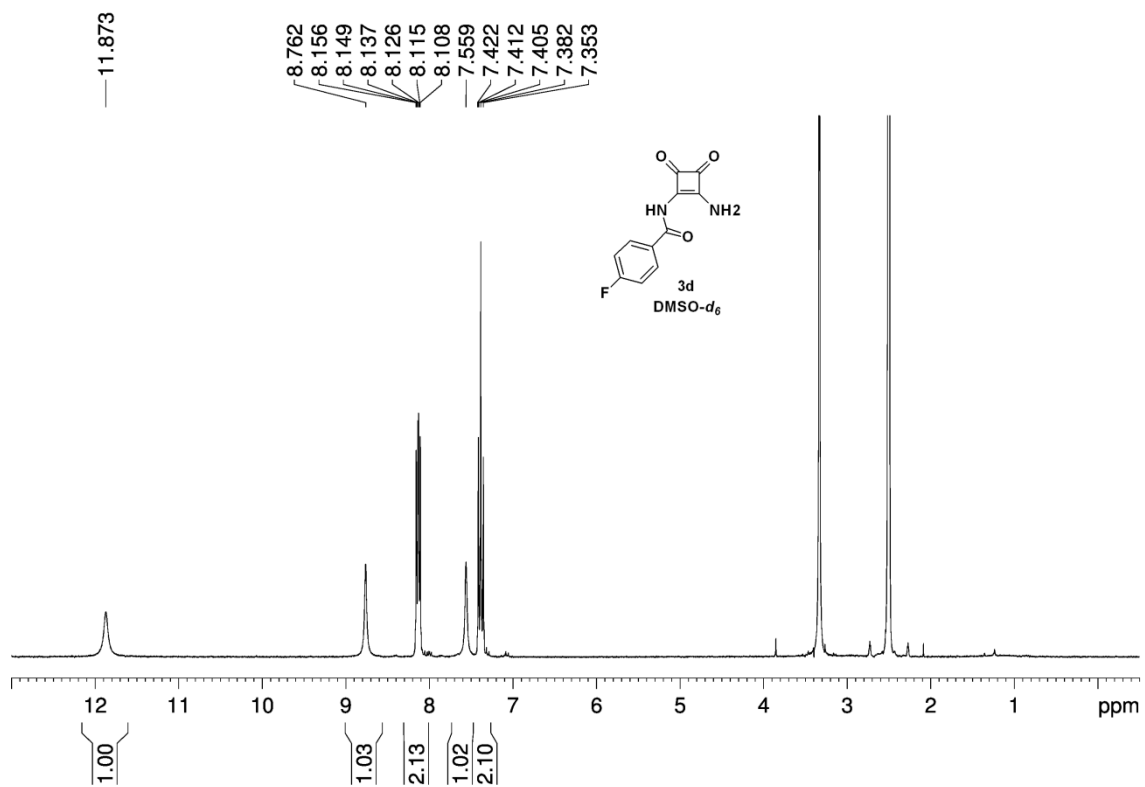


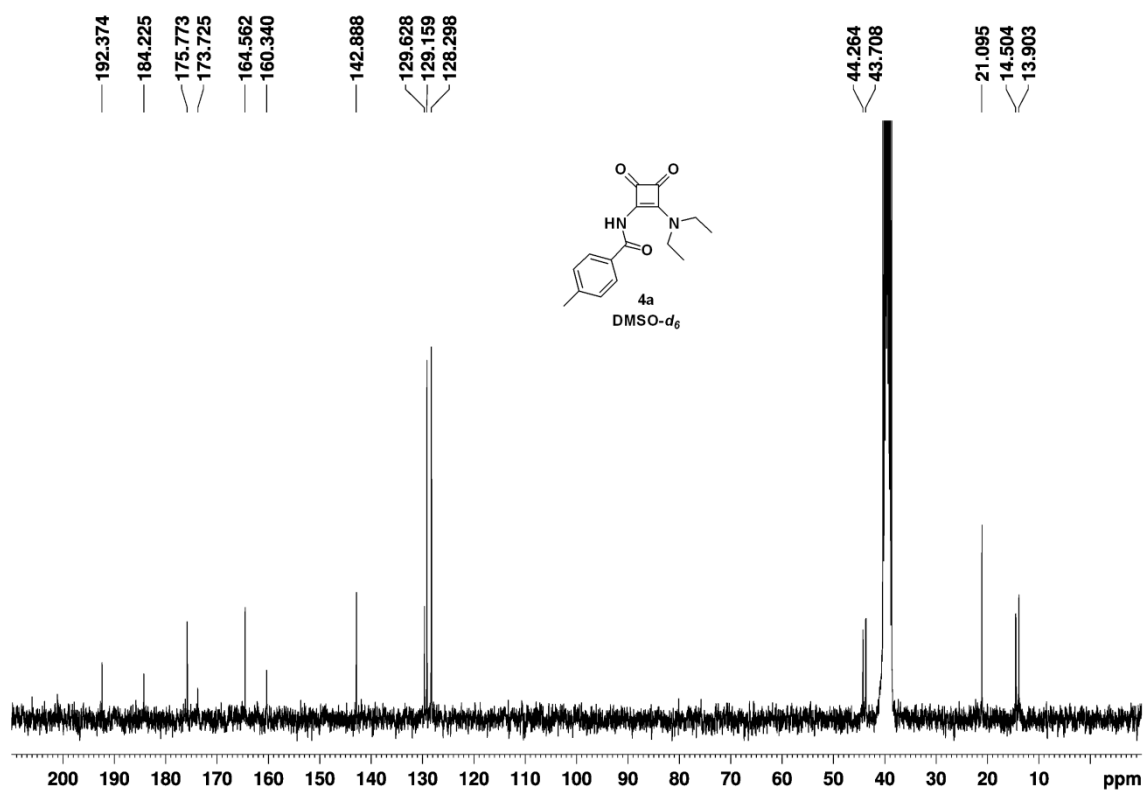
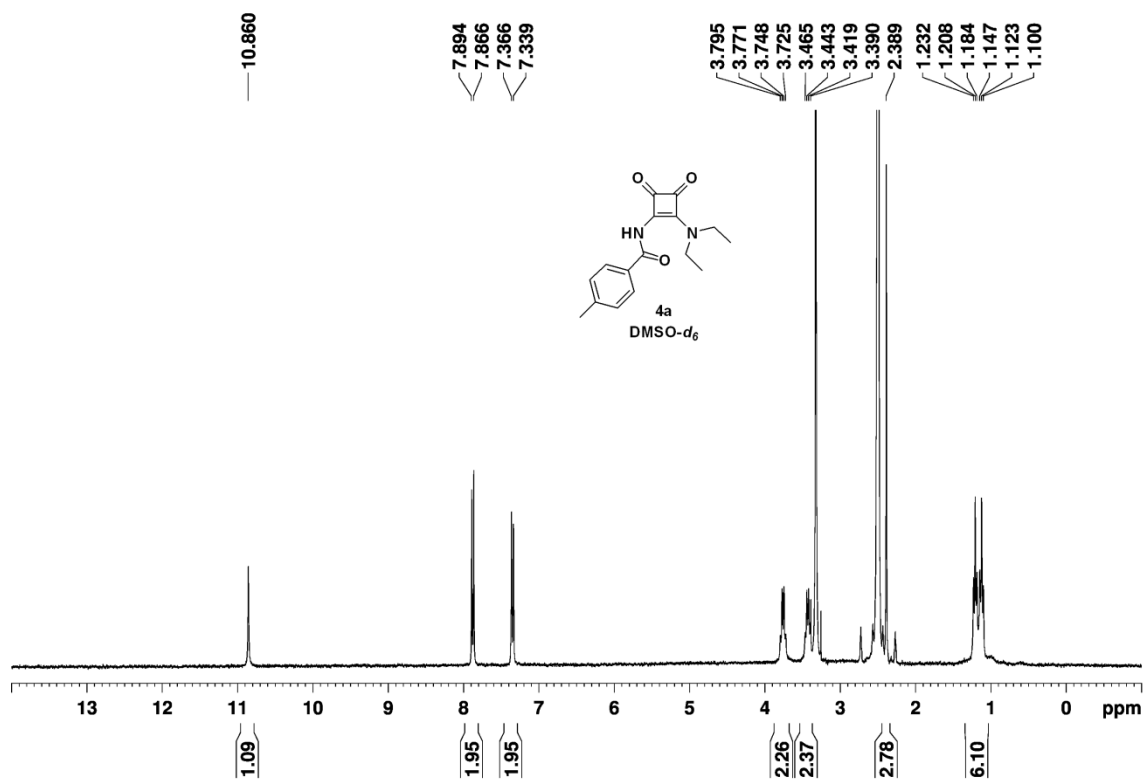


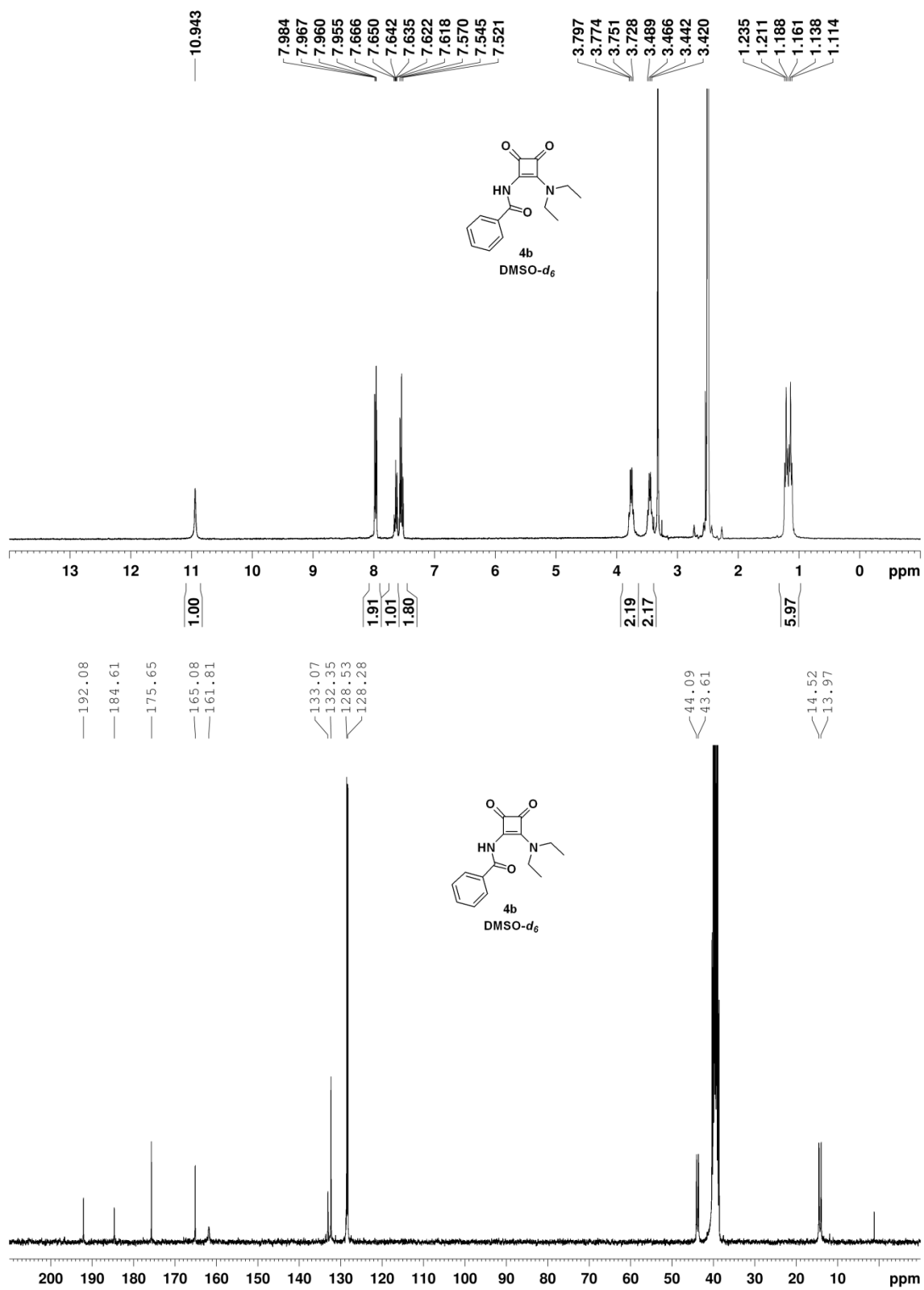


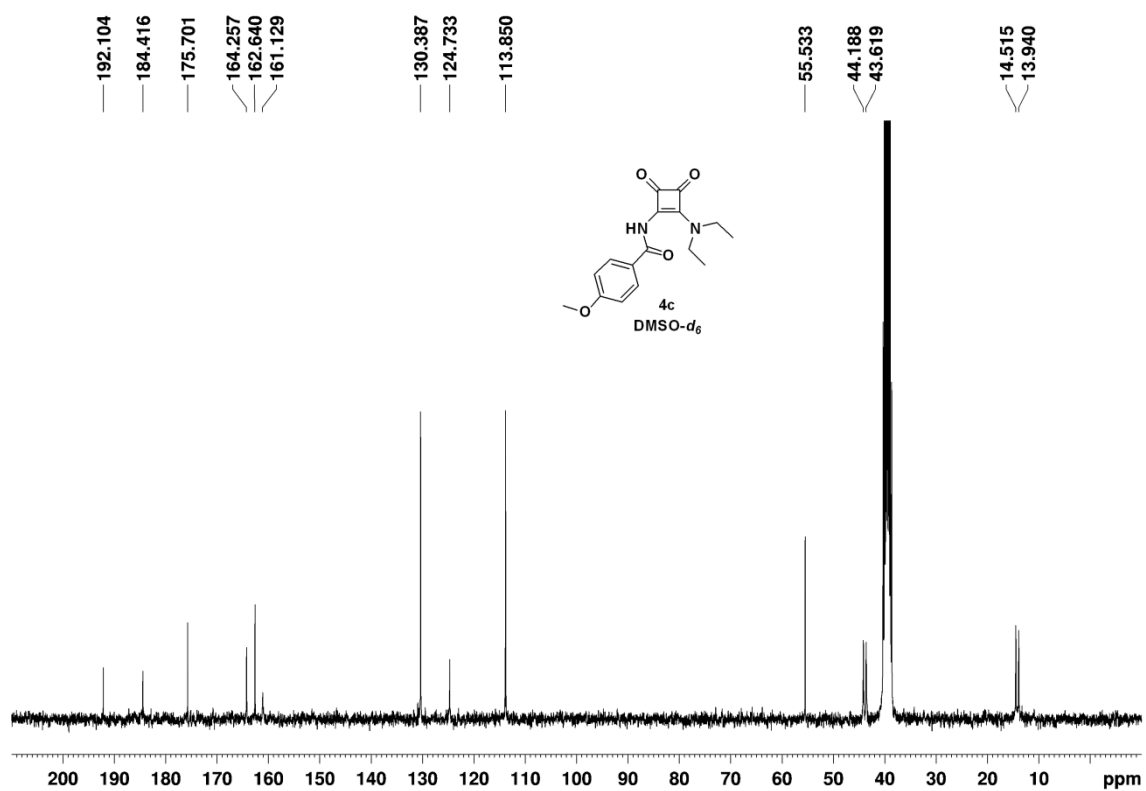
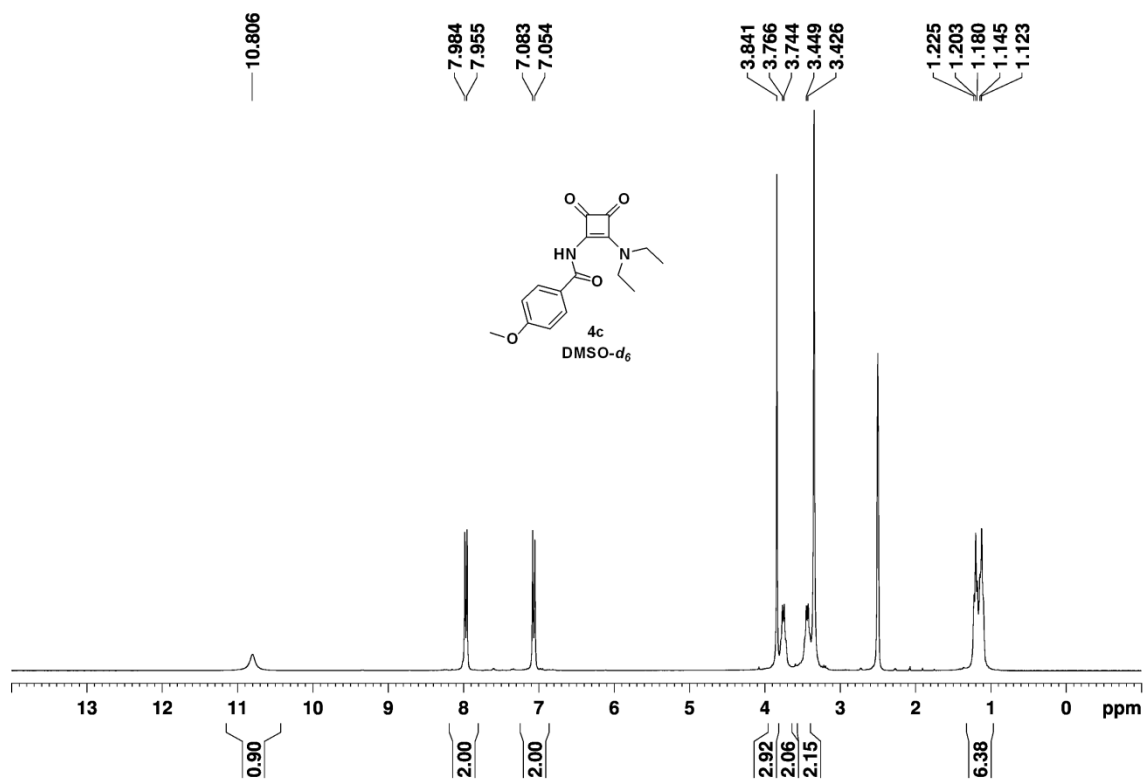


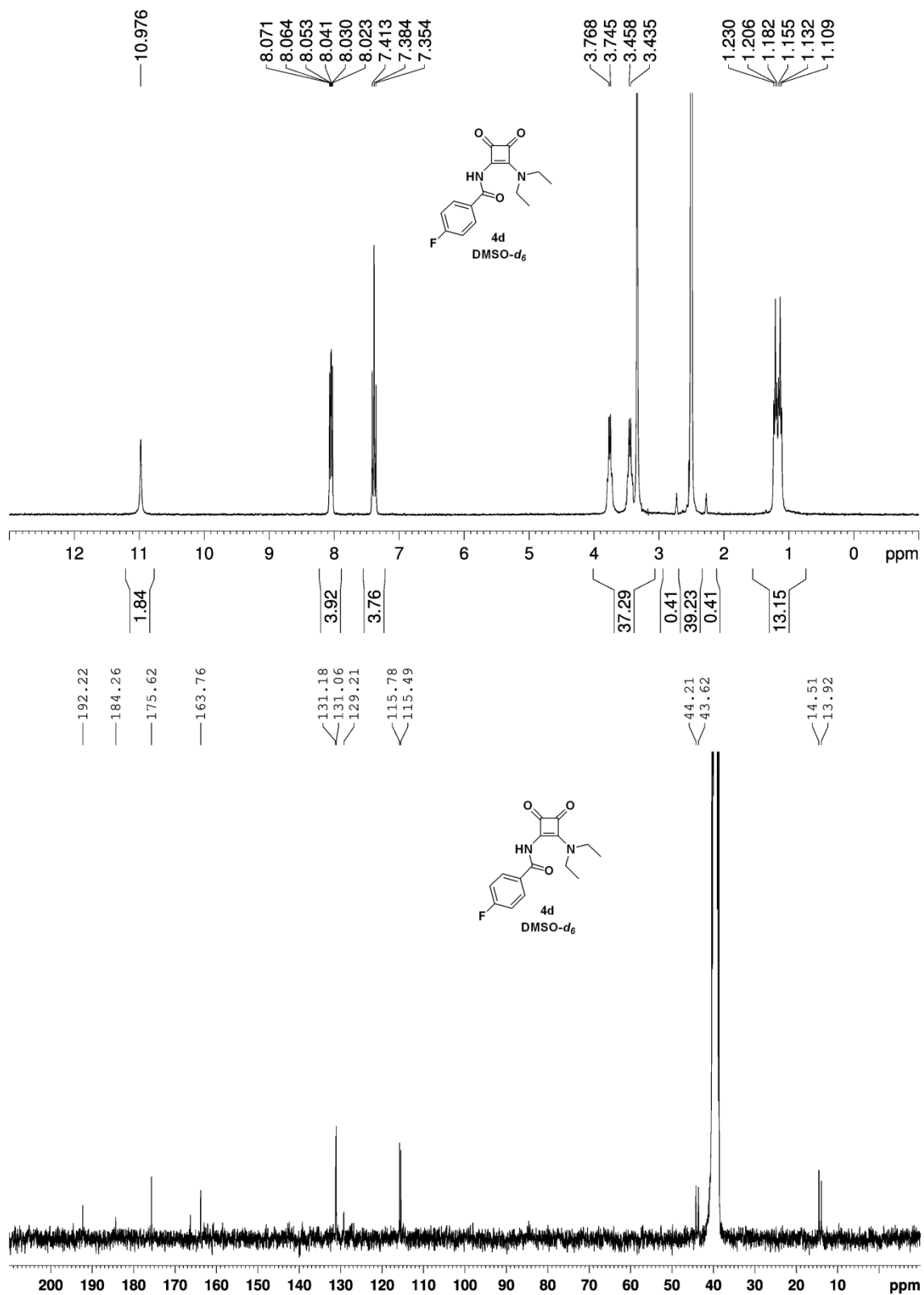












4.5.7.3. HPLC (High performance liquid chromatography) method for the analysis of aroyl squarimides

All the experiments were carried out on a GILSON system equipped with 321 pump and diode array detector (DAD) modules. The column used is a XBridge™ BEH C18 5 μ column (130 Å, 4.6 \times 150 mm). The experimental conditions are listed as follows: flow rate was 1 mL/min, the injection volume was typically 20 μ L and absorbance was monitored simultaneously at 250 and 290 nm. Mobile phase A contains milliQ water and mobile phase B contains MeCN.

The gradient used for the runs was: hold at 30% of phase B 1.8 minutes, increases from 30% to 80% in 8.5 min, hold at 80% for 2.75 minutes, and decreases to 30% in 5 minutes.

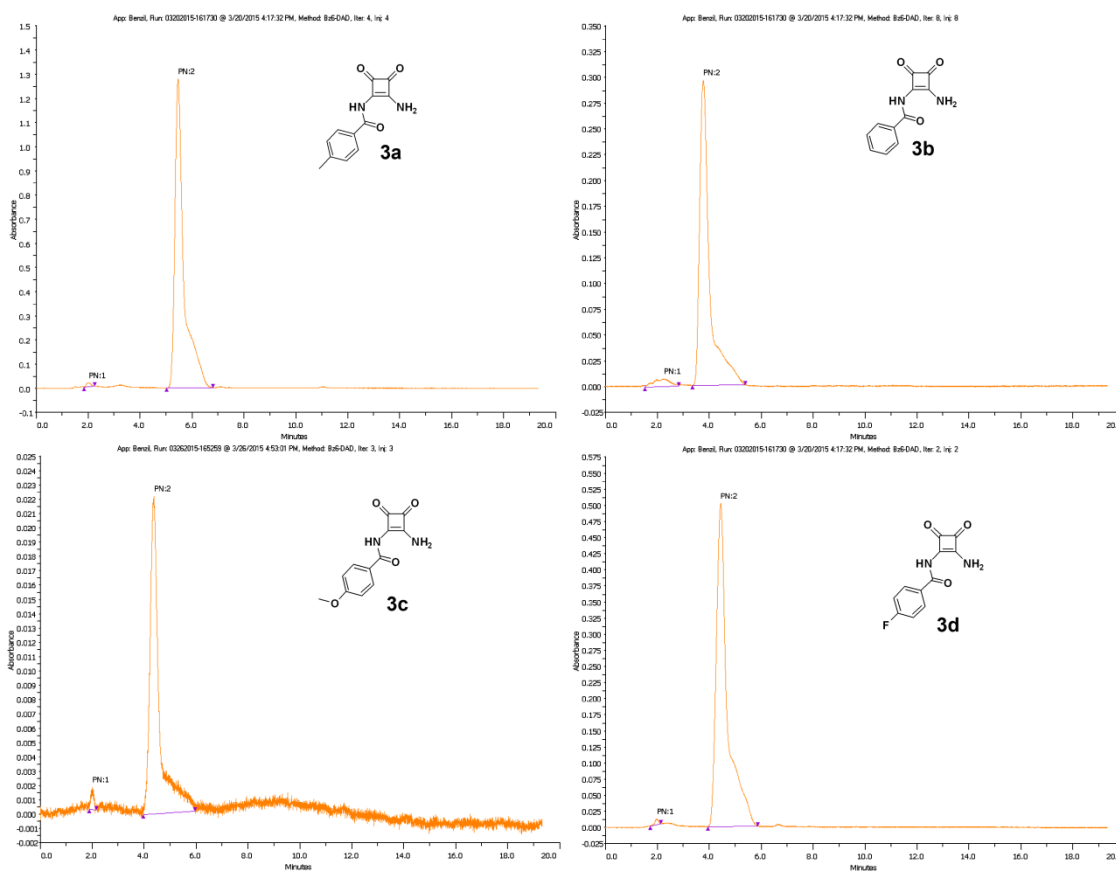


Figure S41. HPLC-traces of **3a-d**.

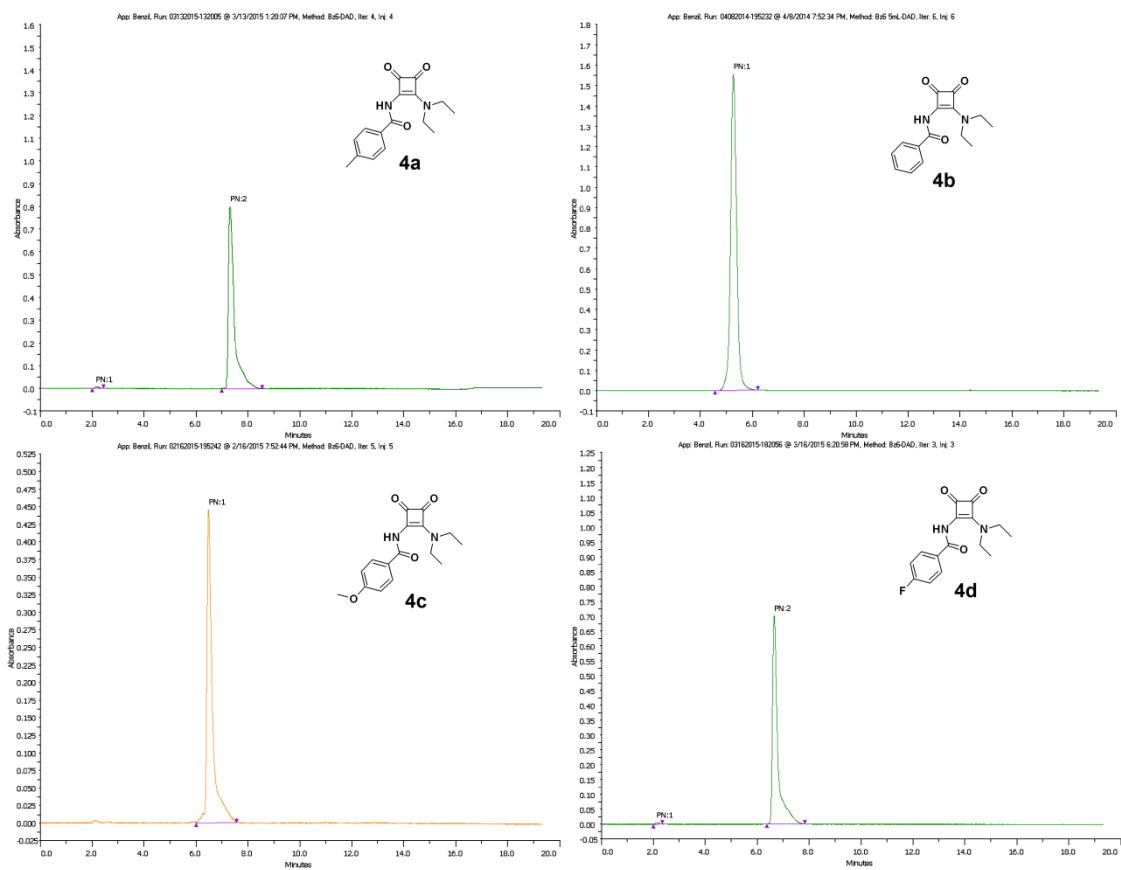


Figure S42. HPLC-traces of 4a-d.

4.4.7.4. X-ray Crystal Structure Analyses

Table S5. Crystallographic data of **3c**.

Empirical formula	C ₁₂ H ₁₀ N ₂ O ₄	
Formula weight	246.22	
Temperature (K)	100(2)	
Wavelength (Å)	0.71073	
Crystal system, space group	Triclinic, <i>P</i> -1	
Unit cell dimensions	a = 7.1800(4)	α = 70.409(2)
	b = 11.3273(7)	β = 76.793(2)
	c = 14.4521(9)	γ = 78.724(2)
Volume (Å ³)	1068.96(11)	
Z, calculated density (Mg/m ³)	4, 1.530	
Absorption coefficient	0.117	
<i>F</i> (000)	512	
Crystal size (mm)	0.22 x 0.12 x 0.03	
θ range for data collection	1.92-30.30	
Index ranges	-10 ≤ <i>h</i> ≤ 9, -15 ≤ <i>k</i> ≤ 16, -20 ≤ <i>l</i> ≤ 19	
Reflections collected (unique)	19379/5659 [<i>R</i> (int) = 0.0261]	
Completeness to θ = 30.30 °	88.4%	
Max. and min. transmission	0.9965 and 0.9747	
Goodness-of-fit on <i>F</i> ²	1.039	
Final <i>R</i> indices [<i>I</i> > 2σ(<i>I</i>)]	<i>R</i> ₁ = 0.0418, <i>wR</i> ₂ = 0.1130	
<i>R</i> indices (all data)	<i>R</i> ₁ = 0.0523, <i>wR</i> ₂ = 0.1208	

Table S6. Crystallographic data of **4c**.

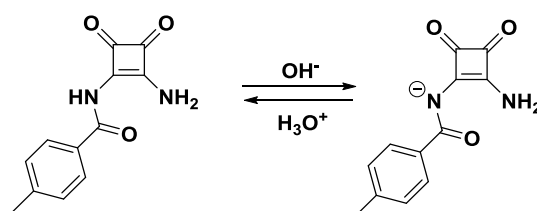
Empirical formula	$C_{16}H_{18}N_2O_4$	
Formula weight	302.32	
Temperature (K)	100(2)	
Wavelength (Å)	0.71073	
Crystal system, space group	Monoclinic, $P2(1)/n$	
Unit cell dimensions	$a = 7.1019(17)$	$\alpha = 90$
	$b = 9.611(2)$	$\beta = 91.783(4)$
	$c = 21.173(4)$	$\gamma = 90$
Volume (Å ³)	1444.4(5)	
Z, calculated density (Mg/m ³)	4, 1.390	
Absorption coefficient	0.101	
$F(000)$	640	
Crystal size (mm)	0.20 x 0.20 x 0.20	
θ range for data collection	2.327-45.215°.	
Index ranges	-9<=h<=14, -19<=k<=18, -41<=l<=37	
Reflections collected (unique)	31153/10513 [$R(\text{int}) = 0.0162$]	
Completeness to $\theta = 45.215$	87.3%	
Max. and min. transmission	0.980 and 0.754	
Goodness-of-fit on F ²	1.133	
Final R indices [$I > 2\sigma(I)$]	$R_1 = 0.0425$, $wR_2 = 0.1176$	
R indices (all data)	$R_1 = 0.0482$, $wR_2 = 0.1202$	

4.4.7.5. UV-vis pKa determination

Solutions of corresponding aryl squarimides **3a** and **4a** ($5 \cdot 10^{-6}$ M) were prepared with nanopure deionized water (MilliQ 16 M Ω) containing 10% MeCN for solubilizing aid and NaCl ionic strength ($5 \cdot 10^{-4}$ M). NaOH solutions were standardized immediately prior its use by titration with potassium hydrogen phthalate to a phenolphthalein end point.

Titration curves were carried out at 22°C with standard acid-base glass equipment covering a pH range from 5 to 10. The glass bulb pH probe (Crison combination pH electrode for microsamples 3 mm o.d.) was calibrated with pH 4 and 7 standard reference buffers. Initial volume was 2 mL. After each addition, the solution was lead to equilibrate at least 60 s and its UV-vis spectra registered. For calculations, the total concentration of the product was readjusted according to the variation of volume produced after each measurement. The whole set of NMR data were fit using HypSpec (Protonic Software, version 2008).²⁸⁴

Table S7. Model used for the determination of the pKa's of aryl squarimide **3a**. LH = aryl squarimide **3a**, L = deprotonated form.



Reaction	Log β	L	H	
L + H = LH	9.009(0.005)	1	1	refined
OH + H = OH ₂	-13.78	0	-1	constant

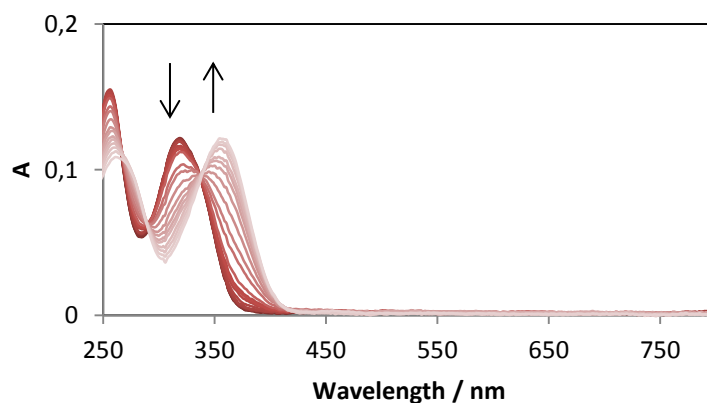
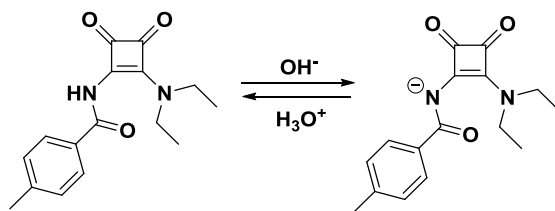


Figure S43. Titration curves of **3a** in H₂O:MeCN 9:1 at 295K.

²⁸⁴ (a) HypSpec 2008 program (Protonic Software; <http://www.hyperquad.co.uk>). Frassinetti, C.; Ghelli, S.; Gans, P.; Sabatini, A.; Moruzzi M. S.; Vacca, A. *Anal. Biochem.* **1995**, *231*, 374-382; (b) Frassinetti, C.; Alderighi, L.; Gans, P.; Sabatini, A.; Vacca A.; Ghelli, S. *Anal. Bioanal. Chem.* **2003**, *376*, 1041-1052.

Table S8. Model used for the determination of the pKa's of aroyl squarimide **3a**. LH = aroyl squarimide **3a**, L = deprotonated form.



Reaction	Log β	L	H	
$\text{L} + \text{H} = \text{LH}$	8.1947(0.0009)	1	1	refined
$\text{OH} + \text{H} = \text{OH}_2$	-13.78	0	-1	constant

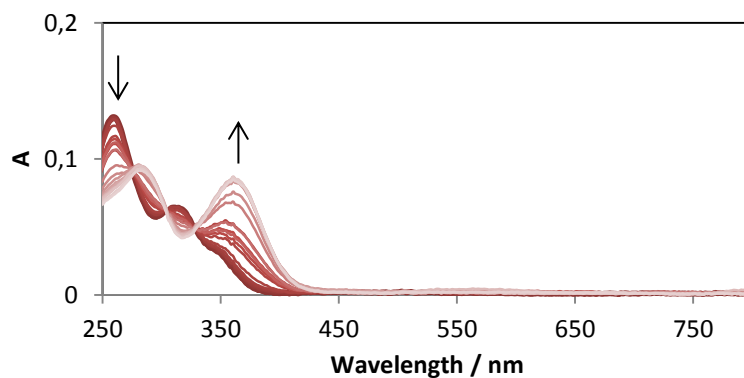


Figure S44. Titration curves of **3a** in $\text{H}_2\text{O}:\text{MeCN}$ 9:1 at 295K.

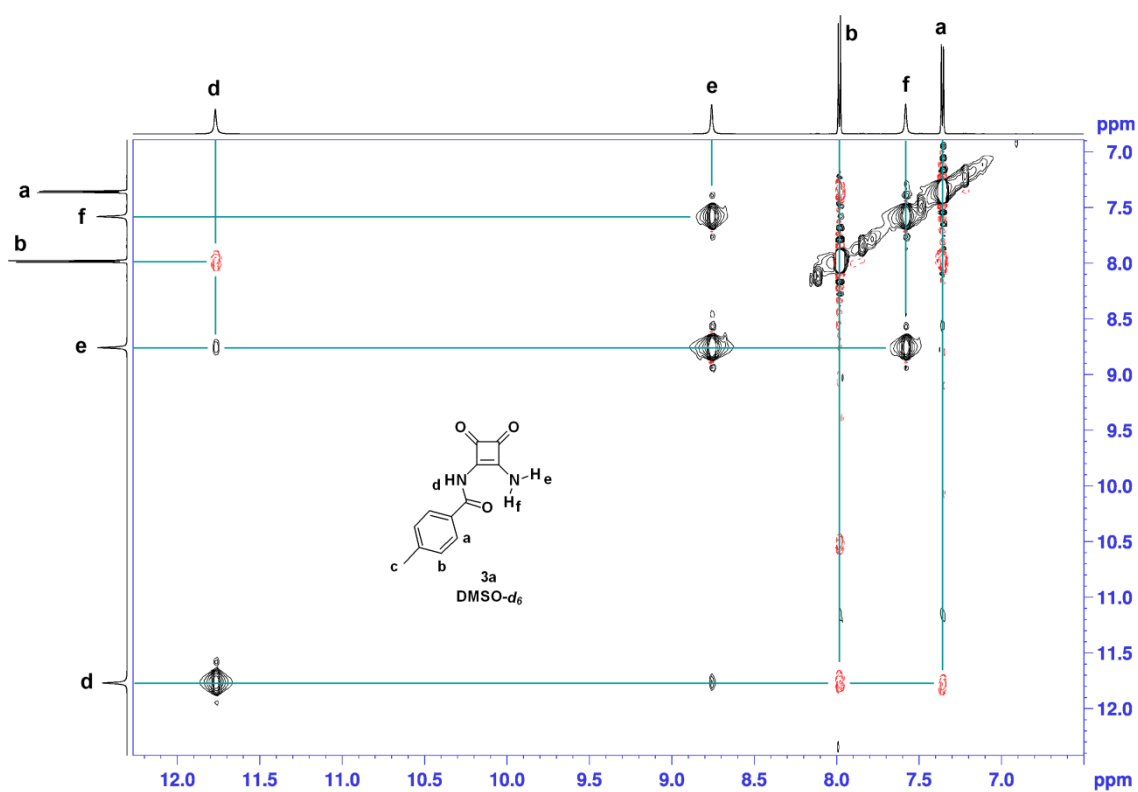


Figure S45. Partial 2D ROESY spectrum of **3a** (50 mM) in DMSO- d_6 at 298 K.

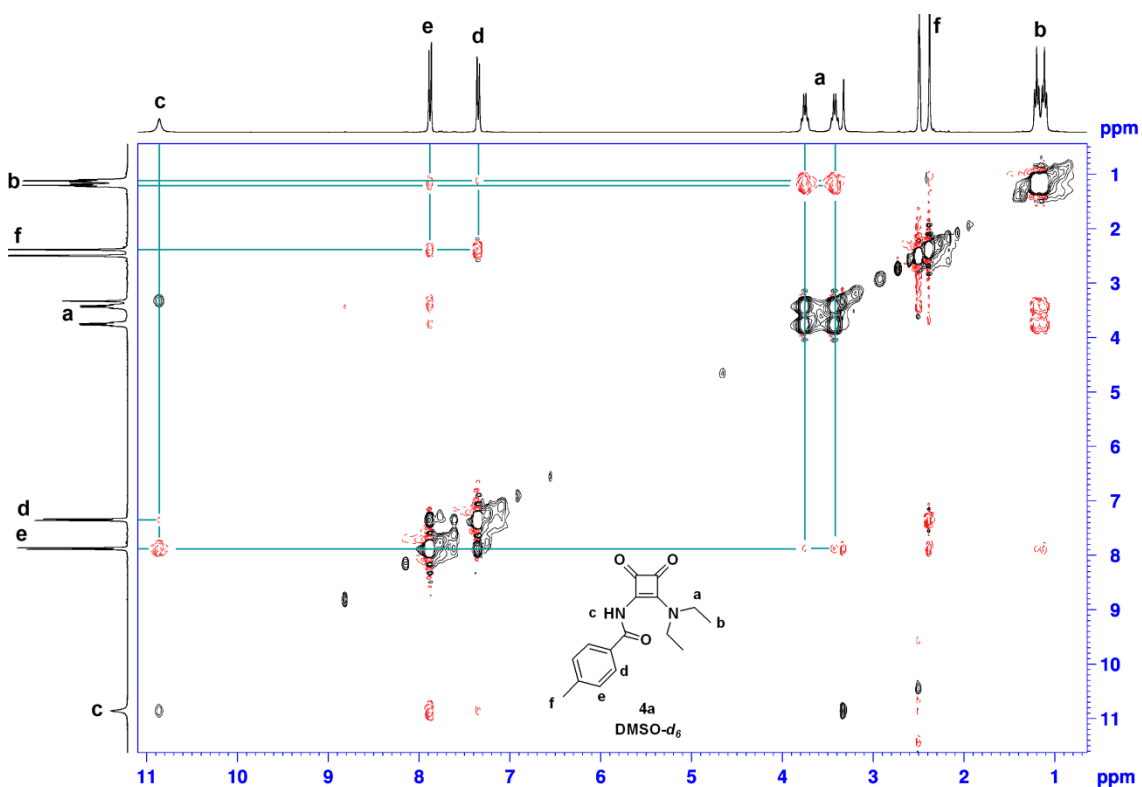


Figure S46. 2D ROESY spectrum of **4a** (50 mM) in DMSO- d_6 at 298 K.



Chapter 5: Squaramide -based dendrimers

5.1 Introduction: The Dendritic Family

In 1978, Vögtle et al. presented the first attempt to design and synthesize dendritic structures or “cascade molecules”.²⁸⁵ Since then, several years passed until Tomalia’s group²⁸⁶ in parallel with Newkome et al.²⁸⁷ were interested in these systems.

Dendritic structures are widely found in biological systems. Based on their architectures, these systems can be divided into different groups namely, hyperbranched polymers, dendrigrafts, dendronized polymers and dendrimers (Figure 109).

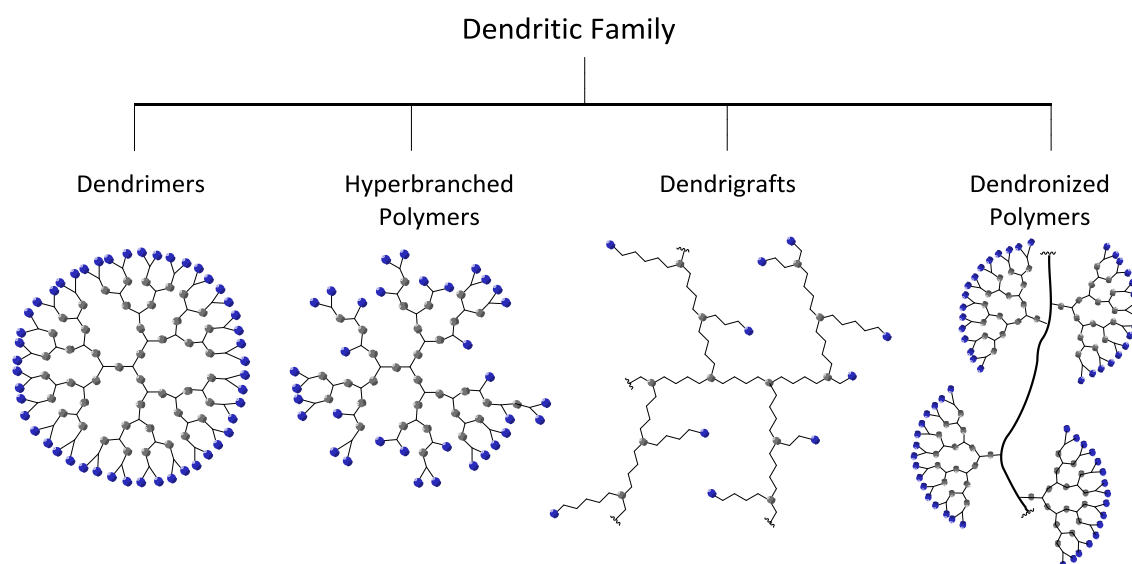


Figure 109. Scheme of the dendritic family that include: dendrimers, hyperbranched polymers, dendrigrafts and dendronized polymers.²⁸⁸

5.2 Dendrimers

The word dendrimer derives from the Greek words *dendron* meaning “tree” or “branch” and *meros* that means “part”. Dendrimers are monodispersed hyperbranched macromolecules with a layer-by-layer structure obtained by an iterative sequence of reaction steps. This process let to obtain molecules with a high level of control in their structure, size and surface functionality.

Owing to their internal structure in which all the bonds grow up radially from the core, dendrimers have a globular shape. Unlike linear polymers they have low viscosity and the functional groups present in their structure can be protected or exposed.

Dendrimers can be classified according to their functionalization as: glycodendrimers,²⁸⁹ peptide dendrimers,²⁹⁰ metallodendrimers,²⁹¹ Janus dendrimers,²⁹² amphiphilic dendrimers,²⁹³ etc. However, the

²⁸⁵ Buhleier, E.; Wehner, W.; Vögtle, F. *Synthesis* **1978**, 155-158.

²⁸⁶ Tomalia, D. A.; Baker, H.; Dewald, J.; Hall, M.; Kallos, G.; Martin, S.; Roeck, J.; Ryder, J.; Smith, P. *Polym. J.* **1985**, *17*, 117-132.

²⁸⁷ Newkome, G. R.; Yao, Z.; Baker, G. R.; Gupta, V. K. *J. Org. Chem.* **1985**, *50*, 2003-2004.

²⁸⁸ Carlmark, A.; Hawker, C.J.; Hult, A.; Malkoch, M.; *Chem. Soc. Rev.* **2009**, *38*, 352-362.

²⁸⁹ a) Bhadra, D.; Yadav, A. K.; Bhadra, S.; Jain, N. K., *Int. J. Pharm.* **2005**, *295*, 221-233, b) Shiao, T. C.; Roy, R. *New J. Chem.* **2012**, *36*, 324-339.

²⁹⁰ Higashi, N.; Koga T.; Niwa, M. *ChemBioChem* **2002**, *3*, 448-454.

²⁹¹ Gorman, C. *Adv. Mat.* **1998**, *10*, 295-295.

most common families of dendrimers are poly(amidoamine) dendrimers (PAMAM) and poly(propilenimine) dendrimers (PPI) that are easily functionalizable and commercially available.

5.3 Dendrimeric structure

The structure of a typical dendrimer can be divided in three parts: core, branches and the periphery (see Figure 110).

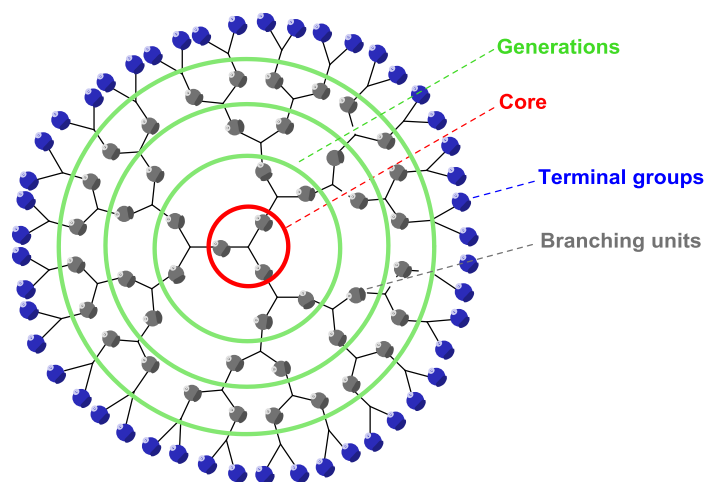


Figure 110. Schematic structure of a G3 dendrimer.

The core can be a single atom, such as the ammonia group of PAMAM dendrimers, or a polyfunctional compound with at least two identical functionalities.

The dendrons or branches radiate from the core to the periphery and they consist of the repetition of branching units. As a result, every new unit implies the exponential growth of the number of functional end groups. The number of units indicates the generation of the dendrimer. Additionally, intermediate products sometimes are denoted as half-generations.

The presence of multiple branching units in the dendrimeric structure leads to the formation of empty internal cavities with different physical properties depending on the nature of the dendrimer. The presence of these cavities is more pronounced in the higher generations with a larger number of branching units as is illustrated in Figure 111. The formation of these hydrophobic cavities in typically hydrophilic dendrimers allows the encapsulation of different host molecules for application in drug and gene delivery as well as catalytic processes.²⁹⁴ In those cases, the voids generated by the dendrimer behave as the cavity of cavitands, cyclodextrins or cucurbiturils. Unlike typical macrocyclic compounds, the size and shape of dendrimeric cavities change with time or variations in the medium such as pH or temperature.

²⁹² Rosen, B.M.; Wilson, C.J.; Wilson, D.A.; Peterca, M.; Imam, M. R.; Percec, V. *Chem. Rev.* **2009**, *109*, 6275–6540.

²⁹³ Shao, S.; Si, J.; Tang, J., Sui, M.; Shen, Y. *Macromolecules* **2014**, *47*, 916-921.

²⁹⁴ a) Natarajan, B.; Gupta, S.; Jayaraj, N.; Ramamurthy, V.; Jayaraman, N. *J. Org. Chem.* **2012**, *77*, 2219-2224. b) Zeng, F.; Zimmerman, S. C. *Chem. Rev.* **1997**, *97*, 1681-1712. c) Ficker, M.; Petersen, J. F.; Hansen, J. S.; Christensen, J. B. *PLoS ONE* **2015**, *10*, e0138706.

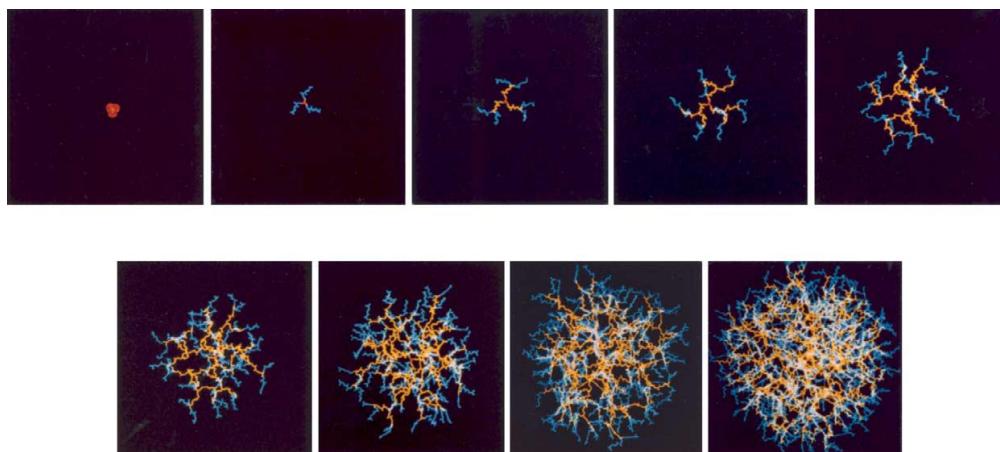


Figure 111. Representation of PAMAM dendrimers growing from the core (left-up) to a seventh generation (G7) (down-right). It can be observed the increase in the diameter and surface functionalization after each generation.²⁹⁵

Until now, there has not been an agreement on the nomenclature of the different families of dendrimers. For example, in the case of PAMAM dendrimers, the amine core is considered the zero generation (G0). On the contrary, in the case of PPI dendrimers, the central core is considered as a half generation (G0.5). In this case, the first generation is the first amido-functionalized product as the Figure 112 shows. This discrepancy in nomenclature generates confusion and it has been discussed the necessity to unify the criteria for the nomenclature of dendrimers to avoid misunderstandings.²⁹⁶ For this reason, in 2015, Jain et al. have proposed to consider the mother dendrimer generation as G0, followed by G1, G2, and so on.

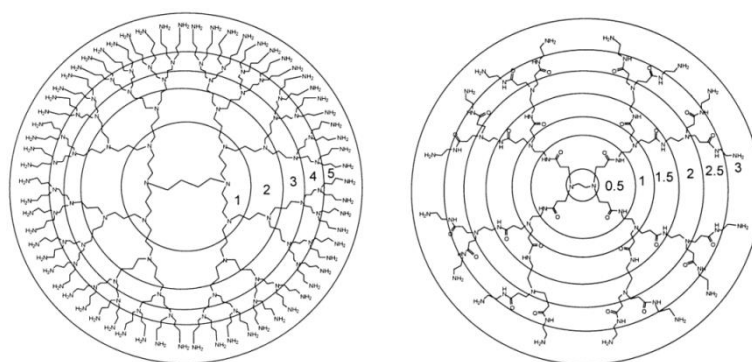


Figure 112. Left: Structure of a G5 PPI dendrimer. Right: Structure of a G3 PAMAM dendrimer.²⁹⁷

5.4 Synthesis of dendrimers

The synthesis of dendrimers is a long and tedious process that implies the use of iterative steps of deprotection/activation of functional groups followed by coupling reactions and exhaustive purification steps. All these processes affect the overall yield and require the use of high yield reactions.

²⁹⁵ Svenson, S.; Tomalia, D. A. *Adv. Drug Deliv. Rev.* **2005**, *57*, 2106-2129.

²⁹⁶ P. Kesharwani, R. K. Tekade, N. K. Jain, *Drug Discov. Today* **2015**, *20*, 497-499.

²⁹⁷ Boas, U.; Heegaard, P. M. *Chem. Soc. Rev.* **2004**, *33*, 43-63.

There are two general routes for the preparation of dendrimers. The divergent approach, also known as starburst method, consists in the synthesis of the dendrimer from the core to the periphery in a sequence of reaction steps generation by generation.

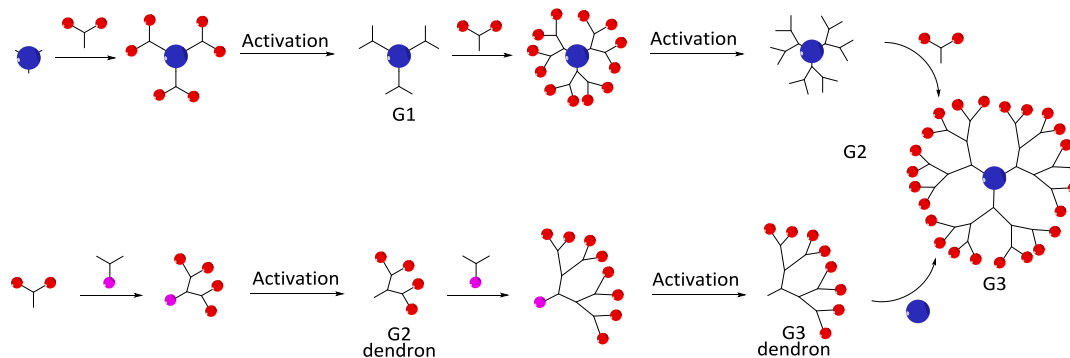


Figure 113. Schematic representation of the two possible synthetic pathways to prepare dendrimers.

In 1985 Tomalia reported the first use of a divergent route, with the description of the PAMAM dendrimer family (Figure 114).²⁸³ In this instance, the synthesis consisted of repetitive steps of Michael addition of methyl acrylate followed by amidation with ethylene diamine as is shown in Figure 113. Here, every new step requires the use of reactions with high yields and high excess of monomer units to avoid defects in the final structure. The purification of these compounds is complicated due to the similarity between products and byproducts of each step. Additionally, the number of reaction sites grows exponentially after the formation of each new generation that leads to slower reactions, and in some cases, to incomplete reactions, hindering to obtain high generation dendrimers.

On the other hand, the convergent approach was introduced by Fréchet and Hawker²⁹⁸ in 1990. This strategy consists in the synthesis of the dendrimer from the periphery to the core where the last step of the reaction is the linkage of the different dendrons or dendrimeric segments to the core (see Figure 113).

This route presents some advantages over the previous one. In this case, the number of reaction sites remains low during all the process enabling faster reactions. The possibility of defects in the dendritic structure during the synthesis for incomplete or unwanted reactions is minimized because the complete dendrons are synthesized and purified before their linkage to the core. The purification is also easier due to larger differences between reactive and products. At the same time, with this strategy, the preparation of asymmetric dendrimers with different functionalization is suitable.

Despite all these advantages, the linkage of the dendrons to the core is difficult and requires the use of very efficient reactions and large cores to avoid defects.

²⁹⁸ Hawker, C. J.; Fréchet, J. M. J. *J. Am. Chem. Soc.* **1990**, *112*, 7638–7647

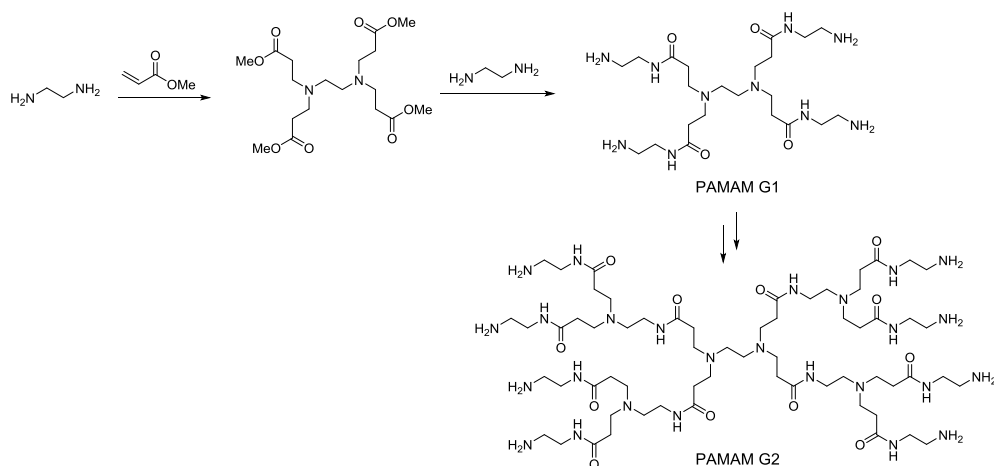


Figure 114. Synthesis of PAMAM dendrimers.

5.5 Applications of dendrimers

In recent years, the use of dendrimers in medicinal chemistry has been increased due to their well-defined structures, monodispersity, specific size and shape, and for their easily tunable properties. The core and the branching units of dendrimers determine the microenvironment inside the cavities formed by the building units of dendritic structure and the functionalization of the periphery determines their solubility. Thanks to these characteristics, they have been used in drug delivery and drug solubility enhancement, but also as MRI contrast agents, gene therapy or as catalysts.²⁹⁹

5.5.1 Dendrimers in drug delivery

Dendritic structures have shown to interact with a variety of drug molecules and transport them into the cell. This characteristic is very useful in the case of compounds with very low solubility and low cell penetrating properties in physiological media. Currently, dendrimers have been applied as carriers of a variety of anticancer, antiviral, antibacterial, antitubercular, and antimalarial drug compounds.³⁰⁰

Dendrimers can interact with different guests by physically entrapping molecules inside the cavities of various sizes and shapes distributed along the dendritic structure through electrostatic, hydrophobic and hydrogen bonding interactions as shown in Figure 115 or, alternatively, by covalent attachment of the drug to the periphery of the dendrimer.

²⁹⁹ Caminade, A. -M.; Turrin, C. -O.; Laurent, R.; Ouali, A.; Delavaux-Nicot, B. "Dendrimers: Towards Catalytic, Material and Biomedical Uses". ISBN: 978-0-470-74881-7, 2011.

³⁰⁰ Kalhapure, R. S.; Kathiravan, M. K.; Akamanchi, K. G.; Govender, T. *Pharm. Dev. Technol.* 2015, 20, 22–40.

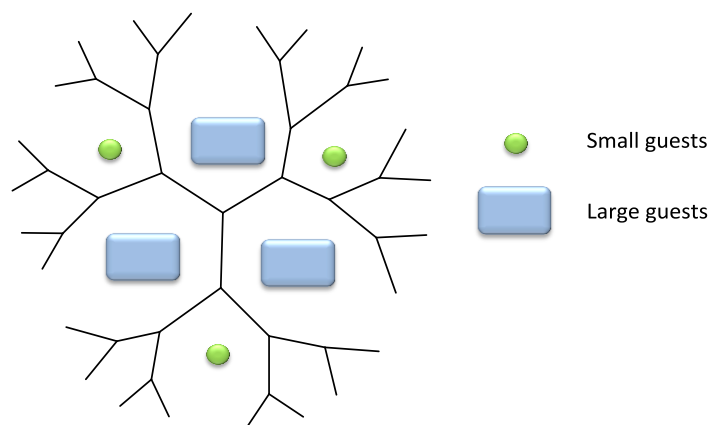


Figure 115. Schematic representation of the interaction of guest molecules with the different cavities present in the dendrimeric structure

Additionally, polyamine-based dendrimers are extremely affected by the pH of the medium due to the “proton sponge effect”. So, under basic pH, the internal tertiary amines of the structure are deprotonated causing a back-folding process giving a denser structure (see Figure 116). Under these conditions, the structure can trap large amounts of guest molecules inside the different void spaces formed in solution. Conversely, at acidic pH, the protonation of the amines causes the repulsion between charges. This repulsion produces the expansion to a more globular conformation leading to the release of the guest molecules.

Commercially available amino-terminated dendrimers are commonly employed for biological applications. The amino groups on the periphery are protonated at physiological pH, and can interact with the negatively charged cell membranes allowing the cell uptake by endocytosis. Higher generations of dendrimers often exhibit higher cytotoxicity originating cellular lysis.

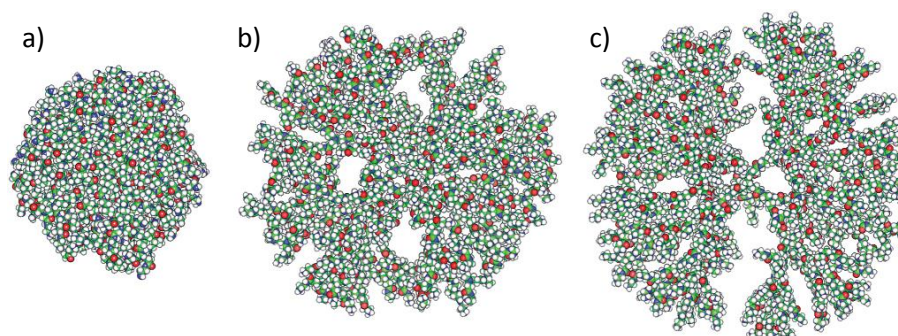


Figure 116. 3D structural representation of a G6 PAMAM dendrimer at: a) basic pH, b) neutral pH and c) acidic pH.³⁰¹

An important issue in the development of dendrimeric systems is the minimization of the toxicity of these compounds. To this end, the functionalization of the surface with polyethylene glycol units (PEGylation) is a common technique.³⁰²

³⁰¹ Lee, I.; Athey, B.; Wetzel, A.; Meixner, W.; Baker, J. *Macromolecules* **2002**, *35*, 4510-4520.

Poly-L-lysine (PLL) dendrimers are a family of dendrimeric compounds used in drug delivery processes due to their lower cytotoxicity compared with PAMAM and PPI dendrimers. PEGylated PLL dendrimers have been charged with different drugs for the treatment of several diseases. In this way, the metastatic breast cancer in rats has been successfully treated with doxorubicin (DOX)-dendrimer complexes (Figure 117).³⁰³

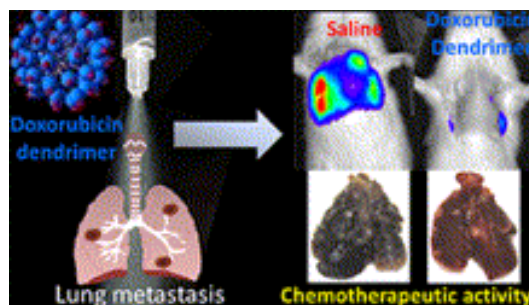


Figure 117. Images showing the reduction in the cancer tumor after treatment with the DOX-Dendrimer complex

Dendrimers can also serve to enhance the solubility of poorly or totally insoluble compounds through the formation of stable dendriplexes. As an example, some PAMAM dendrimers have shown to improve the solubility of niclosamide, an anthelmintic drug active against most tapeworms.³⁰⁴ Other macrocyclic compounds have been used for this purpose, as cyclodextrins, but their use is limited due to toxicity issues and low water solubility.³⁰⁵

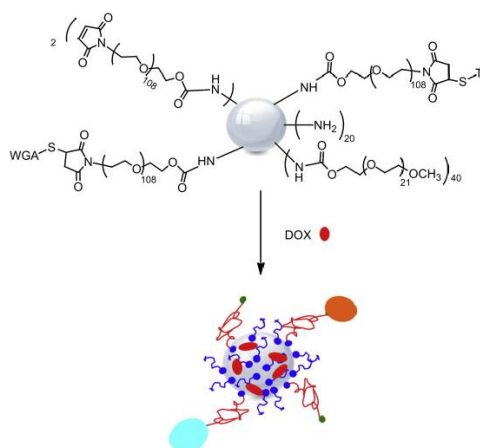


Figure 118. Representation of the complex (PAMAM-PEG-WGA-Tf)-DOX able to cross the blood-brain barrier and reach the brain.

The modulation of physicochemical properties of a dendrimer, allows the design of compounds for target delivery. As an example, PEGylated PAMAM dendrimers decorated with WGA (wheat germ

³⁰² Kulhari, H.; Pooja, D.; Prajapati, S. K.; Chauhan, A. S. *Int. J. Pharm.* **2011**, *405*, 203–209.

³⁰³ Kaminskis, L.M.; McLeod, V. M.; Ryan, G. M.; Kelly, B. D.; Haynes, J. M.; Williamson, M.; Thienthong, N.; Owen, D. J.; Porter, C. J. H. *J. Control. Release* **2014**, *183*, 18–26.

³⁰⁴ Devarakonda, B.; Hill, R. A.; Liebenberg, W.; Brits, M.; de Villiers, M. M., *Int. J. Pharm.* **2005**, *304*, 193–209.

³⁰⁵ Loftsson, T.; Brewster, M. E., *J. Pharm. Sci.* **1996**, *85*, 1017–1025.

agglutinin) and Tf (transferrin) targeting ligands (PAMAM-PEG-WGA-Tf) can encapsulate doxorubicin and cross the blood-brain barrier to accumulate them in the brain (Figure 118).³⁰⁶ The transport ratios of the PAMAM-PEG-WGA-Tf-DOX, PAMAM-PEG-WGA and free DOX were determined by in vitro assays showing values of 13.5%, 8% and 7% of drug loading, respectively. These results, indicate the enhanced ability of the conjugates to cross the BBB. Additional in vitro assays showed that the complex PAMAM-PEG-WGA-Tf delivered an 11% of DOX during the first hour and a 2.5% additional DOX during the second one showing that, in this case, the release of the drug molecule was a very fast process unlike traditional carrier systems showing no toxicity.

Another example is the dendrimeric system functionalized with polyester hydrophobic groups described by Fréchet et al. (Figure 119). This dendrimer can load a 12% weight of doxorubicin molecules inside the inner cavities. Here, the surface of the dendrimer is functionalized with acetal groups as pH-sensitive linkages. The acid hydrolysis of the acetal groups turns the dendrimer more hydrophilic causing the release of the anticancer drug.³⁰⁷ pH-dependent release studies determined that the release rates of the DOX drug were completed after less than ten hours at pH 5 and 7.4. In vitro studies showed that the DOX-dendrimer loaded complexes were located in intracellular organelles after 24 hours, unlike free drug that was situated in the nucleus. It should be noticed that doxorubicin interacts with DNA causing damages. For this reason, it is used for cancer treatment. But in high concentrations, doxorubicin present serious adverse effects as cardiomyopathies.

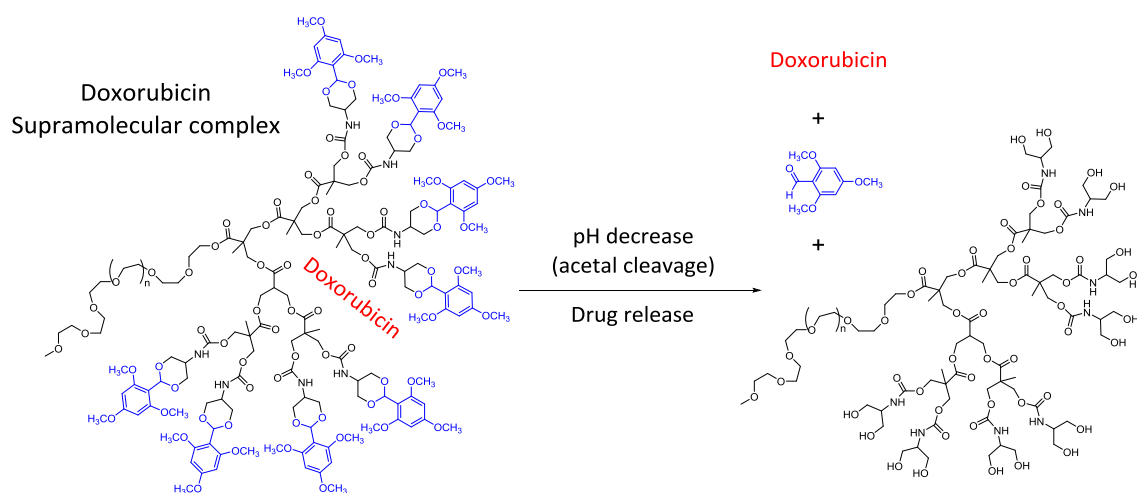


Figure 119. Representation of the supramolecular complex formed between doxorubicin (red) and a polyester dendrimer with acidic cleavage acetal groups. A pH decrease causes the release of the entrapped drug molecules.

Dendrimers can also be used as prodrug molecules through drug condensation with the dendrimer functional groups both, directly or by using appropriate linkers. This strategy relies on a change in the properties of the medium or the chemical or enzymatic cleavage of a functional group at the target organ that could cause the release of the drug responsible for the biological activity. For example, D'Emmanuele et al. reported a series of G0 PAMAM dendrimer-based prodrugs for the enhancement of the drug solubility and bioavailability of naproxen (Figure 120).³⁰⁸ Naproxen, an anti-inflammatory drug,

³⁰⁶ He, H.; Li, Y.; Jia, X. R.; Du, J.; Ying, X.; Lu, W. L.; Lou, J. N.; Wei, Y. *Biomaterials* **2011**, *32*, 478-487.

³⁰⁷ a) Gillies, E.; Fréchet, J. *Bioconjug. Chem.* **2005**, *16*, 361-368. b) Gingras, M., Raimundo, J.-M. M. & Chabre, Y. M. *Angew. Chem. Int. Ed. Engl.* **2007**, *46*, 1010-1017.

³⁰⁸ Najlah, M.; Freeman, S.; Attwood, D.; D'Emmanuele, A. *Int. J. Pharm.* **2007**, *336*, 183-190.

was conjugated to the dendrimer via direct conjugation or a PEG linker. In vitro studies showed that the direct condensation of the naproxen to the G0-PAMAM dendrimer through an amide functionality (**G0-NAP**) resulted in a very stable product. In this case, no traces of drug compound in plasma or liver were detected after treatment. Diethylene glycol linkers produced products with very high rates of drug release (**G0-deg-NAP**). On their turn, compounds with lactate ester linkers (**G0-lact-NAP**) showed slow rates of hydrolysis converting them in good candidates for the release of the drug in vivo.

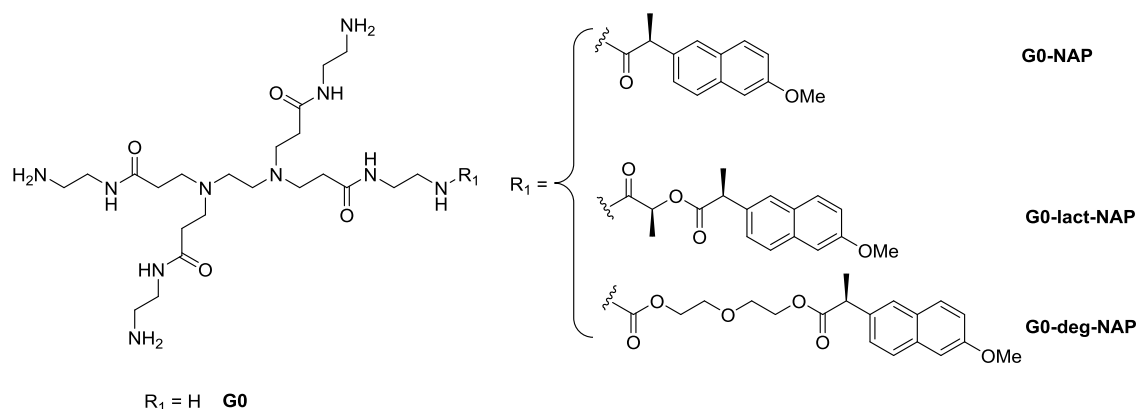


Figure 120. Chemical structure of G0-PAMAM dendrimers used as prodrug systems.

5.5.2 Dendrimers as vectors for biomedical applications

Dendrimers have also been used in gene therapy, magnetic resonance imaging (MRI), X-ray CT (computed tomography) and radionuclide-based contrast agents, among others.

Gene therapy has become a major investigation line in the treatment of some diseases such as cancer, AIDS, Parkinson or Alzheimer's. This approach and newer molecular-target-based approaches involve the use of efficient, but highly labile, agents such as monoclonal antibodies, siRNAs (small interference RNA) or aptamers (single-stranded DNA or RNA). These molecules, that are easily degraded and have limited stability in vivo, bind to a particular target such as small organics, proteins, cells, peptides, or tissues to accomplish their biological function.

Cationic dendrimers can interact with anionic biomolecules to form stable complexes known as "dendriplexes". Dendriplexes show improved transfection efficiencies and can be used as gene delivery systems. The most studied dendrimers in gene delivery are PAMAM dendrimers.

For example, siRNA molecules can be protected from degradation via formation of stable nanoparticles with PAMAM dendrimers. The siRNA/dendrimer nanoparticles facilitate cell uptake via endocytosis as shown in Figure 121. After entering cells, the siRNA molecules escape from the acidic endosome due to the "proton sponge effect" previously described. A net positive charge of the complex dendrimer-biological molecule is necessary to achieve good transfection efficiencies.

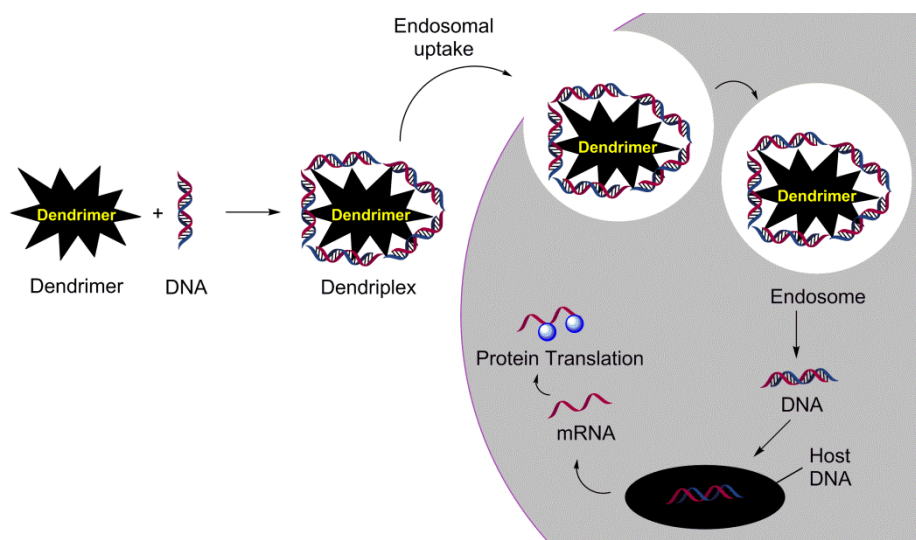


Figure 121. Schematic representation of the endocytosis process of a dendriplex.³⁰⁹

So far, different types of dendrimers have been developed for siRNA delivery, such as PAMAM dendrimers, PPI dendrimers, poly(L-lysine) dendrimers, carbosilane dendrimers, triazine dendrimers, etc. There are also commercially available kits for DNA and siRNA delivery as PolyFects and SuperFects based on PAMAM dendrimers.

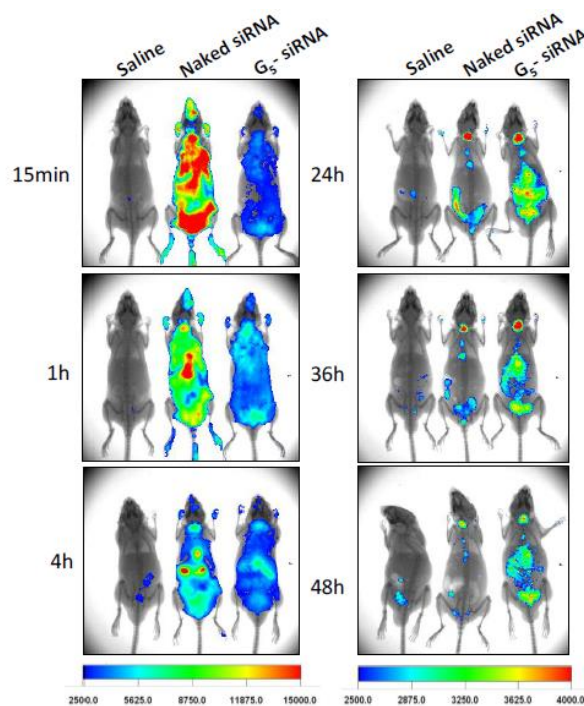


Figure 122. In vivo distribution of G_5 dendrimer-Cy5 siRNA complexes in a C57BL/6 mouse model.

³⁰⁹ Kesharwani, P.; Iyer, A.K. *Drug Discov. Today* **2014**, *20*, 536-547.

For example, complexes of PAMAM-dsiRNA molecules have been used for the treatment of HIV-infected humanized (RAG-hu) mice resulting in the silencing of the HIV replication and host HIV infection (See Figure 122).³¹⁰

Dendritic gadolinium polychelates illustrate the use of dendrimers in MRI. They consist of PPI and PAMAM dendrimers modified with small molecular Gd(II)-chelates, typically diethylenetriamine pentaacetate (DTPA)³¹¹ or tetraazacyclododecane tetraacetic acid (DOTA).³¹² The modulation of their properties let to obtain contrast images of different tissues useful for diagnosis (See Figure 123). Fluorescent dye molecules have been also charged into dendrimers molecules for fluorescence imaging applications.³¹³

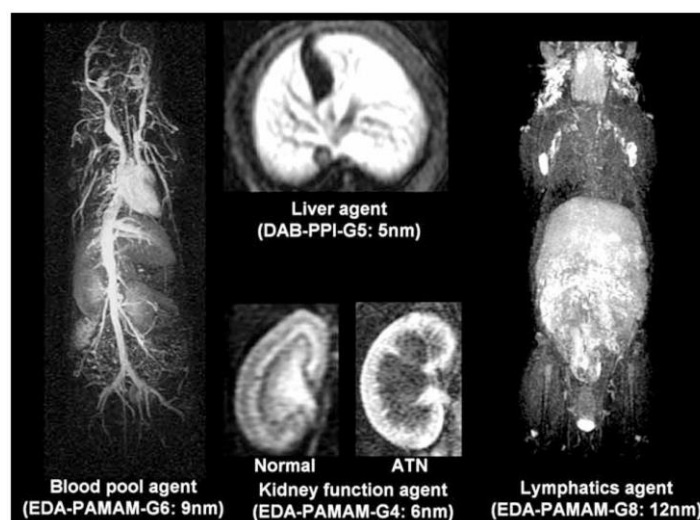


Figure 123. Magnetic resonance images (MRI) of selected organs obtained by using dendrimer-contrast agents.

³¹⁰ Zhou, J.; Neff, C. P.; Liu, X.; Zhang, J.; Li, H.; Smith, D. D.; Swiderski, P.; Aboellail, T.; Huang, Y.; Du, Q.; Liang, Z.; Peng, L.; Akkina, R.; Rossi, J. J. *Mol. Ther.* **2011**, *19*, 2228-2238.

³¹¹ a) Wiener, E., Brechbiel, M. W., Brothers, H., Magin, R. L., Gansow, O. A., Tomalia, D. A.; Lauterbur, P. C. *Magn. Reson. Med.* **1994**, *31*, 1–8. b) Pálinkás, Z.; Baranyai, Z.; Brücher, E.; Rózsa, B. *Inorg. Chem.* **2011**, *50*, 3471-3478

³¹² Lauffer, R. B. *Chem. Rev.* **1987**, *87*, 901-927.

³¹³ Longmire, M.; Choyke, P. L.; Kobayashi, H. *Curr. Top. Med. Chem.* **2008**, *8*, 1180-1186.

5.6 Aims

The main goal of this chapter is the initial design and synthesis of a new family of dendrimers based on squaramides. The specific aims are:

- To design a new set of dendrimeric compounds combining amine and squaramide motifs in their structures.
- To explore the synthesis of squaramide-based dendrimers through both, convergent and divergent approaches.
- To fully characterize the new compounds by NMR spectroscopy, mass spectrometry, and related techniques.
- In particular cases, to study the host-guest properties in front of typical biomolecules and to test the bioavailability (at a cell level) of the new dendrimers and dendriplexes.

Design and synthesis of a new family of squaramido-amino-based dendrimers

Preliminary unpublished results

5.7.1 Abstract

Dendrimers have been widely used in gene and drug delivery processes due to their in vivo stability and low cytotoxicity. Here, we report the design and synthesis of a new squaramido-amino-based dendrimeric family that combine the features of traditional polyamine dendrimers with the host-guest properties of squaramides. Specifically, different G1 and G2 dendrimeric compounds have been synthesized from four different core molecules and two different growing units.

5.7.2 Introduction

Dendrimers are highly branched structures with globular shape and an easily tunable surface that present excellent gene and drug delivery efficiencies.³¹⁴ Different families of dendrimers with different functionalities have been reported, but polyamino-based dendrimers as PAMAM and PPI are particularly attractive.³¹⁵ Both types of compounds possess secondary and tertiary amines that become protonated under weakly acidic conditions allowing the complexation with anionic guests. The resulting dendriplexes can be transferred to the cytosol by endocytosis.³¹⁶ However, in cationic dendrimers, the transport efficiency is closely related to its generation.³¹⁷ So, low generations exhibit minimal toxicities but low transfection efficacies. The modification of low generation polyamino dendrimers to improve their use as non-viral gene vectors is an important goal in dendrimer chemistry. Surface PEGylation or esterification, among others, has proved to reduce their toxicity.³¹⁸

On the other hand, squaramide-based macrocycles with amine functionalization have showed excellent cell internalization properties through endocytotic mechanism.³¹⁹ The observed fast cell internalization is triggered by the macrocycle binding to anionic compounds located on the outer face of the cell membrane. Our group have recently used squaramide-amine based macrocycles in gene-delivery processes showing good transfection efficacy and low toxicities (unpublished results, manuscript in preparation). On these grounds, the aim of this work is the design, synthesis, and characterization at an initial stage of a new family of squaramide-based-dendrimeric compounds featuring polyamino groups. These dendrimers are expected to achieve efficient transfection by a synergistic combination of the proton sponge effect of the amino groups and the high affinity of squaramides for phosphate groups.

³¹⁴ a) Esfand, R.; Tomalia, D. A. *Drug Discov. Today*, **2001**, *6*, 427-436, b) Liu, M; Fréchet, J. M. J.; *Pharm. Sci. Technol. Today* **1999**, *2*, 393-401, c) Dufès, C.; Uchegbu, I. F.; Schätzlein, A. G. *Adv. Drug Deliv. Rev.* **2005**, *57*, 2177-2202.

³¹⁵ a) Eichman, J. D.; Bielinska, A. U.; Kukowska-Latallo, J. F.; Baker Jr, J. R. *Pharm. Sci. Technol. Today* **2000**, 232-245, b) Nanjwade, B. K.; Bechra, H. M.; Derkar, G. K.; Manvi, F. V.; Nanjwade, V. K. *Eur. J. Pharm. Sci.* **2009**, *38*, 138-196.

³¹⁶ a) Behr, J. –P. *Chimia* **1997**, *51*, 34-36, b) Patil, M. L.; Zhang, M.; Taratula, O.; Garbuzenko, O. B.; He, H.; Minko, T. *Biomacromolecules* **2009**, *10*, 258-266.

³¹⁷ a) Lee, I; Athley, B. D.; Wetzel, A. W.; Meixner, W.; Baker Jr., J. R. *Macromolecules* **2002**, *35*, 4510-4520, b) Zinselmeyer, B. H.; Mackay, S. P.; Schätzlein, A. G.; Uchegbu, I. F. *Pharm. Res.* **2002**, *19*, 960-967, c) Shah, N.; Steptoe, R. J.; Parekh, H. S. *J. Pept. Sci.* **2011**, *17*, 470-478.

³¹⁸ a) Luo, D.; Haverstick, K.; Belcheva, N.; Han, E.; Saltzman, W. M. *Macromolecules* **2002**, *35*, 3456-3462, b) Nam, H. Y.; Nam, K.; Hahn, H. J.; Kim, B. H.; Lim, H. J.; Kim, H. J.; Choi, J. S.; Park, J. –S. *Biomaterials* **2009**, *30*, 665-673.

³¹⁹ Sampedro, A. Villalonga-Planells, R.; Vega, M.; Ramis, G.; Fernández de Mattos, S.; Villalonga, P.; Costa, A.; Rotger, C. *Bioconjug. Chem.* **2014**, *25*, 1537–1546.

5.7.3 Results and discussion

The new set of compounds was designed with a polyamine core and polyamino-squaramide branches as is shown in Figure 124. So, each generation combines a tertiary amine and a squaramide unit. Tertiary amines were included to modulate the encapsulation of different substrates as a function of the pH. At the same time, the squaramide moieties would enhance the affinity of these products for oxoanions such as phosphates or carboxylates.³²⁰ Finally, the periphery of the dendrimer was decorated with easily tunable amine groups.

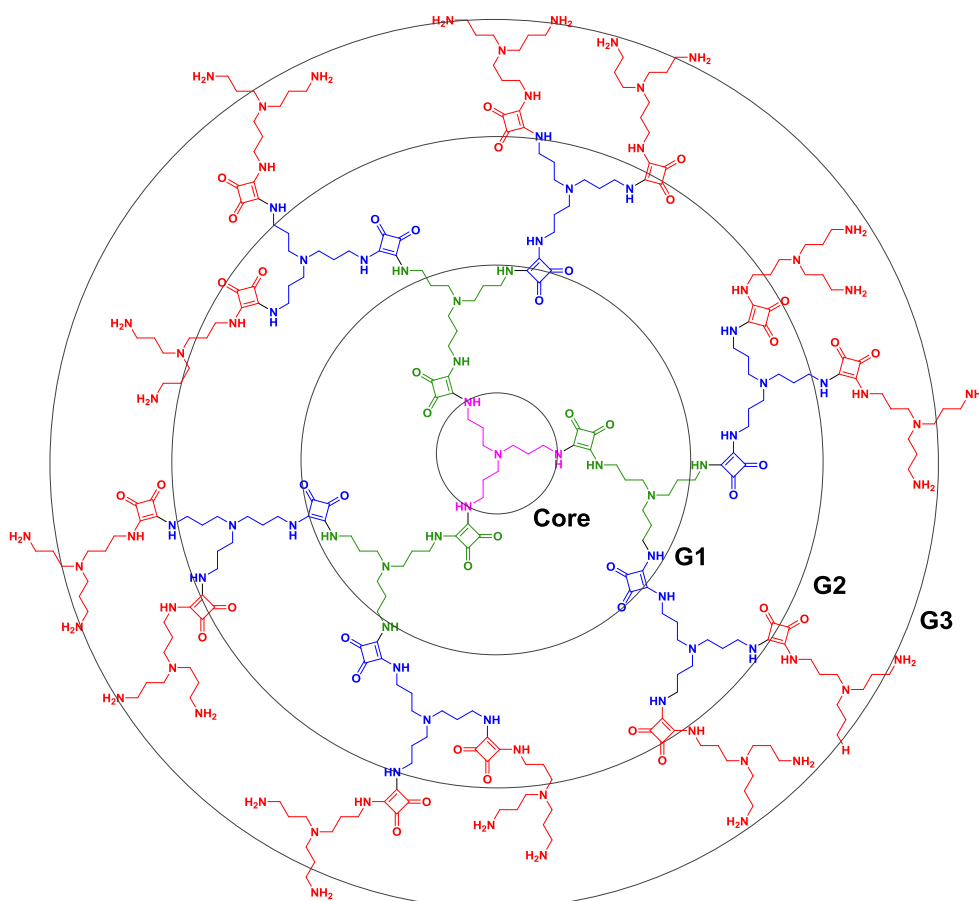


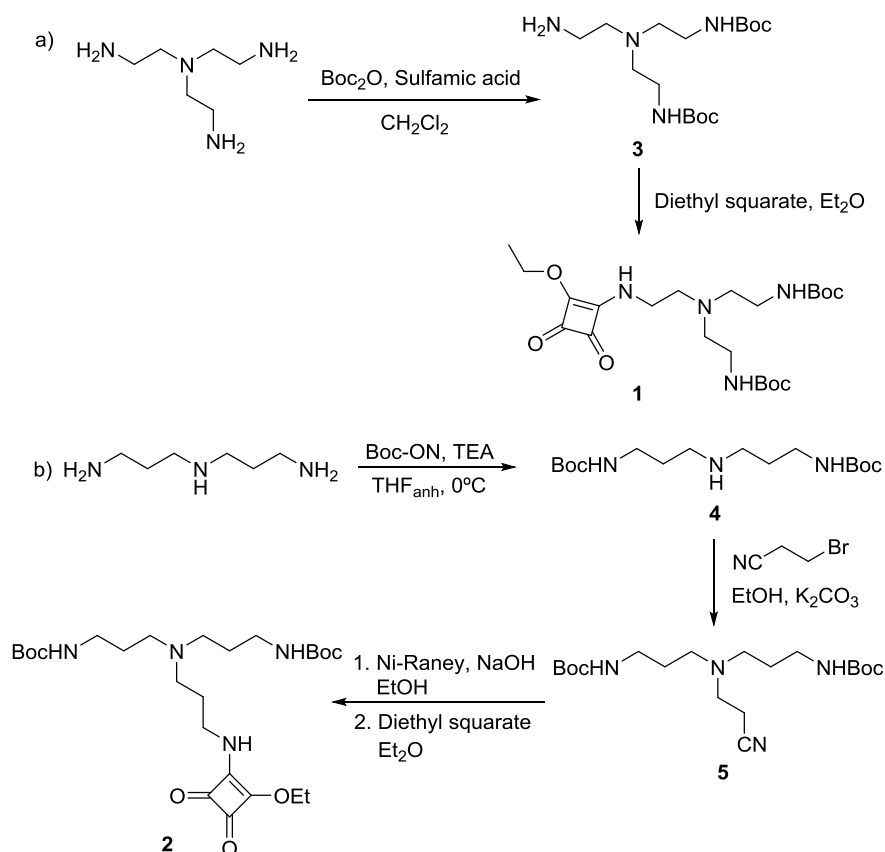
Figure 124. General design of the new squaramide-based dendrimers.

Semiesters **1** and **2** were prepared as growing units (see Scheme 4). They feature a squaramide unit at one end and two amino Boc-protected groups. As a result, the branching is duplicated after each synthetic step. Compound **1** was prepared by condensation reaction of the diprotected amine with diethyl squarate in Et₂O with 80% yield. Semester **2** was obtained following a four-step procedure as described in Scheme 4. First, the N1-(3-aminopropyl)propane-1,3-diamine was Boc-diprotected and, then, the resulting product was coupled with 3-bromopropanenitrile to give the intermediate product **5**.

³²⁰ a) Frontera, A.; Morey, J.; Oliver, A.; Piña, M. N.; Quiñero, D.; Costa, A.; Ballester, P.; Deyà, P. M.; Anslyn, E. V.; *J. Org. Chem.* **2006**, *71*, 7185–7195; b) Piña, M. N.; Soberats, B.; Rotger, C.; Ballester, P.; Deyà, P. M.; Costa, A. *New J. Chem.* **2008**, *32*, 1919–1923.

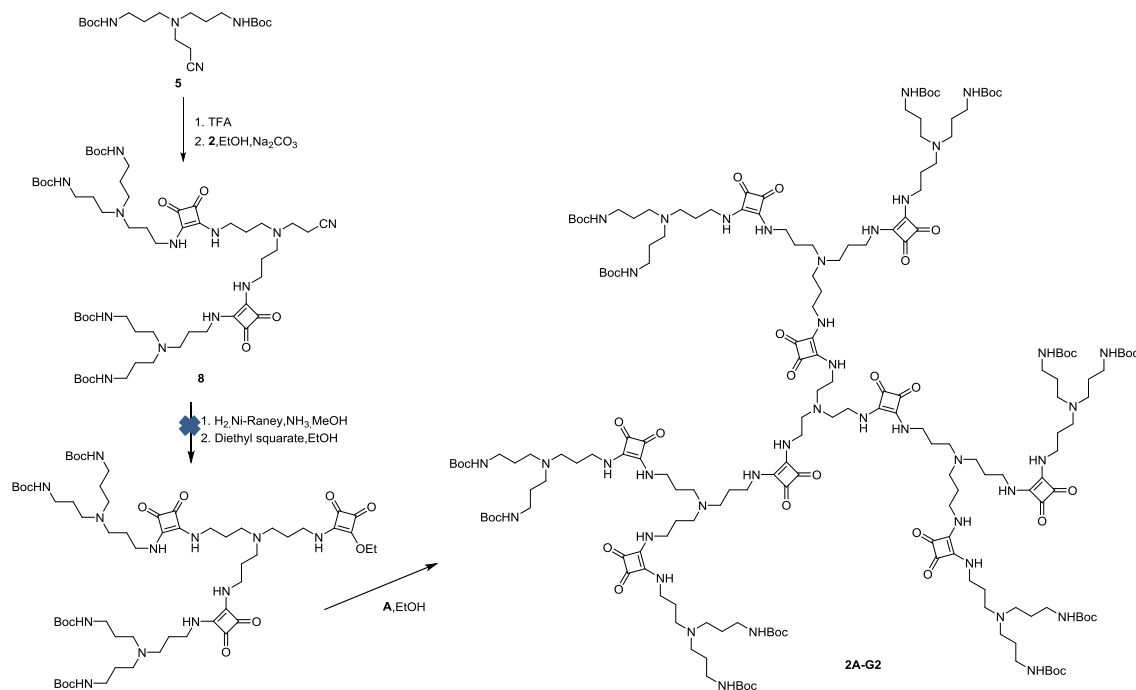
This compound was hydrogenated in the presence of Ni-Raney® and NaOH in ethanolic media. The resulting product was reacted with diethyl squarate in MeCN to afford **2** in 50% overall yield.

Scheme 4. Synthetic pathway to obtain: a) **1** and b) **2**.

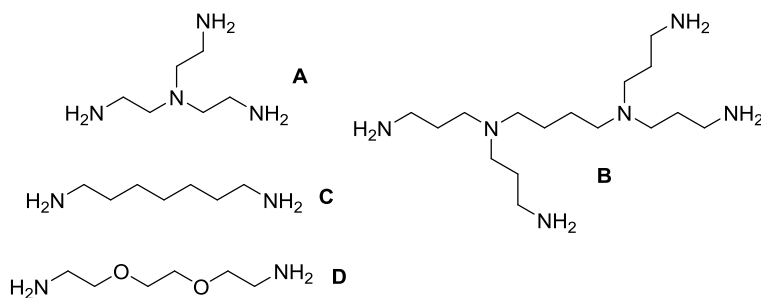


For the preparation of the dendrimers, we decided to follow a convergent approach as it has some advantages, such as the possibility to prepare asymmetric or multifunctional systems.³²¹ For this reason, the initial synthesis was done following this approach. Here, the synthesis of the dendrons starts with the amine deprotection of monomer **5** and the condensation of the resulting product with **2** (Scheme 5). The reduction of the nitrile group followed by the condensation with diethyl squarate gives a second generation dendron. Then, the coupling reaction with the corresponding core would yield the dendrimer. Unfortunately, in the present case, the reduction of the nitrile group failed. The same result was obtained when a Cbz protecting group was used in the place of the nitrile functionality. Following these disappointing results, we moved towards a divergent approach.

³²¹ a) Antoni, P.; Hed, Y.; Nordberg, A.; Nyström, D.; von Host, H; Hult, A.; Malkoch, M. *Angew. Chem. Int. Ed.* **2009**, *48*, 2126-2130, b) Ledin, P. A.; Friscourt, F.; Guo, J.; Boons, G. –J. *Chem. Eur. J.* **2011**, *17*, 839-846, b) Kimoto, A.; Cho, J. –S.; Higuchi, M.; Yamamoto, K. *Macromolecules*, **2004**, *37*, 5531-5537.

Scheme 5. Proposed synthetic pathway for the preparation of dendrimers following a convergent synthesis.

As an alternative, we tried a divergent approach. In this case, we tested several polyamines as core molecules. First, we used N1,N1-bis(2-aminoethyl)ethane-1,2-diamine (**A**) as the core molecule. This route implies the use of a large excess of the growing units to avoid mistakes during the coupling. The first generations (G1) for linkers **1** and **2** were obtained with excellent yields for both linkers, **1** and **2** (**1A-G1** 92%, **2A-G1** 75%). Encouraged by these results, we tried other commercial polyamines to examine the effect of the length and the branching of the core over the properties of the G1 dendrimeric molecules (Figure 125). We tested, tris(2-aminoethyl)amine (**A**), a small triamine; N1,N1'-(butane-1,4-diyl)bis(N1-(3-aminopropyl) propane-1,3-diamine) (**B**), a bigger polyamine with four branches; heptane-1,7-diamine (**C**) and 2,2'-(ethane-1,2-diylbis(oxy))bis(ethan-1-amine) (**D**).

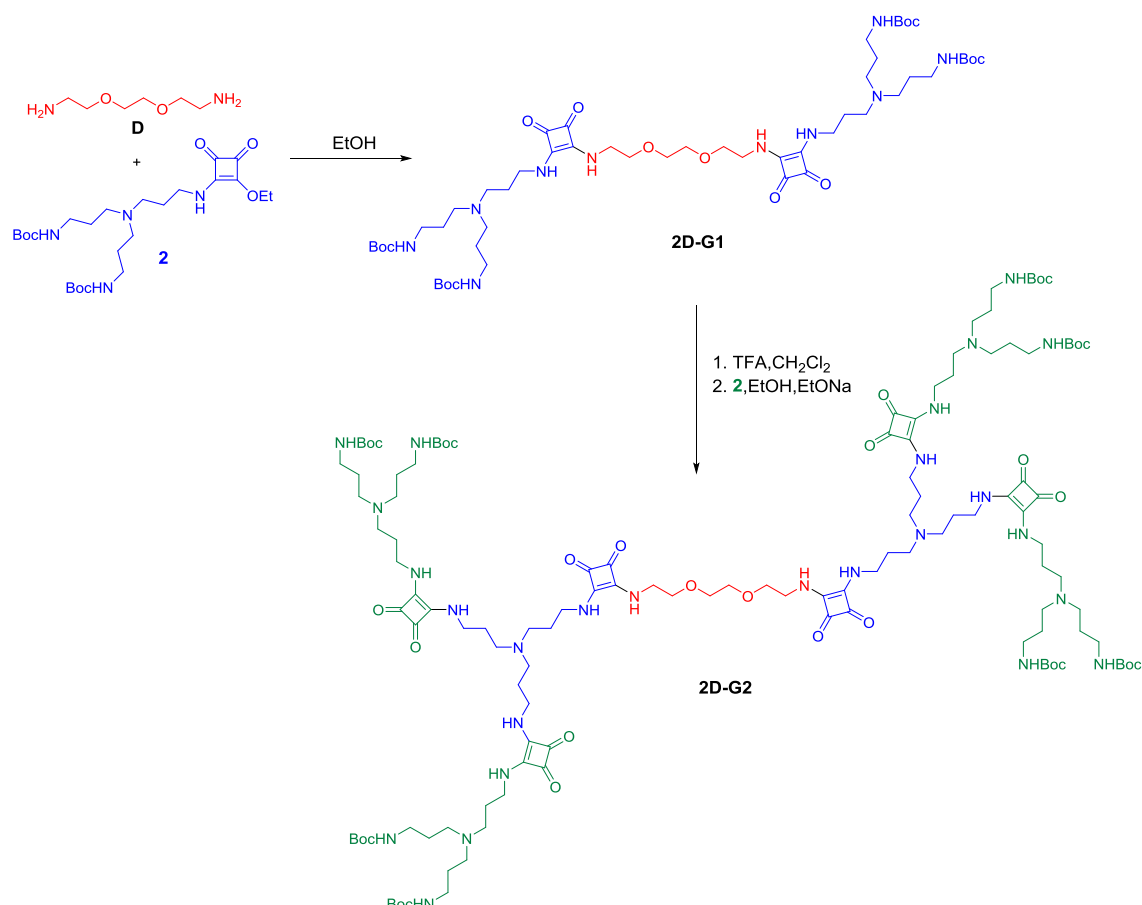
**Figure 125.** Chemical structure of core molecules used in this study.

In this way, dendrimers **1B-G1**, **2B-G1**, **2C-G1** and **2D-G1** were obtained from the direct condensation reaction of the corresponding polyamine with a high excess of semiester **2** in alcoholic media (Scheme

6). After purification by column chromatography (Al_2O_3 , CH_2Cl_2 :MeOH mixtures), the above dendrimers were obtained in excellent yields (75-96%) or at least, in reasonable yields for **1B-G1** (26%) and **2B-G1** (64%), respectively.

Deprotected generations (**G1-NH₂**) can be isolated by dialysis in water or water:ethanol mixtures of the Boc-protected dendrimers previously treated with TFA or CH_2Cl_2 :TFA mixtures.

Scheme 6. Schematic synthetic pathway for the preparation of G1 and G2 dendrimers.



Second generations **1A-G2**, **2B-G2**, **2C-G2** and **2D-G2** were also isolated in fairly good yields ~13-60% yield. The syntheses were carried out by deprotection of the Boc-protected amino groups by treating the Boc-protected G1 dendrimers in TFA or CH_2Cl_2 -TFA mixtures for 2-4 hours. The deprotected products were condensed with the growing unit **2** in an ethanolic solution containing an excess of NaOEt. Remarkably, it was observed that the yield of **2D-G2** increased from 13% to 45% working at a lower temperature of 5 °C instead of at room temperature. Overall, this observation suggests that the condensation of the squaramide units with the amine groups is an exothermic process.

With the most branched cores (**A** and **B**), the yields were unsatisfactory (10% and 12%, respectively). For **B**, the functionalization with the two semiester compounds resulted in mixtures of crowded products hindering their purification by column chromatography. For this reason, the yields were very low compared to other core molecules. On the other hand, core **A** gave **G1** in excellent yield. Conversely, the

yield is drastically diminished in **G2**. Here, partially substituted products were the main products of the synthesis probably because the core is too small to accommodate heavily substituted dendrons.

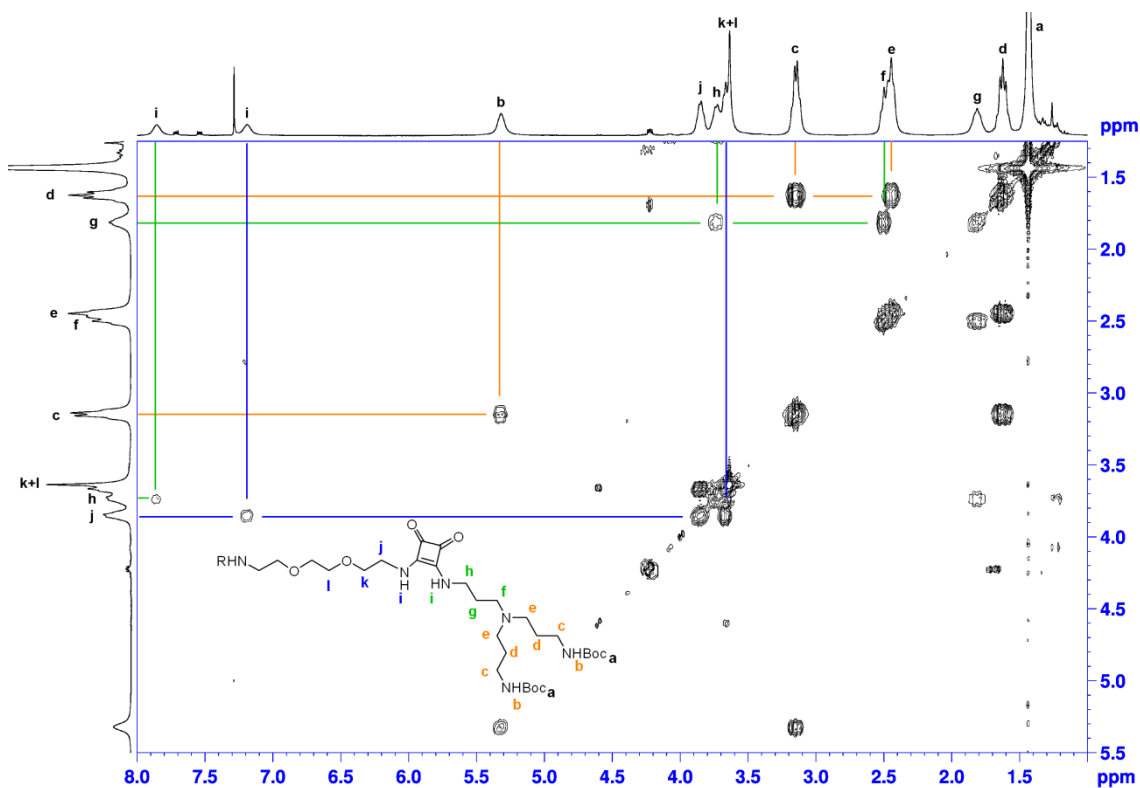


Figure 126. 2D-COSY NMR spectrum of **2D-G1** in CDCl_3 at 298K.

In general, better results were obtained when the reaction was carried out with linker **2** probably because an extra carbon atom gives more flexibility to the resulting dendrimer that can better accommodate the new units.

Mass spectrometry confirmed the molecular weight of each dendrimer. Both, 1D and 2D NMR spectroscopy were used for complete assignments of all synthesized dendrimers. Particularly useful were 2D-COSY and 2D-TOCSY NMR spectra. As an example, the 2D-COSY NMR spectrum of **2D-G1** is shown in Figure 126 in which each spin system is indicated by a different color.

^1H -NMR spectra of synthesized **2**, **2D-G1**, and **2D-G2** are shown in Figure 127 for comparison.

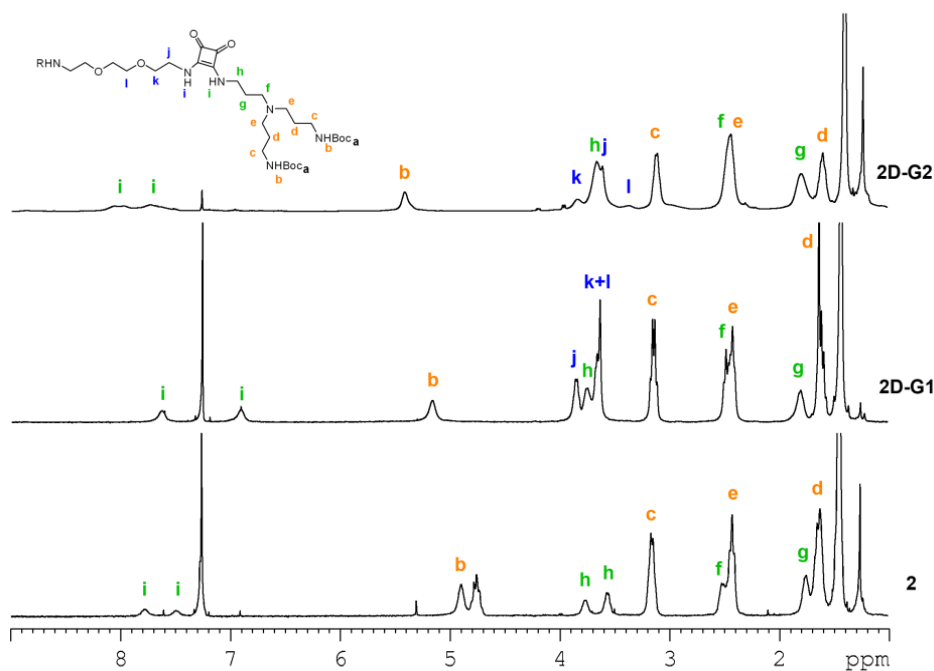


Figure 127. $^1\text{H-NMR}$ spectra (CDCl_3 , 300 MHz) of **2**, **2D-G1**, and **2D-G2**. In each case, the signals are indicated for comparison.

In order to characterize the dendrimer generations, preliminary 2D-DOSY NMR experiments have been carried out on mixtures of **2**, **2D-G1**, and **2D-G2** in methanol. However, the DOSY spectrum is not conclusive (Figure 128).

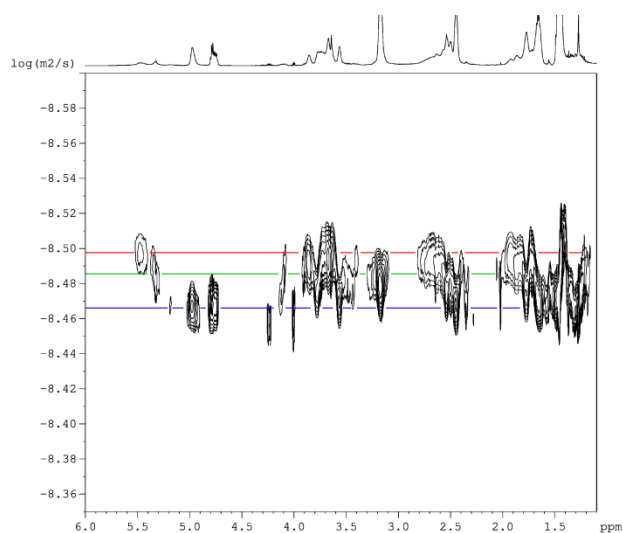


Figure 128. 2D DOSY spectrum of: **2** (3.2 mM) blue, **2D-G1** (3 mM) green and **2D-G2** (3.6 mM) red in CDCl_3 at 298 K.

The surface charge of deprotected dendrimers at different pH values is important for posterior biological applications. The electrostatic potential or zeta potential near the surface of dendrimers in solution is a critical indicator of the stability of colloidal dispersions of the dendrimers. It measures the degree of electrostatic repulsion between adjacent, similarly charged particles. A high value of zeta

potential confers stability while compounds with small values of zeta potential tend to aggregate in solution. As an example, zeta potential values for **2D-G1-NH₂** at different pH values (9.5-6.5) were determined. In this case, as expected, at a basic pH, the surface of the dendrimer is negatively charged while in neutral and in slightly acidic solutions, the amino groups appear protonated. But, in all cases, zeta potential values were very low indicating that in unbuffered aqueous solutions, these compounds tend to aggregate.

Table 14. Zeta potential values for compound **G1Dd** at different pH.

pH	Zeta pot (mV)
9,4	-5,79
9,05	-4,33
8,45	-1,75
7,62	1,33
7,24	3,81
7,04	4,99
6,95	5,5
6,81	6,49

5.7.4 Conclusions

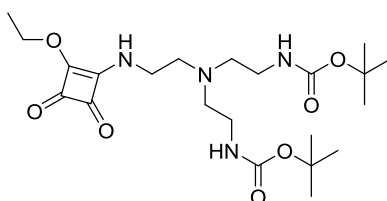
In summary, a new set of G1 and G2 squaramide-based dendrimeric compounds with different core molecules and linkers have been synthesized and partially characterized. Several initial generations have been studied by 2D-DOSY NMR experiments and by zeta potential measurements. Further work is necessary prior to their biological evaluation such as the determination of their purity by HPLC/GPC chromatography or DOSY, AFM, zeta potential and DLS experiments in water at different pH values.

5.7.4 Experimental

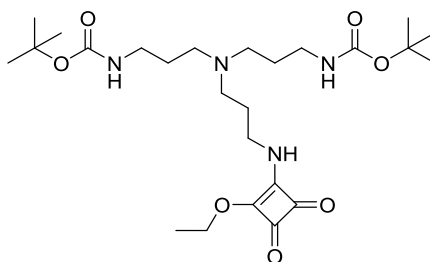
5.7.4.1 General methods

All reagents were purchased commercially and used without further purification. Mass spectra were registered on a MICROMASS Autospec3000 spectrometer equipped with an electrospray module or with a Bruker Autoflex (MALDI-Tof). ^1H and ^{13}C spectra were recorded on Bruker AVANCE 300 (^1H at 300 MHz and ^{13}C at 75 MHz) and on Bruker AVANCE III 600 equipped with a cryoprobe, in CDCl_3 or D_2O solvents and using the residual proton signal as reference. Chemical shifts (δ) are in ppm and coupling constants (J) in Hz. Zeta potential measurements were recorded on a Zetasizer Nano ZS90. pH measurements were carried out on a Crison micropH 2000 pH meter. Elemental analyses (C, H, N) were conducted by the "Centro de Microanálisis Elemental" of the "Universidad Complutense de Madrid" (Spain).

5.7.4.2 Synthesis and characterization of products

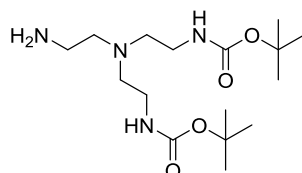


Di-tert-butyl (((2-aminoethyl)azanediyl)bis(ethane-2,1-diyl))dicarbamate (1). 1.36 g (3.93 mmol) of di-tert-butyl (((2-aminoethyl)azanediyl)bis(ethane-2,1-diyl))dicarbamate in 60 mL of Et_2O were added dropwise to a solution of 0.74 g (4.33 mmol) of 3,4-diethoxycyclobut-3-ene-1,2-dione in 50 mL of Et_2O . The resulting solution was stirred overnight at room temperature. After this period, the solvent was removed by rotary evaporation. The resulting yellow oil was dissolved in CH_2Cl_2 and precipitated with hexane (1.5 g, 81%). ^1H NMR (300 MHz, CDCl_3) δ 7.47 (s, 0.5H), 7.15 (s, 0.5H), 4.93 (s, 2H), 4.76 (q, $J = 7.2$ Hz, 2H), 3.71 (s, 1H), 3.48 (s, 1H), 3.15 (q, $J = 5.7$ Hz, 4H), 2.69 (t, $J = 5.7$ Hz, 2H), 2.54 (s, 4H), 1.44 (s, 21H); ESI-HMRS: calc. $\text{C}_{22}\text{H}_{38}\text{N}_4\text{O}_7\text{Na}$: 493.2638; exp. 493.2642 $[\text{M}+\text{Na}]^+$.

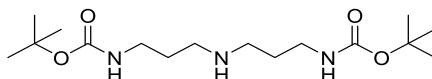


Di-tert-butyl(((3-((2-ethoxy-3,4-dioxocyclobut-1-en-1-yl)amino)propyl)azanediyl)bis(propane-3,1-diyl))dicarbamate (2): 0.715 g (1.859 mmol) of di-tert-butyl (((2-cyanoethyl)azanediyl)bis(propane-3,1-diyl))dicarbamate, 0.197 g of sodium hydroxide and 0.123 g (1.859 mmol) of Raney[®] Nickel were dissolved in 50 mL of EtOH and the dissolution was hydrogenated at 50 psi 48 hours. After this period, the solvent was removed by rotary evaporation affording the deprotected amine that was used without further purification steps. The resulting yellow oil was dissolved in 75 mL of Et_2O , filtered through celite and added dropwise to a solution of 0.381 g (2.239 mmol) of 3,4-diethoxycyclobut-3-ene-1,2-dione in 30 mL of Et_2O . The resulting solution was stirred overnight. The crude solution was concentrated and the

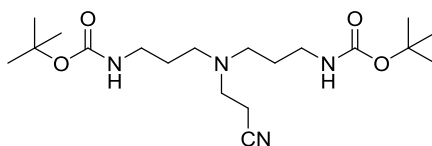
product was purified by column chromatography (silica, CH₂Cl₂:MeOH 2-5%) to afford the product (0.8 g, 84%). mp = 97-99 °C; ¹H NMR (600 MHz, CDCl₃) δ 7.86 (s, 0.5H), 7.53 (s, 0.5H), 4.97 (s, 2H), 4.77 (m, 2H), 3.77 (s, 1H), 3.56 (s, 1H), 3.17 (s, 4H), 2.54 (m, 2H), 2.45 (s, br, 4H), 1.78 (s, 2H), 1.66 (m, 4H), 1.45 (s, 21H); ¹³C NMR (150 MHz, CDCl₃) δ 189.3, 181.1, 177.0, 172.7, 172.4, 156.1, 79.3, 69.4, 52.3, 51.5, 44.0, 43.3, 38.9, 28.4, 27.8, 27.4, 26.7, 15.9; MALDI-TOF(+) m/z (%): calc. C₂₅H₄₅N₄O₇ 513.3288; exp. 513.3300 [M+H]⁺.



Di-tert-butyl (((2-aminoethyl)azanediyl)bis(ethane-2,1-diyl))dicarbamate (3). This compound was prepared by a modification of a reported procedure.³²² 1.48 g (6.8 mmol) of di-tert-butyl dicarbonate in 30 mL of CH₂Cl₂ were added dropwise to a solution of 2.5 g (16.42 mmol) of N1,N1-bis(2-aminoethyl)ethane-1,2-diamine and 0.04 g (0.4 mmol) of sulfamic acid in 20 mL of CH₂Cl₂ at 0 °C. The resulting solution was stirred overnight at room temperature. After this period, 50 mL of water were added and the pH was adjusted to 2-3. The aqueous phase was washed with CH₂Cl₂ (2×20 mL). The pH was readjusted to 8 with NaOH and extracted with CH₂Cl₂ (10×10 mL). The organic phase was dried with Na₂SO₄, filtered and concentrated by rotary evaporation to afford the product as a yellow oil (0.575 g, 50%). ¹H NMR (300 MHz, CDCl₃) δ 5.21 (s, 2H), 3.17 (q, *J* = 5.7 Hz, 4H), 2.73 (t, *J* = 6.0 Hz, 2H), 2.55 (t, *J* = 6.0 Hz, 4H), 2.5 (t, *J* = 6.0 Hz, 2H), 1.44 (s, 18H); ESI-MS(+) m/z (%): 325.2699 [M+H]⁺.



Di-tert-butyl (azanediylbis(propane-3,1-diyl))dicarbamate (4): This compound was prepared following a reported procedure.³²³

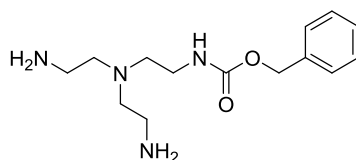


Di-tert-butyl (((2-cyanoethyl)azanediyl)bis(propane-3,1-diyl))dicarbamate (5): This compound was prepared following a reported procedure.³²⁴

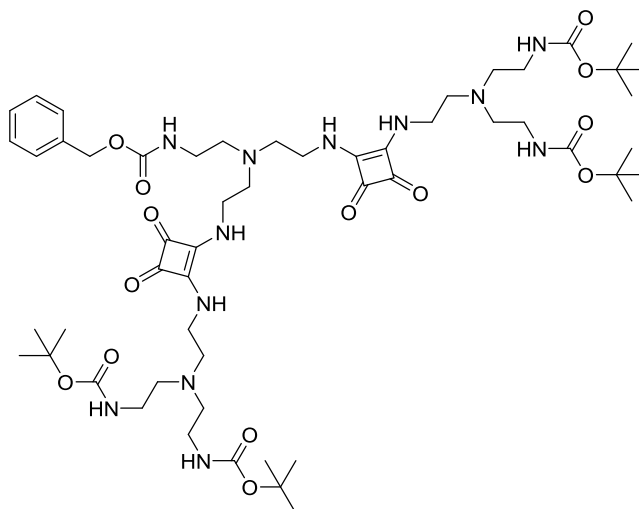
³²² Morin, E.; Nothisen, M.; Wagner, A.; Remy, J. –S. *Bioconjugate Chem.* **2011**, *22*, 1916–1923.

³²³ Deng, B. –L.; Beingessner, R. L.; Johnson, R. S.; Gidhar, N. K.; Danumah, C.; Yamazaki, T.; Fenniri, H. *Macromolecules* **2012**, *45*, 7157–7162.

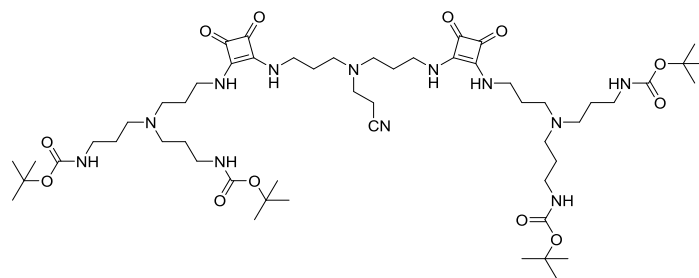
³²⁴ Malabarba, A.; Ciabatti, R.; Kettenring, J.; Scotti, R.; Candiani, G.; Pallanza, R.; Berti, M.; Goldstein, B. P. *J. Med. Chem.* **1992**, *35*, 4054–4060.



Benzyl (2-(bis(2-aminoethyl)amino)ethyl)carbamate (6). 1.03 mL (6.85 mmol) of benzyl chloroformate in 100 mL of anhydrous CH_2Cl_2 were added dropwise during 1 hour to a solution of 2.92 g (19.19 mmol) of N1,N1-bis(2-aminoethyl)ethane-1,2-diamine in 50 mL of anhydrous CH_2Cl_2 at 0 °C. The resulting solution was stirred 1 additional hour at room temperature and the solvent was removed by rotary evaporation. The resulting crude was dissolved in 20 mL of water, the pH adjusted to 3 and washed with CH_2Cl_2 (3×10 mL). The pH was readjusted to 7-8 with NaOH and extracted with CH_2Cl_2 (5×10 mL). The pH was readjusted to 9-10 with NaOH and extracted with CH_2Cl_2 (8×10 mL). The organic phase was dried with Na_2SO_4 , filtered and concentrated by rotary evaporation to afford the product as a yellow oil (0.77 g, 50%). ^1H NMR (300 MHz, CDCl_3) δ 7.35 (m, 5H), 5.91 (s, 1H), 5.09 (s, 2H), 3.26 (s, 2H), 2.73 (t, $J = 6$ Hz, 4H), 2.58 (t, $J = 6$ Hz, 2H), 2.52 (t, $J = 6$ Hz, 4H); MALDI-TOF(+) m/z (%):281.193 $[\text{M}+\text{H}]^+$.

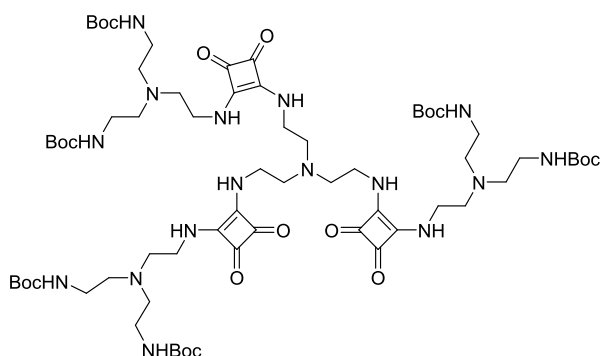


Benzyl (2-(bis(2-((2-(bis(2-((tert-butoxycarbonyl)amino)ethyl)amino)ethyl)amino)-3,4-dioxocyclobut-1-en-1-yl)amino)ethyl)amino)ethyl)carbamate (7): 0.05 g (0.178 mmol) of **3** in 20 mL of EtOH were added dropwise to a solution of 0.21 g (0.446 mmol) of **1** in 10 mL of EtOH. The resulting solution was stirred overnight at room temperature. After this period, the solvent was removed by rotary evaporation. The crude solution was concentrated and the product was purified by column chromatography (silica, $\text{Et}_2\text{O}:\text{MeOH}$ 0-10%) to afford the product as yellow oil (0.1 g, 50%). ^1H NMR (300 MHz, CDCl_3) δ 7.60 (s, 2H), 7.30 (m, 5H), 7.08 (s, 2H), 5.01 (s, br, 5H), 3.68 (s, 8H), 3.14 (s, 10H), 2.61 (m, 18H), 1.41 (s, 36H); MALDI-TOF(+) m/z (%): calc. $\text{C}_{54}\text{H}_{88}\text{N}_{12}\text{NaO}_{14}$ 1151.6441; exp. 1151.6488 $[\text{M}+\text{Na}]^+$.

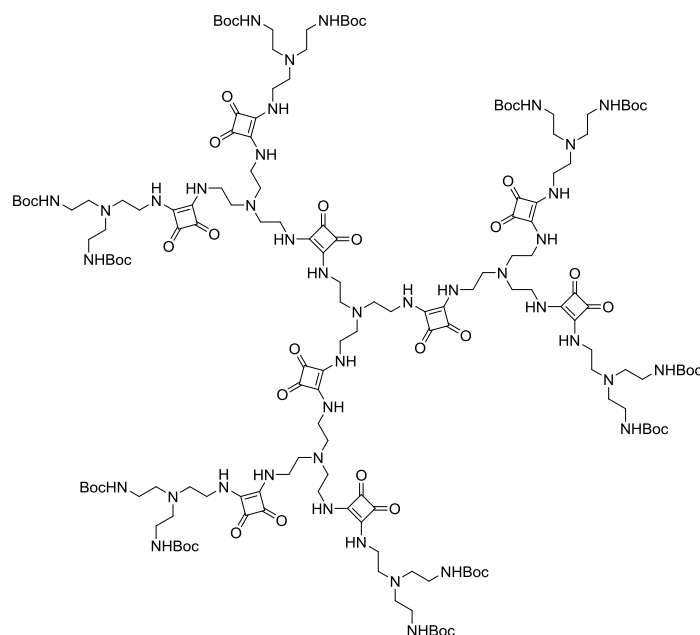


tetra-tert-butyl (((((((((2-cyanoethyl)azanediyl)bis(propane-3,1-diyl))bis(azanediyl))bis(3,4-dioxocyclobut-1-ene-2,1-diyl))bis(azanediyl))bis(propane-3,1-diyl))bis(azanetriyl))tetrakis (propane-3,1-diyl))tetracarbamate (8): 35 mg (0.091 mmol) of **5** were dissolved in 1 mL of trifluoroacetic acid and resulting solution was stirred for 2 hours. After this period, the deprotected amine was precipitated as chloride salt with hydrogen chloride 2N solution in diethyl ether and was used without further purification steps.

0.1 g (0.195 mmol) of **3** in 10 mL of EtOH were added dropwise to a solution of the previous obtained amine in 5 mL of EtOH previously neutralized with Na_2CO_3 . The resulting solution was stirred 24 hours. After this period, the crude solution was filtered and concentrated under vacuum. The product was purified by column chromatography (silica, CH_2Cl_2 :MeOH 8-10%) to afford the product (63 mg, 61%). ^1H NMR (300 MHz, CDCl_3) δ 8.47 (s, 2H), 8.08 (s, 2H), 5.28 (s, 4H), 3.72 (s, 8H), 3.17 (q, 8H), 2.55 (br, 20H), 1.87 (br, 16H), 1.42 (s, 36H); MALDI-TOF(+) m/z (%): calc. $\text{C}_{55}\text{H}_{96}\text{N}_{12}\text{NaO}_{12}$ 1139.7168; exp. 1139.7142 $[\text{M}+\text{Na}]^+$.

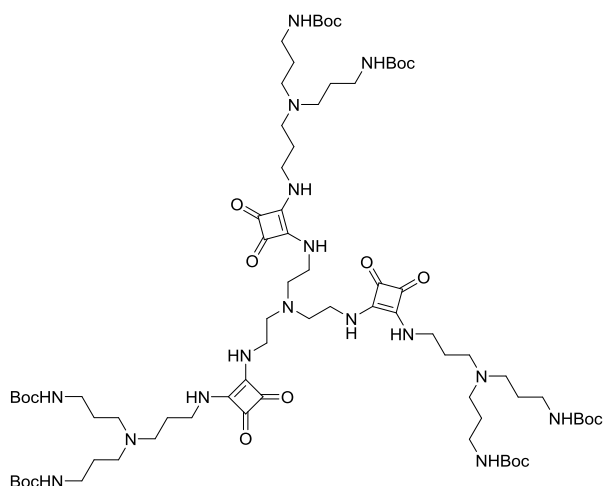


Compound 1A-G1: 0.14 g (0.919 mmol) of N1,N1-bis(2-aminoethyl)ethane-1,2-diamine in 40 mL of EtOH were added dropwise to a solution of 1.352 g (2.87 mmol) of **1** in 50 mL of EtOH. The resulting solution was stirred 3 days at room temperature. After this period, the solvent was removed by rotary evaporation. The crude solution was dissolved in CH_2Cl_2 and the product was precipitated with hexane. The product was isolated as yellow solid by centrifugation (1.2 g, 92%). ^1H NMR (300 MHz, CDCl_3) δ 7.40 (s, 6H), 5.17 (s, br, 6H), 3.69 (s, br, 12H), 3.15 (s, br, 12H), 2.72 (s, br, 12H), 2.59 (s, br, 12H), 1.42 (s, 54H); ^{13}C NMR (75 MHz, CDCl_3) δ 183.1, 181.9, 168.6, 167.2, 156.6, 79.3, 77.3, 54.9, 43.1, 42.2, 39.20, 28.6; ESI-HMRS: calc. $\text{C}_{66}\text{H}_{115}\text{N}_{16}\text{O}_{18}$: 1419.8575; exp. 1419.8584 $[\text{M}+\text{H}]^+$. Anal. Calcd. for $\text{C}_{66}\text{H}_{114}\text{N}_{16}\text{O}_{18}$: C, 55.84; H, 8.09; N, 15.79. Found: C, 55.35; H, 7.83; N, 15.62.



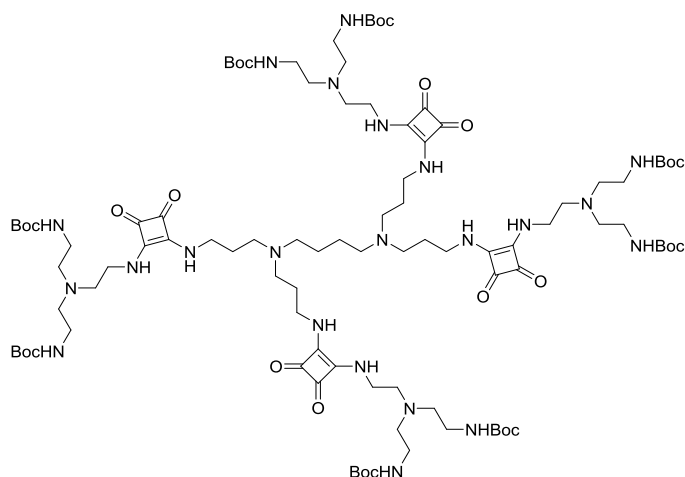
Compound 1A-G2: 200 mg (0.141 mmol) of **1A-G1** were dissolved in 2 mL of CH_2Cl_2 with 0.25 mL of trifluoroacetic acid and the resulting solution was stirred for 4 hours. After this period, the solution is neutralized with Na_2CO_3 and concentrated under vacuum affording the corresponding deprotected compound that was used without further purification.

0.646 g (0.986 mmol) of **1** in 15 mL of EtOH were added dropwise to a solution of the previous obtained amine in 20 mL of EtOH. The resulting solution was stirred overnight. After this period, the crude solution was concentrated under vacuum. The product was dissolved in H_2O and extracted with CH_2Cl_2 (3×10 mL). The organic phase was dried with Na_2SO_4 , filtered and concentrated by rotary evaporation to afford the product as a yellow oil that was solidified with pentane (224 mg, 10%). ^1H NMR (300 MHz, CDCl_3) δ 5.09 (br, 18H), 3.68 (s, br, 24H), 3.15 (s, br, 36H), 2.71 (s, br, 24H), 2.59 (s, 36H), 1.42 (s, 108H).

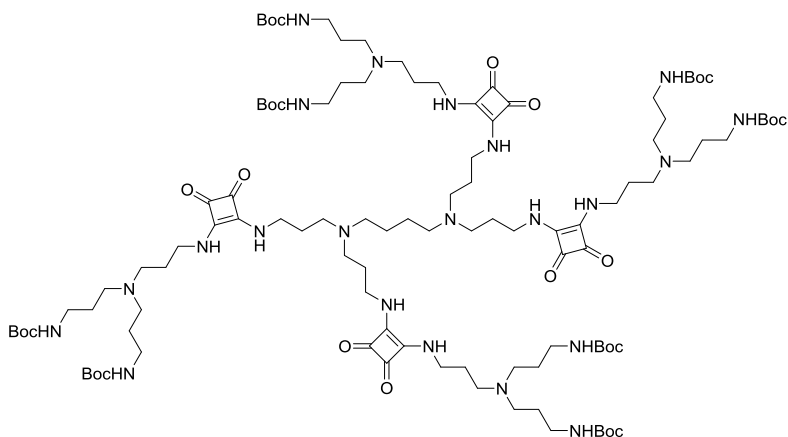


Compound 2A-G1: 0.026 mL (0.46 mmol) of N1,N1-bis(2-aminoethyl)ethane-1,2-diamine in 5 mL of EtOH were added dropwise to a solution of 0.239 g (0.46 mmol) of **2** in 5 mL of EtOH. The resulting solution was stirred 3 days. After this period, the crude solution was concentrated under vacuum. The product was dissolved in CH_2Cl_2 and precipitated again with hexane. The product was isolated as a yellow solid by centrifugation (192 mg, 75%). mp = 158-160 °C; ^1H NMR (300 MHz, CDCl_3) δ 7.94 (s, br,

3H), 7.55 (s, br, 3H), 5.38 (s, br, 6H), 3.70 (s, br, 12H), 3.14 (q, $J = 5.4$ Hz, 12H), 2.78 (s, br, 6H), 2.44 (m, 18H), 1.81 (s, br, 6H), 1.61 (t, $J = 6$ Hz, 12H), 1.43 (s, 72H). ^{13}C NMR (75 MHz, CDCl_3) δ 183.1, 181.5, 169.0, 166.9, 156.4, 79.0, 55.9, 51.6, 51.2, 43.4, 39.1, 28.6, 27.1. MALDI-TOF(+) m/z (%): calc. $\text{C}_{75}\text{H}_{132}\text{N}_{16}\text{NaO}_{18}$ 1567.9798; exp. 1567.9790 $[\text{M}+\text{Na}]^+$.

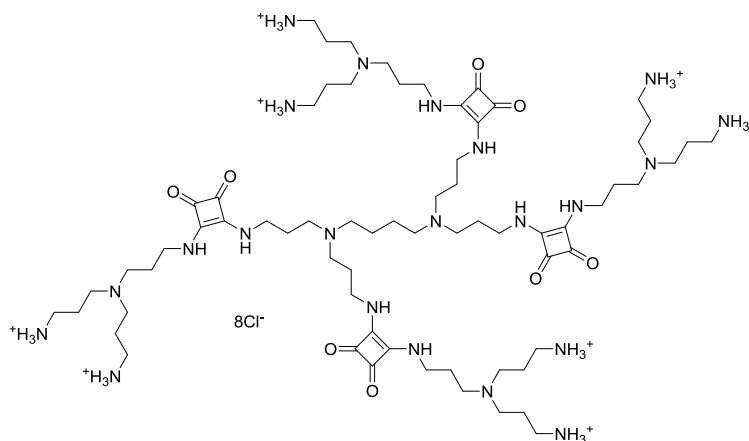


Compound 1B-G1: 0.093 mL (0.283 mmol) of N1,N1'-(butane-1,4-diyl)bis(N1-(3-aminopropyl)propane-1,3-diamine) in 5 mL of MeOH were added to a solution of 0.6 g (1.275 mmol) **1** in 30 mL of EtOH. The resulting solution was stirred at 60 °C 3 days. After this period, the crude solution was concentrated under vacuum. The product was dissolved in CH_2Cl_2 and washed with brine (2 \times 10 mL). The organic phase was dried with Na_2SO_4 , filtered and concentrated by rotary evaporation to afford the product as orange oil (150 mg, 26%). ^1H NMR (300 MHz, CDCl_3) δ 7.75 (s, 4H), 5.25 (s, br, 8H), 3.71 (s, br, 16H), 3.16 (s, br, 16H), 2.75 (s, br, 6H), 2.61 (s, br, 24H), 2.47 (s, br, 6H), 1.80 (s, br, 12), 1.45 (s, 72H); ESI-HMRS: calc. $\text{C}_{96}\text{H}_{168}\text{N}_{22}\text{NaO}_{24}$: 2036.2500; exp. 2036.2494 $[\text{M}+\text{Na}]^+$.

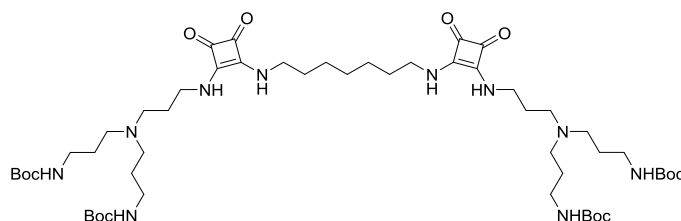


Compound 2B-G1: 0.045 g (0.143 mmol) of N1,N1'-(butane-1,4-diyl)bis(N1-(3-aminopropyl)propane-1,3-diamine) in 5 mL of MeOH were added to a solution of 0.33 g (0.644 mmol) of **2** in 20 mL of EtOH. The resulting solution was stirred at 60 °C for 3 days. After this period, the crude solution was concentrated under vacuum. The product was purified by column chromatography (alumina, CH_2Cl_2 :MeOH 0-4%) to afford the product as orange oil (200 mg, 64%). ^1H NMR (300 MHz, CDCl_3) δ 7.99 (s, br, 4H), 7.59 (s, br, 4H), 5.41 (s, br, 8H), 3.67 (s, br, 16H), 3.11 (m, br, 16H), 2.43 (s, br, 36H), 1.79 (s,

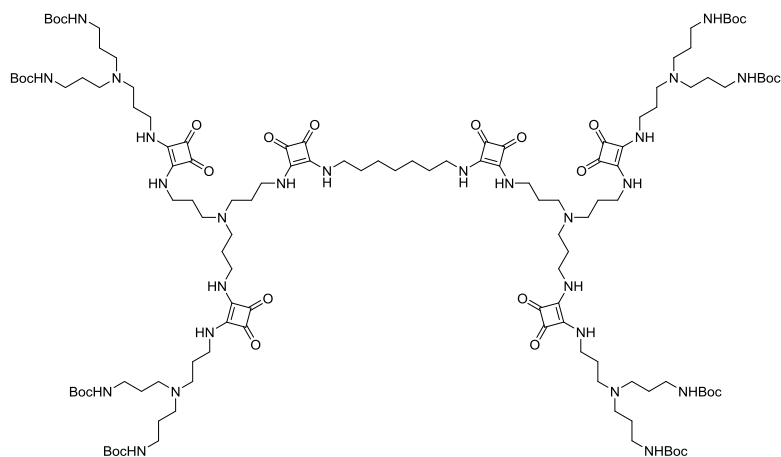
br, 16H), 1.59 (s, br, 16H), 1.40 (s, 72H); ^{13}C NMR (75 MHz, CDCl_3) δ 183.1, 181.4, 169.3, 166.8, 156.3, 78.9, 53.5, 51.6, 51.0, 43.3, 42.6, 39.1, 29.7, 29.1, 28.5, 28.1, 27.0; ESI-HMRS: calc. $\text{C}_{108}\text{H}_{193}\text{N}_{22}\text{O}_{24}$: 2182.4558; exp. 2182.4587 $[\text{M}+\text{H}]^+$.



Compound 2B-G1-NH₂: 0.830 g (0.38 mmol) of **2B-G1** were dissolved in 50 mL of H_2O with 2.5 mL of HCl 37% and the resulting solution was stirred at 50 °C for 12 hours. After this period, the crude solution was concentrated under vacuum to afford the product as hydrochloride salt. ^1H NMR (300 MHz, D_2O) δ 3.74 (s, br, 16H), 3.35 (s, br, 36H), 3.13 (t, $J = 7.5$ Hz, 20H), 2.18 (s, br, 32H).

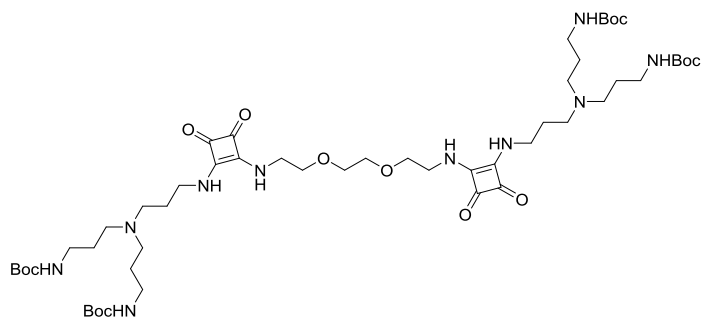


Compound 2C-G1: 0.75 g (1.463 mmol) of **2** in 5 mL of EtOH were added to a solution of 0.075 mL (0.488 mmol) of heptane-1,7-diamine in 10 mL of EtOH. The resulting solution was stirred for 48 hours. After this period, the crude solution was concentrated under vacuum. The product was purified by column chromatography (alumina, CH_2Cl_2 :MeOH 0-5%) to afford the product as yellow solid (390 mg, 75%). mp = 125-127 °C; ^1H NMR (300 MHz, CDCl_3) δ 7.76 (s, br, 2H), 7.41 (s, br, 2H), 5.34 (s, br, 4H), 3.68 (m, br, 8H), 3.14 (q, $J = 5.7$ Hz, 8H), 2.46 (m, br, 12H), 1.83 (m, br, 4H), 1.61 (m, br, 12H), 1.42 (s, 40H), 1.25 (s, 2H); ^{13}C NMR (75 MHz, CDCl_3) δ 183.2, 182.1, 168.9, 167.4, 156.5, 79.2, 51.5, 51.0, 43.4, 43.2, 39.1, 30.1, 29.8, 29.5, 28.8, 28.3, 28.0, 27.0, 25.9, 24.6; ESI-HMRS: calc. $\text{C}_{53}\text{H}_{94}\text{N}_{10}\text{NaO}_{12}$: 1085.6950; exp. 1085.6947 $[\text{M}+\text{Na}]^+$.

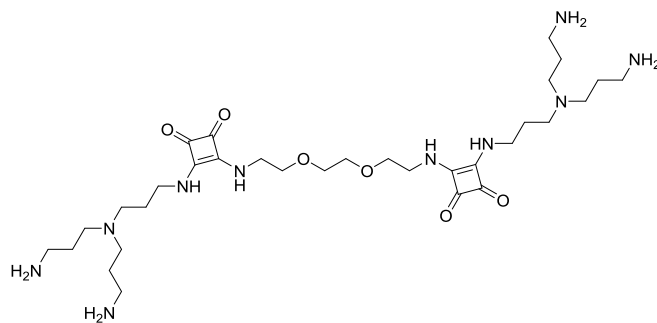


Compound 2C-G2: 100 mg (0.094 mmol) of **2C-G1** were dissolved in 1 mL of CH_2Cl_2 with 0.3 mL of trifluoroacetic acid and the resulting solution was stirred for 4 hours. After this period, the solution is concentrated under vacuum to afford the product as trifluoroacetate salt that was used without further purification.

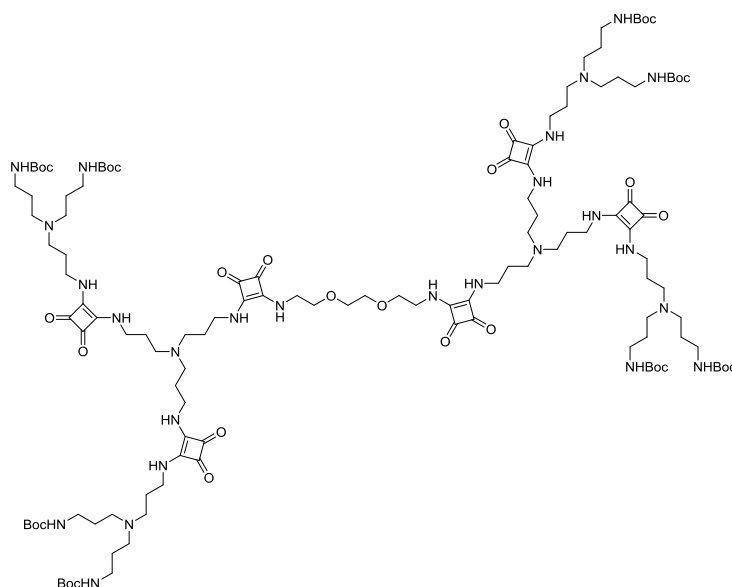
0.240 g (0.468 mmol) of **2** in 5 mL of EtOH were added to a solution of the previous obtained amine **2C-G1** in 15 mL of EtOH previously neutralized with Na_2CO_3 . The resulting solution was stirred for 24 hours. After this period, the crude solution was filtered and concentrated under vacuum. The product was purified by column chromatography (silica, CH_2Cl_2 :MeOH 2-3%) to afford the product (95 mg, 40%). ^1H NMR (300 MHz, CDCl_3) δ 7.74 (s, br, 8H), 5.26 (s, br, 8H), 3.75 (s, br, 40H), 3.16 (q, $J = 5.7$ Hz, 16H), 2.48 (m, 36H), 1.60 (m, 42H), 1.45 (s, 72H), 1.27 (s, 24H); ESI-MS: calc. $\text{C}_{125}\text{H}_{214}\text{N}_{26}\text{NaO}_{28}$: 2550.6019; exp. 2550.5742 $[\text{M}+\text{Na}]^+$.



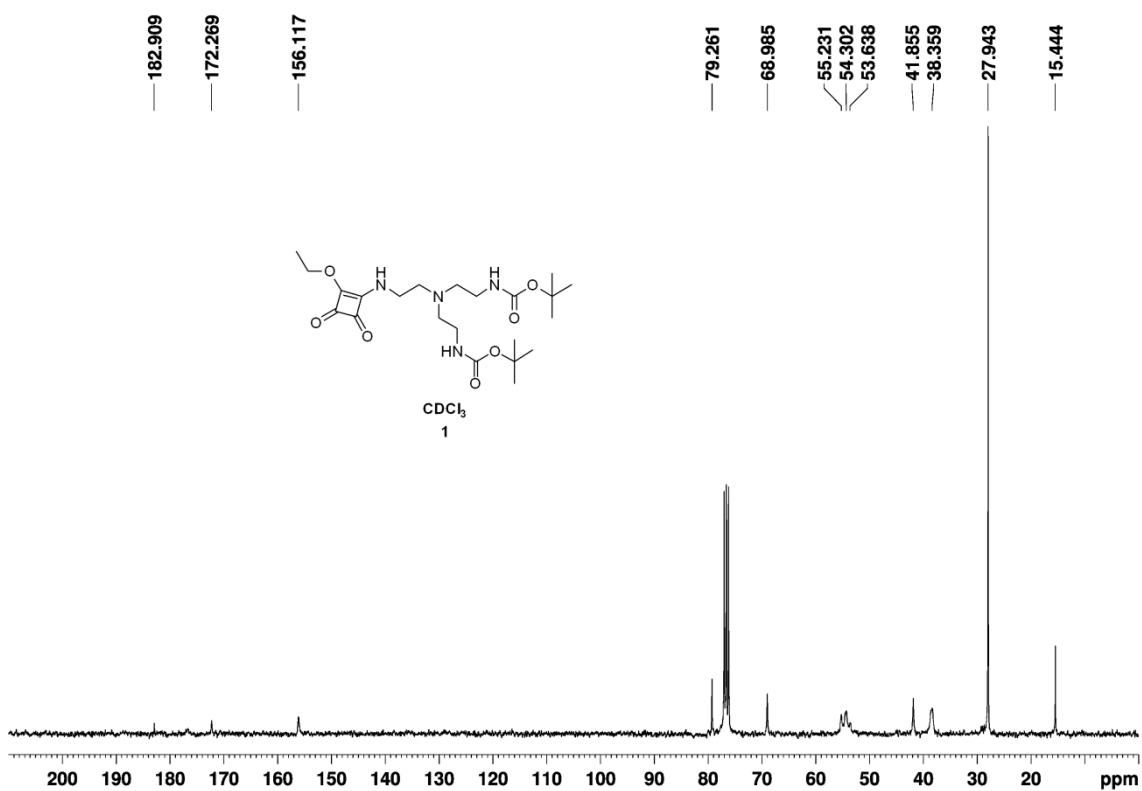
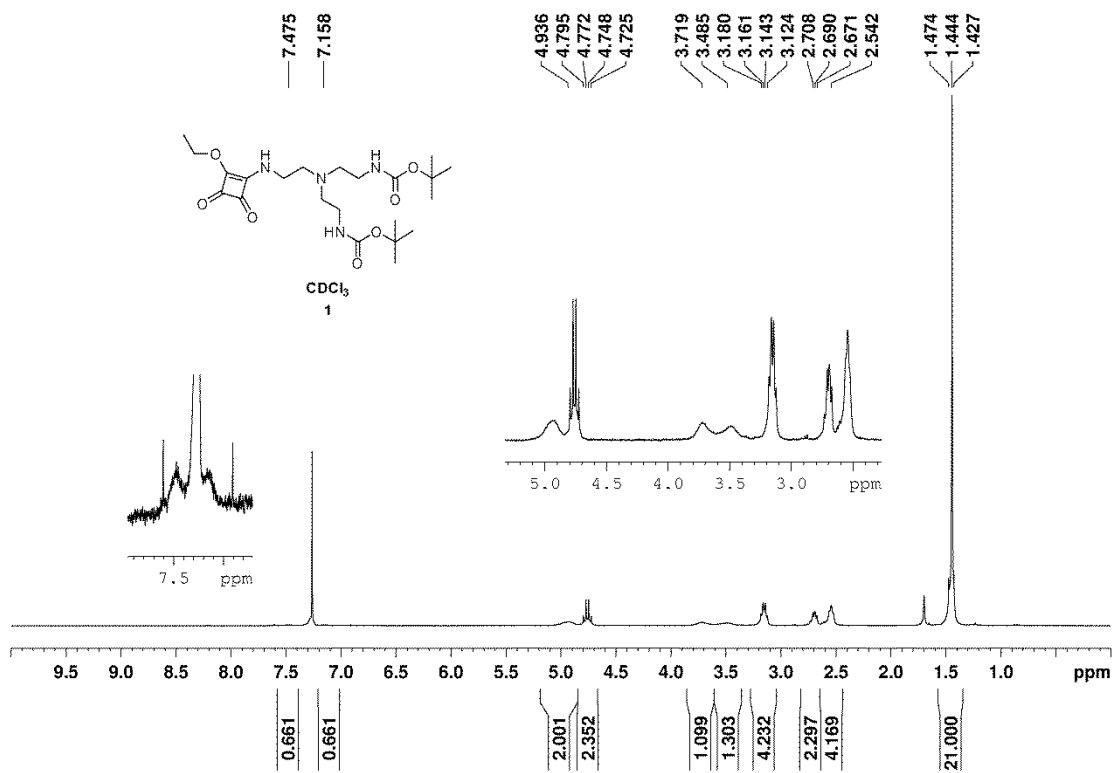
Compound 2D-G1: 0.1 g (0.661 mmol) of 2,2'-(ethane-1,2-diylbis(oxy))bis(ethan-1-amine) in 15 mL of EtOH were added to a solution of 1.017 g (1.984 mmol) of **2** in 15 mL of EtOH. The resulting solution was stirred for 3 days. After this period, the crude solution was concentrated under vacuum. The product was purified by column chromatography (alumina, CH_2Cl_2 :MeOH 0.1-10%) to afford the product as yellow solid (686 mg, 96%). mp = 120 °C; ^1H NMR (300 MHz, CDCl_3) δ 7.65 (s, br, 2H), 6.93 (s, br, 2H), 5.18 (s, br, 4H), 3.77 (m, br, 16H), 3.16 (q, $J = 6$ Hz, 8H), 2.48 (m, br, 12H), 1.82 (s, br, 4H), 1.65 (m, 8H), 1.45 (s, 36H); ^{13}C NMR (75 MHz, CDCl_3) δ 183.2, 182.3, 168.9, 167.6, 156.4, 79.1, 71.0, 70.5, 51.6, 51.1, 44.1, 43.3, 39.1, 28.6, 28.2, 27.1; ESI-HMRS: calc. $\text{C}_{52}\text{H}_{93}\text{N}_{10}\text{O}_{14}$: 1081.6873; exp. 1081.6902 $[\text{M}+\text{H}]^+$.

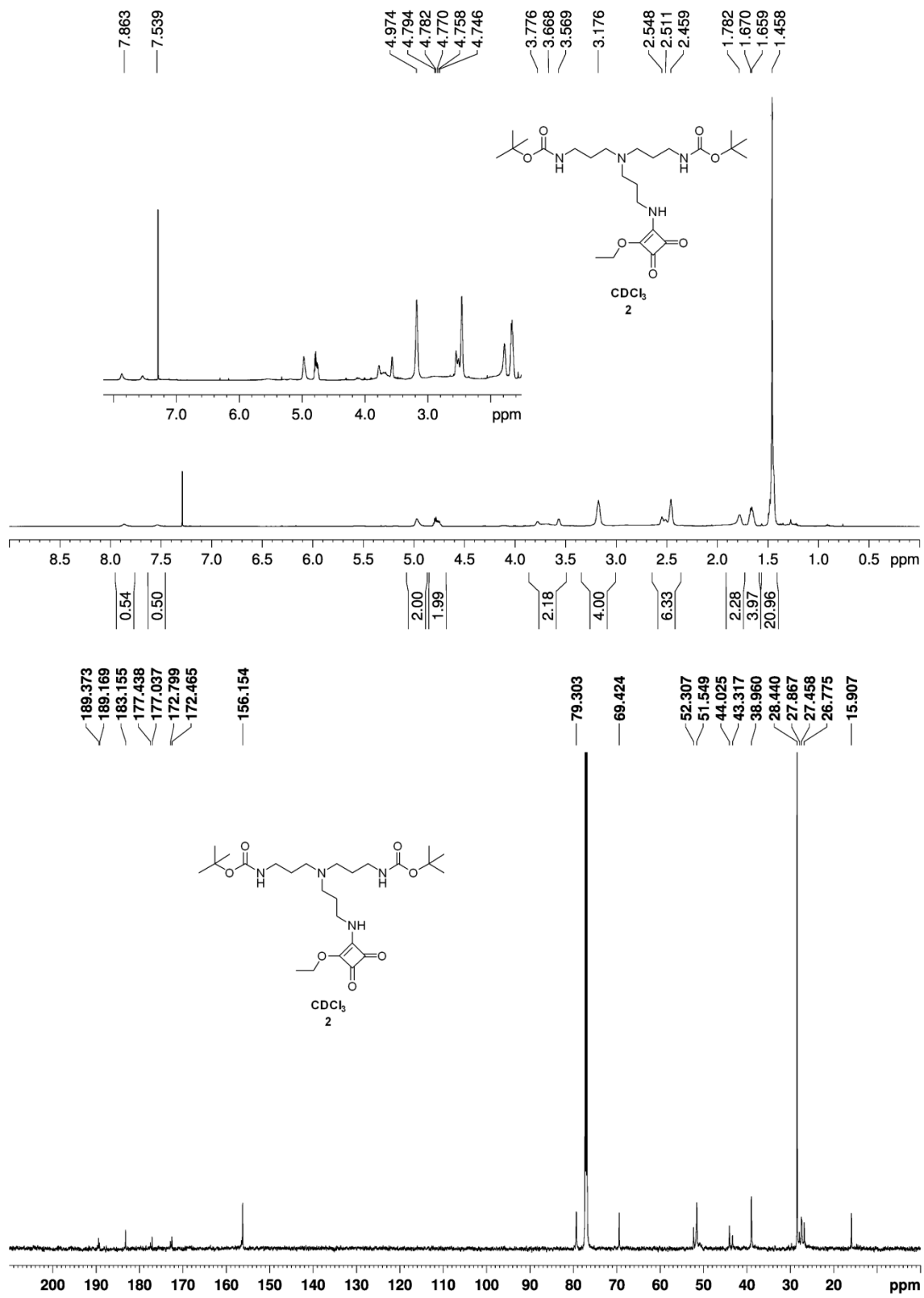


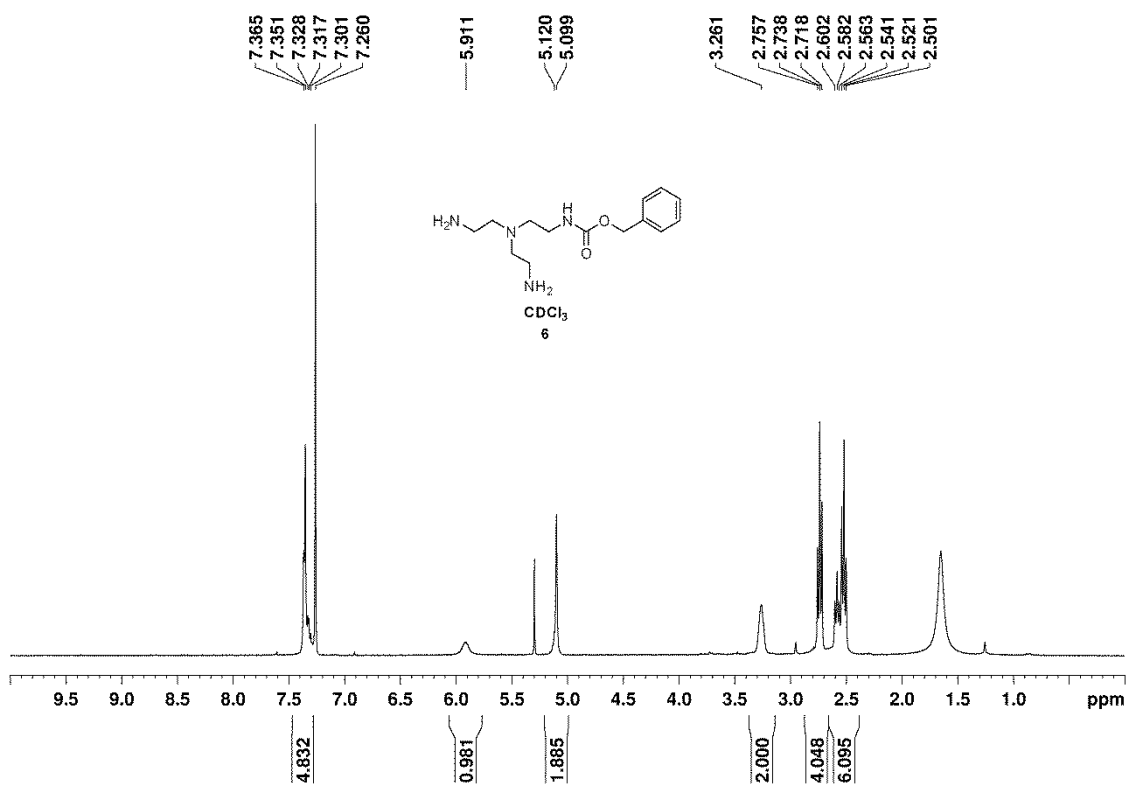
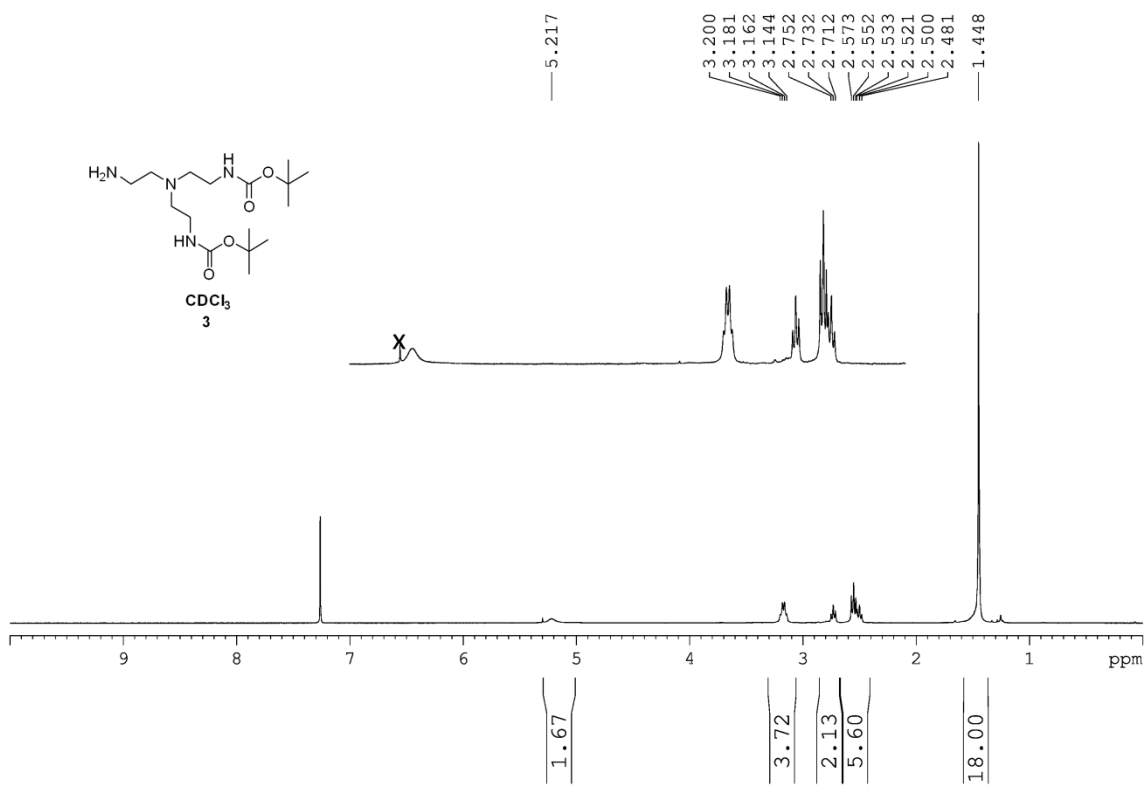
Compound 2D-G1-NH₂: 290 mg (0.268 mmol) of **2D-G1** were dissolved in 25 mL of CH₂Cl₂ with 2.5 mL of trifluoroacetic acid (32.5 mmol) and the resulting solution was stirred for 12 hours. After this period, the solution is concentrated under vacuum. The resulting oil is dissolved in 10 mL of H₂O and the solution is neutralized with Na₂CO₃. The solution is dialyzed with a dialysis membrane with pore size of 100-500 for 48 hours to afford the product as a yellow solid (70 mg, 39%). ¹H NMR (300 MHz, D₂O) δ 3.69 (m, br, 16H), 3.00 (q, 4H), 2.80 (s, br, 4H), 2.56 (s, br, 12H), 1.73 (m, 12H); ¹³C NMR (75 MHz, D₂O-DMSO-*d*₆) δ 180.5, 180.3, 167.6, 167.2, 163.7, 69.1, 68.8, 68.4, 49.4, 49.3, 48.8, 42.8, 39.5, 37.5, 25.7, 25.4, 25.0, 24.8, 24.5, 22.3; MALDI-TOF(+) *m/z* (%): calc. C₃₂H₆₀N₁₀NaO₆ 703.4595; exp. 703.4589 [M+Na]⁺.

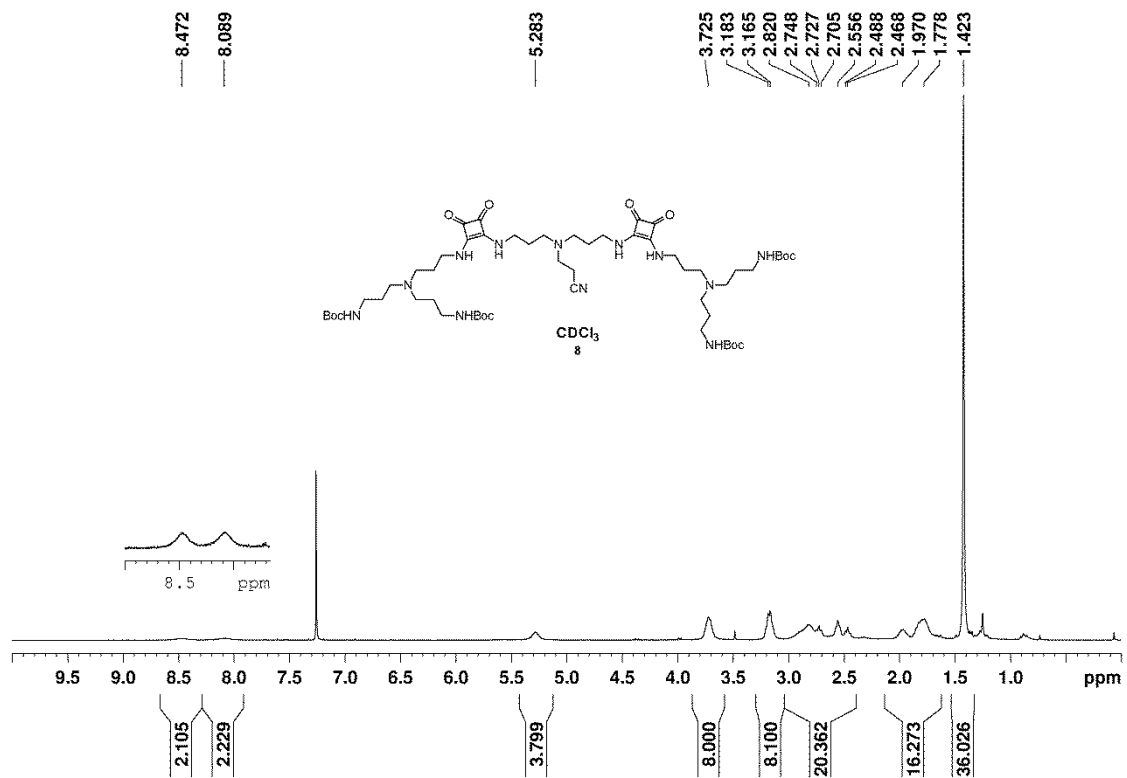
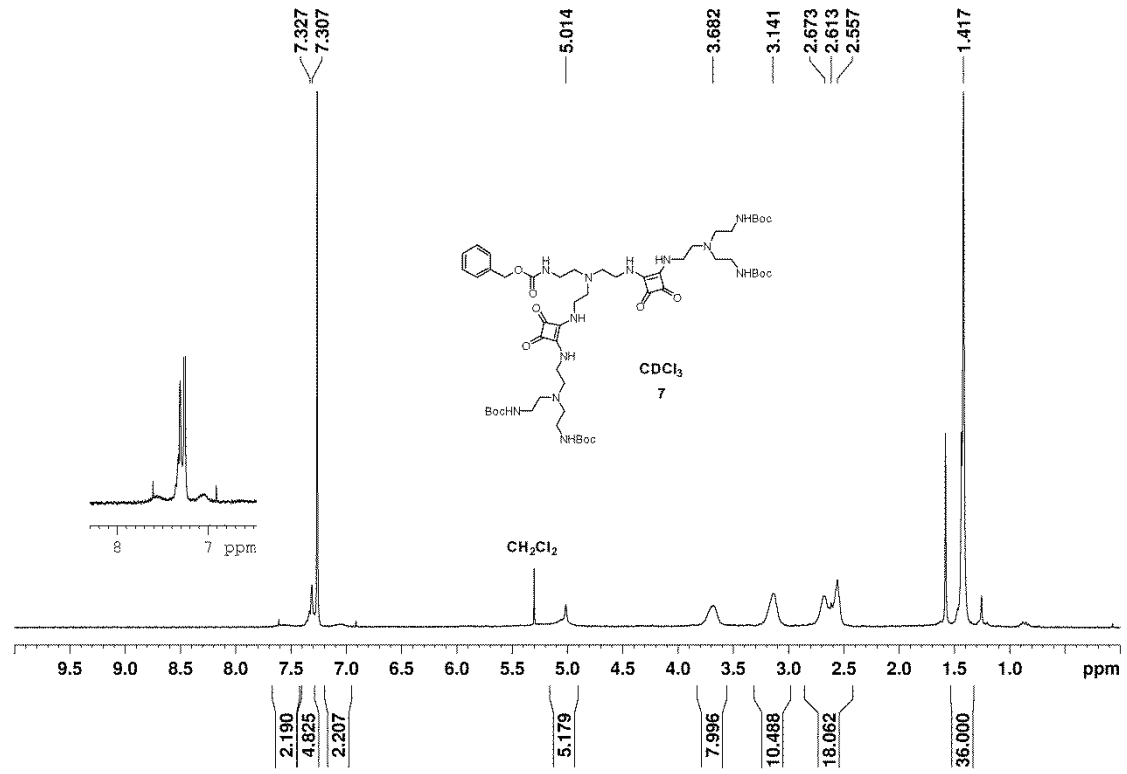


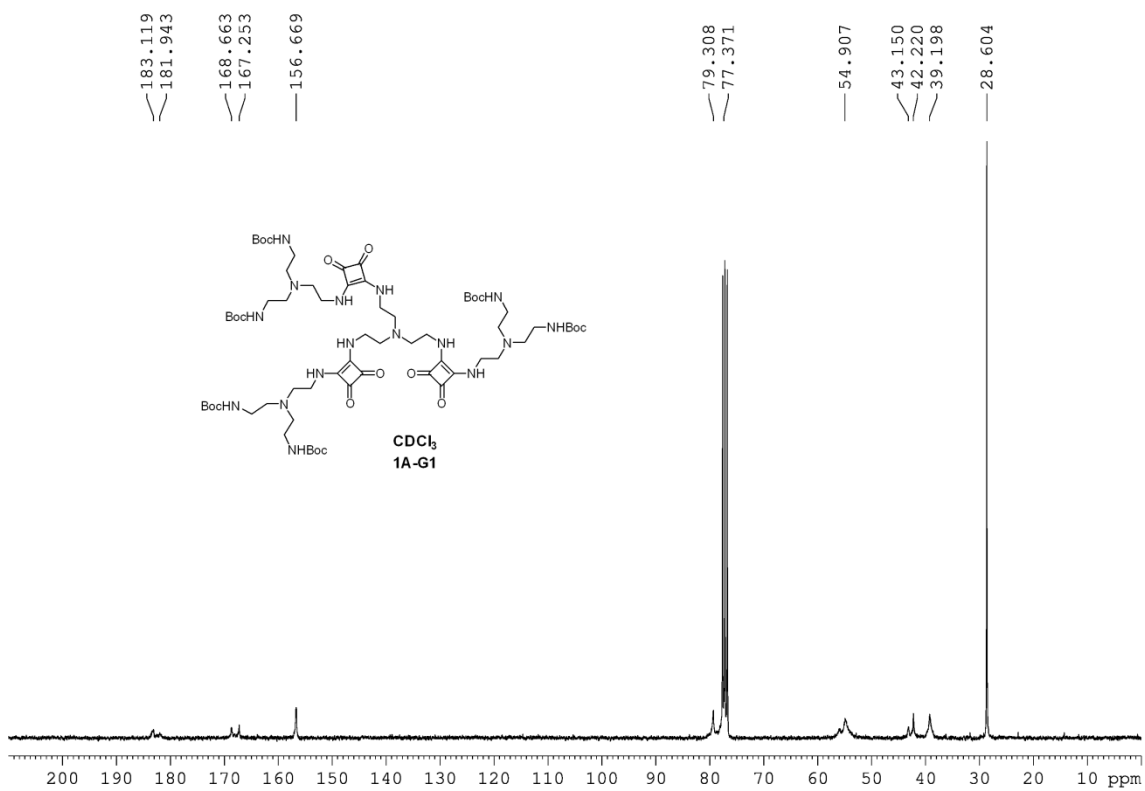
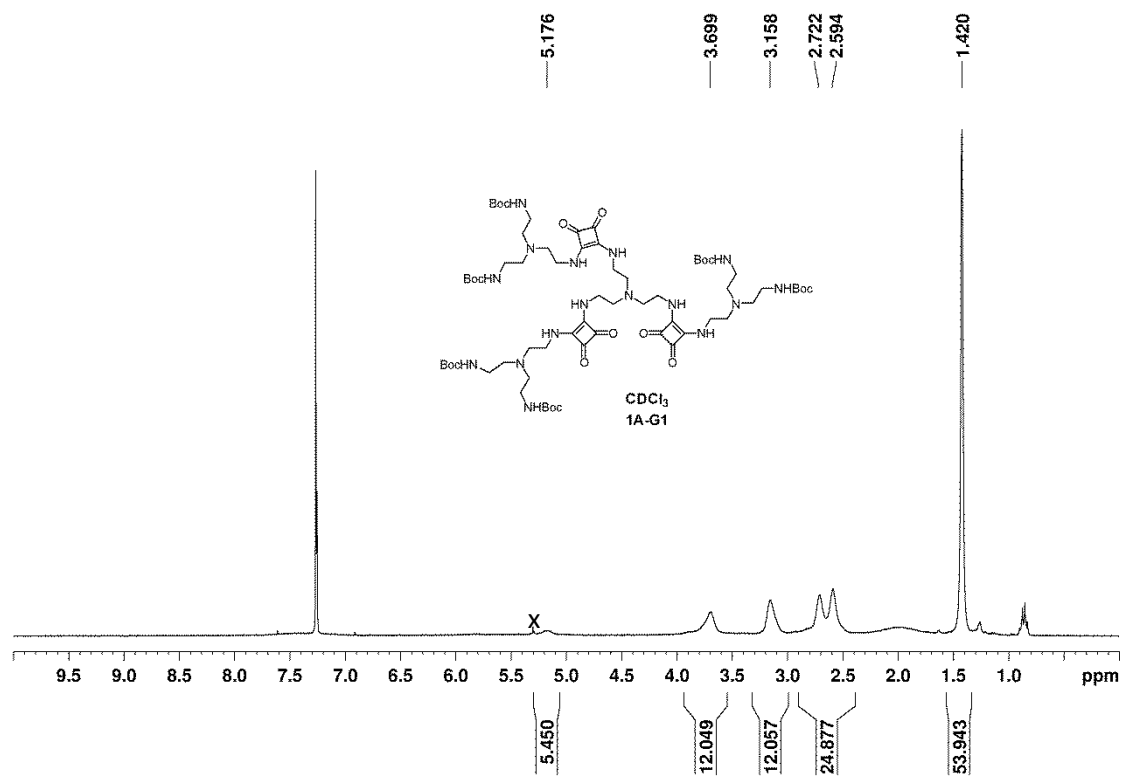
Compound 2D-G2: 1.896 g (3.70 mmol) of **7** in 15 mL of EtOH were added to a solution of 0.5 g (0.44 mmol) of **2D-G1-NH₂** in 10 mL of EtOH with 1.573 g (23.12 mmol) of EtONa. The resulting solution was stirred for 4 days at 5°C. After this period, the crude solution was concentrated under vacuum. The product was purified by column chromatography (alumina, CH₂Cl₂:MeOH 10-50%) to afford the product as yellow solid (500 mg, 43%). *m.p.* > 200 °C (dec.). ¹H NMR (300 MHz, CDCl₃) δ 7.86 (s, br, 6H), 7.43 (s, br, 6H), 5.22 (s, br, 8H), 3.87 (s, br, 4H), 3.64 (m, 24H), 3.49 (m, 4H), 3.14 (m, 16H), 2.45 (m, br, 36H), 1.80 (s, br, 20H), 1.61 (t, 16H), 1.42 (s, 72H); ¹³C NMR (75 MHz, CDCl₃) δ 182.8, 182.4, 181.6, 181.4, 169.0, 168.2, 167.8, 167.1, 167.0, 156.4, 79.0, 70.7, 70.3, 51.5, 51.0, 50.5, 44.3, 43.3, 42.6, 40.5, 39.6, 39.1, 38.7, 29.7, 28.9, 28.9, 26.5, 26.2; MALDI-TOF(+) *m/z* (%): calc. C₁₂₄H₂₁₂N₂₆NaO₃₀ 2568.5760; exp. 2568.5680 [M+Na]⁺.

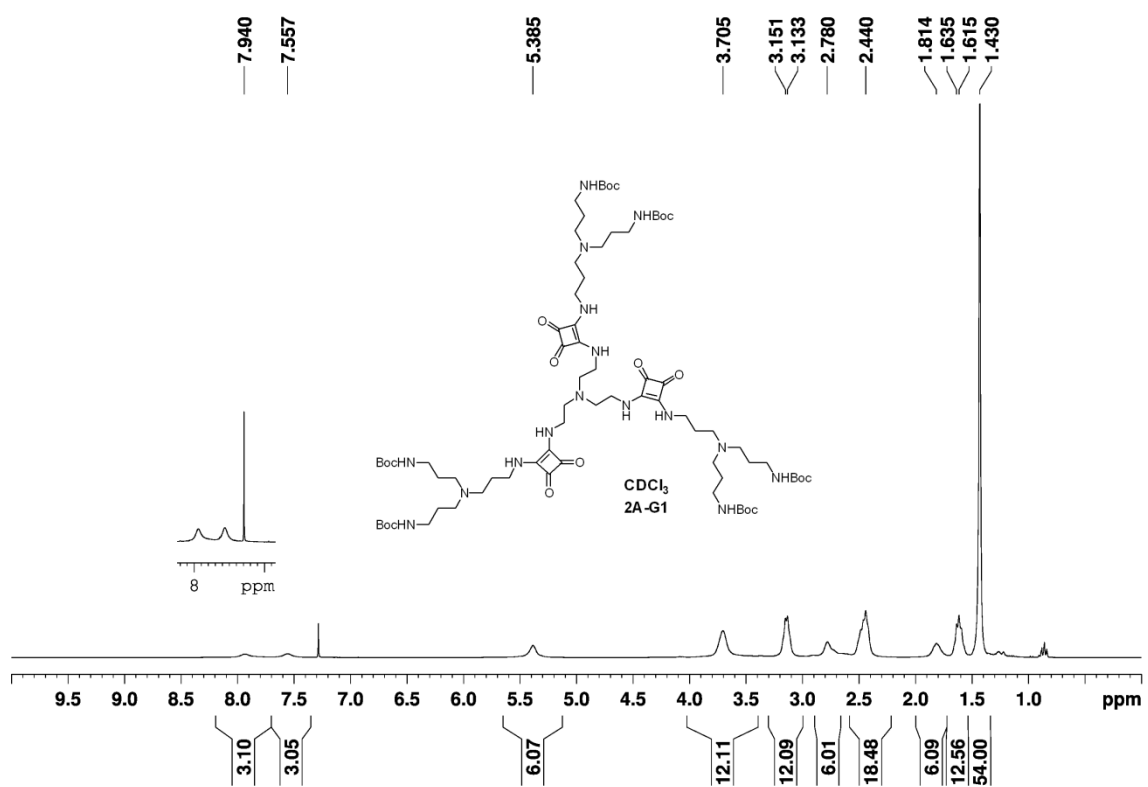
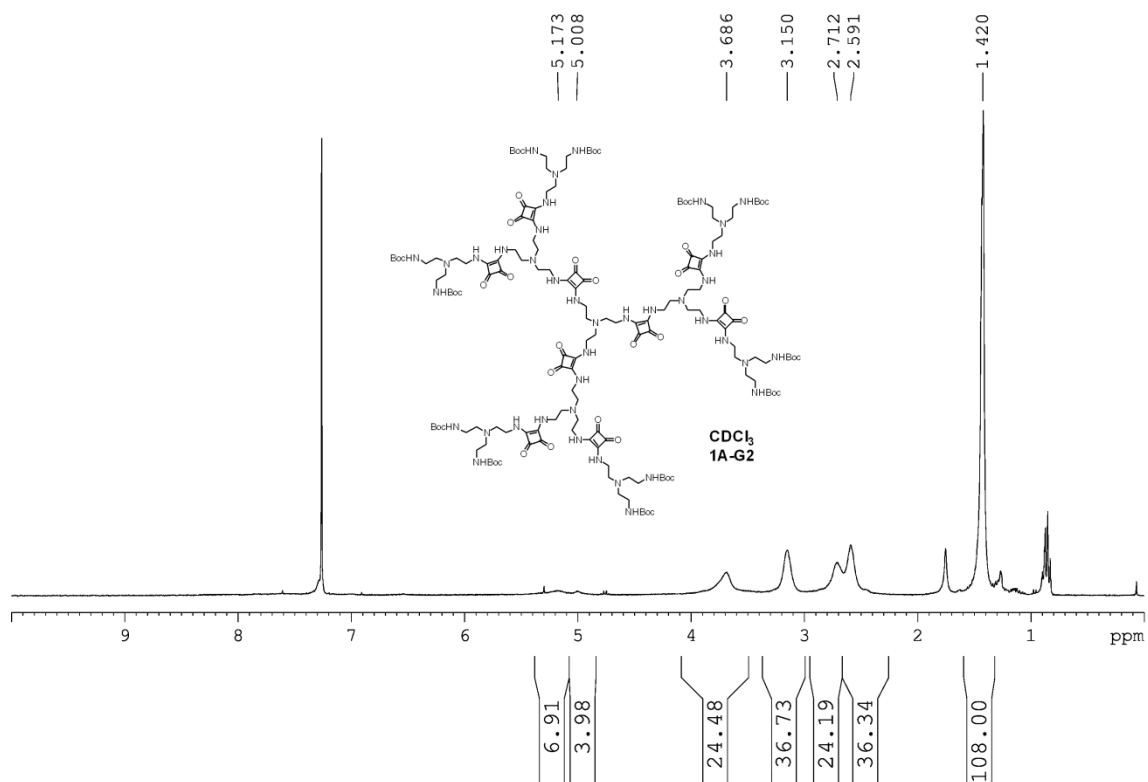


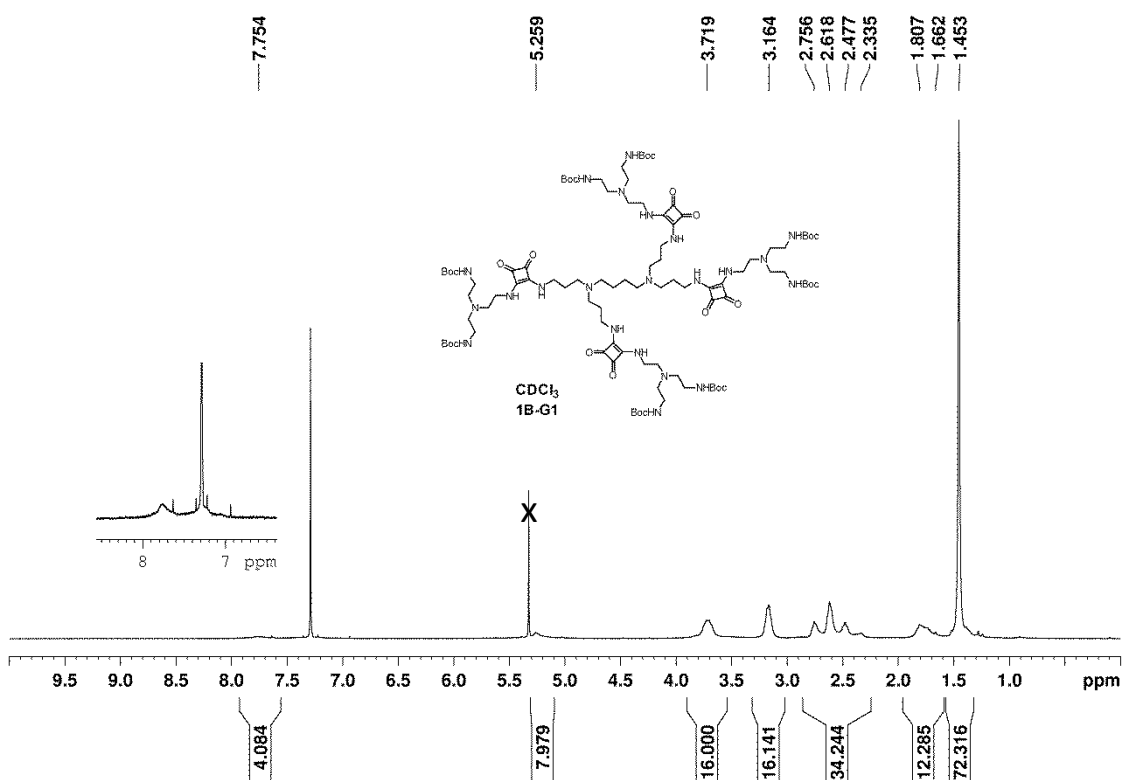
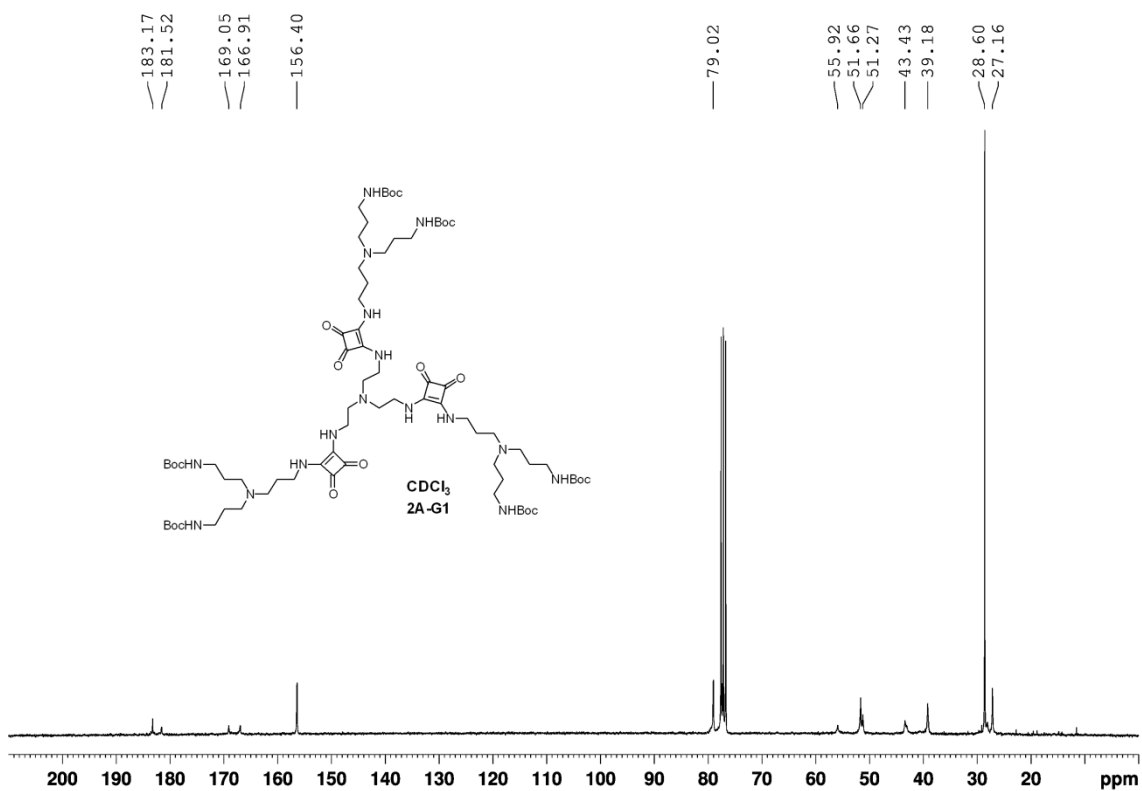


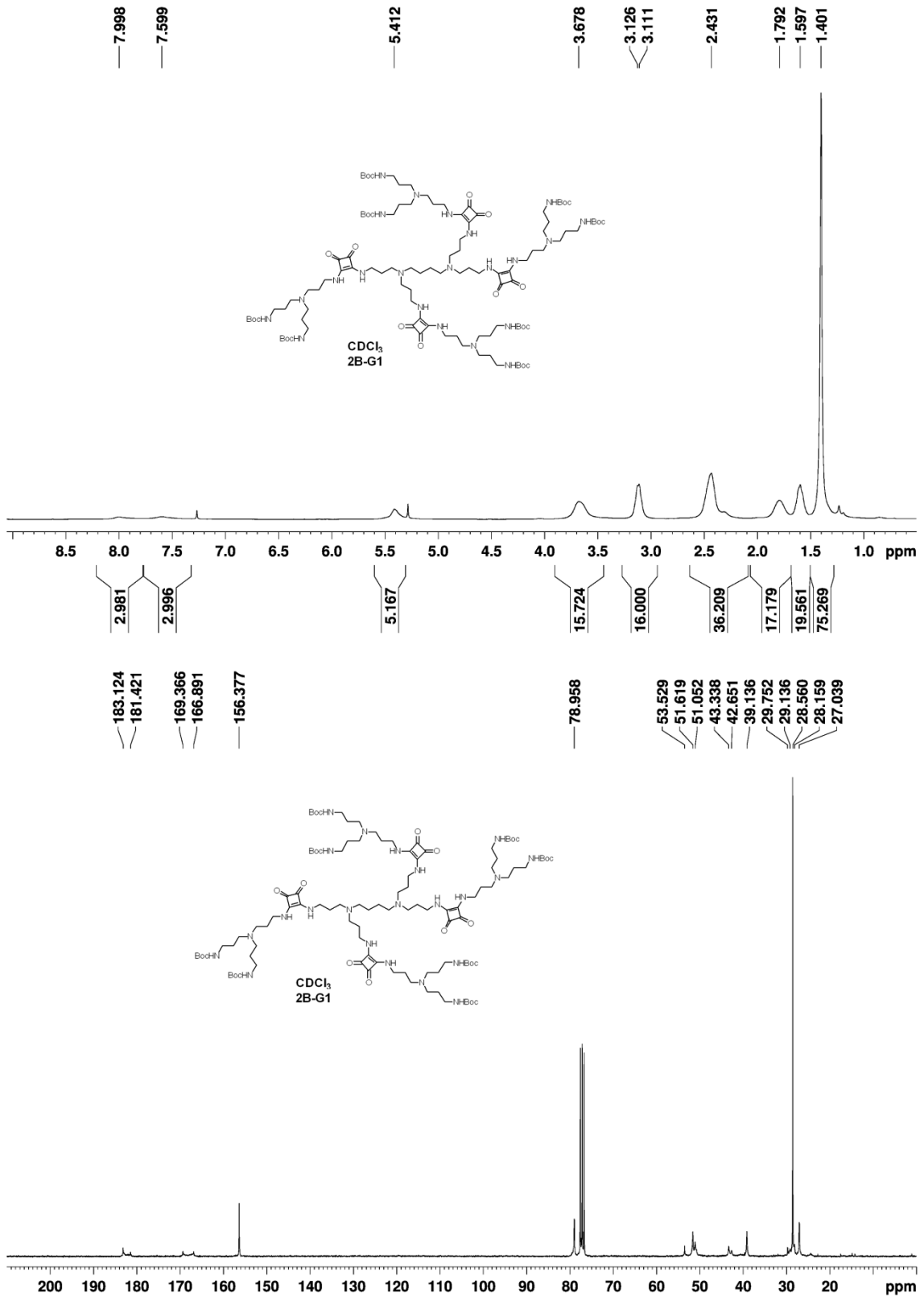


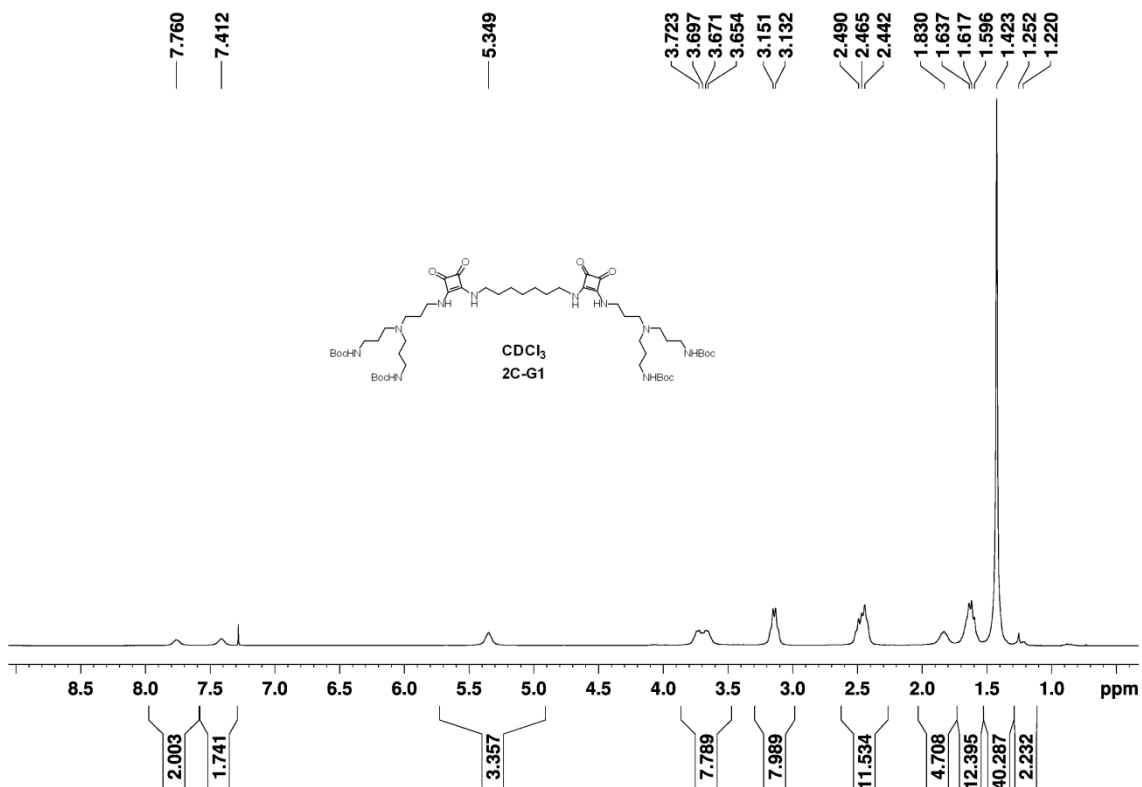
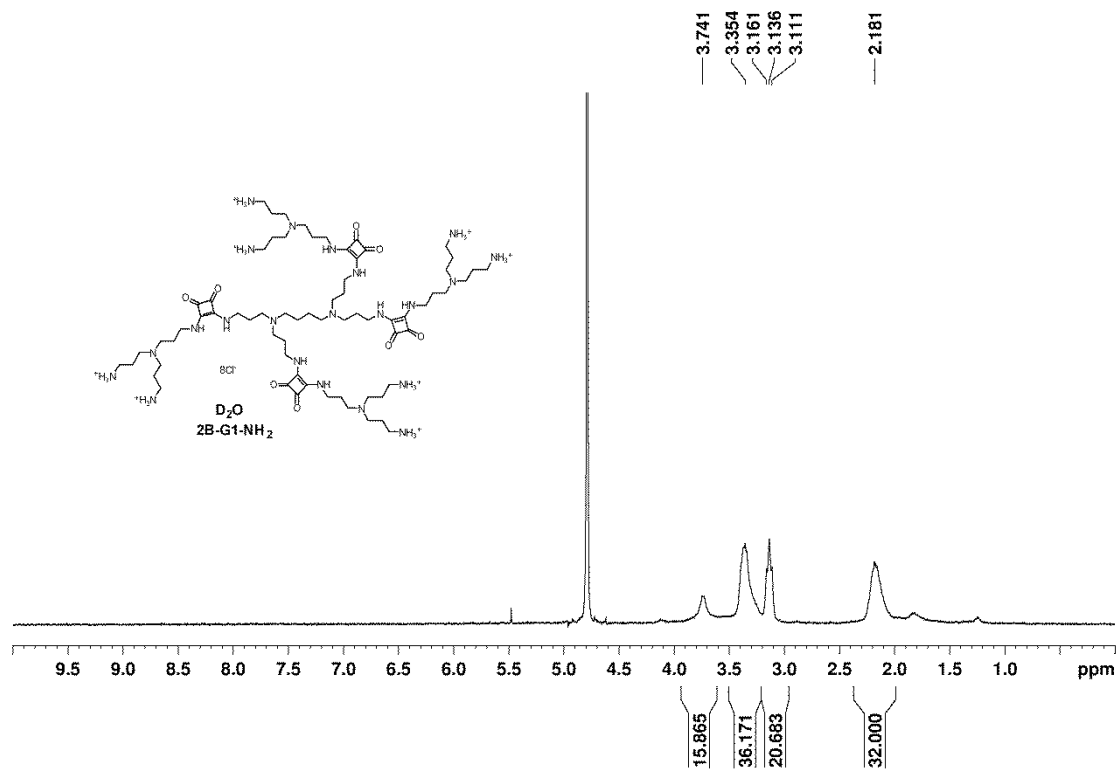


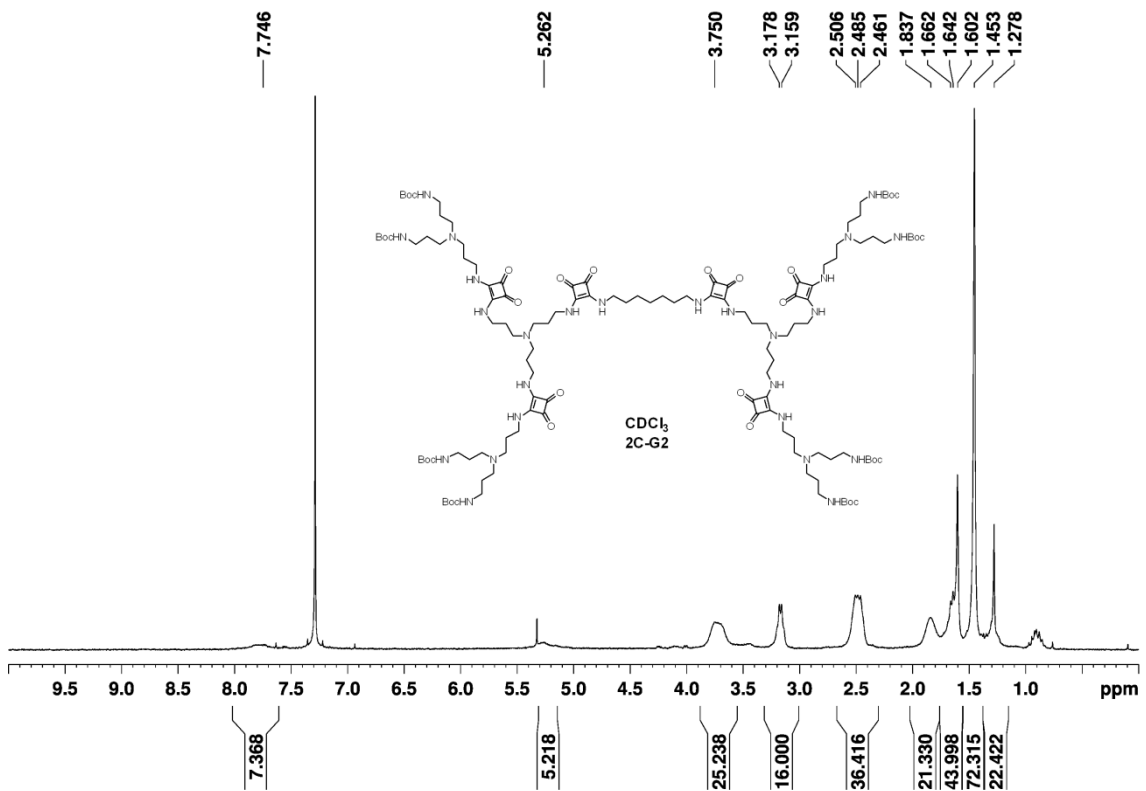
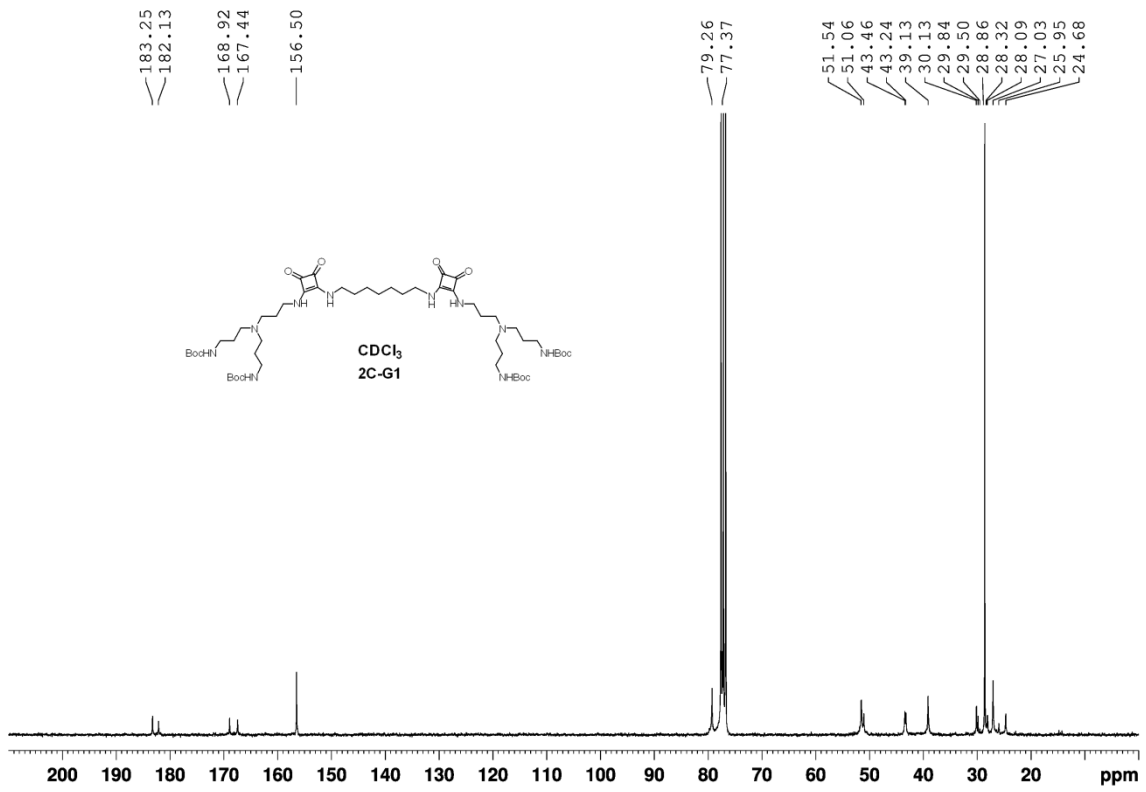


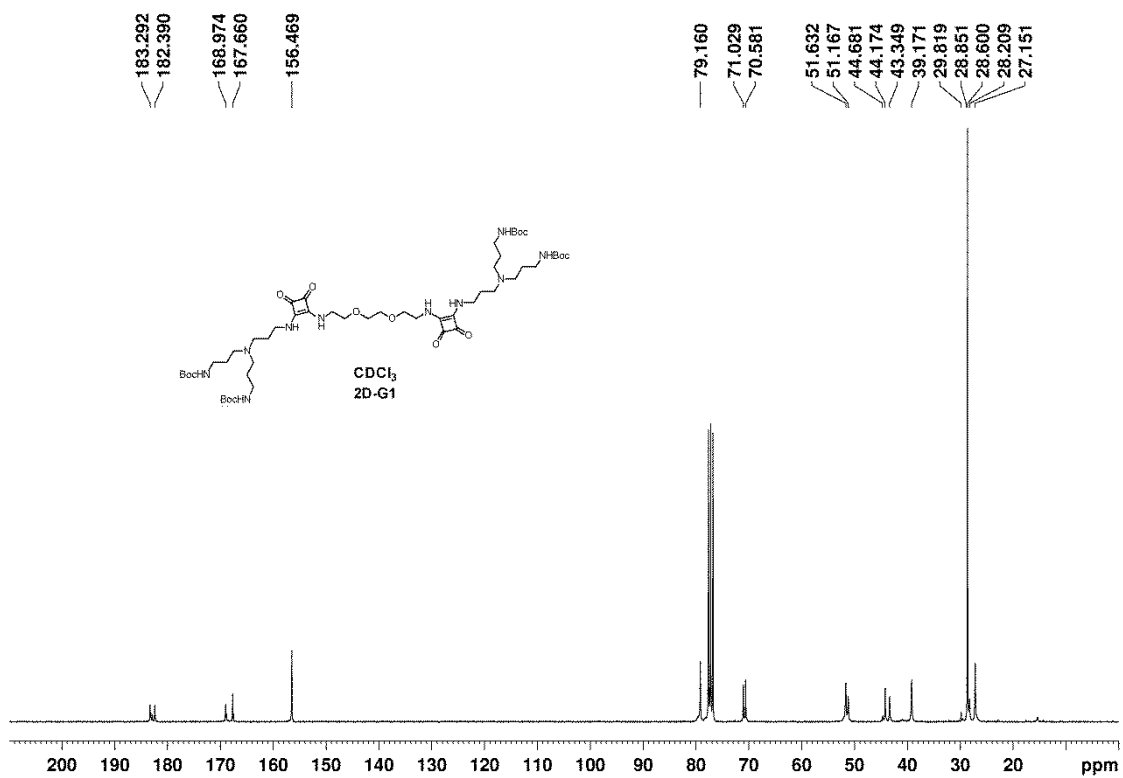
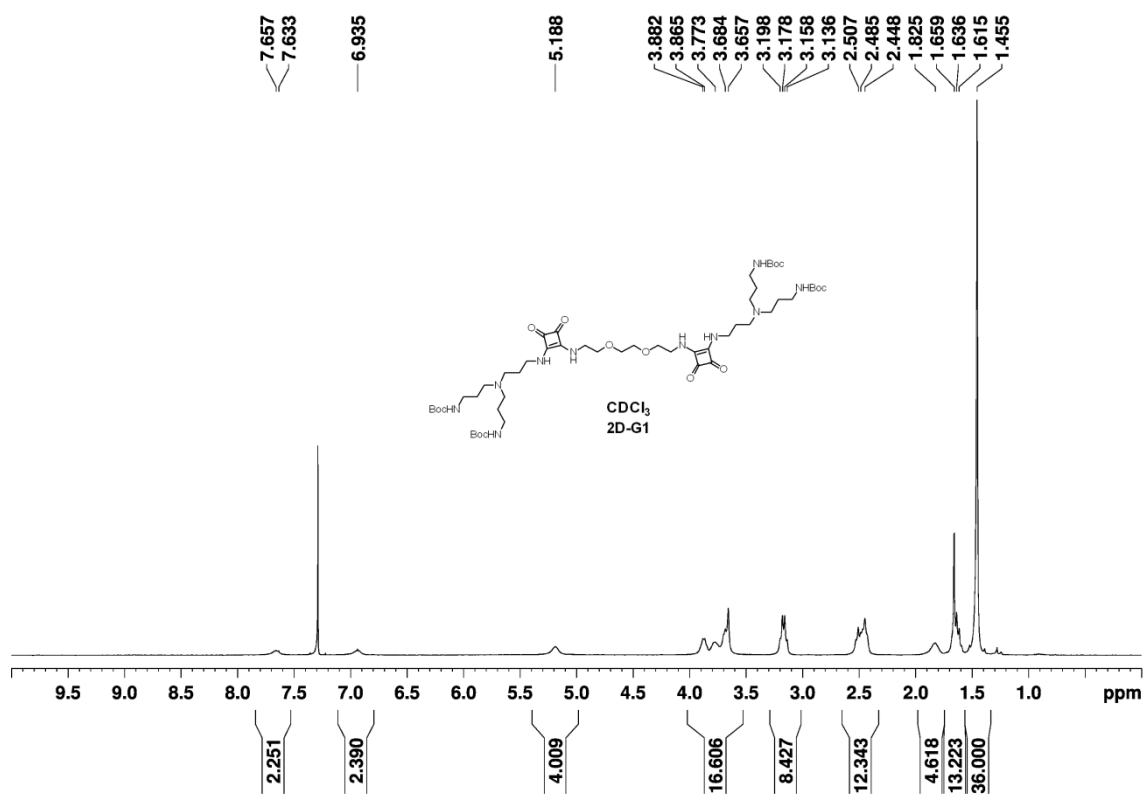


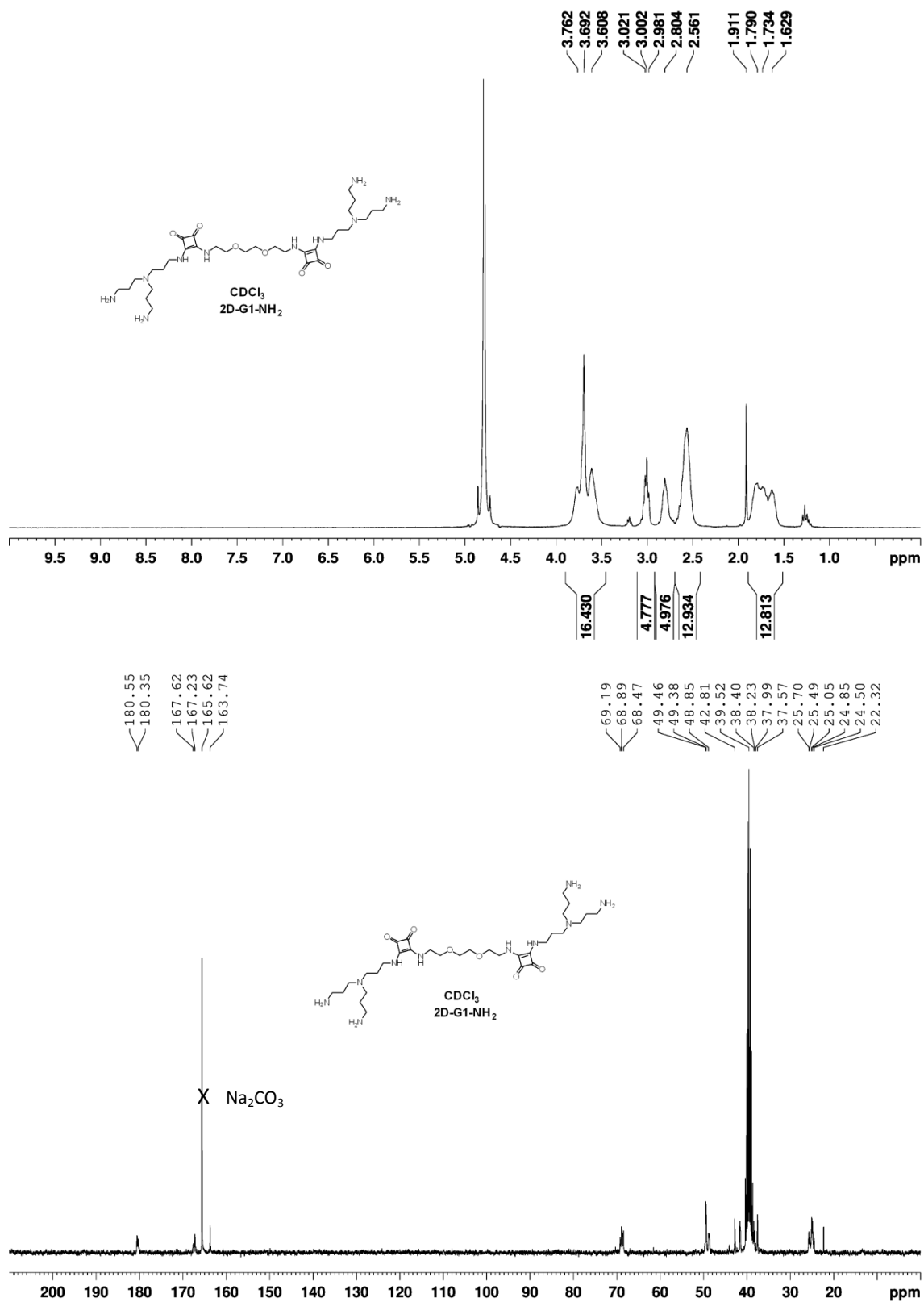












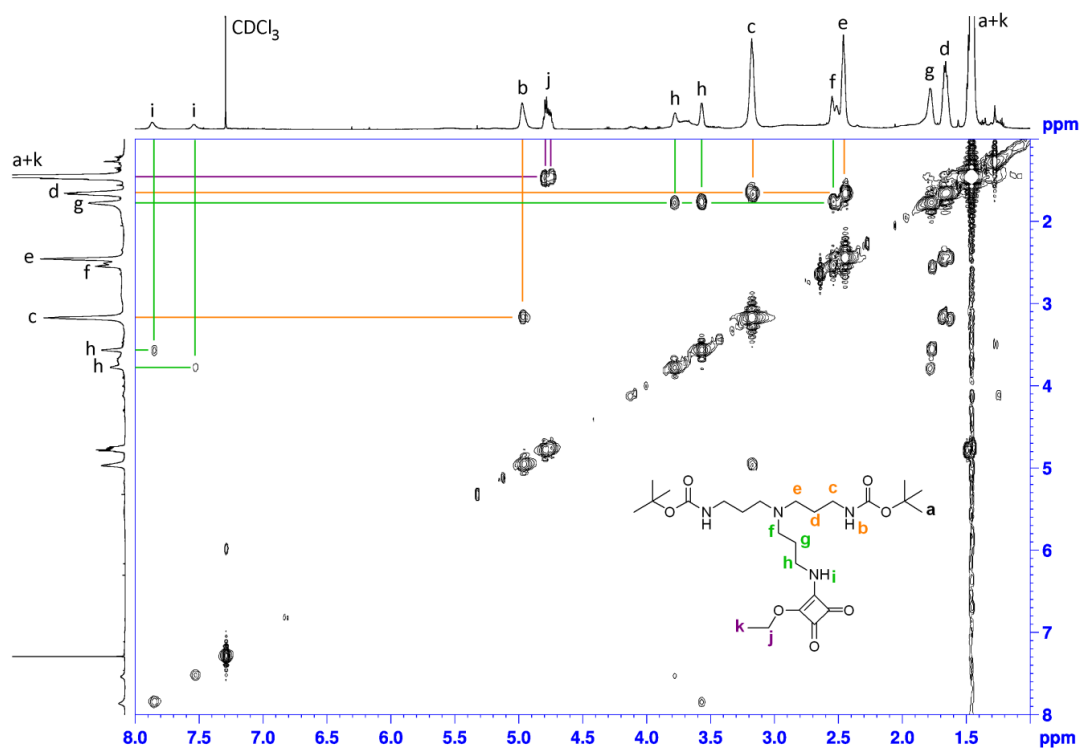


Figure S47. 2D COSY spectrum (3.2 mM) of **2** in CDCl_3 at 298 K.

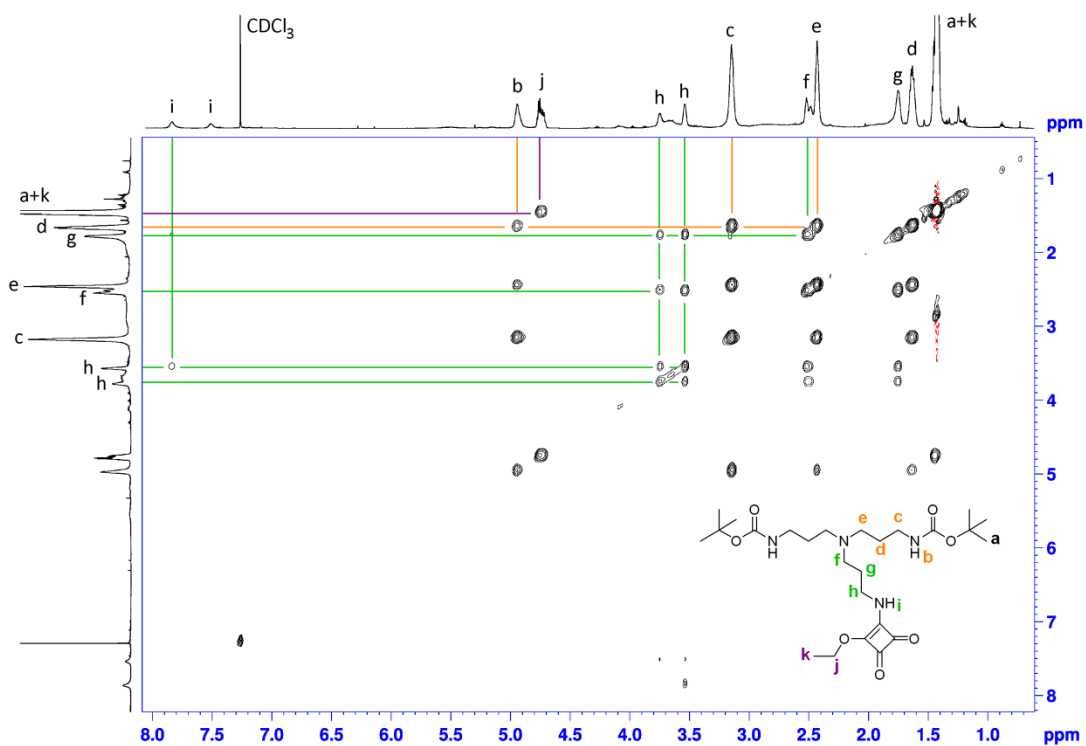


Figure S48. 2D TOCSY spectrum (3.2 mM) of **2** in CDCl_3 at 298 K.

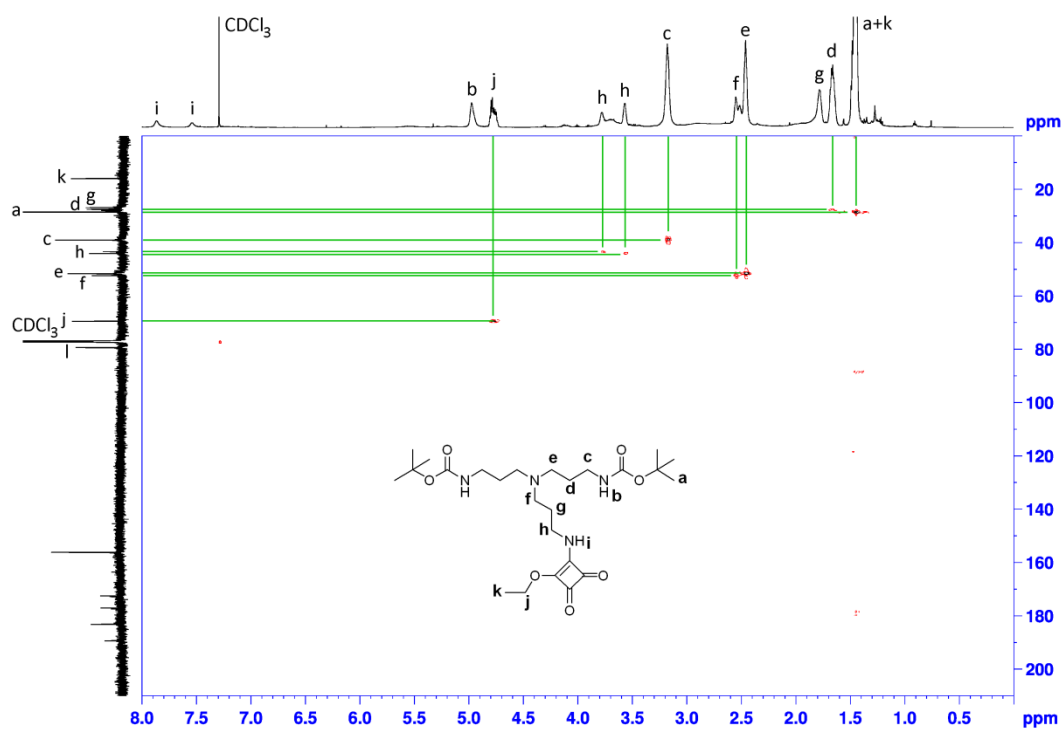


Figure S49. 2D HSQC spectrum (3.2 mM) of **2** in CDCl_3 at 298 K.

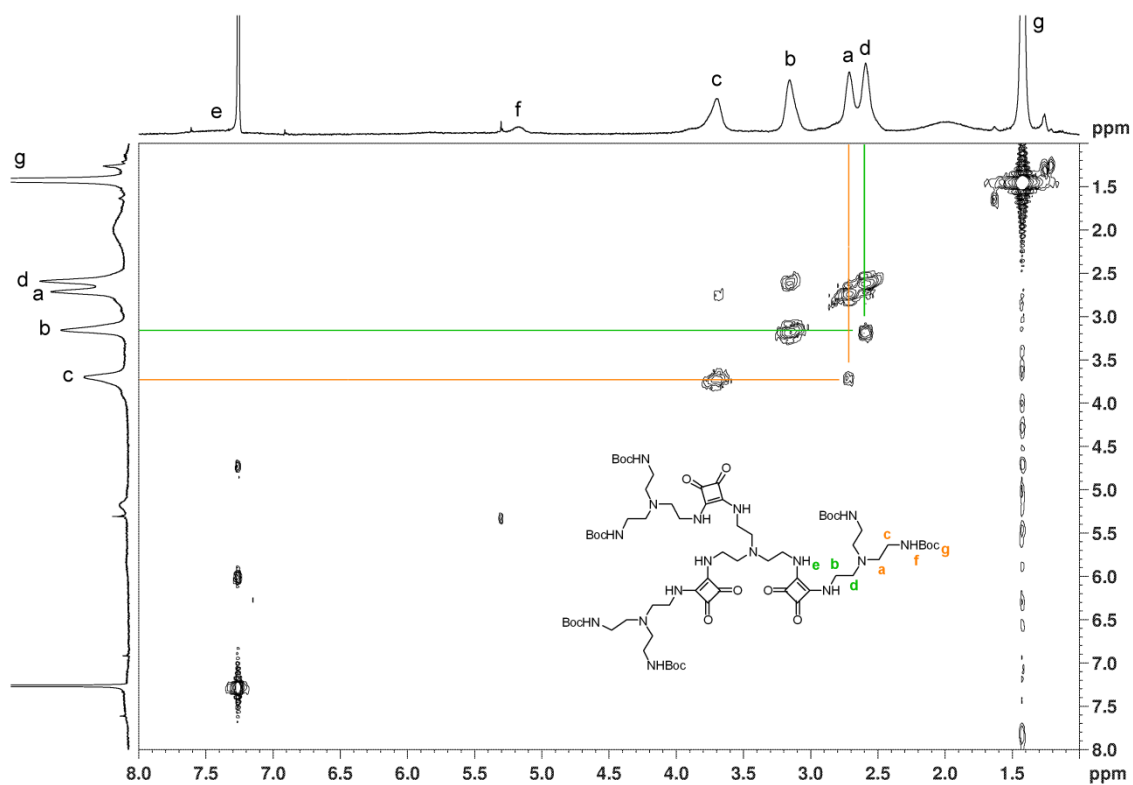


Figure S50. 2D COSY spectrum of **1A-G1** in CDCl_3 at 298 K.

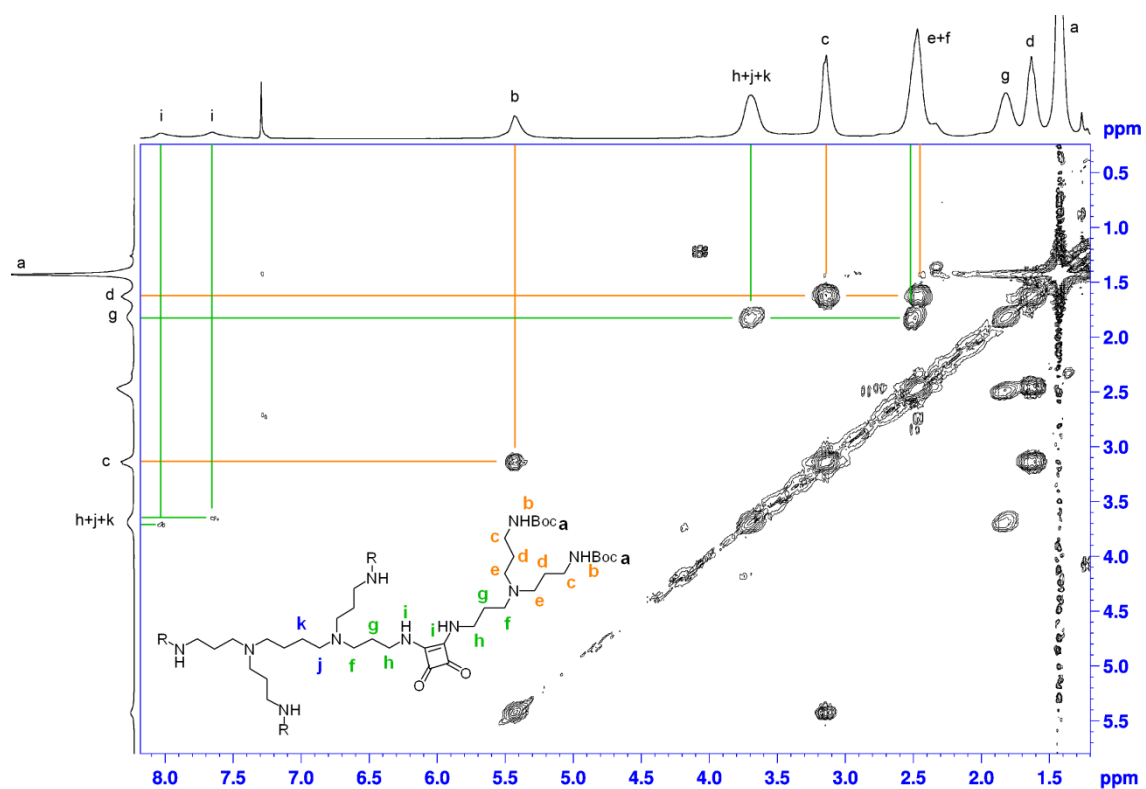


Figure S51. 2D COSY spectrum of **2B-G1** in CDCl_3 at 298 K.

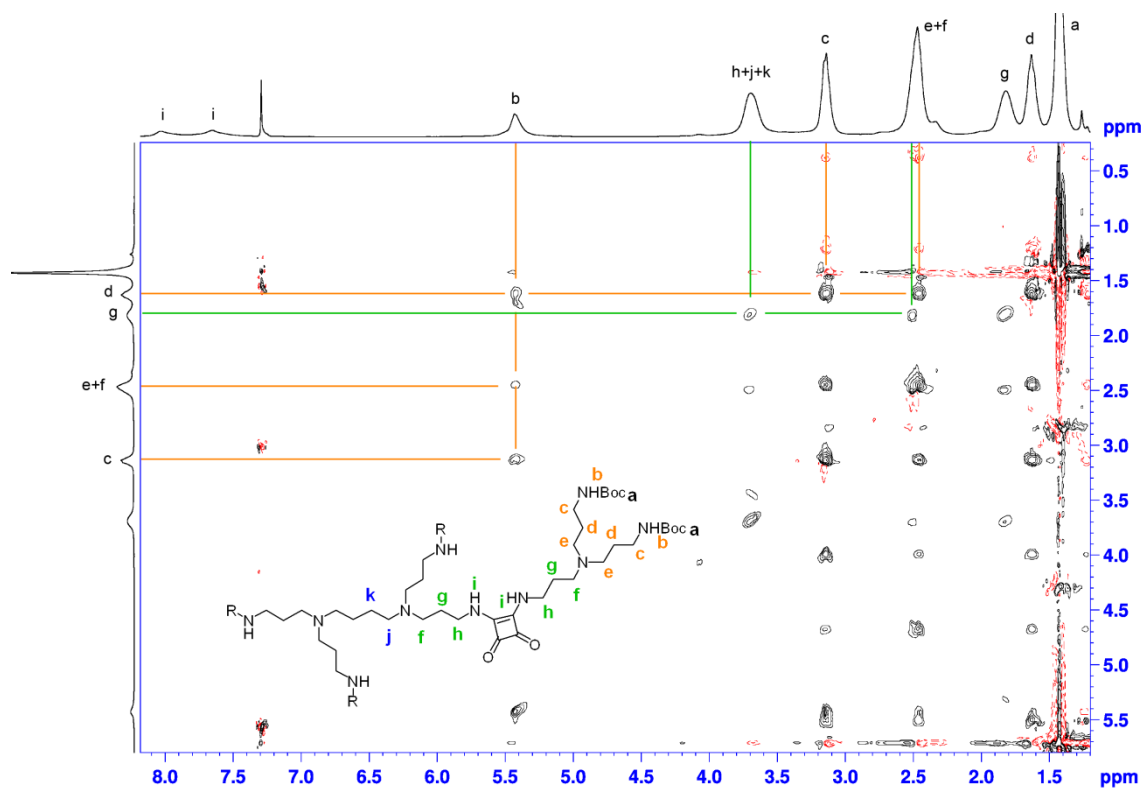


Figure S52. 2D TOCSY spectrum of **2B-G1** in CDCl_3 at 298 K.

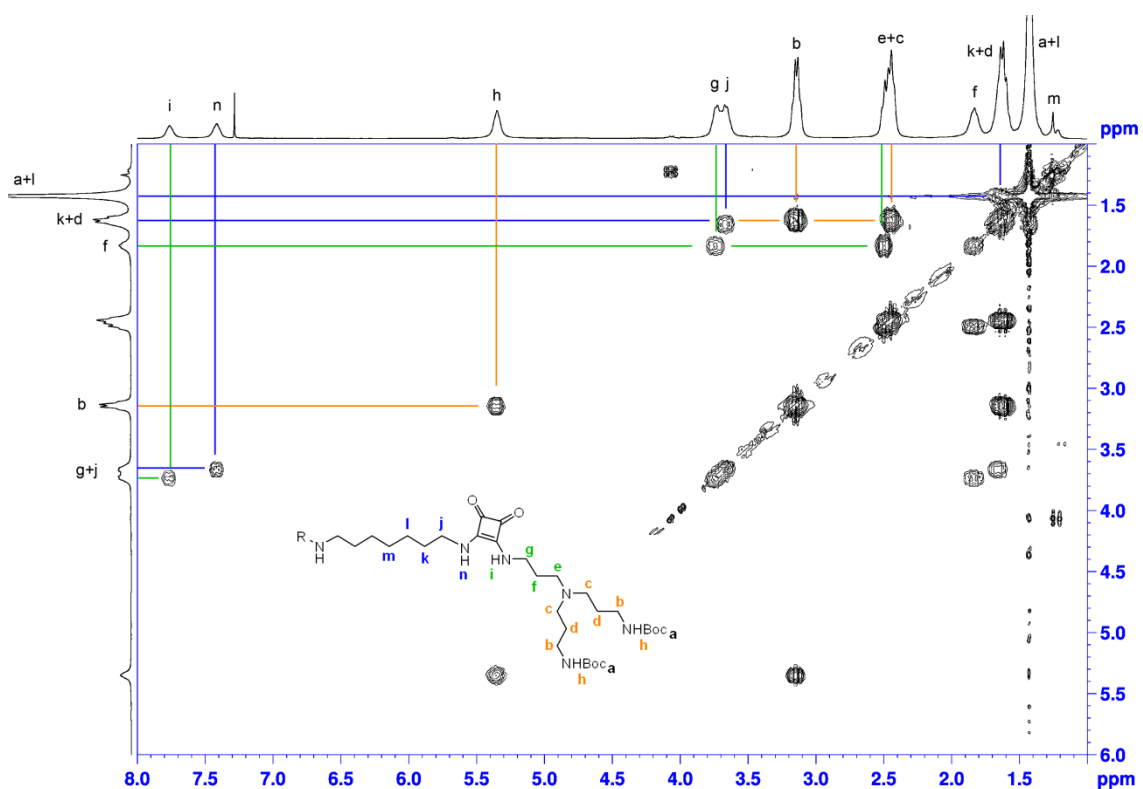


Figure S53. 2D COSY spectrum of **2C-G1** in CDCl₃ at 298 K.

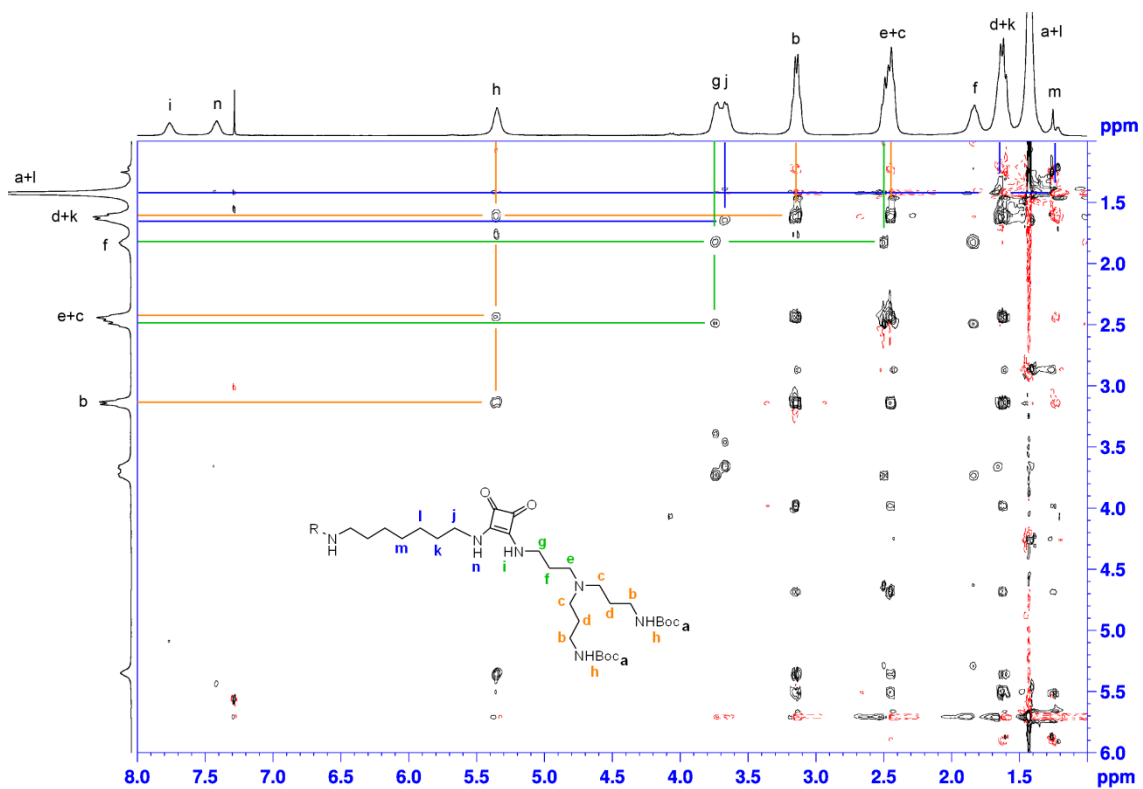


Figure S54. 2D TOCSY spectrum of **2C-G1** in CDCl₃ at 298 K.

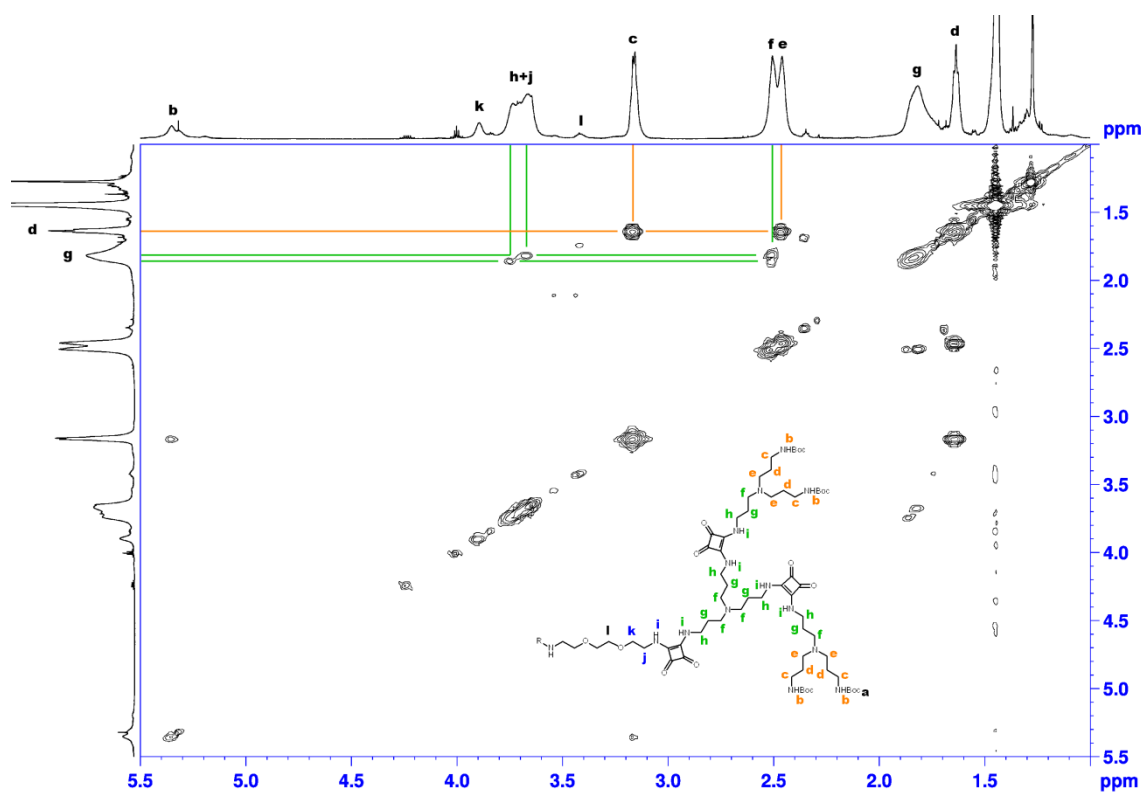


Figure S55. 2D COSY spectrum of **2D-G2** in CDCl_3 at 298 K.

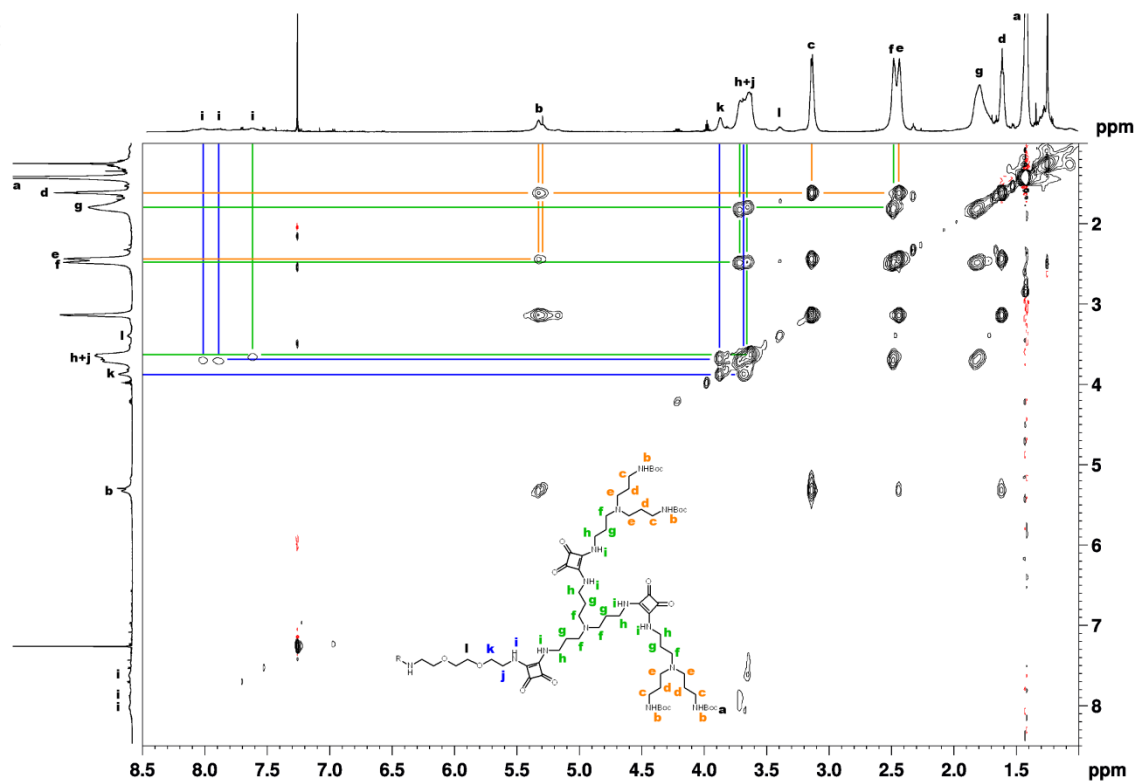


Figure S56. 2D TOCSY spectrum of **2D-G2** in CDCl_3 at 298 K.

Conclusions

Conclusions

The development of new supramolecular systems for applications in molecular recognition, self-assembly processes, molecular transport and catalysis are key features. The present work describes the design, synthesis and characterization of some examples of new supramolecular systems with cavities able to accommodate different guest molecules for different applications. Specifically, this thesis is divided in three sections.

Part I, describes the properties of a 2-aminobenzimidazole functionalized deep cavitand. This cavitand binds choline derivatives inside the cavity in MeCN:H₂O v:v mixtures. Taking advantage of this, it has been studied the hydrolysis of a choline carbamate catalyzed by the cavitand compound proving that the reaction involves three steps. First, the binding of the choline carbonate to the cavity, the carbamylation of one of the aminobenzimidazole groups on the walls of the cavity and the hydrolysis of this intermediate compound by a water molecule located in the walls of the cavity. The process has been studied by UV-vis and ¹H-NMR techniques showing that the last step is very slow and mimics the action of an acetylcholinesterase inhibitor.

Part II, describes six new cycloimine compounds obtained from the slow imination reaction of two propargyldimines with two dialdehydes. Different reaction conditions were tested, but the best results were obtained when the reaction was carried out in AcOEt at room temperature. When the reaction takes place in refluxing MeOH, two diastereoisomers were isolated. The treatment of the mixture of isomers in CHCl₃ at 50°C for 15 hours yields the same product that is obtained when the reaction is carried out in AcOEt and corresponds to the thermodynamic product. It was not possible to isolate the kinetic stereoisomer in any case.

Two of the cycloimines were obtained as crystalline material and were characterized by X-ray, NMR, TGA, DSC and SEM techniques. The X-ray analysis of both compounds showed that one of them crystallizes to form one dimensional channels filled with the reaction solvent (AcOEt). The porous structure was maintained after desolvation. The resulting channels can be filled with different guest molecules only by immersion of the crystals (solvated or desolvated) in the guest solution. The X-ray analysis of the new complexes allows the determination of the structure of the guests. The exchange was also confirmed by NMR, GC, TGA or DSC analysis. Some selectivity studies were performed showing that diethyl phthalate sorption is preferred over other phthalate derivatives.

Part III describes the preparation of different new squaramide-based supramolecular compounds. Chapter 4, reports the design and synthesis of a new set of squaramide-based macrocycles from the condensation of α,α' -Dibromo-*m*-xylene with a bicyclic squaramide. If the same reaction is carried out with formaldehyde and the squaramide derivative, oligomeric chains are obtained. In no case, however, it was possible to isolate the mixture of products.

During the preparation of the squaramides derivatives for the macrocyclization, a new set of squarimide compounds not described in the literature were isolated. These compounds were prepared from the reaction of benzil derivatives with squaramides. The pK_a's of these new compounds were determined in water by UV-vis measurements showing that the NH of the squarimides is more acidic than the same protons of squaramides.

Finally, Chapter 5 describes the synthesis of G1 and G2 squaramide-based dendrimeric compounds for their posterior biological evaluation. To synthesize these dendrimers, four different cores and two squaramide linkers were used. The different generations have been studied by two dimensional NMR experiments and by zeta potential measurements but further experiments are needed.

